Universidade de Aveiro Departamento de Geociências
2002

Maria Teresa Condesso de Melo

modelo matemático de fluxo e transporte de massa do sistema multiaquífero Cretácico da região de Aveiro (Portugal)

flow and hydrogeochemical mass transport model of the Aveiro Cretaceous multilayer aquifer (Portugal)

dissertação apresentada à Universidade de Aveiro para cumprimento dos requisitos necessários à obtenção do grau de Doutor em Geociências, realizada sob a co-orientação científica do Doutor M. A. Marques da Silva, Professor Associado com Agregação do Departamento de Geociências da Universidade de Aveiro e do Doutor W. M. Edmunds, Investigador Principal do St. Peters College da Universidade de Oxford e Professor Convidado da Universidade de Kingston (Reino Unido)

o júri

presidente — Reitora da Universidade de Aveiro

Doutor Emilio Custodio Gimena
professor catedrático da Universitat Politècnica de Catalunya (Barcelona, España)

Doutor Carlos Alberto da Costa Almeida
professor catedrático aposentado da Faculdade de Ciências da Universidade de Lisboa

Doutor Manuel Oliveira da Silva
professor catedrático da Faculdade de Ciências da Universidade de Lisboa

Doutor Fernando Joaquim Fernandes Tavares Rocha
professor catedrático do Departamento de Geociências da Universidade de Aveiro

Doutor Manuel Augusto Marques da Silva (Orientador)
professor associado com agregação do Departamento de Geociências da Universidade de Aveiro

Doutor Wyndham Mike Edmunds (Co-Orientador)
senior research associate, Oxford Centre for Water Research, University of Oxford, Oxford (UK)
honorary research associate, British Geological Survey (Hydrogeology), Wallingford (UK)
visiting professor, Kingston University, Surrey (UK)

agradecimentos/ acknowledgements

It would not have been possible to achieve the objectives of this Ph.D. thesis without the help and disinterested collaboration of a great number of people to whom I am deeply grateful. I would therefore like to express special gratitude to the following people and institutions for their assistance and scientific contribution:

My supervisors, Professors M.A. Marques da Silva and W.M. Edmunds, for their support and invaluable guidance in this project. Their deep interest in the Aveiro Cretaceous aquifer has always been a source of inspiration for me, and I clearly benefited from the many pleasant and fruitful discussions we have had since 1997. I also thank them for providing the unique opportunity of meeting, working with and learning from some of Europe's foremost groundwater scientists.

Praxis XXI and the Science and Technology Foundation (FCT), for having funded this research from its very beginning (BD/9743/96 Praxis XXI). I would like to extend my thanks to the British Council (Windsor Treaty) and the European Union (Projects PALAEAUX ENV4-CT95-0156 and BASELINE EVK1-1999-00032P) for co-funding research projects which widened the scope of the present research. I have learned a lot from co-operating with scientists and institutions involved in these projects.

Professors A.C.J. Appelo, E. Custodio, H. Loosli (v.b.f.f.S.), L. Ribeiro and F.T. Rocha, whose teaching, suggestions and ideas certainly influenced my thinking and the content of this work.

Dr C. Kjoller and Professor D. Postma, for helping me with PHREEQC and the discussion on geochemical modelling.

Thomas Franz and the rest of the Waterloo Hydrogeologic staff, for their unconditional help with Aquifer Test, Visual Modflow and flow modelling.

David Buckley, for coming to Portugal to carry out the depth sampling campaign, teaching me how to use Viewlog and helping with the interpretation of the geophysical logging results. I would also like to thank other colleagues, friends and members of staff of the British Geological Survey, in particular Janice Trafford and Drs C.J. Milne, P. Shand, G. Darling, D. Kinniburgh, P. Smedley, for their full support, good suggestions and helpful scientific discussions in the last five years.

Dr B.A. Barbosa and António Barra, for introducing me to the geology of the study area and allowing me to use their own unpublished notes with unique geological data about it.

Dr A.C. Batista, for her help with using geostatistics to complement the study of groundwater baseline quality.

Luis Galiza, for his help with dealing with GIS maps and databases and other digital information.

D.R.A.O.T. Centro (Dr F. Peixinho de Cristo and J. Serrano, Mr C. Ramos and P. Sobral), Serviços Municipalizados de Aveiro (Eng. A. Roque, R. Ferreira and Mr Carlos Gomes), Ílhavo (Eng. H. Labrincha), Murtosa, Águeda, Vagos and Oliveira do Bairro for letting me use their boreholes for the necessary field work and for supplying all the necessary data about groundwater exploitation. I would like to acknowledge all the other borehole owners, who opened their doors to me to let me get water samples for analysis.

Mr João Graça, for his invaluable collaboration with all the field work and Mrs M.ª da Graça Marques, for her precious help with the final printing. Also the other staff of the UA Geosciences Department, whom it is impossible to acknowledge individually, for the excellent assistance received during the years I have been working with them.

The many colleagues and friends who have inspired me and given me confidence and moral support all these years. They contributed to create a good and supportive working atmosphere around me and to make me smile when I was almost loosing hope. Special encouragement and support came from A. Abranches Marta, A. Ferreira, C. Castelo Branco, C. Abranches Marta, C. Migueis, D. Gusini, D. Terroso, E. Ferraz, E. Ramalho, F. Teixeira-Dias, G. Abranches, G. Cabano, G. Seabra Pereira, I. Abrantes, J. Naudin, J. Serrano, J. Vidinha, J. Baptista Silva, L. Candela, M. Olim, M. Inácio, M. Manzano, M.R. Queiró, M. Iglesias, P. Morgado, P. Blaser (v.b.f.f.S.), S. Mota Leite, S. Rey, T. Trick, V. Martins and Z. Abu Heen. And also from A. Gallina, A. Lamberti, A. Benavides, A. Haria, B. López San Roman, C. Perrin, E. Frank, M. Hodnett, M. Ashworth, N. Alam, R. Cano, S. Catmur and S. Oliveira, whose friendship contributed to make my stay in Oxford a pleasant and unique experience.

Not because of their scientific contribution but because their love, care and relentless confidence were the fundamental encouragement to get on and complete this thesis, I thank Heleno and my parents Clara and Max. Also my grandmother, my brother Chico, my sister Catarina and her husband Francisco (thanks also for the long jogs), my uncles Tó-Zé and João, my aunt Romi and all the rest of the family. For many years, the Ph.D. looked like a never ending lone job, and it was very important to be surrounded by such a family, who understood my absences and made me feel close even when I was miles away.

resumo

Desde meados da década de 1960, que o sistema multiaquífero Cretácico de Aveiro é intensamente explorado, o que conduziu gradualmente a uma acentuada depressão dos níveis piezométricos regionais. Este facto, porque tem lugar num aquífero costeiro e com uma limitada recarga natural, contribui para aumentar o risco de deterioração da qualidade da água subterrânea, quer por fenómenos de intrusão marinha, quer por mistura com águas de níveis aquíferos profundos com elevado grau de mineralização.

Constituindo um recurso de água vital para toda a região, este sistema aquífero adquire um claro valor económico, que exige a adequada avaliação, exploração, gestão e conservação dos seus recursos.

A tese 'Modelo matemático de fluxo e transporte de massa do sistema multiaquífero Cretácico da região de Aveiro (Portugal)' representa nesse sentido um esforço sistemático para reunir e integrar toda a informação geológica, hidrogeológica, geoquímica e paleoclimática disponível sobre este sistema aquífero à escala regional, de modo a analisar e desenvolver um conhecimento mais completo do sistema, que permita criar condições para uma exploração sustentável dos seus recursos. Para isso procedeu-se à construção de um modelo tridimensional de diferenças finitas (MODFLOW) a partir de um modelo conceptual e à sua calibração e utilização para descrever o fluxo subterrâneo no aquífero Cretácico de Aveiro. O programa MODPATH foi usado para determinar e ilustrar as linhas de fluxo advectivo regional subterrâneo.

O desenvolvimento de um modelo de fluxo e transporte de massa permitiu assim desenvolver um melhor conhecimento do sistema hidrogeológico no seu estado natural e avaliar o impacte ambiental resultante das actividades antrópicas. Permitiu ainda descrever: (1) os limites físicos e hidráulicos do sistema aquífero, e (2) as relações entre as águas superficiais e subterrâneas; (3) criar um modelo numérico que calcule o balanço de água subterrânea, a recarga natural ao sistema, as zonas de descarga e descrever a distribuição de fluxo regional; (4) relacionar o quimismo das águas subterrâneas com as principais direcções de fluxo subterrâneo, e (5) fazer uma previsão dos efeitos à escala regional de uma possível variação na recarga ou na bombagem do aquífero.

Os dados geoquímicos foram usados para descrever as relações existentes entre o quimismo da água subterrânea, a mineralogia do aquífero e as principais direcções de fluxo subterrâneo actual e no passado. A variabilidade espacial nas concentrações dos principais solutos foi avaliada e relacionada com a variação das propriedades do aquífero à escala regional. As análises químicas e isotópicas da água subterrânea e do próprio material aquífero ao longo das principais direcções de fluxo foram usadas para avaliar os processos hidrogeológicos e geoquímicos predominantes no aquífero e para fazer a datação das águas subterrâneas.

abstract

The Aveiro Cretaceous aquifer has been exploited for public and industrial supply since the nineteen sixties. Groundwater intensive exploitation is affecting the natural piezometric surface and threatening the balance of this natural system. In recent years, a continuous fall in the piezometric surface has been observed due to intensive groundwater abstraction leading in some areas to values of -25 m below mean sea level. Because it occurs in a coastal aquifer, partially confined and with limited natural recharge, there is the threat of it leading to gradual deterioration of the water quality, either because of salt-water intrusion or due to mixing with very high-mineralised waters from deeper aquifer levels, nowadays with higher water potentials.

This aquifer has proven to be quite unique in Europe from the geochemical point of view. It is very important as an archive of past climate conditions in temperate regions of Europe and is nowadays recognised as a strategic water resource for the Aveiro region. It has clear economic importance requiring an adequate evaluation, exploitation, management and preservation of its resources.

The thesis 'Flow and transport model of the Aveiro Cretaceous multilayer aquifer (Portugal)' represents a systematic effort to assemble geologic, hydrologic, and geochemical information, to analyse and develop an understanding of the system, and to develop predictive capabilities that will contribute to an effective sustainable management of the system. The approach followed required the construction of a three-dimensional finite difference groundwater flow model (MODFLOW), and its calibration and use to describe the regional flow. The particle-tracking program MODPATH was used to determine and illustrate simulated advective regional groundwater flow patterns.

The use of computer simulation contributed to develop an understanding of the natural, undisturbed hydrologic system and the changes brought about in it by human activities. It also contributed to describe: (1) the physical and hydraulic boundaries of the aquifer system, and (2) the regional relations between surface water and groundwater; (3) to devise a numerical model to compute a regional groundwater budget, regional recharge and discharge areas and the patterns of regional groundwater flow; (4) to relate groundwater chemistry to these patterns of regional flow; and (5) to predict the effect of a possible variation in the recharge or volume of abstraction on a regional scale.

Geochemistry data were used to describe the relations between groundwater chemistry, aquifer mineralogy, and present and past patterns of regional flow. The spatial variability in the concentrations of major solutes in groundwater was evaluated and related to aquifer properties at regional scale. Chemical and isotopic analyses of groundwater and aquifer material along with general directions of regional groundwater flow were used to evaluate the important hydrological and geochemical processes controlling groundwater chemistry and to estimate groundwater ages qualitatively.

This thesis is dedicated to my parents,

Clara and Max

and, to *Heleno*.

"The idea that knowing the recharge (by which one generally means the virgin rate of recharge) is important in determining the size of a sustainable groundwater development is a myth. This idea has no basis in fact.

The important entity in determining how a groundwater system reaches a new equilibrium is capture. How capture occurs in an aquifer system is a dynamic process. For this reason, hydrogeologists are occupied in studying aquifer dynamics. The principal tool for these investigations is the groundwater model.

These ideas are not new; Theis spelled them out in 1940. Somehow the ground water community seems to lose sight of these fundamental principles."

J.D.Bredehoeft

(In: 'The Water Budget Myth Revisited: Why hydrogeologists Model'
Groundwater 40, No. 4: 340-345, Issue Paper)

"If sustainable development is to mean anything, such development must be based on an appropriate understanding of the environment – an environment where knowledge of water resources is basic to virtually all endeavours."

(Report on Water Resources Assessment, WMO/UNESCO, 1991)'

CONTENTS

APPENDIX C

APPENDIX D

APPENDIX E

LIST OF FIGURES

CHAPTER 1

CHAPTER 2

CHAPTER 3

CHAPTER 4

CHAPTER 5

CHAPTER 6

CHAPTER 7

LIST OF TABLES

CHAPTER 6

1

INTRODUCTION

Groundwater is a strategic natural resource in Portugal for the present and future generations. Some parts of the country where surface water is deficient or unsuitable are fully or partially dependent on groundwater for water supply (Fig. 1.1). Groundwater is also the source of most of the water used for irrigation, and supplies approximately 60% of the drinking water to urban and rural areas, supports industries and crop irrigation, and contributes to rivers, lakes, springs and streams baseflow, moderating the influence of periods of low precipitation. This contribution provides an important amount of the water that supports fisheries and sustains many of the country wetland ecosystems and has a strong influence on the large variety of their habitats. From an overall national perspective, groundwater resources appear ample, but they are frequently put under pressure or at risk by many human and industrial activities and face increasing demands from growing populations, urbanization (including residential sanitation and solid waste disposal) and intensive agricultural and industrial activities. Furthermore, overpumping is threatening the sustainability of the abstractions, and different types of contamination are producing a general decline in the baseline quality of groundwater systems, often without any strong and effective legal action to protect it.

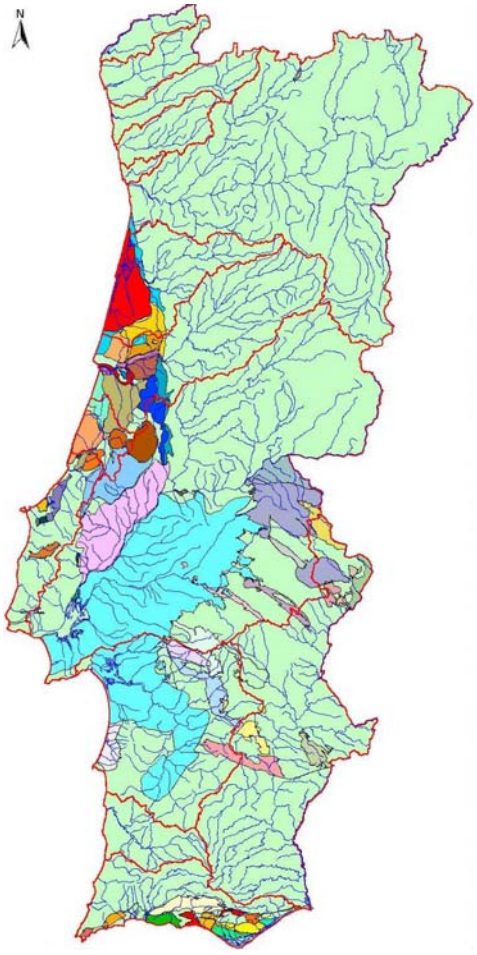

Fig. 1.1 Principal river basins and aquifer systems in Portugal. All together they guarantee an overall availability of more than 25,000 hm^3 of fresh water per year (CE, 1997; PNA, 2002).

The observation of this gradual deterioration has lately led to increased public awareness of the importance and vulnerability of this hidden resource and motivated the Water Authorities to

formulate a National Plan for Groundwater Protection and Sustainable Management. Its public presentation by the Ministry of Environment in April 1999 was interpreted as a clear sign that the preservation of good quality groundwater resources is finally becoming a prior environmental concern. This document called public attention to the importance of groundwater resources at national scale and placed emphasis on the necessity for immediate definition of: (1) the principal aquifer bodies, (2) the main groundwater uses, (3) the well-head protection areas, and (4) the groundwater quality and quantity monitoring networks. Simultaneously, the new European Union (EU) policy concerning the protection of the environment and natural resources assisted the Portuguese authorities in conducting legislative measures that could prevent groundwater mistreatment and ensure a sustainable management of both surface and groundwater quantity and quality in Portugal.

In terms of groundwater, the achievement of these objectives has been facilitated by three important actions carried out in the last two years. These actions included the implementation of the new Water Framework Directive (2000/60/EC) in December 2000 (WFD, 2000), the accomplishment of the River Basin Plans (PBH) late in 2001 and first months of 2002 and recently the approval of the National Plan of Water (PNA, 2002) (D.L. nº 112/2002 17 Abril).

Both the River Basin Plans and the Water National Plan include regional scale hydrogeological studies of a number of the country's is most important aquifer systems which represent an important part of its total water supply. Although these studies are quite detailed they do not foreclose the necessity for further research and for the submission of proposals to European Union (EU) Research and Technological Development Programmes, which would improve the scientific basis for the rational management of national groundwater resources. In this context, it was a great challenge for the Geosciences Department of the University of Aveiro to develop two research projects - *PALAEAUX* and *BASELINE*, funded within EU Fourth and Fifth Framework Programmes in order to carry out further detailed hydrogeological studies in the two principal regional aquifers of the Lower Vouga basin (Aveiro, Portugal).

The *PALAEAUX project - Management of Coastal Aquifers in Europe: Palaeowaters, Natural Controls and Human Influence* (1996-1999) brought together the origin and evolution of palaeowaters in the coastal areas of Europe, from the Baltic region to the Iberian Peninsula (Edmunds & Milne, 2001). The Aveiro Cretaceous Aquifer System (ACAS) was one of the key aquifers selected for this study. During the project the present distribution of palaeowaters in the aquifer was determined, as well as their importance as archives of former climatic conditions, and their potential as valuable sources of good quality drinking water, unaffected by impact of the industrial era.

The ongoing *BASELINE project - Natural Baseline Quality in European Aquifers: A Basis for Aquifer Management* (2000-2003) provided us the opportunity to study the baseline groundwater

quality of both the Aveiro Cretaceous and Quaternary Aquifer Systems (AQAS) taking geochemical considerations and residence times into account. The project aims to provide a Europe-wide scientific approach to the concept of baseline quality of groundwaters and a methodology for the application of scientific data and concepts pertinent to policy decisions, especially with regard to implementing the Water Framework Directive. Such a standard is essential as it makes possible the scientific assessment of groundwater quality natural variation and whether or not anthropogenic pollution is taking place. As well as giving a scientific framework, this project provides a forum for discussion with policy makers and end users and helps to integrate scientific research and policy decisions towards the goal of achieving the sustainability and protection of Europe's high quality groundwater.

This PhD thesis was developed simultaneously with both research projects, which contributed to enlarge its scope and objectives, and provided an opportunity to synthesise earlier work and carry out further investigations using new state-of-art methodologies. The overall research was planned with the principal purpose of bringing together information on the geology, hydrology, geophysics, geochemistry and groundwater flow of the Aveiro Cretaceous aquifer in order to derive a coherent and broad understanding of the aquifer system, to determine the risk of changes brought about in the aquifer by human activities, and to develop predictable capabilities that can contribute to a more effective management of the natural hydrogeologic system.

1.1 Background

The present research focuses on the Aveiro Cretaceous aquifer system, a multilayer coastal aquifer that covers over 1,800 km^2 in the northwest part of the Portuguese mainland and the adjacent continental shelf and is an integral part of the Lower Vouga sedimentary basin (Fig. 1.2). The aquifer is part of a thick sequence of Mesocenozoic sediments underlying Quaternary deposits and one of the largest. And, because of its intensive use in public water supply, industry and also agriculture, in the southern part of the study area, is economically one of the most important aquifers in Portugal.

The Lower Vouga basin was traditionally a mainly rural area, but in the last decade widespread industrial development has occurred and the region is nowadays one of the most industrialised areas in Portugal. The main industries are pulp and paper factories, ceramics, food manufacturing, graphic arts, metallurgy, metalomechanic, transport equipment and footwear. Besides these industries and agriculture itself, which is still responsible for 20% of the total employment in the area, the region offers a wide range of fishing and fish-farming activities. Apart from lagoon-based activities - inshore fishing and the farming of sea bass and sea bream - it

includes one of Portugal's leading fresh-fish and deep-sea fishing ports, which has led to the development of a significant processing industry.

The installation of all these industries in the region led to significant improvements in the services provided and contributed to an increase in job opportunities in both the secondary and tertiary sectors of regional economy, attracting more people to this prosperous region and increasing the population. As a result, the local resident population increased 12% in the last 10 years exceeding 385,000 people in 2001, with over 214 inhabitants per km^2 and a ratio of territory occupation of around 98% (INE, 2002).

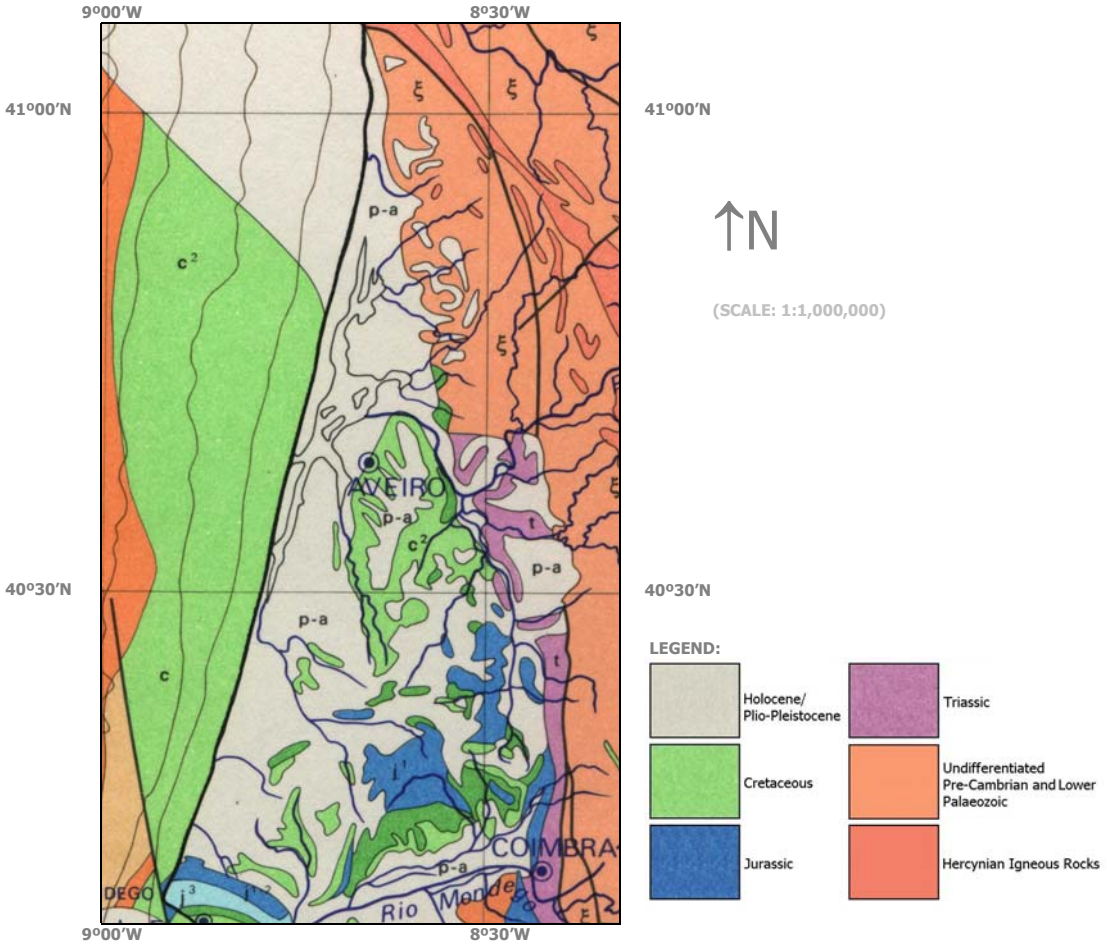

Fig. 1.2 Generalized surficial geology of the Lower Vouga Sedimentary basin and adjacent continental shelf (from Boillot & Mougenot, 1978).

All these rapid social and economic transformations in the Lower Vouga region place a continually increasing demand on water resources in the basin. Historically, the local populations and industries pumped groundwater from the shallow Quaternary aquifer layers or in the case of the Aveiro area, used water from the 'Vale das Maias' mine to supply their water needs. However, in the early forties and fifties water quality problems related to high salinity and contaminated

waters were associated with some poisoning episodes that affected the codfish processing industries, and obliged the local authorities to look for alternative water sources. Further hydrogeological studies carried out in the Quaternary aquifer in the sixties proved that there were water quality problems (mainly high iron and eventually, high chloride) that could limit the use of shallow groundwater for public water supply.

The growing demand for water resources in the basin led progressively to an increased reliance on groundwater from the Cretaceous aquifer formations for most of the urban and industrial water supply. The Vista Alegre porcelain factory (Ílhavo) drilled in 1941/42 one of the very first deep boreholes crossing Cretaceous formations (150 m deep); and since then almost two hundred more boreholes have been drilled in the aquifer (Fig. 1.3).

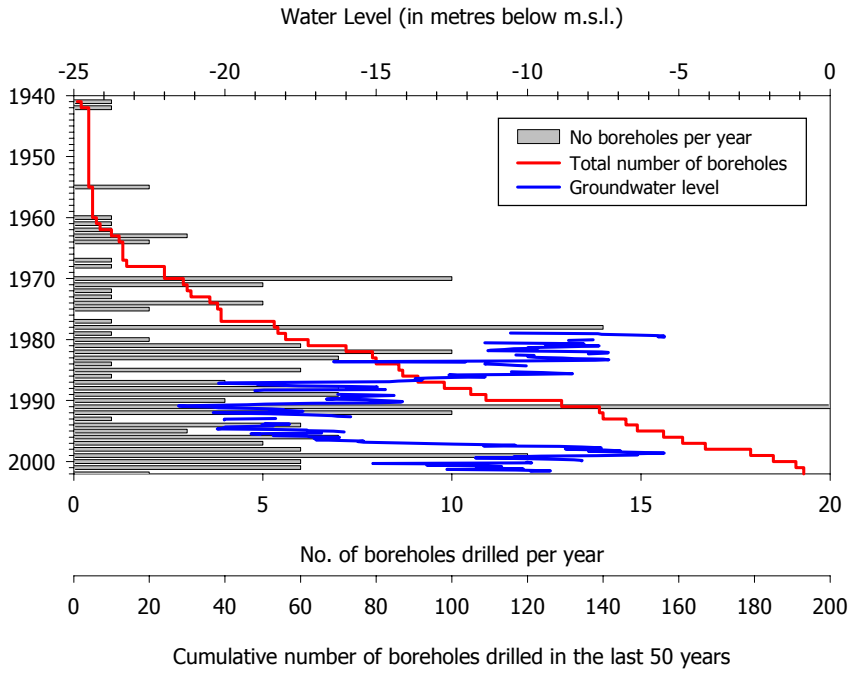

Fig. 1.3 Number of boreholes drilled per year in the Aveiro Cretaceous aquifer and comparison to the evolution of the groundwater level in a piezometer (O2/174/002) of the National Groundwater Quantity Monitoring Network.

Original conditions in the aquifer were those of a confined aquifer in two thirds of its extension, with a smooth decreasing natural gradient from the recharge area in the east towards the sea, where pristine groundwaters with residence times in the order of 18 ka or older have been identified. Radiocarbon ages for the aquifer indicate a smooth gradient across the aquifer, implying continuous flow during the Late Pleistocene and Holocene but suggesting very limited rate of modern recharge.

Artesian conditions prevailed for many years in the flat areas bordering the coastline and may still occur these days in very restricted areas (*e.g.*, south of Vagueira) (Fig. 1.4). However,

beneath the Aveiro – Esgueira - Cacia region, intensive pumpage for municipal and industrial supply since the early sixties has gradually caused natural piezometric surface declines and is now threatening the natural balance of this coastal aquifer system. Long-term hydrographs of several boreholes tapping the Aveiro Cretaceous aquifer show a general downward trend from the late 1980's until mid 1990's (Fig. 1.3). From 1987 to 1995 the piezometric level fell by over 1.5 m per year exceeding locally 40 m below mean sea level (m.s.l.) and contributing to reverse the natural flow direction in the region. Spring flows have also been affected by groundwater development and, in the eastern part of the study area, the natural discharge from the groundwater system in a few springs was reduced gradually until they almost dried up (Marques da Silva, 1990).

Fig. 1.4 Artesian borehole drilled in April 2002 in the Aveiro Cretaceous aquifer at the Areão beach (south of Vagueira).

The significant depletion of water levels in the confined part of the aquifer produced growing concerns about the risk of groundwater quality deterioration in the aquifer due to salt-water intrusion, or to its mixing with very high-mineralised waters from deeper aquifer levels which nowadays have significant higher water potentials.

Worried about the long-term groundwater level declines, the Regional Water Authorities adopted restrictions to the development of groundwater from the aquifer and to the drilling of new boreholes in the region and the local public water supply companies (S.M. Águeda, Albergaria-a-

Velha, Aveiro, Estarreja, Ílhavo and Murtosa) started looking for alternative water resources. These companies were also worried about the increased costs associated with the exploration of deeper water levels and with water of decreasing quality standards (increasing Fe^{2+} and Cl^- contents).

Since 1996, the Carvoeiro Inter-municipal System (SIC) is finally progressively ensuring the water for public supply in the studied region using shallow groundwater from the river Vouga alluvium. The volume of abstractions from the Aveiro Cretaceous aquifer has therefore been gradually reduced and a rapid recovery of the regional piezometric levels is being observed. Increases in spring discharge also have been observed in a few springs located in the outcrop area of the aquifer. However, if the number of new boreholes keeps increasing and the volume of abstraction is not monitored, the precarious equilibrium just attained will soon be threatened again, putting at risk the objective of preserving this aquifer as a strategic water resource for present and future generations in the Aveiro region.

1.2 Purpose and scope

The Aveiro Cretaceous aquifer is probably one of the most studied deep confined aquifers in Portugal but, paradoxically, the knowledge about its hydrodynamical behaviour as a whole multilayer aquifer system cannot be considered satisfactory yet. There are still a number of uncertainties and hypothesis about the aquifer recharge and discharge processes, interlayer flows, and geochemical controls that need further investigation to provide the scientific information needed for accurate groundwater-resources management in the aquifer.

An improved understanding of the hydrogeology of the Aveiro Cretaceous aquifer is important not just from the scientific perspective (this aquifer has already proved to be quite unique from the geochemical point of view and to be a good archive of past climate conditions in temperate regions of Europe) but mostly from the viewpoint of the sustainable development of the Aveiro region.

This deep confined aquifer is a very good quality water resource for the Aveiro region; however, groundwater resources in the Aveiro Cretaceous aquifer should not be considered a completely renewable resource because of the time scales involved. In this sense, the aquifer has a clear economic and strategic importance, which requires an adequate evaluation and sustainable management to guarantee the preservation of its resources.

A multidisciplinary methodology that included three principal approaches: (1) hydrogeology, (2) hydrogeochemistry (including aquifer matrix-water interaction) and (3) modelling was adopted, in order to better address the questions related to the understanding of the aquifer complex hydrodynamics.

These three approaches indeed determine the basic structure of this work, with all the research developing from and around these three main branches. The first part summarises the regional geology of the study area and the hydrogeology of the aquifer. Borehole geophysical data have been integrated with geologic and hydrogeologic information to provide a means for the development of a comprehensive interpretation of the hydrogeologic conditions and a conceptual understanding of groundwater flow. Pumping test interpretation results data are used to extract information about principal hydrological properties (*e.g.*, hydraulic conductivity, specific storage).

The second part of the thesis is the result of the detailed hydrogeochemical study of the aquifer. It included the identification of major groundwater geochemical patterns in the aquifer, study of the aquifer natural stratification, determination of the aquifer natural background levels, and definition of the controlling processes responsible for the downgradient changes in water chemistry, focusing on mixing processes and rock/ water interaction.

This was accomplished by studying and comparing the chemical and isotopic composition of rain and groundwater, through determination of ionic molar and isotopic ratios and residence times, calculation of saturation indexes relatively to most common minerals, and by quantifying the mass balance of solutes along the main flowpaths using a reaction-path geochemical model.

In the final part, a three-dimensional finite-difference groundwater flow model is used to describe regional flow in the Aveiro Cretaceous aquifer. Flow modelling results are validated using long term water level data and carbon-14 calculated ages and are used to predict future scenarios for the aquifer.

1.3 Objectives

This PhD thesis summarises information on the hydrogeology, geochemistry and regional groundwater flow in the Aveiro Cretaceous multilayer aquifer system (Aveiro, Portugal). Groundwater flow and geochemical mole-balance transport modelling was used as a framework for studying aquifer hydrodynamics and for improving the present understanding on regional groundwater flow processes. The specific objectives are the following:

(1) to improve knowledge on the hydrogeologic framework of the aquifer;

(2) to characterize the aquifer boundaries;

(3) to adequately determine the amount of natural recharge to the aquifer using new estimation techniques and assess their usefulness for simulating groundwater flow in regional scale aquifers, verifying the effect of scaling up some specific site-recharge estimates to regional values;

(4) to provide an overview of the water-rock interactions that control the aquifer solute chemistry, and to integrate this information with radiocarbon and environmental isotope results relating to the principal patterns of regional flow;

(5) to integrate the hydrogeological and geochemical information to present a comprehensive analysis of the occurrence and flow of water in the aquifer system;

(6) to build and calibrate a three-dimensional flow model to compute a regional groundwater budget, regional recharge and discharge areas, and patterns of regional groundwater flow;

(7) to provide an additional scientific tool for future decision making on aquifer management.

1.4 Previous hydrogeological investigations

Numerous geologic investigations have been made in the Lower Vouga sedimentary basin but it is beyond the scope of this PhD thesis to list all these research works. Most of the hydrogeology works, however, are referred later in this section and other references are given throughout the text. Some of the major references for stratigraphy, palaeontology, palaeogeography, morphology, structural geology and mineralogy in the study region are listed in Rocha (1993).

The Aveiro Cretaceous aquifer has motivated numerous studies over the last 20 years that produced valuable information for the understanding of the aquifer. The first references to the hydrogeology of the Cretaceous formations can be found in Zbyszewski (1963), Zbyszewski *et al.* (1972) and in the explanatory notes that come with the geological maps of Aveiro (Teixeira & Zbyszewski, 1976) and Vagos (Barbosa, 1981). These geological maps are at a scale of 1:50,000 and were used together with the one for the Ovar region (Teixeira, 1976) and another for the Fermentelos region (Barra, 1998) to compile the geology for the study region.

Saraiva *et al.* (1983) and Lauverjat *et al.* (1983) published the first articles about the aquifer but it was Peixinho de Cristo (1985) who wrote the first synthesis on the hydrogeology and hydrochemistry of the aquifer and suggested an interpretative cross-section for it. Marques (1990) and Reis (1990) estimated the natural recharge for the north and south parts of the aquifer, respectively, using both the conventional Penman-Grindley method and data on shallow groundwater levels.

Marques da Silva (1990) integrated most of the information available at that time on the geology, hydrogeology, hydrochemistry and geophysics of the aquifer, developed a conceptual model for the aquifer and identified palaeowaters in the confined part of the aquifer. This very complete work is still nowadays a reference for any study carried out in the area. Other papers

written by the same author include Marques da Silva (1992) and Marques da Silva *et al.* (1993). Rocha (1993) studied in detail the mineralogy, sedimentology and geochemistry of the fine fraction of the Cretaceous sediments, a very important piece of research for the understanding of the aquifer hydrochemistry. And, Ferreira (1995) and Condesso de Melo *et al.* (2002*a*) studied the hydrogeochemistry of the Aveiro Quaternary aquifer which overlays the Cretaceous formations.

Carreira *et al.* (1996) and Carreira Paquete (1998) are two other reference papers for the aquifer. Using isotopic tools, the author confirmed the occurrence of palaeowaters in the confined part of the aquifer and documented an enrichment in $\delta^{18}O$ and $\delta^{2}H$ in waters recharged during the Late Pleistocene. The same author used noble gas recharge temperatures to prove that this aquifer is very important as an archive of past climate conditions in temperate regions of Europe.

Peixinho de Cristo *et al.* (1997) summarised the groundwater level monitoring data available for the aquifer and Oliveira (1997) used a mass balance model to predict groundwater chemical evolution along a NW-SE cross-section. In Oliveira *et al.* (1998*a, b*) the same author discussed the influence of aquifer layers mineralogy and cation exchange capacities on the hydrochemistry of the aquifer. Other papers about the aquifer include Condesso de Melo *et al.* (1998, 1999, 2001 & 2002*b, c, d*). Figueiredo (2002) used gravity survey data to define the bedrock topography and deep geological structures of the Lower Vouga region.

1.5 Scientific approach and methodology

A multidisciplinary scientific approach was used to develop a three-dimensional model that could simulate regional patterns of groundwater flow in the Aveiro Cretaceous aquifer. This approach allowed the integration of varied information on the hydrogeology and geochemistry of the studied hydrogeologic system benefiting both the conceptual model construction and the calibration processes, crucial steps to achieve an acceptable representation of the field situation.

The methodology followed included several steps summarised in the flow chart illustrated in Fig. 1.5. The study was initiated with the identification of the main goal of the research, which is to provide a new scientific tool that may be used for both interpretative and predictive purposes, assessing decision making, and providing additional insight into the controlling parameters of the aquifer system dynamics.

The second step of the study was the data collection and its organisation in a Microsoft® Access 97 database. At the beginning of the study, there was a lot of information available on the regional geology and hydrology, and aquifer hydrogeology and geochemistry. However, the majority of this information was not in a digital format and required specific data treatment to convert it to a useful and user-friendly format.

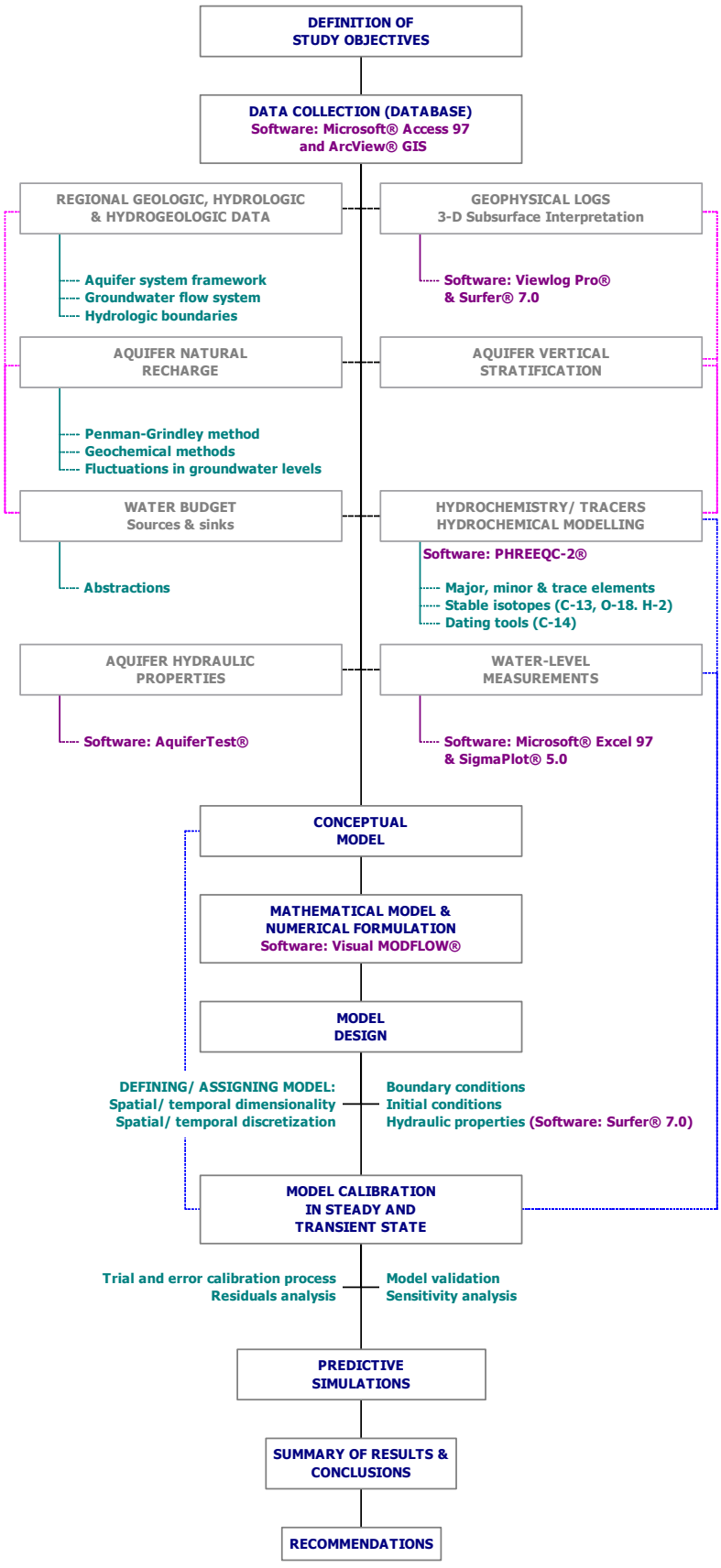

Fig. 1.5 Flow chart describing the methodology followed during the overall research.

The geology for the study area was digitised and integrated with the surface hydrology using a GIS support (ArcView®). Available borehole geophysical logs were digitised and correlated to each other along several aquifer cross-sections, providing unique information on the aquifer layers thickness. Data was spatially integrated using Surfer® 7.0 (Golden Software, Inc) and Viewlog Pro® (Viewlog Systems) and allowed for a three-dimensional interpretation of the aquifer system.

More than two hundred pumping tests were collected from the borehole drilling reports and interpreted using AquiferTest®. The estimated parameters were used to assign the range of aquifer hydraulic properties required for the flow model design.

The Regional Water Authorities provided long-term water levels in the aquifer and the corresponding hydrographs were plotted using Microsoft® Excel 97 and Sigma Plot® 5.0 (SPSS Science) to be used for aquifer calibration. Water levels were also used to determine main groundwater flow directions, location of water-divides and hydrologic boundaries.

The principal water supply companies provided groundwater abstraction volumes, but unfortunately it was not possible to obtain the same type data of data from most of the industries in the region that use groundwater. This limitation will certainly contribute to increase model uncertainty.

Long-series of rainfall data were recompiled for three monitoring sites within the study area and used together with monthly averaged air temperature, wind velocity, relative humidity and insulation data to calculate water balance using the Penman-Grindley method. Besides, other alternative methods were used to assess groundwater recharge. Specific field work carried out in the aquifer recharge area included unsaturated zone profiling, groundwater level weekly monitoring and chloride concentration determination in shallow wells within the area. These data allowed for the use of geochemical methods and of fluctuations in groundwater levels to estimate groundwater natural recharge, and to compare point to areal estimates.

Rainfall chemistry was also monitored monthly onsite for five years and the annual averaged concentrations were used for chloride mass balance calculations. And, considering the available geochemical information on the aquifer, it was decided to carry out three other field campaigns to enlarge the geochemical database to the whole extension of the aquifer. More than 90 boreholes were sampled and analysed for major, minor and trace elements, and stable isotope. Water samples were also collected for carbon-14 dating in parts of the aquifer that have not been studied before.

Hydrogeochemical data was used to determine the regional groundwater quality patterns in the aquifer, to simulate groundwater evolution and water-rock interactions using PHREEQC-2® and to estimate residence times, which later were used to compare to the flow model particle

tracking results. A unique field campaign was carried out to determine aquifer vertical stratification and included detailed geophysical logging and depth sampling in seven non-equipped boreholes in the study area.

With all the above mentioned data collected and interpreted, the third and crucial step consisted in the construction of the conceptual model of the aquifer system. This step implied the identification of the principal aquifer hydrostratigraphic units and boundaries and the identification of a range of aquifer parameters for each specific aquifer layer.

The fourth step included the selection of the computer code with the preference for MODFLOW®, a modular three-dimensional finite-difference groundwater flow model developed by the U.S. Geological Survey (McDonald & Harbaugh, 1988; Harbaugh & McDonald, 1996). The selection of this program may be attributed to the fact that MODFLOW has become the worldwide standard for simulating groundwater flow, is well documented and has been extensively tested. The Visual MODFLOW Pro interface that combines MODFLOW®, MODPATH® (a particle tracking post-processing package for MODFLOW) and ZoneBudget (a program for computing sub-regional water budgets for MODFLOW ground-water flow models) has been used to decrease the complexities typically associated with building three-dimensional groundwater flow models.

The computer code selection was followed by the model design which included the vertical and horizontal grid design, the assignation of aquifer parameters to each layer (varying in space according to kriging estimates), the selection of boundary conditions, time steps and hydrologic stresses, and the setting of initial aquifer conditions. Once finished the model design, the model was run several times and calibrated in steady- and transient-state. Particle-tracking was used to compute three-dimensional flow paths using output from steady-state or transient ground-water flow simulations by MODFLOW.

The model calibration against averaged field-measured heads required occasional reconstruction of portions of the model and was achieved trough both manual trial-and-error adjustment of parameters and automated model calibration using non-linear parameter estimation and predictive analysis (PEST). Calibration was performed to steady-state data sets and evaluated through analysis of residual. A sensitivity analysis was performed to quantify the uncertainty in the calibrated model, identifying the key aquifer parameters, boundary conditions and stresses in the calibration process. Finally, the calibrated model was used to predict the response of the aquifer system to future stresses, in particular to the increase of the volume of abstractions. All the modelling results are reported in Chapter 6.

An overview of the thesis and synthesis of science, with references to the applied significance of results and future directions for research, has been included in Chapter 7 while Chapter 8 summarises the main conclusions of the present research.

2

REGIONAL AND GEOLOGICAL SETTING

The area of northwest Portugal (western Iberian Peninsula) covered by the present research extends between the 40º30'N and 40º53'N latitude parallels, and is bounded to the west by the Atlantic Ocean and to the east by the 8º26'W longitude meridian. It is a gently sloping coastal plain of about 1,800 km^2 on the Portuguese mainland and offshore beneath the Atlantic Ocean, corresponding in its totality to the district of Aveiro (Fig. 2.1).

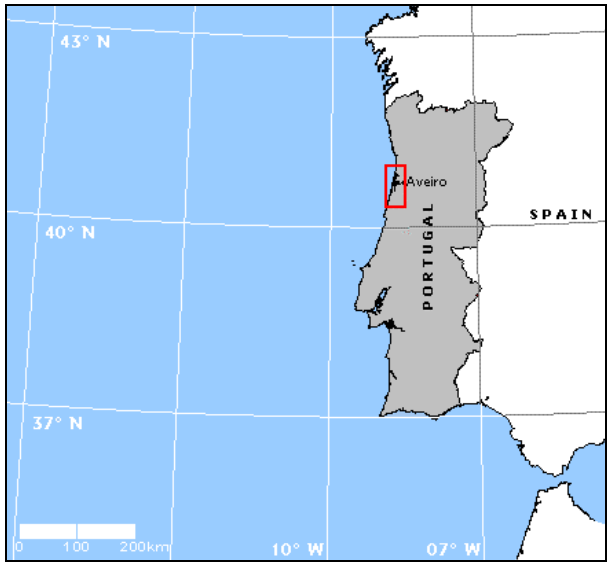

Fig. 2.1 Location of the Aveiro Cretaceous aquifer study area.

2.1 Area and regional framework

The study region is particularly known for the 'Ria de Aveiro', a shallow coastal lagoon with both marine and estuarine waters, separated from the adjacent sea by an elongated barrier of sand and other lose sediments transported by waves, currents, and winds. Today, the lagoon system and adjacent channels encompass an area of approximately 527 km^2, with extensive mudflats, sandbanks and salt marshes developed in its intertidal zone. This diverse area associated to the Aveiro lagoon is regarded as one of the most important humid areas in Portugal providing

wintering areas for more than 20,000 aquatic birds and has recently been classified as Special Protection Area (SPA) under the EC Directive on the Conservation of Wild Birds (PTZPE0004, D.L. nº 384-B/1999 23 Setembro).

The development of the Aveiro lagoon started less than 1,000 years ago but it has been a very dynamic evolution process since from its very beginning. The natural flow of water into the lagoon brought sediment producing its progressive silting up and developing southward a sand bar barrier parallel to the coastline, which helped to further trap the sediments and has almost isolated the lagoon from the Atlantic Ocean on several occasions during the last centuries (Fig. 2.2).

A manmade inlet channel was constructed in the year 1808 to guarantee the permanent direct access to the ocean, and dredging has historically been used to prevent the channel silting up and to keep the lagoon open to tidal flows. The average depth of the lagoon is nowadays 1 to 2 m but may reach 5 to 10 m in the navigation channels where dredging operations are frequently carried out (Dias *et al.*, 1999). However, the construction of the channel increased the tidal prism and current velocity in the Aveiro lagoon, intensifying the erosion processes and putting the natural equilibrium of this system at risk. Erosion processes together with fish-farming activities are in great part responsible for almost extinguishing salt production in the Aveiro region, an ancestral and important economic activity that goes back to the tenth century (Rezende, 1944).

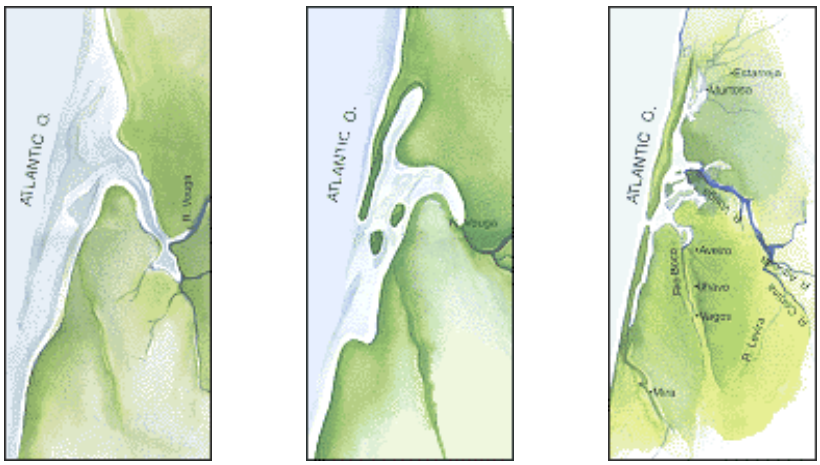

Fig. 2.2 Schematic maps describing the evolution of the 'Ria de Aveiro' lagoon during the last 1,000years (RNDSJ, 2002).

Several rivers flow into the lagoon – the Caster and the Gonde in the north part; the Vouga, the Jardim and the Antuã in the east part; and the Boco in the south part of the lagoon. Altogether they correspond to a total river basin drainage area larger than 3,600 km^2. In summer, when the river flow decreases and evaporation is high, the salinity of the water in the interior part of the lagoon may approach (or may be higher than) that of the ocean.

The river Vouga is the longest (148 km) and the main tributary river in the regional hydrologic system. It has a middle-size catchment area with a dominant east-west orientation that includes the rivers Caima and Sul on the right bank, and the rivers Águeda, Alfusqueiro and Cértima on the left bank, as its principal tributaries (Fig. 2.3). The flat, low-lying alluvial plain of the river Vouga completely dominates the local topography and surface geology in the study area.

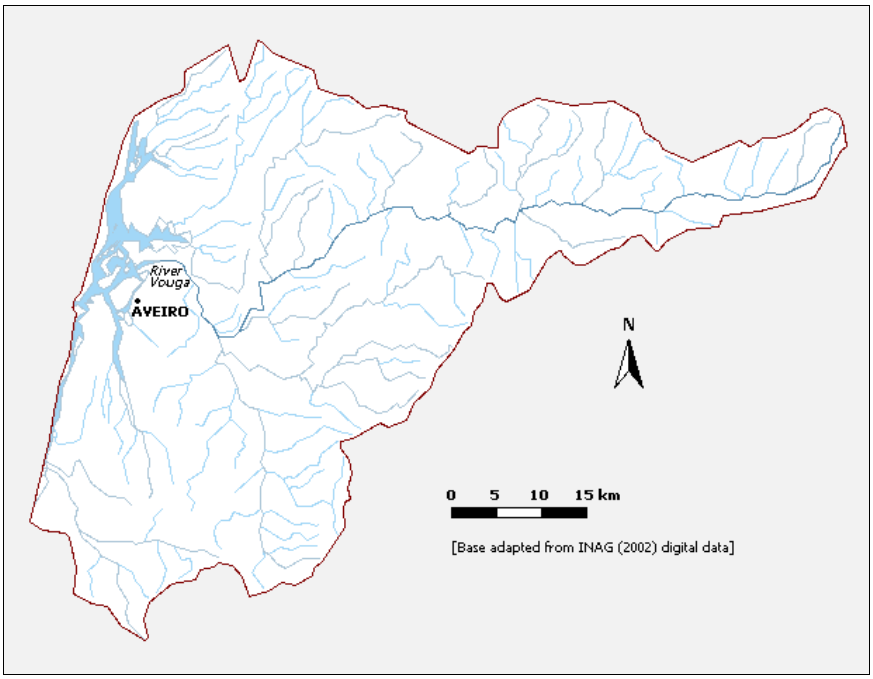

Fig. 2.3 Map of the Vouga river drainage basin.

The Aveiro region is also noted for the extensive and diverse sand-dunes belt along its littoral coast, which plays an important role in protecting the local coastline, acting as a buffer against wave damage during storms and protecting the land behind from salt water inundation, sea spray and strong winds. The S. Jacinto littoral dune system, which extends in the northwest of the study area between the Atlantic Ocean and the 'Ria de Aveiro' lagoon, was declared a Natural Reserve in recognition for its biodiversity (D.L. nº 41/1979 06 Março, D.R. nº 46/1997 17 Novembro).

2.2 Geological Framework

The Lower Vouga basin and the Aveiro Cretaceous aquifer correspond to the north most part of the Lusitanian basin, one of the known Atlantic margin rift-basins formed along the western border of the Iberian Peninsula as a response to Mesozoic active extension and subsequent opening of the North Atlantic Ocean (Fig. 2.4).

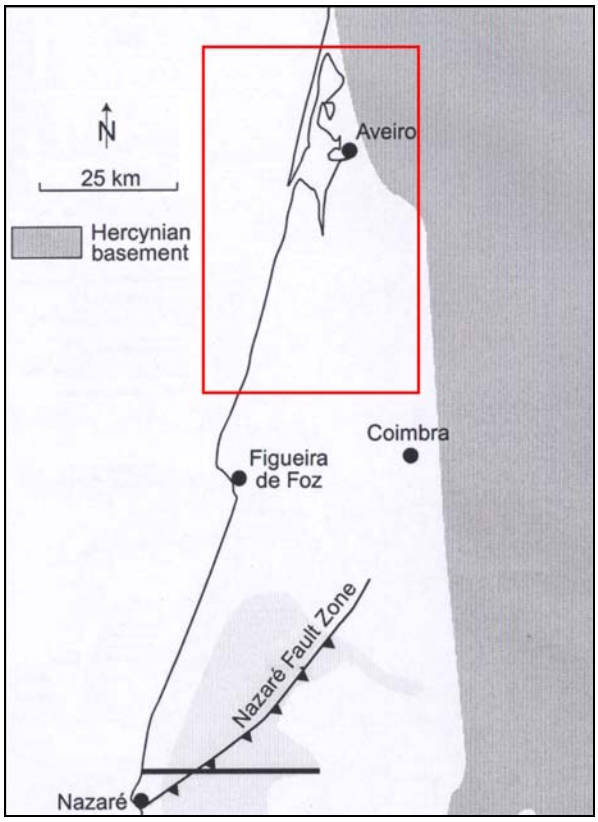

Fig. 2.4 Location of the Aveiro Cretaceous aquifer study area within the north most part of the Lusitanian basin (adapted from Rasmussen, 1998).

For the Lusitanian basin, located at the western end of a convergence zone between tectonic plates, the gradual opening of the North Atlantic is probably the most important factor in the complex pattern of differential motion and intense deformation between Eurasia, Africa and Iberia over the past 120 Ma. Periodically, regional tectonics connected with the opening of the North Atlantic Ocean and resulted in widespread breaks in deposition or erosion associated with uplift on a regional scale (Fig. 2.5).

From the Late Triassic to the Cretaceous, the western Iberian margin experienced two major stages of rifting alternated with intermittent periods of less intense stretching or even tectonic inactivity. The rifting phases strongly influenced the stratigraphy and tectonic evolution of the Meso-Cenozoic inner and outer sedimentary basins individualised along the Portuguese continental margin (Mauffret *et al.*, 1978; Boillot *et al.*, 1979; Ribeiro *et al.*, 1979; Vanney & Mougenot, 1981; Guéry *et al.*, 1986; Wilson, 1990; Rasmussen *et al.*, 1998; Andeweg, 2002).

The inner basins are located in the inner part of the continental margin, often extending offshore, and comprise the Porto, Lusitanian and Algarve basins. The outer basins include the Galicia Interior, Peniche, Alentejo and Sagres basins, the evolution of which is less well known because most data about them have only become available recently.

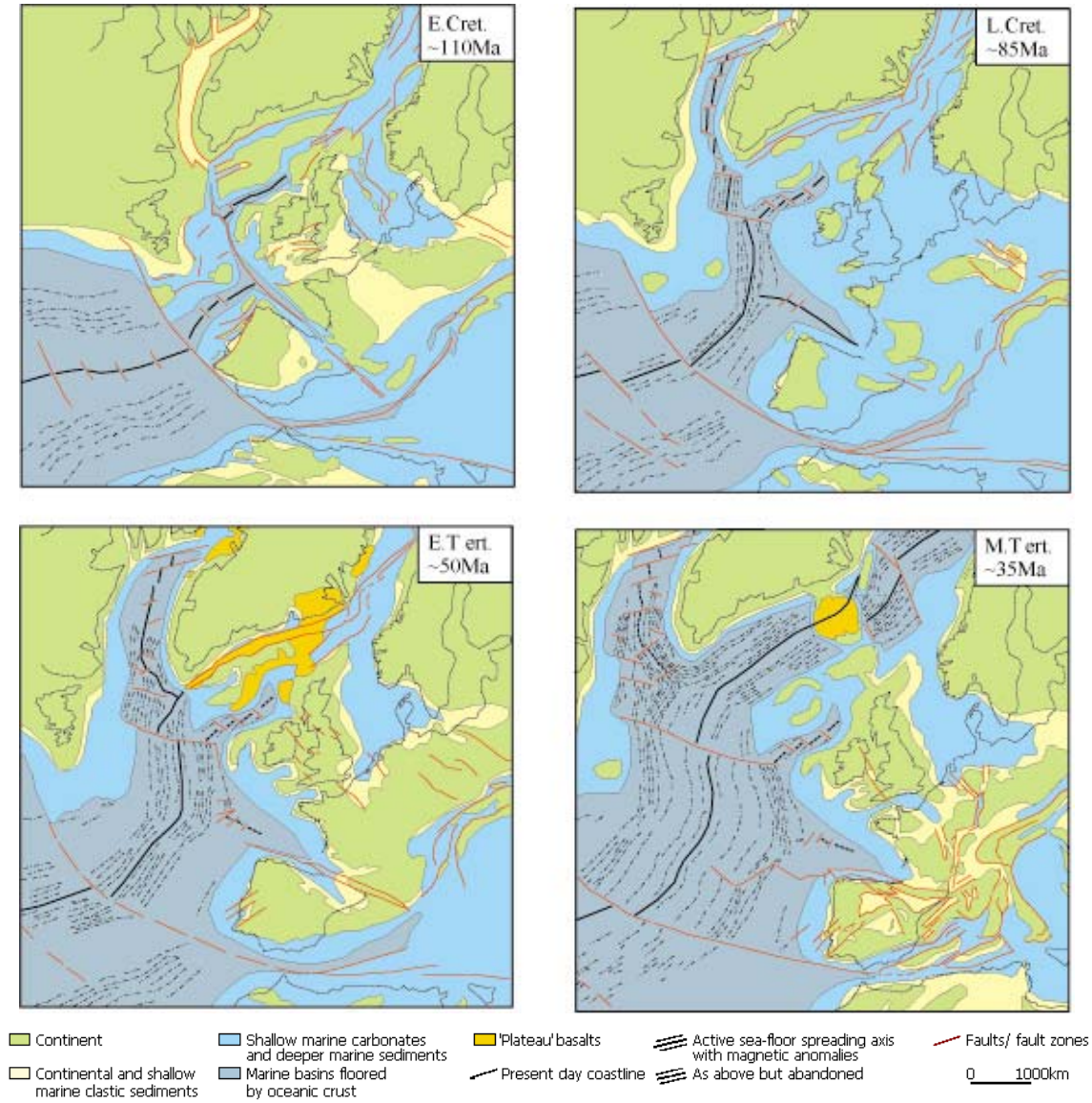

Fig. 2.5 Progressive opening of the North Atlantic Ocean and the related differential motion between the Eurasian, African and Iberian tectonic plates (from Andeweg, 2002).

2.2.1 **Structural evolution and geologic history of the region**

The Lusitanian basin covers over 20,000 km^2 in the west-central part of the Portuguese mainland and the adjacent continental shelf, and is one of the very few basins around the North Atlantic with syn-rift sediments exposed onshore (Stapel, 1996). The development of the basin was characterized by a number of rift and subsidence phases during the Mesozoic, superimposed upon an older Hercynian orogenic terrain of folded Precambrian and Early Paleozoic rocks, and followed by inversion movements during the Cenozoic Alpine collision.

For the Lusitanian basin, the first indications of Mesozoic continental rifting are of Late Triassic age, and although poorly documented, it is possible to infer that deposition of mainly

continental sands and clays of alluvial origin took place in grabens or half-grabens (Mauffret *et al.*, 1978; Vanney & Mougenot, 1981).

Following a period of regional subsidence during the earliest Early Jurassic, when evaporites and carbonates were deposited, a second rifting phase occurred within the Lusitanian basin in the Early Jurassic. This stretching episode is marked by the deposition of a shallow carbonate platform of marine dolomites and evaporites that gradually expanded to the borders of the basin. This is followed by a period of more diffuse extension and less prominent fault-related subsidence, which led the western Iberian margin into a phase of relative tectonic quiescence (Stapel *et al.*, 1996; Ravnås, 1997).

Folds within the Hercynian terrain trend NW-SE, oblique to the primarily NNE-SSW trend of Lusitanian rifting, thus creating pre-rift, cross-basinal arches which were episodically reactivated during subsequent tectonic phases. Similarly, many significant Hercynian faults were used as major rift half-graben boundaries, and hence can define syn-rift, fluvial clastic depocenters. Such faults generally exhibited later episodes of wrench movement as well, particularly at the end of the Middle Jurassic and during Tertiary Alpine orogenesis (Uphoff *et al.*, 2002).

The Late Jurassic deposits are separated from the succession described above by a regional hiatus ranging from the latest Callovian to the earliest Oxfordian. This regional unconformity is probably related to uplift due to the opening of the central Atlantic Ocean and the beginning of oceanic spreading at the Iberian Abyssal Plain (Rasmunsen *et al.*, 1998).

A new phase of rifting was initiated in the Late Jurassic. This rifting phase was more pronounced in the outer basins, and the evolution of the inner and outer basins began to differ markedly. The Lusitanian basin, as well as the other two basins along the western coast of Portugal, became aborted rifts with relatively limited subsidence since then. Regional uplift occurred during the Callovian to Early Oxfordian. In the north part of the Lusitanian basin, this uplift phase was followed by pronounced fault-block rotation and rapid fault-controlled subsidence along NNW-SSE trending faults during the Late Oxfordian-Earliest Kimeridgian that led to the drowning of the subbasin towards SSE and produced an influx of coarse continental sediments.

This resulted in rapid lateral facies changes from shallow carbonate deposits in topographic highs to fluvial-deltaic siliciclastic sediments in lows that gradually interfingered with marginally marine shale and limestone basinwards. This sedimentation process was strongly influenced by the action of diapiric activity and the reactivation of faults, which controlled the source area of the sediments (Bernardes, 1992). Salt pillows were formed above major faults modifying the topography formed by block rotations.

A regional angular unconformity and a marked change in lithology with deposition of conglomerates denote the final phase of extension during the Late Jurassic to Early Cretaceous.

The rift axis shifted further to the west, and eventually resulted in the opening of the north Atlantic. Renewed subsidence took place in the Outer basins, resulting in the deposition of thick sequences of Late Cretaceous to recent sediments, significantly different from their thin equivalents in the inner basins.

During the Early Cretaceous the Lusitanian basin was a complex graben characterized by a post-rifting regime (Dinis *et al.*, 2002) and the deposition of mainly terrestrial clastics proceeded influenced by both fault-controlled subsidence and halokinesis that resulted in a variety of deposits related to a mixed carbonate-siliciclastic system. Diapirism in the central part of the basin was triggered by the Miocene inversion techtonics (Rasmunsen *et al.*, 1998).

Tectonic quiescence followed upon this last tectonic phase and deposition of siliciclastic sediments occurred during the remaining part of the Early Cretaceous. According to Stapel *et al.* (1996) the overall vertical motions appear to be quite homogeneous for the Early Cretaceous suggesting that somewhere during this time span the transition from syn-rift to post-rift takes place. The tectonic quiescence continued during the Late Cretaceous and vertical movements are small when compared to the two proceeding major rifting phases (Stapel *et al.*, 1996).

In contrast to the Mesozoic, the Tertiary and the Quaternary in the Iberian Peninsula are periods dominated by compressive deformation due to the Pyrenean phase of the Alpine orogeny. As a result of the collision of the African and Eurasian plates, the first compression movements were felt in the Eocene and lead to basement shortening and basin inversion, especially in the northern Lusitanian basin. The infilling of the basin as the result of these compression episodes was controlled by pre-existing Hercynian basement faulting and was often amplified by halokinesis which, in extreme instances, led to the formation of diapirs that pierced through the entire sedimentary cover (NPEP, 2001).

The sedimentation processes during the Paleogene were mainly restricted to shallow marine sediments and carbonates, while in the Neogene, the sedimentation is dominated by subsidence and marine transgression, with deposition of mainly sands and conglomerates. Tectonic phases, which may have occurred during the Paleogene, have been overprinted by the strong inversion tectonics that affect the western Iberian Peninsula since the Miocene till the present. The principal thrust faults are striking along a ENE-WSW direction, but as the compression was compensated along former fault trends, thrusting also occurred along NNW-SSE and E-W striking zones.

The Pliocene is marked by consecutive transgression-regression cycles, and the Pliocene sediments have been uplifted and tilted by tectonic movements. During the Quaternary, several erosional surfaces are developed, and the sedimentation deposits are mainly of coarse sand and gravel, often affected by neotectonic movements (Rocha, 1993).

2.2.2 **Lithostratigraphy**

The Lusitanian basin stratigraphy has been extensively studied by several authors (*e.g.* Berthou, 1973; Teixeira, 1976; Teixeira & Zbyszewski, 1976; Mauffret *et al.*, 1978; Boillot *et al.*, 1979; Ribeiro *et al.*, 1979; Berthou & Lauverjat, 1979; Vanney & Mougenot, 1981; Barbosa, 1981; Soares *et al.*, 1982, 1993; Guéry *et al.*, 1986; Wilson, 1990; Bernardes, 1992; Rocha, 1993; Dinis, 1999) and a regional synopsis of the basin is represented in Fig. 2.6.

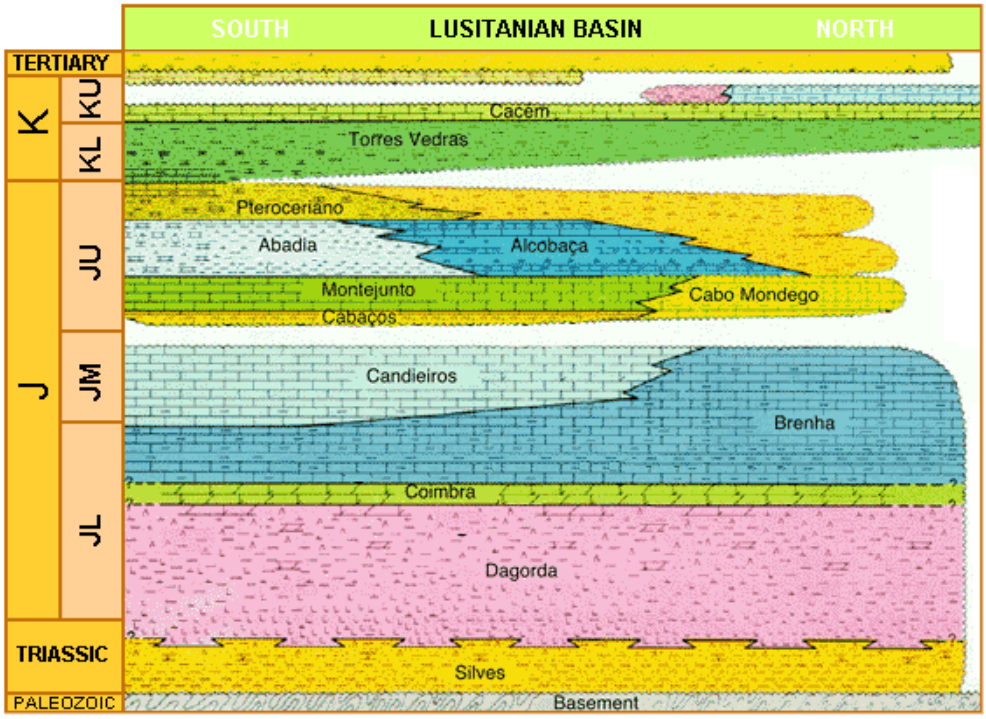

Fig. 2.6 Regional stratigraphy of the Lusitanian basin (modified from NPEP, 2001).

During the Mesozoic, the deposition conditions varied within the Lusitanian basin. In the south and west areas of the basin there was a gradual opening to the marine influence, while in the north and east parts there occurred a predominant detritical infilling of continental origin.

From the tectonic point of view, the development of stretching movements controlled by dominant fracture sets led to the formation of tilting blocks and the definition of two subbasins or sectors divided by the Nazaré parallel: the 'Estremadura' and the 'Beira Litoral' subbasins, in the south and north halfs, respectively. A NNE-SSW direction is dominant in the south sector (Estremadura) while N-S and NNW-SSE fractures are dominant in the north and central part of the basin (Dinis, 1998).

The studied area corresponds to the very north part of the 'Beira Litoral' sector and presents as principal stratigraphic distinguishing features:

- the occurrence of two significant hiatus corresponding to breaks in the stratigraphic sequence during the Carixian – Aptian and Late Cretaceous – Pliocene, although Rocha (1993) refers to the occurrence of Tertiary 'relics' in geological logs of boreholes drilled along the Aveiro region littoral, between the villages of Gafanha and Muranzel;
- the important development/ thickness of Late Cretaceous formations, which is singular not just in the context of the stratigraphic evolution of the north part of the basin, but for the whole Portuguese territory.

The bedrock in the region consists of mica schists and schists of Proterozoic age in most of the studied region with the exception of the north part, where Proterozoic gneisses, migmatites and Palaeozoic granitoids constitute the actual bedrock.

The Precambrian-Early Paleozoic bedrock units are overlain by the Meso-Cenozoic sedimentary cover in most of the study area, being exposed along a NNW-SSE axis close to the border limit with the Iberian Meseta. The bedrock basement dips westward from the eastern border and is affected by several N-S and NNE-SSW faults that produce the gradual sinking of blocks of basement rock forming a complex system of horsts and grabens (Figueiredo, 2001).

The Meso-Cenozoic infilling stratigraphic sequence is discontinuous and ranges in age from Late Triassic to Holocene formations (Fig. 2.7). It includes from bottom to top (Rocha, 1993):

- **Triassic sandstone formation ('Eirol sandstone')**

Red sandstones of Late Triassic age (Rhaetian) are the oldest sediments in the area. They form redbeds that unconformably overlay the Paleozoic and Precambrian bedrock, and outcrop along the eastern part of the study area between the villages of Angeja and Requeixo. Their origin is related to the weathering of rocks of the Hesperic Massif (mainly biotite and chlorite schists and granitoids) and deposition of the loose sediments in a littoral platform. The depositional environment was predominantly continental with a hot and humid climate that evolves to semi-arid.

The Triassic sandstone formation consists of micaceous fine to medium sand sediments (occasionally, coarse), with unrolled pebbles, and an iron rich matrix (hematite, goethite). Conglomerate layers with marly clayey levels have been observed in the bottom part of the formation, while to the top, the formation becomes fine grained.

- **'Dagorda marl formation'**

Unit formed by brown-reddish sandy marls, with abundant halite and anhydrite, and occasionally goethite and hematite. This marl formation has been deposited in a littoral marine environment, with lagoon characteristics, and was affected by stretching movements and long periods of dry climate. They occur essentially in the east and southeast part of the study area.

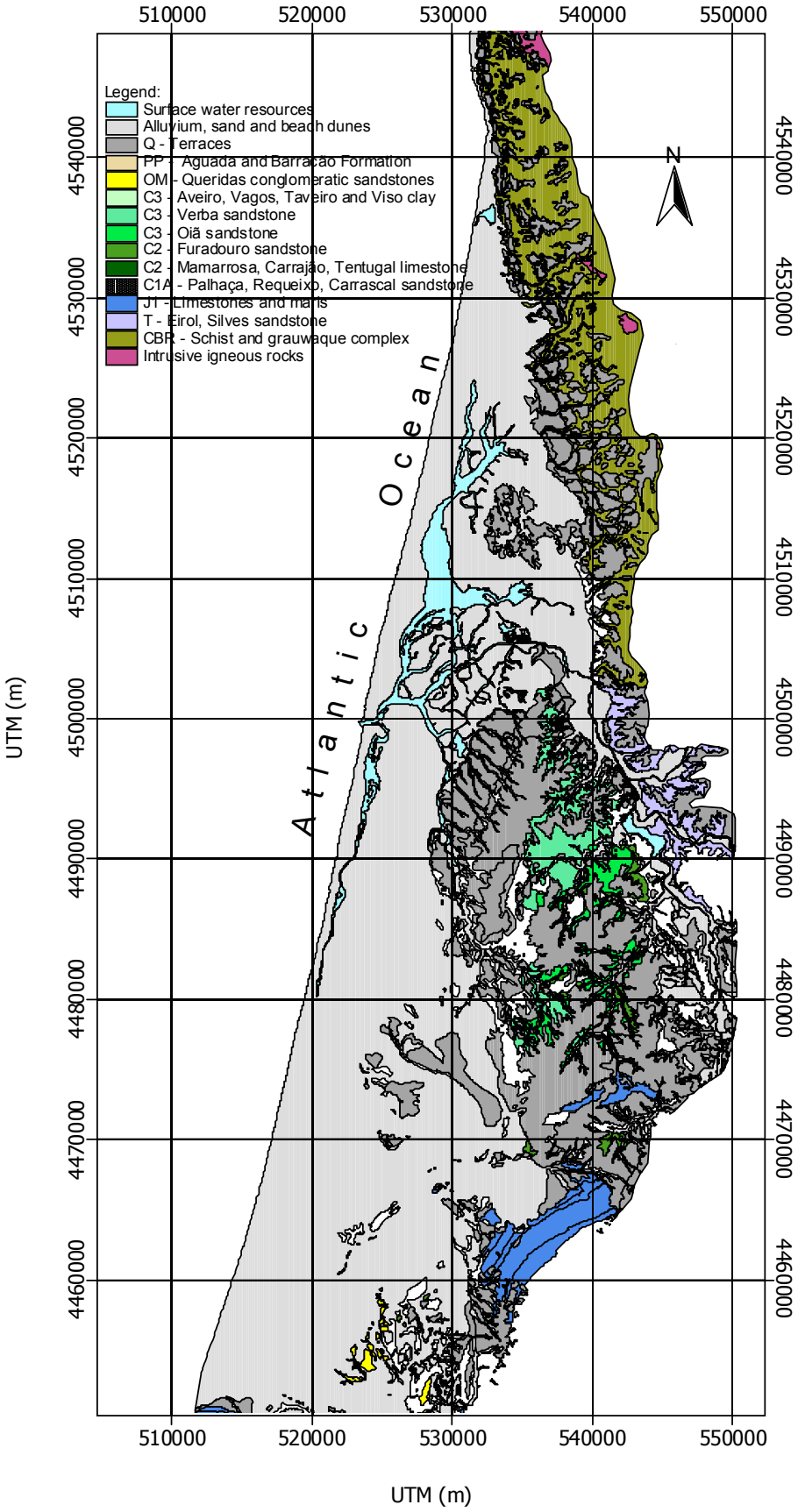

Fig. 2.7 Geological map of the study area. The geological information was digitised from the national geological map sheets no.: 13C-Ovar, 16A-Aveiro, 16C-Vagos and 19A-Cantanhede, and from Barra (1998).

- **'Camadas de Coimbra formation'**

Marly sandstones, sandy marls or marly dolomites of greyish colour essentially form this formation. The origin of this marly sandstone formation is related to the deposition of terrigenous sediments eroded from a nearby continental margin in an open shallow basin with calm waters and with a persisting temperate climate. This formation has been identified in logs of boreholes drilled in the south part of the study area close to Nariz and Bustos and in outcrop areas close to Cantanhede and Vilarinho do Bairro.

- **'Camadas de S. Miguel formation'**

This formation with marly sandstones or sandy marls, greyish colour, was deposited in a marine environment under transgression conditions, with very limited capacity for the transport of sediments (low hydrodinamism) and conditions for preferential settling. A cold and dry climate was dominant at the time. As the immediately overlaid formation, this unit has been identified in logs of boreholes drilled in the south part of the study area close to Nariz and Bustos and in outcrop areas close Cantanhede and Vilarinho do Bairro.

- **'Eiras marl formation'**

This marl formation was deposited in a shallow marine environment, with very low hydrodinamism and with mostly anoxic conditions, typical of a closed lagoon. The abundant presence of carbonate sediments should indicate a temperate rainy climate. Like the two previously described formations, this formation has been identified in logs of boreholes drilled in the south part of the study area close to Nariz and Bustos and in outcrop areas close to Cantanhede and Vilarinho do Bairro.

- **Lower sandstone formation ('Palhaça sandstone formation'), C_{1A}**

The Lower sandstone formation consists of medium to coarse sands of predominantly brown-yellowish colour and continental facies. It usually has interlayered clay levels or coarse sandy levels with pebbles, and increasing clay and carbonate contents towards the top of the unit.

This unit has probably been deposited in a flooding deltaic plain with a complex network of fluvial channels. This is confirmed by the observed extremely high kaolinite content, which also indicates that it was deposited under very hot and humid conditions.

The Lower sandstone formation is present in all the extension of the study area with a maximum thickness close the recharge area (*e.g.* Mamodeiro). It unconformably overlies the schist grauwaque complex in the northeast, the Triassic sandstone in the west part and the Liasic limestones in the south and southeast part. It outcrops in the eastern part, in an area encompassed between Salreu-Taboeira–Azurva–Fermentelos-Vilarinho do Bairro and occasionally along the axes of Palhaça and Mamarrosa fractured structures.

- **Carbonate formation ('Mamarrosa limestone formation'), C_2**

The carbonate formation was deposited during the Cenomanian transgression and is formed by several different lithological types, which may include fine clayey sandstone of greyish colour, marly limestones, marly clays or sandy marls.

The marine influence in this unit is more obvious in the coastal and central parts of the basin, where the dominant clay minerals are illite and smectite, respectively, indicating shallow marine waters with low hydrodinamism. However, the amplitude of the Cenomanian regression in the region is quite small indicating that the sea was just present in the area for a short time.

The carbonate formation is also represented in all the extension of the study area but sometimes it is difficult to recognize it without the detailed study of its mineralogy. The main difference comparing to the Lower sandstone formation is the presence of carbonate cement. However, the presence of this carbonate cement is less relevant in the interior and north sectors of the basin, corresponding these areas to the limit of the Cenomanian transgression. This unit is very abundant in the central eastern part of the study area, close to Fermentelos.

- **Micaceous sandstone formation ('Furadouro sandstone formation'), C_2**

The 'Furadouro sandstone formation' was deposited during the Turonian regression in a predominantly littoral environment, very similar to the deposition environment of the Lower sandstone formation. It consists of medium to coarse micaceous sand, with higher granulometry in the top part, and some interstratified marly clay levels and abundant quartz.

On the top and at the bottom of this formation there are lenticular dark coloured marly-clay layers of variable thickness and high organic matter content. They occur at a regional scale and correspond to erosion surfaces that resulted from the constant variations of the sea level during deposition of the Cretaceous sedimentary column in the Aptian/Albian and the Senonian (Rocha 1993).

This unit outcrops along narrow band in the eastern part of the study area (Taboeira, Azurva, Eixo, Carrajão, Requeixo and Fermentelos). It also outcrops along the axes of Palhaça and Mamarrosa fractured structures.

- **Upper sandstone formation ('Oiã sandstone formation'), C_3**

The deposition of the 'Oiã sandstone' was under a fluvial continental environment due to a regressive movement of the sea during the Upper Turonian-Lower Coniacian. The deposits are characterized by mainly medium sand of brown-yellowish colour and abundant rose quartz. It may present some more clayey levels at the bottom and top of the unit, but the grain size decreases significantly to the top. It has been identified in whole the study area, and outcrops in the southeastern part where it has a good cartographic representation.

- **Upper sandstone formation ('Verba sandstone formation'), C_3**

The 'Verba sandstone formation' is a fine to medium clayey-marly sand interlayered with marls and marly clays deposited under a transgression period. The dominant colour is grey-brownish and the clay content usually increases to the top of the formation. This top part of the Upper sandstone formation has been deposited under transitional continental to fluvial-littoral environments under transgression conditions. It is present in the whole study area and outcrops in Verba and Nariz, and to the SE of Bustos village.

- **Marly clay formation ('Aveiro clay formation'), C_3**

A long regression period under temperate climate allowed for the deposition of the Aveiro clay formation in the study region. These are essentially greyish marly clays, sometimes with an important percentage of sand and with layers of marly limestone.

This unit presents a remarkable lateral homogeneity in terms of clay minerals, and in general illite is the dominant clay mineral followed by calcium smectite. This unit is more or less uniform in the study area with thickness that can be higher than 150 m in the areas close to the coast. Although this is the Cretaceous unit with the most important cartographic representation, this marly clay unit is not present in the eastern part of the study area where uplift led to its erosion.

Mineralogical studies by Rocha (1993) using X-ray Diffraction and Transmission Electronic Microscopy analysis show that the principal mineral assemblages for the different Cretaceous units are largely identical although the relative abundance vary from layer to layer. They are composed mainly of quartz, phyllosilicates, calcite, dolomite, K-feldspar and plagioclase. Gypsum, anhydrite, jarosite, melanterite, pyrite and goethite might occur as accessory minerals. Kaolinite, smectite and illite are the most abundant clay minerals (Table 2.1).

Table 2.1. Principal mineral assemblages for the different aquifer layers (after Rocha, 1993)

Unit	Lithology	Mineralogy† (<38 μm)	Clay Minerals† (<2 μm)
C_3	Marly clays	Phyllosilicates - Quartz - Potassium Feldspar – Plagioclase - Dolomite - (Calcite)	Illite - Kaolinite - (Smectite)
	Upper sandstone formation	Quartz - Potassium Feldspar - Phyllosilicates - Dolomite - (Plagioclase - Calcite)	Kaolinite - Smectite - Illite
		Quartz - Plagioclase - Potassium Feldspar - Phyllosilicates - (Dolomite - Calcite)	Kaolinite - Illite
C_2	Micaceous sandstone	Quartz - Phyllosilicates - Potassium Feldspar - Plagioclase - Dolomite - Pyrite - (Calcite)	Illite - Kaolinite - Sodium Smectite
	Carbonate formation	Calcite - Phyllosilicates - Potassium Feldspar - (Plagioclase - Dolomite - Quartz)	Kaolinite - Illite - Smectite and Sodium smectite
C_{1A}	Lower sandstone formation	Quartz - Potassium Feldspar - Plagioclase - Phyllosilicates - (Dolomite - Calcite)	Illite - Kaolinite - Smectite

† Minerals are written in descending order of their relative abundance. Minerals written in brackets occur as accessories.

The Cretaceous formations have distinct grain sizes, mineralogical compositions and clay contents, forming a multilayer aquifer system with different hydrogeological properties.

- **Plio-Pleistocene and Holocene deposits**

These are mainly recent alluvial deposits and sand dunes (primarily fine sands) of Holocene age and old beach deposits and fluvial terraces (mainly clays and clayey sands in the upper part and coarse sands and pebbles at the bottom) of Pleistocene age. The maximum thickness in the study area does exceed 30 m, and the sediments overlay all the Mesozoic sediments in the study region.

A synopsis of the infilling lithostratigraphic column within the studied area has been included in the following Table 2.2.

Table 2.2. Synopsis of the lithostratigraphy in the north part of the Lusitanian basin.

Era	Period	Stage	Lithostratigraphic Units		Lithology
CENOZOIC	**QUATERNARY** **Holocene**		Sand dunes, eolian and beach sands, alluvials		Fine to medium sands
	Plio-Pleistocene		Old beaches and alluvial terraces		Medium to coarse sands with some clayey levels
MESOZOIC	**CRETACEOUS**	Campanian-Maastrichtian	'Aveiro clay formation', C_3		Clay and marly clay, with some carbonate levels
		Coniacian-Santonian	Upper sandstone formation, C_3	'Verba sandstone'	Marly sandstones and sandy marls
		Upper Turonian-Lower Coniacian		'Oiã sandstone'	Clayey sandstones and sandy clays
		Upper Cenomanian-Turonian	'Furadouro sandstone', C_2		Coarse to medium micaceous sandstone, with some marly-clayey levels
		Cenomanian	Carbonate formation, C_2	'Mamarrosa limestone'	Marly limestone, marls and fine marly sandstone
		Aptian/Albian-Lower Cenomanian	Lower sandstone formation, C_{1A}	'Palhaça sandstone'	Medium to coarse sub-arkosic sandstone
	JURASSIC	Carixian-Domerian	'Eiras marls'		Sandy marls and marly sands
		Upper Lotharingian-Lower Carixian	'Camadas de S. Miguel'		Marly limestone
		Sinemurian-Lower Lotharingian	'Camadas de Coimbra s.s.'		Marly dolomitic limestone
		Hettangian	'Dagorda marls'		Sandy marls
	TRIASSIC	Rhaetian	'Eirol/ Silves sandstone'		Red marly-clayey sandstone
PALEOZOIC	**CAMBRIAN**				Granitoids
PRE-CAMBRIAN	**PROTEROZOIC**		Schist-grauwaque Complex		Mica schists, schists migmatites and gneisses

2.2.3 **Offshore lithostratigraphy of the Cretaceous formations**

An important question for the present study is whether the Lusitanian Basin's onshore exposures are representative of what underlies offshore beneath the Atlantic Ocean. Unfortunately, information available on the offshore stratigraphy of the Cretaceous formations in the north part of the basin is rather limited.

The stratigraphic and sedimentologic relationships between the offshore and onshore sedimentary formations are crucial to have a more correct idea about the extension of the Aveiro Cretaceous aquifer in the adjacent continental shelf.

The recently released data by the Portuguese Geological and Mining Institute (IGM) on the geology and drilling report of a deep-see borehole drilled by Esso Exploration & Production Company offshore the Aveiro region revealed some important stratigraphic and geophysical information. The deep-borehole is located 20.7 km off the Portuguese coast and 40.5 km NNW off Figueira da Foz, approximately in parallel with Vagos (Esso, 1974), and intersected the Cretaceous strata covered by Tertiary sediments (Table 2.3).

Table 2.3. Stratigraphy of the Cretaceous formations in the CARAPAU-1 borehole drilled offshore the studied region (data from Esso, 1974)

Period	Epoch	Stage	Depth (m)	Lithology	Environment	Seal
Tertiary	Eocene		**0** 82		Atlantic Ocean Sea floor	
			82 177	Sand, Clay	Shallow shelf	
			177 219	Limestone		
Cretaceous	Upper Cretaceous	Maestrichtian	**219** 387	Sandstone	Shallow shelf	Porous sandstones and carbonates were noted in the Upper and Lower Cretaceous sections, and these beds were known to have no seal.
		Maestrichtian Campanian	**387** 461	Sandstone, Clay	Shallow to middle shelf	
		Campanian Santonian	**461** 597	Limestone	Shallow shelf	
		Early Santonian	**597** 646	Clay, Shale, Limestone	Shallow shelf to brackish	
		Turonian?	**646** 685	Clay and Shale		
		Turonian Cenomanian	**685** 775	Limestone and Shale	Shallow shelf to brackish	
	Lower Cretaceous	Pre Albian Early Cretaceous	**775** 1135	Sand, Shale, Clay	Brackish to continental	

According to the geological description summarised in the previous Table 2.3, a complete over 1000 m carbonate-rich Late Cretaceous succession with upwards intercalation of siliciclastic beds was penetrated by deep see drilling and showed a very uniform depositional pattern (Esso, 1974; Rasmussen *et al.*, 1998). Therefore, the Late Cretaceous sequence is much thicker offshore than the equivalent sequence identified in the adjacent onshore area, raising the question whether a minor inversion offshore may have produced the erosion of approximately 300 m of Late Cretaceous sediments during the Cenozoic.

This new data is relevant for the study of the aquifer because it confirms the idea that the thickness of the Aveiro Cretaceous aquifer is probably much more important offshore than onshore. However, geophysical logging results for the drilled borehole, which just included resistivity determinations for the very bottom part of the Cretaceous formations and the whole Jurassic column indicate salinities equivalent to those of seawater (~50,000 $\mu S\ cm^{-1}$). These new data seem to discard the possibility of occurrence of freshwater in the deepest part of the Cretaceous formations at least at these distances from the coast.

2.2.4 **Regional syn-sedimentary tectonics**

The syn-sedimentary tectonic structures in the north part of the Lusitanian basin are mainly related to faulting movements. Geological evidences show that folding movements in the area were not intense and had gentle flank slopes. The region may be considered divided into two quite fractured zones, with a vaulted structure and separated by the structural alignment of the Mogofores-Febres-Tocha anticlinal (Barbosa, 1981).

The infilling sequence to the west of this alignment deeps to northwest reflecting the higher inclination of Cretaceous formations, while in the eastern part several sinclinal (*e.g.* Montouro-Mesas and Febres-Vilarinho do Bairro) and anticlinal (*e.g.* Marvão-Malhada, Troviscal-Bunheira-Oiã and Oiã-Mamodeiro) structures are evidenced and are strongly affected by faulting.

The fracturing tectonics is largely represented in the area by rotational and piano key type faults and is often in relation with most of the Cretaceous outcrops. Usually, these types of faults are subvertical direct fractures orientated along two orthogonal systems, which produce a block compartimentation and varied sinking/raising amplitudes along the fault plans.

These tectonic structures are frequently observed in the Mamarrosa, Palhaça, Oiã and Mamodeiro areas, in the southeast part of the study region. An important north-south fault develops from the Palhaça fracturing structure until the Mamodeiro area producing a vertical displacement of about 20 m between the Cretaceous formations.

Barbosa (1981) also suggests the existence of the Febres-Campanas fault between the Aveiro clays and the Lower sandstone formations. This fault would not be visible because the Quaternary sediments overlay it, but would be responsible for a displacement greater than 100 m.

3

HYDROGEOLOGICAL BACKGROUND

The Aveiro Cretaceous aquifer is part of a thick sequence of mainly siliciclastic sediments deposited in the northernmost part of the Lusitanian basin. Deposition was in fluvial, deltaic or shallow marine environments under predominantly transitional or continental depositional conditions. Sea level changes and regional elevation due to basin differential uplift and subsidence resulted in alternated transgression and regression movements of the sea followed by cyclical sedimentation of interbedded sand, clay, silt and limestone deposits. Generally, the more sandy continental deposits have higher permeabilities representative of aquifer layers, and the more clayey transitional (or marine) deposits have lower permeabilities characteristic of confining units.

In the region, Cretaceous sandstone units yield substantial volumes of water and developed an extensive groundwater flow system confined in two thirds of its extension by a low permeability marly clay formation of Upper Cretaceous age, which limits modern recharge to the aquifer. This unit is not present in the eastern part of the study area where the aquifer is unconfined.

The principal elements of the Aveiro Cretaceous aquifer hydrogeology are described in the following sections, and include the characterisation of the geometry and hydraulic properties of the aquifer's hydrogeologic units, the distribution of hydraulic head and the rate of discharge. The description of the stratigraphy, lithology and mineralogy of the Cretaceous formations was already made in Chapter 2 and the analysis of the recharge processes is intentionally left for Chapter 4. These elements are brought into play in the aquifer hydrogeological characterisation and are very important for the development of the aquifer conceptual model used in the numerical flow modelling.

3.1 Definition of the Aveiro Cretaceous aquifer

The Aveiro Cretaceous aquifer system covers over 1,800 km^2 of the northwest part of the Portuguese mainland and adjacent continental shelf. Unfortunately, well yield data are insufficient to define precise offshore and onshore limits of the aquifer, and therefore, geostructural boundaries and hydrogeologic inferences were used to delimit the studied aquifer (Fig. 3.1).

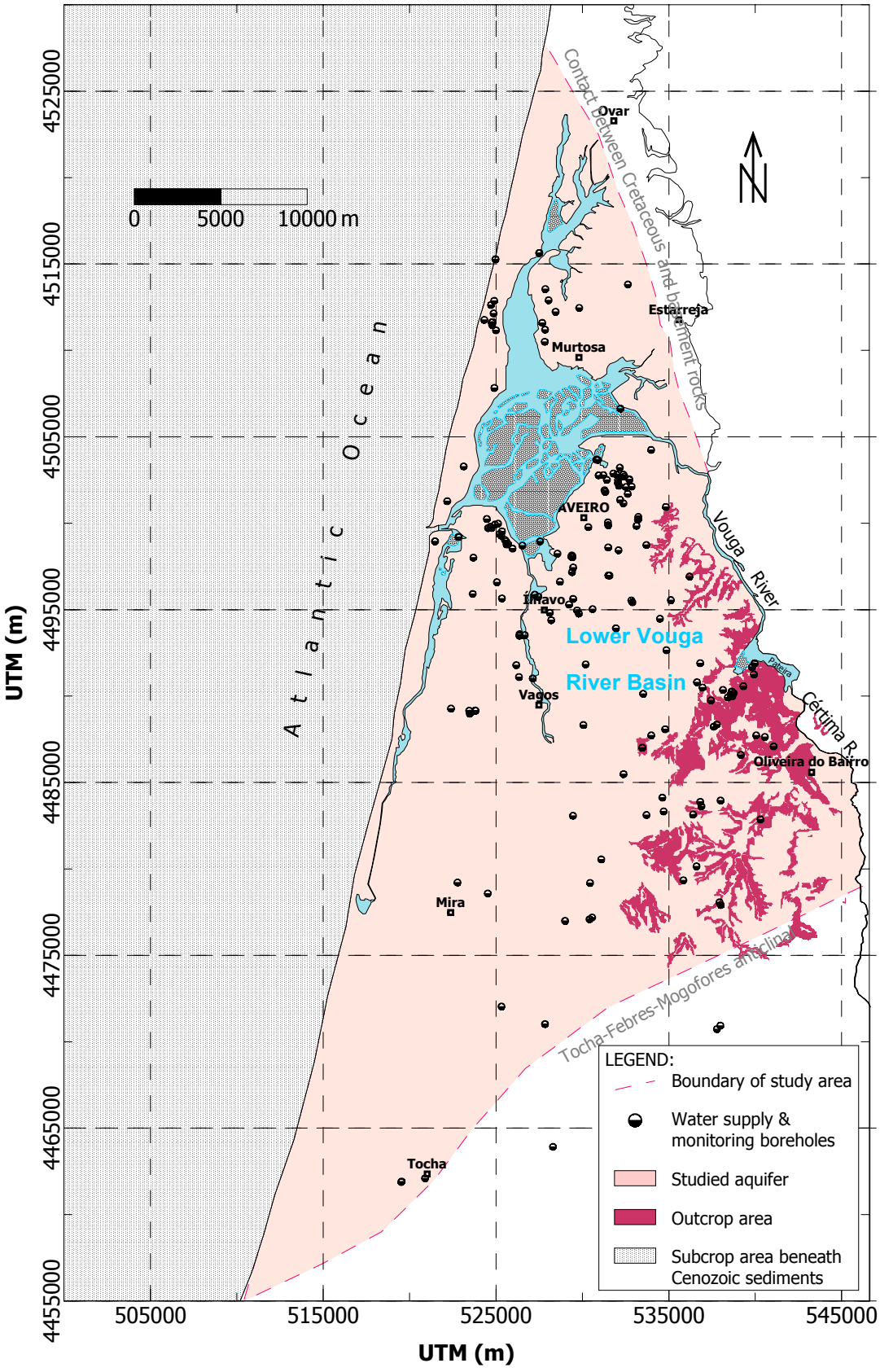

Fig. 3.1 Boundaries of the study aquifer system including outcrop and subcrop areas (the downdip limit of the subcrop area is assumed to be the edge of continental shelf, which is about 50 km from the present day coastline).

The geological contact between the Cretaceous formations and the Palaeozoic-Proterozoic basement rocks was established as the north and northeastern boundaries of the aquifer, because of the difference of permeabilities between both geological formations. The Palaeozoic-Proterozoic formations are believed to be a hydrogeologic boundary to groundwater flow and no significant groundwater flows are expected from one side to the other. The contact between the Cretaceous formations and the underlain Triassic (east), Jurassic (south) and schist-grauwaque complex rocks (in the rest of the area) were established as the lower boundary of the Aveiro Cretaceous aquifer.

The southern border of the aquifer is a geostructural limit formed by the 'Tocha-Febres-Mogofores' anticlinal structure with a predominant WSW-ENE orientation (Fig. 3.1). The Cretaceous infilling sequence to the west of this alignment deepen to northwest, while on the other side of the anticlinal structure the infilling formations deepen southeastwards.

The western boundary of the Aveiro Cretaceous aquifer was defined in two different positions, about 50 km apart. For present day analysis, the limit was assumed to coincide with the present coastline, and when analysing the emplacement of palaeowaters in the aquifer system, the border was considered to be the edge of the continental shelf. The depth of the continental shelf edge in front of the Aveiro region is at about 160 m below mean sea level, which corresponds to an average platform width of approximately 50 km in the region (Magalhães, 1999) (Fig. 3.2).

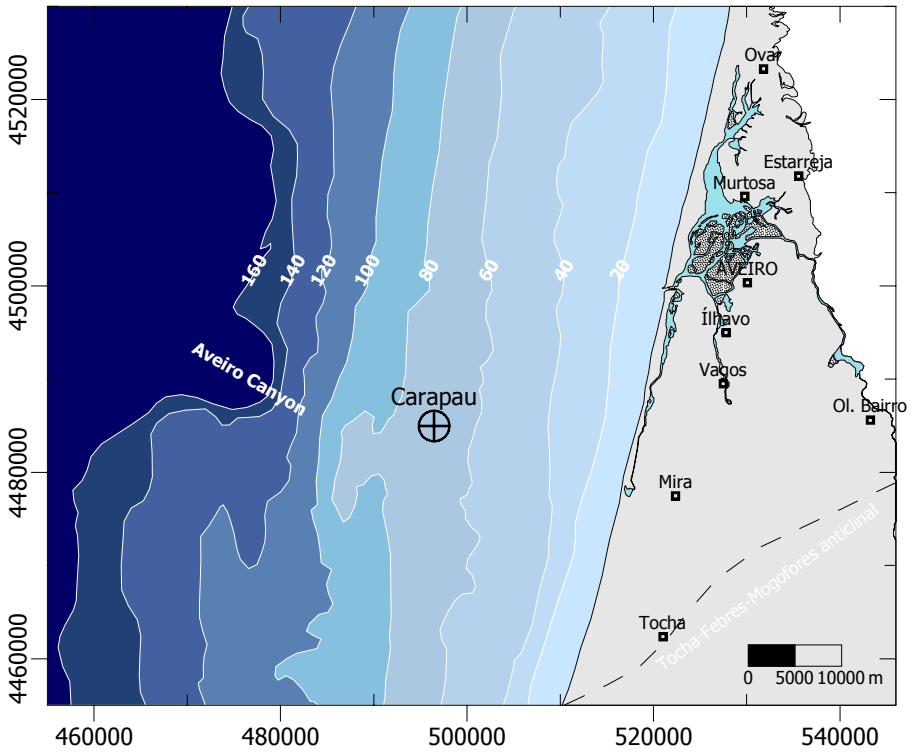

Fig. 3.2 Approximate extension of the continental shelf in front of the Aveiro region, where Upper Cretaceous sediments are known to outcrop and have been intersected in depth (⊕ Carapau deep-sea offshore borehole).

Upper Cretaceous sediments are known to outcrop sporadically in the offshore area to the north of the 'Aveiro canyon', and they might also do along the continental slope (Vanney & Mougenot, 1981). The exact extension of the aquifer in the adjacent continental shelf is not known but as described in Chapter 2, a deep-see borehole (Carapau, UTM Northing: 496471.29; UTM Easting: 4484965.74) drilled by Esso Exploration & Production Company offshore the Aveiro region intersected the Cretaceous strata covered by Tertiary sediments (Fig. 3.2).

The western two-thirds of the aquifer extension are confined where the Cretaceous sandstone formations are overlain by the 'Aveiro marly clay formation'. The average thickness of this confining unit increases towards the coast and may be over 150 m, in the deepest parts of the aquifer (Vagos). Uplift and erosion of the confining marly clay unit in the east defines the unconfined part of the aquifer, where the 'Upper sandstone formation', the 'Furadouro formation' and the 'Lower sandstone formation' crop out at the surface and receive direct recharge from rainfall infiltration. The 'Carbonate formation' ('Mamarrosa limestone'), which also crops out in the recharge area, is of low permeability, indicated by the occurrence of springs and swampy areas in the contact between the 'Carbonate formation' and the overlaying micaceous sandstone unit.

The eastern boundary of the aquifer was defined as the eastern limit of the outcrop of the Cretaceous sandstone formations. The Cretaceous units are in this part underlain by Triassic formations, which have smaller transmissivities and confine the flow system to the overlying units.

3.2 Description of the hydrogeologic units

The Aveiro Cretaceous aquifer is a multilayer aquifer system formed by geologic units with increasing thickness seaward, downdip direction, and distinct hydrogeological properties. In the region, the Cretaceous units are overlain by the Quaternary geologic formations that form themselves another multilayer aquifer system. However, most of the present discussion is directed towards the flow system in the Cretaceous units and the Quaternary deposits are hereby discussed only in general terms, without any detailed analysis of their groundwater flow system or geochemistry. The hydrogeology of the Quaternary deposits has already been described elsewhere by Marques da Silva (1990), Ferreira (1995) and Condesso de Melo *et al.* (2002*a*).

3.2.1 **Principal hydrogeologic units**

The subdivision of the aquifer geologic formations into hydrogeologic units for analysis in the present research followed four main approaches:

- the borehole geophysical logs were used to identify the principal water bearing units and the most significant confining units at a regional scale;

- the logs were also used to identify adjacent aquifer layers with contrasting hydraulic conductivities but not separated by regional confining units;
- the well logs at the time of drilling, showing depth, thickness and lithologic characteristics of the different strata penetrated were used to subdivide the aquifer system in those areas where there were no geophysical logs available;
- the principal aquifer units were extended to areas without any geological or geophysical information by keeping a constant proportion of the total system thickness, therefore preserving horizontal hydrologic continuity.

Overall, 270 geophysical logs corresponding to almost 100 deep boreholes in the region were analysed and used to interpret the hydrogeology of the study area at a regional scale. In most cases, the available geophysical measurements included natural gamma, point resistance and spontaneous potential logs run in the mud-filled hole prior to screening (*e.g.* Hearst *et al.*, 2000).

3.2.1.1 **Quaternary hydrogeologic units**

The Quaternary hydrogeologic units consist of alluvium, sand dunes, and old beach and terrace deposits that occur regionally as a surficial layer or as layers of variable thickness (maximum thickness is 25 to 30 m). These deposits unconformably overlay the bedrock, constituted by Paleozoic and Precambrian rocks in the north of the study area, or the Cretaceous formations in the rest of the region.

- *Alluvium, beach and eolian sands and sand dunes*

These are modern unconsolidated sand deposits of Holocene age continually being eroded, transported and deposited. They are abundant in the western part along the coast and inland along most of the riverbeds. The average thickness ranges between 8 to 10 m, rarely exceeding 20 m of total thickness.

These deposits overlay most of the study region and form a highly permeable (20 to 30 m d^{-1}) shallow aquifer that receives direct recharge from rainfall infiltration. The natural flow pattern in the aquifer is from the east towards the sea with smooth gradients ranging between 0.0012 and 0.0036 in the north and south parts of the aquifer, respectively. The aquifer discharges to the sea, to the rivers that flow in the area and to the underlain semi-confined Quaternary aquifer.

Coarser highly permeable sediments (10 to 20 m d^{-1}) associated to the several river basins of the region form the semi-confined Quaternary aquifer, which is separated from overlaying shallow aquifer by an organic mud layer of variable thickness. This mud layer acts as an aquitard

limiting the natural recharge to the underlain layer. The natural gradient in the semi-confined aquifer layer is about 0.0014 flowing from the east towards the sea.

- *Terrace deposits and old beach deposits*

The terrace deposits associated with rivers in the study area are older alluvial deposits (Plio-Pleistocene) visible in areas where erosion processes have deepened the river valleys and left the terrace deposits topographically above the present day alluvium. These deposits are predominantly coarse sands, gravel and pebbles, which occur mainly along the eastern part of region, where they overlay either Cretaceous or Triassic formations. The thickness of the terrace deposits in the study area ranges between 10 to 20 m and the average permeabilities range from 5 to 10 m d^{-1}.

This study unit receives recharge primarily by infiltration of rainfall, and secondarily by infiltration of excess irrigation. Unlike the other surficial Quaternary deposits, the natural gradient in these terrace deposits is from west to the east (0.004) where they discharge to the principal rivers that flow in the area.

3.2.1.2 **Cretaceous hydrogeologic units**

Beneath the Quaternary alluvium and terrace deposits are the consolidated geological units of Cretaceous age deposited in a series of changing sedimentary fluvial and fluviomarine environments. The Cretaceous strata are formed by mainly siliciclastic sediments and dip gently to northwest beneath the present coastline. The structural geology of the Cretaceous formations is quite simple in the central and northern part of the study area but faults of approximately north-south orientation have been inferred in the geologic maps (Barbosa, 1981) and when drawing interpretative cross-sections in the eastern and southern part of the study aquifer.

- *Marly clay formation ('Aveiro clay formation'), C_3*

This unit consists of low permeability marly clays, occasionally with thin sandy clay interlayered beds, and for practical purposes it is considered to be being an aquiclude. It confines the western two-thirds of the aquifer extension, limiting recharge but protecting the underlain permeable Cretaceous formations from contamination episodes. This marly clay formation is considered as part of the Aveiro Cretaceous aquifer, being its top confining layer.

- *Upper sandstone formation ('Verba sandstone formation'), C_3*

Mainly clays and clayey sandstones form the top part of the Upper sandstone formation, which generally do not yield substantial volumes of water to wells. The high clay content of this unit reduces the transmissivity and increases the groundwater residence times of this formation considerably. Just very few small-yield boreholes around the village of 'Verba', for domestic use,

are completed in this formation. The productivity of these wells is always very limited and the groundwater pumped has usually higher salinities than the baseline values for the aquifer.

This aquifer layer has been often considered an aquitard from the hydrogeological point of view (Marques da Silva, 1990) but for the purpose of the present study, the 'Verba sandstone formation' is considered a low transmissivity aquifer layer.

- *Upper sandstone formation ('Oiã sandstone formation'), C_3*

Stratigraphically below the 'Verba sandstone formation', the bottom part of the Upper sandstone formation is significantly more permeable than the overlaying unit. This unit consists of medium-grained sandstone with some interbedded clayey levels. The sand is predominantly quartz, but because this unit was deposited in a fluvial/deltaic sedimentary environment, the lithologic variability may be very large even in short distances. However, from the hydrogeological point of view this is considered an aquifer unit and it may yield significant volumes of water to wells.

- *Micaceous sandstone formation ('Furadouro sandstone formation'), C_2*

This sandstone formation is undoubtedly the aquifer layer with the highest transmissivities and boreholes completed along a full section of the 'Furadouro sandstone formation' may yield as much as 40 or 60 L s^{-1}. The thickness of the unit ranges from 10 to 30 m with a median thickness of about 20 m, and the sand is predominantly very clear quartz with a wide range of granulometry, thus increasing the grain size to the top of the unit. Most boreholes drilled in the region are completed in this formation, and the screens placed along this unit are responsible for the great majority of the water pumped. The high micaceous content of 'Furadouro sandstone formation' may sometimes create some groundwater quality constraints related to the very fine mica particles in suspension and requires the correct placement of well screens.

- *Carbonate formation ('Mamarrosa limestone formation'), C_2*

The lithology of the Carbonate formation varies significantly within the study region but usually it shows hydrogeological characteristics that permits its exploitation in the majority of the area. However, in the central part of the region, the permeability of this unit is significantly reduced and does not yield much water to boreholes. And as it was already pointed out, the Carbonate formation outcrops in the recharge area are also of low permeability.

- *Lower sandstone formation ('Palhaça sandstone formation'), C_{1A}*

This Lower sandstone formation is uniform and exploited by several boreholes in the eastern part of the study area, where it yields considerable volumes of water to wells. However, in the western part of the region it presents an important lithologic variability with depth and has been divided into three different layers from the hydrological point of view. The top part, which underlains the Carbonate formation, is usually of high transmissivity and has good quality waters.

Most boreholes are completed in this unit. A brown-reddish clay layer separates this top part from an intermediate part, where the clay content and sandstone degree of cementation increase and the well yield is reduced. The water quality decreases due to increasing mineralization. Fewer boreholes are completed in this unit and it usually presents higher hydraulic heads than the upper overlaying layer.

The bottom part of the Lower sandstone formation despite having coarser granulometries, also presents a high degree of cementation, which significantly reduces the permeability of the unit and increases the water mineralization. Usually boreholes avoid exploiting this part because it creates obvious quality constraints. It also presents higher piezometric water levels than the upper layers. These two last aquifer layers still have been considered as making part of the principal aquifer system, but much lower transmissivity values were assigned to both layers when compared to the overlaying layers.

The relation between the regional lithostratigraphic units and the corresponding hydrogeologic units for the study aquifer is summarised in following Table 3.1, which shows the division of the two principal aquifer systems of the Lower Vouga region into eight hydrogeologic units for further flow analysis. For the purpose of this research, the Quaternary deposits are defined as the permeable zone 1 and treated as a whole aquifer system.

From a hydrogeological point of view, the most productive aquifer units and those with the lowest salinities correspond to the top of unit C_{1A}, the entire unit C_2, and the bottom of unit C_3. The top of unit C_3 and the intermediate and bottom parts of unit C_{1A}, due to their low transmissivities and increasing groundwater residence times, have frequently very high-mineralised waters, which may represent a water quality constraint.

Table 3.1. Correlation of aquifer systems and hydrogeologic units for the Aveiro region.

Period	Stage	Lithostratigraphic units		Lower Vouga Region Aquifer-System Analysis	
				Hydrogeologic unit	Aquifer system
Q	Holocene and Plio-Pleistocene	Alluvium, beach and eolian sands and sand dunes		Permeable zone 1	Quaternary aquifer
		Terrace and old beach deposits			
C	Campanian-Maastrichtian	'Aveiro clay formation', C_3		Confining unit 1	Multilayer Cretaceous aquifer
	Coniacian-Santonian	Upper sandstone formation, C_3	Top	Permeable zone 2	
	Upper Turonian-Lower Coniacian		Bottom	Permeable zone 3	
	Upper Cenomanian -Turonian	'Furadouro sandstone', C_2		Permeable zone 4	
	Cenomanian	Carbonate formation, C_2		Permeable zone 5	
	Aptian/Albian-Lower Cenomanian	Lower sandstone formation, C_{1A}	Top	Permeable zone 6	
			Intermediate	Permeable zone 7	
			Bottom		

3.2.2 **Thickness and vertical relation of principal aquifer layers and confining units**

The approximate thicknesses of the principal aquifer layers and confining units were assessed based on the analysis and interpretation of the geophysical logs available for the study region (Fig. 3.3). The unknown bottom elevation values between adjacent boreholes were estimated using linear kriging (e.g. Davis, 1986) and interpolated for the rest of the study region. The results obtained have been represented using contour plots in Fig. 3.4.

The subsurface data integration and interpretation was further improved using cross-sections showing the vertical relation of the basic hydrostratigraphic units and their approximate thicknesses. The logs were first corrected for depth and presented in terms of true vertical depth with respect to sea level and then correlated from one borehole to the next along six approximately east-west hydrogeologic cross-sections (Fig. 3.5 to Fig. 3.10).

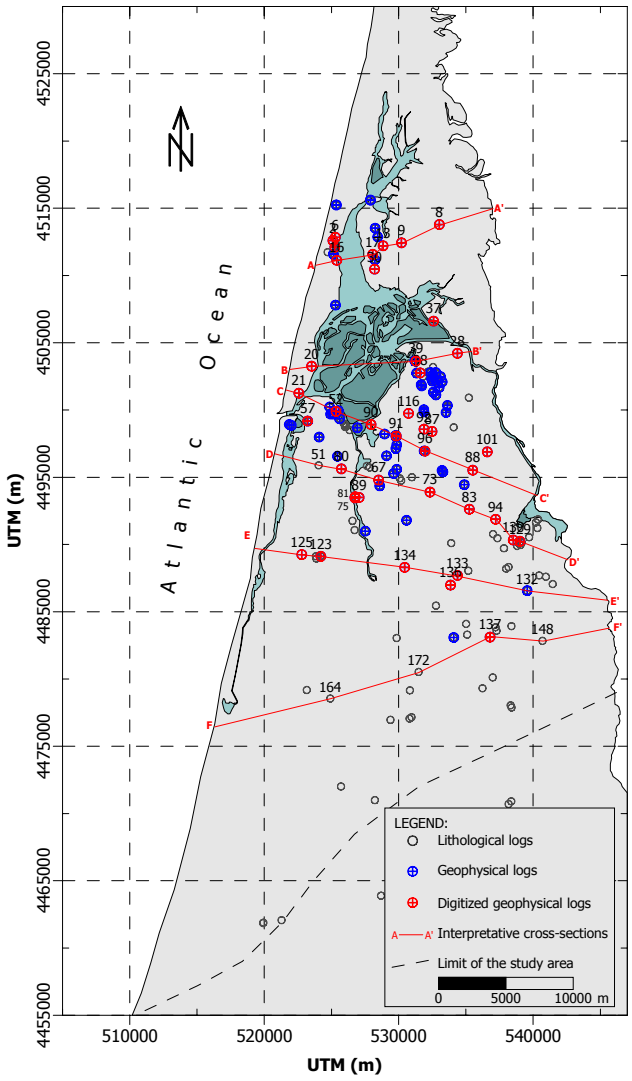

Fig. 3.3 Location of the borehole lithological and geophysical logs used to interpret the hydrogeology of the study area. Also shown are the locations of the hydrogeologic cross-sections (shown in Fig. 3.5 to 3.10).

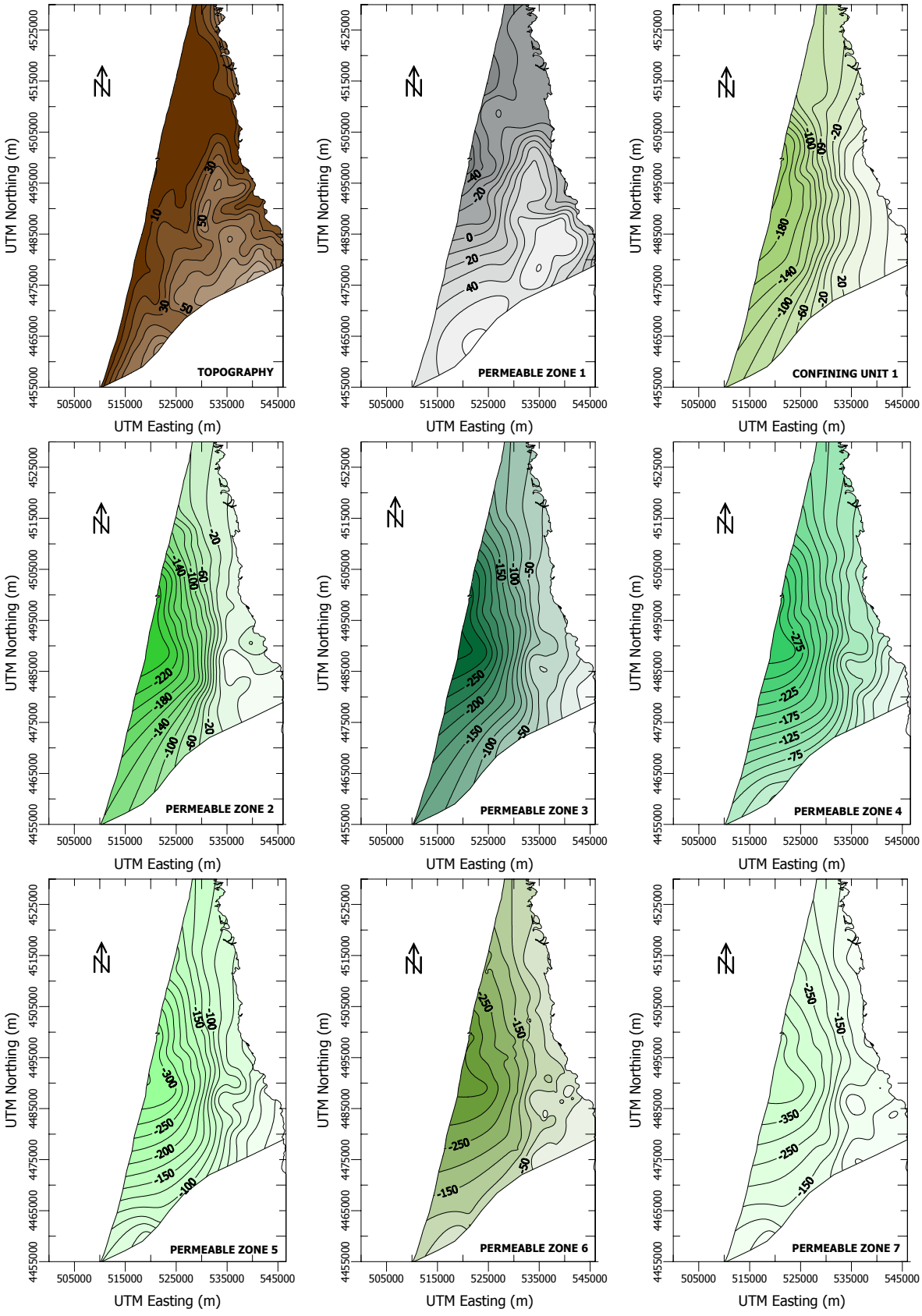

Fig. 3.4 Topography and bottom elevation of the principal aquifer layers and confining units. Values were estimated for the whole region using linear kriging.

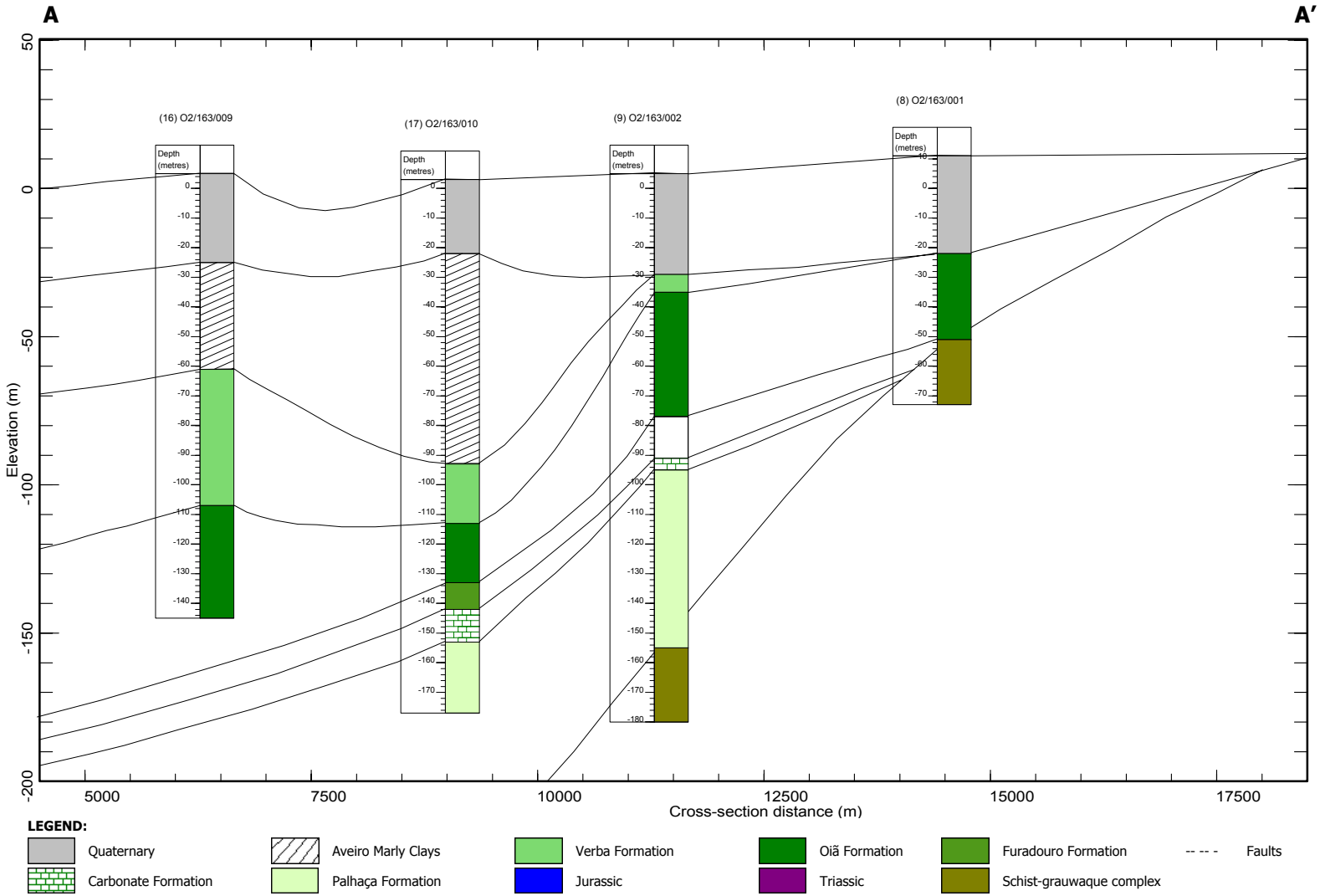

Fig. 3.5 Hydrogeologic interpretative cross-section for the study aquifer showing principal aquifer layers and confining units (A-A').

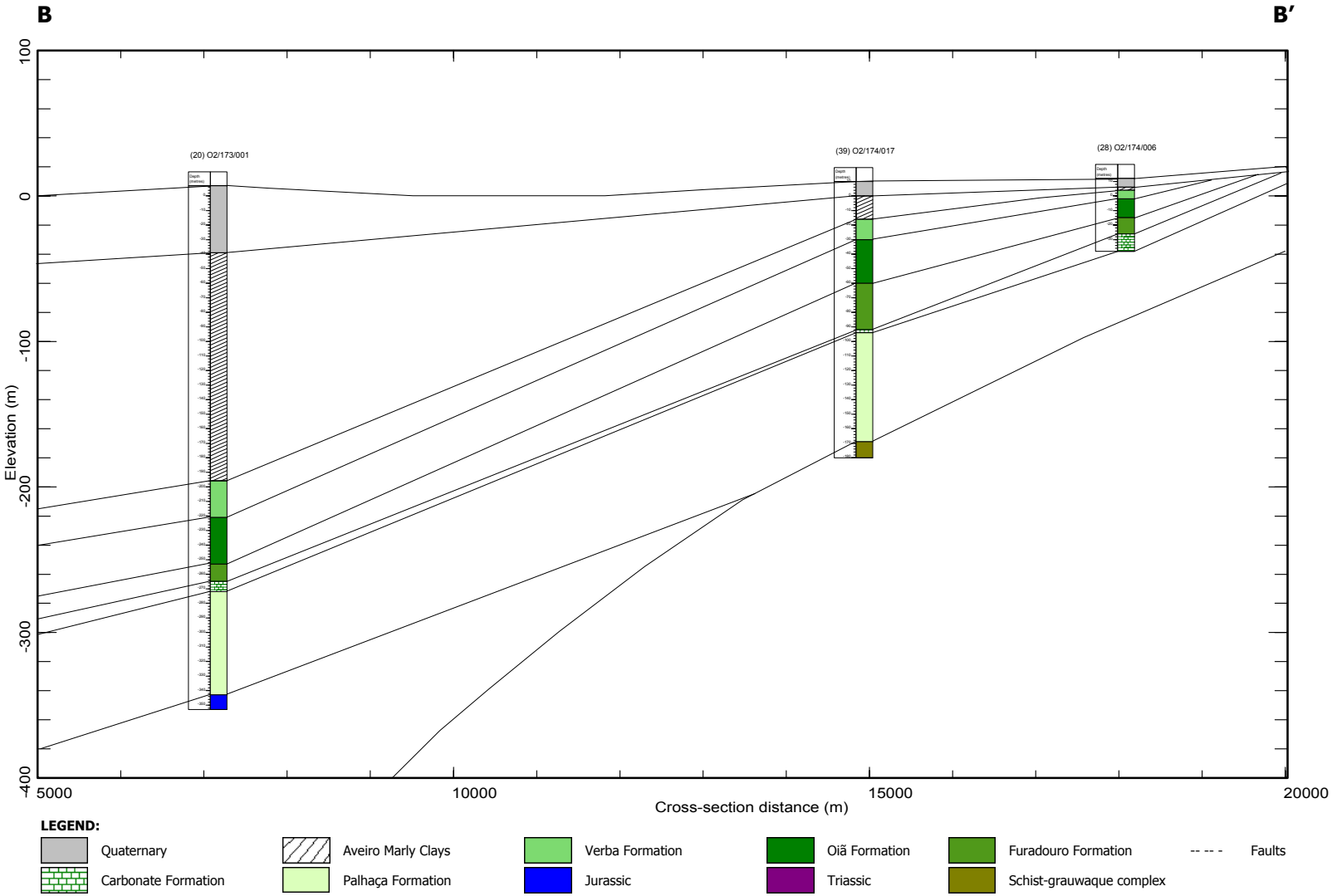

Fig. 3.6 Hydrogeologic interpretative cross-section for the study aquifer showing principal aquifer layers and confining units (B-B').

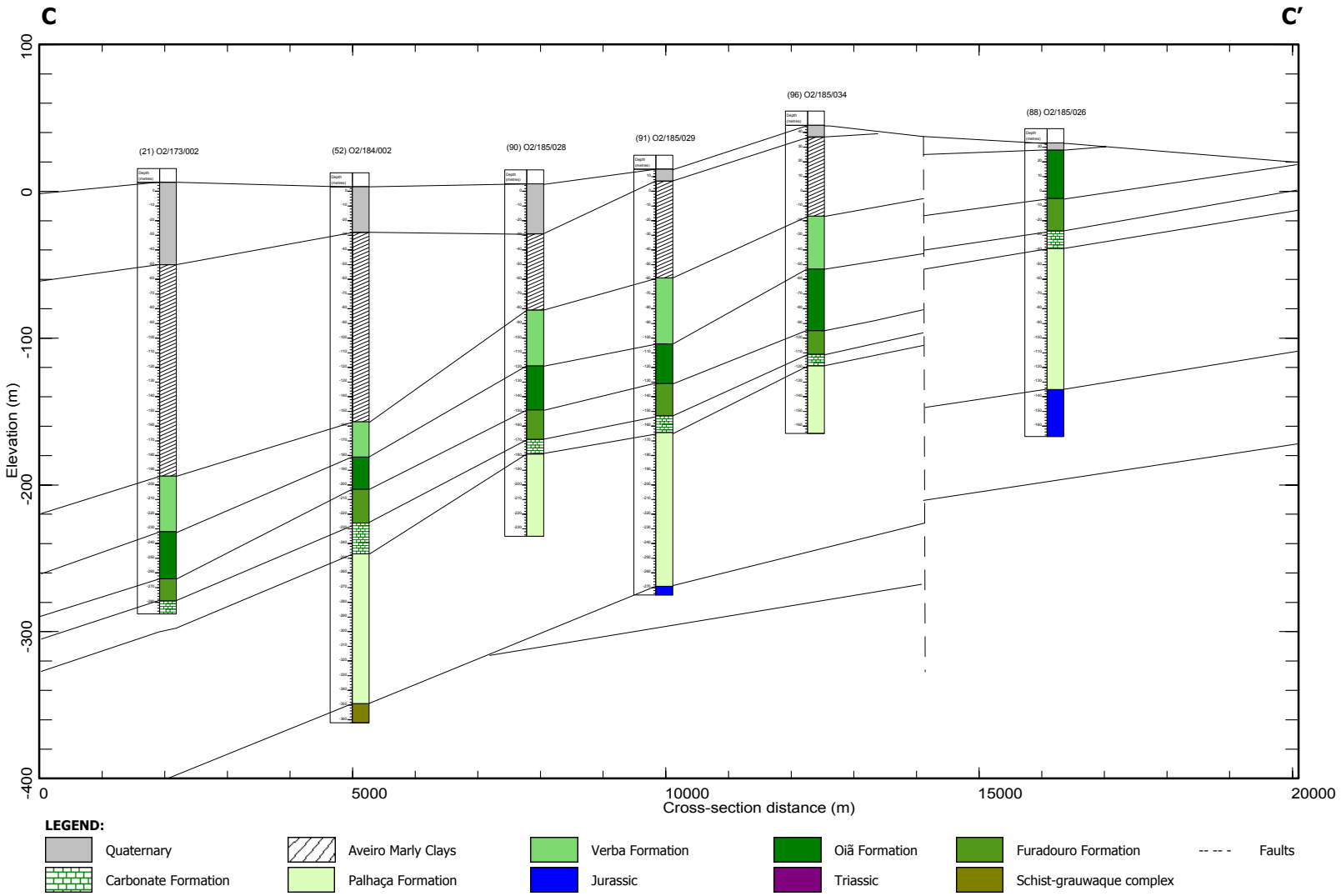

Fig. 3.7 Hydrogeologic interpretative cross-section for the study aquifer showing principal aquifer layers and confining units (C-C').

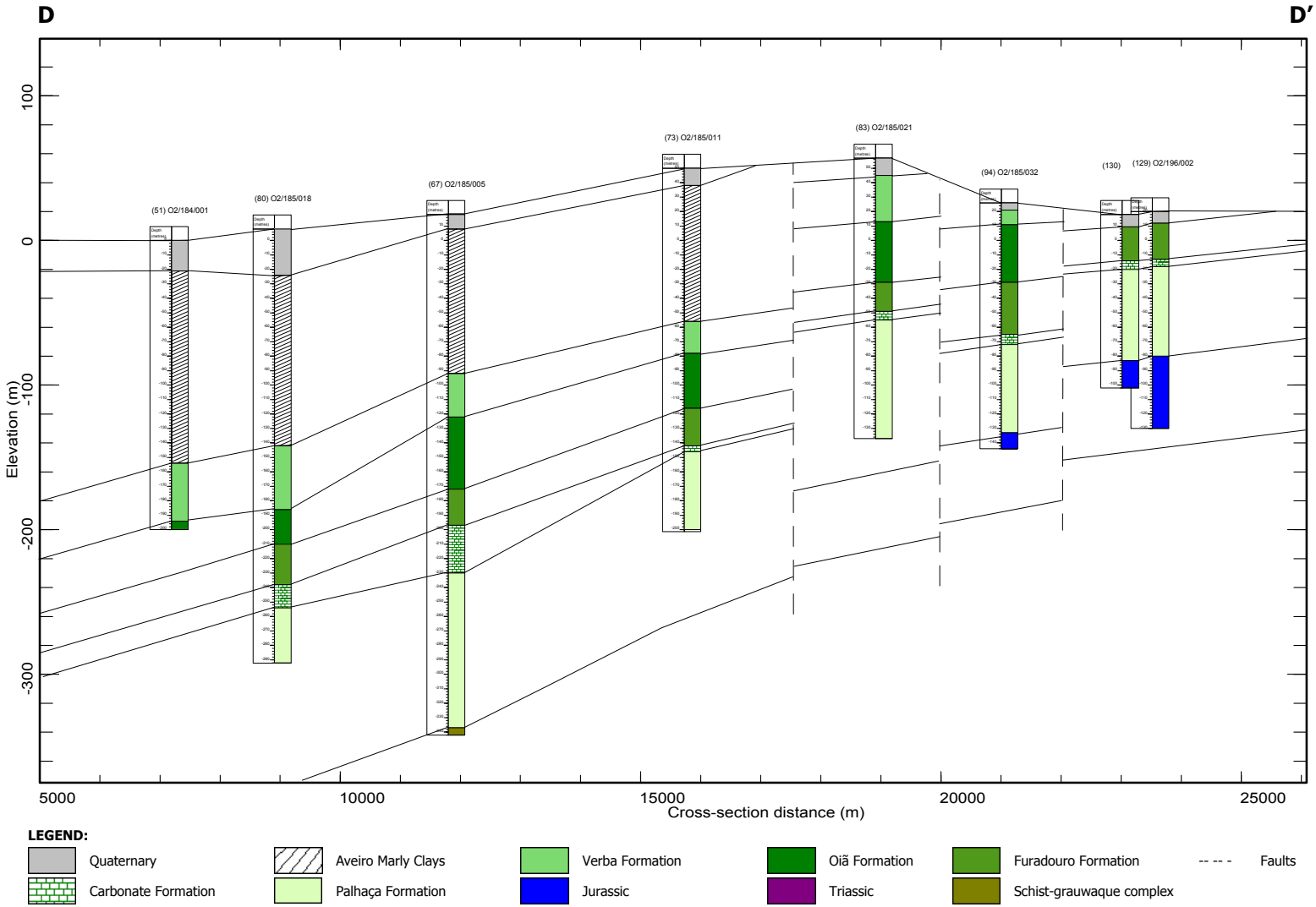

Fig. 3.8 Hydrogeologic interpretative cross-section for the study aquifer showing principal aquifer layers and confining units (D-D').

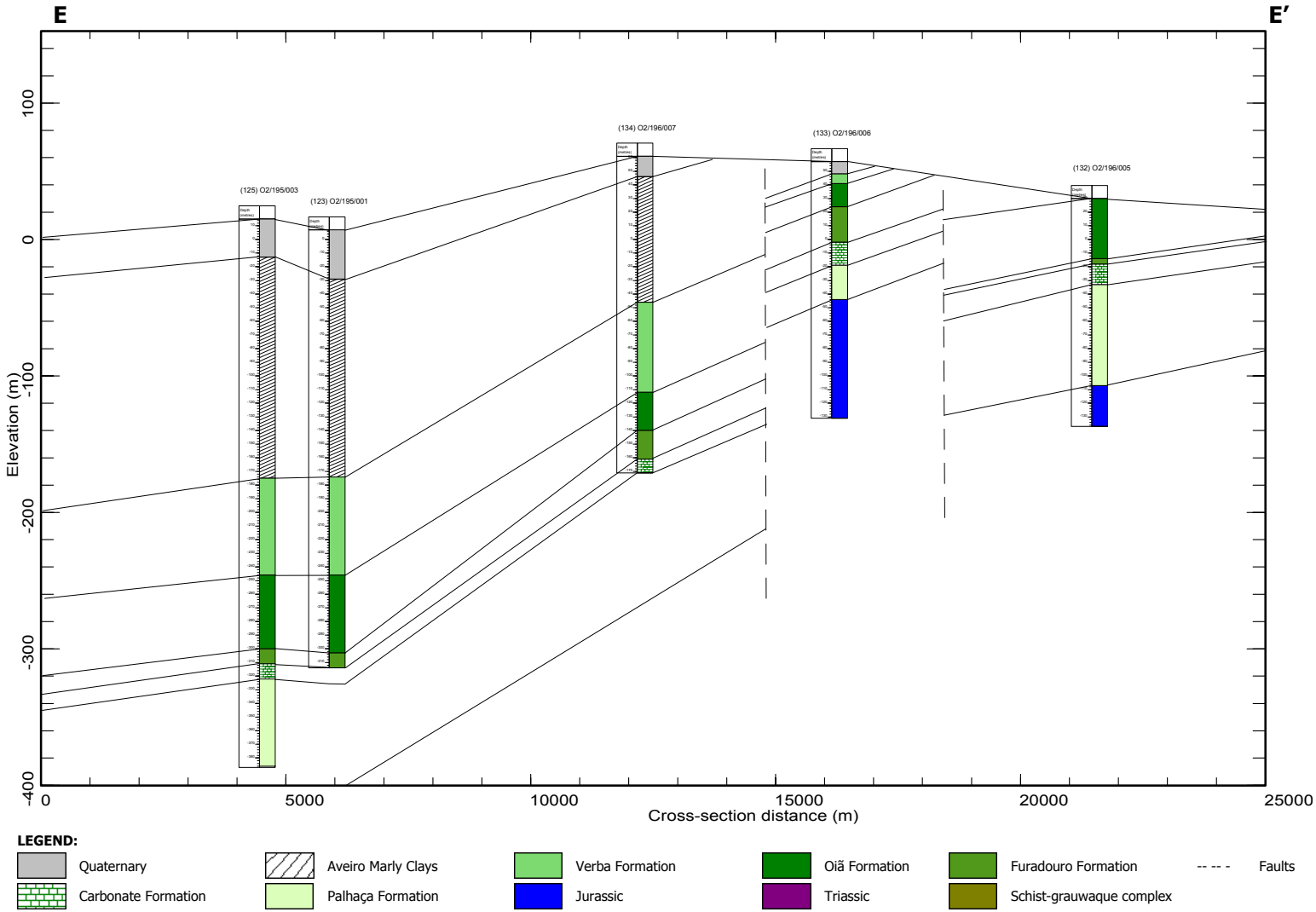

Fig. 3.9 Hydrogeologic interpretative cross-section for the study aquifer showing principal aquifer layers and confining units (E-E').

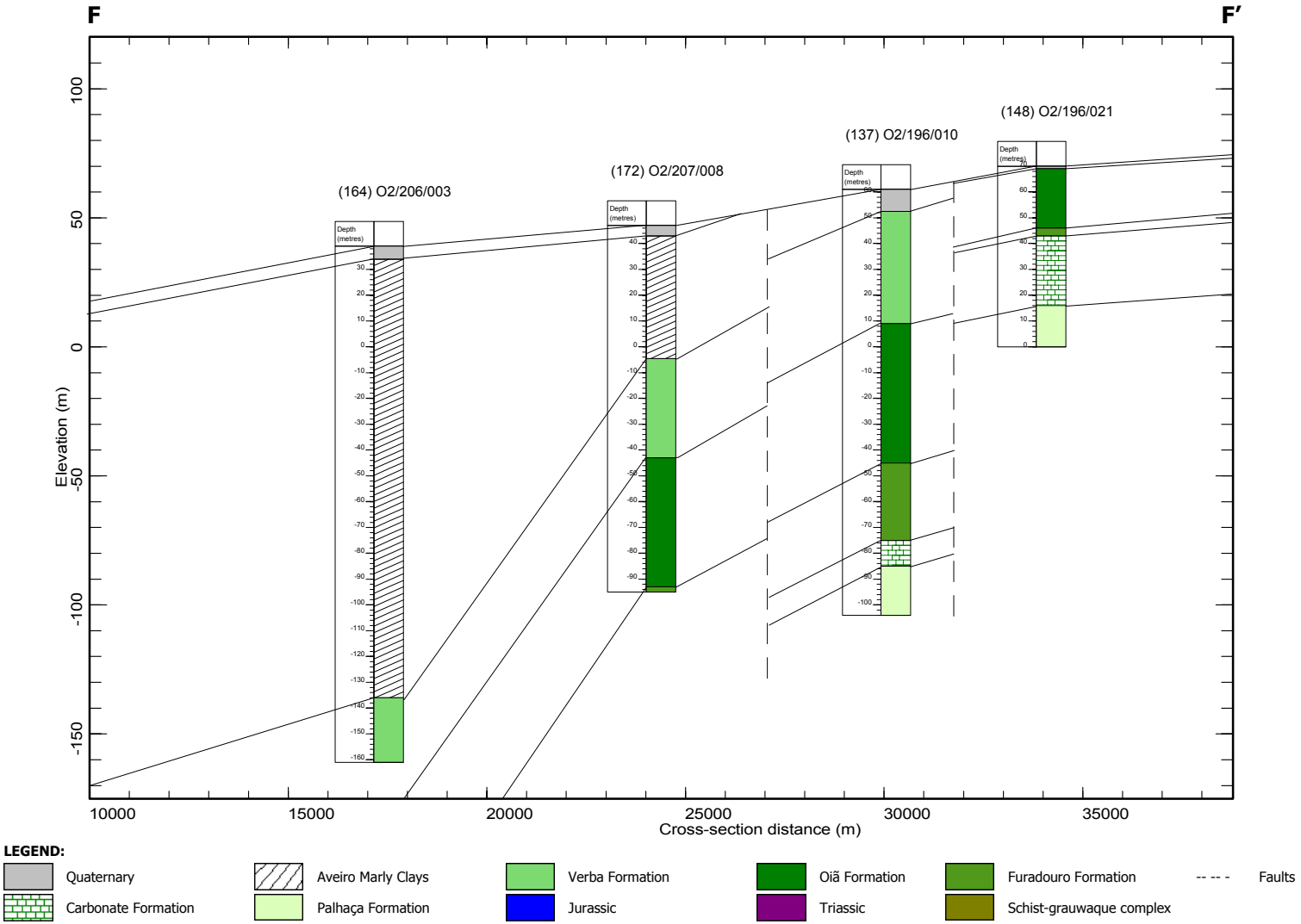

Fig. 3.10 Hydrogeologic interpretative cross-section for the study aquifer showing principal aquifer layers and confining units (F-F′).

3.2.3 **Hydraulic properties**

The simulation of groundwater flow velocity (*v*) in an aquifer requires the definition and (if possible) measurement of two fundamental hydraulic properties, the hydraulic conductivity (*K*) and the porosity (φ). Hydraulic conductivity is a measure of the ability of the aquifer to transmit water, and porosity is the percentage of empty spaces in the aquifer matrix, which may be occupied by water or fluids. The three variables (*v*, *K* and φ) are related by Darcy's law (Darcy, 1856):

$$v = -\frac{K}{\varphi} \text{grad}\, h \qquad [3.1]$$

where *grad h* is the gradient (slope) of the hydraulic head (h) in the water between the top and the bottom of the aquifer formation.

The hydraulic conductivity is a constant of proportionality in the Darcy's law and depends not only on the porous medium and on the fluid, but also varies inversely with its dynamic viscosity. In fact, the real reasons for fluid displacement in a porous medium are, on the one hand, the pressure gradients and, on the other, the external gravity forces (Marsily, 1986). Consequently, *K* [L T^{-1}] can be expressed in the generalized form (Equation [3.2]):

$$K = \frac{k \rho g}{\mu} \qquad [3.2]$$

where *k* is the intrinsic or specific permeability and relates to the porous medium regardless of the characteristics of the fluid (and is only defined on the macroscopic scale) [L^2], ρ the fluid density [M L^{-3}], *g* the acceleration of gravity [L T^{-2}] and μ the dynamic viscosity of the fluid [M $L^{-1}T^{-1}$].

Early measurements of *K* and φ based on pumping tests and/or laboratory studies on field samples, usually cores of some type, suggested that these parameters varied smoothly from one location to another in the aquifer. In general, problems dealing solely with groundwater flow may be modelled fairly well using the parameters of transmissivity ($T=K\,b$; b= aquifer thickness) and storage coefficient (*S*), which is related closely to the porosity. Both parameters involve averages of *K* and φ over the entire vertical thickness of an aquifer (Molz, 2000).

However, more detailed measurements of *K* and φ using several alternative methods (*e.g.* standard and air permeameter tests, borehole flowmeter tests, slug tests, pumping tests, grain-size analysis) indicated that *K* (and, also φ) are often very difficult parameters to measure and may vary widely across relatively short distances. Moreover, there is presently controversial evidence that the *K* parameter is systematically scale-dependent (Schulze-Makuch *et al.*, 1999).

Despite of the above mentioned uncertainties, the characterization of some of the principal hydraulic properties and their areal distribution within the Aveiro Cretaceous aquifer, permeable zones and confining units, had to be carried out based on the interpretation of the available pumping-test data. Porosity and specific storage values to be used in Chapter 6 have been

estimated based on literature values (*e.g.* Anderson & Woessner, 1992; Domenico & Schwartz, 1990 and Marsily, 1986). And, to overcome the lack of data about the vertical hydraulic conductivity values of aquifers and aquitards, these were considered to be approximately 10 and 100 times less than the estimated horizontal hydraulic conductivities, respectively.

The available pumping-test data included 130 pumping tests provided by the well drilling companies and corresponded to more than 80 boreholes within the study region. The tests performed are either variable discharge test methods, using constant-rate stepped change in discharge, or constant discharge test methods, including in both cases the recovery-test measurements.

In their great majority these tests were performed during well construction and development phases, and were planned for determining the well specific capacity and other well characteristics related to their adequate exploitation. Only in 25 of these pumping tests, water level data was monitored not just in the pumping well but also in adjacent observation wells. For these reasons the resulting data was not always the most suitable for the purpose of the present research.

The pumping-test results were interpreted using AquiferTest® 3.0 (Waterloo Hydrologic, Inc.) and the results obtained per group of aquifer layers tested have been summarised in Table 3.2. The estimated hydraulic characteristics are basically the transmissivity, hydraulic conductivity and storage coefficient. These properties are accepted to be: (1) an approximation of their real field distribution, (2) specific to the test method, (3) dependent upon the instrumentation of the field test, the knowledge of the aquifer system and the conformance of the hydrogeologic conditions at the field site to the simplifying assumptions that are implicit in each test method (ASTM, 1996).

The results should be analysed taking into account several limiting factors:

- the short duration of most pumping tests, generally not long enough to determine the existence of nearby boundaries or leakage from different aquifer layers;
- the tidal influence, producing water level oscillations in the boreholes close to the coast, masquerading water level drawdown due to withdrawal;
- the existence of discharging wells in the vicinity of the test sites;
- the majority of the boreholes are multiscreened pumping water from different aquifer layers.

Another important limiting factor is the spatial distribution of the pumping tests. Most of the pumping tests available are for the central and north part of the region, while for the eastern and southern parts of the aquifer there is a clear lack of information.

Table 3.2. Hydraulic parameter for the principal aquifer layers calculated using AquiferTest® 3.0.

Aquifer layers tested	Permeable zone 6 & 7			Permeable zone 5, 6 & 7			Permeable zone 4, 5, 6 & 7			Permeable zone 3, 4, 5, 6 & 7		
Hydraulic parameters	**T**	**K**	**S**	**T**	**K**	**S**	**T**	**K**	**S**	**T**	**K**	**S**
Total no. of data values	15	15	2	8	8	0	104	104	16	90	90	10
Missing values	1	1	14	0	0		0	0	88	1	1	81
Minimum	2	0.1	3.2E-05	1	0.1		0.1	0.004	9.6E-12	0.4	0.02	4.5E-06
Maximum	275	25	3.2E-05	166	13		8165	255	3.6E-01	896	46	4.3E-03
Average	**68**	**5**	**3.2E-05**	**40**	**3**		**388**	**15**	**2.3E-02**	**265**	**10**	**7.6E-04**
Median	**15**	**1**	**3.2E-05**	**13**	**0.5**		**256**	**11**	**9.8E-05**	**235**	**8**	**3.5E-05**
1st Quartil	7	0.5	#N/A	2	0.1		168	6	4.4E-05	117	4	7.7E-06
3nd Quartil	91	6	#N/A	61	5		415	16	6.9E-04	361	12	2.0E-04
Standard deviation	95	8	0.0E+00	57	4		803	25	8.9E-02	198	9	1.5E-03

Aquifer layers tested	Permeable zone 3 & 4			Permeable zone 3, 4 & 5			Permeable zone 4 & 5			Permeable zone 2, 3, 4, 5, 6 & 7		
Hydraulic parameters	**T**	**K**	**S**	**T**	**K**	**S**	**T**	**K**	**S**	**T**	**K**	**S**
Total no. of data values	16	16	3	10	10	2	8	8	1	19	19	5
Missing values	1	1	14	0	0	8	0	0	7	0	0	14
Minimum	66	4	2.8E-05	182	10	1.6E-05	180	11	4.7E-03	16	1	1.1E-05
Maximum	838	43	3.9E-04	877	32	2.2E-05	757	47	4.7E-03	575	21	6.0E-05
Average	**413**	**22**	**1.5E-04**	**427**	**20**	**1.9E-05**	**427**	**24**	**4.7E-03**	**200**	**7**	**3.2E-05**
Median	**368**	**18**	**3.6E-05**	**429**	**21**	**1.9E-05**	**441**	**22**	**#N/A**	**161**	**6**	**3.6E-05**
1st Quartil	253	15	#N/A	220	12	#N/A	300	19	#N/A	63	2	1.3E-05
3nd Quartil	571	28	#N/A	530	27	#N/A	499	25	#N/A	239	9	4.4E-05
Standard deviation	220	11	2.0E-04	213	8	4.1E-06	177	11	#N/A	181	6	2.0E-05

Aquifer layers tested	Permeable zone 2			Permeable zone 2 & 3			Permeable zone 2, 3 & 4			Permeable zone 2, 3, 4 & 5		
Hydraulic parameters	**T**	**K**	**S**	**T**	**K**	**S**	**T**	**K**	**S**	**T**	**K**	**S**
Total no. of data values	5	5	0	6	6	0	2	2	0	2	2	0
Missing values	0	0		0	0		0	0		0	0	
Minimum	9	0.2		1	0.05		645	25		452	13	
Maximum	84	7		461	15		693	27		454	13	
Average	**41**	**3**		**140**	**5**		**669**	**26**		**453**	**13**	
Median	**37**	**3**		**64**	**4**		**669**	**26**		**453**	**13**	
1st Quartil	11	0.3		20	1		#N/A	#N/A		#N/A	#N/A	
3nd Quartil	69	6		230	8		#N/A	#N/A		#N/A	#N/A	
Standard deviation	33	3		178	6		34	1		1	0	

Legend: #N/A - Not applicable T - Transmissivity in $m^2\ d^{-1}$ K - Permeability in $m\ d^{-1}$
S - Storage coefficient

The examination of the pumping test interpretation results summarised in Table 3.2 show that the intermediate part of the aquifer, which includes permeable zones 3, 4 & 5, has the highest hydraulic conductivities (18 to 22 m d^{-1}) and is where most groundwater flow should occur. And, the 'Furadouro sandstone formation' must be the principal contributing unit because when the boreholes do not have a screen placed in front of this aquifer unit the average hydraulic conductivities are almost 60% lower. From these aquifer intermediate layers, the hydraulic conductivity values decrease significantly up and downwards the aquifer to values of 1 to 5 m d^{-1}, which are in agreement with the lithological characterisation. Unfortunately, there are no hydraulic conductivity data available for the confining unit ('Aveiro marly clay formation).

The storage coefficients are characteristic of a confined aquifer showing values varying between 10^{-5} and 10^{-4}.

The calculated transmissivity values have been plotted using a classed post map (Fig. 3.11). This type of representation may not be very correct because it mixes pumping-test data for different aquifer layers, or at least, the aquifer layers tested are not always the same. However, the map is still very important to show the areal distribution of the transmissivity within the study area. The central part of the aquifer (around Ílhavo, Aveiro and Cacia) has the highest

transmissivity values, while in the rest of the region (either to the north, east, south or even along the coast), the transmissivity suffers an important decrease.

The map also puts in evidence the low transmissivities (< 50 m d^{-1}) observed in the aquifer recharge area, which may indicate difficulties for the recharge water to reach the deeper and confined parts of the aquifer.

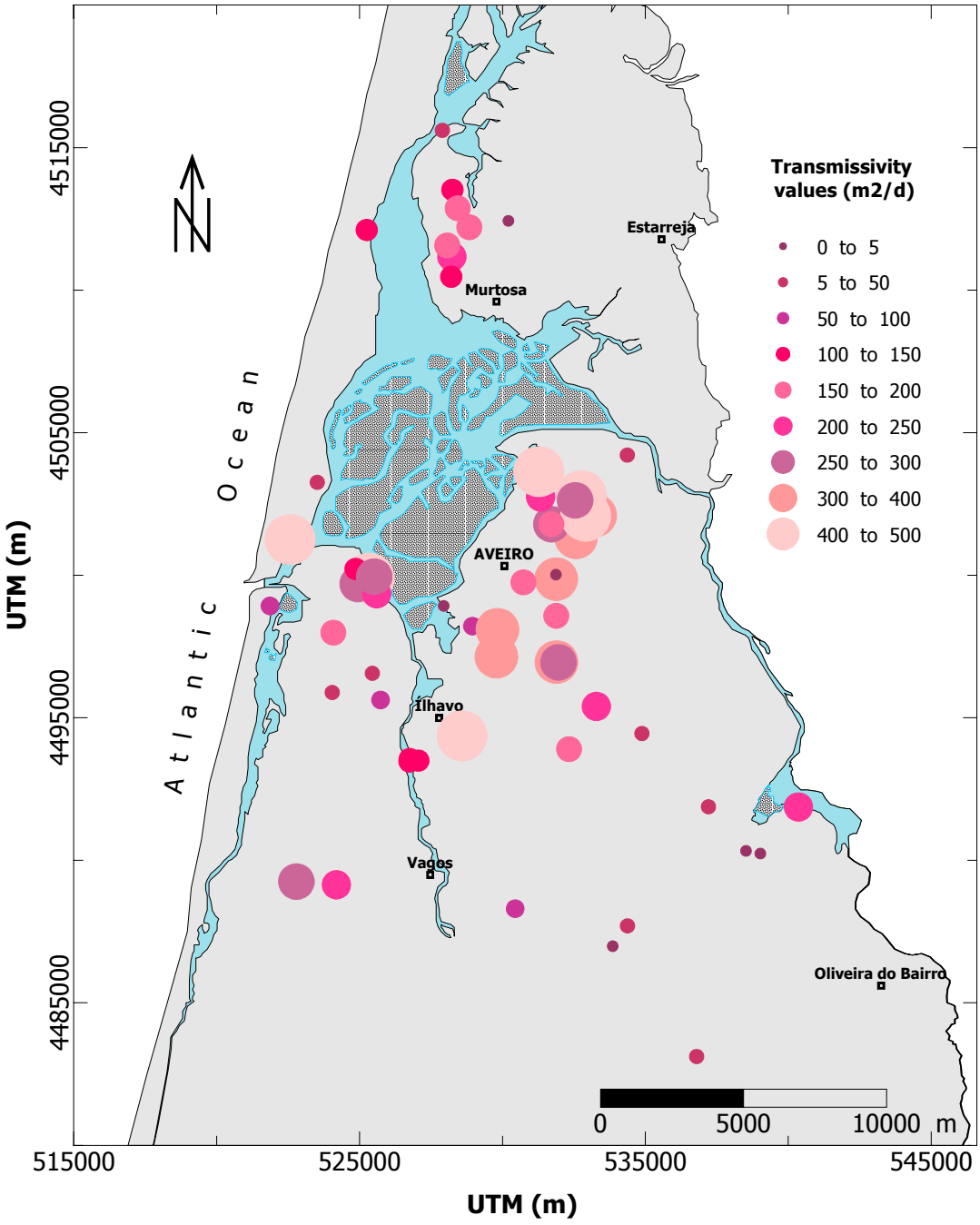

Fig. 3.11 Transmissivity values for the Aveiro Cretaceous multilayer aquifer. Values were calculated from pumping test analyses.

3.2.4 **Water levels**

Monthly measurements of water levels in the Aveiro Cretaceous aquifer were available for 28 monitoring wells distributed throughout the aquifer area. The water levels were measured in deep boreholes, which belong to the National Groundwater Levels Monitoring Network. The monitoring period varies for each well, but for at least 18 of these wells it is longer than 15 years. The corresponding water level hydrographs and a map with their exact location have been included in Appendix A.

Because the water level measurements are not point measurements, no attempt was made to construct potentiometric surface maps for each aquifer layer. Instead a regional potentiometric-surface map of the Aveiro Cretaceous aquifer was constructed by contouring measurements of static (nonpumping) head relatively to the mean sea level measured in June 2002 (Fig. 3.12).

Most of the regional variations observed in groundwater levels are a response to changes in the rates of groundwater discharge and a consequence of the extensive pumpage. The impact of groundwater recharge is just observed in the boreholes located in the outcrop area, and in this part of the aquifer the water levels recover during the winter months. In the rest of the region, water levels generally decline during the summer months due to an increase in groundwater abstraction, and along the coast water levels may change daily due to the influence of sea tides (Marques da Silva, 1990).

The values observed at present show that hydraulic heads are below mean sea level in the central part of the aquifer. Potentiometric highs are in the southeast part of the aquifer close to the recharge area and to the southern limit of the aquifer. A large depression of the piezometric surface and a reversal of the natural flow direction may be observed nowadays in the area between Ílhavo, Aveiro and Cacia.

The groundwater levels distribution does not show any significant contribution of the river Vouga to the aquifer system but do seem to indicate some contribution from the 'Pateira de Fermentelos lagoon' located in the eastern part of the study area. According to Barra (1998) the lagoon overlays the Triassic sandstones and not the Cretaceous formations. However, they do have a lateral contact, so it is possible that depending on the time of the year, the lagoon acts as a recharge/ discharge boundary.

Review of historical groundwater level data indicates that the aquifer has never been in a steady-state condition during the monitoring period. The hydrographs show that in spite of the fast recovery in the water levels (1 to 2 m per year) observed in the late nineties (and as should be expected from a confined aquifer), they are falling again, requiring strong protection measures from the Water Authorities.

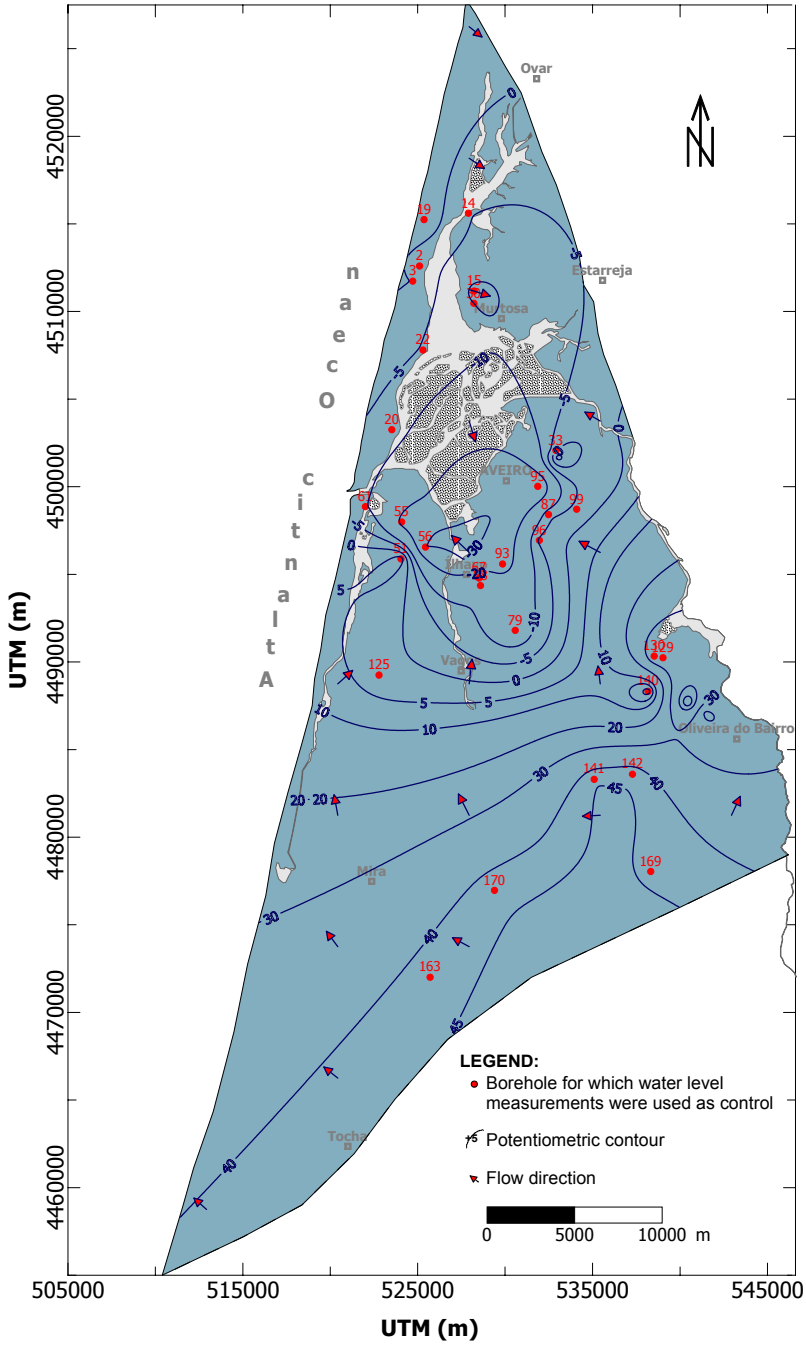

Fig. 3.12 Configuration of the regional piezometric level in the Aveiro Cretaceous aquifer on June 2002. Hydraulic heads are measured relatively to the mean sea level.

3.2.4.1 **Predevelopment potentiometric surface**

Several factors may control the regional groundwater flow in the aquifer systems under predevelopment conditions (Williamson & Grubb, 1998). For the Aveiro Cretaceous aquifer the most important factors were considered to be: (1) topography; (2) outcrop/subcrop pattern and geometry of aquifers, permeable zones, and confining units; (3) variation of hydraulic properties of aquifers, permeable zones, and confining units; and, (4) downdip limits of the aquifer.

Taking into account these several factors and the water levels measured in the first boreholes drilled in the aquifer, an average predevelopment (1950's) potentiometric map was estimated for the study region using linear kriging (Fig. 3.13). The depth of the piezometric levels is a controlling factor for regional groundwater flow (Fig. 3.14), which under natural conditions is from the recharge area in the east towards the sea, with a natural gradient around 0.0015.

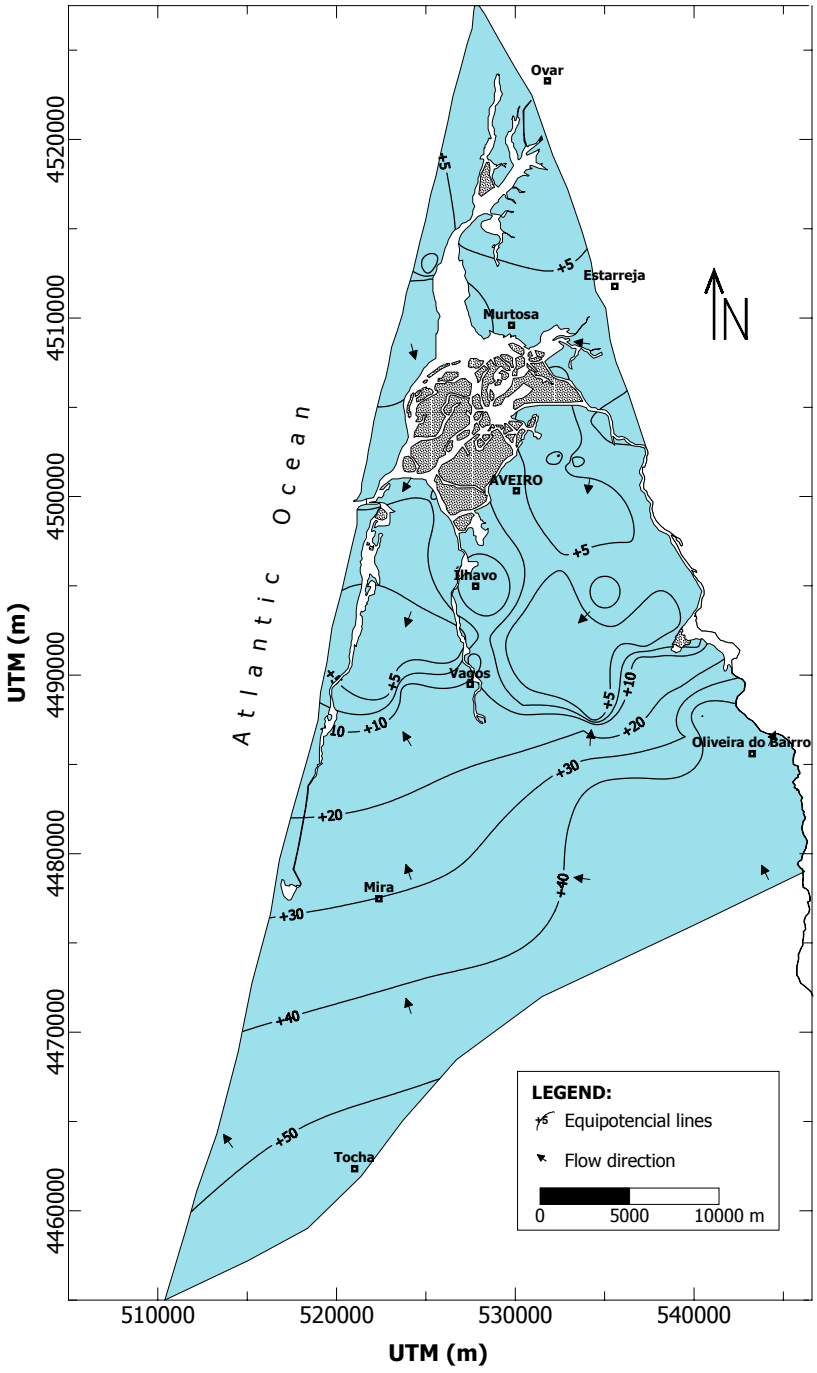

Fig. 3.13 Estimated predevelopment (1950's) potentiometric surface for the Aveiro Cretaceous aquifer using linear kriging.

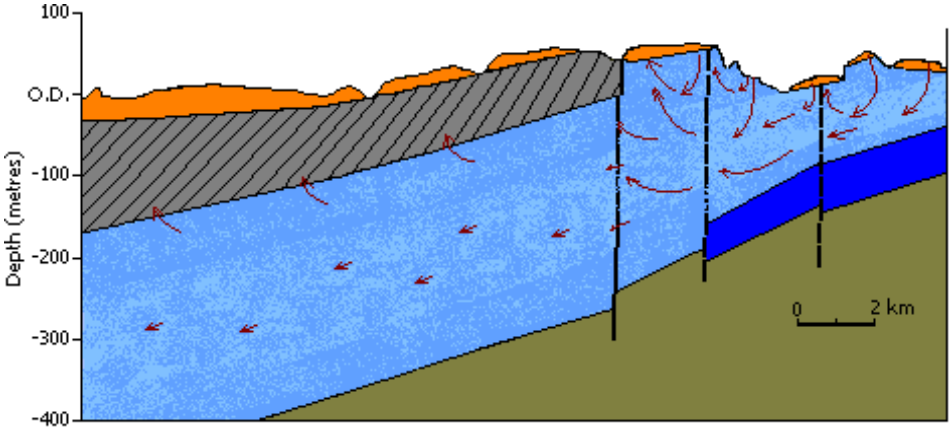

Fig. 3.14 Diagram showing the regional groundwater flow in the region.

3.2.5 **Boreholes and groundwater uses**

Groundwater is withdrawn from the Aveiro Cretaceous multilayer aquifer system by deep multi-screened boreholes, which pump water from the most permeable aquifer layers, at discharge rates varying from a few litres per second to over 50 L s^{-1} (Fig. 3.15).

For the present research 185 boreholes have been inventoried within the studied region and are summarised in Appendix A. These boreholes have variable depths, with total depth values ranging from something about 25 to 35 m, in the recharge area, to over 300 m, along the coastline. The deepest water-supply borehole in the region is 350 m long and has been drilled in the forested area surrounding the town of Vagos.

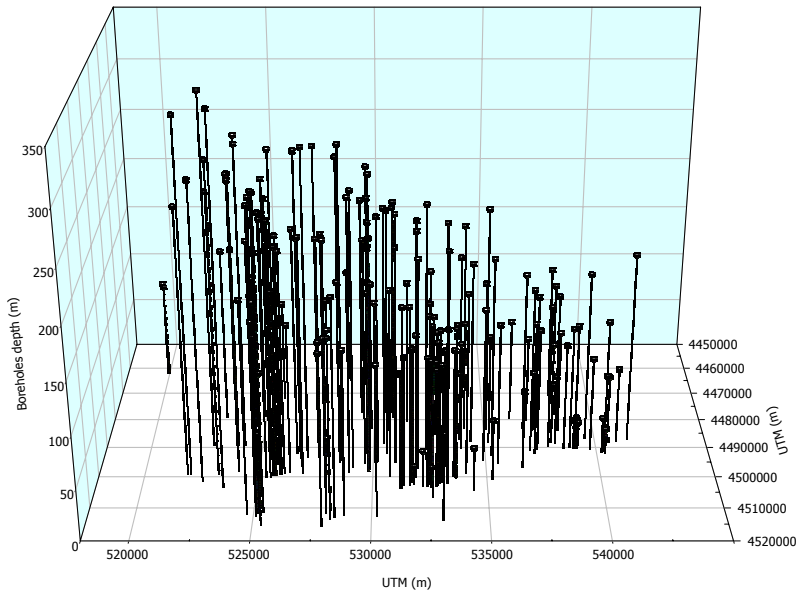

Fig. 3.15 Borehole depth distribution in the Aveiro Cretaceous aquifer.

This type of boreholes has on average 8 screened intervals of about 3-4 m long, which corresponds to a total screen length of about 26 m. The correct placement of the screens is often critical for the borehole productivity and water quality, as inevitably this type of boreholes mix water of different quality and residence times.

The boreholes in the region are mainly used for water supply (75%), while the rest are used as piezometers (4%) or monitoring wells (7%). About 14% of the drilled boreholes have been abandoned in relation to their lack of productivity or to leaks at joints in the blank casing (Fig. 3.16).

Most of these boreholes pump water from the Aveiro Cretaceous aquifer that will be used for industrial (36%), public supply (22%) and domestic supply (15%). The wells used for domestic supply are usually located in areas close to the recharge area, where the average borehole depth is often less than 50 m. In the rest of the region, the necessity to drill deep boreholes to pump good quality water makes this alternative rather expensive, and the local population prefer the public water supply.

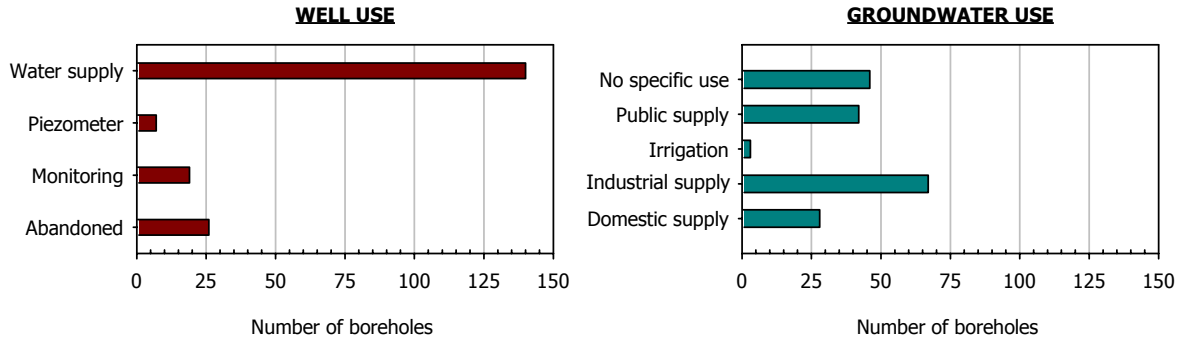

Fig. 3.16 Principal well and groundwater uses in the Aveiro Cretaceous aquifer

3.2.6 **Groundwater discharge**

Mean groundwater discharge from the Aveiro Cretaceous aquifer system is essentially of three types: (1) the water pumped by the boreholes drilled in the aquifer; (2) the discharge to a few springs in the recharge area; and, (3) the possible aquifer discharge to the sea. The greatest volume of groundwater discharge is directly into boreholes.

The calculation of the total volume of aquifer abstractions is one of the uncertainties that limits the present research. The abstraction volumes were just obtained for the two principal water supply companies of the region (S.M. Aveiro & S.M.A.S. Ílhavo). The data provided has been plotted in Fig. 3.17 and confirms the significant reduction observed in the pumped volumes since 1996. Unfortunately, most of the other Water Supply companies and industries located in the

region and using groundwater do not provide regularly any abstraction volumes to local Water Authorities.

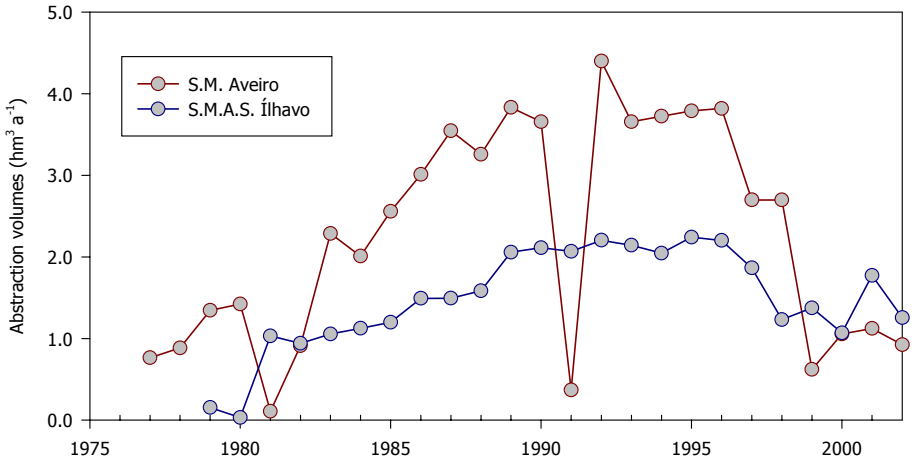

Fig. 3.17 Evolution of the abstraction volumes pumped by the two major water supply companies in the region.

In an attempt to try to approximate the total volume of abstractions in the aquifer and minimise the uncertainty, the specific discharge of each well was taken into account. Then, the total volume of water pumped was calculated considering that a well for: (1) industrial supply works about 12 h per day; (2) domestic supply works about 4 h per day; and, (3) a well for public water supply works almost 16 h per day, all the days of the month. The results are summarised in the pie chart of Fig. 3.18 and give a total volume of abstractions of about 21.3 $hm^3 a^{-1}$, which is possibly still underestimated.

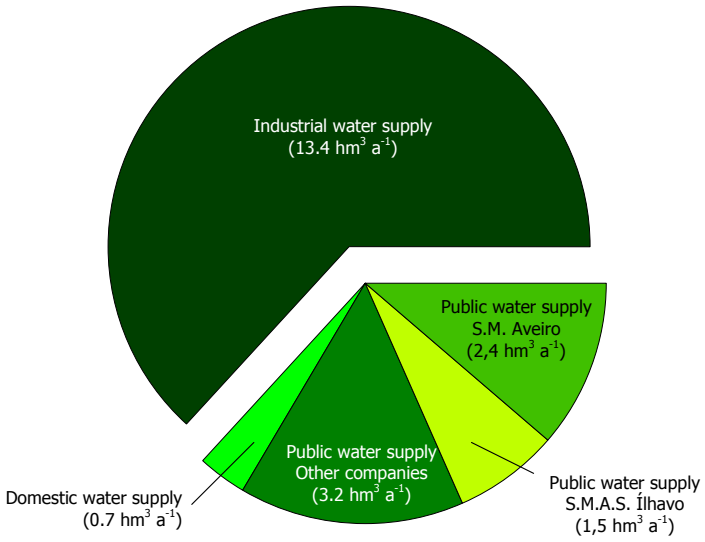

Fig. 3.18 Pie chart showing the estimated mean annual groundwater discharge for water supply in the aquifer.

The aquifer discharge to springs in the recharge area is almost negligible. It has been estimated to be less than 0.01 $hm^3 a^{-1}$, considering a base flow of about 0.2 L s^{-1} measured in the just two springs inventoried in the Cretaceous outcrops.

The natural flow pattern of the aquifer was from the recharge area on the east to northwest, discharging the aquifer to the sea. However, these days the flow to the sea must be minimal, induced by groundwater exploitation for public and industrial supply. To calculate the present day amount of aquifer discharge to the sea, it was assumed that: (1) the total coastline length is approximately 70 km; (2) the average transmissivity for the boreholes along the coast varies between 200-250 $m^2 d^{-1}$; and, (3) the hydraulic gradient is nowadays less than 0.0005.

Based on these values, the total aquifer discharge to the sea was calculated and ranges between 2.6 and 3.2 $hm^3 a^{-1}$. These discharge volumes are quite small when compared to the total borehole abstraction volumes (for industrial, public and domestic water supply) from the aquifer.

3.3 Palaeohydrological conditions during the Late Pleistocene

The Aveiro Cretaceous coastal aquifer serves as a good indicator for changes in the coastal aquifer systems along the Iberian western Atlantic coast since the Last Glaciation because Late Pleistocene-Early Holocene groundwaters have been identified in the deeper and confined part of the aquifer (Carreira *et al.*, 1996). At the Last Glacial Maximum (LGM) the limit between the Polar Front and the Gulf Stream was located close to the Spanish-Portuguese northern border (40°N). For the Iberian Peninsula, the picture emerging for the last 20,000 years is that of a coastal Iberian continental margin periodically intruded during Heinrich events by a pre-Holocene Canary current carrying large amounts of icebergs originating from a collapsing Laurentine Ice Sheet (Baas *et al.*, 1997). On their way along the Portuguese margin, the icebergs rapidly melted, leading to a different climatic response in the Iberian littoral zone, north and south of 40°N, and to a greatly reduced flux of ice rafted debris off southern Portugal.

According to Zazo *et al.* (1996), for the zone north of 40°N, the climatic conditions during the LGM were less humid and generally cool. In this area, the Younger Dryas event is characterised by cool and slightly humid conditions, evolving towards conditions that are more humid. A temperate and humid climate similar to the present day was reached at the beginning of the Holocene. In contrast, the climate for the zone south of 40°N is described as generally dry and cold before 15,000 a BP, followed by amenable climate conditions.

At the time of the Last Glaciation the river basins were much larger and river runoff significantly higher than at present day. Some of them, like the river Vouga in NW Portugal, had even different orientations at their terminal part confirmed by the existence of palaeochanels

identified in bore-drillings (Marques da Silva, 1990). The amount of sediments transported by the rivers also increased resultant from the activation of erosive processes due to favourable weather conditions (Dias *et al.*, 1997).

3.3.1 Sea level rise and impacts on groundwaters

The likely mean sea level evolution during the past 20,000 years along the Iberian western margin is summarised in the relative mean sea level curve of Fig. 3.19. The gradual melting of the polar front and its major or minor northward retreat conditioned the sea level rise and had a considerable impact on the flow regimes and flow paths of rivers and coastal aquifers along the Iberian coast, such as the Aveiro Cretaceous aquifer.

According to the relative sea level curves represented in Fig. 3.19, sea level in the NW of the Iberian Peninsula was at about –130 to –140 m at the LGM (18 ka BP). During the following 2ka sea level rose up to –100 m (at 16 ka BP), stabilising at this level till the very end of the glaciation (14 ka BP). The Flandrian transgression rose the sea level up to –40 m at 12 ka BP, but the cold event known as Younger Dryas dropped the sea level again to –60 m. A gradual rise of sea level has been observed from 10 ka BP onwards, faster in the initial 2 ka and slower then. The present position was reached at around 4 ka BP.

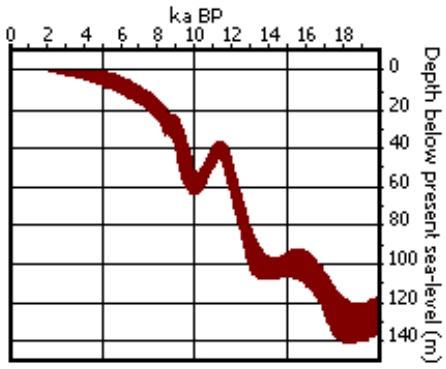

Fig. 3.19 Sea-level curve for the northern part of the Portuguese shelf since the L.G.M. (Dias *et al.*, 2000)

At the time of the LGM sea level was lowered to –130 to –140 m when compared to the present day, producing an increase of at least 35 km more in the length of the Aveiro Cretaceous aquifer flow path and a groundwater flow gradient twice as high as present day. These high flow gradients might have contributed for the complete refreshing of the aquifer, and there is a strong possibility of freshwater or brackish water being preserved in the present confined offshore areas. Fresh groundwater is found at present day at depths over 250 m OD in boreholes next to the coast.

4

GROUNDWATER RECHARGE

Groundwater recharge of an aquifer system may be defined as the volume of water that reaches the saturated zone of the aquifer contributing for replenishing the groundwater reservoir. Recharge is an important component of most groundwater flow models and it may be either specified or estimated during model calibration (Sanford, 2002). However, the idea that knowing the groundwater recharge is important in determining the size of a sustainable groundwater development (long-term safe yield) is a myth because it is an oversimplification of the information that is needed to understand the effects of developing a groundwater system (Alley *et al.*, 1999; Bredehoeft, 2002).

Groundwater recharge can be either a natural or an artificial process. The former occurs when recharge stems from the direct infiltration of rainfall or from the water percolation of adjacent water bodies, and the later when recharge is induced by human activity such as irrigation, urbanisation, construction of injection boreholes, or river spreading. Depending on the route followed by percolating water towards the water table, recharge can be classified as direct recharge when talking about diffuse infiltration of recharge water towards groundwater, or as indirect recharge when along river and other main channels. Some authors, such as Lerner (1997), also refer to localised/ focussed recharge to describe the recharge that suffered some horizontal movement before recharging groundwater, such as streams and lakes. Rushton (1997) also refers to actual and potential recharge to distinguish between the infiltrated water that reaches indeed the water table from that recharge, estimated from surface-water and unsaturated zone studies, which may or may not reach the water table.

Nowadays there are several methods available to estimate natural groundwater recharge, from the well-known physical methods (using either direct techniques based on the use of lysimeters or on the water table fluctuation, or indirect techniques based on the estimate of soil physical parameters) or the geochemical methods (using chemical and isotope techniques), to the so-called inverse methods, using numerical models to solve the groundwater flow equation for recharge instead of groundwater heads. Detailed and critical summaries of all these methods are given in Allison (1988), Sharma (1989), Allison *et al.* (1994), Lerner (1997), Selaolo (1998), Vries (2002) and Scanlon *et al.* (2002).

For the present study, the focus is on natural processes of groundwater recharge of the Aveiro Cretaceous aquifer using different estimation methods. The combined use for the first time in the aquifer of physical methods which rely on direct measurements of hydrological parameters and tracer techniques applied to both unsaturated and saturated zone studies is an attempt to substantiate recharge predictions awaiting for some consistency in results. However, these recharge estimates based on field data still have an important degree of uncertainty and have to be constrained using flux observations (*e.g.* groundwater ages).

Previous recharge investigations in the Aveiro Cretaceous aquifer were done by Marques (1990), Marques da Silva (1990), Reis (1990) and Peixinho de Cristo (1992) and have relied on the use of balance methods such as the soil moisture budgeting or the chloride mass balance methods. These authors suggested values of annual average recharge for the aquifer of 160, 110 and 130 mm H_2O a^{-1}, respectively.

In this chapter before presenting and discussing the results of the different methods used for estimating the Aveiro Cretaceous aquifer natural recharge, a review is made of the background information on the main factors in the hydrologic landscape that potentially control water flow and infiltration. These factors are climate, geomorphology including topography, soil cover and vegetation, hydrology and geology framework.

This review includes a study of the principal environmental variables required by the different recharge estimating methods and the results of a 5-year monitoring programme of the chemical and isotopic composition of present day precipitation in the study region. The understanding of rainfall chemistry is necessary not just for recharge calculations but also to interpret past and present hydrochemical values in groundwater, as rainfall is a major input to groundwater.

4.1 Recharge area

The recharge area of the aquifer is located in the east part of the study area where the aquifer is unconfined and the permeable Cretaceous sediments crop out. It is an area of gentle slopes with altitudes of less than 60 m. The soil cover is thin, consisting mainly of silty clay loam (Rogado, 1995) and, the original vegetation cover of pine and eucalypti forests is slowly being replaced by industrial areas.

The area is limited in the east by the rivers Cértima and Vouga and by the Pateira lagoon. The southern limit is a geostructural limit formed by the Tocha-Febres-Mogofores anticlinal structure with orientation WSW-ENE. Towards the west, the permeable formations are overlaid and confined by the Aveiro marly clay formation that constitute the western limit.

The permeable outcrops encompass a restricted area of approximately 52 km^2 and are mainly formed by fairly homogeneous sediments of the micaceous sandstone formation ('Furadouro sandstone'), the upper sandstone formation ('Oiã sandstone') and the lower sandstone formation ('Palhaça sandstone') (Fig. 4.1).

The limestone formation ('Mamarrosa limestone') that also crops out in the recharge area is of low permeability, indicated by the occurrence of springs in the contact between the carbonate layer and the overlaying micaceous sandstone layer, and was discarded when calculating the aquifer recharge area.

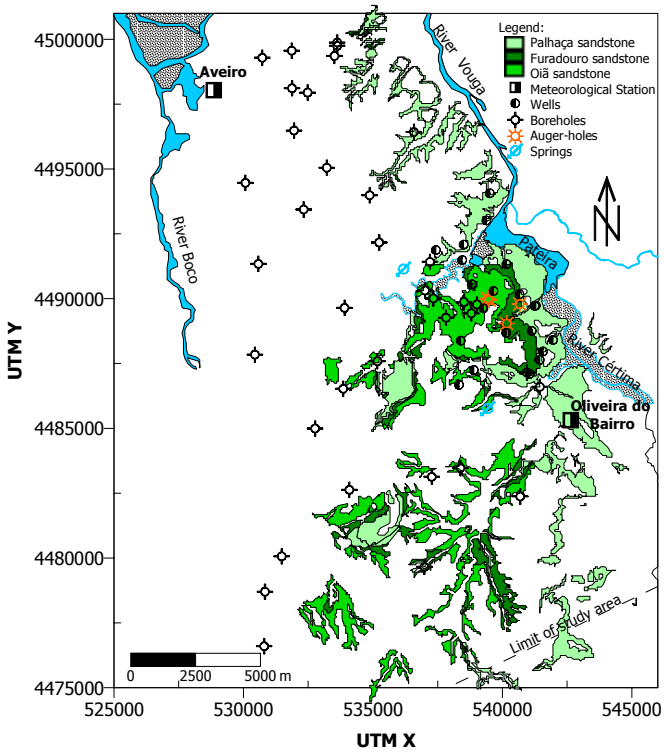

Fig. 4.1 Map of the aquifer recharge area indicating the aquifer outcrop area in green and showing the location of the boreholes, wells, springs and auger-holes used in the different recharge estimation studies presented in this Chapter 4.

4.2 Climate

The study area has a warm humid climate with wet and dry seasons determined in great part by its proximity to the Atlantic Ocean. This Atlantic influence protects this area from the dry and cold winds coming from the Spanish Meseta in winter, and from the hot continental air currents during summer, allowing mild temperatures all over the year (Fig. 4.2).

The mean annual temperature for the last 20 years is 15.5 ºC, ranging from 10.2 ºC in the coldest months of December and January to 20.3 ºC in July and August, usually the hottest

months. The daily average number of hours of sun is six, reaching eight hours per day with sun in June/ July and going down to just four hours with sun in December.

The average annual relative humidity levels are round 76% with little oscillations throughout the year. These high values reflect the cumulative effects of the permanent evaporation from the 'Ria de Aveiro' lagoon as well as the humidity carried in from the sea by the warm westerly winds, which are influenced by the Gulf Stream. Prevailing winds in the area are from the north and northwest all the year round, despite in autumn and winter when the winds might blow often from the south and southeast. The windiest months are usually April and May with average wind velocities of 12 km h^{-1}.

Surface runoff for the Aveiro region is estimated to range from 200 mm a^{-1} in the western part of the study area, closer to the coast, to 300 mm a^{-1} in the eastern part where there is the outcrop area (DGA, 2001).

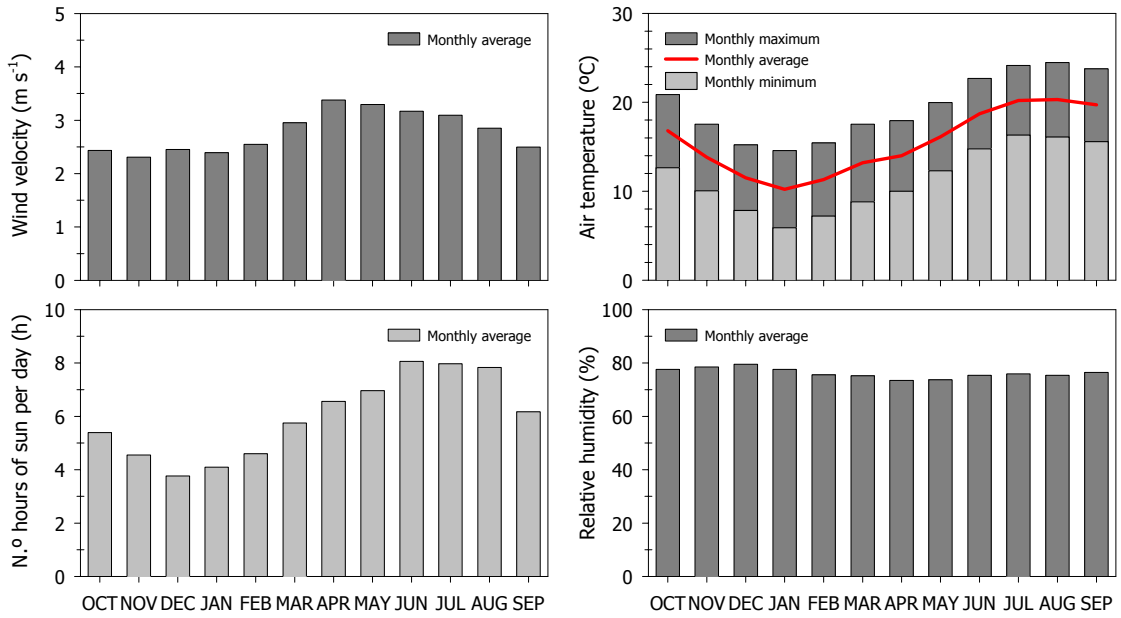

Fig. 4.2 Monthly averaged values for wind velocity, air temperature, number of hours of sun per day and relative humidity in the study region. Values were recorded at the Aveiro National Weather Service station over a period of 20 years (1981-2001).

4.2.1 **Rainfall**

Rainfall data for this study was recorded at three monitoring sites from the Precipitation National Monitoring Network and located at varying distances from the coastline. The northernmost site is located in Albergaria-a-Velha (ALB), in the northeast limit of the study area. The two other sites are located in the University of Aveiro Campus (AVR) in Aveiro city and in Oliveira do Bairro (OBR),

in the southeast part of the study area, neighbouring the aquifer recharge area. All the three sites had long-term rainfall data series and a summary of rainfall statistics for the area has been included in Table 4.1.

Table 4.1. Rainfall statistics of the Aveiro, Oliveira do Bairro and Albergaria-a-Velha stations located at different distances from the coastline.

	Aveiro	Albergaria-a-Velha	Oliveira do Bairro
Latitude	40º38'12" N	40º41'59" N	40º31'15" N
Longitude	8º39'29" W	8º28'51" W	8º29'50" W
Altitude (m.a.s.l.)	3	131	60
Distance to the coastline (km)	8.0	22.0	24.5
Monitoring period	1981-2001	1932-2001	1932-2001
Annual average rainfall (mm)	903	1301	1076
Maximum annual rainfall (mm)	1645	2599	1877
Minimum annual rainfall (mm)	528	585	536

The location of the three sites within a distance of approximately 20 km apart from each other is close enough to allow for a characterization of the areal distribution of precipitation in the study area. The precipitation isohyets were calculated from the mean annual precipitation values for the region and plotted in Fig. 4.3.

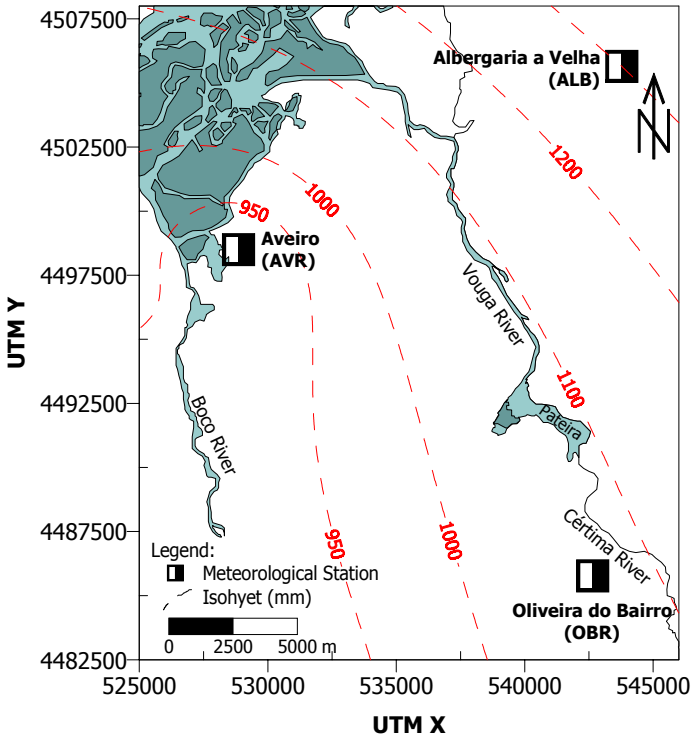

Fig. 4.3 Location of the 3 rainfall monitoring sites referred in text and precipitation isohyets for the studied area.

The areal distribution of rainfall is not uniform within the study area, decreasing significantly from the east towards the coast. The northeast part of the study area is the wettest, while in Aveiro rains almost thirty percent less than in Albergaria-a-Velha. This is also well documented in the summary of rainfall statistics.

Rainfall data series have been plotted on annual and monthly basis in Fig. 4.4. Mean annual rainfall varies between 900 and 1300 mm a^{-1} of which 80% corresponds to the period comprised between October and April. This is indicative of a pronounced seasonality of the rainfall distribution along the year, with December and January being usually the wettest months with monthly average rainfalls over 150 mm and, July and August the driest months with just occasional showers. Besides, annual averages show that rainfall along the past years has not been regularly distributed and series of wet years alternate with dry years.

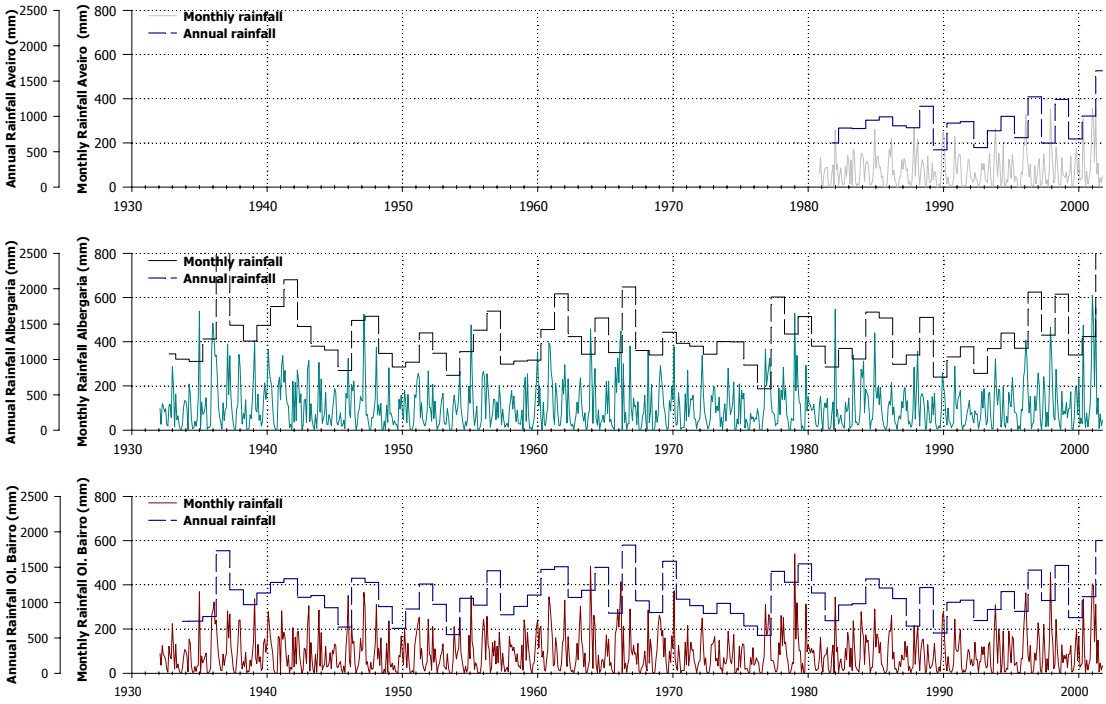

Fig. 4.4 Temporal rainfall distribution at the three monitoring sites referred in the text.

4.2.2 **Rainwater chemistry**

Groundwater recharge and hydrogeological studies require not just the monitoring of rainfall quantity and areal distribution but also the long-term measurement of the chemical composition of precipitation. Rainwater composition when merged with geochemical data in groundwater may be used for tracing infiltrating water in recharge and groundwater studies, to estimate groundwater ages or to help to reconstruct the Late Pleistocene and Holocene climates.

There are a few IAEA stations in the continental Portugal but up to now, long term systematic observation of both chemical and isotopic composition of precipitation in Portugal have been quite limited (*e.g.* Lima, 2000) and none in the Lower Vouga basin. And before this study, there was no data available to establish the recent input or temporal variability of isotopes, or even, chloride in the rainfall of the study region.

For this purpose, rainwater chemistry was monitored monthly from on-site rainfall collected in bulk samplers at the three monitoring sites (AVR, ALB and OBR), over a period of 5 years from 1997-2001. All the sites stay within a distance of less than 25 km from the coastline so it is expected that like in other coastal regions, the contribution of seasalt aerosols dominate the chemical signature of the rain.

Totalisers, large containers with a funnel area of 1000 cm^2 and a capacity of storing 32 L, were used to collect the rainwater on a monthly basis for major ion (Cl, SO_4^{2-}, Br^-, NO_3-N, Na^+, K^+, Ca^{2+}, Mg^{2+}, Si^{4+}, pH), stable isotope ($\delta^{18}O$, δ^2H) and tritium (^3H) analysis. NH_4^+ was not analysed. Evaporation was minimised by filling the container with a thin layer of high-purity vaseline.

Evolution of major ions, pH and silica content in rainfall with time and rainfall quantity for the 3 sites is shown in Fig. 4.5 to Fig. 4.7. The composite rainfall samples collected on a monthly basis correspond to a monthly series of rainfall events. The mean (volume weighted) chemical composition ($\overline{\delta_c}$) was calculated using the following Equation [4.1]:

$$\overline{\delta_c} = \left(\frac{\sum_{i=1}^{n} P_i \, \delta_i}{\sum_{i=1}^{n} P_i} \right) \qquad [4.1]$$

where δ_i is the concentration of the chemical element in the rainwater sample during the *i* th event; P_i the precipitation amount during the *i* th event; and, *n* the number of events in a year.

The values obtained for average concentrations of major ions in the region and some characteristic chemical molar ratios used to compare rainfall compositions with that of sea salt have been summarised in Table 4.2.

Table 4.2 Rainwater annual averaged rainwater composition at the three monitoring sites of the study area. Also shown some characteristic chemical molar ratios for the rainwater.

(all data in mg L^{-1})	Cl^-	SO_4^{2-}	NO_3^--N	Br^-	Na^+	K^+	Ca^{2+}	Mg^{2+}	Si^{4+}	pH
AVR	5.29	3.86	0.124	0.024	4.28	0.28	1.35	0.48	0.23	5.37
ALB	3.57	3.68	0.104	0.023	3.13	0.34	2.98	0.59	0.19	6.15
OBR	3.36	4.87	0.156	0.023	3.14	0.36	3.09	0.60	0.29	6.00

(molar ratios)	Na/Ca	K/Na	Mg/Na	Mg/Ca	K/Mg	Na/Cl	Mg/Cl	Si/Na	Br/Cl
SEAWATER	**44.65**	**0.02**	**0.12**	**5.43**	**0.18**	**0.85**	**0.10**	**0.0002**	**0.0016**
AVR	5.54	0.04	0.11	0.59	0.36	1.25	0.13	0.04	0.0020
ALB	1.83	0.06	0.18	0.33	0.37	1.35	0.24	0.05	0.0029
OBR	1.78	0.07	0.18	0.32	0.37	1.44	0.26	0.08	0.0030

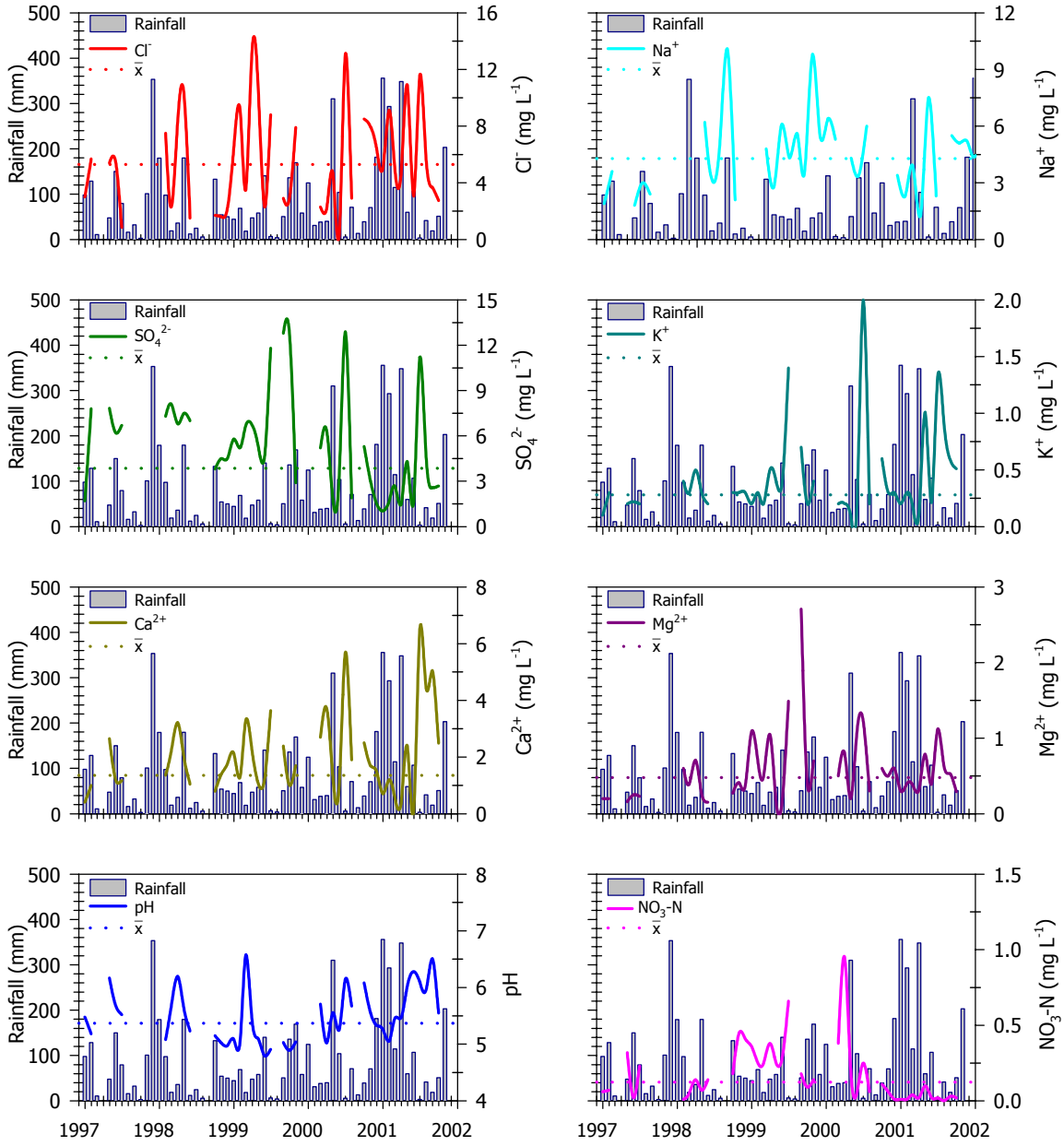

Fig. 4.5 Evolution of major ions, pH and silica content in rain with time and rainfall quantity for the Aveiro precipitation monitoring site ($\bar{x}$ is the weighted mean composition for local precipitation).

The results obtained show that rainfall in the studied region is a slightly acid solution, with a solute content that demonstrates the marine aerosol influence as well as the result of the dissolution of atmospheric gases and solid particles (aerosols). Mean pH values lower than about 5.4 like the ones for Aveiro probably result from reactions of the acid gases, and coincide with the lowest calcium concentrations (< 1.5 mg L^{-1}). Occasionally, rainwater in Aveiro reaches important levels of acidity (pH<5.0), comparable to pH values of acid rain observed in the NE USA and NW Europe (Leeuwen *et al.*, 1996). However, these sporadic very low pH values could not be related to a particular time of the year or to particularly high rainfall events. Rainfall acidity in Europe comes

in most cases from burning fossil fuels that produce sulphur dioxide (SO_2), which dissolves into the water to form sulphuric acid, and various oxides of nitrogen (mainly NO_2 and NO_3, altogether called NO_x).

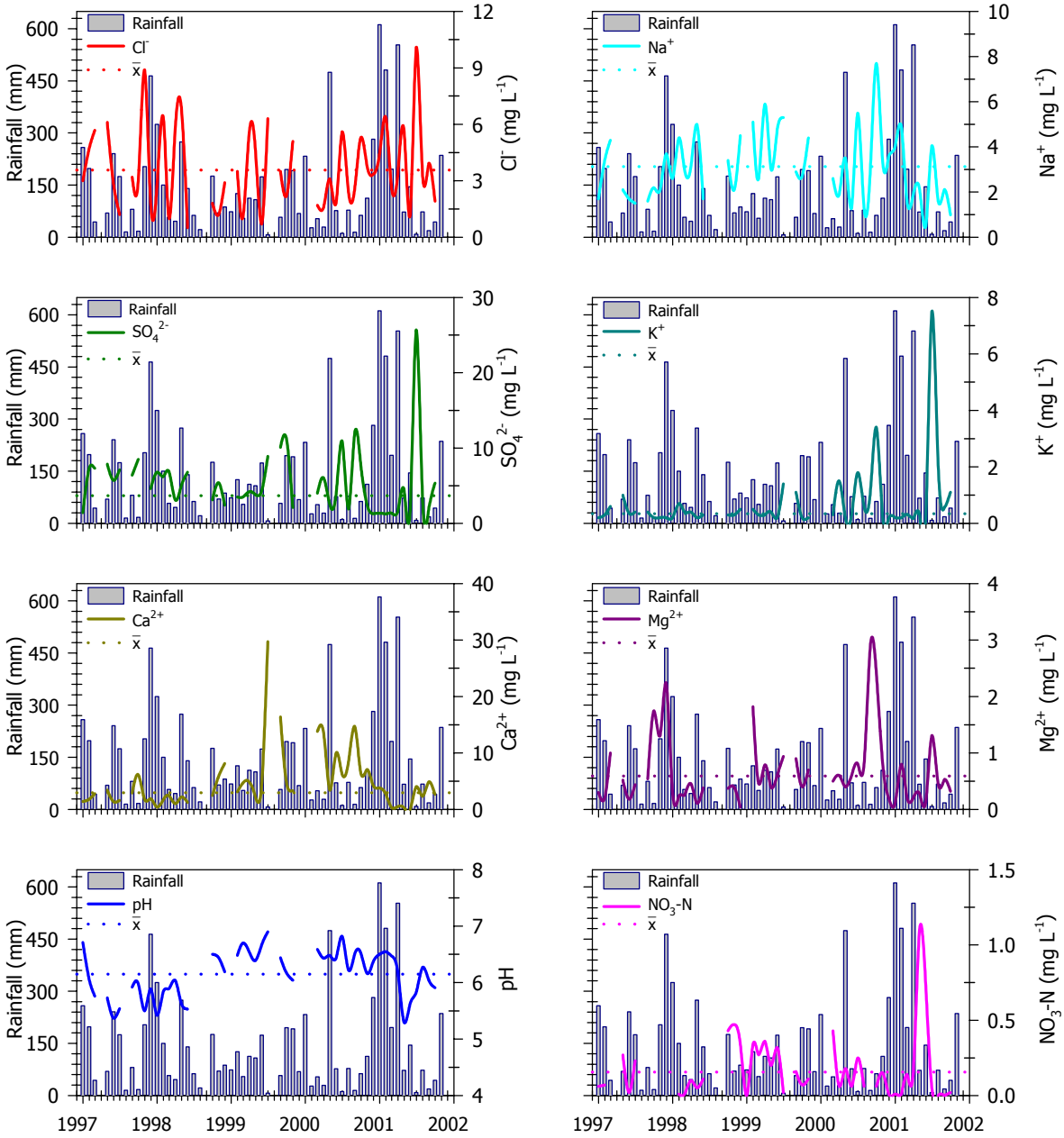

Fig. 4.6 Evolution of major ions, pH and silica content in rain with time and rainfall quantity for the Albergaria-a-Velha precipitation monitoring site ($\bar{x}$ is the weighted mean composition for local precipitation).

Although the pH values determined in the rainwater of the sites located in Oliveira do Bairro and Albergaria-a- Velha are slightly acidic (pH of 6.00 and 6.15, respectively), they are above the reference pH of 5.65 at 15ºC in natural precipitation (Charlson & Rodhe, 1982). Calcium

ion, which shows high values in the rainwater samples of these two sites, must be acting as a neutralizer contributing for an increase in the observed pH values.

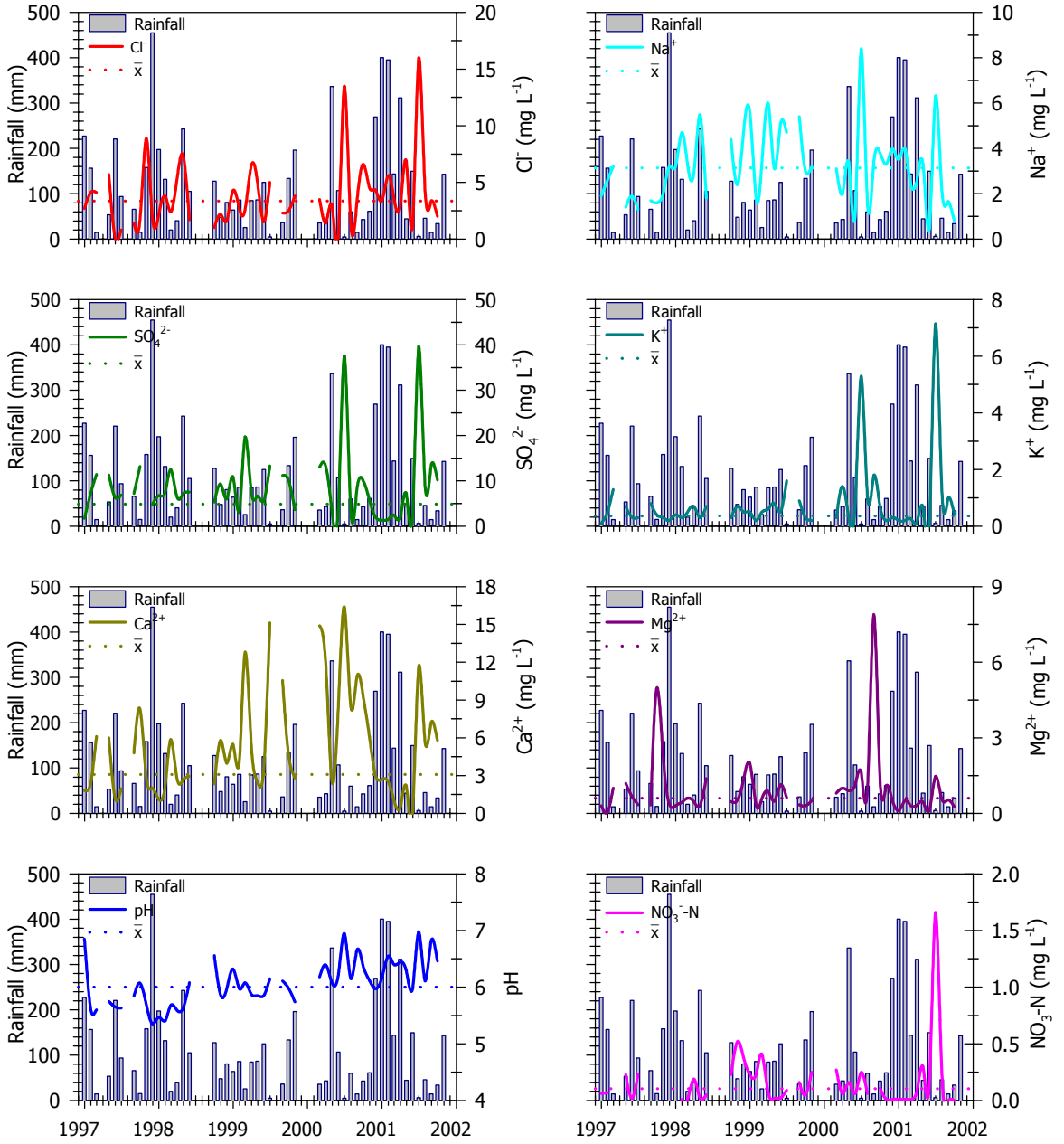

Fig. 4.7 Evolution of major ions, pH and silica content in rain with time and rainfall quantity for the Oliveira do Bairro precipitation monitoring site ($\bar{x}$ is the weighted mean composition for local precipitation).

A seasonal trend can be observed in local precipitation. The highest concentrations of ions in local rain are usually obtained during the summer months, when the rainfall occurs as brief showers. Months with long-term rainfall have lower concentrations of ions and lower pH values

because the release of alkaline elements (*e.g.* from soil dust) into the atmosphere is reduced and the air is cleaner.

The concentration of ions in local rainfall follows a general pattern $Cl^- > SO_4^{2-} > Na^+ > Ca^{2+} > Mg^{2+} > K^+ > NO_3$-N. Sodium and chloride are the dominant ions in Aveiro where the rain is basically a Na-Cl solution. These two ions are closely correlated in coastal regions due to their common origin in seasalt aerosols. In the other two sites further 20 km inland, sodium becomes less abundant, calcium doubles its concentration becoming almost as abundant as sodium and chloride contents decrease approximately 35%. This decrease of Cl inland is usually interpreted as rapid deposition of sea salt in precipitation near the coast (Berner & Berner, 1996).

Following these variations, rainfall composition changes from Na-Cl near the coast to Na-Ca-SO_4 type in the interior, showing that the influence of marine aerosol on local rainfall composition decreases significantly in a short distance from the coast. Rainfall samples from the Oliveira do Bairro site show an increase in sulphate exceeding the chloride concentrations and reflecting, probably, an anthropogenic contribution related to industrial activities. In coastal areas like Aveiro, sulphate is the second most abundant anion and probably mostly derived from seasalt.

The average nitrate concentrations are low and vary between a minimum value of 0.10 mg L^{-1} of NO_3-N and a maximum of 0.16. The highest nitrate amounts were observed in months with less than 100-150 mm of rain, which is consistent with the fact that the rainfall in very wet months contain less near-surface particulate material (Edmunds *et al.*, 2002).

The determined Br/Cl ratios at the Aveiro site are close to marine aerosol composition, while for the other two sites located in agricultural and forest areas further away from the sea this ratio increases relatively to seawater reflecting probably the addition from the biomass during burning and forest fires.

Several other molar ratios were calculated to confirm the main factors influencing rainfall chemistry. Molar ratios relative to chloride (Na/Cl, Mg/Cl), to sodium (K/Na, Mg/Na, Si/Na) or to magnesium (K/Mg) are significantly higher than the marine ratio, and the ratio is also higher for the sites further away from the coast. This shows that soil dust may be contributing inland for the increase in species usually mainly derived from marine aerosols. On the other hand, molar ratios relative to calcium (Na/Ca, Mg/Ca) are smaller than that in seawater decreasing from coast to the inland stations, due to the expected enrichment inland of terrestrial dominated species (Ca^{2+}, K^+).

In coastal areas like the Lower Vouga region, known seawater ratios may be used to estimate the contribution of sea-salt ions to precipitation, assuming no fractionation on aerosol formation from seawater. The depletion or addition of ions in rainwater is reflected by a change in the concentration ratio with respect to seawater and is best illustrated by a fractionation factor relative to a reference species (Berner & Berner, 1996; Appelo and Postma, 1996).

Sodium and chloride have been frequently used as the reference species for the sea salt component assuming that all Cl^- or Na^+ in rainwater are derived from seawater. However, it is known that both species can have also an anthropogenic source. In heavily polluted industrial areas, chloride can be derived from HCl and other pollutive gases in atmosphere, while soil dust can significantly contribute for increasing sodium amount in rainfall.

For the present study chloride was the reference species selected for calculating the fractionation factor relative to sea salt. Sodium was discarded because the data showed some enrichment relative to sea salt ratio, which indicated an additional source of sodium. The calculated fractionation factors relative to Cl^- (F_{Cl}) have been summarised in Table 4.3. Data for seawater composition was based on a compilation by Goldberg *et al.* (1971).

Table 4.3. Fractionation factors for rainwater relative to Cl^- (F_{Cl}) at the 3 sites.

		Na^+	K^+	Mg^{2+}	Ca^{2+}	Cl^-	SO_4^{2-}	NO_3-N	Br^-
	AVR	1.5	2.6	1.3	11.8	1.00	5.1	3.0E+03	1.3
F_{Cl}	**OBR**	1.7	5.3	2.5	42.6	1.00	10.2	3.9E+03	1.9
	ALB	1.6	4.6	2.3	38.7	1.00	7.2	5.5E+03	1.9

In all the three sites the major ions show more or less a significant enrichment with respect to chloride, with increasing fractionation degrees for sites further away from the coast. This denotes that sea salt is only one source of solutes in precipitation, and rainwater composition may differ to varying extents from the ratios in seawater. All the sites in this case show the contribution of terrestrial and anthropogenic inputs besides the known contribution of seawater. The rainfall of the sites inland show higher fractionation factors than the coastal rainfall in Aveiro.

Sodium and bromide average fractionation factors are less than 2 indicating that is primarily derived from seawater, while magnesium and potassium show average fractionation factors of 3 and 5, respectively. Calcium is the element that has the highest fractionation degree, ranging from 15 to 50 times relatively to chloride in seawater, which accounts certainly for the presence of a terrestrial source. Sulphate ion is enriched when compared to seawater ratio, associated probably with soil dust and anthropogenic contribution (industrial and traffic air pollution, fossil fuel burning).

The actual percentage of seawater contribution to final rainwater chemistry was determined for the three sites based again on the concentration of ion chloride. The results summarised in Table 4.4 show that seawater contribution varies according to the ion species but does not exceed in most cases 10%. Even, magnesium, a species considered in a first approach as primarily derived from marine aerosols has a sea salt contribution of just 10%. Just chloride

(assumed 100% sea salt contribution) and sodium (calculated 85% sea salt contribution) are essentially primarily derived from marine aerosols.

Table 4.4. Seawater and additional sources contribution for the rainwater composition in the Aveiro region (units are μmol L^{-1} with exception of seawater composition that is expressed mmol L^{-1}).

Major ions	Seawater composition	AVEIRO			OLIVEIRA DO BAIRRO			ALBERGARIA-A-VELHA		
		Rainfall composition	Seawater contribution	Other source contribution	Rainfall composition	Seawater contribution	Other source contribution	Rainfall composition	Seawater contribution	Other source contribution
Na^+	**456.8**	186.1	158.6	27.5	136.8	116.5	20.2	136.0	115.9	20.1
K^+	**10.0**	7.1	0.1	7.0	9.3	0.2	9.1	8.7	0.2	8.5
Ca^{2+}	**10.2**	33.6	0.6	33.0	77.0	1.5	75.5	74.5	1.4	73.0
Mg^{2+}	**55.5**	19.9	2.1	17.9	24.8	2.6	22.3	24.5	2.5	21.9
Si^{4+}	**0.1**	8.2	0.00	8.2	10.3	0.00	10.3	6.8	0.00	6.8
Cl^-	**536.0**	149.3	149.3	0.0	94.8	94.8	0.0	100.8	100.8	0.0
SO_4^{2-}	**28.1**	40.2	2.1	38.1	50.7	2.7	48.0	38.3	2.0	36.3
Br^-	**0.8**	0.3	0.0005	0.3	0.3	0.0004	0.3	0.3	0.0005	0.3
NO_3^--N	**0.01**	8.9	0.0002	8.9	7.4	0.0001	7.4	11.2	0.0002	11.2

4.2.3 **Rainwater isotopic composition**

Rainwater monthly isotopic composition ($\delta^{18}O$, δ^2H and ^3H) has been also monitored in the 3 monitoring sites of Aveiro, Albergaria-a-Velha and Oliveira do Bairro during the last 5 years (1997-2001).

The isotope analyses were carried out by the Instituto Tecnológico e Nuclear (Lisbon) in the course of a joint research project funded by the Portuguese Ministry of Science & Technology (Praxis-2-2.1-CTA-321-94). The determinations were carried out by mass spectrometry following the methods developed by Friedman (1953) for δ^2H and Epstein & Mayeda (1953) for $\delta^{18}O$. Analytical errors are ±0.1 ‰ for ^{18}O, ±1 ‰ for ^2H. Tritium was measured using a liquid scintillation counter (LSC) following the method suggested by the Hydrology Laboratory of the International Atomic Energy Agency (IAEA, 1976) and carrying an average precision of ±1.02 TU. Standard δ (delta) notation for the stable isotopes is used (Gonfiantini, 1978). Values of $\delta^{18}O$ and δ^2H are expressed in the conventional per mil (‰) notation and reported relative to the Vienna Standard Mean Ocean Water (VSMOW) standard according to Equation [4.2]:

$$\delta_{sample} = \frac{(R_{sample} - R_{std})}{R_{std}} x1000 \qquad [4.2]$$

where R_{sample} is the ratio of $^{18}O/^{16}O$ (or $^2H/^1H$) and R_{std} is the ratio of $^{18}O/^{16}O$ (or $^2H/^1H$) in the international standard.

A graph showing the variation in the rainfall isotopic composition at the three sites for the period comprised between 1997-2001 is represented in Fig. 4.8. Deuterium excess, *d*, was calculated as $d=\delta^2H-8\,\delta^{18}O$ as defined by Dansgaard (1964).

The weighted mean values were calculated for each site using the Equation [4.3], and the results obtained are summarised in Table 4.5.

$$\overline{\delta_w} = \left(\frac{\sum_{i=1}^{n} P_i\,\delta_i}{\sum_{i=1}^{n} P_i} \right) \qquad [4.3]$$

where δ_i is $\delta^{18}O$ or δ^2H (‰) or ^3H activity of the precipitation sample during the *i* th event; P_i is precipitation amount during the *i* th event; and, *n* is the number of events in a year.

Table 4.5. Results for the rainwater isotopic composition ($\delta^{18}O$, δ^2H, ^3H and d-excess) monitored at the 3 sites for the period comprised between 1997-01.

		Number of Samples	Range Min	Range Max	Weighted Mean	Arithmetic Mean	Standard Deviation
AVR	$\delta^{18}O$ (‰)	51	-7.95	-0.48	-4.10	-3.80	1.45
	δ^2H (‰)	51	-54.90	-2.10	-23.73	-21.88	10.38
	d-excess (‰)	51	-3.72	13.00	9.08	8.53	3.18
	^3H (TU)	47	0.50±1.00	6.00±1.40	2.88±1.01	2.93±0.96	1.50
ALB	$\delta^{18}O$ (‰)	51	-7.36	-1.01	-4.20	-3.88	1.43
	δ^2H (‰)	51	-46.20	-0.17	-23.83	-21.53	10.95
	d-excess (‰)	51	3.38	13.20	9.74	9.51	2.35
	^3H (TU)	47	1.00±1.00	8.60±1.50	3.40±0.98	3.83±0.94	1.70
OBR	$\delta^{18}O$ (‰)	51	-6.70	-1.12	-4.32	-3.83	1.48
	δ^2H (‰)	51	-44.30	-2.80	-25.60	-21.97	10.80
	d-excess (‰)	51	3.62	13.66	8.93	8.70	2.59
	^3H (TU)	47	0.30±1.00	8.27±0.81	3.39±0.98	3.77±0.93	1.74

The isotopic composition of precipitation at the three sites varied over a wide range during the analysed period (1997-2001). Values for the stable isotopes $\delta^{18}O$ and δ^2H ranged from –8.0 to –1.0‰ and from –55.0 to -1.0‰, respectively, and deuterium-excess varied from –4 to 14‰ (Table 4.5). However, the weighted mean values are consistent with those interpolated from IAEA monthly precipitation maps for oxygen-18, deuterium and d-excess in Europe (Fig. 4.9).

The isotopic compositions also compare well with data from other IAEA stations in Portugal. The annual weighted mean values for $\delta^{18}O$ and δ^2H in Faro, located on the south coast of Portugal (37º01'N, 7º96'W) is –4.74 and –26.38, respectively, while, in Porto (41º08'N, 8º36'W), located at 60 km further north than Aveiro, the weighted mean values are -4.76 for $\delta^{18}O$ and -27.47 for δ^2H (IAEA/WMO, 2001).

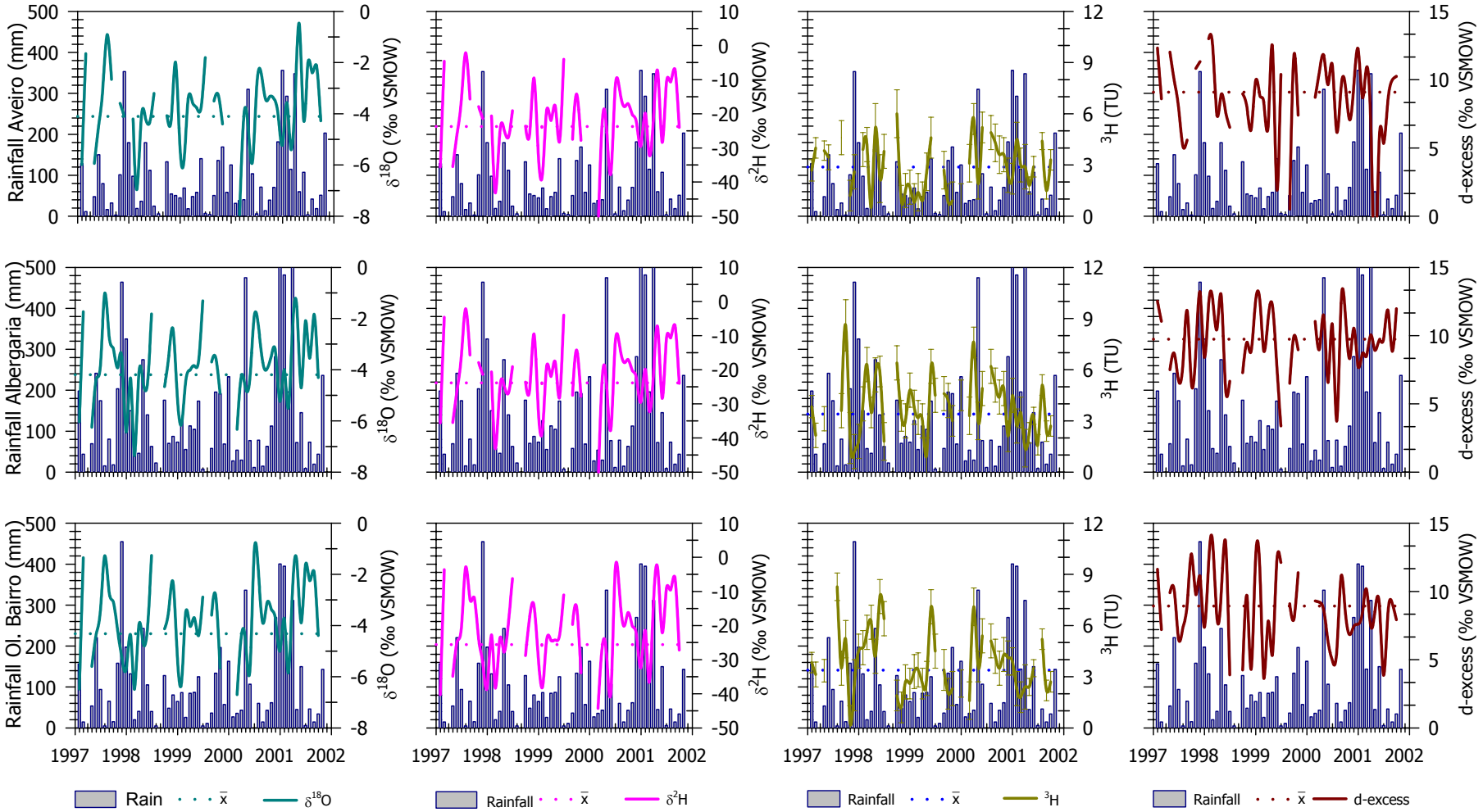

Fig. 4.8 Evolution of stable isotope, tritium activity and d-excess in rainfall during the monitoring period, from January 1997 to September 2001. ($\bar{x}$ is the weighted average annual values for $\delta^{18}O$, $\delta^{2}H$, ^{3}H and d-excess in precipitation monitored at the 3 monitoring stations.

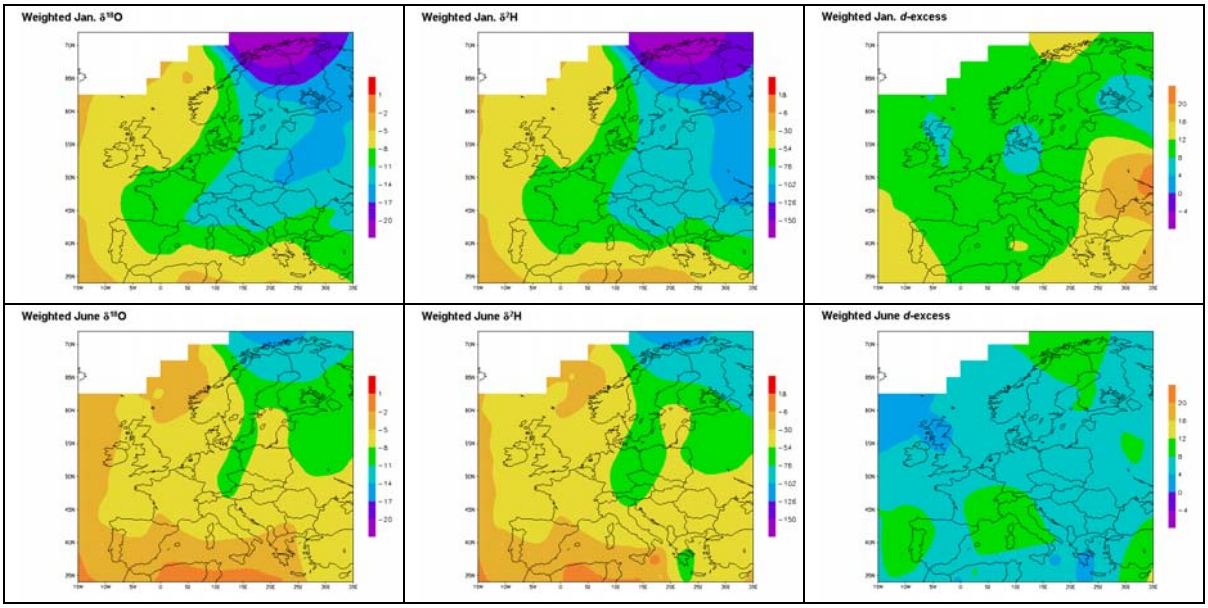

Fig. 4.9 Amount-weighted monthly precipitation maps for oxygen-18, deuterium, d-excess in Europe. Data from GNIP, the IAEA/WMO Global Network for Isotopes in Precipitation managed by the Isotope Hydrology Section of IAEA (IAEA/WMO, 2001).

Tritium activity ranged from 1-9 TU and the weighted mean activity for the last 5 years was around 3.20 TU, but some uncertainty should be attached to this value because of the varying magnitude of the analytical precision. To estimate how representative the 3.20 TU value was for the region, a comparison was made with Porto (4.28 TU) and Faro (5.67 TU).

Both the stable isotopes and the radioisotope show a strong seasonal effect typical of these mid-latitude climates (Fig. 4.10). During the summer months when the temperatures are higher and the average rainfall is often less than 20 mm per month, the stable isotope content in rainfall presents a clear enrichment. This effect has also been observed in other sites worldwide and Rozanski *et al.* (1993) presented seasonal correlations between T and $\delta^{18}O$ for several stations in both hemispheres.

Monthly ^{3}H activities also show a maximum peak during summer. This seasonal trend observed in the radioisotope data is the result of the so-called 'spring leak and could be related to the fact that the greatest transfer of tritium from the stratosphere to the underlying troposphere occurs during the spring, producing higher ^{3}H activities in late-spring and summer precipitation (Gat, 1980; Rozanski *et al.*, 1991; Simpkins, 1995; Clark & Fritz, 1997).

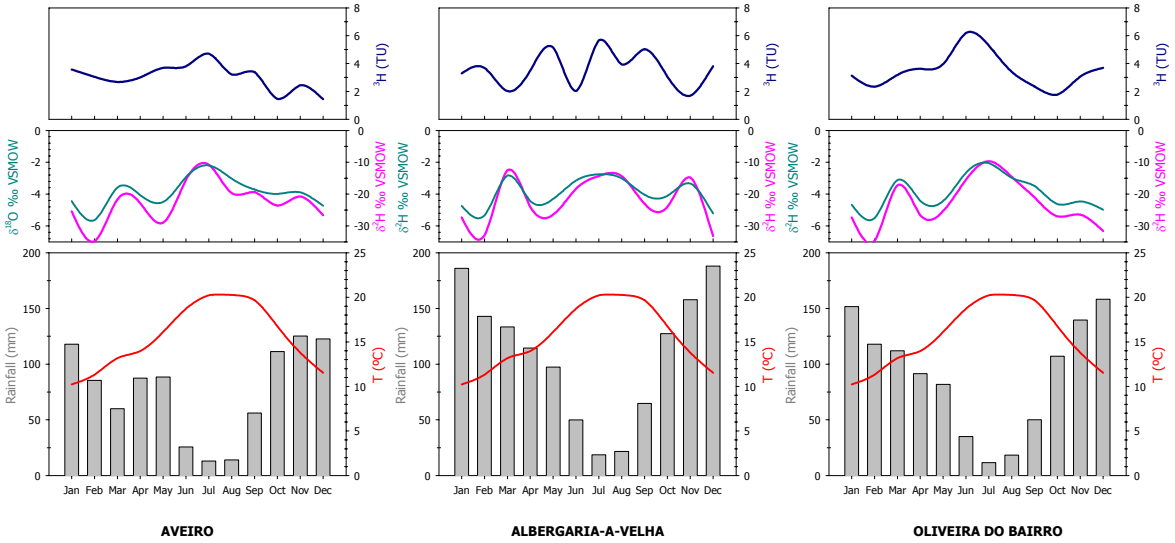

Fig. 4.10 Seasonal variations in $\delta^{18}O$, $\delta^{2}H$, ^{3}H, temperature and amount of rainfall for the 3 monitoring stations (Aveiro, Albergaria-a-Velha and Oliveira do Bairro). Values are monthly averaged and the air temperatures considered are for the Aveiro station as there are no air temperature data for the other two stations.

For hydrological studies it is very useful to determine the local linear correlation between $\delta^{2}H$ and $\delta^{18}O$ for comparison with groundwater stable isotope composition as it is assumed that local meteoric water line provides a baseline for groundwaters. The relationship between these two stable isotopes in precipitation is mainly controlled by condensation and evaporation processes related to Rayleight distillation (Dansgaard, 1964; Gat & Gonfiantini, 1981). Global precipitation values of $\delta^{2}H$ and $\delta^{18}O$ generally plot on or near the Global Meteoric Water Line (GMWL) defined by Craig (1961) as:

$$\delta^{2}H = 8\,\delta^{18}O + 10 \qquad [4.4]$$

Local meteoric water lines (MWL) were constructed from the precipitation data for the 3 monitoring sites in the study area by using a linear regression based upon a least-squares approximation. The regression was significant at r^{2}=0.93 in Aveiro and r^{2}=0.96 in Oliveira do Bairro and Albergaria-a-Velha, and the departures from the line outside the 99% confidence interval were not significant. The calculated MWL were compared to the global meteoric water line (GMWL) in Fig. 4.11.

The local meteoric lines have lower slopes and deviate slightly from the global meteoric water line indicating that some isotopic fractionation has occurred during rainfall evaporation. The smaller deviations from the GMWL are indeed observed in those sites with the highest rainfall rates. Deviations of $\delta^{18}O$ and $\delta^{2}H$ data from the GMWL, particularly lower slope values, have been observed in the precipitation of other IAEA monitoring sites in Portugal (*e.g.* Porto:

$\delta^2H=6.77\delta^{18}O+3.86$; Faro: $\delta^2H=6.14\delta^{18}O+2.62$), and also worldwide (Rozanski *et al.*, 1983; Simpkins, 1995).

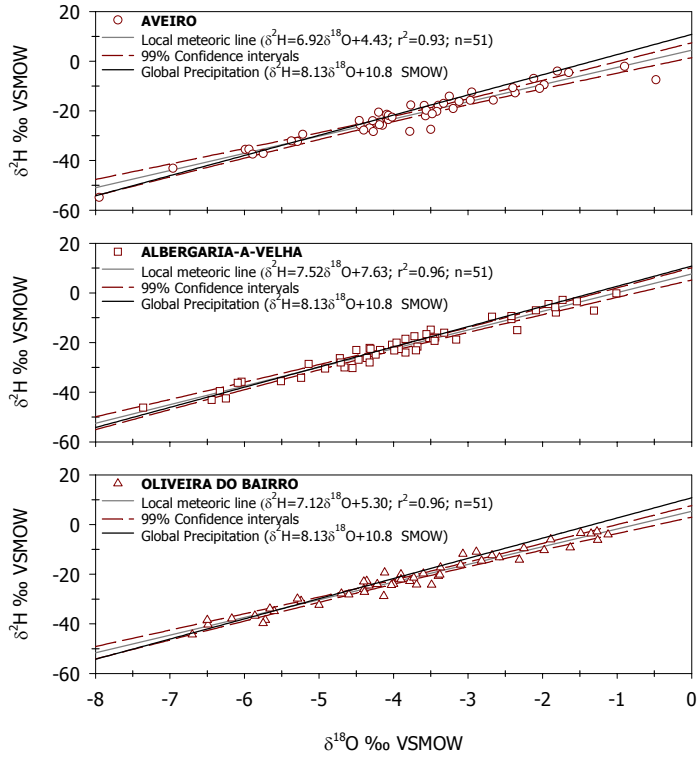

Fig. 4.11 Meteoric water relationship for $\delta^{18}O$ and δ^2H in precipitation monitored at the 3 monitoring stations.

4.3 Groundwater recharge estimation methods

Four different groundwater recharge estimation methods were used to approximate groundwater recharge in the Aveiro Cretaceous aquifer. Two are physical methods and the other two are geochemical methods applied both to the saturated and unsaturated zones. A brief summary of the methods used is presented in the following paragraphs.

4.3.1 **Penman-Grindley method**

The Penman-Grindley (Penman, 1950; Grindley, 1967) is the conventional and most widely used method of estimating recharge. The method was initially developed to calculate soil moisture deficit and actual evaporation, but allows recharge to be calculated as a function of effective rainfall. It conceptualises that water is held in store as soil moisture, which can be increased by rainfall and depleted by evapotranspiration. When the field capacity is attained, excess rainfall is routed to surficial runoff and to groundwater as recharge (Fig. 4.12).

In this method, the soil water balance equation is defined for a uniform zone and certain interval of time as follows:

$$P = E_A + R + \Delta S \qquad [4.5]$$

$$\Downarrow$$

$$\Delta S = P - E_A - R \qquad [4.6]$$

where P is rainfall [L], E_A is the actual evapotranspiration [L], R is the runoff [L L^{-2}] and ΔS is the change in soil water storage [L].

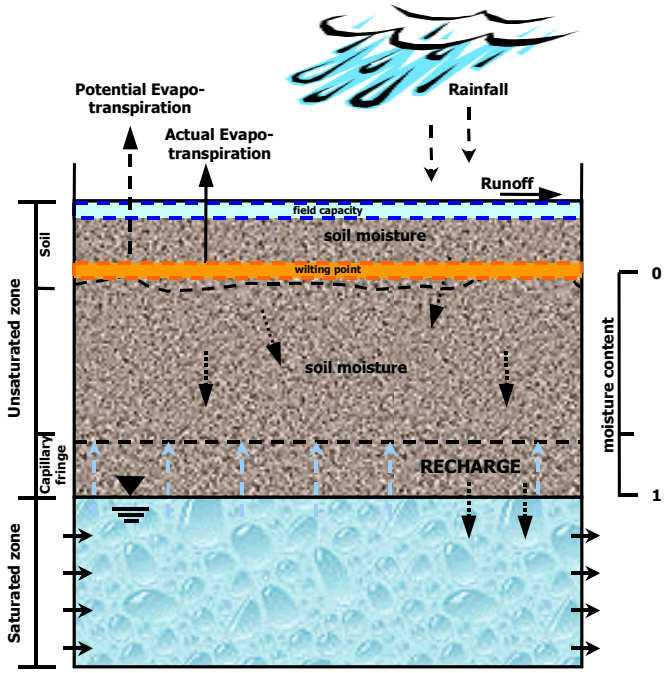

Fig. 4.12 Conceptualisation of the Penman-Grindley soil moisture budgeting model.

The accuracy of this method relies on the accuracy of the initial data. Actual evapotranspiration is one of the critical parameters. It can either be determined directly from open water evaporation pans or irrigated lysimeters, or calculated from meteorological data using for instance the Penman (1948) or the Thornthwaite (1948) formulae, just to mention two of the most used ones. Both methods give a potential rate of evaporation, and a budgeting procedure using soil moisture is used to convert potential to actual evapotranspiration. The essence of the model is actually considered to be the relation between potential (E_P) and actual evapotranspiration.

The method works best for humid climates with seasonal patterns of recharge, widespread and relatively uniform rainfall, in areas with well-developed soils that never dry completely (Lerner, 1997). And, it is unlikely to be successful in semi-arid areas because of the long periods of less

than potential evaporation, when errors in estimating the actual evapotranspiration are greatest, and the precipitation and the actual evapotranspiration are nearly equal (Allison, 1981).

4.3.1.1 **Application of the method**

The Penman-Grindley method was used to estimate the groundwater recharge of the Aveiro Cretaceous aquifer. Water balance calculations were based on rainfall data for the Oliveira do Bairro monitoring site, the closest to the recharge area. Meteorological data (temperature, wind velocity, insulation, humidity) used to calculate the potential evapotranspiration was from the University of Aveiro meteorological station as the Oliveira do Bairro station just provides daily rainfall data. Potential evapotranspiration was determined directly from open water evaporation pans and indirectly, using the Penman and Thornthwaite formulae.

Using data from the open water evaporation pan an average value of 939 mm a^{-1} for the annual potential evapotranspiration was calculated. The calculation with the Penman and Thornthwaite formulae gives average values of 740 and 876 mm a^{-1}, respectively. These values do not exceed the average rainfall inland, but do exceed the average rainfall on the coastal areas.

A comparison of the mean monthly values for potential evapotranspiration calculated using these three different methods is shown in Fig. 4.13, and indicate the lowest values from December to February (E_P~0.7 mm d^{-1}) and the highest in June and July (E_P~3.8 mm d^{-1}). From October to April the rainfall exceeds the potential evapotranspiration but during the summer and autumn months (May-October) rainfall is just 1/3 of the potential evapotranspiration.

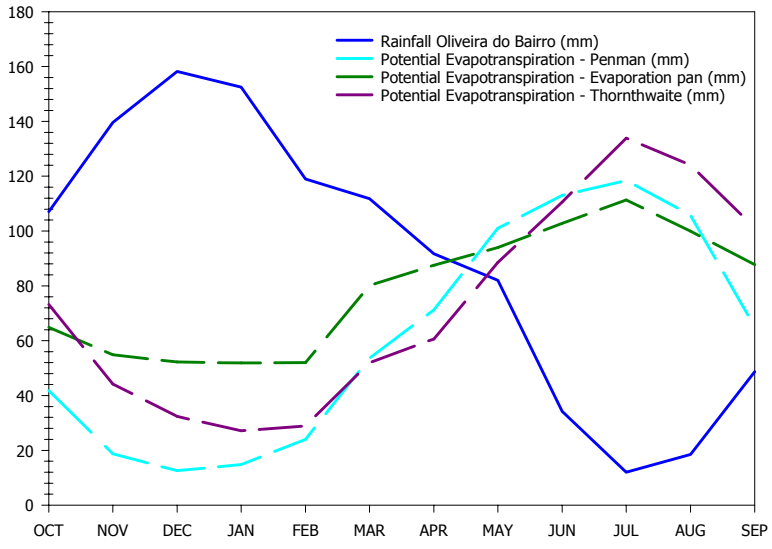

Fig. 4.13 Comparison of the potential evapotranspiration values obtained using data from open water evaporation pans and the Penman and Thornthwaite formulae.

Comparing the three methods, the evaporation pan gives the highest potential evapotranspiration estimates for the winter period and the lowest for the summer period, while the Penman formula gives the lowest estimates in winter and the Thornthwaite gives the highest estimates in summer. The values determined in the evaporation pan seem to be extreme values for the study area and might be affected by other meteorological variables such as wind and rainfall.

Assuming that the maximum volume of stored water for plants use is equal to 100 mm and that the volume of water stored at the beginning of the calculation period in October is null, a sequential water budget was carried out for the three values for potential evapotranspiration. The results obtained are summarised in Table 4.6 and plotted in Fig. 4.14.

Table 4.6. Sequential water budget for the Aveiro region using the evaporation pan, Penman and Thornthwaite estimates for potential evapotranspiration.

	OCT	NOV	DEC	JAN	FEB	MAR	APR	MAY	JUN	JUL	AUG	SEP	TOTAL
P	107.1	139.6	158.2	152.5	119.0	111.8	91.7	82.0	34.2	12.0	18.5	48.7	1075.5
(using Evaporation pan values for potential evapotranspiration)													
E_P	64.9	54.8	52.2	51.8	52.0	80.1	87.5	94.0	102.8	111.3	99.9	87.7	939.1
P- E_P	42.2	84.8	105.9	100.7	67.0	31.8	4.2	-12.1	-68.6	-99.3	-81.4	-39.0	136.4
ΔPl	42.2	100.0	100.0	100.0	100.0	100.0	100.0	87.9	19.3	0.0	0.0	0.0	749.4
E_A	64.9	54.8	52.2	51.8	52.0	80.1	87.5	94.0	102.8	31.3	18.5	48.7	738.7
EXC	0.0	27.1	105.9	100.7	67.0	31.8	4.2	0.0	0.0	0.0	0.0	0.0	336.8
DEF	0.0	0.0	0.0	0.0	0.0	0.0	0.0	0.0	0.0	80.0	81.4	39.0	200.4
(using Penman values for potential evapotranspiration)													
E_P	41.8	18.7	12.5	14.8	24.0	53.6	71.2	101.0	113.0	118.4	105.8	65.1	739.9
P- E_P	65.3	120.9	145.6	137.7	95.0	58.2	20.6	-19.0	-78.8	-106.4	-87.3	-16.3	335.5
ΔPl	65.3	100.0	100.0	100.0	100.0	100.0	100.0	81.0	2.2	0.0	0.0	0.0	748.4
E_A	41.8	18.7	12.5	14.8	24.0	53.6	71.2	101.0	113.0	14.2	18.5	48.7	532.1
EXC	0.0	86.2	145.6	137.7	95.0	58.2	20.6	0.0	0.0	0.0	0.0	0.0	543.3
DEF	0.0	0.0	0.0	0.0	0.0	0.0	0.0	0.0	0.0	104.2	87.3	16.3	207.8
(using Thornthwaite values for potential evapotranspiration)													
E_P	73.2	44.2	32.3	27.1	28.9	51.9	60.6	88.5	110.6	133.9	124.0	101.1	876.4
P- E_P	33.9	95.4	125.9	125.5	90.1	59.9	31.1	-6.6	-76.4	-121.9	-105.5	-52.4	199.1
ΔPl	33.9	100.0	100.0	100.0	100.0	100.0	100.0	93.4	17.0	0.0	0.0	0.0	744.4
E_A	73.2	44.2	32.3	27.1	28.9	51.9	60.6	88.5	110.6	29.0	18.5	48.7	613.6
EXC	0.0	29.3	125.9	125.5	90.1	59.9	31.1	0.0	0.0	0.0	0.0	0.0	461.8
DEF	0.0	0.0	0.0	0.0	0.0	0.0	0.0	0.0	0.0	104.8	105.5	52.4	262.8

Legend: **P** – Rainfall; **E_P**– Potential evapotranspiration; **DEF** – Water deficit; **ΔPl** – Reserve of water for plants; **E_A** – Actual evapotranspiration; **EXC**– Runoff, R + Stored water, ΔS

The water balance shows that from the 1076 mm of rainfall, almost half of it 532 mm (or, 614 mm if we consider the Thornthwaite estimates, or even 739 mm if we consider the evaporation pan estimates) is lost through evapotranspiration, and the rest corresponds to the stored water plus runoff. The stored water in this water balance constitutes the natural recharge to the aquifer and using Equation [4.6] it can be calculated.

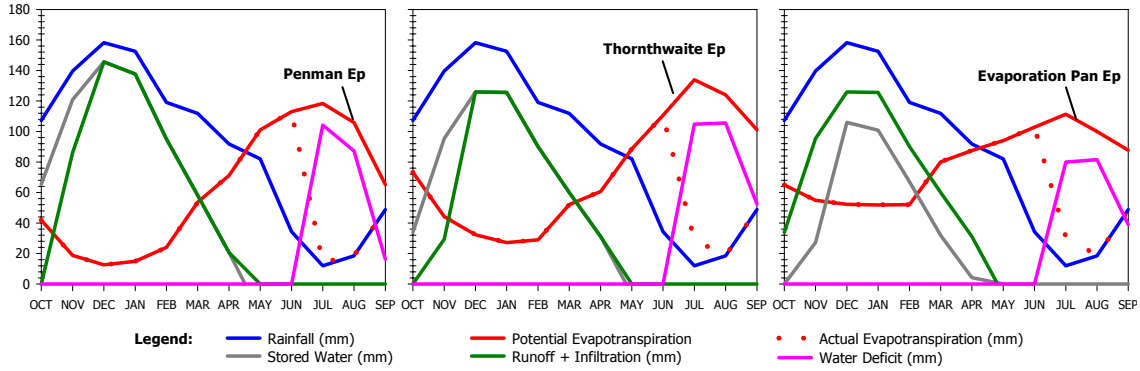

Fig. 4.14 Water budget for the Aveiro Cretaceous aquifer using the Penman-Grindley method and considering the different estimates for the potential evapotranspiration.

Assuming runoff to be equal to 300 mm a^{-1} in the aquifer recharge area, the volume of excess water that will make part of the deep infiltration will vary between 37, 162 and 243 mm a^{-1} (depending if we are using the evaporation pan values, or the Penman and Thornthwaite evapotranspiration estimates, respectively). These values correspond to about 3, 15 and 23 % of the annual rainfall. And while 15 % seems a reasonable estimate and approximately the average of the three values, the 3 and 23 % seem to be under and overestimated values for the region.

4.3.2 **Water table fluctuation method**

The water table fluctuation method for estimating groundwater recharge is based on the premise that rises in groundwater levels in unconfined aquifers are due to recharge water arriving at the water table and going immediately into storage (Healy & Cook, 2002). The recharge rate is calculated as follows:

$$q_w = Sy \frac{dh}{dt} = Sy \frac{\Delta h}{\Delta t} \qquad [4.7]$$

where *Sy* is the specific yield, *h* is the water table height and *t* is time.

This method is very easy to use and has been applied in numerous studies as early as the 1920s. However, the method is not able to account for steady rate of recharge (*e.g.* when rate of recharge is equal to rate of drainage) and works best in areas with shallow water tables that display sharp water level rises and falls. Another very important constraint is the difficulty and uncertainty on the determination of the specific yield, despite the fact that there are several laboratory, field or geophysical methods available to calculate it.

The analysis of the water table fluctuations provides spatially averaged recharge rates as long as the monitoring wells are located such that the water levels are representative of the

catchment as a whole. The time period represented by the recharge estimates will depend on the length of the hydrographic record.

4.3.2.1 **Application of the method**

From October 2000 to September 2001, groundwater table fluctuations were measured in 21 shallow wells within the Aveiro Cretaceous aquifer recharge area on a weekly basis, and thanks to the collaboration of two under-graduated students. Spring discharge was also monitored on a weekly basis in two springs (Bica and Seara). Precipitation was measured daily in the Oliveira do Bairro monitoring station (data from the DRAOT Centro).

Water table lies generally within a few meters from land surface and changes in the water level are assumed to be due to groundwater recharge. The highest water levels are observed in late winter and early spring after the rainy season, while the lowest water levels are usually measured in late summer. A depletion of spring Seara baseflow is also observed in late summer. Data for spring Bica had to be discarded because it was reconstructed during the study and the discharge changed for other reasons than groundwater recharge.

The calculation of the water level rise in each well was done according to Healy & Cook (2002). Δh was assumed to be equal to the difference between the peak of the rise and lowest point of the extrapolated antecedent recession curve at the time of the peak (Fig. 4.15). The observed water table and spring discharge fluctuations for the rest of the monitoring wells and springs have been plotted in Fig. 4.16 and Fig. 4.17.

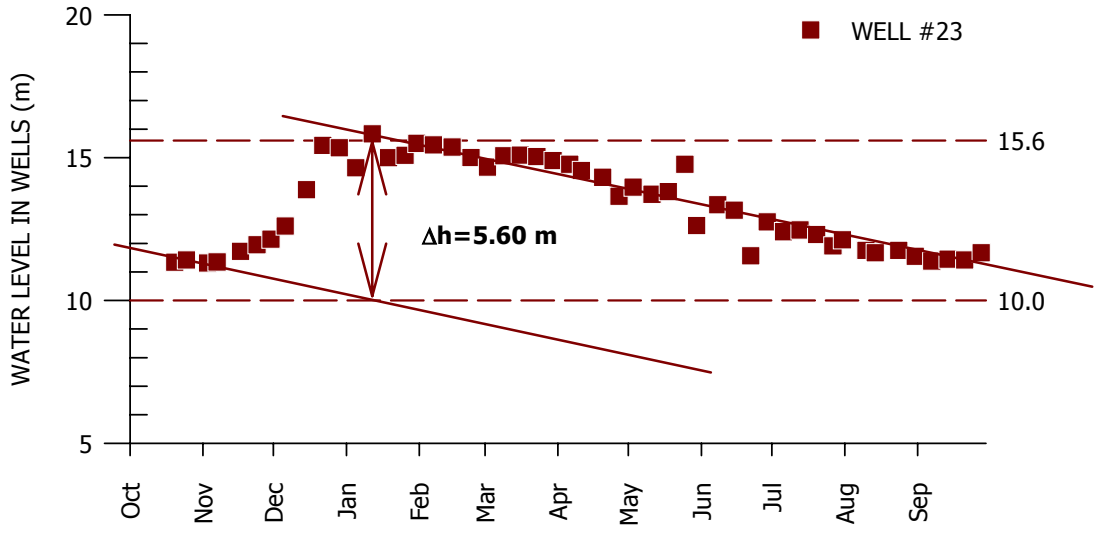

Fig. 4.15 Example of the method used to estimate the water table rise in wells in response to precipitation. Δh is equal to the difference between the peak of the rise late in winter and lowest point of the extrapolated antecedent recession curve at the time of the peak.

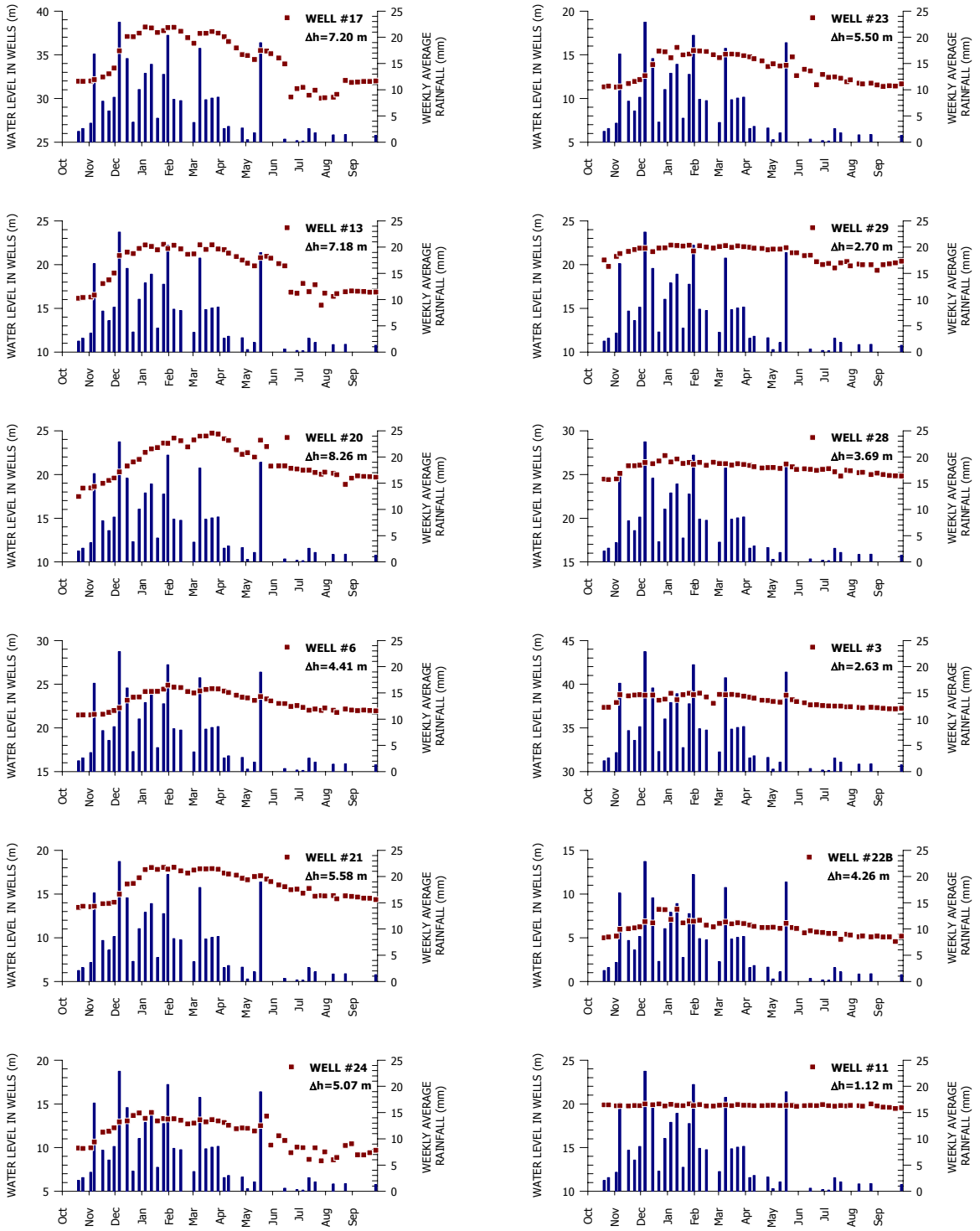

Fig. 4.16 Hydrographs of water levels in wells and bar graphs of weekly average precipitation.

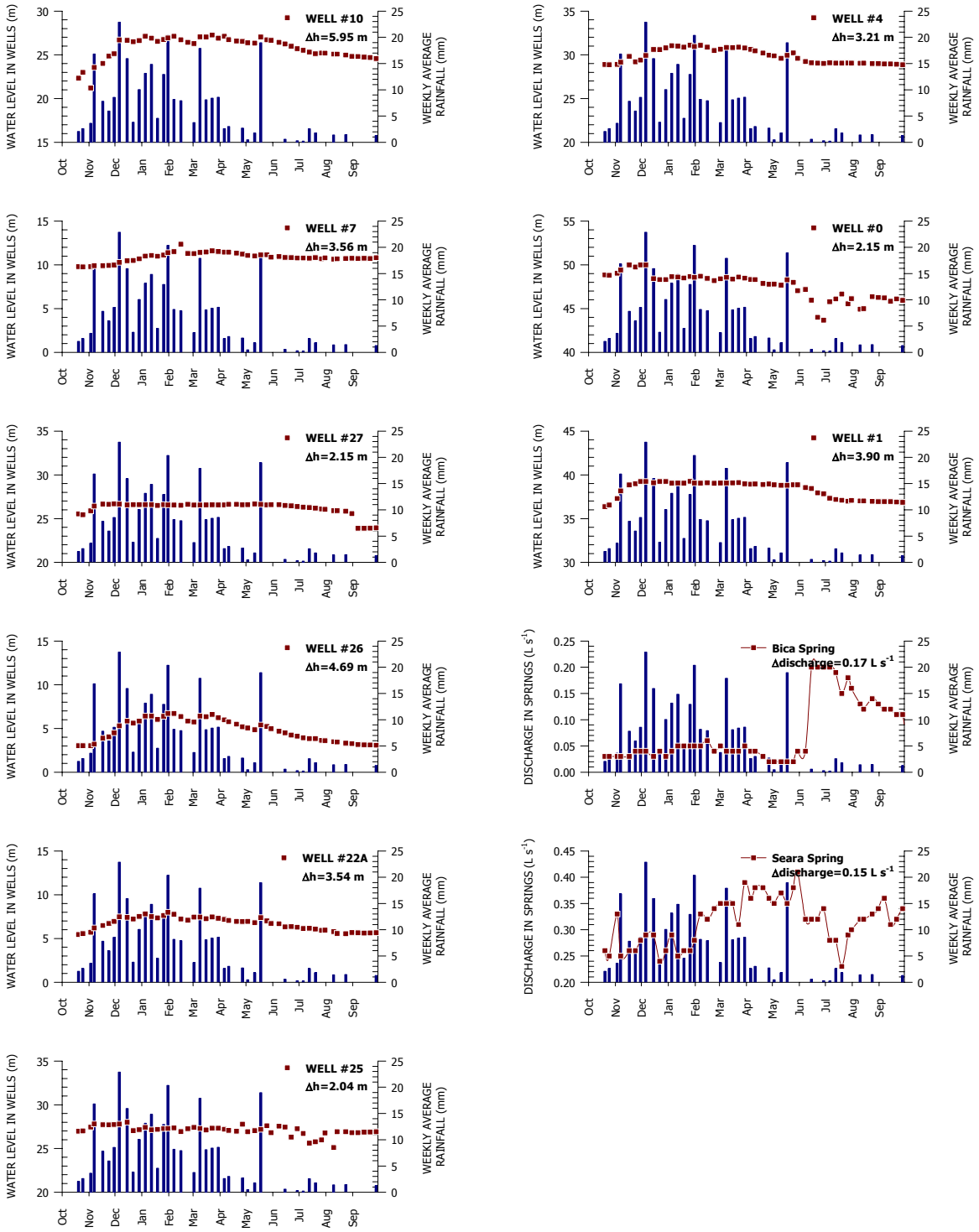

Fig. 4.17 Hydrographs of water levels in wells, spring discharge and bar graphs of weekly average precipitation.

As there was no laboratory or field data available, the specific yield for the study area was estimated to vary between 0.02 and 0.12 according to literature values compiled by Healey & Cook (2000). However, this range of values was validated calculating the specific yield that should correspond to the observed water level fluctuations in the monitoring wells if the net infiltration is 163 mm a^{-1} as calculated previously using the Penman-Grindley method. Using this last method specific yield values ranging between 0.02 and 0.14 are obtained for the region, with average and mean values of 0.05 and 0.04, respectively. These values are remarkably similar to the estimated ones using literature values and contribute to validate them.

The net recharge over the monitoring period was calculated applying Equation [4.7] and assuming *Sy* equal to the median value for the region (Sy=0.04). Recharge estimates varied significantly in space (higher values in the area closer to the 'Pateira de Fermentelos' lagoon) and a contour map for recharge values was plotted in Fig. 4.18 to describe the spatial variability. The median and average recharge value for the region using the water table fluctuation method is 156 and 169 mm a^{-1}, respectively.

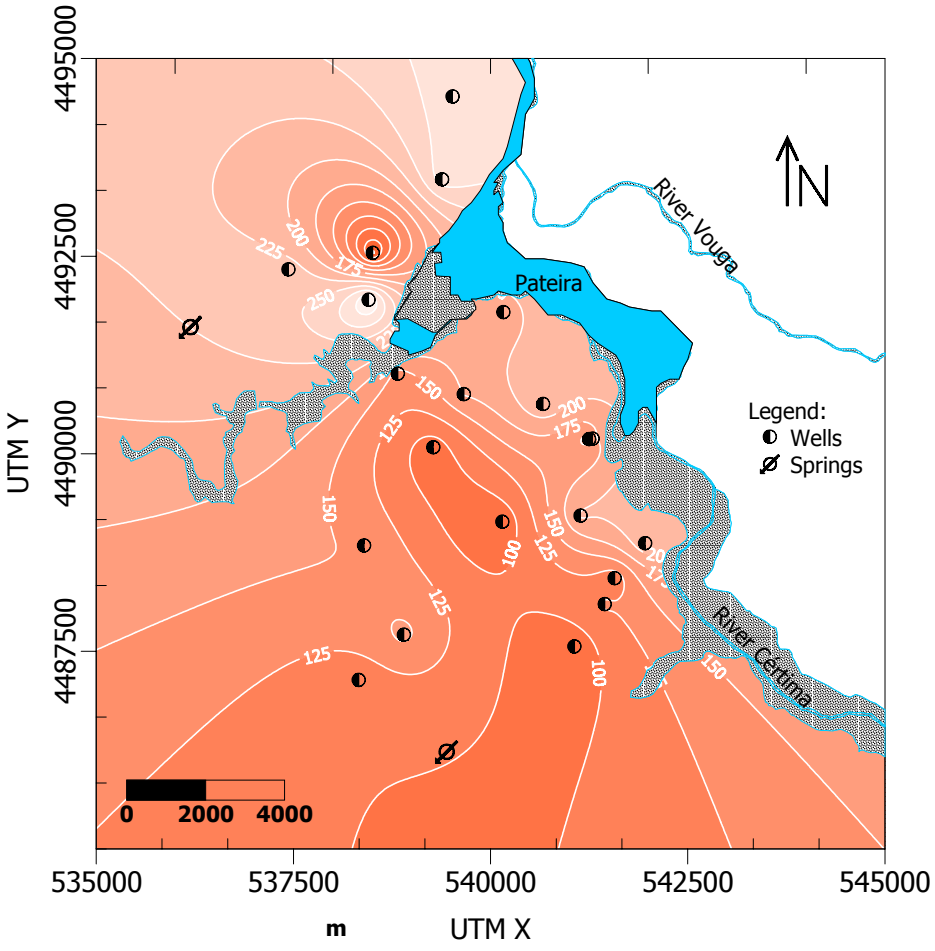

Fig. 4.18 Spatial distribution of recharge rates estimated using the water table fluctuation method (Median, $Y_{0.50}$= 156 mm a^{-1}; Mean, μ= 169 mm a^{-1}; Maximum, MAX= 330 mm a^{-1}; Minimum, MIN= 49 mm a^{-1}).

4.3.3 **Geochemical methods**

The geochemical methods applied use the chemical characteristics of rainfall and infiltrating water as tracers of groundwater recharge. Solute profiling techniques in the unsaturated zone as well as a solute mass balance approach in the saturated zone have been used for the determination of local recharge rates.

4.3.3.1 **Chloride mass balance in the unsaturated zone**

In the last 20 years there have been an increasing number of studies that use geochemical solute profiling techniques for the study of water movement along the unsaturated zone in order to assess groundwater recharge (Allison & Hughes, 1978; Sukhija and Reddy, 1988; Gee & Hillel, 1988; Gardner *et al.*, 1991; Cook *et al.*, 1992; Edmunds *et al.*, 1992; Edmunds and Gaye, 1994; Allison *et al.*, 1994; Gee *et al.*, 1994; Gaye and Edmunds, 1996; Bazuhair and Wood, 1996; Njitchoua *et al.*, 1997; Selaolo 1998; Edmunds & Tyler, 2002).

The recharge estimates based on unsaturated zone studies have been applied to a wide range of semi-arid and arid environments for reconstructing palaeoclimatic variations and recharge histories over time-scales of up to 50,000 years but never before in a humid temperate climate as the one of the Aveiro region. The best records are often obtained where the unsaturated zone is 10-30 m thick, and where sediments and flow are relatively homogeneous. In temperate zones, however, the time-scale range will be more limited as the vadose zone is less thick and the moisture fluxes are much higher, and the typical record may extend for 5-50 years.

The solute profiling methodology is based on the evidence that recharge water usually reaches the underlying groundwater body after moving downwards through the unsaturated zone. Along its pathway, recharge water reacts with vegetation, soil minerals, organic matter and fertilisers, leaving behind a signature in the soil interstitial solution. The study of this signature under favourable conditions and using natural tracers may contribute to assess the quantitative value of recharge and its variation in time. Some of the most widely used natural tracers are Cl, ^{36}Cl, ^{3}H, ^{14}C, ^{15}N, ^{18}O, ^{2}H and ^{13}C.

For the present research, recharge was calculated studying the chloride natural signature in sand-clay profiles through the vadose zone of the Aveiro Cretaceous aquifer recharge area. Chloride was selected as a tracer owing to its conservative (non-adsorbed) behaviour in most soils and groundwaters, that let it preserve the signature of recharging precipitation, providing the atmospheric inputs in the form of wet and dry deposition are known, and there are no geological or marine inputs. However, in some heavier textured soils anion exclusion may be a problem and chloride will appear to move more rapidly than the infiltrating water being traced.

The chloride mass balance techniques assume steady state conditions for the atmospheric input of chloride (wet and dry fallout) and conservation of mass between the atmospheric chloride input and the chloride flux in the subsurface. The method requires long-term monitoring of the wet and dry chloride deposition at the ground surface, and knowledge of the long-term annual averaged rainfall and chloride concentration in soil moisture and groundwater. Even though, long term rainfall studies in the eastern fringe of the Botswana Kalahari by Selaolo (1998) prove that chloride deposition may vary significantly in time and from site to site.

The principal constraints to the application of the chloride mass balance method are the uncertainty in establishing the base of the root zone and the zero flux plane (plane of zero hydraulic gradient in the soil), which separates upward (E_a) from downward (deep infiltration) water movement. Also limiting is the assumption of a piston flow regime ignoring constraints/ enhancement of downward moisture transport by lower permeability layers or by preferential flow zones, respectively. And, there are actually an increasing number of examples, which suggest that water movement in the unsaturated zone occurs along preferred pathways. A further limiting issue is created by the fact that these unsaturated zone techniques quantify potential groundwater recharge and generally apply to small spatial scales (local recharge) not being able to characterize the variation in rates of recharge over even short distances.

Most plant species do not take up significant quantities of chloride from soil water, thus chloride concentration in soil water increases through the root zone by evaporation. The expected evolution of the chloride depth profiles after the base of the root zone depends on the dominant process of water flow in the unsaturated zone and have been schematised in Fig. 4.19 according to Allison (1988).

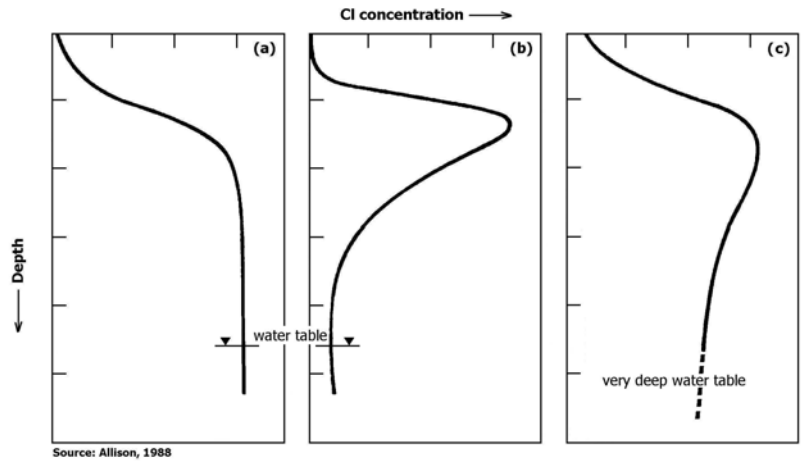

Fig. 4.19 Schematic depth profiles of the chloride concentration of soil water (Allison, 1988). (a) Piston flow with abstraction of soil moisture by roots; (b) Abstraction of soil moisture by roots with either preferred flow of water to beneath the root zone or diffusive loss of chloride to the water table; (c) A profile which may reflect different recharge rates and conditions for one site.

Assuming that water and solute (chloride ion) behave conservatively and that their downward movement is by piston flow below the surface mixing layer, the total chloride content C_{Tz} [M L^{-2}] down to a depth z can be calculated according to (*e.g.* Allison *et al.* 1985; Allison *et al.* 1992; Selaolo, 1998):

$$\overline{C_{Tz}} = 10\sum_{i=1}^{Z} h_i C_i \frac{\theta_G \rho_i}{\rho_w} = 10\sum_{i=1}^{Z} h_i C_i \theta_w \qquad [4.8]$$

where h_i is the depth interval [L]; C_i is the chloride content in soil moisture [M L^{-1}]; θ_G the gravimetric moisture content and is expressed as grams of moisture per 100 g of dry sediment and ρ_i the bulk density [M L^{-3}]. The term $\theta_G \rho_i / \rho_w = \theta_w$ where θ_w is the volumetric moisture content. ρ_w [M L^{-3}] is the water density and is considered ~1.

Similarly, the total moisture content θ_{Tz} [M L^{-2}] is given by:

$$\theta_{Tz} = 10\sum_{i=1}^{Z} h_i \frac{\theta_G \rho_i}{\rho_w} \qquad [4.9]$$

Furthermore, if the average annual total chloride fallout $C_{fallout}$ [M L^{-2} T^{-1}] at the surface is assumed to be constant over the long term, then the vertical soil moisture flux q_w [L T^{-1}] can be expressed as:

$$q_w = \frac{C_{fallout} \cdot \theta_{Tz}}{C_{Tz}} \qquad [4.10]$$

And the actual soil moisture velocity v_w is given by:

$$\upsilon_w = \frac{q_w}{\theta_w} \qquad [4.11]$$

To study changing environmental conditions with time, cumulative chloride content (C_T) is plotted against cumulative soil moisture content (θ_T), and the moisture flux q_w becomes:

$$q_w = C_{fallout} \cdot \left(\frac{\partial \theta_T}{\partial C_T} \right)_z \qquad [4.12]$$

If the total chloride deposition is assumed to be constant in time, the soil moisture age t_{w_z} [T] at the point of interest within a profile can be calculated as follows:

$$t_{w_z} = \frac{C_{Tz}}{C_{fallout}} \qquad [4.13]$$

4.3.3.1.1 **Application of the method**

The present investigation was located at four different sites situated all within the permeable outcrop area of the aquifer and shown already in Fig. 4.1. The three initial solute profiles were augered in Fermentelos (#HA1), Alto de Fermentelos (#HA2) and the last one, in Barreira de Perrães (#HA3) at the end of the hydrological year, in September 1997. The other two profiles were augered in Quintas and once again in Alto de Fermentelos at the end of winter season in February 2000. Site descriptions are summarised in the following Table 4.7.

Table 4.7. Site descriptions of the five solute profiles in the Aveiro Cretaceous aquifer recharge area.

Profile No.	Sampling date	Depth (m)	UTM Coordinates X	Y	Site location	Native vegetation	Geomorphological feature
#HA1	03/09/1997	6.0	540438	4490050	Fermentelos	Bare soil in the sampling area with pine trees within a distance of ±10 m.	Flat area
#HA2	05/09/1997	21.5	539500	4490400	Alto de Fermentelos		Top of a hill
#HA3	08/09/1997	4.5	540175	4489500	Barreira de Perrães		Flat area
#HA4	28/02/2000	7.5	539450	4490470	Alto de Fermentelos		Middle of a hill
#HA5	28/02/2000	5.5	540675	4490250	Quintas		Flat area

The continuous unsaturated zone profiles are mainly fine to medium sand with some intercalated thin clayey layers and were drilled at different depths by hand auguring. Samples were taken every 25 cm, bulked, homogenised and immediately sealed for taking to the laboratory for water content determination and chloride analysis.

Gravimetric water contents were determined by drying 100 mg of sample at 105°C for 24 h. Interstitial waters were extracted directly by centrifugation using an immiscible liquid ('Arklone' – CCl_3CF_3, not available since the Montreal Protocol on substances that deplete the ozone layer).

The moisture content in 90% of the samples was sufficiently high to extract enough water for the chemical analysis and provided the sample for chloride analysis. For each sampling interval, the interstitial water sample obtained was filtered through 0.45 μm membrane filters and analysed for Cl^- by automated colorimetry at the British Geological Survey laboratories (Wallingford, UK).

In any interpretation using unsaturated zone profiles it is important to be aware that the definition of the mixing zone for a profile is not always easy and that preferential flow is a common flow path. Although for the interpretation of the profiles and to simplify the system we are assuming steady state flow conditions and conservative behaviour for the unsaturated zone these conditions are not often prevalent. The shorter the profile is, the noisier will be the information given by the profile and the more difficult to interpret. However, to apply these methods to

temperate humid regions where the water levels are usually much less deep than in arid zones this is a reality we have to deal with.

Results obtained for gravimetric water contents and chloride concentrations of soil moisture are plotted for the five profiles in Fig. 4.20, showing variation with depth and from site to site. Most of the gravimetric water content profiles show some more or less significant variation in depth, with average values of less than 13% for all the profiles and just the samples closer to the water level have gravimetric water contents higher than 20%. Profile #HA2 augered at the Alto de Fermentelos site in 1997 presents anomalous high volumetric water contents (θ_V>50%) at the bottom because it reached at the depth of 20 m a saturated level of dark organic clay. For the other profiles, the minimum water content varies between 2 and 9%, while the maximum value ranges between 14 and 25%.

Most of the hand-augered profiles show an increase in chloride concentration in the top part due probably to evaporation. Cook *et al.* (1992) suggests that this top part of the profile forms a separate reservoir within a surface mixing layer. After this initial peak chloride contents decrease but still show variations along the profile that should reflect inputs of wet and dry years. However, and given that there are continuing solute inputs in rainfall and there has been minimal disturbance of vegetation, only selectively cut for lumber at the time of sampling at each site, it seems reasonable to consider that below the root zone the solute concentration profiles are close to steady state.

The maximum (MAX_{Cl}), minimum (MIN_{Cl}) and averaged ($\bar{x}_{Cl}$) values over the profiles depth interval are summarised in Table 4.8. Average chloride contents in soil moisture are significantly higher in the profiles augered in September 1997 at the end of the dry season ($\bar{x}_{Cl}$~25.3 mg L^{-1}) than in the ones augered in February 2000, at the end of the wet season ($\bar{x}_{Cl}$~7.4 mg L^{-1}). This is justified by a dilution effect by rainfall. The minimum and maximum values for chloride in soil moisture vary between 8.4 and 82.3 mg L^{-1}, respectively, in September 1997, and between 0.7 and 23.6 in February 2000. These lower values in the profiles of year 2000 will certainly imply much higher recharge rates.

Table 4.8. Maximum, minimum and averaged soil moisture chloride concentrations over the sampled depths.

Profile No.		Depth Interval (m)	$\bar{x}_{Cl}$ (mg L^{-1})	MIN_{Cl} (mg L^{-1})	MAX_{Cl} (mg L^{-1})
#HA1	1997	0.0 – 6.0	19.0	8.4	38.0
#HA2		0.0 – 21.5	32.9	10.0	82.3
#HA3		0.0 – 4.5	24.0	10.8	30.5
#HA4	2000	0.0 – 7.5	6.8	0.7	19.4
#HA5		0.0 – 5.5	7.9	2.4	23.6

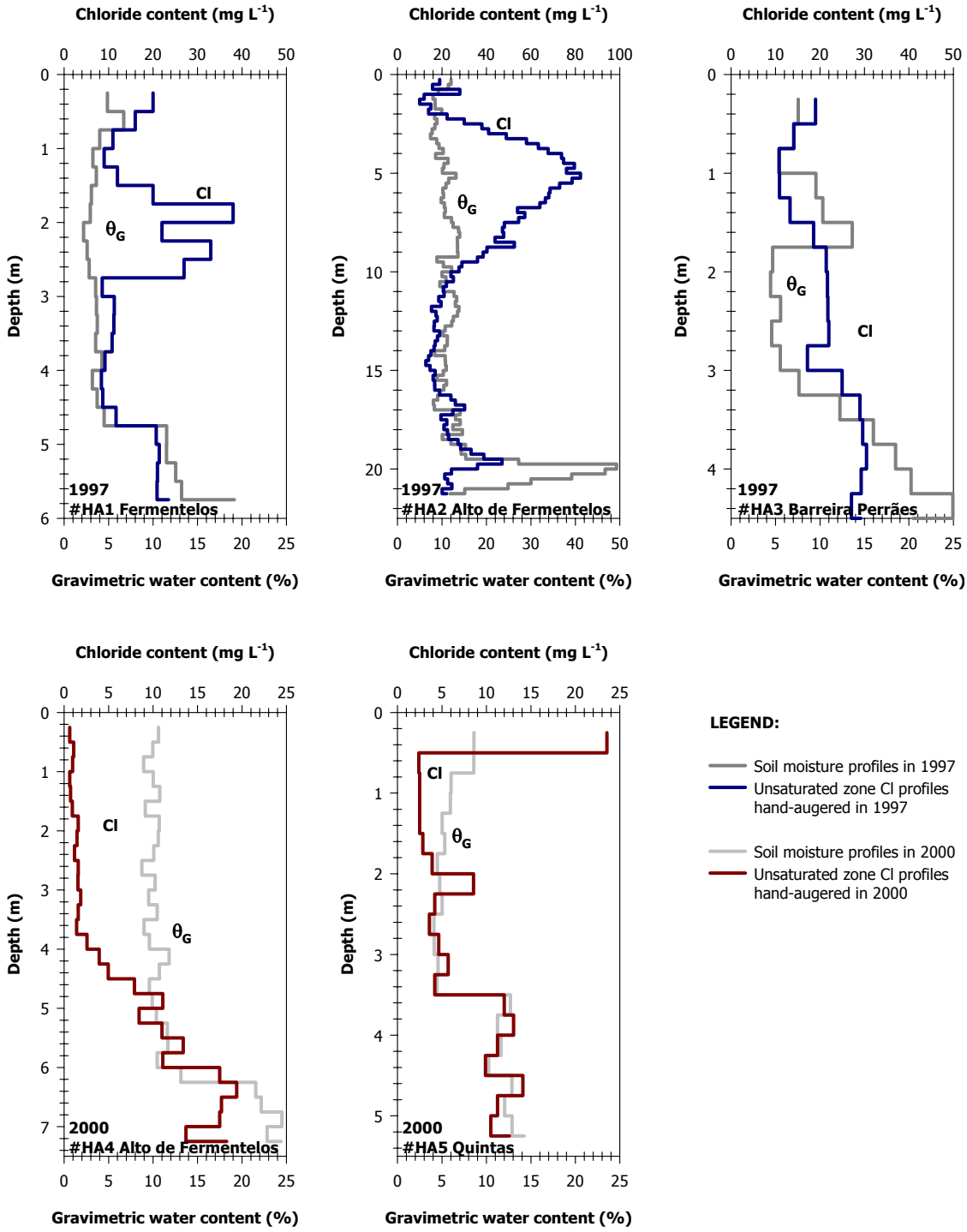

Fig. 4.20 Gravimetric water contents and chloride concentrations of soil moisture along the six hand-augered profiles and used in this chapter for recharge calculations.

Plots of inverse chloride contents, proportional to recharge, versus cumulative chloride contents, proportional to time, are shown for the four sites in Fig. 4.21 and Fig. 4.22. Time intervals recorded by each profile were calculated using Equation [4.13] and assuming an average

chloride deposition of 3.61 g m^{-2} a^{-1}. The corresponding dates were calculated considering the date the unsaturated zone profile was augered and the equivalent time interval for each depth interval.

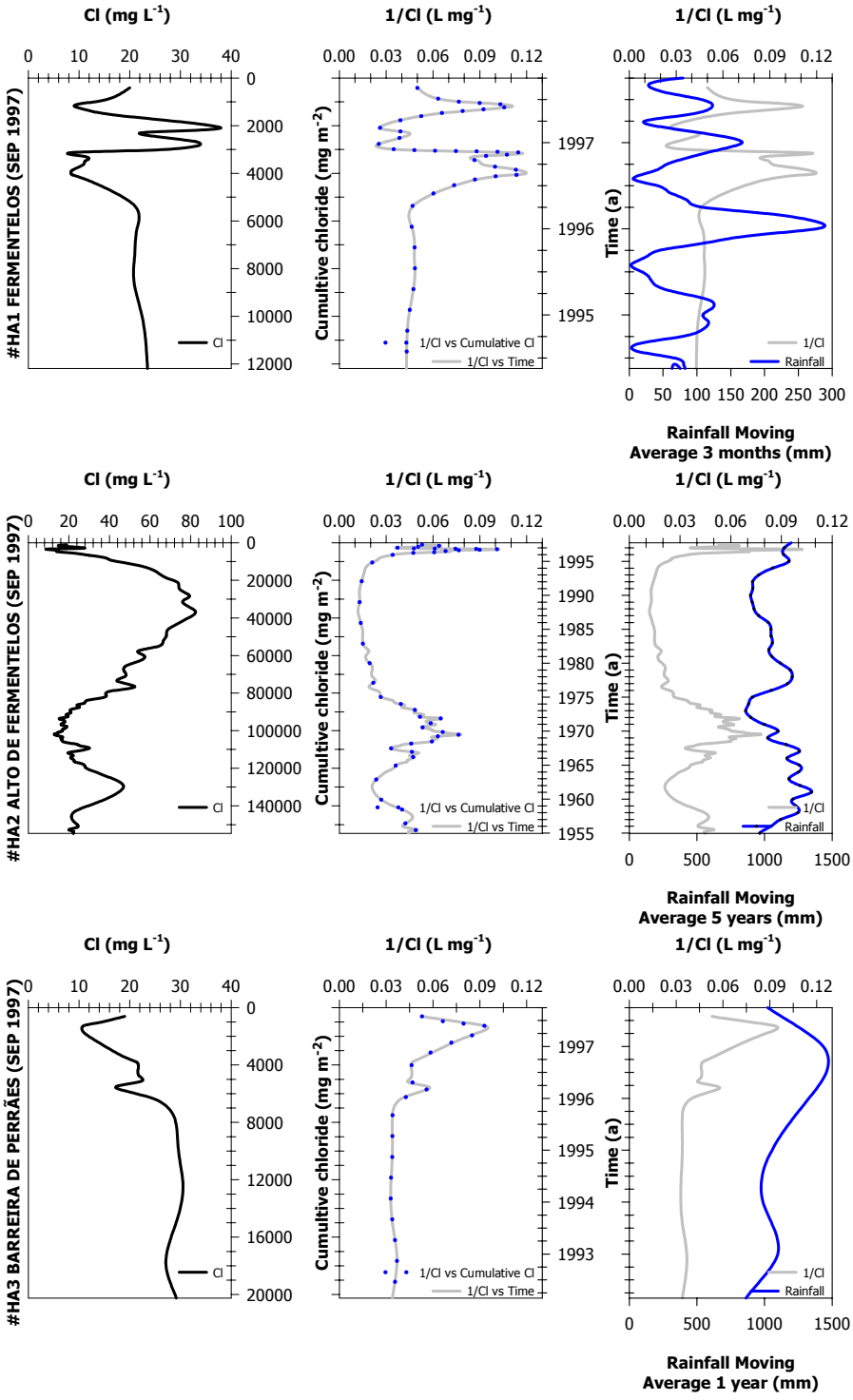

Fig. 4.21 Measured chloride profiles at bores #HA1, #HA2 & #HA3 compared with rainfall at Oliveira do Bairro. Plotting versus cumulative chloride rather than depth normalises the profile with respect to time. The profiles are scaled relative to the rainfall record assuming a chloride fallout of 3.61 g m^{-2} a^{-1}.

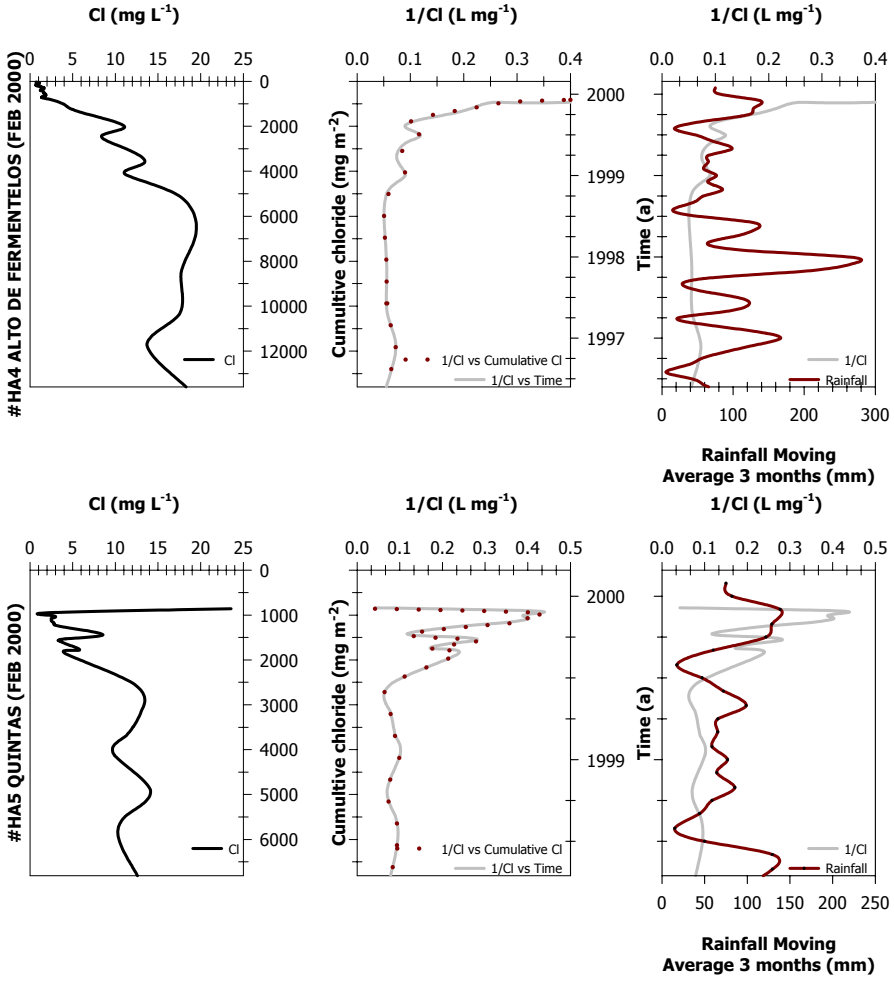

Fig. 4.22 Measured chloride profiles at bores #HA4 & #HA5 compared with rainfall at Oliveira do Bairro. Plotting versus cumulative chloride rather than depth normalises the profile with respect to time. The profiles are scaled relative to the rainfall record assuming a chloride fallout of 3.61 g m^{-2} a^{-1}.

Recharge estimates were obtained for the five profiles using Equation [4.12] and the results are summarised in the following Table 4.9. The estimates correspond in all cases to a series of several years or even decades depending on the depth of the profile. Calculated recharge fluxes were compared with rainfall values for the same period to verify if rainy periods were followed by periods of higher recharge rates. To make this comparison easier a rainfall moving average of 5 years was considered for the longest profile, while for the shorter profiles, because they correspond to shorter time intervals, a rainfall moving average of just 3 months and 1 year was considered. Thus, this proved to be an almost impossible mission for very short profiles.

The mean recharge rate since 1955 has been estimated to be 110 mm a^{-1}. However, estimated recharge values increase for shorter time intervals (shorter profiles), and in the case of profiles #HA2 and #HA3, the mean recharge rates have been estimated to be 151 mm a^{-1} (since 1992) and 191 mm a^{-1} (since 1994), respectively. The same calculations for profiles augered in

2000 give mean recharge rates that vary from a minimum value of 381 mm a^{-1} (since 1998) to a maximum of 411 mm a^{-1} (since 1996).

Table 4.9. Recharge estimates derived for all interstitial chloride profiles.

Site No	Interval, h_i (m)	Mean rainfall, P (mm)	Mean Cl in rainfall, C_P (mg L^{-1})	Mean Cl in profile, C_{Tz} (mg L^{-1})	Mean annual recharge, q_w (mm a^{-1})		Time interval of profile, t_{w_z} (a)	Rainfall in the time interval (mm)
September 1997:					q_w	v_w (m a^{-1})		
#HA1	0.0 – 6.0	1075.5	3.36	19.0	191	1.78	3.6	1201
#HA2	0.0 – 21.5	1075.5	3.36	32.9	110	0.50	42.8	1090
#HA3	0.0 – 4.5	1075.5	3.36	24.0	151	0.80	5.6	1122
February 2000:								
#HA4	0.0 – 7.5	1075.5	3.36	6.8	411	2.00	3.8	1215
#HA5	0.0 – 5.5	1075.5	3.36	7.9	381	2.92	1.9	1105

The high recharge values obtained for the profiles hand-augered in February 2000 are considered too high for the region. The profiles were hand-augered during the wet season in February 2000, when the rainfall is higher and the recharge is also higher. Over the depth interval augered (5-7 m) a record of just 2 to 4 years can be obtained. Infiltrating water moved during this period at 2 to 3 m a^{-1} which is at least two times faster than the velocities calculated for the profiles drilled in 1997 (0.5 to 2 m a^{-1}).

While profile #HA2 is an estimate covering 43 years, all the other profiles are estimates covering less that 6 years. Taking into account that these are point estimates with difficult spatial integration and that vegetation is similar for all the sites and cannot justify the differences observed, it is not advisable to use all the profiles to calculate an average recharge value for the region. Instead it was decided to accept the estimate that covers the longer period of time as the best value for potential recharge in the study region.

4.3.3.2 **Chloride mass balance in the saturated zone**

The groundwater chloride mass-balance method is frequently used for estimating groundwater recharge, specially related to the fact that it is a inexpensive method, does not require sophisticated instrumentation and is independent of whether recharge is focused or diffuse. The method yields recharge estimates that are integrated in the space and in time, and was originally applied in the late sixties to estimate recharge rates in the coastal plain of Israel (Eriksson & Khunakasem, 1969).

The use of the chloride mass balance approach in groundwater requires the knowledge of three environmental variables, which are: (1) the mean annual rainfall for the study region; (2) the

average annual total chloride fallout; and (3) the average groundwater chloride concentrations in the study area.

The method assumes that chloride ion behaves as a conservative, non-adsorbed environmental tracer under steady-state conditions, and the validity of its application is restricted by several assumptions:

- the only origin of groundwater chloride is either from rainfall or from dry deposition, and it doesn't occur any recycling of chloride within the aquifer;
- rainfall and atmospheric input of chloride (wet and dry fallout) is considered to be constant with time over long periods of time;
- rainfall is evaporated and/ or recharged to groundwater without any significant surface runoff;
- no groundwater evaporation occurs upgradient from the groundwater sampling points.

According to the chloride mass-balance method, the mean annual recharge flux (q_w) is calculated as stated by the basic equation (*e.g.* Allison & Hughes,1978):

$$\overline{q_R} = \frac{\overline{P}\left(\overline{C_p} + \overline{C_D}\right)}{\overline{C_{gw}}} \qquad [4.14]$$

where P is the long-term mean annual precipitation [L T^{-1}], C_P is the weighted mean concentration of chloride in rainfall [M L^{-3}], C_D is the amount of chloride in the dry deposition [M L^{-2} T^{-1}] and C_{gw} [M L^{-3}] is the average chloride concentration in groundwater within the recharge area.

4.3.3.2.1 **Application of the method**

Chloride concentrations in groundwater in the unconfined part of the Aveiro Cretaceous aquifer provided a basis for estimating local recharge. Nine wells and 2 springs within the recharge area were monitored for chloride concentrations during one hydrological year (Oct 00 to Sep 01) (Condesso de Melo *et al.*, 2002b). Chloride concentration determined in 34 boreholes located within or nearby the aquifer recharge area were also used to estimate groundwater recharge.

The average chloride concentrations in the springs and wells have average values of 33.7 mg L^{-1}, while in the boreholes is 31.7 mg L^{-1}. However, for the calculation of this last value it was discarded a borehole with 213 mg L^{-1} of chloride, as this value is an outlier for the area and reflects the local groundwater contamination by a septic tank. Altogether the groundwater chloride results for the wells, springs and boreholes have a median and an arithmetic mean value of 32.2 and 29.4 mg L^{-1} of Cl, respectively (Fig. 4.23). These low mean chloride values will imply moderately high local infiltration rates according to Equation [4.14].

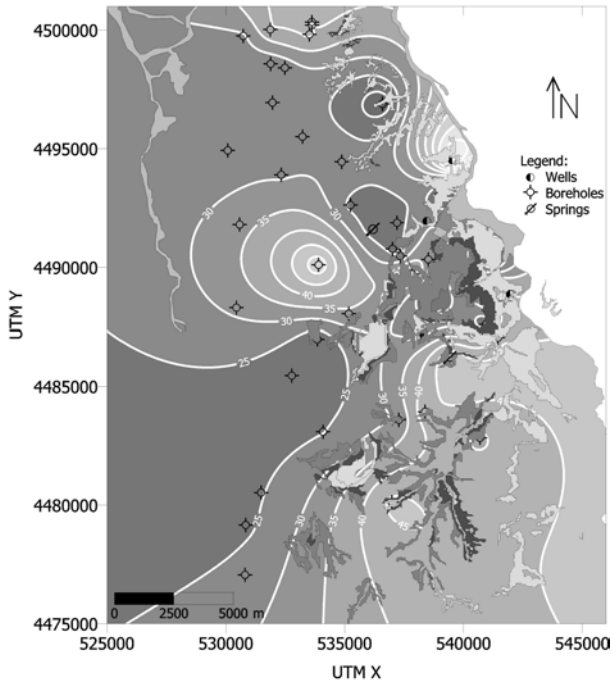

Fig. 4.23 Contour map of groundwater chloride concentration in the unconfined part of the Aveiro Cretaceous aquifer recharge area (Median, $Y_{0.50}$= 29.4 mg L^{-1} Cl; Mean, μ= 32.2 mg L^{-1} Cl; Maximum, MAX= 67.1 mg L^{-1} Cl; Minimum, MIN= 15.9 mg L^{-1} Cl)

Assuming that the mean annual rainfall for the study region is 1075.5 mm a^{-1} and the average annual chloride deposition (including wet and dry deposition) in the area is 3.61 g m^{-2} a^{-1}, the long-term groundwater recharge was calculated using Equation [4.14]. A local infiltration rate of 123 mm a^{-1} was obtained, corresponding approximately to 11% of the annual precipitation under today's climate (Table 4.10).

Table 4.10. Long-term groundwater recharge calculations based on the chloride mass balance method applied to the saturated zone (all chloride concentrations in mg L^{-1}).

	UTM_X	UTM_Y	Cl		UTM_X	UTM_Y	Cl	UTM_X	UTM_Y	Cl	Recharge
Springs & Wells ($Y_{0.50}$= 29.5 mg L^{-1} Cl; μ= 32.2 mg L^{-1} Cl)	539518	4494522	67.14	**Boreholes** ($Y_{0.50}$= 29.4 mg L^{-1} Cl; μ= 31.7 mg L^{-1} Cl)	535252	4492627	23.8	537208	4491877	23.5	Rainfall= 1075.5 mm; $Cl^-_{fallout}$= 3.61 g m^{-2} a^{-1}; $Cl^-_{groundwater}(Y0.50)$= 29.4 mg L^{-1} **Recharge (q_R)= 123 mm a^{-1}**
	539385	4493473	18.72		534879	4494447	29.8	537019	4490775	23.6	
	538453	4491949	29.06		533224	4495506	28.4	535177	4488048	33.9	
	539661	4490755	37.92		531960	4496943	27.9	533858	4486986	20.8	
	540666	4490630	23.06		532483	4498408	26.9	537830	4489724	46.5	
	541294	4490192	18.98		531870	4500021	39.6	534096	4483089	24.8	
	541141	4489218	44.89		531883	4498574	26.7	540696	4482834	39.0	
	541960	4488869	40.29		530582	4491801	33.1	537280	4483590	30.6	
	541574	4488426	37.30		537342	4490469	25.2	536994	4480119	46.2	
	538396	4488840	19.13		538523	4490330	33.5	533907	4490105	53.9	
	538328	4487139	29.49		538807	4489893	24.4	538386	4483931	43.4	
					533626	4500338	42.7	533628	4500209	39.5	
					530733	4499750	29.3	533521	4499818	41.1	
					536589	4496889	15.9	530081	4494925	26.8	
	539444	4486229	49.95		530807	4477059	26.7	530446	4488301	31.2	
	536195	4491603	22.22		530836	4479159	23.9	541454	4487060	43.7	
					532330	4493898	29.4	540949	4487605	20.4	

4.4 Conclusions

The use and comparison of multiple independent approaches to estimate groundwater recharge in the study area was extremely important because besides helping to confirm that recharge estimates do vary depending on the method used, it also called attention to:

- the importance of the actual evapotranspiration estimate when you are calculating recharge applying the Penman-Grindley method;
- the danger of extrapolating point estimates to a whole recharge area (*e.g.* the use of unsaturated zone profiles to calculate the recharge for a whole area);
- the difficulty of discriminate rainfall events in the unsaturated zone profiles augered in areas with humid climates, high infiltration rates and shallow water levels;
- the nonsense of comparing results provided by the same methodology but that cover different time intervals of recharge (*e.g.* to compare results from two unsaturated zone profiles with different total lengths);
- the importance of using methods that account for the spatial variability (*e.g.* both the chloride mass balance in the saturated zone and the water table fluctuation method provide not just spatially averaged recharge rates but also allow for point estimates).

The four methods provided average estimates for recent recharge in the unconfined part of the Aveiro Cretaceous aquifer that fall in an interval varying between 110 and 162 mm a^{-1}, with a mean value of 140 mm a^{-1} (Table 4.11). These values correspond to about 14% of the annual rainfall, which is usually a reasonable estimate of groundwater recharge in humid climates. However, the volume of recharge to the confined part of the aquifer might be a small percentage of the total modern recharge, as deep percolation depends also on the permeability and thickness of the geological formations, and on the geological structure. And in Chapter 3 it was already pointed out the low hydraulic conductivity of the sediments in the eastern part of the aquifer, and the occurrence of regional faults that could limit net recharge and flow to the aquifer confined part.

Table 4.11. Summary of modern groundwater recharge estimates obtained for the Aveiro Cretaceous aquifer using different methods.

	Recharge Estimation Method	Interval of recharge estimates (mm a^{-1})	Final recharge estimates (mm a^{-1})	
Spatial integrated estimate	Penman-Grindley	37 – 162 - 243	**162**	138
	Water table fluctuation	156 - 169	**156**	
	Chloride mass balance in the saturated zone	123	**123**	
Point estimate	Chloride mass balance in the unsaturated zone	110 – 151 - 191 381 - 411‡	**110**	

‡ Values discarded for reasons justified in the text

5

HYDROGEOCHEMISTRY AND GEOCHEMICAL MODELLING

The Aveiro Cretaceous aquifer has been the subject of detailed hydrogeochemical studies during the present investigation. Geochemical data were collected to study the relations between the groundwater chemistry, aquifer mineralogy, and present and past patterns of regional flow.

The approach followed included the identification of major groundwater geochemical patterns in the aquifer, study of the aquifer natural stratification, determination of the aquifer natural background levels, and definition of the controlling processes responsible for the downgradient changes in water chemistry, focusing on mixing processes and water/ rock interactions.

This was accomplished by studying and comparing the chemical and isotopic composition of rain and groundwater, through determination of ionic, molar and isotopic ratios and residence times, calculation of saturation indices relative to most common minerals, and by quantifying the mass balance of solutes along the main flowpaths using a geochemical reaction path transport model.

Previous investigations based on major ions and isotopic analysis (Peixinho de Cristo 1985, Marques da Silva 1990; Carreira *et al.* 1996; Carreira Paquete 1998) always revealed a consistent hydrogeochemistry for the aquifer and a remarkable constancy in the groundwater quality.

The aquifer was re-sampled during four field campaigns carried out in October 1996, September 1997, August 2000 and December 2000, and groundwater samples for laboratory analysis were collected from 90 public supply and private deep boreholes. The analysis included the determination of major, minor and trace elements, with radiocarbon and stable isotope contents determined in pre-selected samples. For the present discussion the isotopic database for this aquifer was increased with 23 sets of stable isotope and radiocarbon groundwater analysis ($\delta^{2}H$, $\delta^{18}O$, $\delta^{13}C$ and ^{14}C) published by Carreira *et al.* (1996) over the data sets obtained during the current study. Noble gases analysis (He, Ne, Ar, Kr and Xe) for this aquifer have also been reported previously by Carreira Paquete (1998).

All the groundwater sampling points discussed in this chapter are shown in Fig. 5.1. The hydrogeochemical database and plots for the baseline values have been included in Appendix B.

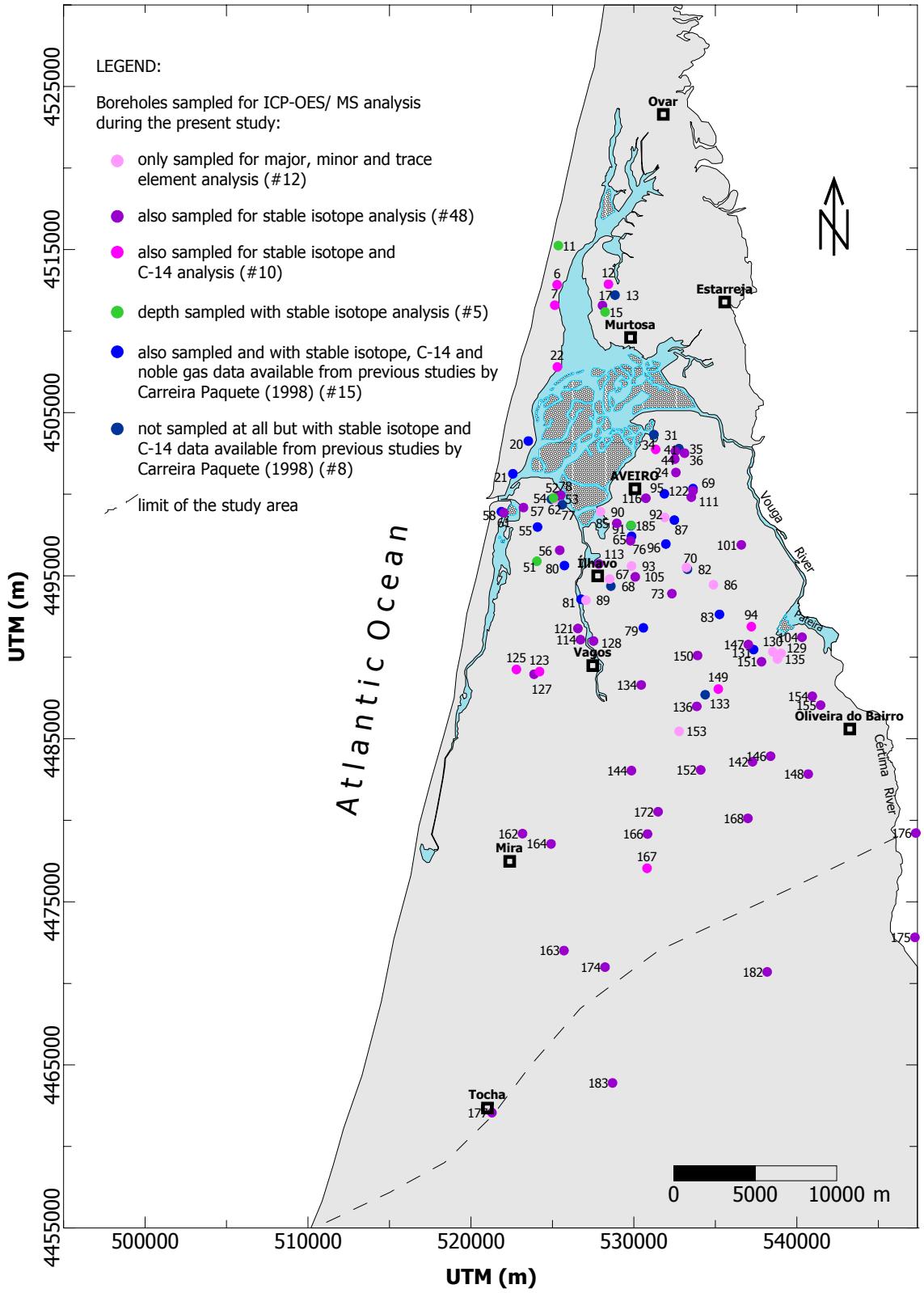

Fig. 5.1 Map of the study area with location of groundwater sample sites. Numbered sample sites refer to those mentioned in the text, tables and figures included in this chapter.

As is common in the region, most boreholes have increasing depths towards the coast following the aquifer thickening and are multi-screened, pumping water from the different aquifer layers with known distinct hydrochemistry and residence times. The borehole specific capacity and the good quality of the water pumped will depend on a great extent on the ability of the hydrogeologist to define the well design and the correct placement of the well screens. Often, higher salinity groundwaters from the Aveiro Cretaceous aquifer are associated with wrongly positioned well screens, either too shallow or too deep (Fig. 5.2).

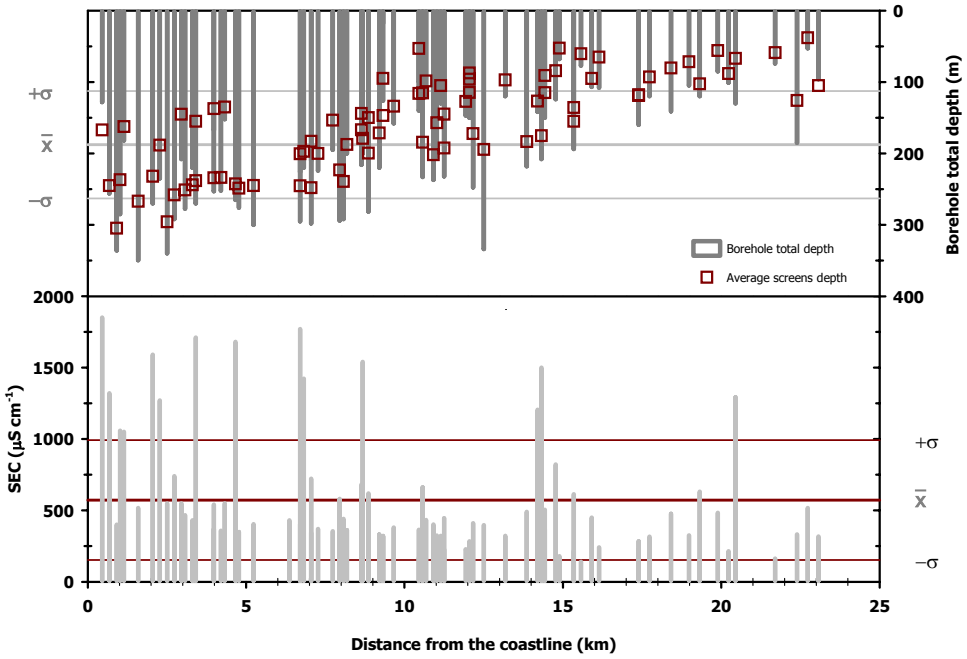

Fig. 5.2 Relation between the well design and screens placement and groundwater total dissolved salts (expressed here as SEC in µS cm^{-1}).

For these reasons, water samples collected from the discharge during the pumping were initially assumed to correspond to a mixture of waters with different chemical characteristics. To better address this problem or this uncertainty, it was decided that during the final field campaign and in collaboration with the British Geological Survey (Wallingford, UK), seven non-equipped boreholes within the study area would be selected for geophysical logging studies and depth sampling.

The detailed description of the geophysical logging studies and depth sampling campaign carried out in the aquifer, as well as the discussion of the principal hydrogeochemical results, has been included in Appendix C. However, the main findings and key points that arise from this specific field investigation are presented in this chapter after the discussion of the regional results in view of their importance in clarifying the possibilities of mixing of pumped samples.

5.1 Groundwater sampling and analytical methods

Groundwater samples were collected from 90 boreholes located within the aquifer study area. A multiport flow-through cell connected in-line to the sampling points was used to obtain reliable geochemical field. Water samples were taken from the discharge during pumping conditions and once stabilisation of the principal field parameters – pH, temperature (T), specific electrical conductance (SEC), reduction-oxidation potential (Eh) and dissolved oxygen (DO) under anaerobic conditions was observed. Redox readings, which were measured by platinum electrode and referenced to ZoBell's solution, are reported relative to the standard hydrogen electrode (SHE).

On-site measurements also included the determination of alkalinity (quoted as HCO_3^-) by acid titration using standard colorimetric titration HACH® kit method. The method involved titrating 100 mL of the sample with sulphuric acid 1.6 N (or, 0.16 N if sample pH was less than 6.0) to pH~4.5 using bromocresol green indicator.

Samples were also collected for subsequent major, minor, trace element and isotopic analysis. Aliquots were filtered in the field through 0.45 μm Milipore® HA membrane filters into two separate acid-washed high-density polyethylene Nalgene® bottles with polypropylene screw closure. An acidified 30 mL sample (1% v/v HNO_3 Aristar® grade) was analysed for major cations, total S (quoted as SO_4), total P and trace elements by inductively coupled plasma-atomic emission spectroscopy (ICP-AES) and inductively coupled plasma-mass spectroscopy (ICP-MS). The second 60 mL aliquot was kept unacidified for chloride (Cl^-), total oxidised nitrogen (NO_3-N), nitrite (NO_2^-), ammonium (NH_4^+), bromide (Br^-), fluoride (F^-) and total iodine (I^-) analysis by automated colorimetry or ion chromatography (depending if the analysis were done by BGS or Activation Laboratories, respectively).

The inorganic determinations in the samples for the two initial field campaigns were performed by the Groundwater Systems and Water Quality Group laboratories of the British Geological Survey (BGS) at Wallingford (UK) in batches of 26 and 30 samples. The chemical analysis of the two last field campaigns were performed by Activation laboratories in Ontario (Canada) in batches of 29 and 16 samples, respectively. Analyses were corrected for blanks and instrumental drift and regular checks were made using standard reference materials. Table 5.1 summarises the 6σ detection limits applied by both laboratories.

The electro-neutrality (E.N) condition expressed in Equation [5.1] (all data in meq L^{-1}) was used as a quality control for all the determinations, and ionic mass balances with closing errors between ± 5% were considered to be acceptable.

$$\text{E.N. (\%)} = \frac{\sum(Na^+, K^+, Ca^{2+}, Mg^{2+}) + \sum(Cl^-, HCO_3^-, SO_4^{2-}, NO_3 - N)}{\sum(Na^+, K^+, Ca^{2+}, Mg^{2+}) - \sum(Cl^-, HCO_3^-, SO_4^{2-}, NO_3 - N)} \cdot 100 \qquad [5.1]$$

Ionic charge imbalances were in all cases less than 5%. For the first batch 100% of the samples were within ±3%, the second and third batches had 60% of the samples within ±3% and the rest 40%, above 3% but still below 5%. The last batch of samples had closing errors within 3 to 5% for 70% of the samples and of less than 3% for the rest. Fig. 5.3 shows the result of electro-neutrality calculations for all the analysed samples and discussed in the following sections.

Table 5.1. Detection limits (6σ) for the inorganic analysis performed by the BGS Groundwater Systems and Water Quality Group laboratories (Wallingford, UK) and by the Activation Laboratories (Ontario, Canada).

ICP-AES/ ICP-MS	ACTALAB	BGS LABS	ICP-AES/ ICP-MS	ACTALAB	BGS LABS	ICP-AES/ ICP-MS	ACTALAB	BGS LABS
(all values in μg L^{-1})								
Li	1	0.2	**Se**	0.2	1	**Pr**	0.001	0.004
Be	0.1	0.05	**Br**	3	-	**Nd**	0.004	0.009
B	1	7	**Rb**	0.005	0.03	**Sm**	0.002	0.008
Na	5	20	**Sr**	0.04	0.08	**Eu**	0.001	0.004
Mg	1	40	**Y**	0.003	0.01	**Gd**	0.002	0.010
Al	2	0.8	**Zr**	0.01	6	**Tb**	0.001	0.003
Si	50	40	**Nb**	0.005	0.12	**Dy**	0.001	0.007
K	10	200	**Mo**	0.1	0.1	**Ho - Lu**	0.001	0.002
Ca	50	20	**Ru**	0.01	-	**Hf**	0.002	-
Sc	1	0.8	**Rh**	0.02	-	**Ta**	0.001	-
Ti	0.1	0.01	**Pd**	0.01	-	**W**	0.02	-
V	0.05	6	**Ag**	0.2	0.04	**Re**	0.001	-
Cr	0.5	0.3	**Cd**	0.01	0.1	**Os, Ir, Au**	0.002	-
Mn	0.1	0.1	**In**	0.001	-	**Pt**	0.01	-
Fe	5	6	**Sn**	0.1	-	**Hg**	0.2	-
Co	0.005	0.01	**Sb**	0.01	0.06	**Tl**	0.005	0.02
Ni	0.3	0.2	**Te**	0.01	-	**Pb**	0.1	0.07
Cu	0.2	0.3	**I**	1	1	**Bi**	0.01	0.077
Zn	0.5	0.7	**Cs**	0.002	0.029	**Th**	0.001	-
Ga	0.01	0.034	**Ba**	0.1	0.12	**U**	0.001	0.016
Ge	0.01	0.049	**La**	0.001	0.02	**P**	-	200
As	0.03	0.3	**Ce**	0.002	0.004	**SO_4**	-	200

OTHER METHODS†	ACTALAB	BGS LABS	OTHER METHODS†	ACTALAB	BGS LABS	OTHER METHODS†	ACTALAB	BGS LABS
(all values in μg L^{-1})								
F	0.5	0.02	**NO_2-N**	0.5	0.02	**NO_3-N**	0.5	0.05
Cl	0.5	0.05	**Br**	0.5	0.005	**P**	1	-
HCO_3	-	1.0	**NH_4-N**	-	0.0005	**SO_4**	1	-

†*Other methods include: Ion chromatography, automated titrimetry and automated colorimetry.*

Groundwater samples for total organic carbon (TOC) analysis were collected from all the boreholes sampled during the 3rd field campaign. Samples were collected without any filtration or acidification into 10 mL glass vials handled with laboratory gloves and immediately stored at 4°C. TOC analyses were also carried out by the BGS Groundwater Systems and Water Quality Group laboratories (Wallingford, UK) using a phase separation TOCSIN-II aqueous carbon analyser.

Inorganic carbon was sparged using 2% nitric acid and the remaining organic carbon converted to CO_2 in a furnace held 900°C. The CO_2 was then converted to methane by hydrogenation over a nickel catalyst prior to analysis by a Flame Ionisation Detector (FID).

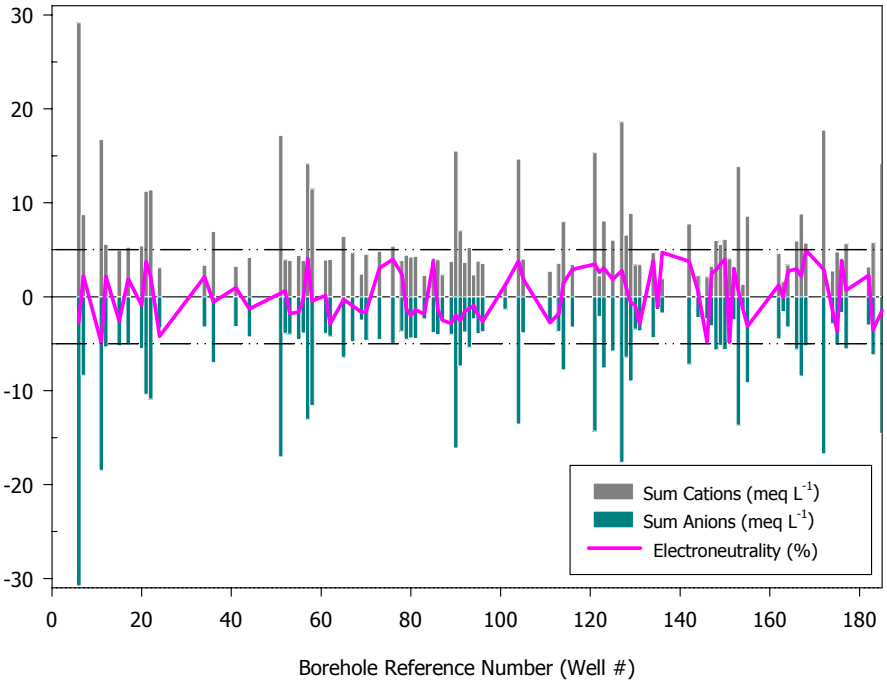

Fig. 5.3 Ionic mass balance for the all the aquifer analysed groundwater samples.

Considering the available isotopic data for the aquifer, just sixty-three of the ninety boreholes sampled for inorganic analysis were selected for collecting water samples in glass bottles for stable isotope analysis of oxygen ($^{18}O/^{16}O$), hydrogen ($^{2}H/^{1}H$) and carbon ($^{13}C/^{12}C$). Fourteen extra samples were also collected for isotope analysis of radiocarbon (^{14}C).

Four samples representative of the aquifer matrix (Palhaça, Furadouro and Oiã sandstone formations) were collected in two recently drilled boreholes for stable isotope analysis of carbon ($^{13}C/^{12}C$) and oxygen ($^{18}O/^{16}O$).

Determinations of stable isotopes were carried out by mass spectrometry by BGS Groundwater Systems and Water Quality Group laboratories Wallingford (UK) following the methods developed by Coleman *et al.* (1982) for $\delta^{2}H$, Epstein & Mayeda (1953) for $\delta^{18}O$ and as described in Clark & Fritz (1997) for $\delta^{13}C$. Deuterium, oxygen and carbon-13 results are reported as parts per thousand (‰) with respect to Vienna Standard Mean Ocean Water (VSMOW) standard and Vienna Pee Dee Belemnite (VPDB), respectively, using the standard δ (delta) notation (Gonfiantini 1978). The analytical precision for stable isotope analysis is ±0.2‰ for ^{18}O, ±2.0‰ for ^{2}H and ±0.3‰ for ^{13}C.

The groundwater samples for radiocarbon analysis were prepared to graphite at NERC Radiocarbon Laboratory in East Kilbride (Scotland) and then analysed by ^{14}C AMS at the University of Arizona NSF facility (USA). The pre-treatment involved the hydrolysis of the raw samples in sealed systems with 85% H_3PO_4 to obtain CO_2. CO_2 was then cryogenically separated from any water present and then graphitised using Fe/Zn reduction.

In keeping with international practice the radiocarbon activities are expressed as a percentage of modern carbon (pMC) and reported ages are calculated as conventional radiocarbon years BP (before AD 1950), both expressed at the $\pm 1\sigma$ level for overall analytical confidence.

5.2 Groundwater hydrogeochemical evolution

The chemical evolution of groundwater is due to geochemical reactions between water, minerals and gases within the unsaturated and saturated zones of the aquifer. The main purpose of the geochemical investigations is to try to identify and quantify these geochemical reactions occurring in the aquifer system (Parkhurst *et al.*, 1996).

In this section, the baseline quality and geochemical reactions in the Aveiro Cretaceous aquifer are investigated and identified based on: the analysis of the chemical and isotopic composition of the groundwater samples; and the information about the petrography and mineralogy of the aquifer matrix. This type of study also requires background knowledge on the geological and hydrogeological properties of the physical framework of the system being studied (Chapter 2 & 3); the regional patterns of groundwater flow (Chapter 3); and the rainfall chemistry, as rainfall is a major input to groundwater (Chapter 4).

The results of this hydrogeochemical study can help in delineating the groundwater flow system, distinguishing the aquifer recharge and discharge areas, identifying areas of groundwater mixing, and estimating relative rates of groundwater flow, providing tracer based timescales to be used to calibrate the numerical groundwater flow model (Chapter 6). Moreover, some of the major and minor dissolved solids and isotopic tracers in the aquifer, can also be used to infer the important chemical and hydrologic processes in the aquifer, as well as being used as early-warning indicators of groundwater quality changes in the system (for future monitoring purposes).

A general description of the chemical composition of groundwater in the studied aquifer is initially presented, followed by the explanation of the possible origin and natural evolution of the groundwater in the system, focussing on the controlling geochemical processes. Finally, the redox environment in the study units is discussed and a brief description on the occurrence of trace elements in the aquifer is presented.

5.2.1. **Major hydrogeochemical patterns**

Identification of hydrochemical facies in the Aveiro Cretaceous aquifer system was based on the distribution of water types and used to divide the Aveiro Cretaceous aquifer in three main zones (*'groundwater bodies according to the WFD (2000)?'*) with gradually different hydrogeochemical characteristics (Fig. 5.4).

From the recharge area in the eastern part towards the coast we can identify:

1) Modern groundwater is limited to the outcrop area of the aquifer under unconfined conditions (eastern part of the study area). These are recently recharged oxygenated groundwaters of predominantly Ca-HCO_3 hydrochemical facies, with *p*H values lower than 7.0 and water temperatures less than 20°C. Nitrate concentrations are generally low but some occasional higher concentrations have been detected and reflect modern human impact. However, just two boreholes exceeded the limit of potability. Groundwater ages vary from recently recharged up to 7,000 years BP waters, that may occur in the western limit of this part of the aquifer, just 10 km from the outcrop area. Salinity is low with chloride median values around 30 mg L^{-1} and SEC<650 μS cm^{-1}.

2) Holocene to pre-industrial groundwater occurs in the intermediate, confined part of the aquifer. Redox potential and dissolved oxygen progressively decreases along the flowpath with groundwater changing from oxidising to reducing conditions. These are groundwaters with either Ca-HCO_3 or Na-HCO_3 hydrochemical facies, pH values higher than 6.2 but lower than 8.3 and groundwater temperatures around 21.3 ºC. P_{CO2} decreases in this part of the aquifer from 0.04 to 0.001 down flowpath. Background chloride contents increase to 40 mg L^{-1} but SEC still does not exceed the 400 μS cm^{-1}. This is mainly unpolluted groundwater, enriched in $\delta^{18}O$ compositions and with modelled ages lying in the range of 3,500 to 18,000 years BP.

3) Late Pleistocene-Early Holocene groundwaters have been identified in the deeper and confined part of the aquifer, well protected by the thick overlying aquitard. They are Na-HCO_3 or Na-Cl type waters, with *p*H in the range from 7.1 to 8.9, and average groundwater temperatures higher than 22°C, eventually reaching values higher than 30ºC in the deepest part of the sedimentary basin (W of the town of Vagos). The negative Eh values reflect anaerobic (reducing) conditions and the water is unpolluted. The specific electrical conductance indicates that the confined groundwater in the Aveiro aquifer is fresh, with background chloride contents around 115 mg L^{-1}. Fresh groundwater with SEC<500 μS cm^{-1} and Cl^-<40 mg L^{-1} is found down to a depth over 300 m below OD in the Barra camping site borehole, just 900 m from the present coastline.

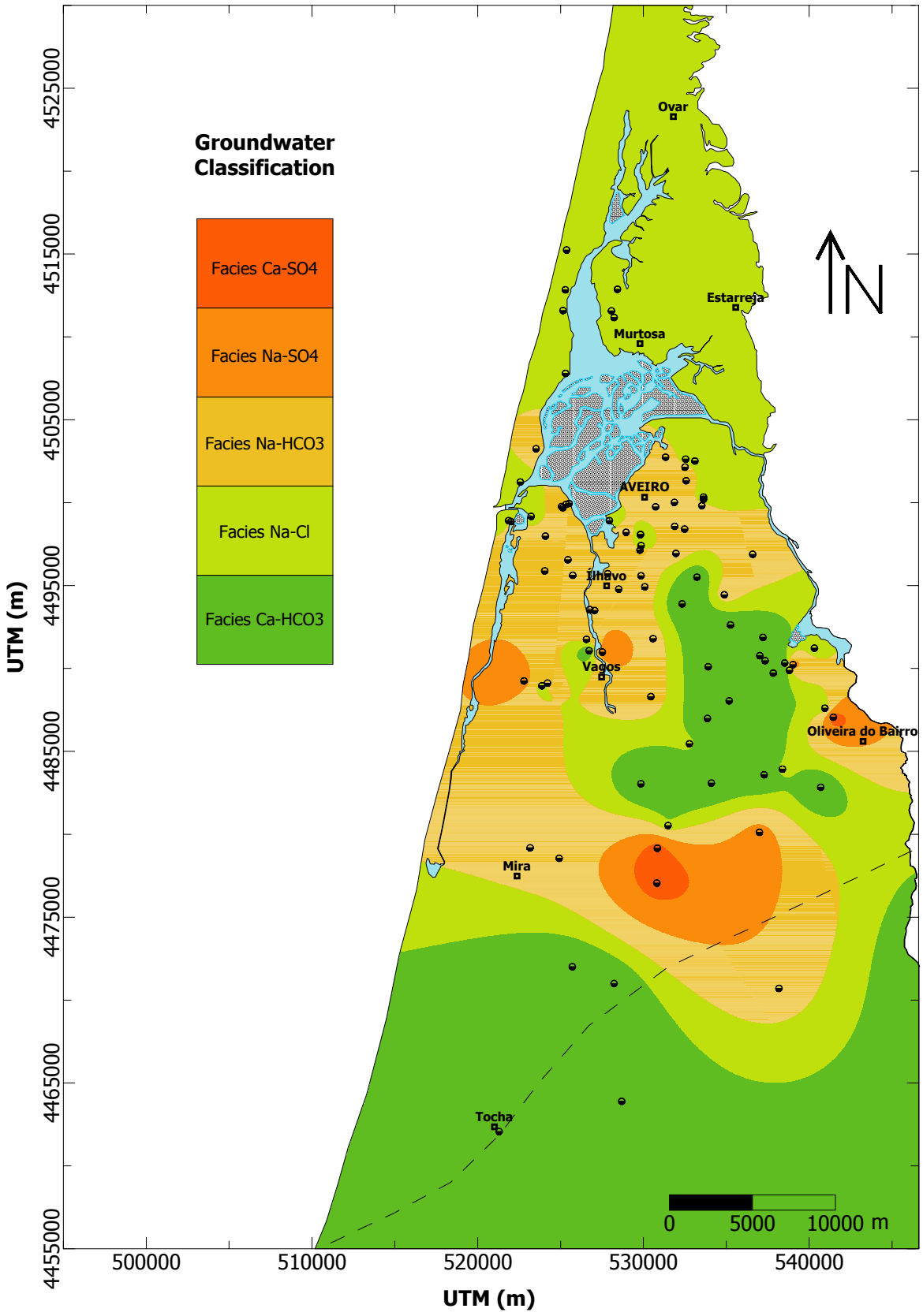

Fig. 5.4 Distribution of the principal hydrochemical facies within the Aveiro Cretaceous multilayer aquifer. The water types follow main aquifer pathlines from the recharge are in the east towards the coastline.

The subdivision of the aquifer in three distinct parts may be confirmed by the analysis of the evolution of the principal field parameters when plotted against the distance from the coastline, as illustrated in Fig. 5.5. Data used to plot these diagrams does not correspond to all the boreholes sampled but just to those along the same flow lines and with increasing depths towards the coast in order to prevent data scattering (as we will see in some of the following diagrams, as long as it does not affect data interpretation).

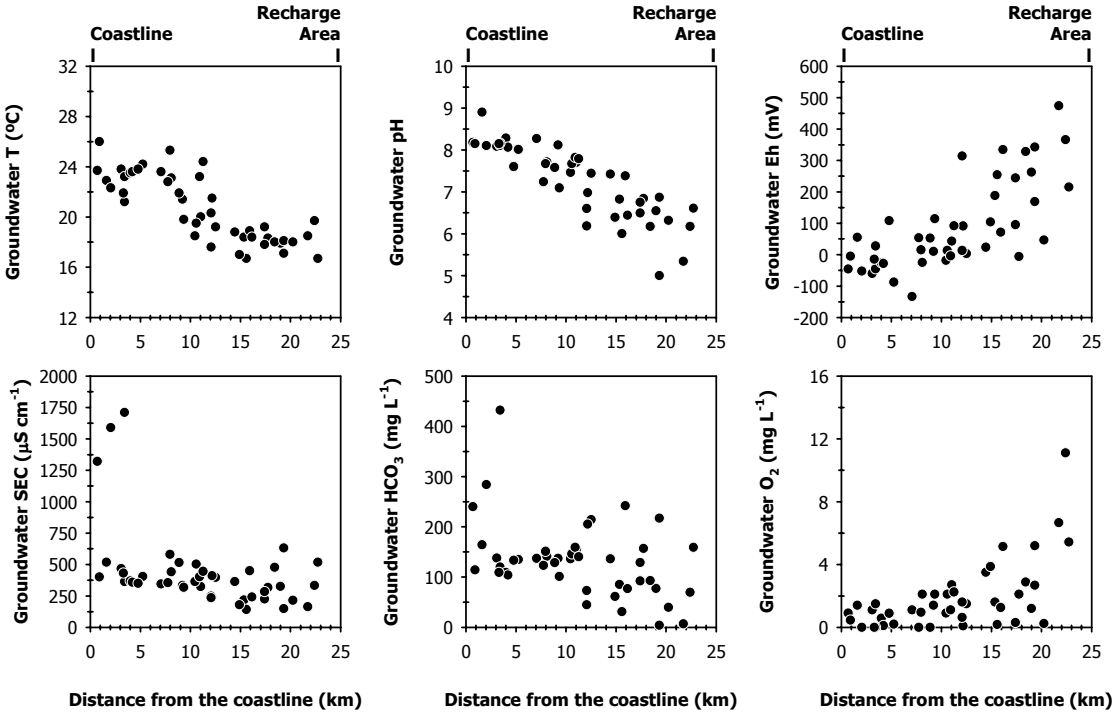

Fig. 5.5 Evolution of the principal aquifer field parameters with distance from the coastline.

The studied groundwaters have their origin in part associated with the infiltration of rainwater of Atlantic origin (which is essentially diluted seawater) and the gradual flushing of older formation waters (eventually, old seawater trapped in the sediments). Infiltrating rainwater percolates through the unsaturated zone to reach the underlying groundwater body, reacting with silicate and carbonate minerals in a system initially open to CO_2. Because carbonate dissolution kinetics are much faster than the silicate weathering reactions, a fresh groundwater dominated by Ca^{2+} and HCO_3^- initially prevails. Ca^{2+} average concentrations in this part of the aquifer are about 33 mg L^{-1} while Na^+ concentration is less than 14 mg L^{-1}.

As the water moves downward along the flow path into the deeper and confined part of the aquifer, Ca^{2+} ions are taken up from groundwater by cation exchangers that make part of the aquifer matrix (mainly, clay minerals), in return for Na^+. In the areas closer to the coast average calcium concentrations are quite small, around 4 mg L^{-1}, while Na^+ becomes the dominant cation

with concentrations higher than 110 mg L^{-1}. Calcium is clearly being taken up from water, in return for Na^{+}, which is being released in solution. With exception to the areas within the outcrop area where calcium is the most abundant cation, sodium is the dominant solute in the aquifer. Its concentrations vary from a minimum 14 to a maximum of 400 mg L^{-1} with increasing residence time, and the same trend is observed for sodium/calcium molar ratios.

The natural hydrogeochemical evolution reflects these processes trending from Ca-HCO_3 type waters near the recharge area to Na-HCO_3 or Na-Cl type waters in the areas close to the coast. The evolution of the groundwater towards an evolved Na-HCO_3 water type indicates that ion exchange and calcite dissolution are dominant geochemical processes in the aquifer.

This pattern of cation exchange is evident when groundwater samples are plotted in a Piper trilinear diagram (Fig. 5.6). However, if the observed pattern of cation exchange is combined with the dilute nature of the aquifer, then we might associate this phenomenon in great part to the initial phases of dilution of saline water trapped in the clay minerals.

It is also noticeable that modern recharge waters plot on the hypothetical fresh-sea water mixing line indicating the influence of the marine aerosols. In the same diagram, there is a group of samples distinguishable from the rest for their high Ca^{2+} and SO_4^{2-} concentrations. These are samples located in the south-east part of the aquifer and whose chemistry reflects mixing with waters from adjacent Jurassic formations.

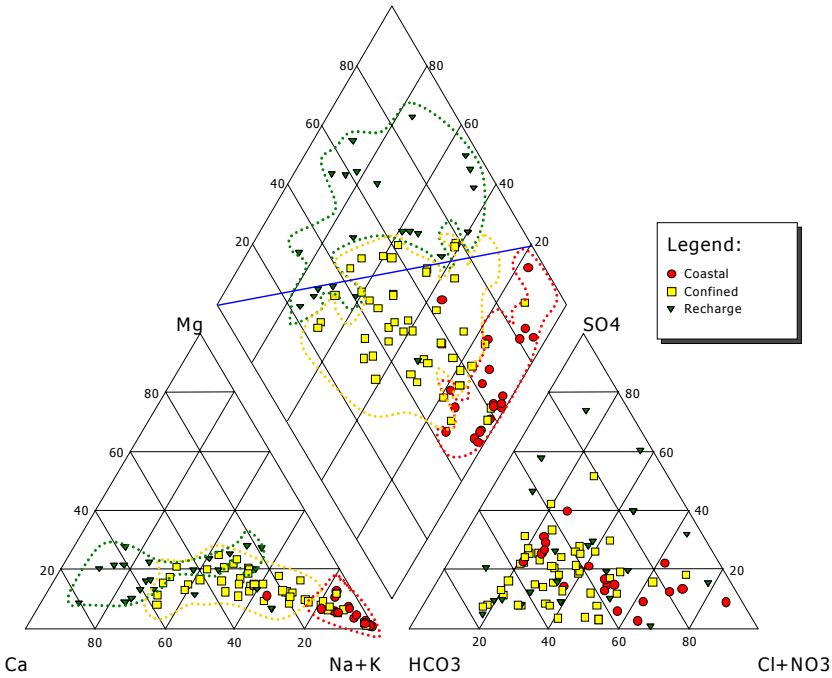

Fig. 5.6 Piper plot of studied groundwater samples in the Aveiro Cretaceous multilayer aquifer in which cation exchange is visible. The hypothetical fresh-sea water mixing line is drawn in blue colour.

At present, the baseline of fresh groundwater in the Aveiro Cretaceous aquifer is of remarkably low salinity (below 50 mg L^{-1} Cl^-), considering that it was, at least in part, of marine origin. The low chloride concentrations (minimum 16 mg L^{-1}, which is about 4x the mean rainfall value) over most of the aquifer is consistent with the main input to groundwaters being derived from atmospheric inputs after allowing for evapotranspiration, and at depth the remaining Cl^- is little more than 1-2% of that probably derived from (marine) formation water.

The dilute nature of the Aveiro groundwaters thus indicates previous freshening of the coastal aquifer since at least the Late Pleistocene or even earlier. Higher hydraulic gradients (~0.004) during the Last Glacial Maximum (LGM) or even before LGM imposed by a sea level lowered by approximately 130-140 m compared to present day would have accelerated the complete refreshing of the aquifer, with fresh water flushing the original formation water.

The analysis of chemical patterns of dissolved species along evolutionary groundwater flow paths was performed using elemental molar ratios. For the Aveiro aquifer, bromide/chloride ratios were useful for the reconstruction of groundwater origin (Fig. 5.7). Late Pleistocene and Early Holocene waters show approximately constant values for the Br/Cl ratio, and samples plot on a mixing line between the rainwater and sea water ($[Br^-]/[Cl^-]$ = 0.0016). This is consistent with Cl^- being mainly of marine (aerosol) origin. Recent recharged waters have a Br/Cl ratio slightly enriched in bromine over the palaeowaters that could reflect the anthropogenic influence.

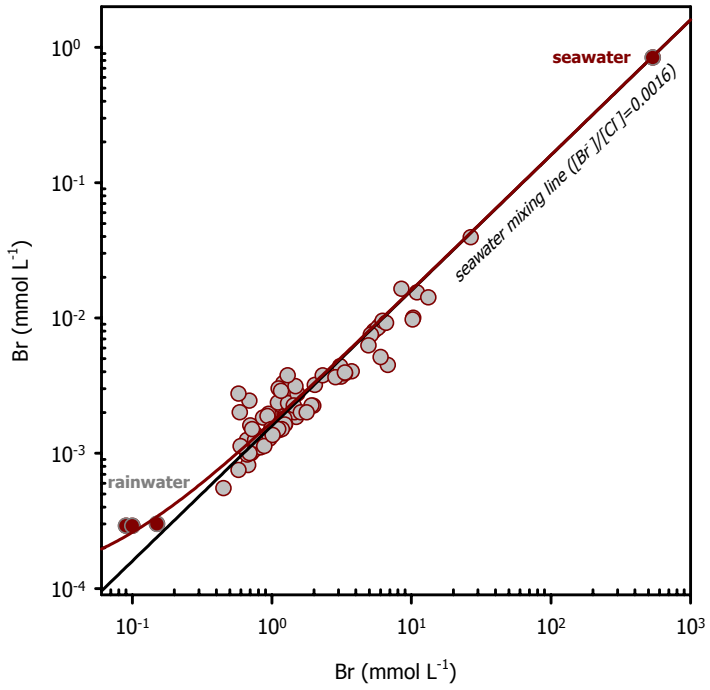

Fig. 5.7 Relation between Br^- and Cl^- content in the groundwater samples. Also plotted are the seawater mixing line (in black) and the rainwater line (in red).

However, the presence of Na^+ is not totally compensated by Cl^-, as would be expected if seawater and aerosol effect were the only sources of sodium, and Na/Cl molar ratio is not consistent with a simple fresh/sea water mixing process. Local rainwater has annual averaged Na/Cl ratios (1.25 to 1.44) higher than the characteristic value for the seawater (0.85) and reflecting not just the marine aerosol but also the soil dust. In this region however only the recently recharged groundwaters have Na/Cl ratios close to 1.0. These groundwaters are the result of rainwater infiltration, reflecting just the chemical composition of local rain, as the residence times have not been long enough to show any significant chemical evolution due to water-rock interaction. Sodium feldspar dissolution is likely to be one of the geochemical processes responsible for liberating extra Na^+ to solution, leading to Na/Cl ratios higher than one and high ratios of Na^+ relative to Ca^{2+} as shown in Fig. 5.8.

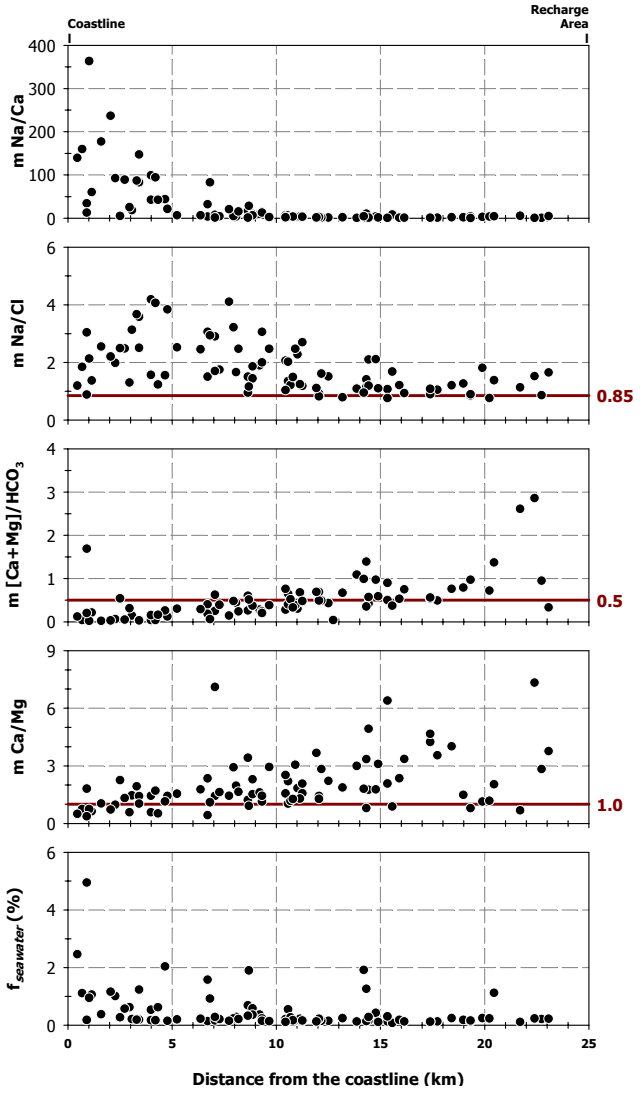

Fig. 5.8 Variation in molar Na/Ca, Na/Cl, $[Ca+Mg]/HCO_3$ and Ca/Mg molar ratios, and in the fraction of seawater in the studied aquifer with increasing distances from the coastline.

It is well known that aquifer silicate minerals can be a source of solutes through dissolution and a sink via the processes of adsorption and precipitation (*e.g.* White & Brantley, 1995; Lasaga, 1995; Brady & Walther, 1989; Bland & Rolls, 1988). Taking account of the mineralogy of the aquifer matrix and the long residence times, alumino-silicate weathering and carbonate minerals dissolution are likely to be the other processes responsible for cation variation in the Aveiro aquifer. Besides, the observed decrease of P_{CO_2} along the flowpath confirms that mineral reaction is taking place (Fig. 5.9).

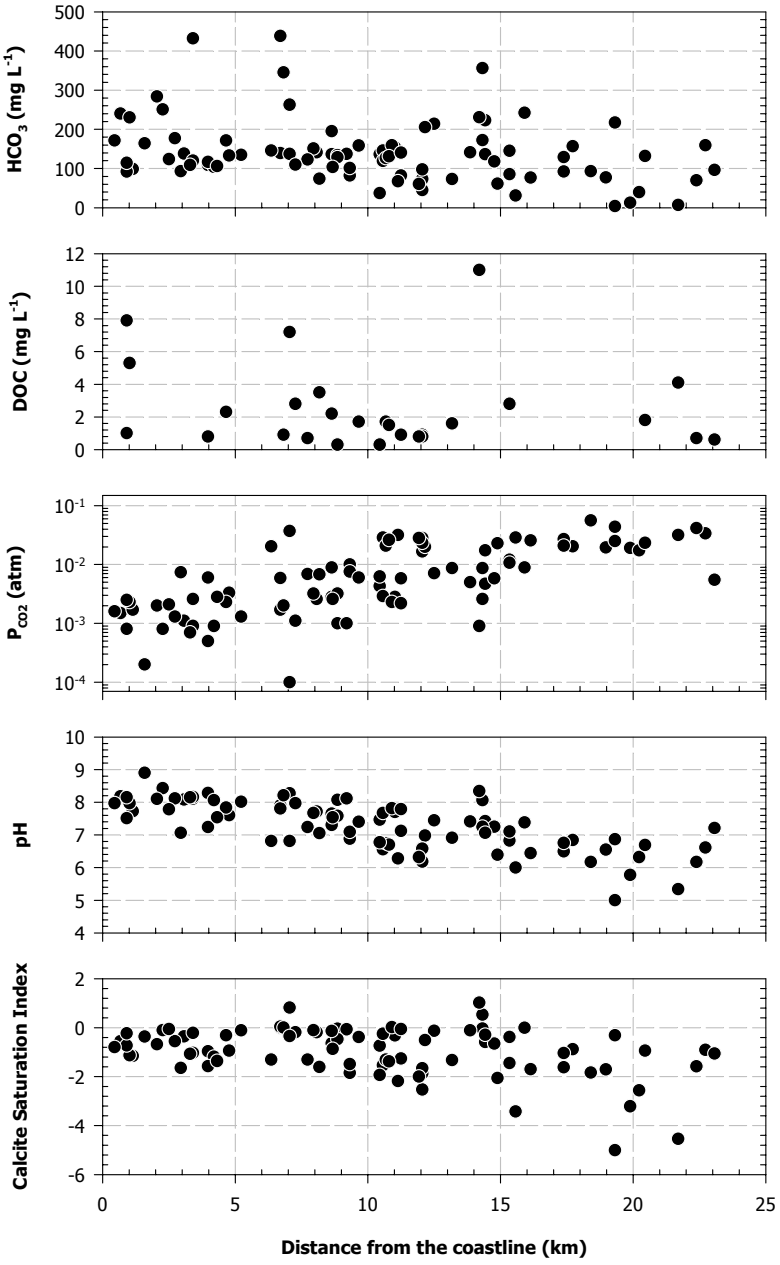

Fig. 5.9 Groundwater pH, P_{CO_2}, TOC, HCO3 and calcite saturation index evolution along the aquifer flow path.

When such weathering reactions dominate the aquifer chemistry, the apparent P_{CO_2} ranges from near atmospheric values (0.06 atm) in the recently recharged waters to 0.0002 atm in the palaeowaters, while pH increases from 5.0 to 8.9 over a 25 km distance downdip. This is because both alumino-silicate and carbonate minerals dissolution consumes CO_2 and is also a major H^+ consuming process. And, the aquifer goes from an open system to CO_2 in the outcrop area to a closed system reaction in the confined part.

The low *p*H of recharge waters is then buffered by mineral weathering, as both the alteration of silicate minerals to clays (more slowly) and calcite and/or dolomite dissolution (comparatively faster) consume H^+. The origin of the carbon dioxide required for silicate dissolution is presumably obtained from the decay of traces of organic matter present in the aquifer matrix. This may lead to the reduction of Fe and S to form pyrite, an accessory mineral in the studied aquifer.

Dolomite dissolution in the sandstone cement causes increases in the concentration of magnesium in the water and is reflected in the increase of Mg/Ca ratios in the initial 10 km of the aquifer flowpath. The observed depletion of calcium and magnesium shown before in Fig. 5.8 relative to bicarbonate ($[Ca+Mg]/[HCO_3]<0.5$) in the last 15 km of the aquifer is due to the cation exchange phenomenon.

For a mainly silicate aquifer system, groundwater silicon concentrations (~5.5 mg L^{-1}) are remarkably uniform for the whole aquifer. Silica is being released into solution by silicate alteration but with a proportion being retained as secondary minerals (kaolinite and smectite); any excess of silica is likely to be removed initially as colloidal silica to maintain the apparent equilibrium with chalcedony or quartz.

The molar ratio of Si to Na^+ can be interpreted as a reflection of the dominant weathering processes (Appelo & Postma, 1996). Si/Na ratio decreases along the flow path, from values around 0.40 in the recharge area to values of 0.02 in the deeper part of the aquifer. Considering just the sodium due to silicate reaction and neglecting Na derived from seawater (either rain or connate water), a ratio of Si^{4+} to Na^+ still lower than two is derived (Fig. 5.10). The weathering of common rocks to kaolinite or gibbsite cannot generate that value; therefore a 2:1 silicate such as smectite must be forming. This is consistent with the clay minerals observed in the mineral assemblage of the aquifer layers.

The aquifer is formed of predominantly siliceous material with very slow dissolution kinetics that may not be expected to produce significant variations in the water chemistry. Besides the minerals do not necessarily contribute to the solutes in groundwater in proportion to their abundance in the bedrock.

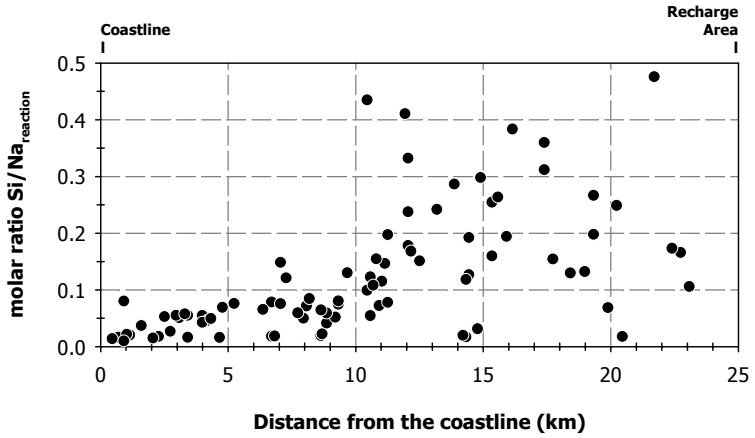

Fig. 5.10 Evolution of $Si/Na_{reaction}$ content along the flowpath

5.2.2. **Redox patterns and their impact on groundwater chemistry**

The natural redox conditions in the Aveiro multilayer aquifer change along the flowpath becoming gradually anoxic and affecting the solubility and transport of some major and minor constituents in groundwater (Fig. 5.11).

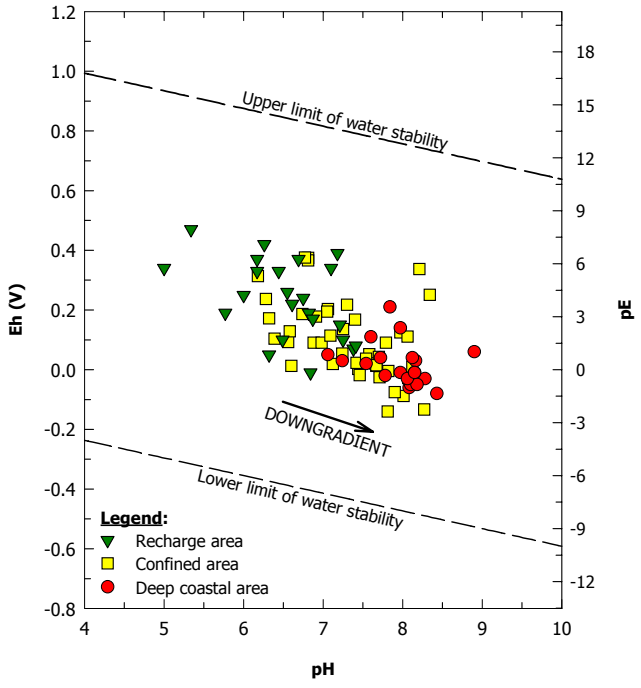

Fig. 5.11 Eh-pH-pE stability diagram for the Aveiro multilayer aquifer.

Decreasing Eh, NO_3 and U groundwater values along the aquifer main flow path were used to indicate the presence of a redox boundary, which was observed close to the unconfined-confined boundary (Fig. 5.12). Oxidising conditions may generally be recognised by Eh values ≥

300 mV and reducing groundwaters below 100 mV, with some of the most evolved groundwaters in the deeper part of the aquifer with negative measured Eh values.

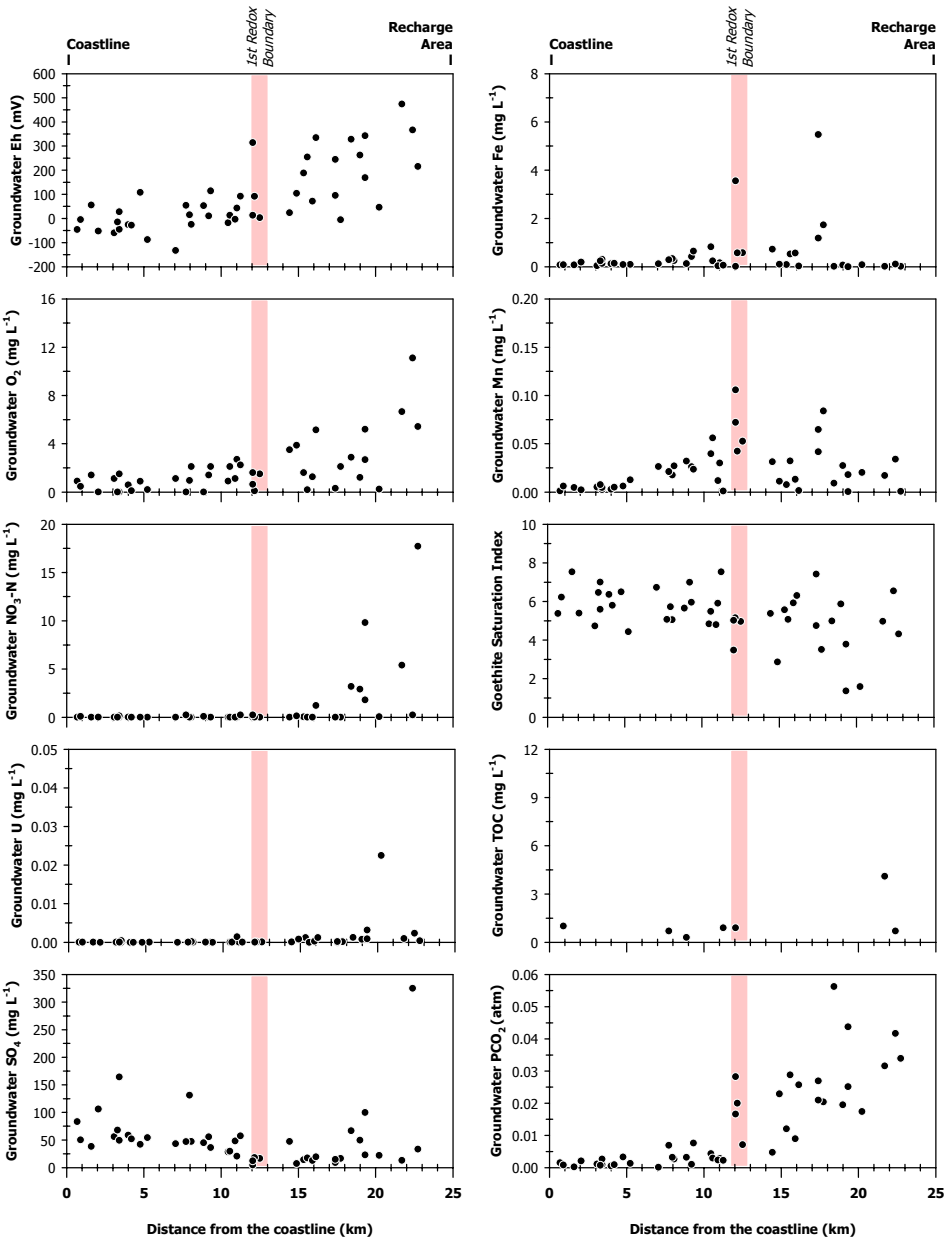

Fig. 5.12 Evolution of groundwater Eh, temperature, NO_3_N (total oxidised nitrogen), U content and other redox indicators along aquifer flowpath.

Values for dissolved oxygen in the unconfined part are commonly less than 6 mg L^{-1}, not reaching groundwater saturation. Deeper confined groundwaters tend to become gradually anaerobic because traces of organic matter and/ or Fe(II) and sulfide in minerals at depth deplete

the oxygen introduced in groundwater recharge. Values of DO<0.2 mg L^{-1} have been determined through out the aquifer confined sections.

Nitrate concentrations in groundwater are just detected in the unconfined part of the aquifer and in three 'dubious' boreholes in the confined aquifer. To the west of the redox boundary, NO_3-N concentrations are below detection limit, which confirm the existence of the redox barrier, coincident with the drop in Eh values to around +100 mV. Uranium, another good indicator of redox conditions, is also below the detection limit beyond the aquifer outcrop area. The concentrations of NO_2-N in the aquifer is below detection levels indicating that denitrification is minimal. Positive values of NH_4-N occur just in three boreholes close to the coast (<7 km), with Cl^- values higher than 200 mg L^{-1}, and are likely to be related to desorption of NH_4^+ ions from clay minerals. Identical phenomenon was observed by Smedley & Edmunds (2002) in the East Midlands Triassic Sandstone aquifer (UK). Total organic carbon concentrations are variable in the aquifer and without a clear trend, but it is possible to associate some higher values with oxidising waters.

Total dissolved Fe concentrations (≤0.45μm fraction) are low or even below detection limit (< 5 μg L^{-1}) in unconfined oxygenated waters, but increase in the anaerobic confined aquifer to >1 mg L^{-1}. The same trend is observed for Mn, which concentrations reach values over 0.05 mg L^{-1} under anaerobic conditions. These high concentrations of Fe and Mn coincide with SO_4 values in the aquifer lower than 50 mg L^{-1} and an increase in As values to over 0.01 mg L^{-1} (Fig. 5.13).

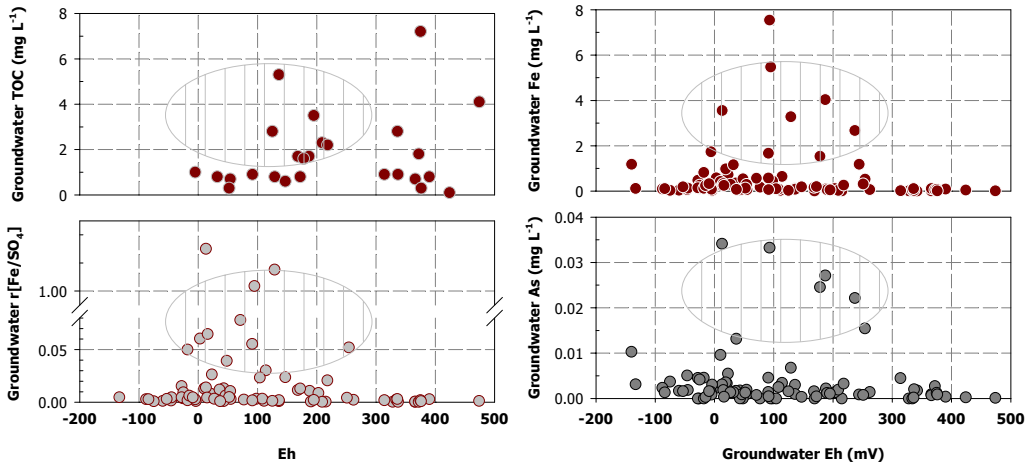

Fig. 5.13 Evolution of groundwater TOC, SO_4, Fe and As in the studied aquifer. Special attention is recalled for the Cacia region where concentrations of Fe well over the MAC value have been detected.

The highest concentrations of dissolved ferrous iron are observed in the area of Cacia where mineralogical studies by Rocha (1993) identified fairly abundant pyrite in the aquifer sediments. The TOC values determined in the available samples for this area are also relatively

high (>2 mg L^{-1}) when compared to background values, so the aquifer has a higher reducing capability in this area. Arsenic concentrations are also higher in this part of the aquifer.

5.2.3. **Minor and trace elements in the aquifer**

An important number of minor and trace elements have been investigated in the aquifer to enrich the understanding of water chemical evolution. These are briefly described here to follow trends with the Aveiro Cretaceous aquifer (Fig. 5.14).

The concentrations of these elements are controlled in groundwater under natural conditions by atmospheric precipitation and the weathering processes, while their speciation, reactivity and mobility depends mostly on the groundwater redox conditions. Some of these elements are considered to be almost inert, as the halogen elements, and are good tracers of groundwater. Others, such as Li, Rb, Cs, Mn and Mo are more reactive, but under very controlled conditions can still be used as residence time indicators (Edmunds *et al.*, 2000).

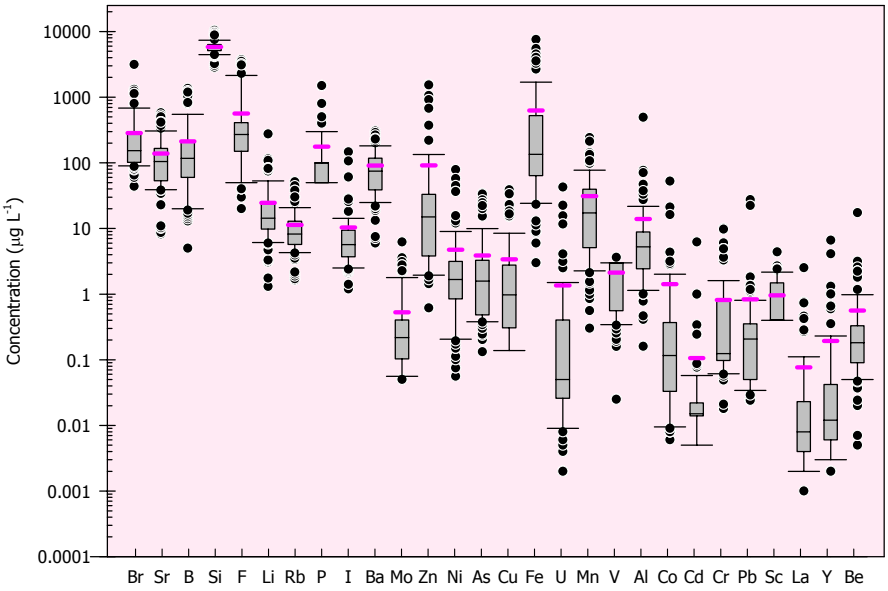

Fig. 5.14 Range of minor and trace element concentrations in the Aveiro Cretaceous aquifer groundwaters. Data is from database included in Appendix B.

Large concentrations of fluoride, iron, manganese and barium are evident in some parts of the aquifer, exceeding occasionally the maximum admissible concentration values for human consumption. Besides fluoride, the other halogen elements also increase with residence time in relation to the mixing with old formation water trapped in the clay minerals present in the aquifer matrix.

On the contrary, lithium concentrations do not show any increase with residence time and do not follow the geochemical behaviour of sodium, behaving differently from what was observed in other sandstone aquifers, where it has been used as a residence time indicator (Edmunds & Smedley, 2000).

Boron is also quite abundant especially around Cacia where it is related to the high rubidium, cesium, iron and manganese concentrations. Boron concentrations are also very high in the most cation-exchanged groundwaters (close to the coast) possibly as a result of mixing with old formation waters and further water-rock interaction. The same trend was observed in the Lower Greensand aquifer in the UK (Mather & Porteous, 2001). However, the concentrations in the Aveiro Cretaceous aquifer are still lower than maximum permissible concentrations in drinking water (300 $\mu g\ L^{-1}$).

Most of the other minor and trace elements are present in concentrations very close to the detection limit, which is indicative of the low reactivity of the Aveiro Cretaceous aquifer.

5.2.4. **Mineral saturation indices**

Saturation indices (SI) with respect to siliceous, carbonate and clay minerals, and activities of soluble species were calculated using PHREEQC-2 (Parkhurst & Appelo, 1999). The validity of the results obtained for the saturation indices of the different minerals relies on the accuracy of the analytical data and specially pH (Nordstrom *et al.*, 1979). When calculating the saturation of silicate minerals, dissolved aluminium concentrations (<0.45 μm) are taken into account. The concentration of total dissolved aluminium in most groundwater samples was less than 6 $\mu g\ L^{-1}$ (3σ detection limit is 0.32 $\mu g\ L^{-1}$). These values are considered close to the true concentration for dissolved total aluminium (Langmuir, 1971) although there is the possibility that some colloidal Al (<0.45 μm) may be included in the analysis.

Speciation calculations suggest that just a few minerals are at saturation. Groundwater from all sites was in equilibrium with chalcedony and saturated with respect to quartz and for some of the common clay minerals - kaolinite, smectite and illite (Fig. 5.15). Subsaturation persists for plagioclase and other feldspar minerals.

In two thirds of the aquifer, groundwater is undersaturated with respect to calcite, with saturation index values increasing from –5.0 to –1.0 with increasing residence time (Fig. 5.16). This means that calcite dissolution is still taking place in this system, increasing the degree of saturation of this mineral with groundwater residence time. The same trend was observed for dolomite.

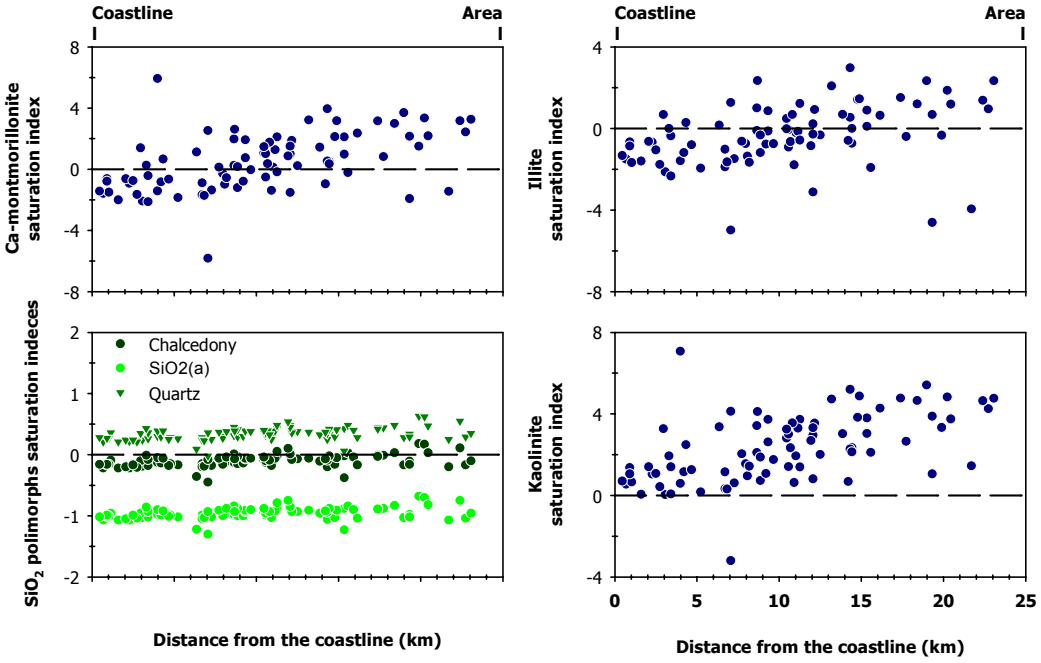

Fig. 5.15 Saturation indices for SiO_2 polimorphs and for some clay minerals.

Saturation with calcite is just achieved in quite a few boreholes closer to the coast where calcite dissolution led to a *p*H of around 8.3. Calcite dissolution is perhaps the most common and effective *p*H buffering reaction. This is a significant observation, showing that flow is mainly in the 'Furadouro sandstone formation' and that the Carbonate formation does not have an important effect on the overall hydrochemistry.

In most groundwaters however the $SI_{calcite}$ lies between –2.0 and 0.0 indicating that the majority of groundwaters are significantly undersaturated with respect to carbonate minerals (Fig. 5.16). In these areas, the observed increase of the anion HCO_3^- (from concentrations of 75 mg L^{-1} in the recharge area to values of 280 mg L^{-1} next to the coast) is an indirect consequence of the processes of cation exchange. The reduction of the amount of Ca^{2+} in solution resulting from cation exchange leads to further calcite dissolution.

Sulphate concentrations in groundwater increase downflow from 20 to 100 mg L^{-1}. Groundwater samples from areas close to the Triassic outcrops (NE part of the study area) show an anomalous increase in SO_4^{2-} concentrations, due to the dissolution of gypsum. However, saturation with gypsum is never attained.

Most silicate minerals dissolve incongruently with the formation of clay minerals – illite, kaolinite and eventually, smectite. The formation of secondary minerals however complicates the interpretation of solute concentrations in the aquifer, and it seems questionable whether true equilibrium with these secondary phases is ever attained and the reaction kinetics are important over this time scales (Appelo & Postma 1996).

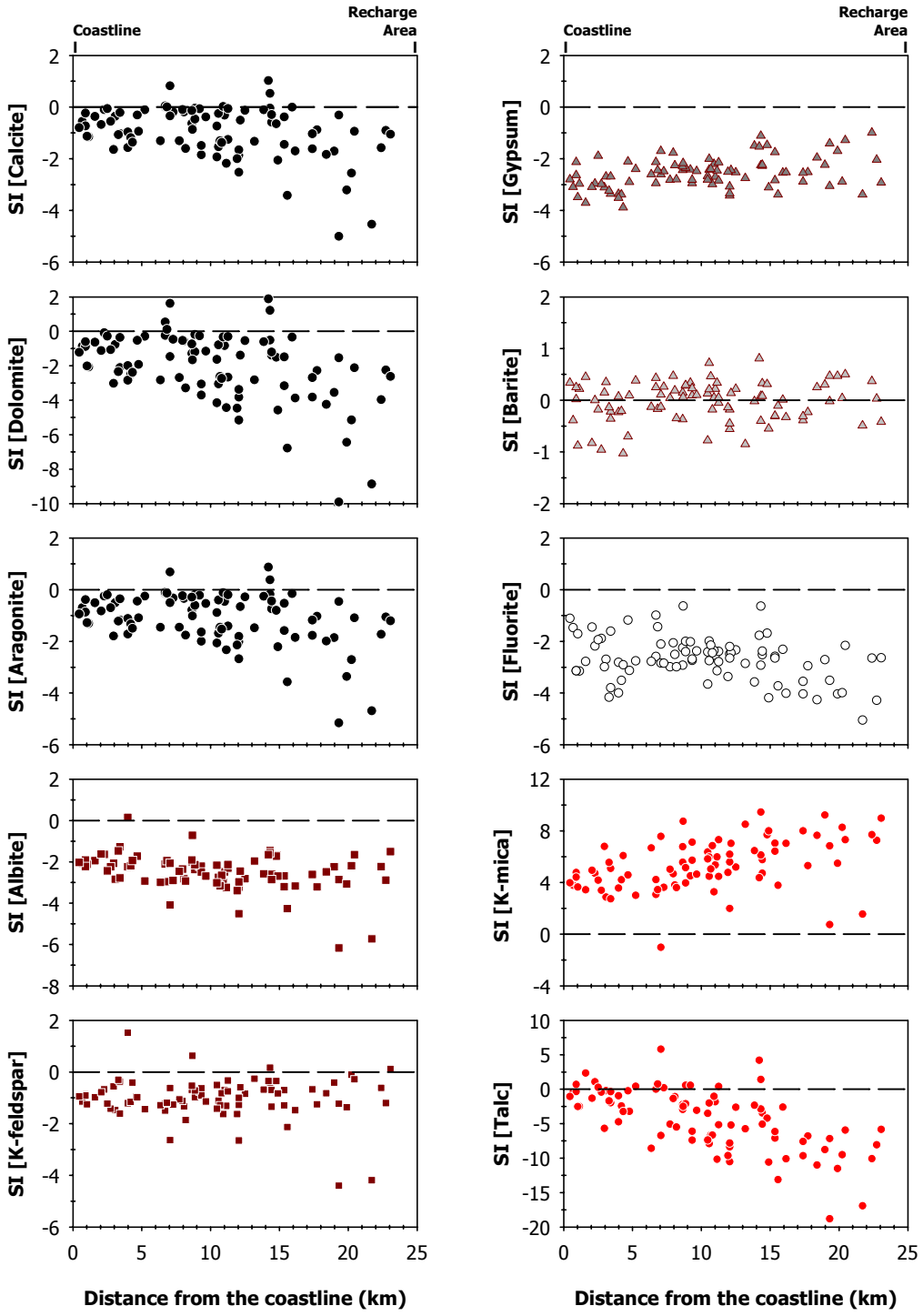

Fig. 5.16 Saturation indices for fluorite and principal carbonate, k-feldspar, sulphate and mica minerals.

5.2.5. **Groundwater isotopic signature**

Palaeowaters have been clearly identified in the confined part of the aquifer combining the use of radiocarbon dating and recharge temperatures calculated by Carreira Paquete (1998) using noble gases determinations. The combined sets of radiocarbon activities from the present study and

Carreira Paquete (1998) are shown in Fig. 5.17 relative to distance from the coastline. These results may be classified on the basis of their carbon stable isotope ratios and three principal groupings of groundwaters are found:

$A^{14}C$ (CITD) < 6 pMC and $\delta^{13}C$ varying from -10 to -13 ‰

$A^{14}C$ (CITD) between 6-15 pMC and $\delta^{13}C$ varying from -12 to -15 ‰

$A^{14}C$ (CITD) > 15 pMC and $\delta^{13}C$ < -15 ‰

representing Late Pleistocene-Early Holocene, Holocene and modern groundwaters, respectively.

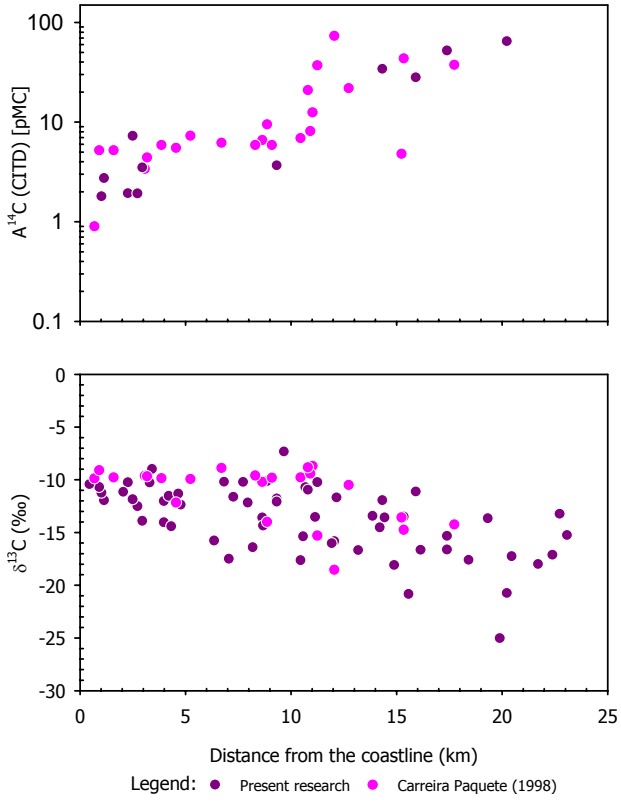

Fig. 5.17 Evolution of $A^{14}C$ (CITD) and $\delta^{13}C$ content along the flow path.

Groundwater ages have been derived applying the correction procedure of the ^{14}C value using the measured $\delta^{13}C$ values following the IAEA model (Salem *et al.,* 1980). This model is based on the chemical balance of Tamers (1975) with a correction factor due to secondary chemical and isotopic exchange reactions between the groundwater and the soil/aquifer matrix lime during water circulation. This simple model was selected considering the aquifer chemistry, undersaturated relative to calcite, but several other methods were applied (*e.g.* Evans et al., 1979) without significant changes in the calculated (differences were less than 0.2 ka) . A value of –25±2‰ was assumed for soil CO_2 together with a carbonate value of –0.72±1.0‰ (which corresponds to the

average of $\delta^{13}C$ values determined in the samples from the 'Furadouro sandstone formation') and an isotopic enrichment factor of 9±0.5‰ that accounts for fractionation.

The oldest age calculated for this set of groundwaters was 34.9 ka BP from an initial activity of 1.92 and $\delta^{13}C$ of –12.5‰. This compares with an age maximum calculated in the paper of Carreira *et al.* (1996) of 35 ka BP using the same model. Thus the timespan for groundwaters in the Aveiro aquifer is likely to be at least 35 ka. And this age information can be used to constraint groundwater flow directions and velocities, fluxes, recharge rates, hydraulic conductivities, and effective porosity.

Modern groundwaters sampled from the eastern outcrop study area are chemically and isotopically distinct from the palaeowaters and these waters have moved up to 5 km from the outcrop into the section. However, groundwaters containing radiocarbon have moved westward for at least 20 km under natural gradients implying that there used to be and possibly still is an outlet offshore. The smooth gradient in radiocarbon ages across the aquifer indicates continuity of recharge and flow through the LGM (Fig. 5.18). This is in contrast for example to the UK East Midlands aquifer where a gap in groundwater ages between approximately 10 ka and 20 ka is interpreted to indicate cessation of recharge at the height of the LGM due to ice cover or permafrost (Edmunds *et al.*, 2001).

The distribution of groundwater ages in the aquifer confirm the sudden change of groundwater flow velocities that took place the LGM when the lowered sea level contributed for much higher hydraulic gradients in the aquifer and probably to the almost complete flushing of seawater from the aquifer. Nowadays there is probably just old formation water trapped in the low permeability formations of the aquifer.

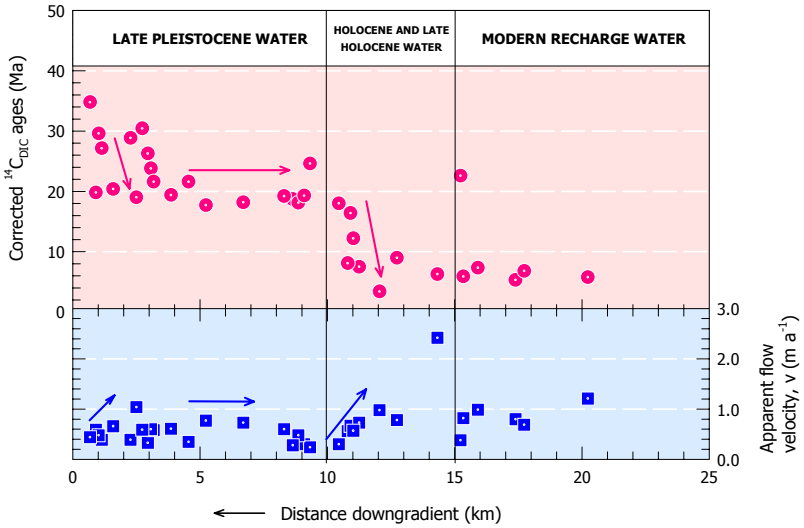

Fig. 5.18 Evolution of groundwater age and apparent flow velocities in the studied aquifer.

In Fig. 5.19 the Cl^- concentrations have been plotted against ^{14}C activities. The rather constant Cl^- values (~1 mmol L^{-1}) throughout much of the time period of >30 ka suggest constant inputs from marine aerosols from the present day through till at least the LGM. Little if any Cl^- contamination is recognisable in the modern groundwaters. Mixing with more saline formation waters is only observed in the oldest groundwaters, which confirms that increasing salinities in the aquifer are related to increasing residence time and not to modern salt water intrusion.

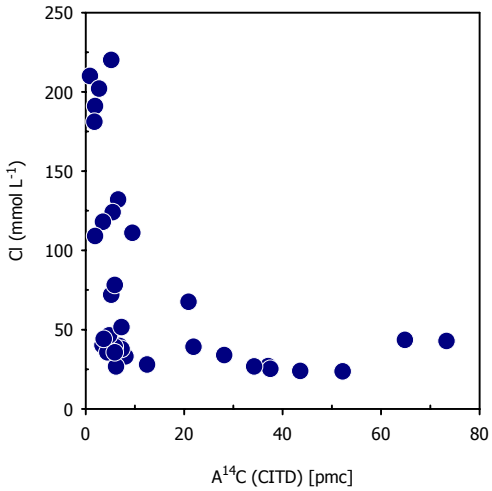

Fig. 5.19 Evolution of chloride content in the aquifer with increasing residence time.

The groundwater noble gas results indirectly indicate that there have been significant variations in climate during the Late Pleistocene and Holocene, notably in mean annual temperature (Fig. 5.20).

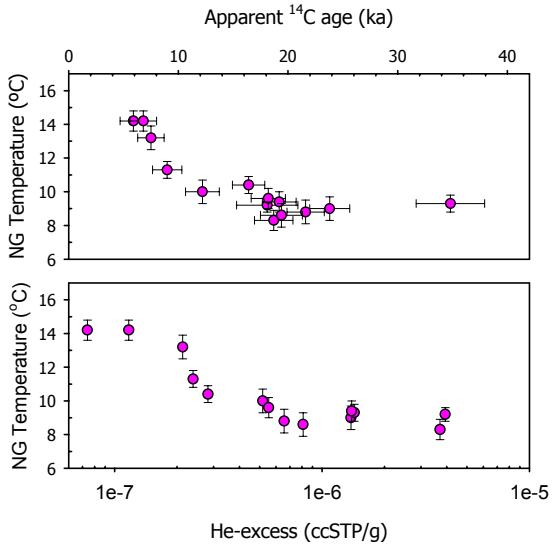

Fig. 5.20 Noble gas recharge temperatures for the Aveiro aquifer (Carreira Paquete, 1998).

The change of 5-6ºC in surface temperature indicated by inert gas ratios, between groundwaters with calculated radiocarbon ages around 18 ka BP and those representing present day recharge temperatures. These values are similar to the climatic amelioration documented by Zazo *et al.* (1996) for the NW part of Iberian Peninsula.

Temperate latitude climates have experienced significant changes in temperature during the Late Pleistocene that may be identified by a shift in the stable isotope content of precipitation, and in deuterium excess. This palaeoclimatic effect, shown by environmental isotopes is one of the most important tools in identifying palaeowaters Clark & Fritz (1997).

The ^{18}O and ^{2}H contents for all the investigated groundwaters are plotted in the classical $\delta^{18}O$-$\delta^{2}H$ diagram together with the global meteoric water line (GMWL) (Fig. 5.21). The $\delta^{18}O$-$\delta^{2}H$ relation provides some valuable information on the origin of these groundwaters and conditions at the time of recharge. The values for palaeowaters are positively displaced with respect to modern recharge water and plot along a line with the same slope as the GMWL (slope s ≈ 8). This implies that Late Pleistocene groundwaters are characterised by a slight enrichment in ^{18}O and ^{2}H with respect to modern waters. This is in contrast to most records of palaeowaters in continental regions, which record an isotopic depletion relative to the present day (Clark & Fritz, 1997; Edmunds & Milne, 2001).

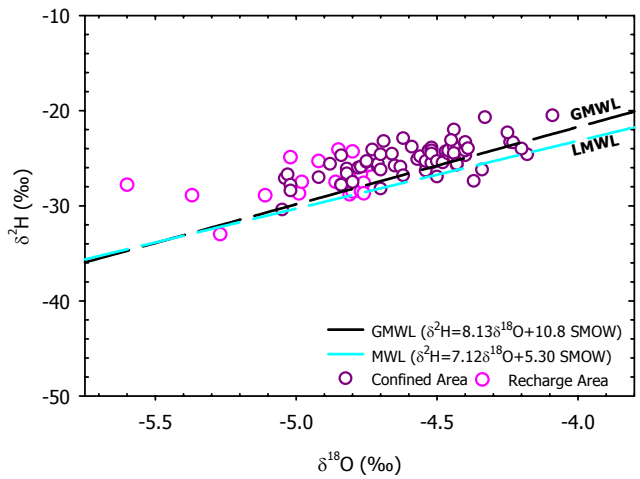

Fig. 5.21 Relationship between $\delta^{2}H$ and $\delta^{18}O$ contents in groundwater samples. GMWL, Global meteoric water line and LMWL, Local meteoric water line calculated for the recharge area in Chapter 4.

This heavy isotope enrichment is confirmed by plotting $\delta^{18}O$ and $\delta^{2}H$ with increasing residence time (Fig. 5.22). The isotopic composition of the Late Pleistocene-Early Holocene waters varies on average from -4.7 to -4.1‰ for $\delta^{18}O$ and from -23 to -22‰ for $\delta^{2}H$. Holocene groundwaters show values for $\delta^{18}O$ between -4.9 and -4.7 ‰, and for $\delta^{2}H$ averaging from -27 to

-25‰. In Fig. 5.23 these isotopic data are combined with hydrochemical data to define approximately the interface between modern and old water in the aquifer.

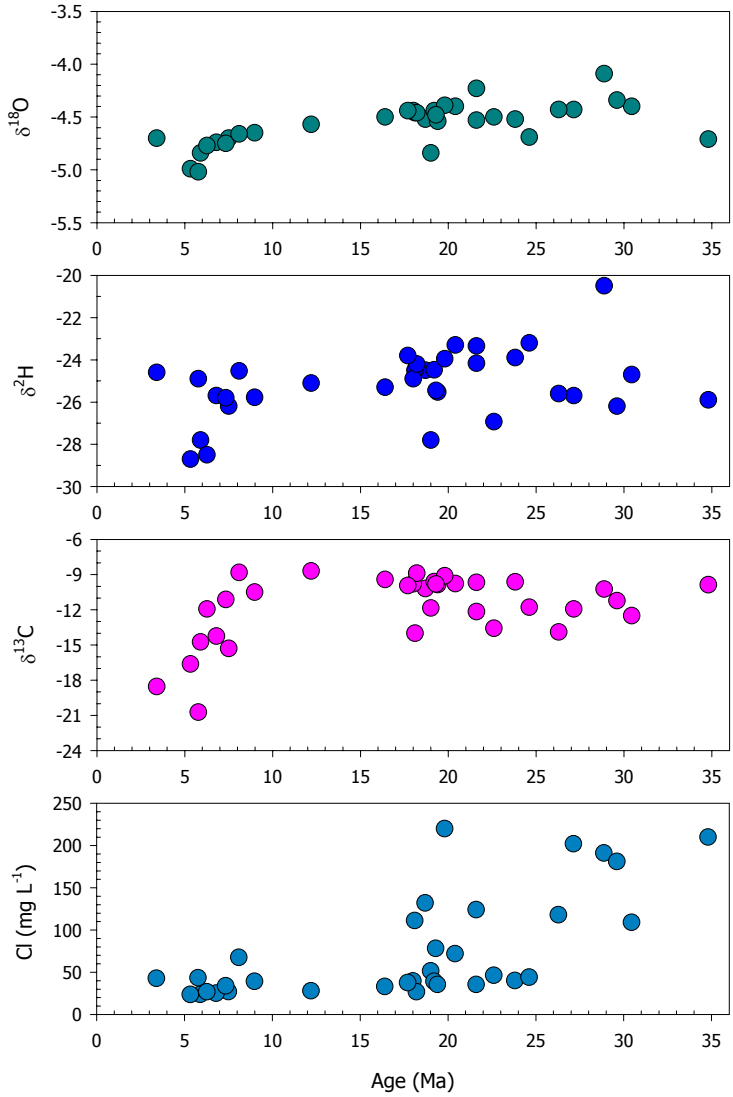

Fig. 5.22 Heavy isotope and chloride enrichment along the flow path with increasing residence time.

This observed enrichment, more common in countries with arid climates, might be related according to Carreira *et al.* (1996) to heavy isotope enrichment of global ocean during glacial times, as at that time large quantities of isotopically depleted waters were trapped in the polar ice sheets. Groundwaters in coastal aquifers reflect necessarily the fluctuations of the isotopic composition of the ocean in the adjacent regions. This phenomenon, associated with the fact that the increase in the Aveiro aquifer flowpath length due to sea level lowering during the LGM was not as significant as in other parts of the European coastline and thus not producing obvious continentally effects, may explain the different heavy isotope pattern observed.

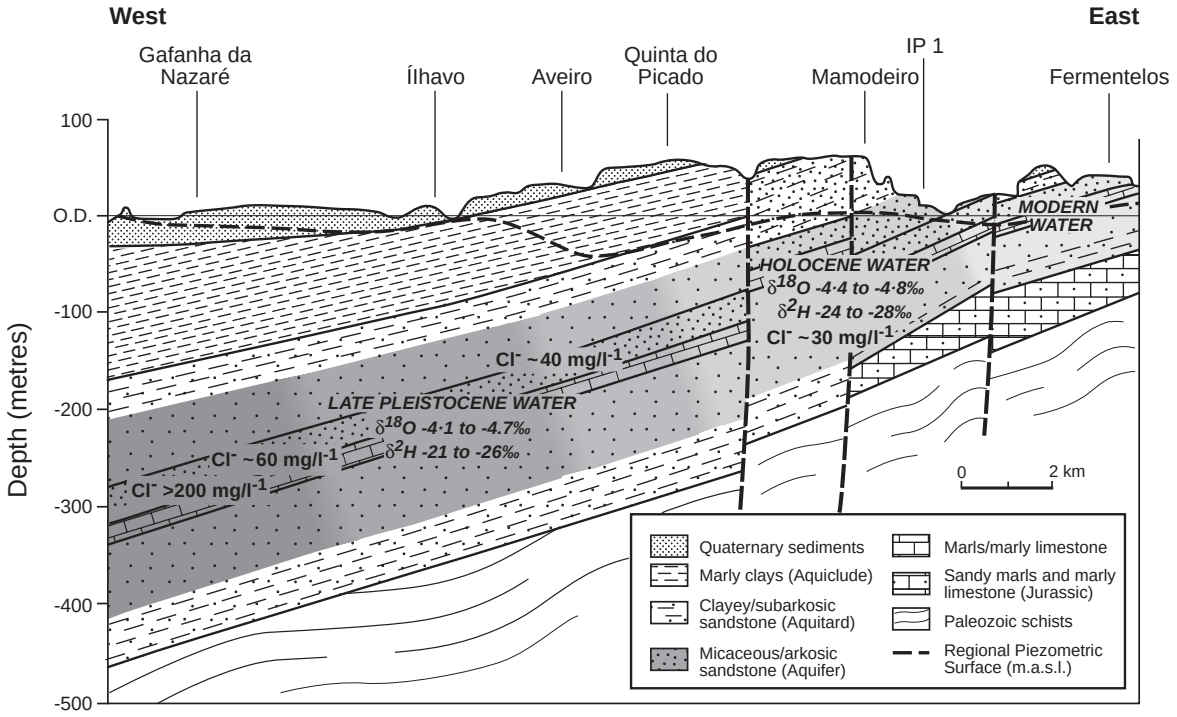

Fig. 5.23 Modern-old water interface in the Aveiro Cretaceous aquifer.

5.3 Aquifer hydrogeochemical natural stratification

The use of conventional methods of groundwater sampling from pumping multiscreened boreholes in the Aveiro Cretaceous multilayer aquifer inevitably leads to water mixing between the different aquifer layers, making the understanding of the water quality patterns more difficult, and eventually, leading to misinterpretations. To minimise this problem, the present study was planned to include not just the study of groundwater quality spatial variability but also the analysis of groundwater vertical stratification arising from geological layering.

However, this type of study required the use of specific geophysical well logging and depth sampling methods not available yet at the University of Aveiro. It also required the availability of non-equipped (preferably) boreholes within the study area, as the logging in equipped boreholes is much more difficult and there is always the risk of a probe getting trapped. Finally, and benefiting from an Anglo-Portuguese Joint Research Project with the British Geological Survey, funded by the Treaty of Windsor Programme, a depth sampling campaign was carried out in December 2000 using the only non-equipped boreholes available within the study area (Fig. 5.24). These included two boreholes recently drilled for industrial and public water supply and five piezometer wells from the National Groundwater Level Monitoring Network. Unfortunately these piezometers have not been pumped since drilling and so their state of preservation was totally unpredictable.

Detailed description of the geophysical logging and depth sampling in each borehole, as well as a description of the principal hydrogeochemical results obtained have been included in Appendix C. A summary is presented in the following section.

This depth sample campaign and all the geophysical and fluid log interpretation discussed in the Appendix C and summarised in the following sections resulted from a work in close collaboration with D. Buckley (BGS, UK) and benefited from his experience of more than 30 years using geophysical logging applied to hydrogeology. More technical details about the geophysical logging equipment and field practices can be found in Buckley (2001).

Fig. 5.24 Logger and tripod set up at borehole #62 (PS1 Gafanha da Nazaré). Also visible the electric hoist used to install the submersible pump and the pump itself.

5.3.1. **Main results from the depth sampling campaign**

The most important inference arising from the depth sampling and flow logging campaign is probably that the 'Furadouro sandstone formation' is contributing with most of the water supplied by the aquifer. The ratio for the transmitted flow could be as high as 9:1 when compared to the other aquifer layers, and implies that samples taken from the discharge during pumping conditions can be assumed to correspond in great part (~90%) to the 'Furadouro sandstone formation'. The chemical composition of the flow samples is also dominated by the chemistry of this aquifer layer.

Summarising the observed vertical stratification it can be said that the lower salinities were observed for the intermediate part of the 'Palhaça sandstone formation' and for the 'Furadouro sandstone formation', except where leaks at joints in the blank casing were observed. In these cases, the high salinity water entering from the Quaternary sediments diffuses along the borehole penetrating in the most permeable and lower salinity aquifer layer ('Furadouro sandstone formation') due to favourable hydraulic and density gradients. Major elements determined in the different samples and corresponding to the different aquifer layers have been plotted in a Piper diagram to help to summarise them (Fig. 5.25).

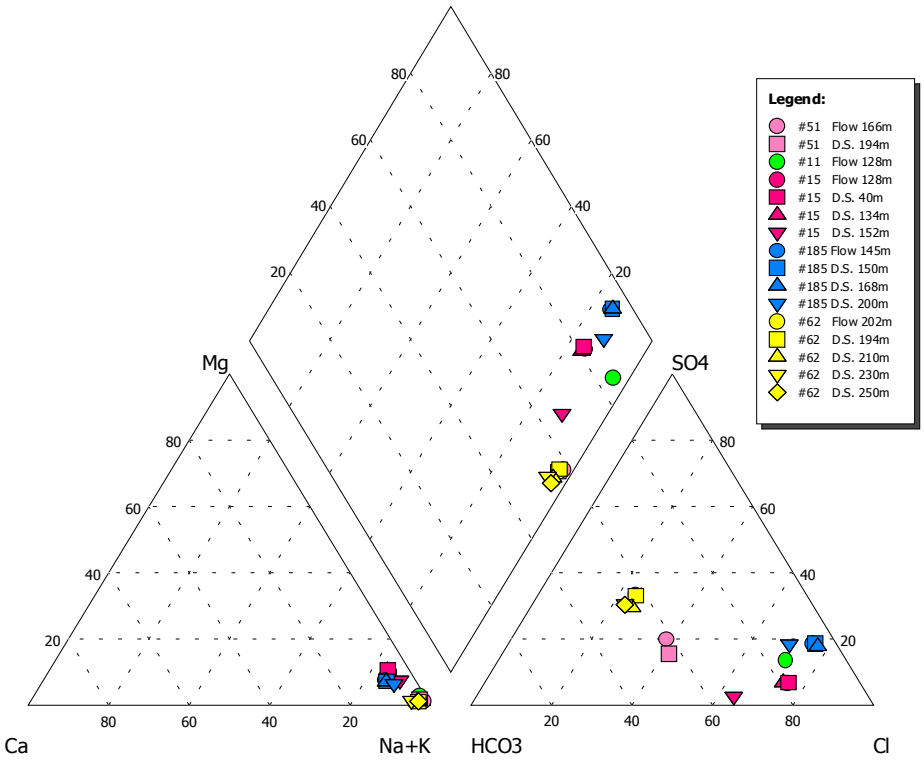

Fig. 5.25 Piper plot of the water samples collected from the discharge (○ Flow) and the corresponding depth samples (□△▽◇ D.S.) for each of the boreholes sampled during the depth sampling campaign in December 2000.

Moderately fresh groundwater of Na-HCO_3 facies appears to exist in the '**Verba sandstone formation'**. The pH values are typically greater than 8.1 and groundwater temperatures higher than 21ºC. Calcium and magnesium have been practically removed from solution due to ion exchange reactions with clay minerals and sodium is the dominant cation, showing increasing concentrations with depth (>375 mg L^{-1} Na). Average chloride (~250 mg L^{-1}) and sulphate (150 mg L^{-1}) contents are higher than aquifer baseline values, but bicarbonate is the dominant anion with concentrations over >400 mg L^{-1} and revealing a freshening pattern for this aquifer layer. Carbon-13 contents (-8.7±0.3‰) are clearly enriched which could indicate increased reaction with marine bicarbonate. Stable isotope composition indicates depletion both in $\delta^{18}O$ (-4.9

±0.04‰) and in δ^2H (-26.1±0.5‰) contents, that could indicate that these are post-Holocene waters. Trace elements do not show any significant increase. The only exception is fluoride, that is probably associated with the clay minerals (kaolinite and illite are abundant in this aquifer layer), with high concentrations well above the maximum admissible concentration (MAC) for human consumption (>2.2 mg L^{-1}).

The '**Oiã sandstone formation'** contains Na-HCO_3 type waters with pH values between 7.6 and 8.0 and groundwater temperatures between 19.5 and 20ºC. When compared to the overlying aquifer, the calcium concentrations are still low (<5 mg L^{-1}) but bicarbonate values do not exceed the 120 mg L^{-1}. The groundwater is low salinity (SEC is less than 500 μS cm^{-1}) with chloride rarely exceeding the 40 mg L^{-1}. Sodium is the dominant cation with concentrations exceeding the 80 mg L^{-1}. No particular enrichment is observed in the trace elements. Carbon-13 contents (-10.5±0.3‰) are still enriched but less than in the overlying layer and a slight enrichment ($\delta^{18}O$=-4.5±0.1‰ and δ^2H=-24.9±0.6‰) observed for stable isotopes, that probably indicates longer residence times.

The **'Furadouro sandstone formation'** is considered the best aquifer layer, for its high permeabilities and low salinities, but for this reason is one the most vulnerable aquifer layer. Groundwater is fresh Na-Cl type water, with SEC values lower than 450 μS cm^{-1} and pH values between 7.1 and 7.7, but rarely exceeding the 7.5 value. Groundwater temperatures are slightly cooler than in the less permeable layers (usually lower than 19.3ºC), which could be related to the shorter residence times. Average HCO_3^- concentrations are around 100-120 mg L^{-1}, calcium concentrations do not exceed 12 mg L^{-1} and strontium is lower than 0.12 mg L^{-1}. Some minor elements Ba, Mn and Fe are enriched in this layer. Total iron often exceeds the MAC values of water for human consumption and is the result of the oxidation of traces of pyrite that are more abundant in this aquifer layer. Fluoride is usually below MAC values in this aquifer layer and that might be because the clay content is much less in this aquifer layer.

Carbon-13 contents are around -13.0±1‰ which is in agreement with stoichiometric dissolution of the marine calcite, and stable isotopes contents show some enrichment ($\delta^{18}O$=-4.2±0.1‰ and δ^2H=-24.4±2‰) when compared to modern recharge.

The **Palhaça sandstone** has Na-Cl type waters with pH values varying in the narrow interval between 7.5 and 7.7 and groundwater temperatures similar to those of the 'Furadouro sandstone formation' (< 19.3ºC). Groundwater quality in the upper zone of this aquifer layer has high salinity (SEC>3100 μS cm^{-1}) and should correspond to traces of saline water of an older generation. This hypothesis is supported by the observed enrichment in many trace elements (*e.g.*, I, Be, Li, F). In the intermediate part of the aquifer layer groundwater is of lower salinity (~500 μS cm^{-1}), chloride concentrations can be lower than 40 mg L^{-1}. This salinity stratification

corresponds probably to different percentages of old sea water trapped in the sediments before the sea level rise during the Late Pleistocene-Early Holocene. Bicarbonate does not show any stratification in this layer (~120 mg L^{-1}) and sulphate concentrations are less than 60 mg L^{-1}. This aquifer layer still shows some enrichment in minor elements such as Si and Li that are related to increasing residence times. The same enrichment can be observed for the stable isotope.

Stable isotope data obtained for the various depth samples collected have been plotted in the following Fig. 5.26 and show the vertical stratification for the different aquifer layers. This stratification should reflect different recharge conditions and residence times for the groundwater flowing in the aquifer layers.

Groundwater samples which inorganic chemistry suggested mixing with Quaternary aquifer water plot indeed on the meteoric line confirming that mixing with modern recharge is taking place. All the rest of the samples show some stable isotope enrichment plotting above or below the local meteoric water line, but following a trend from right to left that reflects their geological origin.

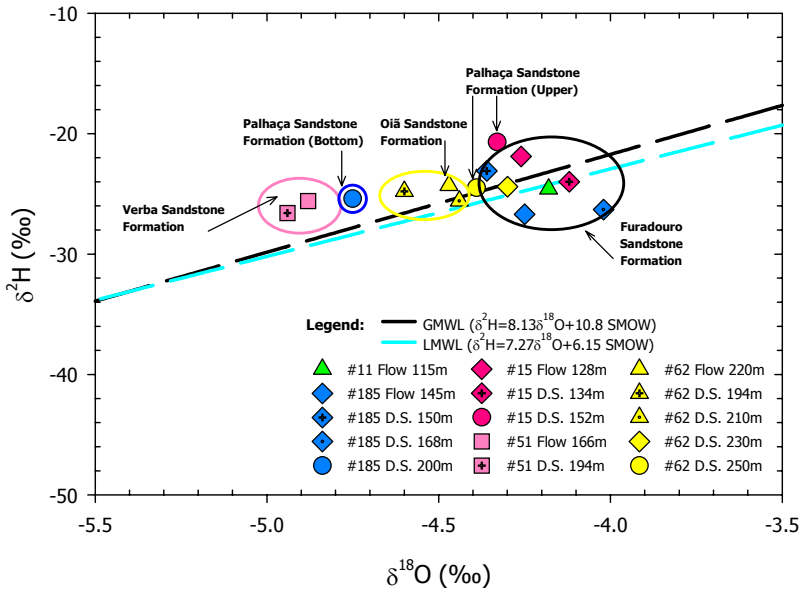

Fig. 5.26 $\delta^{18}O$- $\delta^{2}H$ plot of the water samples collected from the discharge and the corresponding depth samples for each of the boreholes sampled during the depth sampling campaign in December 2000. Different symbology is used for each of the aquifer layers (□ for the Verba sandstone formation, △ for the Oiã sandstone formation, ◇ for the 'Furadouro sandstone formation' and ○ for the 'Palhaça sandstone formation').

5.4 Complementing the study of groundwater baseline quality using geostatistics

Groundwater chemical composition as other important hydrogeological variables are function of space (and/ or time) and very often highly variable. However, this spatial variability is, in general, not purely random but there is some kind of correlation in the spatial distribution. Matheron (1971)

has given the name of regionalised variables to this type of variables, which have properties intermediate between truly random variables and the ones completely deterministic.

Typical regionalised variables are functions describing natural random processes that have geographic distributions and show continuity from point to point. However, the degree of spatial dependence between samples is so complex that can't be described using a deterministic function but requires a geostatistic measure.

This probabilistic approach assumes that adjacent samples are correlated to one another and that the degree of spatial dependence between samples along a specific direction can be analytically and statistically translated in a function known as the semivariogram $\gamma(\mathbf{h})$:

$$\gamma(h) = \frac{1}{2} E\left\{ [Z(x+h) - Z(x)]^2 \right\} \qquad [5.2]$$

where **Z(x)** is a measurement of a regionalised variable taken at location **x**, and **Z(x+h)** is another measurement taken at a distance **h**, **E{Z(x)}** is the expected value of the random variable **Z(x)**, and **γ(h)** is the mean quadratic increment of **Z** between two points separated by the distance **h**.

In principle, the experimental semivariogram could be used directly to provide values for the estimation process, but in practice it is modelled by a continuous function that can be evaluated for any desired distance (Davis 1986). The model chosen has the following properties:

$$\begin{aligned} &\gamma(0) = c_0 \ , \ c_0 \geq 0 \\ &\gamma(a) = c > c_0 \ , \ a > 0 \\ &\gamma(h) = c, \ h \geq a \end{aligned} \qquad [5.3]$$

where, the constant $\mathbf{c_0}$ is called the nugget effect and represents any small-scale data variability or possible sampling errors, the constant **c** is called the sill and should roughly equal the sample variance. The smallest distance at which the variogram reaches the sill (h=a), is called the range and represents the distance upon which the samples are independent (or uncorrelated).

The experimental variogram can be fitted using different models, but usually in geosciences the spherical model is the most widely used (Equation [5.4]):

$$\gamma(h) = \left(\frac{3}{2}\frac{h}{a} - \frac{1}{2}\frac{h^3}{a^3} \right) \sigma^2 \ , \text{ for } 0 \leq h \leq a \quad \vdots \quad \gamma(h) = \sigma^2 \ , \text{ for } h > a \qquad [5.4]$$

Detailed descriptions of this and other common models (Gaussian model, hole-effect model, pure nugget-effect model, power model, linear model and logarithmic model) can be found in specialised literature (Goovaerts, 1997; Houlding, 2000).

The theory of regionalised variables has been used for the study of groundwater baseline composition of the Aveiro Cretaceous. Sampled data for geochemical characterisation of the aquifer was unevenly distributed within the study area and did not follow necessarily a regular grid. Ideally, the values of the variables were desired on a much more regular and eventually finer grid to assess correctly the spatial variability of the data.

This presented the geostatistical problem of estimating the behaviour of the variables in unsampled regions of the study area or where geochemical data was scarce. A good estimator was considered to be the procedure or formula that used the observable spatial correlation between the available sample points to find a representative and reliable value, or estimate, of the unknown quantity.

Kriging, which is a geostatistic estimation technique and was the optimal estimating technique selected for the present study and involves applying the general methodology known as best linear unbiased estimation (BLUE) to intrinsic functions. In other words, kriging is a method for optimising the estimation of a magnitude, which is distributed in space and is measured at a network of points.

The theory of kriging as well as its implementation on a computer is straightforward, despite the intimidating equations it involves. A detailed description of the method can be found for example in Davis (1986), Cressie (1991) or Clark & Harper (2000), and for specific applications to hydrogeology in Marsily (1986) or Kitanidis (1997).

The principal features of this interpolation method are considered to be:

- the estimator is a linear function of the data with weights calculated according to the specifications of unbiasedness and minimum variance, that means that on the average, the error of estimation is zero and the square estimation error is as small as possible.
- the weights are determined by solving a system of linear equations which coefficients depend only on the variogram that describes the variables spatial structure.
- kriging system will always have a unique solution providing we have used a mathematically acceptable variogram and there are no redundant measurements;
- kriging is an 'exact' interpolator in the case of continuous functions reproducing the measured value and having a mean square estimation error equal to zero. However, when the variogram has a nugget effect, the estimate at the measurement points is a discontinuous function but is continuous everywhere else.

Kriging major advantages, when compared to other methods used in interpolation and spatial averaging, are:

- It's flexibility. The weights are not selected on the basis of an arbitrary rule but take into account the relative distance between measurements and from the locations where an estimate is sought;
- The possibility of evaluating the magnitude of the estimation error through the calculation of the mean square error.

The main limitation of kriging and other equivalent linear estimation methods is that they implicitly assume that the available information about the spatial structure of the spatial function can be described adequately through a variogram.

5.4.1. **Exploratory data analysis**

The principal objectives of this exploratory data analysis was to familiarise with the data, check data quality, and in particular to detect patterns of regularity highlighting interesting features of the data set.

This was achieved for Aveiro Cretaceous aquifer using a straightforward methodology, that included the calculation of data summary statistics, such as the:

- arithmetic mean (μ) and the median ($\mathbf{y_{0.50}}$);
- maximum (**MAX**) and minimum (**MIN**) values;
- variance (σ^2), lower ($\mathbf{y_{0.25}}$)/ upper ($\mathbf{y_{0.75}}$) quartiles, 10th ($\mathbf{y_{10}}$)/ 90th ($\mathbf{y_{90}}$)/ 95th ($\mathbf{y_{95}}$) percentiles and standard deviation (σ);
- first Pearson skewness coefficient (**FCS**).

for 71 elements or parameters, that include 5 field parameters (T, pH, Eh, DO, SEC), 9 major elements (Na, K, Ca, Mg, Si, Cl, HCO_3, SO_4, NO_3-N), 39 minor and trace elements (NO_2-N , NH_4-N, TOC, Ag, Al, As, B, Ba, Be, Bi, Br, Cd, Co, Cr, Cs, Cu, F, Fe, Ga, Ge, I, Li, Mn, Mo, Ni, P, Pb, Rb, Sb, Sc, Se, Sr, Th, Ti, U, V, Y, Zn, Zr), 14 rare earth elements (La, Ce, Pr, Nd, Sm, Eu, Gd, Tb, Dy, Ho, Er, Tm, Yb, Lu) and 4 isotopes (^{18}O, ^{2}H, ^{13}C and ^{14}C).

Summary statistics calculated are shown in Table 5.2 and outline conveniently the most important features of experimental distribution of data population, providing a selection of representative central and extreme values, and a measure of the spread and degree of symmetry of the observations in the data set.

The experimental data do not follow a normal distribution for any of the elements or parameters. However, pH data distribution almost approximates a normal distribution shifting slightly to the left. The trace element vanadium and the stable isotopes also are the other

parameters that also show a negative skewness, but all the rest show a positive skewness with a long tail of high values and calculated mean values higher than the corresponding median values.

Complementary, graphical methods were used to represent in a concise yet informative way the experimental distribution of the data. The two graphical methods preferred were the:

- **box plot diagrams**, which are very useful display for summarising the distribution of data set. The upper and lower quartiles of the data define the top and bottom of a rectangle (the 'box'), and horizontal lines segments inside the box portray the median and the mean (Fig. 5.27). The lower and upper inner fence values are the lowest and largest observed values, respectively, provided that they are less than 1.5 times the interquartile range.

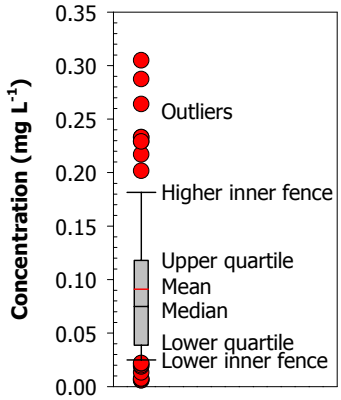

Fig. 5.27 Box plots of concentration data

The obtained box plots confirm that the data are distributed in a highly asymmetric way and also show the existence of outliers. These values exceed 1.5 times the interquartile range but going back to the data source it was concluded that they are not errors, but rather correspond to samples from boreholes that are pumping higher salinity waters due to the inadequate placement of the screens. As these data were considered reliable it was decided to keep these outlier values although they affect the mean and the variance values of the population.

- **histograms**, are very important graphs for ascertaining asymmetry in the experimental distribution of measured data. Histogram plots result from plotting the number of measurements (**n**) that belong to the **k-th** interval or the frequency of occurrence in the k-th interval ($\mathbf{n_k/n}$) as a bar diagram Data distribution for field parameters, major, minor and trace elements, and isotopes were divided in 10 intervals of equal frequency. Histograms showed the non-normal distribution of the data set with the data distributions shifting towards the high values. This tendency should reflect the existence of some high salinity samples and not be produced by analytical errors.

Table 5.2. Extreme values and measures of central tendency, spread and degree of symmetry of groundwater geochemical data.

	T (°C)	pH	Eh (mV)	O_2	SEC	Na	K	Ca	Mg	Si	Cl	HCO_3	SO_4	NO_3-N	NO_2-N	NH_4-N	DOC	Ag
No of data values	88	90	88	86	88	90	90	90	90	90	90	90	90	90	64	85	29	90
No of values < DL[a]	0	0	0	0	0	0	0	0	0	0	0	0	0	71	59	76	0	87
Minimum	16.7	5.0	-140.0	0.0	70.0	13.5	2.0	1.2	0.5	2.9	15.9	4.2	0.8	0.005	0.003	0.010	0.1	0.000022
Maximum	30.8	9.2	691.4	15.6	1850.0	538.0	27.4	125.0	45.1	10.4	941.0	438.0	325.0	17.700	0.400	1.770	11.0	0.000200
Mean, μ	20.9	7.3	122.6	2.1	558.9	91.6	8.3	26.7	7.9	5.8	88.9	139.7	61.1	1.041	0.030	0.041	2.3	0.000095
Variance, σ^2	8.4	0.6	24141	8.3	172520	10598	17.8	760.9	50.1	1.7	16473	6331	3638	7.891	0.009	0.037	6.6	6.84E-09
Standard deviation, σ	2.9	0.8	155.5	2.9	415.8	103.5	4.2	27.7	7.1	1.3	129.1	80.0	60.7	2.731	0.096	0.193	2.6	0.000083
Lower quartile ($y_{0.25}$)	18.5	6.8	12.3	0.2	321.8	24.3	5.5	7.0	3.7	5.1	29.0	93.0	20.8	0.020	0.003	0.010	0.8	0.000022
Median ($y_{0.50}$)	20.7	7.3	92.0	1.1	420.5	54.5	7.9	17.6	6.1	5.7	40.6	131.4	46.1	0.105	0.005	0.010	1.5	0.000040
Upper quartile ($y_{0.75}$)	23.0	7.9	210.6	2.9	588.3	93.4	9.9	30.5	8.3	6.3	79.4	159.0	67.7	0.500	0.005	0.020	2.8	0.000200
10th Percentile (y_{10})	17.9	6.3	-33.3	0.0	222.9	16.9	3.8	3.6	2.4	4.5	24.4	60.9	12.8	0.005	0.003	0.010	0.5	0.000022
90th Percentile (y_{90})	24.3	8.2	349.1	5.2	1301.1	250.1	12.4	69.4	15.8	7.3	213.7	231.4	131.1	2.930	0.010	0.020	5.7	0.000200
95th Percentile (y_{95})	26.0	8.2	375.4	6.6	1572.5	323.9	16.6	87.4	22.2	8.8	333.5	274.4	184.4	5.130	0.346	0.036	7.6	0.000200
Skewness Coef., FCS	0.8	-0.3	0.9	2.5	1.8	2.1	1.7	1.9	2.6	1.0	4.0	1.5	2.1	4.1	3.7	8.8	2.1	0.5

	Al	As	B	Ba	Be	Bi	Br	Cd	Co	Cr	Cs	Cu	F	Fe	Ga	Ge	I	Li
No of data values	90	90	90	90	90	90	90	90	90	90	90	90	90	90	90	90	90	90
No of values < DL[a]	6	13	1	0	12	81	0	60	9	34	2	12	0	2	37	3	0	0
Minimum	0.000319	0.000132	0.000000	0.006000	0.000010	0.000010	0.044000	0.000010	0.000010	0.000036	0.000037	0.000139	0.020000	0.006000	0.000008	0.000010	0.001200	0.001306
Maximum	0.493000	0.034097	1.350000	0.305000	0.017392	0.000236	3.150000	0.006229	0.052494	0.009978	0.002492	0.038646	3.700000	7.530000	0.000278	0.000448	0.147000	0.274000
Mean, μ	0.014035	0.003917	0.200983	0.091081	0.000568	0.000065	0.283294	0.000114	0.001420	0.000856	0.000327	0.003414	0.563889	0.625616	0.000044	0.000158	0.010362	0.024680
Variance, σ^2	0.002741	0.000049	0.084369	0.004149	3.71E-06	4.89E-09	0.151007	4.37E-07	0.000037	0.000003	1.63E-07	0.000043	0.724915	1.572290	3.17E-09	9.49E-09	0.000375	0.001182
Standard deviation, σ	0.052604	0.006814	0.287896	0.064502	0.001879	0.000070	0.397505	0.000661	0.006141	0.001731	0.000405	0.006654	0.856189	1.260805	0.000041	0.000095	0.019474	0.034582
Lower quartile ($y_{0.25}$)	0.002447	0.000762	0.050197	0.040063	0.000100	0.000010	0.102250	0.000018	0.000034	0.000120	0.000100	0.000311	0.157500	0.065000	0.000015	0.000091	0.003700	0.009826
Median ($y_{0.50}$)	0.005266	0.001581	0.111531	0.074918	0.000182	0.000024	0.153500	0.000029	0.000116	0.000196	0.000196	0.000971	0.270000	0.135500	0.000039	0.000142	0.005674	0.014374
Upper quartile ($y_{0.75}$)	0.008816	0.003237	0.197500	0.117250	0.000324	0.000172	0.293000	0.000032	0.000364	0.000772	0.000355	0.002685	0.410000	0.512750	0.000047	0.000197	0.009397	0.023819
10th Percentile (y_{10})	0.001903	0.000482	0.015556	0.027389	0.000075	0.000010	0.090000	0.000010	0.000016	0.000062	0.000060	0.000275	0.050000	0.024889	0.000010	0.000059	0.002580	0.006194
90th Percentile (y_{90})	0.021155	0.009658	0.442000	0.171500	0.000952	0.000172	0.672900	0.000052	0.001922	0.001503	0.000686	0.007709	2.119000	1.676000	0.000085	0.000293	0.014129	0.047817
95th Percentile (y_{95})	0.035456	0.021167	0.944449	0.223600	0.002033	0.000172	0.789534	0.000085	0.003053	0.004331	0.001049	0.016098	2.740000	3.428500	0.000105	0.000341	0.026864	0.081100
Skewness Coef., FCS	8.7	3.1	2.7	1.2	8.3	0.9	4.8	9.1	7.1	3.9	3.0	3.4	2.5	3.4	3.0	0.8	5.5	4.9

	Mn	Mo	Ni	P	Pb	Rb	Sb	Sc	Se	Sr	Th	Ti	U	V	Y	Zn	Zr	
No of data values	90	90	90	90	90	90	90	90	90	90	90	90	90	90	90	90	90	
No of values < DL[a]	0	31	3	77	20	0	68	57	29	0	34	31	16	59	14	6	50	
Minimum	0.000301	0.000100	0.000056	0.100000	0.000029	0.001640	0.000010	0.000800	0.000200	0.008213	0.000001	0.000010	0.000002	0.000050	0.000003	0.001227	0.000010	
Maximum	0.242000	0.006228	0.078524	3.000000	0.027334	0.051667	0.001218	0.004387	0.024047	0.576000	0.000398	0.014127	0.042747	0.006000	0.006601	1.560000	0.179000	
Mean, μ	0.031192	0.000554	0.004758	0.311111	0.000842	0.011364	0.000414	0.001210	0.002692	0.139070	0.000049	0.000817	0.001365	0.003989	0.000194	0.091855	0.006314	
Variance, σ^2	0.001760	0.000001	0.000134	0.349313	0.000013	0.000090	2.82E-07	4.29E-07	0.000017	0.013827	5.82E-09	2.74E-06	0.000029	1.07E-05	6.80E-07	0.075080	0.000358	
Standard deviation, σ	0.042165	0.000925	0.011635	0.591027	0.003669	0.009544	0.000531	0.000655	0.003596	0.118247	0.000064	0.001656	0.005395	0.002635	0.000829	0.275512	0.018917	
Lower quartile ($y_{0.25}$)	0.005344	0.000142	0.000855	0.100000	0.000100	0.005799	0.000016	0.000800	0.000775	0.054025	0.000007	0.000033	0.000028	0.000563	0.000007	0.003823	0.000042	
Median ($y_{0.50}$)	0.017247	0.000217	0.001670	0.200000	0.000207	0.008219	0.000053	0.000800	0.002298	0.104413	0.000013	0.000082	0.000066	0.006000	0.000012	0.014982	0.006000	
Upper quartile ($y_{0.75}$)	0.038145	0.000400	0.003120	0.200000	0.000352	0.012924	0.001148	0.001486	0.003042	0.166000	0.000131	0.001313	0.000400	0.006000	0.000041	0.032463	0.006000	
10th Percentile (y_{10})	0.002393	0.000111	0.000243	0.100000	0.000048	0.004334	0.000010	0.000800	0.000214	0.039290	0.000003	0.000010	0.000009	0.000348	0.000005	0.001986	0.000014	
90th Percentile (y_{90})	0.073048	0.001594	0.007958	0.300000	0.000791	0.020656	0.001218	0.002125	0.005070	0.304600	0.000131	0.001692	0.001423	0.006000	0.000213	0.124731	0.008000	
95th Percentile (y_{95})	0.106462	0.002247	0.014488	0.665000	0.001147	0.028114	0.001218	0.002372	0.007971	0.393750	0.000131	0.002167	0.003657	0.006000	0.000627	0.540396	0.009550	
Skewness Coef., FCS	2.9	3.7	4.7	4.3	6.6	2.5	0.8	1.9	4.1	1.7	2.2	6.1	6.1	-0.6	6.6	4.3	8.7	

	La	Ce	Pr	Nd	Sm	Eu	Gd	Tb	Dy	Ho	Er	Tm	Yb	Lu	^{18}O (‰)	^{2}H (‰)	^{13}C (‰)	^{14}C (pmC)
No of data values	90	90	90	90	90	90	90	90	90	90	90	90	90	90	78	78	78	24
No of values < DL[a]	20	28	51	52	59	53	58	75	63	73	69	78	66	79	0	0	0	0
Minimum	0.000001	0.000002	0.000001	0.000004	0.000002	0.000001	0.000002	0.000001	0.000001	0.000001	0.000001	0.000001	0.000001	0.000001	-5.60	-33.00	-25.02	0.91
Maximum	0.002515	0.006845	0.001554	0.009061	0.002339	0.000460	0.002480	0.000312	0.001554	0.000235	0.000653	0.000081	0.000469	0.000072	-4.09	-20.50	-7.32	73.29
Mean, μ	0.000077	0.000184	0.000051	0.000223	0.000076	0.000031	0.000080	0.000023	0.000049	0.000021	0.000034	0.000018	0.000030	0.000016	-4.68	-25.74	-13.38	16.48
Variance, σ^2	8.45E-08	6.20E-07	3.14E-08	1.08E-06	7.40E-08	3.49E-09	8.75E-08	1.80E-09	3.33E-08	1.30E-09	6.63E-09	7.00E-10	3.86E-09	5.66E-10	0.08	4.27	11.15	161.22
Standard deviation, σ	0.000291	0.000786	0.000177	0.001039	0.000272	0.000059	0.000296	0.000042	0.000183	0.000036	0.000081	0.000026	0.000062	0.000024	0.28	2.15	3.38	19.63
Lower quartile ($y_{0.25}$)	0.000005	0.000007	0.000004	0.000009	0.000006	0.000004	0.000005	0.000001	0.000004	0.000001	0.000002	0.000001	0.000002	0.000001	-4.84	-27.33	-15.67	3.47
Median ($y_{0.50}$)	0.000008	0.000020	0.000006	0.000017	0.000008	0.000006	0.000010	0.000003	0.000007	0.000002	0.000007	0.000002	0.000006	0.000002	-4.71	-25.60	-12.87	7.08
Upper quartile ($y_{0.75}$)	0.000023	0.000056	0.000054	0.000064	0.000089	0.000065	0.000083	0.000059	0.000051	0.000058	0.000062	0.000060	0.000064	0.000054	-4.46	-24.27	-10.49	29.67
10th Percentile (y_{10})	0.000003	0.000004	0.000001	0.000004	0.000002	0.000004	0.000002	0.000001	0.000001	0.000001	0.000001	0.000001	0.000001	0.000001	-5.02	-28.50	-17.75	1.92
90th Percentile (y_{90})	0.000093	0.000125	0.000054	0.000131	0.000089	0.000065	0.000083	0.000059	0.000051	0.000058	0.000062	0.000060	0.000064	0.000054	-4.36	-23.27	-9.79	41.79
95th Percentile (y_{95})	0.000359	0.000574	0.000149	0.000776	0.000181	0.000065	0.000193	0.000059	0.000106	0.000058	0.000062	0.000060	0.000064	0.000054	-4.25	-22.64	-9.29	50.92
Skewness Coef., FCS	7.1	7.3	7.4	7.6	7.2	5.2	7.1	4.1	7.2	3.0	5.9	1.0	4.9	1.0	-0.4	-0.3	-0.8	1.5

[a]DL = Detection Limit

[b]Unless stated, all values for major, minor and trace elements are in mg L^{-1} and SEC is in μS cm^{-1}

5.4.2. **Variogram Analysis**

The spatial variability and continuity of the analysed samples was characterised by determining an average measure of variable correlation, such as the covariance, and through the calculation of the experimental variograms. The elements and parameters considered for this type of analysis were those ones that had at least 60% of the results above detection limit, and so the compounds NO_2-N, NH_4-N, the trace elements Ag, Bi, Cd, P, Sb, Sc, Zr and the rare earth elements (Pr, Nd, Sm, Eu, Gd, Tb, Dy, Ho, Er, Tm, Yb, Lu) were not included. Although, NO_3-N content was below detection limit in 79% of the analysed samples it was exceptionally considered for the spatial continuity characterisation as this compound is considered to be a good indicator of the human impact on the pristine palaeowaters.

The omni-directional (90 degree angular tolerance) and directional (0º, 45º, 90º and 135º, with a 15 degree angular tolerance) experimental variograms for each variable were calculated using Variowin® (Pannatier, 1996) a programme for exploratory variography in 2-D. The directions selected (in particular, the 0º and 135º) were considered to include the principal aquifer flowpaths.

A choice of distance class and number of lags were experimented, based on sampling density (~1 sample/ 16 km^2) and taking into account half of the maximum E-W and N-S distances of the study area, respectively 13 km and 27 km. The optimum number of lags was considered to be 5, for a maximum lag spacing of 2.6 km in the E-W direction and 5.4 km in the N-S direction. Intermediate lag spacing were considered for the remaining directions.

5.4.3. **Variogram modelling**

Experimental variograms were modelled using the programme Model®, an application from Variowin® package that includes interactive modelling of geometric and zonal anisotropies. The modelling process included: (1) the identification and approximate estimation of principal graphical characteristics (nugget effect, sill and range) of the experimental variogram; (2) selection of the adequate variogram model; (3) determination of the covariance; (4) semi-automatic curve fitting of the experimental variograms by supplying the values of the nugget effect, sill and range, and considering that the sum of the nugget effect plus the sill should approximate the variance; (5) verification of the final fitting error as indicative of the goodness of the fit. The fitting parameters are summarised in the following Table 5.3.

With the exception of radioisotope carbon-14 experimental data that was best fitted using a linear variogram, the experimental variograms for the other variables were approximated using a spherical model and in most cases showed a discontinuity at the origin (nugget effect). Just Al, Ce, Li, NO_3-N, Se, T, Ti and Y experimental variograms had no nugget effect. These discontinuities

were interpreted as indicative of fluctuations at a scale smaller than the sampling interval and the hypothesis of measurement errors was discarded.

Table 5.3. Experimental variogram modelling results and fitting parameters.

Parameter	Covariance	Model	C_0 (1)	C_1 (2)	a_{min} (3)	Direction	Geometric Anisotropy
^{13}C	1.12E+01	Spherical	4.50E+00	6.65E+00	9500	0º	2.90
^{14}C	1.61E+02	Linear	1.61E+02				1.00
^{18}O	7.29E-02	Spherical	4.00E-02	3.29E-02	16000	0º	1.00
^{2}H	4.27E+00	Spherical	2.50E+00	1.77E+00	16000	0º	1.00
Al	2.74E-03	Spherical	0.00E+00	2.74E-03	13000	0º	1.00
As	4.90E-05	Spherical	2.80E-05	2.10E-05	8500	0º	1.00
B	8.44E-02	Spherical	2.00E-02	6.44E-02	6500	135º	2.00
Ba	4.15E-03	Spherical	3.00E-04	3.85E-03	5750	90º	2.00
Be	3.71E-06	Spherical	1.60E-06	2.11E-06	10000	0º	1.00
Br	1.51E-01	Spherical	2.00E-02	1.31E-01	27000	135º	1.50
Ca	7.61E+02	Spherical	1.80E+02	5.81E+02	19500	0º	1.00
Ce	6.20E-07	Spherical	0.00E+00	6.20E-07	10000	0º	1.00
Cl	1.65E+04	Spherical	2.00E+03	1.45E+04	15500	45º	2.10
Co	3.73E-05	Spherical	6.00E-06	3.13E-05	13000	45º	1.40
Cr	3.23E-06	Spherical	2.00E-07	3.03E-06	14000	90º	2.50
Cs	1.63E-07	Spherical	3.00E-08	1.33E-07	5000	45º	4.00
Cu	4.43E-05	Spherical	8.00E-06	3.63E-05	7920	135º	3.03
Eh	2.41E+04	Spherical	4.00E+03	2.01E+04	10000	0º	1.00
F	7.25E-01	Spherical	2.00E-01	5.25E-01	4500	135º	2.00
Fe	1.57E+00	Spherical	8.00E-01	7.72E-01	4550	45º	2.86
Ga	3.17E-09	Spherical	1.20E-09	1.97E-09	12000	0º	2.00
Ge	9.49E-09	Spherical	2.00E-09	7.49E-09	6000	90º	2.00
HCO_3	6.33E+03	Spherical	2.00E+03	4.33E+03	6300	90º	1.67
I	3.75E-04	Spherical	1.00E-04	2.75E-04	9000	135º	1.50
K	1.78E+01	Spherical	6.00E+00	1.18E+01	11000	45º	2.70
La	8.41E-08	Spherical	2.20E+00	6.21E-08	12000	0º	1.00
Li	1.18E-03	Spherical	0.00E+00	1.18E-03	6875	45º	1.82
Mg	5.01E+01	Spherical	8.00E+00	4.21E+01	18000	45º	1.11
Mn	1.76E-03	Spherical	2.00E-04	1.56E-03	4600	45º	4.35
Mo	9.52E-07	Spherical	5.00E-07	4.52E-07	20000	0º	1.00
Na	1.06E+04	Spherical	2.80E+03	7.80E+03	11900	45º	1.43
Ni	1.34E-04	Spherical	8.00E-05	5.40E-05	5000	0º	1.00
NO_3-N	7.89E+00	Spherical	0.00E+00	7.89E+00	18000	0º	1.00
Pb	1.34E-05	Spherical	2.00E-06	1.14E-05	18000	135º	1.50
pH	5.95E-01	Spherical	1.50E-01	4.45E-01	9800	0º	3.90
Rb	9.03E-05	Spherical	1.00E-05	8.03E-05	4000	45º	4.00
Se	1.74E-05	Spherical	0.00E+00	1.74E-05	2800	0	1.00
SEC	1.73E+05	Spherical	1.20E+05	5.25E+04	6500	45º	2.00
Si	1.73E+00	Spherical	8.00E-01	9.31E-01	20000	0º	1.00
SO_4	3.64E+03	Spherical	1.00E+03	2.64E+03	11000	0º	2.00
Sr	1.38E-02	Spherical	3.00E-03	1.08E-02	7750	0º	2.00
T	8.43E+00	Spherical	0.00E+00	8.43E+00	12000	0º	2.00
Th	5.82E-09	Spherical	2.00E-09	3.82E-09	17500	45º	1.43
Ti	2.74E-06	Spherical	0.00E+00	2.74E-06	12000	0º	1.00
U	2.88E-05	Spherical	5.00E-06	2.38E-05	12000	0º	1.00
V	1.07E-05	Spherical	6.00E-06	4.70E-06	13000	45º	1.50
Y	6.80E-07	Spherical	0.00E+00	6.80E-07	10000	0º	1.00
Zn	7.51E-02	Spherical	3.00E-02	4.51E-02	4000	0º	2.50

(1) Nugget Effect (2) Sill (3) Minimum range

The following variables (Al, As, Be, Ca, Ce, Eh, La, Mo, Ni, NO_3-N, Se, Si, Ti, U, Y, ^{18}O and ^{2}H) show isotropic distributions within the study area with increasing range values. The rest of the variables show different degrees of anisotropy, being the principal direction of continuity along the

main flow path (135º). That is case of the alkali group metals (Li, Na, K, Rb and Cs), alkali earth group metal Mg, transition elements (V, Mn, Fe, Co), chloride ion (Cl), thorium (Th) and field parameter defined as specific electrical conductance (SEC). With the same type of anisotropy (45º-135º) but with the maximum range along the 45º axe contrasting with chloride behaviour, are the other halides, iodide, bromide and fluoride. All the rest of the parameters have anisotropy 0º-90º.

5.4.4. **Kriging estimates**

With the experimental variograms modelled, the ordinary kriging equations were set up and solved for the estimation on a fine grid over the site. The grid chosen is a 767 by 1555 rectangular grid with origin at (509 175, 4 452 300). This gives a grid spacing of about 50 metres in both directions. No specific search radio was used, which means that all the available data points were considered when interpolating each grid node. The minimum and maximum number of samples to include in the estimation was set to be equal to the number of data sets available, without applying any data exclusion filter.

The maps showing the kriged values of the different parameters over the site are included in Annex D. The system of kriging equations was singular for the elements Ce and Y so the correspondent contour maps could not be plotted.

The contour maps neatly show the spatial distribution of groundwater geochemical composition in the Aveiro Cretaceous aquifer, clearly identifying the deeper part of the aquifer between the town of Vagos and the coast. Some of these spatial trends were masqueraded and difficult to infer from the previously used scatter plots. And although the kriging process smoothed the data, the principal areas of higher salinity are clearly identified in the northwest (due to increased time residence, mixing with higher salinity waters and the proximity of the sea) and in the East in the adjacent areas to the Pateira de Fermentelos lagoon.

Inflows of fresh low salinity water are visible in the south and southeast and agree with the previous definition of the recharge area. Unfortunately these recharge waters are also easily traced by the human impact signature. They show detectable levels of nitrate and nitrite concentration, although still below the maximum admissible concentration (MAC) for human consumption.

The physical boundaries of the aquifer coinciding with different lithologies are also easily identified. The presence of Jurassic limestone layers underneath the aquifer in the southeast and adjacent to the aquifer in the south is clearly shown by the increase in calcium, magnesium, strontium and sulphate contents in groundwaters of these areas.

Iron contour map shows that excluding a cross-section along the central part of the study area all the rest of the area exceeds the iron MAC value. Besides, it calls attention in particularly to the region of Cacia where significant high iron concentrations have been determined (exceeding 2.5 mg L^{-1}). The same trend is corroborated by the manganese contour map, which in this area also exceeds manganese MAC value (50 mg L^{-1}). Although unconfined in this area, measurable dissolved oxygen indicates a suboxic environment (O_2< 0.12 mg L^{-1}). Average Eh value is higher than 90 mV, pH shows relative constancy around 6.5 and groundwater total organic carbon is about 1.5 mg L^{-1}. Besides the upper and lower aquifer layer contain abundant goethite and traces of pyrite. Pyrite is also present in the principal aquifer layer. The high concentration of manganese and iron in this area suggests Mn (IV) and Fe(III) reduction.

5.4.5. **Classed post maps**

As the kriging process attenuated the extreme values of the studied population, it was decided to use classed post maps to determine the distribution and density of 25 major, minor and trace elements (Al, As, B, Ba, Be, Ca, Cd, Cl, Cr, Cu, F, Fe, Mn, Mo, Na, NH_4-N, Ni, NO_2-N, NO_3-N, Pb, Sb, Se, SO_4, U, Zn) and the total hardness. Some of these elements/ compounds are of health significance and others can give aesthetic characteristics to the groundwater having guideline values (GV) or even maximum admissible concentration (MAC) values in drinking water.

The maps have been included in Annex E and alerting for areas of particularly high concentrations. Chemical data values were grouped into eight different classes. The ranges of these classes were set to correspond to the minimum, the 5th/25th/50th/75th/90th/95th/98th percentiles, and the maximum value of the distribution. The legend of these maps includes as a guideline the European Commission (EC) MAC values for drinking water in agreement with the new Water Framework Directive (98/83/EC).

These maps show that within the studied aquifer, a range of naturally occurring concentrations for the different elements/ compounds is found and occasionally, in some parts these concentrations are found to be at concentrations above the present EC maximum admissible concentrations for drinking water. This range of concentrations is considered to reflect natural conditions, resulting from water-rock interaction and not to indicate pollution, except in a few extreme cases located in the unconfined part of the aquifer.

However, if baseline values are defined for the aquifer corresponding to the median ($Y_{0.50}$) concentrations and these were summarised before in Table 5.2, then the baseline values for all the studied elements/ compounds are below the EC MAC values, although positive data are analysed in most boreholes. The baseline values quoted can be regarded as the best single value of the natural unpolluted background for an element in the aquifer.

If instead of the median the 90th percentile ($Y_{0.90}$) was considered, then five elements (Na, Cu, F, Fe, Mn) already exceed the MAC value. In the case of taking into account the 98th percentile ($Y_{0.98}$) then besides the previous mentioned five elements, also chloride, arsenic, nickel, selenium and boron would exceed the MAC value. Iron concentrations exceed EC drinking-water guidelines in at least 42% of the boreholes, while manganese MAC value is exceeded in 13% of the wells. Nutrients (NO_3-N) were detected in low concentrations throughout the aquifer. But just about 20% of the boreholes had positive values of NO_3-N, but only 2% exceeded the MAC value.

5.5 Geochemical modelling

The main geochemical processes that account for the observed water chemistry evolution in the Aveiro Cretaceous aquifer were quantified and simulated using a geochemical reaction-path model.

A geochemical model quantifies the main geochemical processes that occur in the aquifer in combination with the transport characteristics of groundwater flow. Reaction-path models are oriented towards system equilibrium rather than just aqueous equilibrium. Essentially, all of the moles of each element in the system are distributed among the aqueous phase, pure phases, solid solutions, gas phase, exchange sites and surface sites to attain system equilibrium (Parkhurst & Appelo, 1999).

The computer program used to make the reaction-path calculations was PHREEQC version 2 (Parkhurst & Appelo, 1999). PHEREEQC-2 was selected because it is considered the state of art reactive transport model, is chemically well founded and is versatile, and thereby a powerful code to analyse geochemical processes occurring in natural systems. Its robustness compensates the weakness of not being a two dimensional model, which are usually more computer time consuming and not yet free from numerical problems.

PHREEQC-2 is designed to perform a wide variety of low-temperature aqueous geochemical calculations and is based on an ion-association aqueous model. It has capabilities for (1) speciation and saturation-index calculations; (2) reaction-path and 1D-transport calculations involving reversible and irreversible reactions; and (3) inverse modelling. PHREEQC-2 has also the capability to model several one-dimensional transport processes including (1) diffusion, (2) advection, (3) advection and dispersion, and (4) advection and dispersion with diffusion into stagnant zones (dual porosity media). All of these processes can be combined with equilibrium and kinetic chemical reactions.

Previous geochemical modelling exercises in the aquifer used mass-balance models (Oliveira, 1997; Carreira Paquete, 1998; Condesso de Melo *et al.*, 2001). These models use a set of minerals that, when dissolved or precipitated in specified quantities, account for the change in

composition between two groundwaters. The basic assumptions of this type of models are that the two groundwater compositions are representative of waters along a single flowpath and that the final water composition evolved from the initial water composition. Plausible mass-balance models account for the chemical differences between the two waters, and in addition, should be consistent with petrographic and isotopic data and saturation indices (Parkhurst *et al.*, 1996).

5.5.1. **Transport model**

Conservation of mass for a chemical that is transported (Fig. 5.28), yields the advection-reaction-dispersion (ARD) equation, which is solved by the geochemical transport models:

$$\frac{\partial C}{\partial t} = -v\frac{\partial C}{\partial x} + D_L\frac{\partial^2 C}{\partial x^2} - \frac{\partial q}{\partial t} \qquad [5.5]$$

where C is the concentration in water (mol kgw^{-1}), t is time (s), v is pore water flow velocity (ms^{-1}), x is distance (m), D_L is the hydrodynamic dispersion coefficient [m^2 s^{-1}, $D_L=D_e+\alpha_L v$, with D_e the effective diffusion coefficient, and α_L the dispersivity (m)], and q is concentration in the solid phase (expressed as mol kgw^{-1} in the pores). The term $-v(\partial C/\partial x)$ represents advective transport, $D_L(\partial^2 C/\partial x^2)$ represents dispersive transport, and $(\partial q/\partial t)$ is the change in concentration in the solid phase due to reactions (q in the same units as C). The usual assumption is that v and D_L are equal for all solute species, so that C can be the total dissolved concentration for an element, including all redox species.

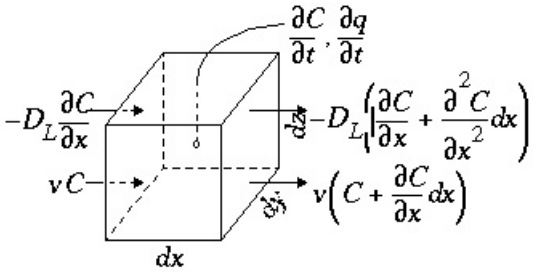

Fig. 5.28 Diagram of terms in the advection-reaction-dispersion.

The transport part of Equation [5.5] is solved with an explicit finite difference scheme that is forward in time, central in space for dispersion, and upwind for advective transport (cf. Appelo & Postma, 1996). The chemical interaction term for each element $(\partial q/\partial t)$ is calculated separately from the transport part for each time step and is the sum of all equilibrium and non-equilibrium reaction rates. The numerical approach follows the basic components of the ARD equation in a

split-operator scheme. With each time step, first advective transport is calculated, then all equilibrium and kinetically controlled chemical reactions, thereafter dispersive transport, which is followed again by calculation of all equilibrium and kinetically controlled chemical reactions. The scheme differs from the majority of other hydrogeochemical transport models in that kinetic and equilibrium chemical reactions are calculated both after the advection step and after the dispersion step. This reduces numerical dispersion and the need to iterate between chemistry and transport.

A major advantage of the split-operator scheme is that numerical accuracy and stability can be obtained by adjusting time step to grid size for the individual parts of the equation. Numerical dispersion is minimized by always having the following relationship between time and distance discretization:

$$(\Delta t)_A = \frac{\Delta X}{v} \qquad [5.6]$$

where $(\Delta t)_A$ is the timestep for advective transport, and Δx is the cell length. Numerical instabilities (oscillations) in the calculation of diffusion/dispersion are eliminated with the constraint:

$$(\Delta t)_D = \frac{(\Delta X)^2}{(3D_L)} \qquad [5.7]$$

where $(\Delta t)_D$ is the time step (s) for dispersive/diffusive transport calculations. The two conditions of equation [5.6]and [5.7] are the Courant condition for advective transport and the Von Neumann criterion for dispersive transport calculations, respectively (*e.g.*, Marsily, 1986). Numerical dispersion is in many cases negligible when $\Delta X \leq \alpha$, because physical dispersive transport is then equally or more important than advective transport.

These and more details about the PHREEQC-2 code can be found in (Parkhurst & Appelo, 1999).

5.5.2. **Conceptualization of the reaction-path transport model**

The hydrogeochemical study of the Aveiro Cretaceous aquifer confirmed the division of the aquifer in three main parts with gradually different hydrogeochemical characteristics. The outcrop area in the east part of the study area, where the infiltrating rainwater percolates through the unsaturated zone to reach the underlying groundwater body, reacting with silicate and carbonate minerals in a system initially open to CO_2. Because carbonate dissolution kinetics are much faster than the silicate weathering reactions, a fresh groundwater dominated by Ca^{2+} and HCO_3^- initially prevails. Thus the recently recharged oxygenated groundwaters are of predominantly Ca-HCO_3 hydrochemical facies, with *p*H values lower than 7.0 and water temperatures less than 20°C.

Further down the flowpath, the aquifer becomes gradually confined and with very limited modern recharge. Holocene to pre-industrial groundwater occurs in the intermediate, confined part of the aquifer. Redox potential and dissolved oxygen progressively decreases along the flowpath with groundwater changing from oxidising to reducing conditions. These are groundwaters with either Ca-HCO_3 or Na-HCO_3 hydrochemical facies and pH values higher than 6.2 but lower than 8.3 and groundwater temperatures around 21.3 ºC. P_{CO2} decreases in this part of the aquifer from 0.04 to 0.001 down flowpath and the aquifer is gradually under closed system conditions. Late Pleistocene-Early Holocene groundwaters have been identified in the deeper and confined part of the aquifer. They are Na-HCO_3 or Na-Cl type waters, with *p*H in the range from 7.1 to 8.9, and average groundwater temperatures higher than 22ºC. The negative Eh values reflect anaerobic (reducing) conditions.

Although the isotopic and chloride data show that the aquifer has been fresh for more than 18 ka, the freshening chemical pattern of the aquifer and the evolution of pH and alkalinity suggest that the aquifer has had previously sea water and that there is probably still an outlet offshore. This seawater has been almost completely flushed from the aquifer by higher hydraulic gradients during the geological periods of lowered sea level and just occurs nowadays as traces of formation water in the low permeability parts of the aquifer.

The calculated apparent flow velocities for the aquifer based on the C-14 dating indicate a gradual decrease of flow velocities along the flowpath. Flow velocities decrease from a few metres per year in the areas closer to the recharge area to less than half a metre per year in the very confined part of the aquifer (Fig. 5.29).

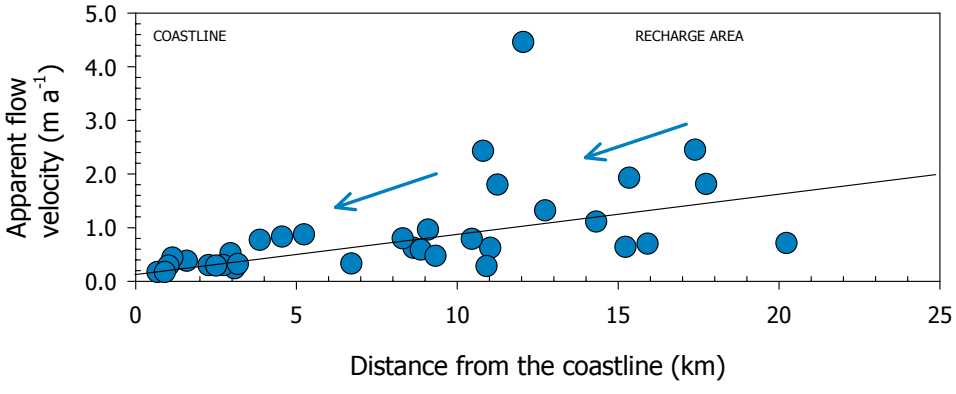

Fig. 5.29 Calculated apparent flow velocities in the Aveiro Cretaceous aquifer based on C-14 data.

Based on these evidences a conceptual model was derived for the geochemical evolution of the water in the Aveiro Cretaceous aquifer (Fig. 5.30). The conceptual model assumes that calcium bicarbonate water, which originated from rainwater infiltration and dissolution of soil CO_2,

recharges the aquifer. This water moves along the flow path reacting very slowly under closed system conditions with the carbonate and silicate minerals and mixing with traces of formation water trapped in the clay minerals, evolving to a sodium bicarbonate type water in the areas close to the coast.

The cation-exchange reaction puts calcium and magnesium onto the clays and releases sodium into solution. The cation-exchange measurements on clay samples are consistent with this cation-exchange reaction (Oliveira, 1997). The loss of calcium and magnesium from solution owing to the exchange reaction should cause some dissolution of carbonate minerals to maintain equilibrium.

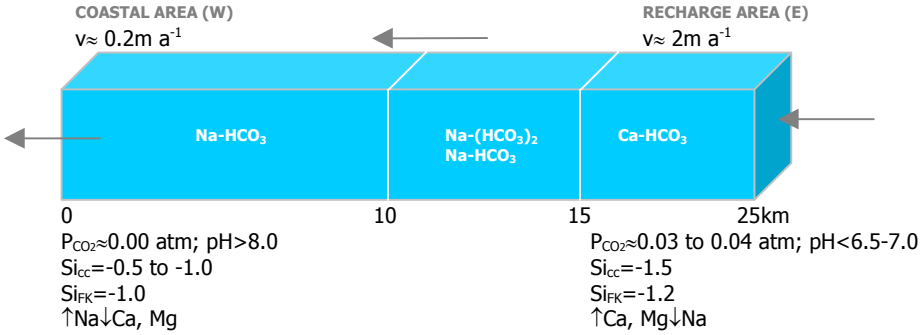

Fig. 5.30 Conceptual transport model along one W-E flow line in the Aveiro Cretaceous aquifer.

5.5.3. **Groundwater samples used for geochemical modelling**

Initial and final water compositions are needed for the reaction-path model. In this study, the initial water composition is the measured composition of a groundwater sample collected in a borehole (well#154) within the aquifer outcrop area. This sample was considered to be representative of the local recharge as it is substantially undersaturated with dolomite, calcite and most mineral phases. Its chloride content is about 20 mg L^{-1} and the sample chemical composition corresponds approximately to five-fold evaporated rainwater.

Considering the aquifer palaeohydrology (Chapter 3), seawater was assumed as the end-term. The hydrochemical data of the two water samples used in the geochemical modelling are summarised in Table 5.4.

Table 5.4. Initial and final water compositions used for geochemical modelling. The hydrochemical composition for the seawater is from Nordstrom *et al.* (1979)

Well Ref.	*p*H	T (ºC)	Na (mM)	K (mM)	Ca (mM)	Mg (mM)	Si (mM)	Al (mM)	HCO_3 (mM)	Cl (mM)	SO_4 (mM)	$\delta^{13}C$ (‰)
154	5.34	18.5	0.65	0.05	0.12	0.18	0.15	$1.0\ 10^{-3}$	0.12	0.58	0.13	-17.99
Seawater	8.22	16	468.4	10.21	10.29	53.14	0.15	$3.7\ 10^{-5}$	2.32	546	28.23	1.5

5.5.4. **Reactants used for geochemical modelling**

The potential reactants and products in the groundwater system required by the reaction-path model were defined based on the previous petrographic and mineralogic information (Chapter 2), the determined saturation indices (this Chapter 5, section 5.2.4) and on the previous results of inverse mass-mole balance modelling for the aquifer (Condesso de Melo *et al.*, 2001). The phases identified as major reactants include carbon dioxide, calcite, potassium feldspar, calcium/sodium exchange and calcium-magnesium/ sodium exchange. Dolomite, gypsum and other mineral phases had minor contributions.

The evaluation of petrographic, mineralogic and saturation indices data also helped to determine which of these mineral phases were dissolving or precipitating within the aquifer system. According to Parkhurst *et al.* (1996) the reaction-path models need to be consistent with these determinations, or otherwise, they can not be considered plausible. The chemical formulae for each reactant and the dissolution constraints, used in the modelling are summarised in Table 5.5.

Table 5.5. Mineral phases, exchange species and constraints used in the geochemical modelling.

Phases	CO_2 (+), calcite (+),K-feldspar (+)
Exchange species	CaX_2, MgX_2, NaX
Balance	Na, K, Ca, Mg, Al, Si, SO_4, Cl, TIC, Alk

(+) enters solution; (TIC) total inorganic carbon; (Alk) alkalinity

The exchangeable cations and the cation exchange capacity (CEC) of the aquifer sediments required for the model were determined in four samples of the principal aquifer layer ('Furadouro sandstone formation') by ion displacement using separately a 1 M NaCl solution and a 1 M NH_4Cl solution (*e.g.*, Andersen, 2002). The results obtained varied from a minimum value of 0.25 meq per 100 g to a maximum value of 0.56 meq per 100 g of total sediment confirming the very low cation exchange capacity, and thus the low reactivity of the aquifer matrix. These low CEC values are in agreement with the previous hydrogeochemical data, which indicated very slow kinetics for the aquifer geochemical reactions.

5.5.5. **Reaction-path model design**

In setting up the reaction-path model, a 1D column corresponding to a 25 km long flow tube was modelled. The column was discretized using two different approaches: (1) dividing the column in 25 cells of 1000 m long; and (2) dividing the upstream 10 km of the flowline in 10 cells of 1000 m long while the downstream 15 km were divided in 150 cells of 100 m long. This second model was

an attempt to model the varying flow conditions within the aquifer system, which indicate flow velocities in the confined part the aquifer about ten times lower than the flow velocities in the aquifer outcrop area. In addition, a dispersivity of about 4% (900 m) was used in both models, and was adjusted to the chloride breakthrough curve in the aquifer. The diffusion coefficient was set to 3 10^{-10} m^2 s^{-1} based on the literature values (Marsily, 1986).

The cation exchange capacity (CEC) of the aquifer sediments was recalculated assuming a total aquifer porosity of 0.20 and a bulk density of 1.8 kg per litre of sediment, and was set to vary between 0.020 and 0.050 mol L^{-1}. These CEC values are about ten times lower than those determined for the aquifer by Oliveira (1997). The observed differences are related to the methodology used to determine the CEC, as Oliveira (1997) calculated the CEC using the fine fraction of the sediments instead of the total sediment. However, when attempting to model the aquifer hydrogeochemical patterns using such high CEC values, the results indicated that the aquifer has been fresh since about 1 million years, which was not in agreement with the geological history of the study area.

The initial solution corresponding to the recharge water was allowed to initially equilibrate with CO_2, calcite and K-feldspar, but subsaturation with respect to calcite (SI=-1.5) and K-feldspar (SI=-1.2) was imposed. After this initial equilibrium, the recharge water was allowed to start flushing gradually the seawater, which filled initially the flow column. A time step of 1000 years was considered and the total number of time steps was set to 100. This is equivalent to about 4 pore volumes of column leached.

During the transport process the recharge water had to equilibrate with an exchanger of very limited CEC capacity (0.020 and 0.050 mol L^{-1}) while calcite and k-feldspar kept dissolving, but never reaching sobresaturation.

5.5.6. **Reaction-path model results**

The best fit for the field results was obtained by trial and error, trying to find the best combination of parameters that could simulate the observed field data. The model with the differentiated discretization completely failed to describe the observed hydrogeochemistry, since it could not reproduce the ion exchange fronts nor the pH or bicarbonate evolution in the aquifer.

The best results are shown in Fig. 5.31 and were obtained for the uniform cell model assuming a minimum value for the CEC of 0.020 mol L^{-1}. The model describes the observed hydrochemical evolution quite satisfactorily confirming that the dominant reactions in the aquifer are calcite and K-feldspar dissolution, and cation exchange. Feldspar dissolution is slowly releasing some aluminium and silica into solution but they will precipitate in silica minerals, kaolinite and illite.

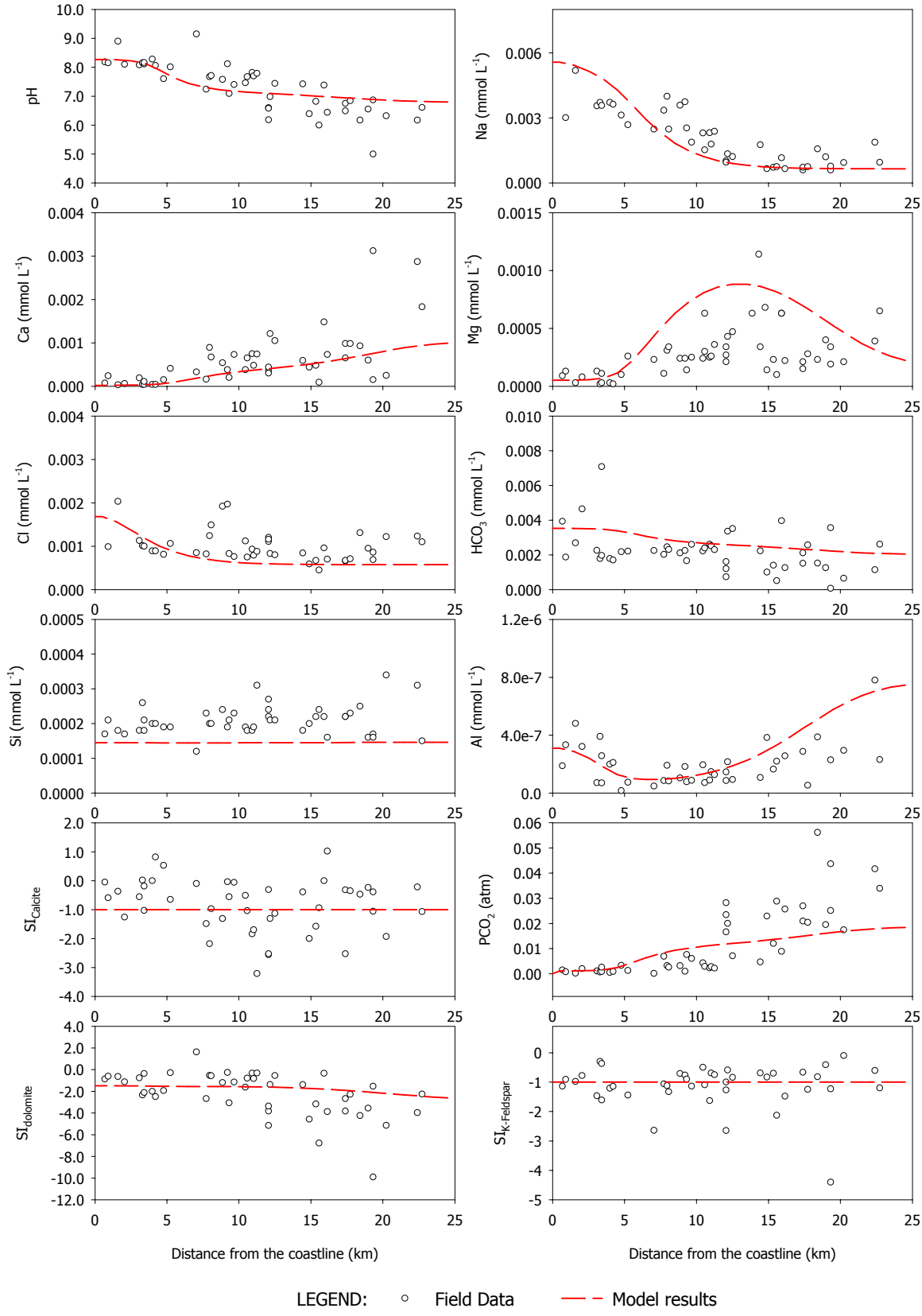

Fig. 5.31 Results of modelling the hydrogeochemical evolution of the Aveiro Cretaceous aquifer using a reaction-path geochemical model (time step= 50 ka; CEC= 0.020 mol L^{-1})

The model reproduces the ion exchange fronts with the calcium from the flushing solution displacing initially magnesium from the ion exchange complex, and further downstream, both calcium and magnesium displacing sodium. However, it does fail to describe the correct extension of the magnesium peak and eventually needed some extra silicate dissolution to be able to reproduce slightly higher Si concentrations in solution.

The effect of varying the P_{CO_2} in the initial solution influenced the calcium, pH and bicarbonate breakthrough curves in the column. When the saturation index of calcite is decreased in the initial solution, the P_{CO_2} also decreases in the column since more calcite is dissolved in the first cell of the column. Thereby the pH also increases due to the lower P_{CO_2}. Thus the concentration of HCO_3 seems more likely to be controlled by the amount of TIC generated in the initial solution.

The use of the highest determined CEC values accelerated the cation exchange process, with the Ca and Mg ions being uptaken faster from the solution and the sodium ions released sooner into solution, but did not succeed to reproduce the observed values.

According to the model, the present day hydrogeochemical pattern is the result of 50 ka of geochemical evolution in the aquifer, which means that the aquifer has been fresh since the Late Pleistocene. This is in agreement with carbon-14 and chloride data for the aquifer that revealed fresh water since at least 35 ka, and also with the geological data. And this proves that the palaeohydrology is still dominating the aquifer geochemistry, which is not yet affected by the extensive abstractions and over pumping since the late sixties.

Thus the reaction-path modelling in the Aveiro Cretaceous aquifer helped to confirm the principal processes contributing to the hydrogeochemical evolution of the aquifer and gave some more evidence about the time scale for the aquifer freshening. At the detailed level however the interpretations may be complicated by the mixing inevitably caused by the pumping regime in the multilayer aquifer.

5.6 Conclusions

The Aveiro Cretaceous aquifer is considered unique from the geochemical and isotopic point of view and important as an archive of past climate conditions in temperate regions of Europe. In contrast to what is observed in northern Europe aquifers, enrichment in $\delta^{18}O$ (Δ= 0.8-1.0 ‰) and $\delta^{2}H$ (Δ= 5-7 ‰) is found in the Late Pleistocene recharge waters of the Aveiro aquifer. This is considered to reflect the enrichment in the Pleistocene ocean water as well as the constancy of the predominant source of moisture from the Atlantic westerly flow.

The groundwaters contain a smooth record of radiocarbon ages indicating continuity of recharge through the LGM and over a period in excess of 30 ka. Noble gas recharge temperatures indicate that atmospheric cooling of 5-6^{o}C occurred during the LGM. The presence of fresh palaeowaters at the present coastline implies that groundwater flow was controlled by an offshore outlet, possibly the outcrop at the continental shelf. It is therefore likely that freshwaters exist beneath the sea to the west of Aveiro.

For an aquifer with residence times in excess of 30 ka, the Aveiro Cretaceous aquifer reveals a significantly slow chemical kinetics for the water-rock interactions resulting from the mainly siliciclastic composition of the aquifer sediments and from a very low cation exchange capacity. Silicate weathering, calcite dissolution and cation exchange in the initial phases of seawater flushing are considered to be the processes responsible for the gradual groundwater chemical composition and were confirmed by the geochemical modelling, which also confirmed that the aquifer has been fresh since about 50 ka.

The most important inference arising from the depth sampling and flow logging campaign is probably that the 'Furadouro sandstone formation' is contributing with most of the water supplied by the aquifer. The ratio for the transmitted flow could be as high as 9:1 when compared to the other aquifer layers, and implies that samples taken from the discharge during pumping conditions can be assumed to correspond in great part (~90%) to the 'Furadouro sandstone formation'. Therefore, the samples obtained from the boreholes discharge while pumping during the previous sampling campaigns are considered to be representative of chemical characteristics of the principal aquifer layer.

6

FLOW MODELLING

Groundwater flow modelling is nowadays routinely employed for environmental resource management decisions and to assess hydrogeologists on the prediction of the behaviour of groundwater systems. The model supporting these decisions must be scientifically defensible and decision-makers and end-users must be informed of the degree of uncertainty in the model predictions.

A protocol for modelling includes definition of study objectives, code selection and verification, model design, calibration, sensitivity analysis, and finally prediction (ASTM, 1996). But for a flow model to be able to approximate field conditions it requires the correct formulation of the aquifer conceptual model, selection of the parameter values to describe spatial variability within the groundwater flow system, as well as spatial and temporal trends in hydrologic stresses and past and future trends in water levels (Anderson & Woessner, 1992).

And it is essential for any groundwater model to be interpreted and used properly that its limitations are understood. In addition to strictly technical limitations, such as accuracy of computations (hardware/ software), the following is true for any model (Kresic, 1997):

- it is based on various assumptions regarding the real natural system being modelled;
- hydrogeologic and hydrologic parameters used by the model are always just an approximation of their actual field distribution which can never be determined with total accuracy;
- theoretical differential equations describing groundwater flow are replaced with systems of algebraic equations that are more or less accurate.

Modelling is an excellent way to help organize and synthesize field data but it is important to recognize that modelling is only one component in a hydrogeological assessment and not an end itself. Good field data are essential when using a model for predictions but a model may also be used to guide data collection. An attempt to model a system with inadequate field data may serve to identify those areas where detailed field data are critical to the success of the model (Wang & Anderson, 1982).

6.1 Groundwater flow models

A model is a tool designed to represent a simplified version of the reality. In hydrogeology, a numerical flow model simulates groundwater flow indirectly by means of a governing equation thought to represent the physical processes that occur in the system, together with equations that describe heads or flows along the boundaries of the model (boundary conditions). For time-dependent problems an equation describing the initial distribution of heads in the system also is needed (initial conditions) (Anderson & Woessner, 1992).

In a numerical model, aquifers and confining units within an aquifer system are represented by cells organized into layers. Hydraulic heads and flow in each layer and the exchange of water between adjacent layers and across the boundaries are computed simultaneously. These calculations are most commonly accomplished by use of a computer code that solves the finite-difference or finite-element approximations of the partial differential equations (three dimensional groundwater flow equation, boundary conditions and initial conditions) that form the numerical model.

6.1.1 **Governing equations for groundwater flow**

The Darcy's law (Equation [6.1]) summarizes much of the physics of groundwater flow by relating the velocity vector to the gradient of potential:

$$\mathrm{q} = -\mathrm{K}\,\mathrm{grad}\,h \qquad [6.1]$$

where q is the velocity vector and has components q_x, q_y and q_z, K the hydraulic conductivity, h the hydraulic head and *grad h* the gradient vector which has components ∂h/∂x, ∂h/∂y and ∂h/∂z.

Continuity or conservation is the second important law. For steady-state conditions, continuity requires that the amount of water flowing into a representative elemental volume be equal to the amount flowing out. The existence of steady-state conditions implies that head is independent of time. The continuity equation for steady-state conditions can be written as follows (Equation [6.2]):

$$\frac{\partial \mathrm{q_x}}{\partial \mathrm{x}} + \frac{\partial \mathrm{q_y}}{\partial \mathrm{y}} + \frac{\partial \mathrm{q_z}}{\partial \mathrm{z}} = 0 \qquad [6.2]$$

The left-hand side of Equation [6.2] represents the net change in the volume rate of flow per unit volume. As such, it is called the divergence of q and written:

$$\mathrm{div}\,\mathrm{q} = \frac{\partial \mathrm{q_x}}{\partial \mathrm{x}} + \frac{\partial \mathrm{q_y}}{\partial \mathrm{y}} + \frac{\partial \mathrm{q_z}}{\partial \mathrm{z}} \qquad [6.3]$$

Laplace's equation combines Darcy's law and the continuity equation into a single second-order differential equation. Darcy's law is substituted component by component into Equation [6.2] to give:

$$\frac{\partial}{\partial x}\left(-K\frac{\partial h}{\partial x}\right)+\frac{\partial}{\partial y}\left(-K\frac{\partial h}{\partial y}\right)+\frac{\partial}{\partial z}\left(-K\frac{\partial h}{\partial z}\right)=0 \qquad [6.4]$$

where $K=K(x,y,z)$. If the region is assumed to be homogeneous as well as isotropic, then K is assumed to be independent of x, y and z, and the Equation [6.4] becomes:

$$\frac{\partial^2 h}{\partial x^2}+\frac{\partial^2 h}{\partial y^2}+\frac{\partial^2 h}{\partial z^2}=0 \qquad [6.5]$$

Equation [6.5] is Laplace's equation - the governing equation for groundwater flow through an isotropic, homogeneous aquifer under steady-state conditions (Wang & Anderson, 1982).

In the derivation of the governing equation for transient conditions (the unknown variable is time dependent), the continuity equation is modified such that the volume outflow rate equals the volume inflow rate plus the rate of release of water from storage. Therefore, an expression for the rate of release of water from storage must be introduced. This expression involves the use of the storage coefficient S, which represents the volume of water released from storage per unit area of aquifer per unit decline in head. That is:

$$S=\frac{-\Delta V_w}{\Delta x\,\Delta y\,\Delta z} \qquad [6.6]$$

where ΔV_w is the volume of water released from storage within the elemental volume whose area is $\Delta x\,\Delta y$ and whose thickness is b.

The rate of release from storage is $\Delta V_w/\Delta t$ and can be written as $-S\Delta x\Delta y(\Delta h/\Delta t)$. As $\Delta t\rightarrow 0$ this expression becomes $-S(\partial h/\partial t)(\Delta x\Delta y)$. Therefore, the form of the continuity equation (Equation [6.2], for transient conditions is:

$$\frac{\partial q_x}{\partial x}\Delta x(b\Delta y)+\frac{\partial q_y}{\partial y}\Delta y(b\Delta x)=R(x,y,z)\Delta x\Delta y-S\frac{\partial h}{\partial t}(\Delta x\Delta y) \qquad [6.7]$$

where $R(x,y,z)$ is the volume of water added per unit time per unit aquifer area to the infinitesimal volume around the point (x,y,z).

Substituting Darcy's law for q_x and q_y and dividing through by $-T\Delta x\Delta y$, where $T=K\,b$, yields the transient flow equation:

$$\frac{\partial^2 h}{\partial x^2}+\frac{\partial^2 h}{\partial y^2}+\frac{\partial^2 h}{\partial z^2}=\frac{S}{T}\frac{\partial h}{\partial t}-\frac{R(x,y,z)}{T} \qquad [6.8]$$

6.1.2 **Boundary conditions**

The solution of Laplace's equation requires specification of boundary conditions, which constrain the problem and make solutions unique. The different types of boundary conditions are:

a) Type 1 – Specified head. Head is known for surfaces bounding the flow region (Dirichlet conditions);

b) Type 2 – Specified flow. Flow is know across surfaces bounding the region (Neumann);

c) Type 3 – Head-dependent flow. Some combination of (a) and (b) is known for surfaces bounding the region (Cauchy or mixed conditions).

6.2 Purpose of the flow model

Groundwater numerical flow modelling was used to describe the Aveiro Cretaceous aquifer system, to test and improve the conceptual model developed for the aquifer and to gain a better understanding of the present and past regional-scale flow dynamics in the aquifer. Specifically, a regional groundwater budget was computed and natural regional groundwater flow patterns and relative magnitudes of regional groundwater flow were determined.

The simulation process included a comparison between the simulated variables from the numerical flow model and the observed field values. When they approximated each other the numerical flow model was considered to be a good approximation of the flow system, and it was assumed that the conceptual model reasonable described the studied aquifer.

6.3 Computer code

The specific computer code selected for this investigation is a modular finite-difference groundwater flow model (MODFLOW®) developed by the U.S. Geological Survey (USGS) (McDonald & Harbaugh, 1988; Harbaugh & McDonald, 1996). MODFLOW® is designed to simulate aquifer systems in which (1) saturated-flow conditions exist; (2) Darcy's law applies; (3) the density of groundwater is constant; and the principal directions of horizontal hydraulic conductivity or transmissivity do not vary within the system. Nowadays, MODFLOW® is the most widely used program in the world for simulating groundwater flow.

MODFLOW® simulates groundwater flow in aquifer systems using the finite-difference method and each simulation feature in the programme has been extensively tested and verified. The model uses the input data to construct and solve equations of groundwater flow in the aquifer system. Visual MODFLOW Pro was used to analyse field data and construct input data sets, as well as to read output from MODFLOW® and graphically present model results.

6.4 Conceptual model

A conceptual model was developed for the Aveiro Cretaceous aquifer with the purpose of simplifying the field problem and organizing the associated field data so that the system could be analyzed more readily. The formulation and geometry of the conceptual model of the aquifer system was based on the hydrogeologic framework described in Chapter 3 and is an interpretation of the main characteristics and dynamics of the physical hydrogeologic system.

A schematic representation of the model is shown in Fig. 6.1. and includes information on the defined aquifer limits, boundary conditions, the number of model layers and the described regional patterns of groundwater flow.

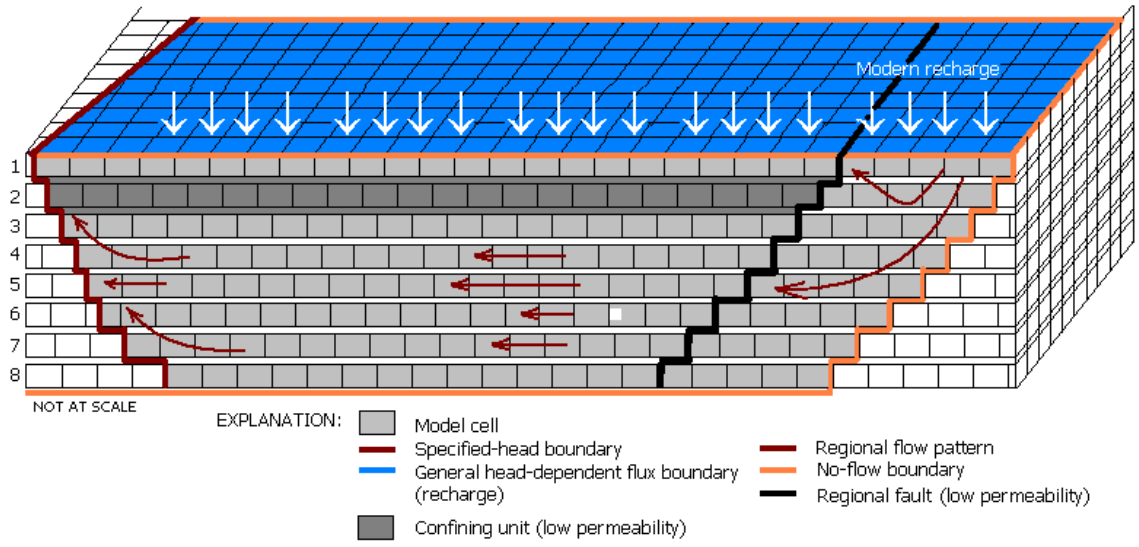

Fig. 6.1 Conceptual model for the Aveiro Cretaceous aquifer showing the areal extent and boundaries of the model layers used to simulate the aquifer system.

The development of the aquifer conceptual model included:

1) definition of the area to be modelled and identification of the boundaries;

The modelled area corresponds to the total aquifer area defined in Chapter 3 (over 1,800 km^2) and is shown in Fig. 6.2. Geostructural boundaries and hydrogeologic inferences were used to delimit the studied aquifer. When trying to simulate the palaeohydrology of the aquifer the modelling area is extended to the downdip limit of the subcrop area, which is assumed to be the edge of continental shelf. Thus the western boundary of the Aveiro Cretaceous aquifer was defined in two different positions, about 50 km apart. For present day analysis, the limit was assumed to coincide with the present coastline, and when analysing the emplacement of palaeowaters in the aquifer system, the border was extended to the edge of the continental shelf.

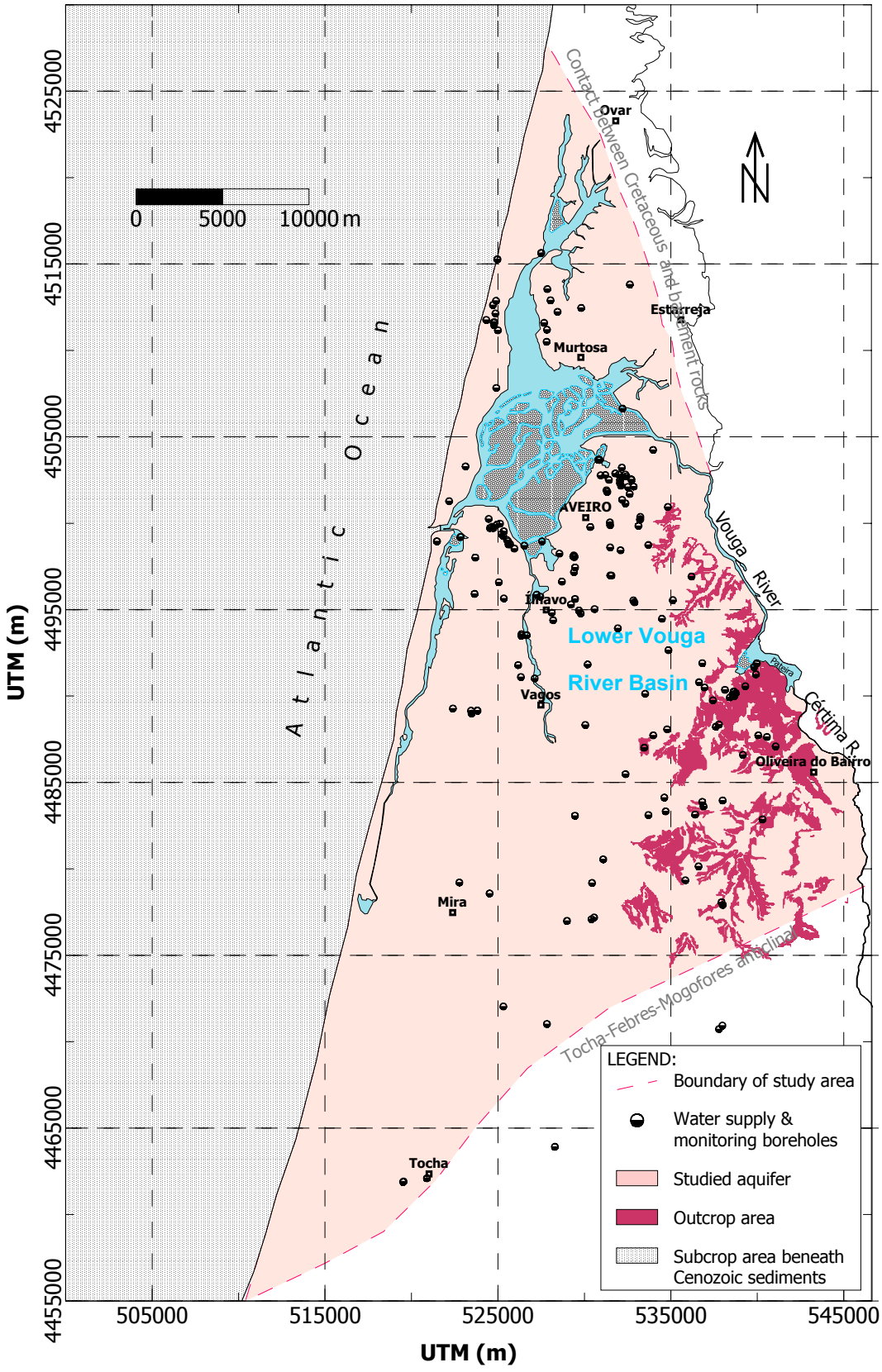

Fig. 6.2 Boundaries of the study aquifer system including outcrop and subcrop areas considered for the flow modelling (the downdip limit of the subcrop area is assumed to be the edge of continental shelf, which is about 50 km from the present day coastline).

The geological contact between the Cretaceous formations and the Palaeozoic-Proterozoic basement rocks was established as the north and northeastern boundaries of the aquifer, because of the difference in permeabilities between both geological formations. The contact between the Cretaceous formations and the underlying Triassic (east), Jurassic (south) and schist-grauwaque complex rocks (in the rest of the area) were established as the lower boundary of the Aveiro Cretaceous aquifer. The southern border of the aquifer is a geostructural limit formed by the 'Tocha-Febres-Mogofores' anticlinal structure with a predominant WSW-ENE orientation (Fig. 6.2). The eastern boundary of the aquifer was defined as the eastern limit of the outcrop of the Cretaceous sandstone formations. The Cretaceous units are in this part of the study area underlain by Triassic formations, which have smaller transmissivities and confine the flow system to the overlying units.

2) definition of the hydrostratigraphic units;

In modelling regional flow systems, aquifers and confining layers are defined using the concept of hydrostratigraphic unit ('geological units of similar hydrogeologic properties') (Maxey, 1964; Seaber, 1988). Geologic information including geologic maps (Fig. 2.7, Chapter 2) and cross-sections (Fig. 3.5 to 3.10, Chapter 3) showing the areal and vertical extent and boundaries of the system, borehole geological and geophysical logs (Appendix A) were combined with information on hydrogeologic properties to define hydrostratigraphic units for the conceptual model (Table 6.1).

Table 6.1. Correlation of aquifer systems, hydrogeologic units and model layers for the Aveiro region.

Period	Stage	Lithostratigraphic units		Lower Vouga Region Aquifer-System Analysis		
				Hydrogeologic unit	Model layer	Aquifer system
Q	Holocene and Plio-Pleistocene	Alluvium, beach and eolian sands and sand dunes		Permeable zone 1	1	Quaternary aquifer
		Terrace and old beach deposits				
C	Campanian-Maastrichtian	'Aveiro clay formation', C_3		Confining unit 1	2	Multilayer Cretaceous aquifer
	Coniacian-Santonian	Upper sandstone formation, C_3	Top	Permeable zone 2	3	
	Upper Turonian-Lower Coniacian		Bottom	Permeable zone 3	4	
	Upper Cenomanian -Turonian	'Furadouro sandstone', C_2		Permeable zone 4	5	
	Cenomanian	Carbonate formation, C_2		Permeable zone 5	6	
	Aptian/Albian-Lower Cenomanian	Lower sandstone formation, C_{1A}	Top	Permeable zone 6	7	
			Intermediate	Permeable zone 7	8	
			Bottom			

3) water budget;

The sources and sinks of water to the aquifer system impact the regional pattern of groundwater flow in the Aveiro Cretaceous aquifer. After identifying the main sources and sinks in

the aquifer, a water budget was prepared for the system that provides an estimate of the current balance between total aquifer withdrawals and discharge and aquifer recharge.

The field estimated inflows to the aquifer include mainly groundwater recharge. This has been calculated in Chapter 4 using several different estimation methods and an average value of 140 mm a^{-1} was obtained. However, depending on the estimation method used the calculated recharge values for the region may vary between 110 and 162 mm a^{-1}, and there is also a well-documented spatial variability. Besides, there are several signs that these high recharge rates may not correspond to effective recharge to the deep part of the aquifer system.

Thus considering that the permeable outcrops in the aquifer recharge area encompass a restricted area of approximately 52 km^2 and that the annual average groundwater recharge is 140 mm a^{-1}, the total inflow volume to the aquifer is approximately 7.3 hm^3 a^{-1}. The outflows from the aquifer may include spring flow, pumping and the possible aquifer discharge offshore. The total annual volume of aquifer discharge was calculated in Chapter 3 to be about 24 hm^3 a^{-1}, exceeding more than three times the total calculated inflows for the aquifer system. The difference in the balance is too high to be significantly affected by the uncertainty in the estimation of the pumping volumes.

The water balance shows an apparent decrease in aquifer storage of approximately 17 hm^3 a^{-1} and indicates that present groundwater withdrawals are affecting the aquifer's long-term storage (Fig. 6.3). The observed net difference is almost two times more than the total recharge, and is well within the estimated margin of error for some of the individual component estimates. The overall error associated with individual water budget component estimates is expected to decrease, as more information about pumping volumes becomes available.

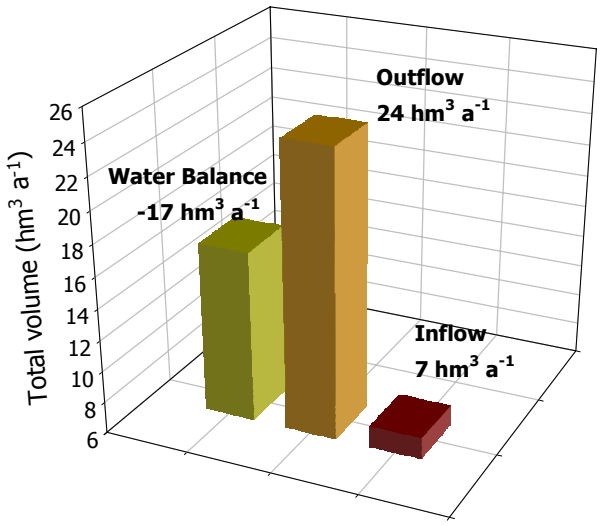

Fig. 6.3 Annual water balance for the Aveiro Cretaceous aquifer (Water balance = inflows-outflows).

The observed negative net difference is in agreement with the extensive groundwater abstraction during the last ten years in the aquifer and with the large depression of the piezometric surface with reversal of the natural flow direction observed nowadays in the area between Ílhavo, Aveiro and Cacia (Fig. 3.12, Chapter 3).

If the observed depression of the regional piezometric surface is combined with carbon-14 results and nitrate data determined for the aquifer in Chapter 5, and with tritium results presented by Carreira Paquete (1998), there is the generalised idea that hardly any modern recharge reaches the confined part of the aquifer, where pristine waters occur. This could mean that the net water balance for the aquifer is probably even more negative that the one presented.

In other European aquifers where palaeowaters have been identified, such as the Valreas basin aquifer in southern France (Huneau, 2000) or the East Midlands aquifer in the UK (Edmunds *et al.,* 2001), detailed hydrogeological investigations showed that just about 10% of the modern recharge reached the confined part of the aquifer. If a similar situation is observed for the Aveiro Cretaceous aquifer, then the inflow to the aquifer system would be just 0.7 $hm^3\ a^{-1}$ and the net balance would be even more negative with over -23 $hm^3\ a^{-1}$. In any case it seems reasonable to state that groundwater sustainability in the Aveiro Cretaceous aquifer requires strong protection measures to prevent irreversible damage.

4) Regional flow system

According to the estimated predevelopment (1950's) potentiometric surface for the Aveiro Cretaceous aquifer presented in Chapter 3 and shown again here in Fig. 6.4, the regional groundwater flow pattern in the region is under natural conditions from the recharge area in the east towards the sea, with a natural gradient around 0.0015. There is some uncertainty associated with the definition of the initial situation for the aquifer as there was hardly any water level data at that time. However, the suggested map should approximate the reality and is similar to other predevelopment maps presented for the aquifer (Marques da Silva, 1990).

Apparent flow velocities for the aquifer calculated from carbon-14 data indicate decreasing flow velocities down the flowpath, from about 2 $m\ a^{-1}$ in the areas close to the outcrop to approximately 0.2 $m\ a^{-1}$ in the deepest part of the aquifer along the coastline.

6.5 Model Design

Model design is the process of transforming the conceptual model into a mathematical form. Fundamental components of the design of a groundwater flow model include: dimensionality, discretization, boundary and initial conditions and hydraulic properties (ASTM, 1996).

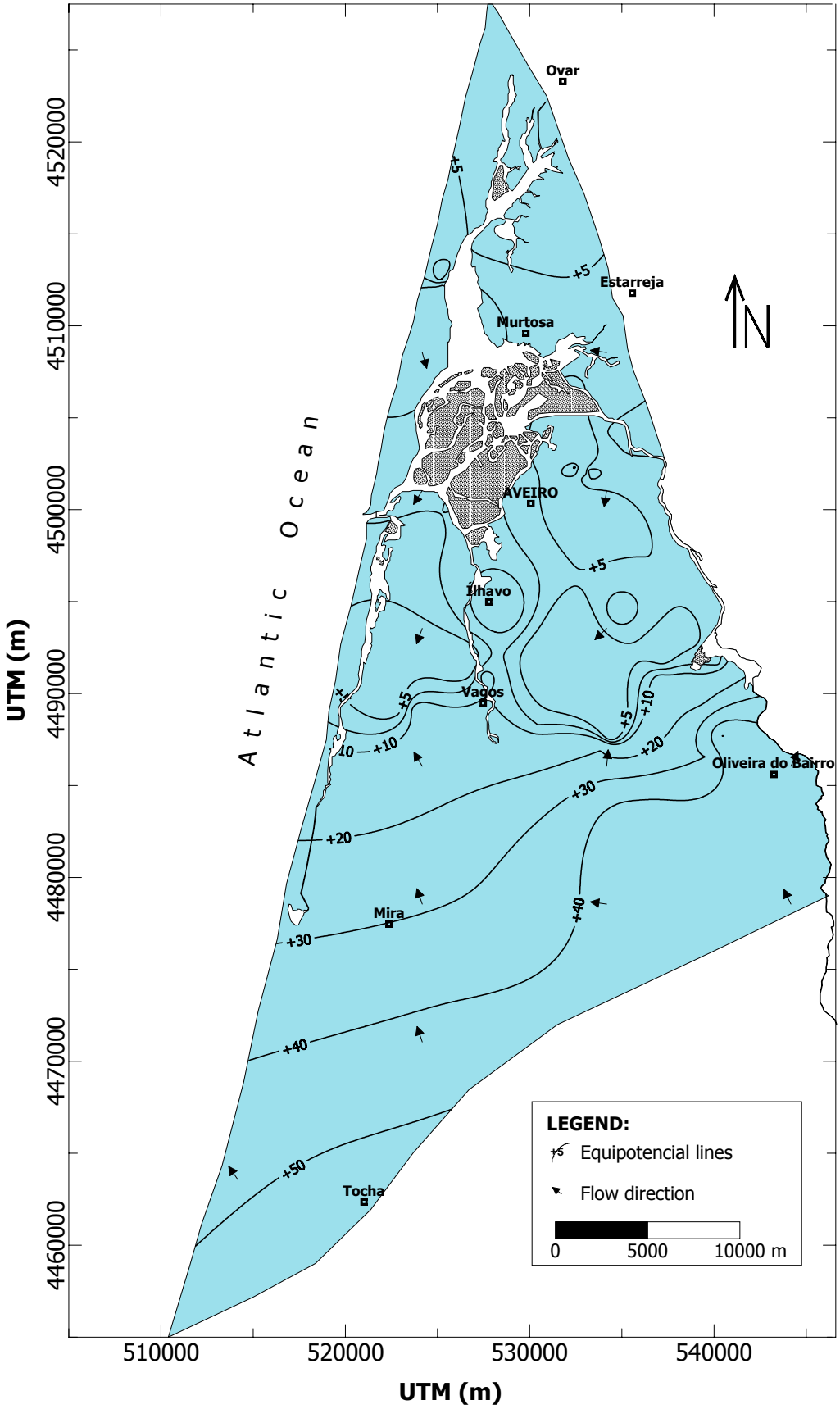

Fig. 6.4 Estimated predevelopment (1950's) potentiometric surface for the Aveiro Cretaceous aquifer using linear kriging.

6.5.1 **Spatial and temporal dimensionality**

A three-dimensional model built based on the previously described conceptual model was used to simulate flow in the Aveiro Cretaceous aquifer using a framework of 8 layers. The land topography was defined as the top elevation of the aquifer model. The approximate thicknesses of the principal model layers corresponding to each hydrostratigraphic unit were determined in Chapter 3, based on the analysis and interpretation of the geophysical logs available for the study region. The unknown bottom elevation values between adjacent boreholes were estimated using linear kriging (*e.g.* Davis, 1986) and interpolated for the rest of the study region. The results obtained have been represented using contour plots in the following Fig. 6.5 and were directly imported to the model using Surfer® grid files.

In terms of temporal discretization, the first step was to approximate the model to pre-pumping steady-state conditions, which correspond in the region to the beginning of the fifties. The flow model at steady-state conditions was then converted to simulate transient conditions using the steady-state heads as initial heads. Pumpage was incrementally entered from the 1960's, and discharge and recharge are represented.

The number and the length of the stress periods were automatically defined by the used pre-processing program, which automatically merges all the different time period data defined for each pumping well and boundary condition into the stress period format required by MODFLOW®. It also calculates the length of each stress period for a transient simulation. In this case, the total number of stress periods was of 327 and correspond to a period of simulation comprised between 1955 and 2035.

For each stress period a total number of five time steps was assumed and a time step multiplier of 1.5 was used to increment the time step size within each stress period. A multiplier factor greater than 1 will produce smaller time steps at the beginning of a stress period resulting in a better representation of the transient changes of the flow field. Thus increasing the number of time steps in a simulation may result in smoother head or drawdown versus time curves (WHI, 2002).

6.5.2 **Grid**

The study area of about 75 km x 36.5 km was divided into a three-dimensional grid of 150 rows, 73 columns and 8 layers (Fig. 6.6). The grid was aligned orthogonal to the flow system and each cell of the model is square, measuring 500 m on a side and representing an area of about 0.25 km^2. The rows in the model are numbered in a southerly direction, and the columns in an easterly direction.

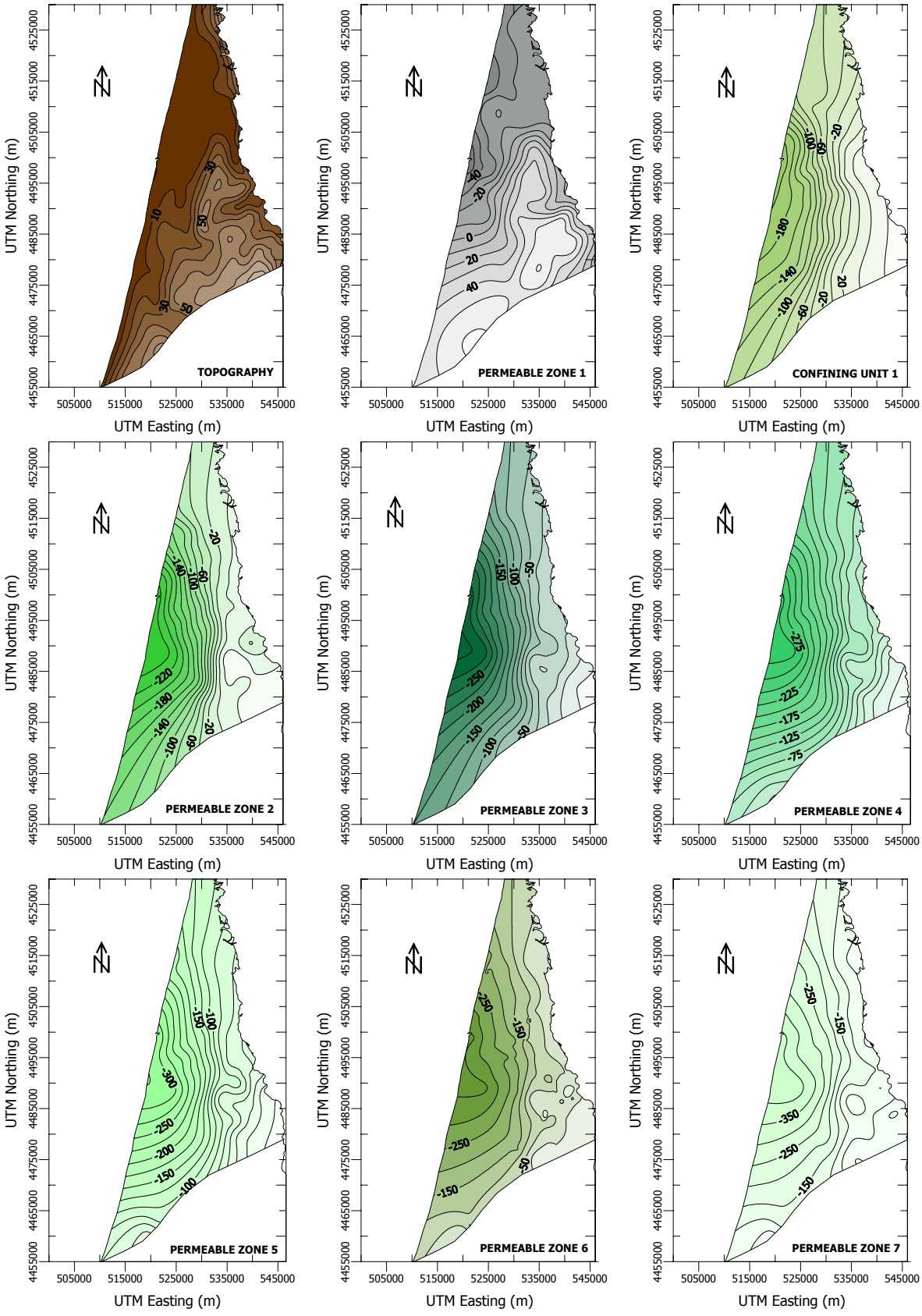

Fig. 6.5 Topography and bottom elevation of the principal model layers and confining units. Values were estimated for the whole region using linear kriging.

The decision to rely on a uniform grid was a compromise between the accuracy of the model and the available computer resources when designing a finite-difference grid. Models that rely on a uniform grid are usually more stable but a finer grid will normally give more precise results. However, the hypothesis of refining the grid when introducing the well fields was discarded because the grid would become too complex taking into account the number of wells and their uneven distribution.

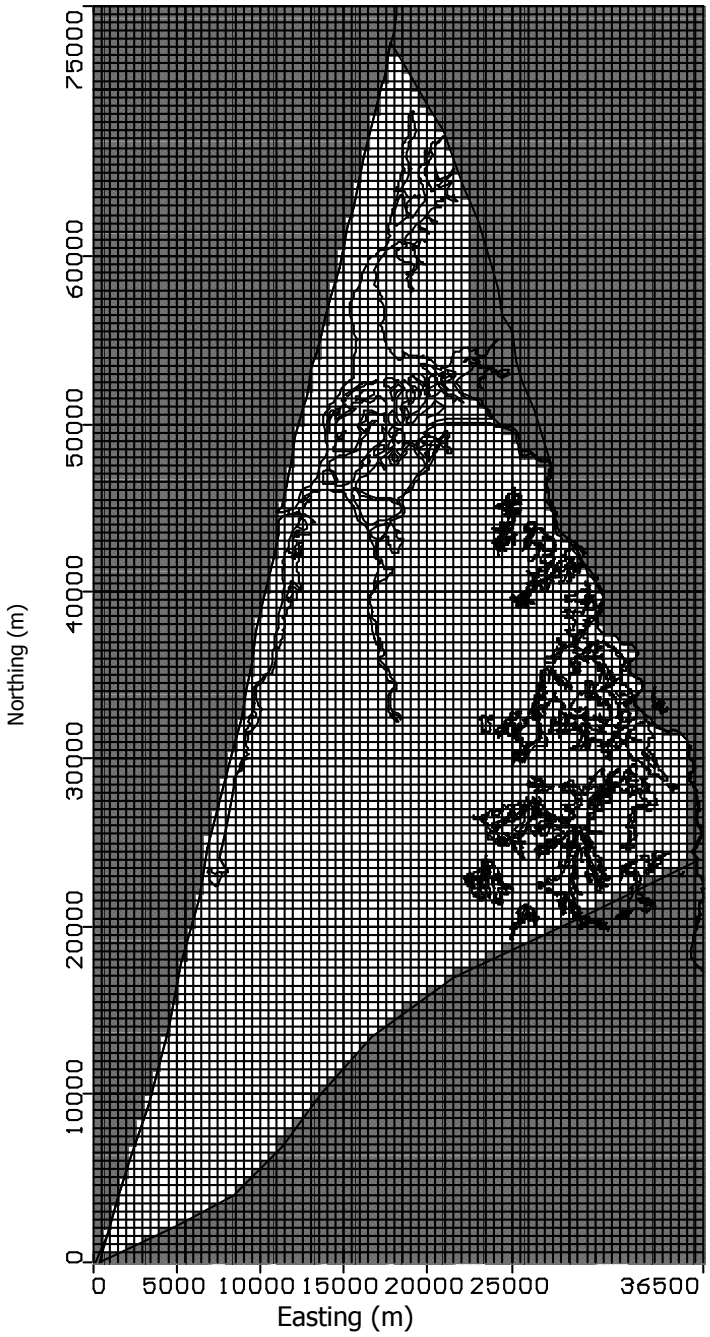

Fig. 6.6 Defined x-y grid for the flow model with 73 columns and 150 rows. The map shows the modelled area in white and the cells defined as inactive in grey. The Cretaceous outcrop area is shown in the east part of the map.

The aquifer system was divided vertically into 8 layers of cells, each layer representing one modelled aquifer or confining unit. When importing the bottom elevations of each aquifer layer, a minimum thickness of 10 m was assigned to each layer to guarantee grid smoothing by preventing discontinuities between the cells. The final vertical discretization of the aquifer model is shown in Fig. 6.7 along a west-east (row 77) and south-north (column 37) cross-section, both in the central part of the modelled area. The layers of the model reflect the thickening of the aquifer towards the coastline and from the north and south borders to the central part of the aquifer.

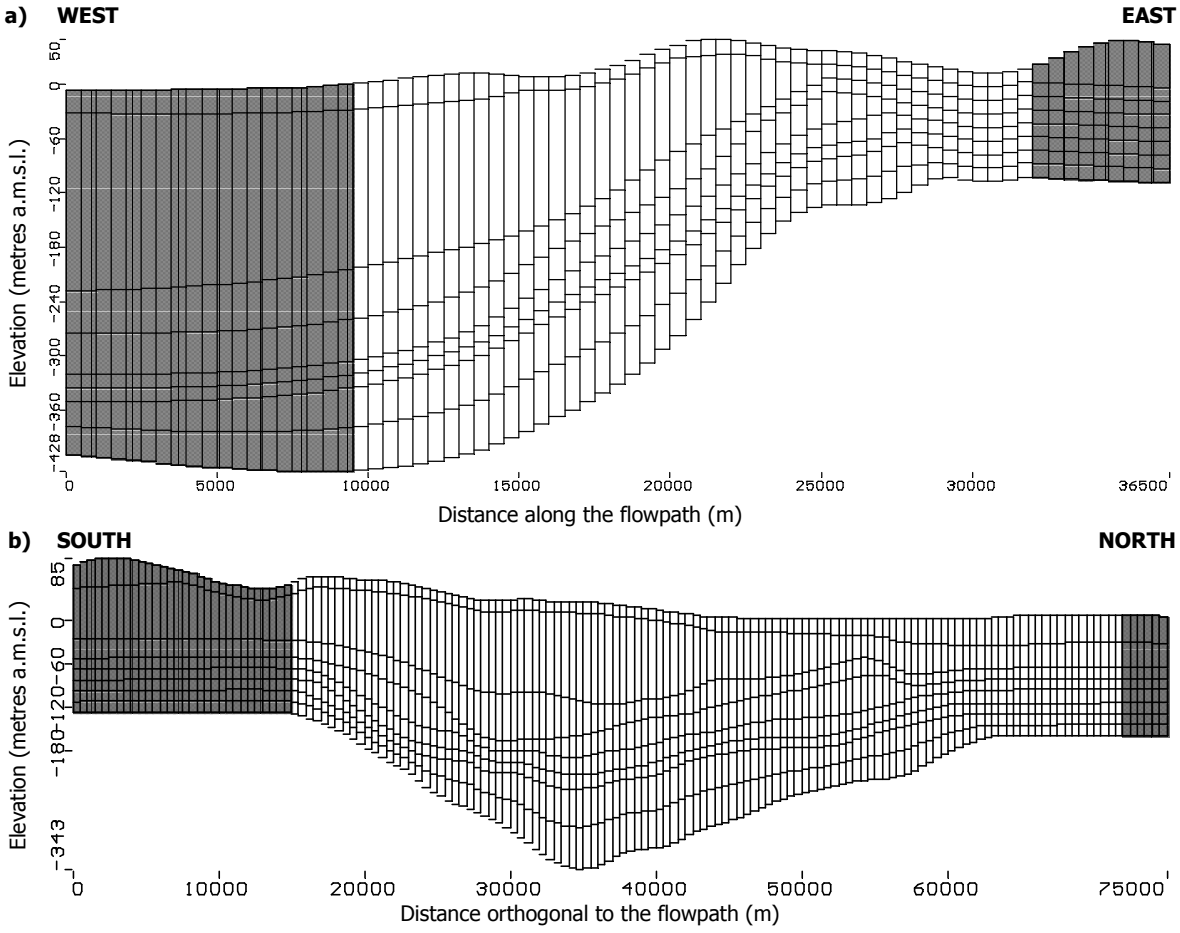

Fig. 6.7 Vertical discretization of the aquifer flow model in 8 layers, 73 columns and 150 rows along a west-east and a south-north cross-section. The figure shows the modelled area in white and the cells defined as inactive in grey for row 77.

6.5.3 **Initial heads**

The initial heads for the steady-state simulation corresponded to the estimated predevelopment (1950's) potentiometric surface for the aquifer (Fig. 6.4). Then the heads calibrated during the simulation of steady-state prepumping conditions were entered as initial heads for the simulation of transient conditions.

6.5.4 **Boundary conditions**

Model boundaries were set for a given model construction and were not automatically adjusted by the nonlinear regression. The following types of boundaries have been included in the numerical model (Fig. 6.8):

a) No-flow boundaries

The boundaries represented in the model by the outline of inactive cells are no-flow boundaries, as groundwater flow is not simulated through inactive cells. Furthermore the outside of the model domain is also a no-flow boundary.

The north and northeastern parts of the model, which represent the contact between the aquifer and the Palaeozoic-Proterozoic basement rocks were established as no flow boundaries, because of the significant difference of permeabilities between both geological formations. The contact in depth between the Cretaceous formations and the basement rocks (Triassic formations in the east, Jurassic formations in the south and schist-grauwaque complex rocks in the rest of the area) were also established as no flow boundaries and correspond to the bottom part of the model.

The southern border of the aquifer is a geostructural limit formed by the 'Tocha-Febres-Mogofores' anticlinal structure with a predominant WSW-ENE orientation, which acts as a groundwater divide. Groundwater divides are frequently simulated as no-flow boundaries in groundwater flow models to limit the areal extent of the system being analyzed (Reilly, 2001). And was also here defined as a no-flow boundary.

b) Specified–head boundaries

Groundwater flows from the eastern towards the coastline. For this reason, a specified-head boundary condition ($h(x,y,z,t)$=1.025 m) is imposed on the western boundary of the aquifer. The justification for considering the freshwater head value as 1.025 m is related to seawater density and is the minimum head necessary for the aquifer to discharge to the sea (Custodio & Llamas, 1983). Rigorous treatment of the saltwater interface requires a model that allows for density effects as well as diffusion and dispersion of saltwater. However, standard flow codes can simulate a saltwater interface approximately as a streamline boundary represented either by no-flow condition (Anderson & Woessner, 1992), and in specific situations by a constant fresh water head (Langevin, 2002).

c) Specified–flux boundaries

The upper boundary of the model was simulated as a flux boundary as recharge was assigned to the top layer of the aquifer. The layer was designated as unconfined and an array of recharge rate of 140 mm a^{-1} was specified to the entire layer. To deal with the possibility of the water table cutting across layers, recharge was applied to the uppermost active model layer.

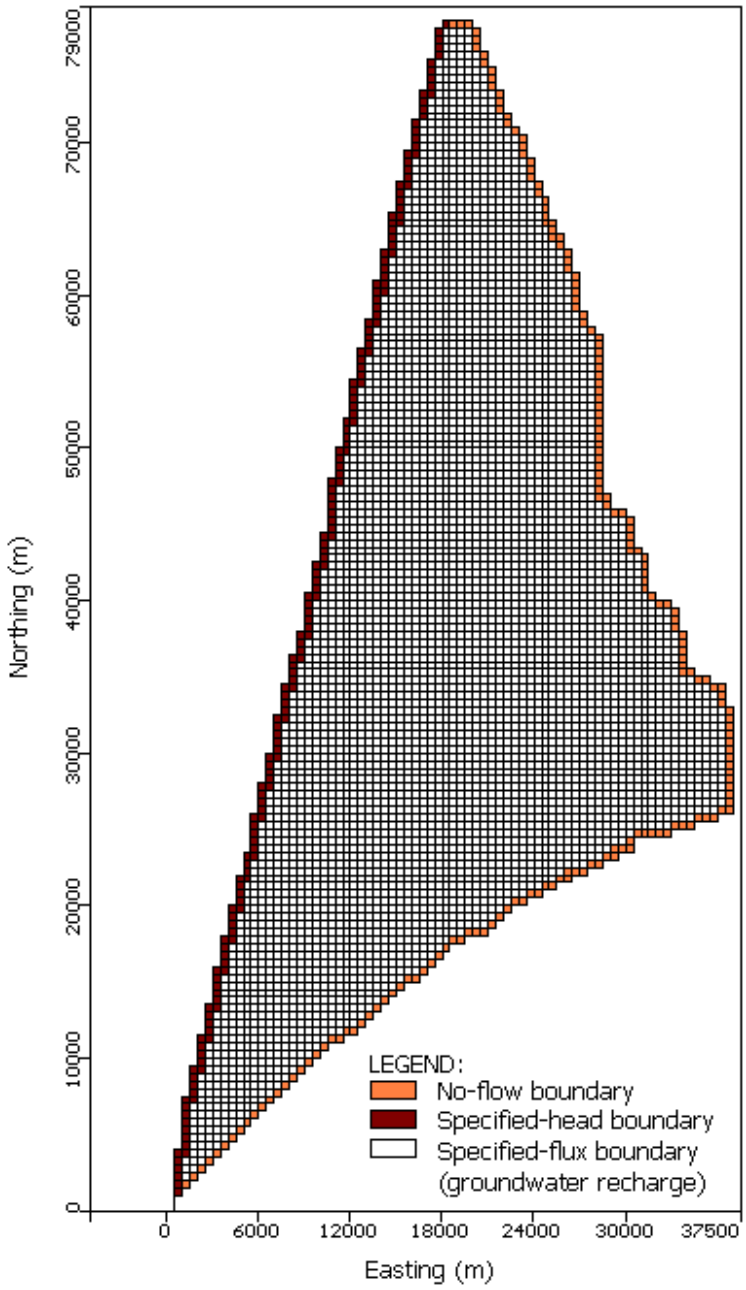

Fig. 6.8 Defined boundary conditions in the numerical flow model of the Aveiro Cretaceous aquifer.

6.5.5 **Model parameters**

The following parameters were used to simulate steady-state and transient regional groundwater flow in the aquifer system:

- horizontal hydraulic conductivity (K_x, K_y): initial estimates were based on the interpretation of the pumping test results (Table 3.2 & Fig. 3.11 in Chapter 3);

- vertical hydraulic conductivity (K_z): estimated assuming K_z to be about 100 and 5-10 times lower than the K_x, K_y in the aquifer layers and confining units, respectively;
- specific aquifer storage (S_s): initial estimates from pumping test data interpretation;
- specific yield (S_y), in the absence of site-specific field or laboratory measurements, initial estimates were taken from values published in the literature (*e.g.* Anderson & Woessner, 1992; Domenico & Schwartz, 1990 and Marsily, 1986);
- effective and total porosities were also quoted from published values in the literature literature (Marsily, 1986).

Table 6.2 is a synthesis of the initial input values assigned to each aquifer layer during the construction of the flow model and later adjusted for a best fit during model calibration process.

Table 6.2. Initial input parameters for the flow model.

Model Layer	$K_x = K_y$ (m d^{-1})	K_z (m d^{-1})	S_s (1)	S_y (1)	n_t (1)	n_e (1)
1	15.0	0.15	1E-3	0.3	0.25	0.15
2	1.0E-4	2E-5	1E-8	0.1	0.50	0.01
3	0.05	0.01	1E-6	0.15	0.35	0.05
4	3.0	0.03	3E-5	0.3	0.15	0.10
5	15.0	0.15	1E-4	0.4	0.30	0.20
6	1.0	0.01	1E-5	0.2	0.12	0.06
7	4.0	0.04	3E-5	0.2	0.15	0.10
8	0.1	0.02	1E-6	0.15	0.35	0.05
9 Fault (2)	0.001	0.0001	1E-8	0.1	0.50	0.01

(1) Values quoted from Anderson & Woessner, 1992; Domenico & Schwartz, 1990 and Marsily, 1986
(2) Regional fault simulated as a low permeability zone

Most of the values are approximations to the field values determined, because the pumping tests tested always more than one layer and there are no individual values for each layer. No pumping test included layer 8 so its values are just an estimate based on the observation of the lithology.

Horizontal conductivity in layer 1, used to simulate the Quaternary aquifer in the western part and the Cretaceous outcrop in the eastern part of the aquifer, is simulated using five different values because of the Cretaceous layers pinching out in the eastern part of the study area. For the same reason, layers from number 2 to 6 have also different hydraulic conductivities in the very eastern part of the model area.

The number of parameter zones reduces in depth and the bottom model layers (7 & 8) have uniform hydraulic conductivity values for the all area. The corresponding parameter zones (areas over which a parameter is applied uniformly) are shown in Fig. 6.10.

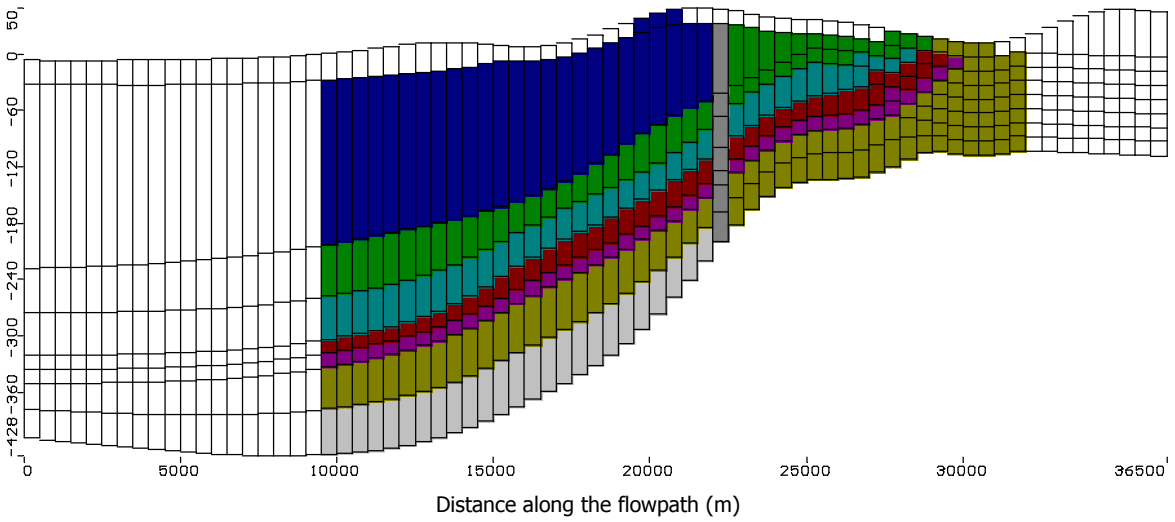

Fig. 6.9 Vertical distribution of the hydraulic conductivity in model row 77. The confining layer (2) and the permeable zone 8 do not exist in the unconfined part of the aquifer.

6.5.6 **Model assumptions and limitations**

The model designed corresponds to the previously described conceptual model, which is always a simplification of the physical system. This simplification is necessary not just for the mathematical analysis to be possible but also because of the scarcity of detailed field data (vertical and areal distributions of the permeabilities, storage coefficient, total and effective porosities, specific yields, hydraulic heads for each aquifer layer) in certain parts of the studied aquifer aquifer.

For these reasons, the flow model was designed making several assumptions, as follows:

- the head in each cell represents an average head for the aquifer in that cell. Since the area of each cell is 0.25 km^2 and the gradients are not steep, the average head should be a reasonable approximation;
- the heads in the uppermost active layer represent the water table in the Quaternary aquifer;
- the groundwater recharge was applied to the uppermost active layer;
- the principal directions of horizontal hydraulic conductivity or transmissivity do not vary within the system;
- the hydraulic properties in the aquifers are defined as isotropic in a first approximation, and the flow within the aquifers is horizontal. There is no detailed information on the exact distribution of the hydraulic properties so this was considered a reasonable approximation. However, an exception was made when aquifers pinch out laterally in the outcrop area, where it was assigned the corresponding hydraulic conductivity of

the aquifer layer pinching out instead of that corresponding to the top layer (Fig. 6.10);

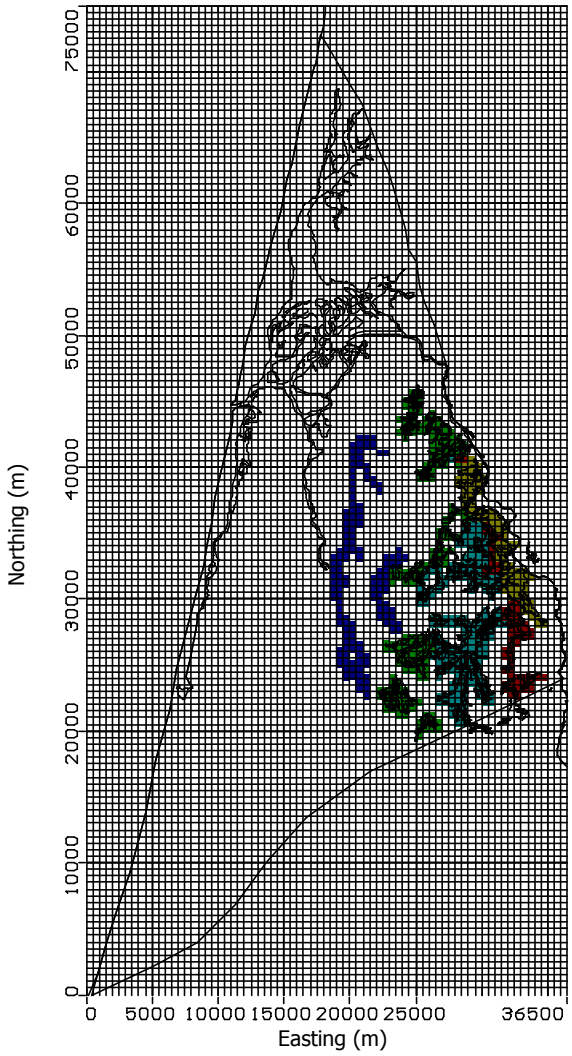

Fig. 6.10 Spatial distribution of the hydraulic conductivity in the model layer 1 corresponding to the Quaternary aquifer and to the Cretaceous outcrops in the eastern part of the aquifer.

- the vertical hydraulic conductivity in the aquifer layers was considered 100 times lower than the corresponding horizontal hydraulic conductivity. In the case of low permeability layers, the vertical hydraulic conductivity was considered lower than the horizontal hydraulic conductivity by a factor of 5 or 10;
- the surficial aquifer and outcrops are treated as unconfined aquifers and the transmissivity is a function of the saturated thickness; the other aquifer layers are treated as confined aquifers and the transmissivity is a constant;

- the confining layer was simulated using a very low permeability value, starting with a value about 1000 times lower than the adjacent units;
- the bedrock underlying the Cretaceous formations was simulated as a no-flow boundary;
- the western boundary (coastline) was simulated as a constant head boundary with a head of 1.025 m. However, the constant head condition was not assigned to the confining layer;
- the regional fault area that approximately coincides with the confined-unconfined limits of the aquifer was modelled as a low permeability area as it reduces the flow to the confined part of the aquifer and because MODFLOW® does not simulate faults directly;
- to introduce the vertical displacement of the layers produced by regional faulting in the eastern part of the aquifer, the vertical distribution of the hydraulic conductivities was displaced one layer up in this part of the aquifer;
- the multi-screened boreholes were replaced by boreholes with a single screen placed in front of the bottom of layer 4 and top of layer 7, and along all layer 5 & 6. The reason for this decision is that MODFLOW® does not have any special considerations for multiple well screens or grid cells containing partially penetrating well screens. And, although Visual MODFLOW Pro can use a group of single layer wells to represent multi-screened boreholes, using the length of the well screen intersecting each model layer to determine the proportion of the total well pumping rate assigned to each well grid cell in the model, this may cause the solution of the model to oscillate. This approach fails to take into account the inter-connection between various layers provided by the well but was preferred to guarantee the model to converge;
- a similar approach was used for the observation wells. The model just accepts point observations while in reality the recorded water level data in the studied aquifer correspond to an average of all aquifer layers. The screens of the observation wells were located in the middle of permeable zone number 5;
- instead of introducing the 185 pumping wells inventoried in the region and their corresponding pumping scheme, which would require a lot of computer RAM memory, it was decided to merge the adjacent pumping wells into a single well. This well corresponds in reality to several wells and the total volume pumped is the sum of the partial volumes pumped by each well represented.

6.6 Model execution

The execution of the model required entry of input data, running the model several times until getting the first error-free output and interpretation of the modelling results. The process also involved a synthesis of some of the field data required for the model, such as: (1) the definition of pumping fields corresponding to several adjacent wells; (2) the definition of the location of the well screens replacing partial screens by a corresponding whole screen; and (3) the extrapolation of some of the hydraulic data for aquifer properties.

6.6.1 **Error criterion**

The simulated heads include errors arising from truncation or discretization error and round-off error (Anderson & Woessner, 1992). The nodal spacing and time step have been selected to minimize discretization errors and avoid instability. The errors caused by space discretization were minimised relying on a uniform grid, and the temporal discretization was controlled by the pre-processing program.

The final error criterion to judge the convergence of the model included the following parameters for the solver:

- maximum outer iterations: 50 (steady state)/ 25 (transient)
- maximum inner iterations: 25 (steady state)/ 15 (transient)
- head change criterion: 0.01 (steady state)/ 1 (transient)
- residual criterion: 0.01
- relative residual criterion: 0

The choice of error criterion controls the size of the iteration residual and influences the number of iterations performed to achieve a solution within the specified error tolerance (Anderson & Woessner, 1992). The head change criterion was initially assumed to be about 10% of the head change in the aquifer (5 m) to make the model converge. After several simulations the head change criterion was gradually reduced till managing to run the model and making it converge assigning a head criterion less than 0.01 and 1.0 for steady state and transient simulations, respectively.

6.6.2 **Calibration process**

Calibration is a procedure of adjusting input parameters until the model is a reasonable representation of the physical system. For this study, calibration was achieved by adjusting the

input parameters for the model within a reasonable range until simulated values of head and net recharge approximated values observed in the field. In addition to these quantitative comparisons, the general flow patterns simulated by the model were qualitatively inspected to ensure that the model reasonably represents groundwater discharge in the Aveiro Cretaceous aquifer.

The numerical model was calibrated to field data to ensure that it is a reasonable representation of the physical system. Calibration is a subjective process that requires solving the inverse problem, which is altering the parameters of the numerical model until model results compare with field observations. The calibration process is needed because of uncertainties in formulating the conceptual model of the aquifer and because of measurement uncertainties associated with the determinations of the aquifer properties.

When an acceptable match between simulated results and field observations is obtained and realistic aquifer parameters are used in the model, it is assumed that the model is a reasonable representation of the physical system. Solving the inverse problem is complicated because more than one set of model parameters can produce an equally well calibrated model. To minimize the potential for this problem, the simplest spatial distribution of model parameters was used to calibrate the numerical models.

6.6.3 **Simulated heads for the aquifer**

The running, convergence and calibration of the flow model for the Aveiro Cretaceous aquifer proved to be a difficult task because of the many uncertainties related to the aquifer parameters, discharge volumes and some of the boundary conditions.

The calibration process consisted of the following phases:

- adjusting the aquifer hydraulic conductivities;

The model did not converge with the initial input hydraulic properties. The main problem was the huge contrasts in the hydraulic conductivity of model layers, and in particular because the values assigned to the fault region and some intermediate layers were very tight compared to the rest of the domain. As long as the permeabilities for the intermediate layers were increased the model immediately converged. However, the hydraulic conductivity for the top aquifer layer and for the layer corresponding to the 'Furadouro sandstone formation' were always kept constant, while for the confining layer had to be reduced by one order of magnitude.

The hydraulic conductivity of the zone between the confined part of the aquifer and the outcrop area (regional fault) was initially too low and besides producing very high hydraulic heads in that region also contributed for almost 100% of the flow to go from the outcrop area to the top

unconfined aquifer layer. The hydraulic conductivity values were then increased by one order of magnitude but can still be considered quite low (0.01 m d^{-1}).

- adjusting the aquifer specific storage;

All the initially assigned specific storage values had to be decreased by one order of magnitude to reproduce approximately the observed drawdown in the aquifer, that is to say to increase drawdown. On the contrary, the specific storage values in the unconfined part of the aquifer were increased to reproduce the unconfined conditions in that part of the aquifer.

- adjusting groundwater recharge;

It was impossible to make the model converge with recharge rates lower than the estimated 140 mm a^{-1} and also lower values of recharge would produce dry cells (water table below the bottom of the cell) in the top layer of the model. However, when assigning this very high recharge rates to the whole aquifer they would produce very high head values in the outcrop area, which did not agree with the field values. To solve this problem recharge in the cells corresponding to the less permeable Cretaceous outcrops ('Verba sandstone formation') was considered just 10% of the average recharge estimated for the all area. This improved the estimated water level results not just in the recharge area but also in the southern border of the aquifer, approximating field values (Fig. 6.11). The highs for the water table values in the aquifer top layer are located in the southern and eastern part of the aquifer (50 m a.m.s.l) and gradually reduce in the central part, where flow to the sea is very limited.

The adjustment of these parameters was checked using a non-linear parameter estimation programme (PEST) but did not contribute to improve the modelling results, which are shown in the following figures for the principal aquifer layer ('Furadouro sandstone formation').

Under steady state conditions (1955's) the flow in the aquifer is from the east part to the sea (Fig. 6.12). The border between the confined-unconfined part of the aquifer limits the flow to the confined part of the aquifer, with an important part (60%) of this flow discharging to the top aquifer layer or to any surficial water body in that region (Fig. 6.13). The effect of this boundary on the head distribution is more significant the lower the permeabilities of the aquifer layers are. The simulated heads considered as the best estimate are still a bit too high in the recharge area but this problem could not be solved and is probably related to the boundary conditions. If the permeability of the fault region was increased the heads would go down but the flow to the confined part of the aquifer would increase and the residence times obtained for the aquifer (varying between a minimum of 2.65E+6 and 1.10E+7) would decrease significantly, increasing also the average velocities in the aquifer (maximum velocities estimated are 1.7 m d^{-1}).

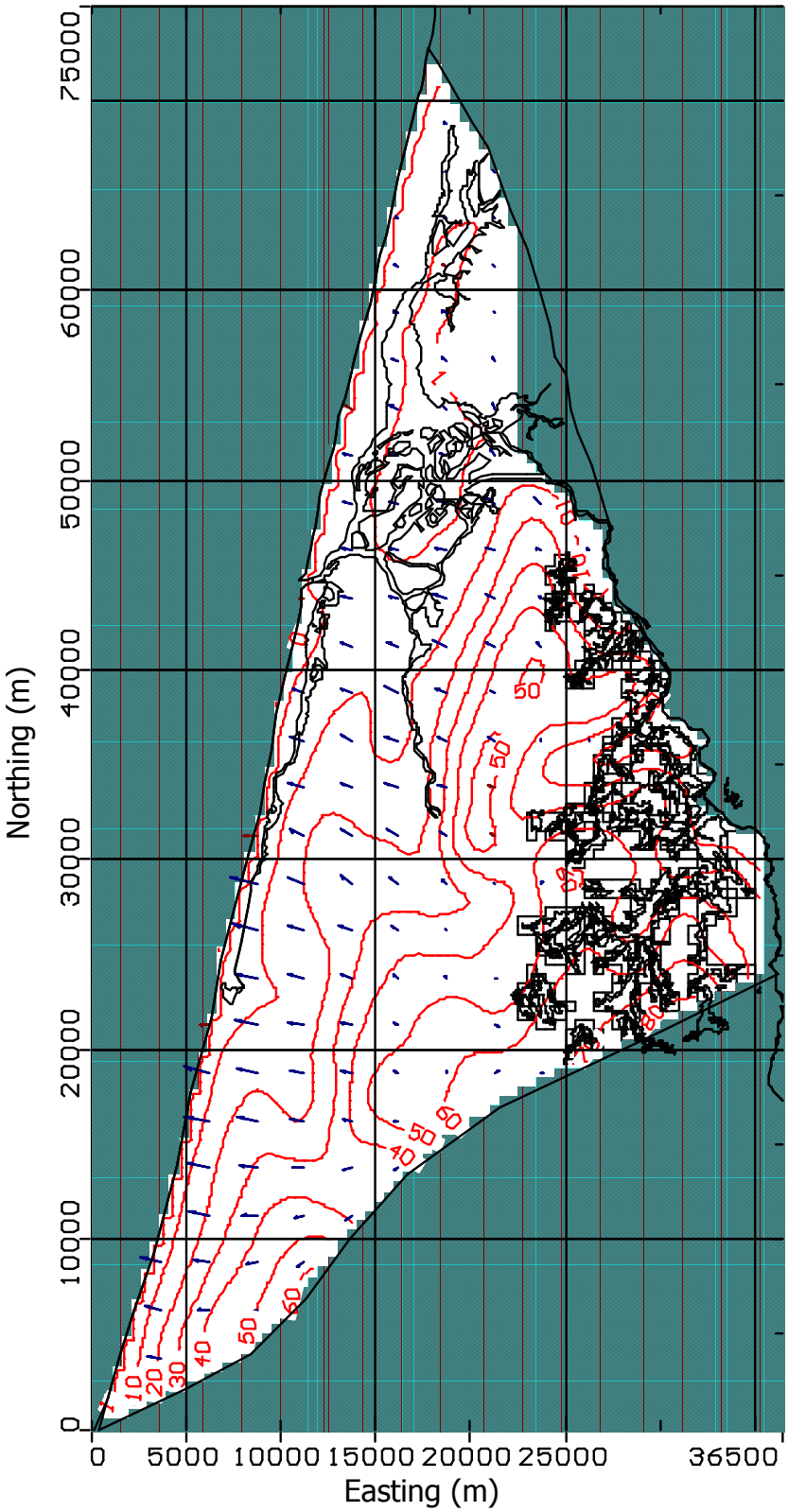

Fig. 6.11 Water table simulation under steady state conditions for the aquifer top layer and recharge area.

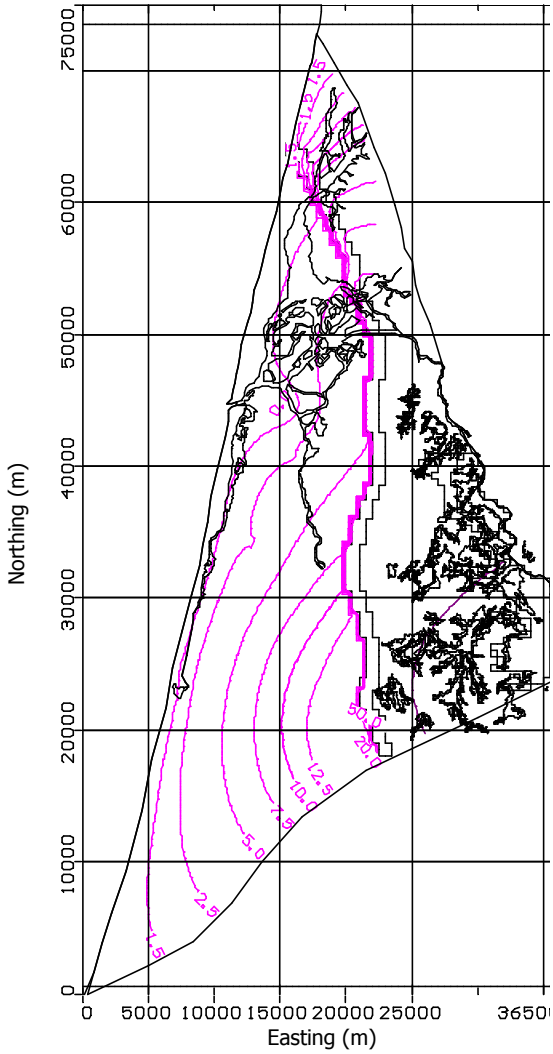

Fig. 6.12 Simulated heads for aquifer layer 5 under steady conditions.

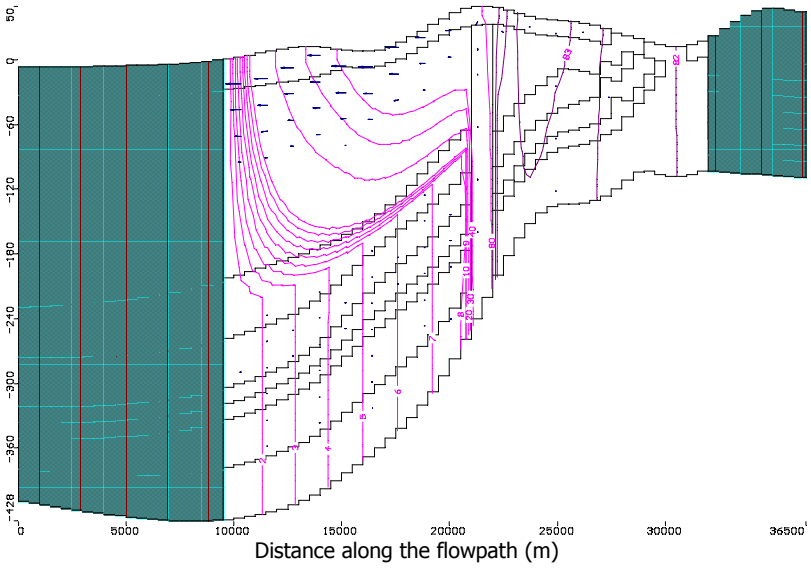

Fig. 6.13 Results presented in cross-section for the steady simulation (row 77).

Pumping was gradually introduced in the aquifer since the early sixties, and the flow model was used to simulate the present day situation in the aquifer under transient simulation conditions and considering the pumping rates supplied by the local Water-Supply companies and the estimated pumping rates of the boreholes for industrial and domestic use supply (Fig. 6.14).

The results of the simulation show a depression in the central part of the aquifer with heads below mean sea level (-10 m). The present day observed head values in that part of the aquifer are even lower and the difference is probably related to the underestimation of the pumping rates.

The computed water budget for present day indicates that an approximated volume of water of 3 E^{-8} m^3 is entering the aquifer through the constant head boundary along the coastline. And although the discharge volume along the coastline is one order of magnitude higher, this confirms the inversion in the flow direction observed in the central part of the aquifer.

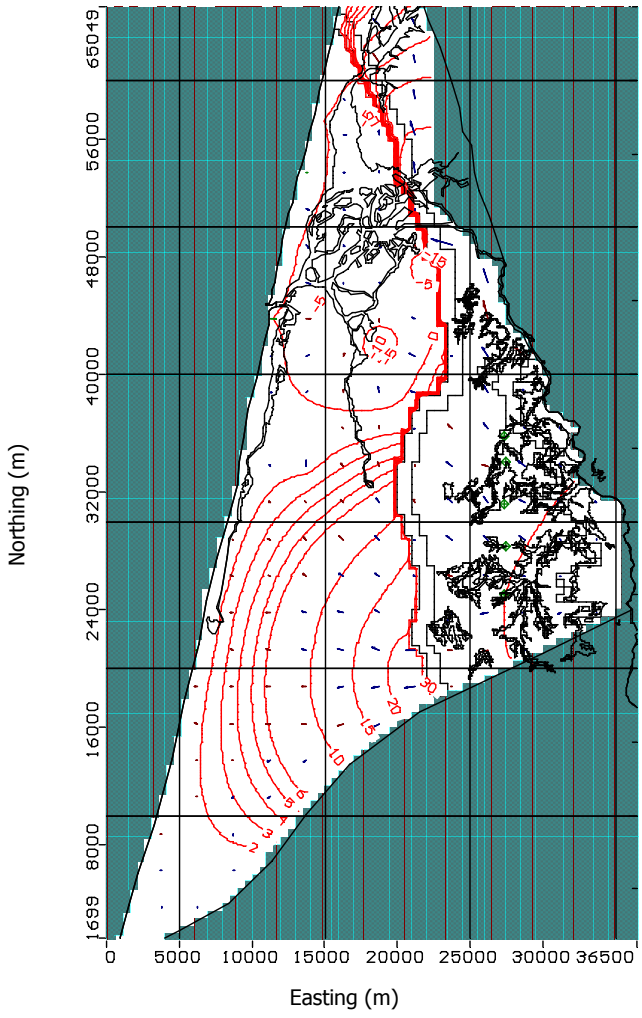

Fig. 6.14 Estimated heads for the aquifer layer number 5 at present day simulated under transient conditions.

6.6.4 **Prediction results for the year 2035**

The flow model was then used to predicted the water levels for the future assuming that the local Water-Supply companies keep their present day abstraction volumes and the industrial areas double their groundwater needs. The result of the simulation for the year 2035 is presented in Fig. 6.15 and shows the extensive depression in the central part of the aquifer.

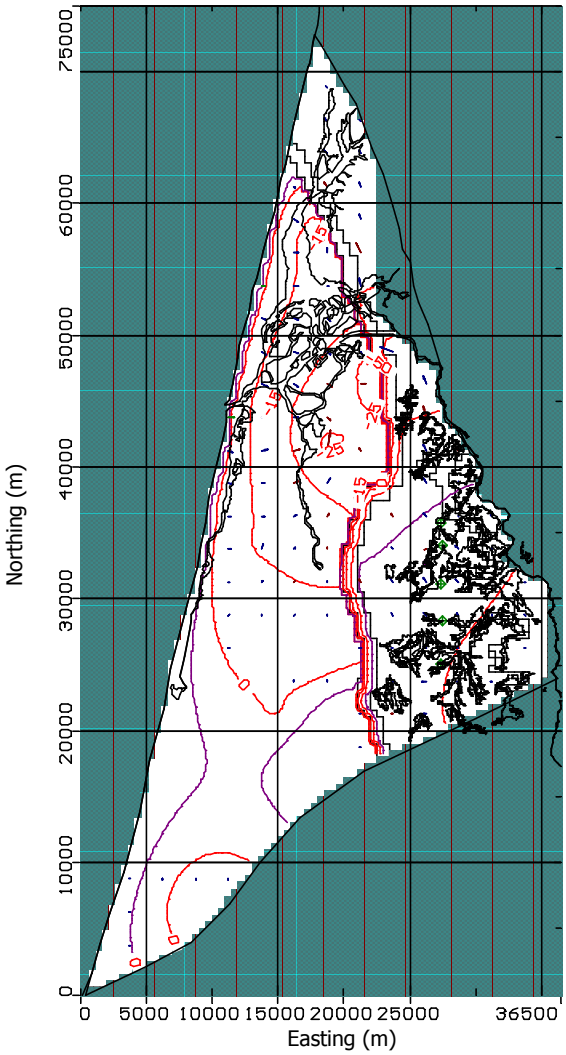

Fig. 6.15 Estimated heads for the aquifer layer number 5 for the year 2035 under transient conditions.

6.6.5 **Sensitivity Analysis**

A sensitivity analysis was performed with the regional-scale model to determine the effects of various boundary conditions and aquifer parameters on the simulated estimates of groundwater discharge to the Atlantic Ocean. And the conclusions is that although recharge and permeabilities

are important with the discharge increasing with their increase, the role of the unconfined-confined boundary is critical and increases drawdown in the aquifer reducing outflow to the sea.

6.7 Offshore continuation of the Aveiro Cretaceous aquifer

The issue of estimating groundwater resources in the Aveiro Cretaceous aquifer has always faced the obstacle of not knowing the offshore continuation of the groundwater system nor the submarine groundwater discharge. Although there are several geological and geochemical evidences that the aquifer system extends beyond the present coastline, the question about how far into the offshore can fresh groundwater be carried remains answered. However, there is the strong possibility of freshwater or brackish water being preserved in the present confined offshore areas.

Numerous studies have reported observation of fresh and/ or brackish groundwater far offshore, beneath continental shelfs and other shallow seas (Reilly & Goodman, 1985; Kooi & Groen, 2001). The results of these studies indicate that there are three main factors which may contribute for the development of an extensive freshwater wedge in the offshore: (1) a high head or freshwater discharge at the coastline; (2) a thick, high-permeability semi-confined aquifer; and (3) the existence of a thick, low permeability confining layer near the seafloor.

The Aveiro Cretaceous aquifer fulfils two of these three requirements, which indicates the possibility of occurrence of low salinity groundwater in the offshore area as a relic of freshwater recharged from precipitation during periods of low sea level at the LGM and that became trapped during the Holocene sea-level rise (Fig. 6.16).

The mathematical simulation of flow and salinity conditions at the offshore would require elaborated analytical solutions and numerical variable-density flow and transport modelling, which use were beyond the objectives of present research. However, a simple modelling approach was used to verify the hydraulic head distribution in the aquifer and check the time span of groundwater to discharge along the continental slope.

The flow system was conceptualised as consisting of a regionally extensive aquifer overlain by a continuous low permeability confining layer. The aquifer outcrops in the recharge area that is located about 20 km and 70 km from the coast at present day and at the LGM, respectively. The flow system dips uniformly seaward and steady-state conditions were assumed.

A cross-section model was designed consisting of four layers, as follows:

- layer 1: top layer of the model corresponding to the high conductivity Quaternary sandy deposits (K_x= 15 m d^{-1}; K_z= 0.15 m d^{-1});

- layer 2: it corresponds to the thick confining layer, which limits modern infiltration from the top aquifer unit (K_x= 10^{-5} m d^{-1}; K_z= 2 10^{-6} m d^{-1});
- layer 3: it is the all set of aquifer layers, which as assigned an average hydraulic conductivity lower than that just corresponding to the 'Furadouro sandstone formation (K_x= 10 m d^{-1}; K_z= 0.01 m d^{-1});
- layer 4: corresponds to the aquitard layer and was assigned a lower hydraulic conductivity (K_x= 0.1 m d^{-1}; K_z= 0.02 m d^{-1});

The recharge conditions were assumed constant for the simulation period and approximate the regional value of 140 mm a^{-1} on top of the Quaternary sediments and 10% of this value in the Cretaceous sediments outcrop area. A constant head value of 5.125 m and 1.025 m was assigned to the offshore limit of the aquifer for simulating the conditions of groundwater flow in the aquifer at 18 ka BP and present day, respectively. Both constant heads account for the differences between sea and freshwater densities and assume that the column of seawater at the edge of the continental shelf is nowadays approximately 200 m.

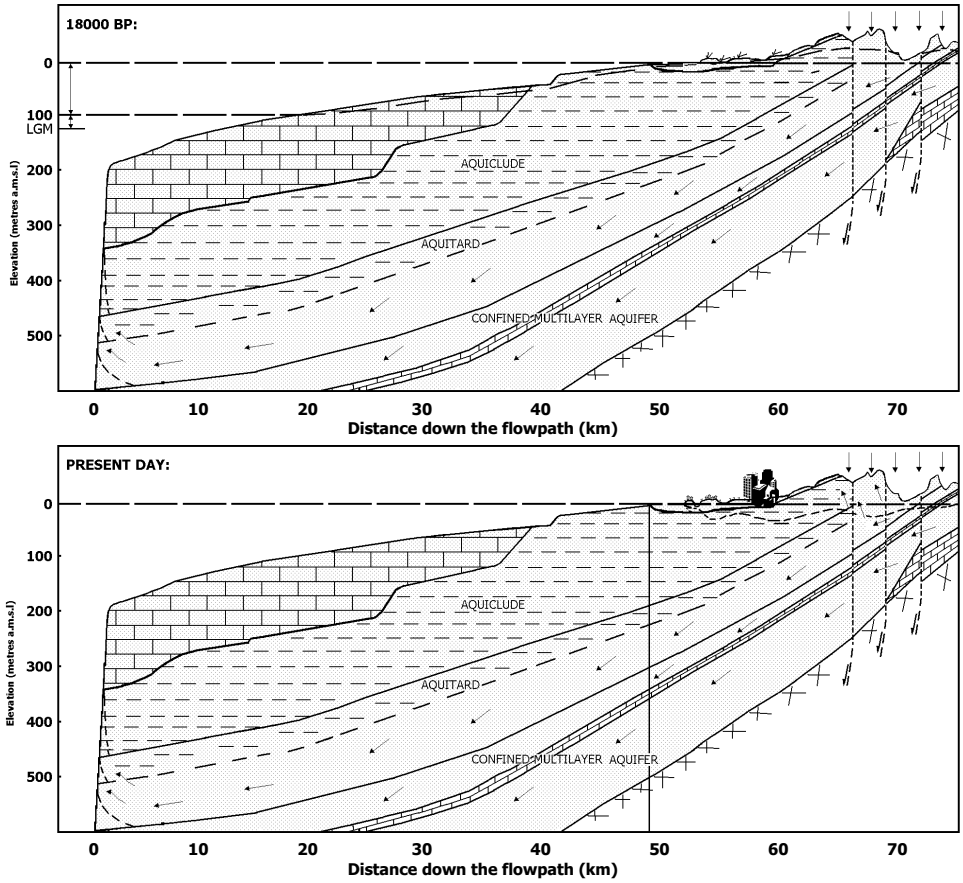

Fig. 6.16 Schematic representation of the impact of sea level rise on the extension of the Aveiro Cretaceous aquifer since the LGM. The distance to the coastline was at the LGM about 50 km further offshore.

The flow modelling results are shown in Fig. 6.17 and prove that for steady state conditions in the aquifer and even with low hydraulic heads along the coastline there were hydraulic conditions for offshore discharge. However, present day offshore discharge would require heads over 7 m at the coastline, which could have existed under pre-development conditions, but not anymore nowadays.

The estimated ages using particle tracking exceed 70 ka for the whole flowpath (around 75 km) and correspond to about 25-30 ka at present coastline, which is in agreement with the observed distribution of carbon-14 ages in the aquifer.

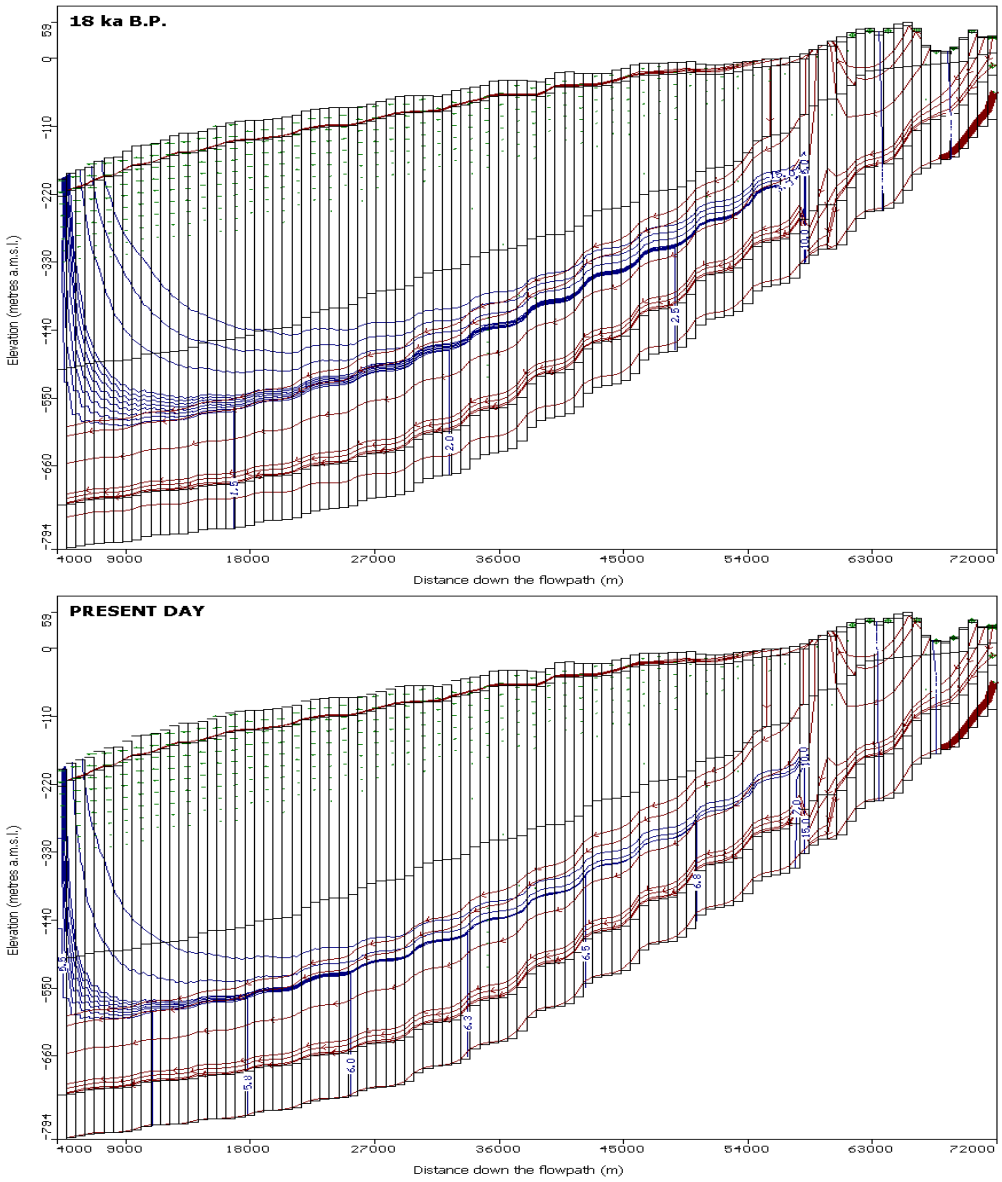

Fig. 6.17 Results for the simulation of the head distribution in the off-shore part of the aquifer at 18 ka B.P. and at present day. Particle tracking results are in agreement with groundwater ages for the aquifer (each arrow along the red pathlines corresponds to 5,000 years).

6.8 Conclusions

The flow model of the Aveiro Cretaceous aquifer should be accepted as a preliminary attempt to build a three-dimensional groundwater flow model for the aquifer that certainly needs further discussion and investigation. The aquifer flow model managed to approximate the spatial distribution of hydraulic heads for the central part of the aquifer although they are slightly underestimated, but it fails to describe the head distribution in the southern part of the aquifer.

The difference between the observed and the estimated heads in the central part of the aquifer could be justified by the uncertainty in the estimation of the total volume of borehole abstraction in the aquifer, which is nowadays probably much higher than 24 $hm^3 a^{-1}$. This reason cannot be used to justify the difference in the southern part, where the model probably requires a different type of boundary condition. A constant head boundary of about 50 m does improve the head distribution but requires further investigation.

The model demonstrated that the contribution of modern recharge to the deep confined part of the aquifer is practically null and that most of the modern recharge goes into the surficial aquifer or to surface water bodies in the region.

The model confirms the present day inversion of the hydraulic heads in the central part of the aquifer indicating that water is coming from the offshore part of the aquifer. The future increase in the pumping rates will contribute for the decrease in the hydraulic heads and to increase gradually the income of water stored offshore.

The flow simulation extending the model till the continental edge showed that a large volume of fresh water should exist in the offshore area of the aquifer. Assuming a steady state for the aquifer, the results indicate that despite the low hydraulic heads along the coastline, the aquifer could discharge to the sea under predevelopment conditions. However, the model also indicates that nowadays with the observed depletion of the hydraulic heads this is highly improbable.

The use of this preliminary flow model for water management would require the clarification of several uncertainties:

- the role of the unconfined-confined boundary of the aquifer;
- the relation between surficial water bodies and groundwater bodies in the unconfined part of the aquifer;
- the type of boundary in the southern part of the aquifer. A constant-head boundary does approximate better the head distribution in the southern part of the aquifer but a justification needs to be found for the high hydraulic heads in this part of the aquifer;

- the use of a constant head to simulate the coastline;
- the estimated predevelopment potentiometric surface based on field data is probably already affected by initial pumping in the aquifer and underestimates the hydraulic heads along the coastline which were expected to be much higher;
- the total volume of aquifer discharge.

7

OVERVIEW OF THE THESIS

This PhD thesis describes in nine chapters the results of detailed hydrogeological, geochemical, flow and transport modelling investigations carried out in the Aveiro Cretaceous aquifer. The overall research was planned with the principal purpose of bringing together information on the geology, hydrology, geophysics, geochemistry and groundwater flow of the Aveiro Cretaceous aquifer in order to improve the understanding of the aquifer system.

Chapter 1 gives an introduction to the study area and summarises the previous hydrogeological investigations in the study region, explains the purpose and scope of the thesis, defines the main objectives and presents the scientific approach and methodology followed to achieve these objectives.

Chapter 2 presents a synthesis of the regional and geological setting of the study area, explaining the structural evolution, geologic history and tectonics of the region. In this chapter, it is also summarised the lithostratigraphy of the sedimentary basin and particular reference is made to the mineralogy of the principal aquifer layers.

Chapter 3 gives the hydrological background of the studied aquifer, defines its limits and describes the principal hydrogeological units and their vertical relation based on the interpretation of borehole geophysical logs. Pumping test results are used to calculate the hydraulic properties of the aquifer and water levels from the National Monitoring Network are interpolated using kriging to estimate the present-day and predevelopment potentiometric surfaces for the aquifer. The principal well and groundwater uses are inventoried and an approximate estimate of the volumes of groundwater discharge is presented with the scarce data available. Most of the hydrogeological information used in this chapter has been compiled in **Appendix A**.

The studied aquifer is part of a thick sequence of mainly siliciclastic sediments deposited in fluvial, deltaic or shallow marine environments under predominantly transitional or continental depositional conditions. Sea level changes and regional elevation due to basin differential uplift and subsidence resulted in alternated transgression and regression movements of the sea followed by cyclical sedimentation of interbedded sand, clay, silt and limestone deposits. Generally, the more sandy continental deposits have higher permeabilities representative of aquifer layers, and the

more clayey transitional (or marine) deposits have lower permeabilities characteristic of confining units (Fig. 7.1).

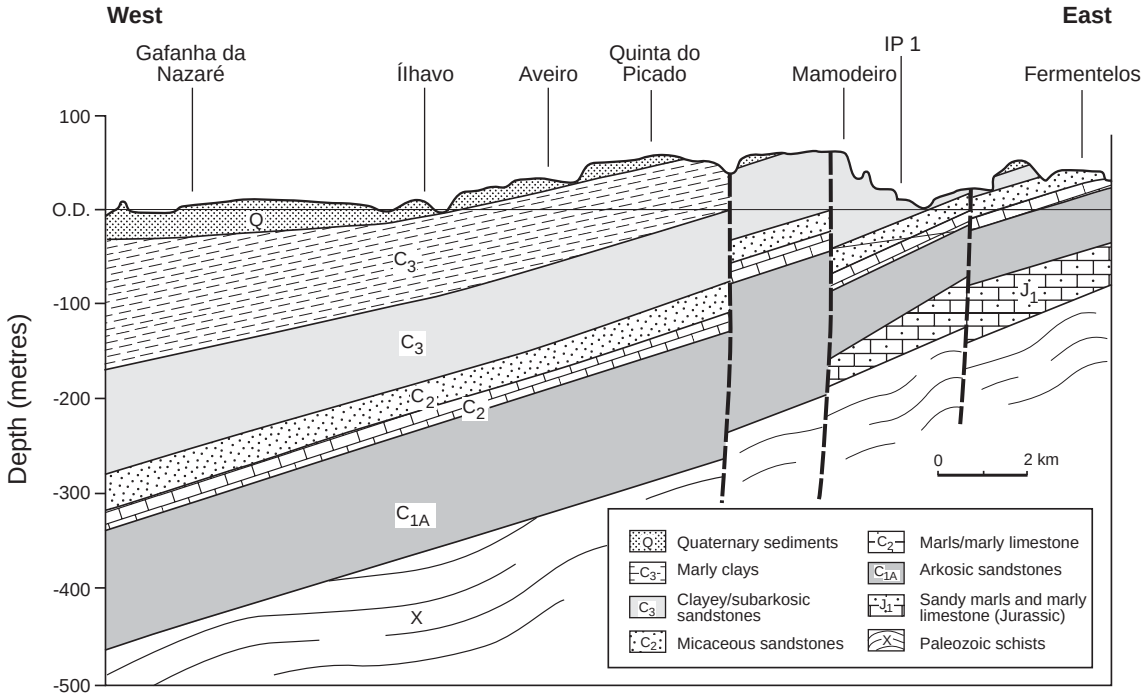

Fig. 7.1 W-E Aveiro multilayer Cretaceous aquifer cross-section (the principal aquifer layers are the top of unit C_{1A}, units C_2 and the bottom of unit C_3)

In the study region, Cretaceous sandstone units yield substantial volumes of water and developed an extensive groundwater flow system confined in two thirds of its extension by a low permeability marly clay formation of Upper Cretaceous age, which limits modern recharge to the aquifer. This unit is not present in the eastern part of the study area where the aquifer is unconfined. Groundwater is withdrawn from the Aveiro Cretaceous multilayer aquifer system by deep multi-screened boreholes, which pump water from the most permeable aquifer layers, at discharge rates varying from a few litres per second to over 50 L s^{-1}.

The three following chapters have been prepared as almost independent review papers, with an introduction, description of the methodology, presentation and discussion of the main results and a final section with the conclusions. However, each chapter gives results and provides interpretations absolutely essential for the following chapters.

Chapter 4 provides the long-term characterisation of rainwater chemistry in the region and estimates of modern groundwater recharge to the aquifer system using different methods.

The predominant source of modern recharge to the aquifer is rainfall. Rainfall quantity and areal distribution and also the long-term measurement of the chemical and isotopic composition of

precipitation in the region were monitored during 5 years. The understanding of rainfall chemistry is necessary not just for recharge calculations but also to interpret past and present hydrochemical values in groundwater, as rainfall is a major input to groundwater.

The results obtained showed that rainfall in the studied region is a slightly acid solution, with a solute content that demonstrates the marine aerosol influence as well as the result of the dissolution of atmospheric gases and solid particles. The concentration of ions in local rainfall follows a general pattern $Cl^- > SO_4^{2-} > Na^+ > Ca^{2+} > Mg^{2+} > K^+ > NO_3$*-N and the rainfall composition changes from Na-Cl near the coast to Na-Ca-*SO_4 *type in the interior. The isotopic composition of rainfall in the region varied over a wide range during the analysed period. Values for the stable isotopes* $\delta^{18}O$ *and* $\delta^{2}H$ *ranged from –8.0 to –1.0‰ and from –55.0 to -1.0‰, respectively, and deuterium-excess varied from –4 to 14‰. However, the weighted mean values are consistent with those interpolated from IAEA monthly precipitation maps for oxygen-18, deuterium and d-excess in Europe.*

The chemical characteristics of rainfall and infiltrating water were used as tracers of groundwater recharge in the region. Four different groundwater recharge estimation methods were used to approximate groundwater recharge in the Aveiro Cretaceous aquifer. Two are physical methods (Penman-Grindley and the water table fluctuation method) and the other two are geochemical methods (chloride mass balance) applied both to the saturated and unsaturated zones. The combined use for the first time in the aquifer of physical methods which rely on direct measurements of hydrological parameters and tracer techniques applied to both unsaturated and saturated zone contributed to substantiate and give some consistency to recharge predictions. However, recharge estimates did vary depending on the method used.

The combination of the four recharge estimation methods provided median values for natural recharge in the region that fall in a relatively narrow interval (110 to 162 mm a^{-1}*) and showed the importance of using estimation methods that account for the recharge spatial variability. Moreover, the results of the investigation confirmed the uncertainty of extrapolating recharge point estimates to a whole recharge area.*

Chapter 5 presents the main results of the hydrogeochemical study and geochemical modelling of the aquifer system. This chapter has been divided in five different sections. In the first section the groundwater sampling and analytical methods used are presented and their limitations discussed. In the following section, the groundwater hydrogeochemical evolution of the aquifer is interpreted giving evidence to the aquifer major hydrogeochemical and redox patterns, minor and trace elements, saturation indices and isotopic signature. All the hydrogeochemical database has been included in **Appendix B**. The third section focused on the aquifer vertical stratification and its impact on groundwater hydrochemistry, and a more detailed description of the specific field work carried out in the aquifer (geophysical logging and depth sampling) was left for **Appendix C**.

In the forth section, geostatistics are used to complement the study of groundwater baseline quality and the results are presented in **Appendix D** and **E** using contour and classed post maps, respectively. These maps are a sort of geochemical atlas for the study aquifer. In the final section, a reaction-path transport model is used to simulate the observed patterns of groundwater chemistry and to confirm the dominant geochemical processes in the aquifer.

The Aveiro Cretaceous aquifer has been the subject of detailed hydrogeochemical studies during the present investigation to characterize both the groundwater quality spatial variability and vertical stratification arising from geological layering. Geochemical data were collected from 90 pumping multiscreened boreholes in the region to study the relations between the groundwater chemistry, aquifer mineralogy, and present and past patterns of regional flow. The approach followed included the identification of major groundwater geochemical patterns in the aquifer, study of the aquifer natural stratification, determination of the aquifer natural background levels, and definition of the controlling processes responsible for the downgradient changes in water chemistry, focusing on mixing processes and water/ rock interactions.

This was accomplished by studying and comparing the chemical and isotopic composition of rain and groundwater, through determination of ionic, molar and isotopic ratios and residence times, calculation of saturation indices relative to most common minerals, and by quantifying the mass balance of solutes along the main flowpaths using a geochemical reaction path transport model. Complementary, the theory of regionalised variables was applied to study the groundwater baseline composition of the aquifer, and contour and classed post maps were used to show the spatial distribution of groundwater geochemical composition.

Identification of hydrochemical facies in the Aveiro Cretaceous aquifer system was based on the distribution of water types and used to divide the Aveiro Cretaceous aquifer in three main zones with gradually different hydrogeochemical characteristics down the flowpath. A redox boundary was defined corresponding approximately with the unconfined-confined boundary in the aquifer. This boundary also separates the pristine groundwaters observed in the confined part of the aquifer from the waters with signs of human impact in the recharge area.

The studied groundwaters have their origin in part associated with the infiltration of rainwater of Atlantic origin (which is essentially diluted seawater) and the gradual flushing of older formation waters (eventually, old seawater trapped in the sediments). Infiltrating rainwater percolates through the unsaturated zone to reach the underlying groundwater body, reacting with silicate and carbonate minerals in a system initially open to CO_2. Because carbonate dissolution kinetics are much faster than the silicate weathering reactions, a fresh groundwater dominated by Ca^{2+} and HCO_3^- initially prevails. Ca^{2+} average concentrations in this part of the aquifer are about 33 mg L^{-1} while Na^+ concentration is less than 14 mg L^{-1}.

As the water moves downward along the flow path into the deeper and confined part of the aquifer, Ca^{2+} ions are taken up from groundwater by cation exchangers that make part of the aquifer matrix (mainly, clay minerals), in return for Na^{+}. In the areas closer to the coast average calcium concentrations are quite small, around 4 mg L^{-1}, while Na^{+} becomes the dominant cation with concentrations higher than 110 mg L^{-1}. Calcium is clearly being taken up from water, in return for Na^{+}, which is being released in solution. With exception to the areas within the outcrop area where calcium is the most abundant cation, sodium is the dominant solute in the aquifer.

The groundwaters contain a smooth record of radiocarbon ages indicating continuity of recharge through the LGM and over a period in excess of 30 ka. The dilute nature of the Aveiro groundwaters thus indicates previous freshening of the coastal aquifer since at least the Late Pleistocene or even earlier. Higher hydraulic gradients during the past geological times imposed by a lowered sea level compared to present day would have contributed for the complete refreshing of the aquifer, with fresh water flushing the original formation water. The presence of fresh palaeowaters at the present coastline implies that groundwater flow was controlled by an offshore outlet, possibly the outcrop at the continental shelf. It is therefore likely that freshwaters exist beneath the sea to the west of Aveiro.

For an aquifer with residence times in excess of 30 ka, the Aveiro Cretaceous aquifer reveals a significantly slow chemical kinetics for the water-rock interactions resulting from the mainly siliciclastic composition of the aquifer sediments and from a very low cation exchange capacity. Silicate weathering, calcite dissolution and cation exchange in the initial phases of seawater flushing are considered to be the processes responsible for the gradual groundwater chemical composition and were confirmed by the use of a reaction-path geochemical model.

Thus the reaction-path modelling in the Aveiro Cretaceous aquifer helped to confirm the principal processes contributing to the hydrogeochemical evolution of the aquifer and gave some more evidence about the time scale for the aquifer freshening, suggesting that the present day hydrogeochemical pattern is the result of 50 ka of geochemical evolution in the aquifer.

The results of a geophysical logging and depth sampling campaign were used to characterize from the geochemical point of view each aquifer layer and confirmed that the 'Furadouro sandstone formation' and the top part of the 'Palhaça sandstone formation' are the best aquifer layers and present the lowest salinities for the aquifer. The 'Furadouro sandstone formation' is indeed contributing with most of the water supplied by the aquifer, in a ratio for the transmitted flow that could be as high as 9:1 when compared to the other aquifer layers. This implies that samples taken from the discharge during pumping conditions can be assumed to correspond in great part (~90%) to the 'Furadouro sandstone formation'. For this reason, and although each aquifer layer has a characteristic chemical and isotopic composition as

demonstrated, the chemical composition of the flow samples is dominated by the chemistry of 'Furadouro sandstone formation'.

However, the data arising from the study of the aquifer vertical stratification also showed that the 'Furadouro sandstone formation' is highly vulnerable to groundwater contamination because of its high transmissivities and depleted hydraulic heads. In the boreholes where leaks at joints in the blank casing were producing inflow of high salinity water from the base of the Quaternary aquifer, it was observed that this water was leaving the borehole through the screens placed in front of the 'Furadouro sandstone formation'. This problem was detected in several boreholes used for monitoring purposes in the region and puts in risk the groundwater quality of the aquifer.

Chapter 6 includes the regional flow modelling of the study aquifer. This chapter uses hydrogeological and hydrogeochemical information discussed in all the other chapters to build a robust conceptual model for the aquifer. Chapter 3 provided the hydrostratigraphic information, aquifer properties and boundaries, water levels and volumes of discharge. Chapter 4 gave the areal distribution of modern recharge and Chapter 5 assisted with the calculated residence times for the aquifer. All these information was integrated and the conceptual model simulated using Visual MODFLOW. Main results show that the aquifer has important reserves of fresh water and still discharges offshore. However, the modelling results also show that nowadays just a very limited percentage of modern recharge enters the aquifer and calls attention for the necessity of limiting abstractions to guarantee the groundwater sustainability in this aquifer.

The Aveiro Cretaceous aquifer is considered quite unique from the geochemical and isotopic point of view and important as an archive of past climate conditions in temperate regions of Europe. And although the groundwater resources in the Aveiro Cretaceous aquifer can not be considered a nonrenewable resource, it has to be accepted that they are not completely renewable in the timeframe of this and future generations.

7.1 Applied significance of results

The improved understanding of the Aveiro Cretaceous aquifer system that resulted from this hydrogeological and hydrogeochemical investigation is an important basis for present day and future water management in the region. The applied significance of the results obtained is ample and hopefully will be of some help to assess the Regional Water Authorities and Water Supply Companies to take decisions about the protection of the aquifer water resources:

- the study provides a consistent description of current water-quality and baseline values in the aquifer. This information may be used to establish the aquifer reference values when defining the groundwater quality monitoring network for the aquifer;
- the major factors that affect the observed water-quality conditions and trends were identified, described and explained and this is also very important for monitoring purposes. Some of the natural baseline values (Fe, Mn, F) exceed the maximum admissible concentrations for human consumption but they are related to natural geochemical processes and not the result of the impact of human activity;
- the division of the aquifer in three different parts with distinct water chemistries could be used to assess the definition of groundwater bodies in the region;
- the calculated residence times for the aquifer show that there is no point in monitoring the groundwater quality in the confined part of the aquifer every month or even every six months. It would be more reasonable to decrease the monitoring frequency and introduce early warning indicators that could indicate, for example, mixture with younger waters (*e.g.*, ^{3}H, $^{3}H/^{3}He$, ^{85}He, SF_6, CFC). In aquifers like the Aveiro Cretaceous aquifer, when concentrations of nitrate are detected is already too late to take any preventive measure;
- the results of geophysical logging and depth sampling campaign showed that some of the boreholes drilled in the aquifer and used nowadays for groundwater monitoring purposes are blocked or present high salinity fluid at shallow depths. This salinity is a result of leaks at joints in the boreholes blank casing allowing high salinity water to enter from the base of Quaternary aquifer and then diffusing along the borehole due to density settling. These results question not only the significance of the water levels measured but also show that some of the monitoring boreholes need to be reconstructed or sealed to prevent them from contaminating the aquifer. This is also the case of the borehole used for supply to the village of Torreira;
- The vertical stratification of the water quality in the aquifer is responsible for the mixing of waters of different qualities in a borehole. When the borehole is pumping, the most transmissible layers provide 90% of the water. However, when the boreholes are left without pumping for a long time they get filled with water coming from the lower transmissivity layers but nowadays with higher hydraulic gradients. This means that the water supply boreholes should be use to pump water every so often, even when this water is not necessary, or otherwise they will deteriorate and contribute to salinize the aquifer;

- the flow modelling results show that the aquifer receives very limited modern recharge and confirms the gradual decreasing in the water levels. These results should be looked attentively by the Regional Water Authorities because they indicate that strong measures should be taken in order to monitor the volumes of abstractions and to limit the construction of new boreholes in the region. The present day volume of abstractions and the increasing number of new wells cannot be considered sustainable;
- the limitations of the model require specific field work and further modelling exercise to clarify all the questions and doubts raised during the modelling process;
- the model could be used in collaboration with the Water Authorities to be improved to be able to test various management schemes and to predict the effects of certain actions.

7.2 Future directions for research

This PhD thesis uses a varied range of conventional and modern scientific tools to study in detail the Aveiro Cretaceous aquifer. For this reason, some of the new methodologies used can certainly be improved or applied in different conditions. Future directions for research in the aquifer should consider:

- to investigate in detail the behaviour of the trace elements in the aquifer, explaining their evolution down the flowpath;
- to try to improve the geochemical modelling results introducing kinetics to describe the water-rock interactions;
- to concentrate on the study of the hydraulic heads and well yield data of the boreholes located along the coastline to infer if there are any further indications of aquifer flow offshore, and to define precise offshore limits of the aquifer;
- to plan a specific campaign including isotopic investigations and pumping tests to try to define the exact position of the unconfined-confined boundary of the aquifer;
- to study the relation between groundwater and surface waters in the aquifer recharge area;
- to integrate all the hydrogeological three-dimensional information of this thesis with previous results from Marques da Silva (1990), Rocha (1993) and Figueiredo (2002) to develop a consistent three-dimensional model for the north most part of the Lusitanian basin.

8

CONCLUSIONS

The Aveiro Cretaceous aquifer represents a main water resource of an important industrialized area of northwestern Portugal with a high population density and intense agricultural activity. The growing demand for water resources in the region led progressively to an increased reliance on groundwater from the Cretaceous aquifer formations for most of the urban and industrial water supply. Intensive pumpage since the early sixties has gradually caused natural piezometric surface declines and is now threatening the natural balance of this coastal aquifer system.

The Aveiro Cretaceous multilayer aquifer system covers over 1,800 km^2 of the northwest part of the Portuguese mainland and adjacent continental shelf and is part of a thick sequence of mainly siliciclastic sediments deposited in fluvial, deltaic or shallow marine environments under predominantly transitional or continental depositional conditions.

The aquifer has been the subject of detailed hydrogeological and geochemical studies during the present investigation, which were complemented by the use of flow and reaction-path transport modelling. These studies contributed to derive a coherent and broad understanding of the aquifer system and to clarify several aspects about the aquifer present day hydrodynamics and palaeohydrology.

A summary of the main conclusions of the present investigation are presented in the following paragraphs:

1) The Aveiro Cretaceous aquifer is a multilayer aquifer system formed by geologic units with increasing thickness seaward, downdip direction, and distinct hydrogeological properties. The deepest part of the sedimentary basin is near Vagos where the whole Cretaceous column can present thicknesses over 400 m. The boreholes in this part of the aquifer pump waters with temperatures higher than 27ºC, the highest observed in the study region, which are in agreement with the depth of the aquifer layers in this area;

2) The western two-thirds of the aquifer extension are confined where the Cretaceous sandstone formations are overlain by the 'Aveiro marly clay formation'. The average thickness of this confining unit increases towards the coast and may be over 150 m, in the deepest parts of the aquifer (Vagos). Uplift and erosion of the confining marly clay unit in the east defines the

unconfined part of the aquifer, where the 'Upper sandstone formation', the 'Furadouro formation' and the 'Lower sandstone formation' crop out at the surface and receive direct recharge from rainfall infiltration. The 'Carbonate formation' ('Mamarrosa limestone'), which also crops out in the recharge area, is of low permeability, indicated by the occurrence of springs and swampy areas in the contact between the 'Carbonate formation' and the overlaying micaceous sandstone unit;

3) The structural geology of the Cretaceous formations is quite simple in the central and northern part of the study area but faults of approximately north-south orientation have been inferred in the geologic maps and when drawing interpretative cross-sections in the eastern and southern part of the study aquifer. These faults contribute for the vertical partitioning of the aquifer and limit the inflow of modern recharge to the aquifer;

4) The natural groundwater flow is under natural conditions from the recharge area in the east towards the sea, with a natural gradient around 0.0015. However, the values observed at present show that hydraulic heads are below mean sea level in the central part of the aquifer. Potentiometric highs are in the southeast part of the aquifer close to the recharge area and to the southern limit of the aquifer. A large depression of the piezometric surface and a reversal of the natural flow direction may be observed nowadays in the area between Ílhavo, Aveiro and Cacia;

5) The examination of the pumping test interpretation results show that the intermediate part of the aquifer, which includes the Oiã and Furadouro formations and the top part of the Palhaça sandstone formation, has the highest hydraulic conductivities (18 to 22 m d^{-1}) and is where most groundwater flow occurs. The other aquifer layers have hydraulic conductivities lower than 5 m d^{-1}. Detailed geophysical logging studies confirm that the ratio for the transmitted flow by the 'Furadouro sandstone formation' could be as high as 9:1 when compared to the other aquifer layers;

6) Samples taken from the discharge during pumping conditions can thus be assumed to correspond in great part (~90%) to the 'Furadouro sandstone formation'. Therefore, the samples obtained from the boreholes discharge while pumping during the sampling campaigns are considered to be representative of chemical characteristics of the principal aquifer layer;

7) The central part of the aquifer (around Ílhavo, Aveiro and Cacia) has the highest transmissivity values, while in the rest of the region (either to the north, east, south or even along the coast), the transmissivity suffers an important decrease. The aquifer recharge area shows remarkably low transmissivities (< 50 m d^{-1}), which is another factor limiting the inflow of modern recharge to the aquifer;

8) Review of historical groundwater level data indicates that the aquifer has never been in a steady-state condition during the monitoring period. The hydrographs show that in spite of the fast recovery in the water levels (1 to 2 m per year) observed in the late nineties (and as should be

expected from a confined aquifer), they are falling again, requiring strong protection measures from the Water Authorities;

9) Mean groundwater discharge from the Aveiro Cretaceous aquifer system is essentially of three types: (1) the water pumped by the boreholes drilled in the aquifer; (2) the discharge to a few springs in the recharge area and in some periods of the year to the Pateira lagoon and surrounding wetlands; and, (3) the possible aquifer discharge to the sea. The greatest volume of groundwater discharge is directly into boreholes. Due to the lack of data, the calculation of the total volume of aquifer abstractions is one of the uncertainties that limits the present research. The total aquifer discharge was calculated to be about 21.2 $hm^3\ a^{-1}$;

10) Modern groundwater recharge has been estimated to vary temporally and spatially, and the interval of values estimated for the region (110 to 162 mm a^{-1}). The use and comparison of multiple independent approaches to estimate groundwater recharge in the study area was extremely important because besides helping to confirm that recharge estimates do vary depending on the method used, it also called attention to: the importance of the actual evapotranspiration estimate when you are calculating recharge applying the Penman-Grindley method; the danger of extrapolating point estimates to a whole recharge area (*e.g.* the use of unsaturated zone profiles to calculate the recharge for a whole area); the difficulty of comparing rainfall events to unsaturated zone profiles in areas with humid climates and shallow water levels; the nonsense of comparing results provided by the same methodology but that cover different time intervals of recharge (*e.g.* to compare results from two unsaturated zone profiles with different total lengths); the importance of using methods that account for the spatial variability (*e.g.* both the chloride mass balance in the saturated zone and the water table fluctuation method provide not just spatially averaged recharge rates but also allow for point estimates);

11) The hydrogeochemical study of the Aveiro Cretaceous aquifer confirmed the division of the aquifer in three main parts with gradually different hydrogeochemical characteristics. The outcrop area in the east part of the study area, where the infiltrating rainwater percolates through the unsaturated zone to reach the underlying groundwater body, reacting with silicate and carbonate minerals in a system initially open to CO_2. Because carbonate dissolution kinetics are much faster than the silicate weathering reactions, a fresh groundwater dominated by Ca^{2+} and HCO_3^- initially prevails. Thus the recently recharged oxygenated groundwaters are of predominantly Ca-HCO_3 hydrochemical facies, with *p*H values lower than 7.0 and water temperatures less than 20°C. Further down the flowpath, the aquifer becomes gradually confined and with very limited modern recharge. Holocene to pre-industrial groundwater occurs in the intermediate, confined part of the aquifer. Redox potential and dissolved oxygen progressively decreases along the flowpath with groundwater changing from oxidising to reducing conditions and defining a redox boundary. These are groundwaters with either Ca-HCO_3 or Na-HCO_3

hydrochemical facies and pH values higher than 6.2 but lower than 8.3 and groundwater temperatures around 21.3 ºC. P_{CO2} decreases in this part of the aquifer from 0.04 to 0.001 down flowpath and the aquifer is gradually under closed system conditions. Late Pleistocene-Early Holocene groundwaters have been identified in the deeper and confined part of the aquifer. They are Na-HCO_3 or Na-Cl type waters, with *p*H in the range from 7.1 to 8.9, and average groundwater temperatures higher than 22°C. The negative Eh values reflect anaerobic (reducing) conditions;

12) The evolution of the groundwater towards an evolved Na-HCO_3 water type near the coastline indicates that ion exchange and calcite dissolution are dominant geochemical processes in the aquifer. Taking into account the mineralogy of the aquifer matrix and the long residence times, alumino-silicate weathering is likely to be the other process responsible for cation variation in the Aveiro aquifer. Besides, the observed decrease of P_{CO_2} along the flowpath confirms that mineral reaction is taking place;

13) Speciation calculations for the aquifer suggest that just a few minerals are at saturation in the aquifer. Groundwater from all sites was in equilibrium with chalcedony and saturated with respect to quartz and for some of the common clay minerals - kaolinite, smectite and illite. Subsaturation persists for plagioclase and other feldspar minerals. In two thirds of the aquifer, groundwater is undersaturated with respect to calcite, with saturation index values increasing from –5.0 to –1.0 with increasing residence time. This confirms that calcite dissolution is still taking place in this system, increasing the degree of saturation of this mineral with groundwater residence time. The same trend was observed for dolomite;

14) The baseline of fresh groundwater in the Aveiro Cretaceous aquifer is of remarkably low salinity (below 50 mg L^{-1} Cl^-), considering that it was, at least in part, of marine origin. The low chloride concentrations (minimum 16 mg L^{-1}, which is about 4x the mean rainfall value) over most of the aquifer is consistent with the main input to groundwaters being derived from atmospheric inputs after allowing for evapotranspiration, and at depth the remaining Cl^- is little more than 1-2% of that probably derived from (marine) formation water;

15) Hydrogeochemical data for the aquifer indicate very slow kinetics for the aquifer geochemical reactions. This is in agreement with low CEC values determined for the aquifer, which confirmed the very low cation exchange capacity, and thus the low reactivity of the aquifer matrix;

16) Although the isotopic and chloride data show that the aquifer has been fresh for more than 18 ka, the freshening chemical pattern of the aquifer and the evolution of pH and alkalinity suggest that the aquifer has had previously seawater and that there is probably still an outlet offshore which is confirmed by the flow modelling results. The dilute nature of the Aveiro groundwaters thus indicates previous freshening of the coastal aquifer since at least the Late Pleistocene or even earlier. Higher hydraulic gradients (~0.004) during the Last Glacial Maximum

(LGM) or even before LGM imposed by a sea level lowered by approximately 130-140 m compared to present day would have accelerated the complete refreshing of the aquifer, with fresh water flushing the original formation water;

17) The isotopic results of the present study confirm the existence of palaeowaters in the confined part of the aquifer and the documented enrichment of stable isotope content down the flowpath;

18) The distribution of groundwater ages in the aquifer confirm the sudden change of groundwater flow velocities that took place the LGM when the lowered sea level contributed for much higher hydraulic gradients in the aquifer and probably to the almost complete flushing of seawater from the aquifer;

19) The calculated apparent flow velocities for the aquifer based on the C-14 dating indicate a gradual decrease of flow velocities along the flowpath, from a few metres per year in the areas closer to the recharge area to less than half a metre per year in the very confined part of the aquifer;

20) The rather constant Cl^- values (~1 mmol L^{-1}) throughout much of the time period of >30 ka suggest constant inputs from marine aerosols from the present day through till at least the LGM. Little if any Cl^- contamination is recognisable in the modern groundwaters (except in the case of leaks at borehole columns). Mixing with more saline formation waters is only observed in the oldest groundwaters, which confirms that increasing salinities in the aquifer are related to increasing residence time and not to modern salt water intrusion;

21) The transport model describes the observed hydrochemical evolution quite satisfactorily confirming that the dominant reactions in the aquifer are calcite and K-feldspar dissolution, and cation exchange. Feldspar dissolution is slowly releasing some aluminium and silica into solution but they will precipitate in silica minerals, kaolinite and illite.

22) The model reproduces the ion exchange fronts with the calcium from the flushing solution displacing initially magnesium from the ion exchange complex, and further downstream, both calcium and magnesium displacing sodium;

23) According to the model, the present day hydrogeochemical pattern is the result of 50 ka of geochemical evolution in the aquifer, which means that the aquifer has been fresh since the Late Pleistocene. This is in agreement with carbon-14 and chloride data for the aquifer that revealed fresh water since at least 35 ka, and also with the geological data. And this proves that the palaeohydrology is still dominating the aquifer geochemistry, which is not yet affected by the extensive abstractions and over pumping since the late sixties;

24) Both the interpretation of the geological and hydrogeological information and the results of the numerical simulation confirm that the flow model reproduces reasonably the groundwater flow patterns for the central part of the aquifer taking into account the assumptions and the conceptual model limitations. Nevertheless it also points out the necessity for further investigation;

25) The flow model results show that overpumping is affecting the aquifer storage and contributing for an inversion of the flow direction. Because of the large volume of freshwater stored offshore this change in the flow pattern is still not detected by the analysis of the chemical patterns in the aquifer;

26) The flow modelling results also show that the discharge is not compensated by natural recharge because most of it goes to the surficial Quaternary aquifer and to surface water bodies;

27) The 2-D off-shore model confirms that there were conditions for aquifer flow offshore under predevelopment conditions and even with low hydraulic heads along the coastline. However, the model also shows that nowadays the hydraulic heads are not high enough to guarantee aquifer offshore discharge if there is an offshore outlet for groundwater flow in the aquifer;

28) The predictions of the flow model for the year 2035 indicate a pronounced depression of the hydraulic heads in the aquifer that requires strong measures by the Regional and National Water Authorities.

9

REFERENCES

Alley, W.M., Reilly, T.E. & Franke, O.L. 1999. Sustainability of ground-water resources. U.S. Geological Survey Circular 1186, 79 pp.

Allison, G.B. 1981. The use of natural isotopes for measurement of groundwater recharge. Proceedings Groundwater Recharge Conference, Townsvill. Australian Water Resources Council, Australian Government Publication Service, Camberra*,* 203-214.

Allison, G.B. 1988. A review of some of the physical, chemical and isotopic techniques available for estimating groundwater recharge. *In:* I. Simmers (ed). Estimation of natural groundwater recharge. Nato ASI Series C 222, D. Reidel Publishing Company, Dordrecht*,* 49-72.

Allison, G.A. & Hughes, M.W. 1978. The use of environmental chloride and tritium to estimate total recharge to an unconfined aquifer. *Aust. J. Soil. Res.*, **16***,* 181-195.

Allison, G.A., Gee, G.W. & Tyler, S.W. 1994. Vadose-zone techniques for estimating groundwater recharge in arid and semiarid regions. *Soil Sci. Soc. Am.*, **58***,* 6-14.

Allison, G.B., Barnes, C.J., Hughes, M.W., Leaney, F.W.J. 1984. Effect of climate and vegetation on oxygen-18 and deuterium profiles in soils. *In:* Isotope Hydrology 1983, IAEA Symposium 270, September 1983. International Atomic Energy Agency, Vienna, 105-123.

Amorim, I. 2001. Aveiro e os caminhos do sal. Câmara Municipal de Aveiro, Aveiro, 123 pp.

Andersen, M.S. 2002. Geochemical processes at a seawater-freshwater interface. PhD thesis, Technical University of Denmark, Denmark, 250 pp.

Anderson, M.P. & Woessner, W.W. 1992. Applied groundwater modelling. Simulation of flow and advective transport. Academic Press, San Diego, 381 pp.

Andeweg, B. 2002. Cenozoic tectonic evolution of the Iberian Peninsula, causes and effects of changing stress fields. PhD thesis, Vrije Universiteit Amsterdam, The Netherlands, 178 pp.

Appelo, C.A.J. & Postma, D. 1996. Geochemistry, groundwater and pollution. 3rd Edition. A.A. Balkema, Rotterdam, 536 pp.

ASTM 1996. ASTM standards on analysis of hydrologic parameters and ground water modelling. Sponsored by ASTM Committee D-18 on Soil and Rock. Philadelphia, 146 pp.

Baas, J.H., Mienert, J., Abrantes, F., Prins, M.A. 1997. Late Quaternary sedimentation on the Portuguese continental margin: climate-related processes and products. *Palaeogeography, Palaeoclimatology, Palaeoecology*, **130**, 1-23.

Barbosa, B.P. 1981. Carta geológica de Portugal na escala de 1/50 000. Notícia explicativa da folha 16-C - Vagos. Direcção-Geral de Geologia e Minas, Serviços Geológicos de Portugal, Lisboa.

Barra, A.J.P. 1998. Cartografia geológica dos depósitos Meso-Cenozóicos do sector Pateira de Fermentelos – Anadia (Aveiro): dados preliminares. Internal report. Faculdade de Ciências da Universidade do Porto, Portugal, 88 pp.

Bazuhair, A.S. & Wood, W.W. 1996. Chloride mass-balance method for estimating ground water recharge in arid areas: examples from western Saudi Arabia. *Journal of Hydrology*, **186**, 153-159.

Bernardes, C. (1992). A sedimentação durante o Jurássico superior entre o Cabo Mondego e o Baleal (Bacia Lusitaniana): modelos deposicionais e arquitectura sequencial. PhD thesis, Universidade de Aveiro, Portugal, 261 pp.

Berner, E.K. & Berner, R.A. 1996. Global Environment: water, air and geochemical cycles. Prentice-Hall, London, 376 pp.

Berthou, P.Y. 1971. Le Crétacé supérieur de l'Éstremadure portugaise. PhD thesis, Paris, 472 pp.

Berthou, P.Y. & Lauverjat, J. 1979. Essai de synthèse paléogéographique et paléobiostratigraphique du Bassin Occidental Portugais au cours du Crétacé Supérieur. *Ciências da Terra*, **5**, 121-144.

Bland, W. & Rolls, D. 1998. Weathering. An introduction to the scientific principles. Arnold, London, 271 pp.

Boillot, G. & Mougenot, D. 1978. Carta geológica da plataforma continental (Escala 1/1 000 000). Instituto Hidrográfico, Serviço de Fomento Mineiro e Serviços Geológicos de Portugal, Lisboa.

Boillot, G., Malod, J.A. & Mougenot, D. 1979. Évolution géologique de la marge ouest-ibérique. *Ciências da Terra*, **5**, 215-222.

Brady, P.V. & Walther, J.V. 1989. Controls on silicate dissolution rates in neutral and basic pH solutions at 25ºC. *Geochimica et Cosmochimica Acta*, **53**, 2823-2830.

Bredehoeft, J.D. 2002. The water budget myth revisited: why hydrogelogists model? *Ground Water*, **40**, 4, 340-345.

Buckley, D.K. 2001. Geophysical logging of 7 observation boreholes near Aveiro, Portugal. British Geological Survey Report CR/01/023, Keyworth, 20 pp.

Carreira Paquete, P.M.M. 1998. Paleoáguas de Aveiro. PhD thesis, Universidade de Aveiro, Portugal, 377 pp.

Carreira, P.M.M., Soares, A.M.M., Marques da Silva, M.A., Araguás, L.A., Rozanski, K. 1996. Application of environmental isotope methods in assessing groundwater dynamics of an intensively exploited coastal aquifer in Portugal. *Isotopes in Water Resources Management*, **2**, 45-58.

Charlson, R.J. & Rodhe, H. 1982. Factors controlling the acidity of natural rainwater. *Nature*, **295**, 667-673.

Clark, I. & Fritz, P. 1997. Environmental Isotopes in Hydrogeology. Lewis Publishers, CRC Press LLC, Boca Raton, 328 pp.

Clark, I. & Harper, W.V. 2000. Practical Geostatistics 2000. Ecosse North America Llc, 342 pp.

Coleman, M.L., Shepherd, T.J., Durham, J.J., Rouse, J.E., Moore, G.R. 1982. Reduction of water with zinc for hydrogen isotope analysis. *Analytical Chemistry*, 54, 993-995.

Condesso de Melo, M.T., Marques da Silva, M.A. & Edmunds, W.M. 1998. Evolução hidrogeoquímica do sistema multiaquífero Cretácico do Baixo Vouga - Aveiro, Portugal. Proceedings 4º Congresso da Água, Lisboa, 23-28 Março [CD-Rom].

Condesso de Melo, M.T., Marques da Silva, & Edmunds, W.M. 1999. Hydrochemistry and Flow Modelling of the Aveiro Multilayer Cretaceous Aquifer. *Physics and Chemistry of the Earth (B)*, **24**, 331-336.

Condesso de Melo, M.T., Carreira Paquete, P.M.M. & Marques da Silva, M.A. 2001. Evolution of the Aveiro Cretaceous aquifer (NW Portugal) during the Late Pleistocene and present day:

evidence from chemical and isotopic data. *In:* Edmunds, W.M. & Milne, C.J. (eds). Palaeowaters in Coastal Europe: evolution of groundwater since the Late Pleistocene. Geological Society, London, Special Publications, **189**, 139-154.

Condesso de Melo, M.T., Cabano, G. & Marques da Silva, M.A. 2002*a*. Evolução hidrogeoquímica do sistema multiaquífero Quaternário de Aveiro. Proceedings 6º Congresso da Água, Porto, 18-22nd March [CD-Rom].

Condesso de Melo, M.T., Batista, A.C. & Marques da Silva, M.A. 2002*b*. Estudo da qualidade química natural do aquífero Cretácico de Aveiro utilizando métodos geostatísticos. Proceedings 6º Congresso da Água, Porto, 18-22nd March [CD-Rom].

Condesso de Melo, M.T., Edmunds, W.M. & Marques da Silva, M.A. 2002*c*. Groundwater recharge in the Aveiro Cretaceous aquifer using soil moisture balance, unsaturated zone profiles and chloride mass-balance method. Proceedings International Groundwater Conference on Balancing the Groundwater Budget, Darwin, 12-17th May [CD-Rom].

Condesso de Melo, M.T., Mendes Lopes, A.M., Cabano, G., Marques da Silva, M.A., Duarte, E. 2002*d*. Estimating spatial and temporal variability of groundwater recharge during one hydrological year: the Aveiro Cretaceous Aquifer, Portugal. Proceedings International Groundwater Conference on Balancing the Groundwater Budget, Darwin, 12-17th May [CD-Rom].

Cook, P.G., Edmunds, W.M. & Gaye, C.B. 1992. Estimating paleorecharge and paleoclimate from unsaturated zone profiles. *Water Resources Research*, **28**, 10, 2721-2731.

Craig, H. 1961. Isotopic variations in meteoric waters. *Science*, **133**, 1702-1703.

Cressie, N.A.C. 1991. Statistical for spatial data. John Wiley & Sons, Inc., New York, 900 pp.

Custodio, E. & Llamas, M.R. 1983. Hidrología subterránea. Tomo II, Sección 13. Ediciones Omega, Barcelona, 1317-1389.

Dansgaard, W. 1964. Stable isotopes in precipitation. *Tellus XVI*, 4, 436-468.

Darcy, H. 1856. Les fontaines publiques de la ville de Dijon. Victor Dalmont, Paris.

Davis, J.C. 1986. Statistics and data analysis in geology. John Wiley & Sons, Inc., New York, 646 pp.

DGA 2001. Atlas do Ambiente. World Wide Web Address: http://195.22.0.189/atlas/c_escoamento.html.

Dias, J.M., Lopes, J.F. & Dekeyser, I. 1999. Hydrological characterisation of Ria de Aveiro, Portugal, in early summer. *Oceanologica Acta*, **22**, 5, 473-485.

Dias, J.M.A., Boski, T., Rodrigues, A., Magalhães, F. 2000. Coast line evolution in Portugal since the Last Glacial Maximum until present – a synthesis. *Marine Geology*, **170**, 177-186.

Dinis, J. 1999. Estratigrafia e sedimentologia da formação de Figueira da Foz. Aptiano a Cenomaniano do sector norte da bacia Lusitânica. Universidade de Coimbra, Portugal, 381 pp.

Dinis, J., Rey, J. & Gracianski, P.C. 2002. Le Bassin lusitanien (Portugal) à l'Aptien supérieur – Albien: organisation séquentielle, proposition de corrélations, évolution. *C.R. Geoscience*, **334**, 757-764.

Domenico, P.A. & Schwartz, F.W. 1990. Physical and chemical hydrogeology. John Wiley & Sons, Inc., New York, 824 pp.

Eberts, S. & George, L.L. 2000. Regional ground-water flow and geochemistry in the Midwestern basins and Arches aquifer system in parts of Indiana, Ohio, Michigan, and Illinois. Regional Aquifer-System Analysis. U.S. Geological Survey Professional Paper 1423-C, 103 pp.

EC (European Commission) 1997. Avaliação dos recursos hídricos de Espanha e Portugal. Relatório final. Office for Official Publications of the European Communities, Luxembourg, 79 pp.

Edmunds, W.M. & Gaye, C.B. 1994. Estimating the spatial variability of groundwater recharge in the Sahel using chloride. *Journal of Hydrology*, **156**, 47-59.

Edmunds, W.M. & Milne, C.J. (eds) 2001. Palaeowaters in coastal Europe: evolution of groundwater since the Late Pleistocene. Geological Society, London, Special Publications, **189**, 327 pp.

Edmunds, W.M. & Smedley, P.L. 2000. Residence time indicators in groundwater: the East Midlands Triassic Sandstone aquifer. *Applied geochemistry*, **15**, 737-752.

Edmunds, W.M. & Tyler, S.W. 2002. Unsaturated zones as archives of past climates: toward a new proxy for continental regions. *Hydrogeology Journal*, **10**, 1, 216-228.

Edmunds, W.M., Faye, S. & Gaye, C.B. 1992. Solute profiles in unsaturated Quaternary sands from Senegal: Environmental information and water-rock interaction. Proceedings 7th International Symposium on Water-Rock Interaction, Utah, 719-722.

Edmunds, W.M., Fellman, E., Goni, I.B., Prudhomme, C. 2002. Spatial and temporal distribution of groundwater recharge in northern Nigeria. *Hydrogeology Journal*, **10**, 1, 205-215.

Edmunds, W.M., Buckley, D.K., Darling, W.G., Milne, C.J., Smedley, P.L., Williams, A.T. 2001. Palaeowaters in the aquifers of the coastal regions of southern and eastern England. *In:* Edmunds, W.M. & Milne, C.J. (eds). Palaeowaters in Coastal Europe: evolution of groundwater since the Late Pleistocene. Geological Society, London, Special Publications, **189**, 71-92.

Edmunds, W.M., Hinsby, K., Marlin, C., Condesso de Melo, M.T., Manzano, M., Vaikmae, R., Travi, R. 2001. Evolution of groundwater systems at the European coastline. *In:* Edmunds, W.M. & Milne, C.J. (eds). Palaeowaters in Coastal Europe: evolution of groundwater since the Late Pleistocene. Geological Society, London, Special Publications, **189**, 289-311.

Epstein, S. & Mayeda, T.K. 1953. Variations of the $^{18}O/^{16}O$ ratio in natural waters. *Geochimica et Cosmochimica Acta*, **4**, 213-223.

Eriksson, E. & Khunakasem, V. 1969. Chloride concentration in groundwater, recharge rate and rate of deposition of chloride in the Israel Coastal Plain. *Journal of Hydrology*, **7**, 178-197.

Esso 1974. Geological and drilling report. Well Completion Carapau-1. Esso Exploration & Production Portugal Inc, 20 pp.

Evans, G.V., Otlet, R.L., Downing, R.A., Monkhouse, R.A., Rae, G. 1979. Some problems in the interpretation of isotope measurements in the United Kingdom aquifers. Isotope Hydrology 1978, Vol.II. International Atomic Energy Agency, Vienna, 679-708.

Ferreira, P.L.O. 1995. Hidrogeologia do Quaternário da região Norte da Ria de Aveiro. MSc thesis, Universidade de Aveiro, Portugal, 102 pp.

Figueiredo, F.P.O.O. 2002. Gravimetria aplicada à organização geométrica da cobertura Meso-Cenozóica (Baixo Vouga). PhD thesis, Universidade de Coimbra, Portugal, 213 pp.

Fleck, W.B. & Vroblesky, D.A. 1996. Simulation of ground-water flow of the coastal plain aquifers in parts of Maryland, Delaware, and the district of Colombia. Regional Aquifer-System Analysis. U.S. Geological Survey Professional Paper 1404-J, 41 pp.

Friedman, I. 1953. Deuterium content of natural waters and other substances. *Geochimica et Cosmochimica Acta*, **4**, 89-103.

Gardner, C.M.K., Bell, J.P., Cooper, J.D., Darling, W.G., Reeve, C.E. 1991. Groundwater recharge and water movement in the unsaturated zone. *In:* Downing, R.A. & Wilkinson, W.B. (*eds*). Applied Groundwater Hydrology. Clarendon Press, Oxford, 54-63.

Gat, J.R. 1980. The isotopes of hydrogen and oxygen in precipitation. *In:* Fritz, P. & Fontes, J.C. (*eds*). Handbook of Environmental Isotope Geochemistry. Elsevier, New York, 21-40.

Gat, J.R. & Gonfiantini, R. 1981. Stable isotope hydrology: deuterium and oxygen in the water cycle. IAEA Technical Reports 210. International Atomic Energy Agency, Vienna, 335 pp.

Gaye, C.B. & Edmunds, W.M. 1996. Groundwater recharge estimation using chloride, stable isotopes and tritium profiles in the sands of northwestern Senegal. *Environmental Geology*, **27**, 246-251.

Gee, G.W. & Hillel, D. 1988. Groundwater recharge in arid regions: review and critique of estimation methods. *Hydrological Processes*, **2**, 255-266.

Gee, G.W., Wiering, P.J., Andraski, B.J., Young, M.H., Fayer, M.J., Rockhold, M.L. 1994. Variations in water balance and recharge potential at three western desert sites. *Soil Sci. Soc. of Am. J.*, **58**, 63-72.

Goldberg, E.D., Broecker, W.S., Gross, M.G., Turekian, K.K. 1971. Marine Chemistry. *In:* Radioactivity in the marine environment, 137-146. Washington, D.C., National Academy of Sciences.

Gonfiantini, R. 1978. Standards for stable isotope measurements in natural compounds. *Nature*, 271, 534-536.

Goovaerts, P. 1997. Geostatistics for natural resources evaluation. Oxford University Press, Oxford, 483 pp.

Grindley, J. 1967. The estimation of soil moisture deficits. *Meteorol. Mag.*, **96**, 97-108.

Guéry, F., Montenat, C. & Varchard, D. 1986. Evolution tectono-sédimentaire du bassin Portugais au Mésozoic suivant la transversale de Peniche (Estrémadure). *Bull. Centr. Réch. Explor. Prod. Elf Aquitaine*, **10**: 83-94.

Harbaugh, A.W. & McDonald, M.G. 1996. User's documentation for MODFLOW-96, an update to the U.S. Geological Survey modular finite-difference ground-water flow model: United States Geological Survey Open-File Report 96Ð485, 56 pp.

Harrar, W.G., Williams, A.T., Barker, J.A., Van Camp, M. 2001. Modelling scenarios for the emplacement of palaeowaters in aquifer systems. *In:* Edmunds, W.M. & Milne, C.J. (eds). Palaeowaters in Coastal Europe: evolution of groundwater since the Late Pleistocene. Geological Society, London, Special Publications, **189**, 213-229.

Healy, R.W. & Cook, P.G. 2002. Using groundwater levels to estimate recharge. *Hydrogeology Journal*, **10**, 1, 91-109.

Hearst, J.R., Nelson, P.H. & Paillett, F.L. 2000. Well logging for physical properties. A handbook for geophysicists, geologists and engineers. 2nd Edition. John Wiley & Sons, Inc., New York, 483 pp.

Houlding, S.W. 2000. Practical Geostatistics: modeling and spatial analysis. Springer-Verlag Berlin, 159 pp.

Huneau, F. 2000. Fonctionnement hydrogéologique et archives paléoclimatiques d'un aquifère profond méditerranéen. Etude chimique et isotopique du bassin miocène de Valréas (Sud-Est de la France). PhD thesis, Université d'Avignon, France, 192p.

IAEA 1976. Procedure and technique critique for tritium enrichment by electrolysis at the IAEA laboratory. Isotope Hydrology Laboratory, Technical Procedure Note 19. International Atomic Energy Agency, Vienna, 30 pp.

IAEA/WMO 2001. Global network of isotopes in precipitation. The GNIP Database. World Wide Web Address: http://isohis.iaea.org/.

INAG 2002. Atlas da Água. Bacia Hidrográfica do Vouga. World Wide Web Address: http://snirh.inag.pt/snirh/atlas/main_nav_fr.html.

INE (Instituto Nacional de Estatística) 2002. Unidades territoriais - Baixo Vouga. World Wide Web Address: http://www.ine.pt/prodserv/pesqut/quadro2.asp.

Kitanidis, P.K. 1997. Introduction to geostatistics: applications in hydrogeology. Cambridge University Press, Cambridge, 249 pp.

Kooi, H. & Groen, J. 2001. Offshore continuation of coastal groundwater systems; predictions using sharp-interface approximations and variable-density flow modelling. *Journal of Hyrdology*, **246**, 19-35.

Kresic, N. 1997. Quantitative solutions in hydrogeology and groundwater modelling. Lewis Publishers. Boca Raton, 461 pp.

Langevin, C.D. 2002. Simulation of Ground-Water Discharge to Biscayne Bay, Southeastern Florida. U.S. Geological Survey, Water-Resources Investigations, 00-4251.

Langmuir, D. & Whittemore, D.O. 1971. Variations in the stability of precipitated ferric oxy-hydroxides. *In:* Hem, J.D. (ed.). Non-equilibrium systems in natural water chemistry. American Chemical Society. *Advances in Water Chemistry Series*, **106**, 209-234.

Lasaga, A.C. 1995. Fundamental approaches in describing mineral dissolution and precipitation rates. *In:* White, A.F. & Brantley, S.L. (eds). Chemical weathering rates of silicate minerals. Mineralogical Society of America. *Reviews in Mineralogy*, **31**, 23-86.

Lauverjat, J., Martins de Carvalho, J. & Marques da Silva, M.A. 1983. Contribuição para o estudo hidrogeológico da região de Aveiro. *Bol. Soc. Geol. Portugal*, **24**, 295-304.

Lerner, D.N. 1997. Groundwater recharge. *In:* Saether, O.M. & de Caritat, P. (*eds*). Geochemical processes, weathering and groundwater recharge in catchments. A.A. Balkema, Rotterdam, 109-150.

Lima, A.S. 2002. Hidrogeologia de terrenos graníticos. Minho – noroeste de Portugal. (Portugal). PhD thesis, Universidade do Minho, Portugal, 451 pp.

Magalhães, F.M.Q. 1999. Os sedimentos da plataforma continental portuguesa: contrastes espaciais, perspectiva temporal, potencialidades económicas. PhD thesis, Universidade de Lisboa, Portugal, 287 pp.

Mather, J.D & Porteous, N.C. 2001. The geochemistry of boron and its isotopes in groundwaters from marine and non-marine sandstone aquifers. *Applied Geochemistry*, **16**, 821-834.

Marques, M.P.L. 1990. Contribuição para o cálculo da recarga natural do sistema aquífero Cretácico de Aveiro. Graduation Research Project, Universidade de Aveiro, Portugal, 104 pp.

Marques da Silva, M.A. 1990. Hidrogeología del sistema multiacuífero Cretácico del Bajo Vouga – Aveiro (Portugal). PhD thesis, Universidad de Barcelona, Spain, 436 pp.

Marques da Silva, M.A. 1992. Camadas-guia do Cretácico de Aveiro e sua importância hidrogeológica. *Geociências*, **7***,* 111-124.

Marques da Silva, M.A., Custódio, E. & Bayó, A. 1993. Saline water in the Aveiro deep aquifer system. *In:* Custodio, E. & Galofré, A. (eds). Studying and modelling of saltwater intrusion into aquifers. CIMNE, Barcelona.

Marsily, G. de 1986. Quantitative hydrogeology. Groundwater hydrology for engineers. Academic Press, London, 440 pp.

Matheron, G. 1971. The theory of regionalized variables and its applications. Cahiers du Centre de Morphologie Mathematiquede Fontainebleau, **5**. Ecole des Mines, Paris, 211 pp.

Mauffret, A., Boillot, G., Auxietre, J.L., Dunand, J.P. 1978. Evolutión structurale de la marge continentale au Nord-Ouest de la Peninsule Ibérique. *Bulletin Société Géoloqique de France*, **20**, 4, 375-388.

Maxey, G.B. 1964. Hydrostratigraphic units. *Journal of Hydrology*, **2**, 124-129.

McDonald, M.C., & Harbaugh, A.W. 1988. A modular three-dimensional finite-difference ground-water flow model. U.S. Geological Survey, Techniques of Water-Resources Investigations, Chapter 1A, Book 6, 586 pp.

Molz, F.J. 2000. Nature and measurement of hydraulic properties: overview of evolving results, methodology and concepts. Proceedings Hydrology Symposium and Workshop, Columbia, SC, January 20-21.

Njitchoua, R., Dever, L., Fontes, J.Ch., Naah, E. 1997. Geochemistry, origin, and recharge mechanisms of groundwaters from the Garoua sandstone aquifer, northern Cameroon. *Journal of Hydrology*, **190***,* 123-140.

Nordstrom, D.K., Plummer, L.N. & Wigley, T.M.L. 1979. Comparison of computerized chemical models for equilibrium calculations i n aqueous systems. *In:* Jenne, E.A. (ed). Chemical Modelling in Aqueous Systems. *American Chemical Society Symposium Series*, **93**, 815-835.

NPEP 2001. Oil exploration and exploitation in Portugal. Data analysis and compilation by the 'Núcleo para a Pesquisa e Exploração de Petróleo'. World Wide Web Address: http://www.igm.pt/departam/npep/default.htm.

Oliveira, T.I.F. 1997. Capacidade de troca catiónica no Cretácico de Aveiro e sua influência no quimismo da água. MSc thesis, Universidade de Aveiro, Portugal, 132 pp.

Oliveira, T., Rocha, F.T. & Marques da Silva, M.A. 1998*a*. Influência da troca catiónica no quimismo da água do Aquífero Cretácico de Aveiro. Proceedings 4.º Congresso da Água, Lisboa, 23-28 Março [CD-Rom].

Oliveira, T., Condesso de Melo, M.T., Rocha, F.T., Marques da Silva, M.A. 1998*b*. Influência de parâmetros mineralógicos e químicos da matriz dos sedimentos no quimismo das águas subterrâneas. O caso das camadas argilo-margosas Cenomanianas/ Turonianas de Aveiro. *Geociências*, **12***,* 83-101.

Pannatier, Y. 1996. Variowin - Software for spatial statistics. Analysis in 2D. Springer-Verlag, New York, 91 pp.

Parkhurst, D.L. & Appelo, C.A.J. 1999. PHREEQC (Version 2) – a computer program for speciation, reaction-path, 1D-transport, and inverse geochemical calculations. U.S. Geological Survey, Water-Resources Investigations Report 99-4259.

Parkhurst, D.L., Christenson, S. & Breit, G.N. 1996. Ground-water quality assessment of the Central Oklahoma aquifer, Oklahoma. Geochemical and geohydrologic investigations. Capter C. United States. U.S. Geological Survey Water-Supply Paper 2357, 101 pp.

Peixinho de Cristo, F. 1985. Estudo hidrogeológico do sistema aquífero do Baixo Vouga. Divisão de Geohidrologia, Direcção-Geral dos Recursos e Aproveitamentos Hidráulicos, Ministério do Equipamento Social, Coimbra, 57 pp.

Peixinho de Cristo, F. 1992. Sistema multiaquífero Cretácico do Vouga. *In:* Plano Regional de Ordenamento do Território do Centro Litoral*,* 131-137. M.P.A.T., Comissão de Coordenação da Região Centro, Coimbra, 175 pp.

Peixinho de Cristo, F., Serrano, J. & Garcia, P. 1997. Piezometria da região Centro. Direcção Regional do Ambiente e Ordenamento do Território do Centro, Ministério do Ambiente e Ordenamento do Território.

Penman, H.L. 1948. Natural evaporation from open water, bare soil and grass. *Proc. R. Soc. London*, Ser. A **193**, 120-145.

Penman, H.L. 1950. The water balance of the Stour catchment area. *J. Inst. Water Eng.*, **4**, 457-469.

PNA 2002. Plano nacional da água, elaborado nos termos do Decreto Lei nº 45/94 de 22 de Fevereiro. Ministério do Ambiente e do Ordenamento do Território, Lisboa, [CD-Rom].

Rasmussen, E.S., Lomholt, S., Andresen, C., Vejbæk, O.V. 1998. Aspects of the structural evolution of the Lusitanian Basin in Portugal and the shelf and slope area offshore Portugal. *Tectonophysics*, **300**, 199-225.

Ravnås, R., Windelstad, J., Mellere, D., Nøttvedt, A., Stuhr Sjøblom, T., Steel, R.J., Wilson, R.C.L. 1997. A marine Late Jurassic syn-rift succession in the Lusitanian basin, western Portugal – tectonic significance of stratigraphic signature. *Sedimentary Geology*, **114**, 237-266.

Reilly, T.E. 2001. System and boundary conceptualization in groundwater flow simulation. Techniques of Water-Resources Investigations of the U.S. Geological Survey, Book 3, Applications of Hydraulics, Chapter B8, 30 pp.

Reilly, T.E. & Goodman, A.S. 1985. Quantitative analysis of salt-water-freshwater relationships in groundwater systems – a historical perspective. *Journal of Hydrology*, **80**, 125-160.

Reis, M.E.D. 1990. Contribuição para o cálculo da recarga natural do Sistema Aquífero Cretácico de Aveiro. Graduation Research Project, Universidade de Aveiro, Portugal, 104 pp.

Rezende, J.V. 1944. Monografia da Gafanha. Instituto para a Alta Cultura. Reedição Fac-Similada pela Câmara Municipal de Ílhavo em 1989, 365 pp.

Ribeiro, A., Antunes, M.T., Ferreira, M.P., Rocha, R.B., Soares, A.F., Zbyszewski, G., Moitinho de Almeida, F., Carvalho, D., Monteiro, J.H. 1979. Introduction à la géologie générale du Portugal. Serviços Geológicos de Portugal, Lisboa, 114 pp.

RNDSJ (Reserva Natural Dunas de S. Jacinto) 2002. Ria de Aveio. World Wide Web Address: http://camarinha.aveiro-digital.net/ria001.htm.

Rocha, F.T. 1993. Argilas Aplicadas a Estudos Litoestratigráficos e Paleoambientais na Bacia Sedimentar de Aveiro. PhD thesis, Universidade de Aveiro, Portugal, 399 pp.

Rogado, N. 1995. Solos do Baixo Vouga de origem aluvionar. D.R. Agricultura da Beira Litoral, Coimbra, 55 pp.

Rozanski, K., Gonfiantini, R. & Araguás-Araguás, L. 1991. Tritium in the global atmosphere: distribution patterns and recent trends. *J. Phys. G. Nucl. Particle Phys. (Suppl.)*, **17**, S523-S536.

Rozanski, K., Araguás-Araguás, L. & Gonfiantini, R. 1993. Isotopic patterns in modern global precipitation. *In:* Continental Isotope Indicators of Climate, American Geophysical Union Monograph.

Rushton, K. 1997. Recharge from permanent water bodies. *In:* Simmers (ed). Recharge of phreatic aquifers in semi(arid) areas. A.A. Balkema, Rotterdam, 215-255.

Salem, O., Visser, J.M., Deay, M. and Gonfiantini, R. 1980. Groundwater flow patterns in the western Lybian Arab Jamahitiya evaluated from isotope data. *In:* Arid Zone Hydrology: Investigations with Isotope Techniques. International Atomic Energy Agency, Vienna, 165-179.

Sanford, W. 2002. Recharge and groundwater models: an overview. *Hydrogeology Journal*, **10**, 1, 110-120.

Saraiva, M.P.S., Barradas, J. & Marques da Silva, M.A. 1983. Aquífero Cretácico de Aveiro – subsídios para a sua caracterização hidrogeológica. *Hidrogeologia y Recursos Hidraulicos*, VII, AEHS, Madrid, 41-49.

Scanlon, B.R., Healy, R.W. & Cook, P.G. 2002. Choosing appropriate techniques for quantifying groundwater recharge. *Hydrogeology Journal*, **10**, 1, 18-39.

Schulze-Makuch, D., Carlson, D.A., Cherkauer, D.S., Malik, P. 1999. Scale dependency of hydraulic conductivity in heterogeneous media. *Ground water*, **37**, 6, 904-919.

Seaber, P.R. 1988. Hydrostratigraphic units. *In:* Back, W. Rosensshein, J.S. & Seaber, P.R. (eds). The geology of North America. Geological Society of America, **0-2**, 9-14.

Selaolo, E.T. 1998. Tracer studies and groundwater recharge assessment in the eastern fringe of the Botswana Kalahari. The Letlhakeng-Botlhapatlou area. PhD thesis, vrije Universiteit te Amsterdam, The Netherlans, 229 pp.

Serrano, J.A.P.F. & Mendes, I.C.L. 2002. Caracterização dos sistemas de abastecimento público de água do distrito de Aveiro. Direcção Regional do Ambiente e Ordenamento do Território do Centro, Ministério do Ambiente e Ordenamento do Território, Coimbra, 103 pp.

Sharma, M.L. 1989. Use of applied tracers in studies of natural groundwater recharge. *In:* Sharma, M.L. (ed). Groundwater recharge. Proceedings Symposium on Groundwater Recharge, Mandurah. A.A. Balkema, Rotterdam, 11-23.

Sharma, M.L. (ed) 1989. Groundwater recharge. Proceedings Sysposium on Groundwater Recharge. Mandurah, Mandurah, Western Australia. A.A. Balkema, Rotterdam, 323 pp.

Simpkins, W.W. 1995. Isotopic composition of precipitation in central Iowa. *Journal of Hydrology*, **172**, 185-207.

Smedley, P.L. & Edmunds, W.M. 2002. Redox patterns and trace-element behavior in the East Midlands Triassic Sandstone aquifer (UK). *Ground water*, **40**, 1, 44-58.

Soares, A.F., Barbosa, B.P. & Pena dos Reis, R. 1982. Esboço do enquadramento cronostratigráfico das unidades líticas pós-Jurássicas da Orla Meso-Cenozóica Ocidental entre os paralelos de Pombal e Aveiro. *Mem. Not. Mus. Lab. Min. Geol. Univ. Coimbra*, **93**, 77-81.

Soares, A.F., Rocha, R.B., Elmi, S., Henriques, M.H., Mouterde, R. Almeras, Y., Ruget, C., Marques, J., Duarte, L., Carapito, M.C., Kullberg, J.C. 1993. Le sous-bassin nord-Lusitanien (Portugal) du Trias au Jurassique Moyen: histoire d'un rift avorté. *C.R. Acad. Sci. Paris*, **317**, 2, 1659-1666.

Stapel, G., Cloetingh, S. & Pronk, B. 1996. Quantitative subsidence analysis of the Mesozoic evolution of the Lusitanian basin (western Iberian Peninsula). *Tectonophysics*, **266**, 493-507.

Sukhija, B.S., Reddy, D.V., Nagabhushanam, P., Chand, R. 1988. Validity of the environmental chloride method for recharge evaluation of coastal aquifers, India. *Journal of Hydrology*, **99**, 349-366.

Tamers, M.A. 1975. Validity of radiocarbon dates on groundwater. *Geophysical Survey*, **2**, 217-239.

Teixeira, C. 1963. Carta geológica de Portugal na escala de 1/50 000. Notícia explicativa da folha 13C - Ovar. Direcção-Geral de Minas e Serviços Geológicos, Serviços Geológicos de Portugal, Lisboa.

Teixeira, C. & Zbyszewski 1976. Carta geológica de Portugal na escala de 1/50 000. Notícia explicativa da folha 16A - Aveiro. Direcção-Geral de Minas e Serviços Geológicos, Serviços Geológicos de Portugal, Lisboa.

Thornthwaite, C.W. 1948. An approach toward a rational classification of climate. *Geologic. Rev.*, **38**, 55-94.

Thorstenson, D.C. & Fisher, D.W. 1979. The geochemistry of the Fox Hills-Basal Hell Creek aquifer in Southwestern North Dakota and Northwestern South Dakota. *Water Resources Research*, **15**, 6, 1479-1498.

Uphoff, T.L., Stemler, D.P., Stearns, M.J., Monteleon, P.H. 2002. Recent exploration drilling results highlight significant potential for Portugal's Lusitanian basin. Report. Mohave Oil and gas Corporation, Houston, Texas, 5 pp.

van Leeuwen, E.P., Draaijers, G.P.J. & Erisman, J.W. 1996. Mapping wet deposition of acidifying components and base cations over Europe using measurements. *Atmospheric Environment*, **30**, Issue 14, 2495-2511.

Vanney, J.R. & Mougenot, D. 1981. La plate-forme continentale du Portugal et les provinces adjacentes: analyse geomorphologique. Memórias dos Serviços Geológicos de Portugal, 28. Direcção Geral de Geologia e Minas, Lisboa, Portugal, 86 pp.

Vries, J.J. & Simmers, I. 2002. Groundwater recharge: an overview of processes and challenges. *Hydrogeology Journal*, **10**, 1, 5-17.

Wang, H.F. & Anderson, M.P. 1982. Introduction to groundwater modeling. Finite difference and finite element methods. Academic Press, San Diego, 237 pp.

WFD 2000. Water framework directive 2000/60/EC of the European Parliament and of the Council of 23rd October 2000. Official Journal of the European Communities. Brussels, 72 pp.

White, A.F. & Brantley, S.L. 1995. Chemical weathering rates of silicate minerals: an overview. *In:* White, A.F. & Brantley, S.L. (eds). Chemical weathering rates of silicate minerals. Mineralogical Society of America. *Reviews in Mineralogy*, **31**, 1-22.

Williamson, A.K. & Grubb, H.F 1998. Ground-water flow in the Gulf Coast aquifer systems, south central United States. U.S. Geological Survey Professional Paper 1416-F, 173 pp.

Wilson, R.C.L., Hiscott, R.N., Willis, M.G., Gradstein, F.M. 1990. The Lusitanian basin of west central Portugal: Mesozoic and Tertiary tectonics, stratigraphy and subsidence history. *In:* Tankard, A.L. & Balkwill, H.R. (eds). Extensional Tectonics and Stratigraphy of the North Atlantic Margins. *Amer. Assoc. Petrol. Geol. Mem.*, **46**, 341-361.

Zazo, C., Goy, J.L., Lario, J. & Silva, P.G. 1996. Littoral zone and rapid climatic changes during the last 20,000 years. The Iberia study case. *Z. Geomorph. N.F.*, Suppl.-Bd. **102**, 119-134.

Zbyszewski, G. 1963. Considerações acerca das possibilidades de se realizar uma nova captação de água para o abastecimento de Aveiro. Grupo de Estudos dos Recursos Hídricos Subterrâneos da Beira Litoral, Montemor-o-Velho. Relatório interno, 6 pp.

Zbyszewski, G., Alves, A.M. & Chaves, J.B. 1972. Contribuição de algumas sondagens de pesquisa e captação de água para o conhecimento hidrogeológico da região de Aveiro. Proceedings I Congresso Hispano-Luso-Americano de Geologia Económica, Lisboa, 793-805.

Zhu, C. Estimate of recharge from radiocarbon dating of groundwater and numerical flow and transport modeling. *Water Resources Research*, **36**, 2067-2620.

A

HYDROGEOLOGICAL BACKGROUND INFORMATION

A.1 BOREHOLE DATABASE

Well Ref	Well Name	UAVR_N	DRA_N	Localisation	Well Description	Drilling Date	Owner
1	AC1	O2/162A/001	162A/002	Torreira	Borehole	07/08/73	Colónia de Férias da Praia da Torreira
2	JK1	O2/162A/002	162A/001	Torreira	Monitoring well	19/09/78	Câmara Municipal da Murtosa
3	1-RN	O2/162A/003	162A/009	Torreira	Monitoring well	01/07/88	Colónia de Férias da Praia da Torreira
4	4-RN	O2/162A/004		Torreira	Borehole	01/12/88	Colónia de Férias da Praia da Torreira
5	5-RN	O2/162A/005		Torreira	Borehole	01/01/89	Colónia de Férias da Praia da Torreira
6	AC1	O2/162A/006		Torreira	Borehole	28/11/83	Câmara Municipal da Murtosa
7	INAG1	O2/162A/007		Torreira	Borehole	11/02/94	Colónia de Férias da Praia da Torreira
8	ACC15	O2/163/001		Chão do Curgo	Borehole	19/05/78	Quimigal Química Portugal, SA
9	ACC16	O2/163/002		Chão do Monte	Borehole	19/05/78	Quimigal Química Portugal, SA
10	ACC17	O2/163/003		Marinhas E. Esteiros	Monitoring well	19/05/78	Quimigal Química Portugal, SA
11	ACC01A	O2/163/004		Quintas do Sul	Monitoring well	14/01/81	Quimigal Química Portugal, SA
12	ACCP1	O2/163/005		Pinhal do Mancão	Borehole	05/08/82	Quimigal Química Portugal, SA
13	ACCP2	O2/163/006		S. Silvestre	Borehole	05/08/82	Quimigal Química Portugal, SA
14	ACCP3	O2/163/007	163/005	Ponte da Varela	Monitoring well	05/08/82	Quimigal Química Portugal, SA
15	ACCP5	O2/163/008	163/006	Bestida	Monitoring well	05/08/82	Quimigal Química Portugal, SA
16	AC2	O2/163/009		Torreira	Borehole	05/08/82	Colónia de Férias da Praia da Torreira
17	JK2	O2/163/010		Mamaparda	Borehole	05/08/82	Câmara Municipal da Murtosa
18	ACCP3	O2/163/011		Ponte da Varela	Monitoring well	05/08/82	Quimigal Química Portugal, SA
19	ACC01B	O2/163/012	162A/007	Quintas do Sul	Monitoring well	14/01/81	Quimigal Química Portugal, SA
20	JK1	O2/173/001		Reserva S. Jacinto	Borehole	18/10/74	Serviços Municipalizados de Aveiro
21	AC1	O2/173/002		S. Jacinto	Borehole	06/08/81	Batalhão Operacional de Tropas Paraquedistas
22	RN6	O2/173/003	173/013	Muranzel	Borehole	24/02/94	Clube Fim de Semana da Ria
23	AC1	O2/174/001	174/021	Junqueira, Aveiro	Borehole	23/10/63	Renault Portuguesa Soc. Ind. Comercial, SARL
24	AC1	O2/174/002		Aveiro	Borehole	01/12/71	Aleluia - Cerâmica, Comércio e Indústria, SA
25	AC49	O2/174/003	174/027	Arrocheira	Borehole	22/02/78	Portucel Industrial Emp. Produtora Celulose, SA
26	AC50	O2/174/004	174/026	Cabeço	Borehole	22/02/78	Portucel Industrial Emp. Produtora Celulose, SA
27	AC51	O2/174/005	174/024	Paço	Borehole	22/02/78	Portucel Industrial Emp. Produtora Celulose, SA
28	AC52	O2/174/006		Cacia	Borehole	22/02/78	Portucel Industrial Emp. Produtora Celulose, SA
29	AC1	O2/174/007		Cacia	Borehole	11/05/79	Vulcano Termo Domésticos, SA
30	ACCP4	O2/174/008	174/002	Arrotas	Monitoring well	05/08/82	Quimigal Química Portugal, SA
31	AC69	O2/174/009		Marinha da Póvoa	Borehole	26/02/83	Portucel Industrial Emp. Produtora Celulose, SA
32	AC70	O2/174/010		Afrocheiras	Borehole	26/02/83	Portucel Industrial Emp. Produtora Celulose, SA
33	JK4	O2/174/011		Cacia	Monitoring well	28/02/75	Serviços Municipalizados de Aveiro
34	AC81	O2/174/012		Paço	Borehole	26/05/85	Portucel Industrial Emp. Produtora Celulose, SA
35	AC1-A	O2/174/013		Cacia	Borehole	20/02/87	Funfrap Fundição Portuguesa, SA
36	AC2	O2/174/014		Cacia	Borehole	01/01/92	Renault Portuguesa Soc. Ind. Comercial, SARL
37	PS1	O2/174/015		Sarrazola, Aveiro	Borehole	03/02/92	Inst. Hidraulica, Eng. Rural e Ambiente (IHERA)
38	AC43	O2/174/016		Paço	Borehole	01/12/63	Portucel Industrial Emp. Produtora Celulose, SA
39	AC44	O2/174/017	174/025	Paço	Borehole	01/01/64	Portucel Industrial Emp. Produtora Celulose, SA
40	AC42	O2/174/018		Mataduços	Borehole	01/01/63	Portucel Industrial Emp. Produtora Celulose, SA
41	CA7	O2/174/019		Estrada de Cacia	Borehole	28/12/96	Vulcano Termo Domésticos, SA
42	FD2	O2/174/020		Cacia	Borehole	12/04/84	Funfrap Fundição Portuguesa, SA
43	SJS1	O2/174/021		Junqueira, Cacia	Borehole	10/09/93	Funfrap Fundição Portuguesa, SA
44	PS1	O2/174/022		Renault	Borehole	12/11/99	Renault Portuguesa Soc. Ind. Comercial, SARL
45	CA17	O2/174/023		Ervideiros, Monte Cacia	Borehole	15/03/99	Lusaveiro - Im/Exportação Máq. Acessórios Ind.
46	CA12	O2/174/024		Quinta do Simão	Borehole	02/04/98	Junta Autónoma de Estradas - Distrito de Aveiro
47	CA11	O2/174/025		Estrada de Cacia	Borehole	28/12/97	Vulcano Termo Domésticos, SA
48	AC46	O2/174/026		Póvoa do Paço	Borehole	30/03/71	Portucel Industrial Emp. Produtora Celulose, SA
49	AC47	O2/174/027		Póvoa do Paço	Borehole	30/03/71	Portucel Industrial Emp. Produtora Celulose, SA
50	AC48	O2/174/028		Póvoa do Paço	Borehole	30/03/71	Portucel Industrial Emp. Produtora Celulose, SA
51	AC1	O2/184/001		Gafanha Encarnação	Monitoring well	15/05/62	Serviços Mun. Água e Saneamento de Ílhavo
52	AC1	O2/184/002	184/003	Porto de Aveiro	Borehole	15/06/67	Administração Porto Aveiro, SA
53	AC1	O2/184/003		Gafanha da Nazaré	Borehole	28/03/74	Bresfor-Indústria de Formol, Lda.
54	AC2	O2/184/004		Gafanha da Nazaré	Borehole	28/03/74	Bresfor-Indústria de Formol, Lda.
55	AC3	O2/184/005		Gafanha da Nazaré	Borehole	07/05/81	Serviços Mun. Água e Saneamento de Ílhavo
56	JK2	O2/184/006		Gafanha de Aquém	Borehole	01/03/87	Serviços Mun. Água e Saneamento de Ílhavo
57	AC2	O2/184/007		Porto de Aveiro	Borehole	17/03/89	Administração Porto Aveiro, SA
58	AC4	O2/184/008		Camping Barra	Borehole	01/09/89	Serviços Mun. Água e Saneamento de Ílhavo
59	PS1	O2/184/009		Porto de Aveiro	Borehole	06/04/98	Administração Porto Aveiro, SA
60	PS2	O2/184/010		Porto de Aveiro	Borehole	23/04/99	Administração Porto Aveiro, SA
61	PS1	O2/184/011		Camping Barra	Borehole	01/07/00	Serviços Mun. Água e Saneamento de Ílhavo
62	PS1	O2/184/012		Gafanha da Nazaré	Borehole	15/09/00	Bresfor-Indústria de Formol, Lda.
63	AC1	O2/185/001	185/080	Aveiro	Borehole	26/12/61	Serviços Municipalizados de Aveiro
64	JK3	O2/185/002	185/061	Fermentelos	Borehole	27/04/70	Serviços Municipalizados de Águeda
65	AC2	O2/185/003		Eucalipto, Aradas	Borehole	04/07/70	Serviços Municipalizados de Aveiro
66	AC3	O2/185/004	185/076	Passal, Esgueira	Borehole	04/07/70	Serviços Municipalizados de Aveiro
67	AC1	O2/185/005		Ílhavo	Borehole	04/04/70	Serviços Mun. Água e Saneamento de Ílhavo
68	AC2	O2/185/006		Ílhavo	Borehole	04/04/70	Serviços Mun. Água e Saneamento de Ílhavo
69	AC1	O2/185/007	185/014	Aveiro	Borehole	02/09/72	Jerónimo Pereira de Campos - Fáb. Cerâmicas, SA.
70	JK2	O2/185/008		Oliveirinha	Borehole	18/10/74	Serviços Municipalizados de Aveiro
71	JK3	O2/185/009		Aveiro	Borehole	25/07/75	Serviços Municipalizados de Aveiro
72	AC4	O2/185/010		S. Bernardo	Borehole	19/04/78	Serviços Municipalizados de Aveiro
73	AC5	O2/185/011		Quinta do Picado	Borehole	19/04/78	Serviços Municipalizados de Aveiro
74	1AH	O2/185/012		Verdemilho, Aradas	Borehole	30/09/78	Estação de Fomento Pecuário
75	AC1	O2/185/013	185/020	Ílhavo	Borehole	11/08/78	Fábrica de Porcelana da Vista Alegre, Lda
76	AC1	O2/185/014		Vale das Aradas	Borehole	27/10/80	Extrusal - Companhia Portuguesa de Extrusão, SA
77	AC1	O2/185/015		Gafanha da Nazaré	Borehole	27/01/81	Frilca Frigo Luso Canadianos, Lda
78	AC1	O2/185/016		Gafanha da Nazaré	Borehole	29/06/81	Empresa de Pesca de Aveiro, SA
79	JK1	O2/185/017		Moitinhos	Borehole	16/07/82	Serviços Mun. Água e Saneamento de Ílhavo
80	AC1	O2/185/018		Ílhavo	Borehole	26/11/85	Ilhavense-Soc. Industrial Papel, Lda.
81	AC2	O2/185/019		Ílhavo	Borehole	25/06/87	Fábrica de Porcelana da Vista Alegre, Lda
82	AC8	O2/185/020		Silval, Oliveirinha	Borehole	02/05/88	Serviços Municipalizados de Aveiro
83	AC9	O2/185/021		Mamodeiro	Borehole	02/05/88	Serviços Municipalizados de Aveiro
84	AC7	O2/185/022		S. Tiago	Borehole	02/05/88	Serviços Municipalizados de Aveiro
85	JK1	O2/185/023		Aveiro	Borehole	01/01/89	Universidade de Aveiro
86	JK5	O2/185/024		Granja de Cima	Borehole	12/10/90	Serviços Municipalizados de Aveiro
87	JK6	O2/185/025	185/074	Sol Posto	Borehole	21/12/90	Serviços Municipalizados de Aveiro
88	JK7	O2/185/026		Picoto	Borehole	27/04/91	Serviços Municipalizados de Aveiro
89	AC3	O2/185/027		Ílhavo	Borehole	08/02/91	Fábrica de Porcelana da Vista Alegre, Lda

Well Ref	Well Name	UAVR_N	DRA_N	Localisation	Well Description	Drilling Date	Owner
90	AC1	O2/185/028		Gafanha	Borehole	01/02/91	Tirtife - Terminais de Aveiro, SA.
91	JK9	O2/185/029		Aveiro	Borehole	21/03/91	Serviços Municipalizados de Aveiro
92	JK10	O2/185/030		Quinta do Gato	Borehole	16/05/91	Serviços Municipalizados de Aveiro
93	PS1	O2/185/031		Bom Sucesso	Borehole	30/09/92	Serviços Municipalizados de Aveiro
94	JK11	O2/185/032		Z. Ind. Mamodeiro	Borehole	26/06/92	Serviços Municipalizados de Aveiro
95	AC10	O2/185/033		Esqueira	Borehole	05/08/92	Serviços Municipalizados de Aveiro
96	AC6	O2/185/034		S. Bernardo	Borehole	04/03/85	Serviços Municipalizados de Aveiro
97	LF1	O2/185/035		Gafanha Nazaré	Borehole	01/01/55	Seca de Bacalhau Testa e Cunha
98	DP1	O2/185/036		Gafanha Nazaré	Borehole	01/01/55	João Maria Vilarinho (ou Baltazar)
99	RN5	O2/185/037	185/069	Azurva	Monitoring well	01/03/89	Dir. Regional Ambiente Recursos Naturais Centro
100	SJS5	O2/185/038		Jardins de Santiago	Borehole	15/09/90	Serviços Municipalizados de Aveiro
101	AC82	O2/185/039		Quinta S. Francisco	Borehole	29/09/85	Raiz - Instituto de Investigação da Floresta e Papel
102	CA22	O2/185/040		Taboeira, Esqueira	Borehole	11/11/99	António Manuel Laranjeiro Nunes Gonçalves
103	SJS3	O2/185/041		Fermentelos	Borehole	23/07/91	João Carlos Matos Martins
104	SJS4	O2/185/042		Fermentelos	Borehole	28/10/91	Alcino Moreira Dias
105	SJS1	O2/185/043	185/071	Aradas, Ilhavo	Borehole	23/07/87	Porcelanas Quinta Nova, SA
106	SJS2	O2/185/044	185/084	Aradas, Ílhavo	Borehole	15/07/88	Porcelanas Quinta Nova, SA
107	PS3	O2/185/045		Gafanha da Nazaré	Borehole	23/02/00	Administração Porto Aveiro, SA
108	SP1	O2/185/046	185/014	Gafanha Nazaré	Borehole	24/04/96	Empresa de Pesca Ribau
109	SP2	O2/185/047		Gafanha Nazaré	Borehole	20/12/96	Manuel Carvalho
110	JK1	O2/185/048		Chousa Nova, Ilhavo	Borehole	21/04/83	Maronagres - Comércio e Indústria Cerâmica, SA
111	AC1	O2/185/049		Z. Ind. da Taboeira	Borehole	22/02/88	Indasa - Abrasivos Flexiveis, SA
112	FD1	O2/185/050		Taboeira, Esgueira	Borehole	02/07/85	Cerexport Cerâmica Exportação, SA
113	CA1	O2/185/051		Bolho, Malhada	Borehole	03/10/96	Esbal
114	CA2	O2/185/052		Cardais, Vagos	Borehole	06/09/96	João Paulo Simões Graça
115	CA8	O2/185/053		Cais Bacalhoeiros	Borehole	17/01/97	Pascoal & Filhos, SA
116	AC1	O2/185/054		Aveiro	Borehole	14/08/64	Luzostela Indústria Serviços, SA
117	CA20	O2/185/055		Bolho, Malhada	Borehole	15/07/99	Senamar - Produtos Alimentares, Lda
118	CA15	O2/185/056		Quinta do Picado	Borehole	28/12/98	António dos Santos Gomes
119	CA10	O2/185/057		Gafanha da Nazaré	Borehole	04/09/97	A Ribeira do Peirxe - Comércio de Peixe, Lda
120	CA27	O2/185/058		Cais Bacalhoeiros	Borehole	18/05/00	Pascoal & Filhos, SA
121	CA9	O2/185/059		Cardais, Vagos	Borehole	21/08/97	Lénia Lourenço
122	FDG1	O2/185/060		Taboeira, Esqueira	Borehole	29/02/00	Cerexport Cerâmica Exportação, SA
123	SJS1	O2/195/001		Zona Industrial Vagos	Borehole	09/04/92	Porcelanas Costa Verde, SA
124	SJS2	O2/195/002		Zona Industrial Vagos	Borehole	25/10/92	Porcelanas Costa Verde, SA
125	PS-3A	O2/195/003	195/041	Zona Florestal	Borehole	10/01/96	Câmara Municipal de Vagos
126	CA13	O2/195/004		Zona Industrial Vagos	Borehole	21/09/98	Cerbran - Cerâmica Artística, Lda
127	CA16	O2/195/005		Zona Industrial Vagos	Borehole	11/02/99	Teccer - Tecnologia Cerâmica, Lda
128	AC1	O2/196/001		Abrigada	Borehole	02/06/77	Novagro - Agro Pecuária Valenta, Lda
129	JK4	O2/196/002		Fermentelos	Borehole	04/02/78	Serviços Municipalizados de Águeda
130	JK5	O2/196/003		Fermentelos	Borehole	04/02/78	Serviços Municipalizados de Águeda
131	ASS1	O2/196/004		Mamodeiro	Borehole	01/10/92	Sanindusa - Indústria de Sanitários, Lda.
132	MAMB1	O2/196/005		Seara, Ol. Bairro	Borehole	30/04/99	Câmara Municipal de Oliveira do Bairro
133	JK8	O2/196/006		Nariz	Monitoring well	27/06/91	Serviços Municipalizados de Aveiro
134	PS-1	O2/196/007	196/219	Lavandeira, Sosa	Borehole	28/02/92	Câmara Municipal de Vagos
135	TC1	O2/196/008		Monte Grande	Borehole	28/02/95	Metalfer- Metalúrgica de Fermentelos, Lda
136	JK4	O2/196/009	196/218	Palhaça	Borehole	03/07/91	Câmara Municipal de Oliveira do Bairro
137	JK5	O2/196/010		Vale da Marinha	Borehole	01/05/96	Câmara Municipal de Oliveira do Bairro
138	JK2	O2/196/011	196/208	Fermentelos	Borehole	27/04/70	Serviços Municipalizados de Águeda
139	CA19	O2/196/012		Qta. dos Duartes, Oiã	Borehole	15/05/99	Fernando Duarte
140	6RN	O2/196/013	196/212	Oiã	Monitoring well	15/04/89	Dir. Regional Ambiente Recursos Naturais Centro
141	7RN	O2/196/014	196/213	Bustos	Monitoring well	15/01/90	Dir. Regional Ambiente Recursos Naturais Centro
142	JVN1	O2/196/015	196/136	Troviscal	Monitoring well	01/12/80	José Vieira Nunes
143	TC1	O2/196/016	196/144	Póvoa Forno	Borehole	22/10/86	Manuel Ferreira da Cruz
144	SJS5	O2/196/017		Rio Tinto, Ouca	Borehole	02/08/91	João Reis Arada
145	SJS1	O2/196/018		Carris, Oiã	Borehole	26/02/91	Isaura Jesus
146	SJS4	O2/196/019		Póvoa Forno	Borehole	12/09/91	Rui Manuel Fontes Coelho
147	SJS1	O2/196/020		Mamodeiro	Borehole	20/02/91	Onix Cristal Esmaltes Cerâmicos, SA
148	SJS1	O2/196/021		Serena, Ol. Bairro	Borehole	11/11/83	Albertina Pereira Ferreira
149	SJS1	O2/196/022	196/061	Nariz	Borehole	15/10/82	Junta de Freguesia de Nariz
150	SJS1	O2/196/023	196/019	Verba, Nariz	Borehole	15/11/83	Eurico Martins Saraiva
151	FD1	O2/196/024		Zona Industrial de Oiã	Borehole	19/10/92	Câmara Municipal de Oliveira do Bairro
152	FD1	O2/196/025		Cabeço de Bustos	Borehole	18/06/91	Câmara Municipal de Oliveira do Bairro
153	AM1	O2/196/026		Palhaça	Borehole		Amadeu Jesus Plácido
154	AC1	O2/196/027		Oiã	Borehole	15/01/89	Porcel - Indústria Portuguesa de Porcelanas, SA
155	TC1	O2/196/028		Silveiro	Borehole.	09/03/99	União Desportiva Cultural e Recreativa do Silveiro
156	JK1	O2/196/029	196/207	Fermentelos	Borehole	27/04/70	Serviços Municipalizados de Águeda
157	JK3	O2/196/030		Sobreiro	Borehole	23/04/74	Câmara Municipal de Oliveira do Bairro
158	G-01	O2/196/031		Fermentelos	Borehole	10/10/94	Serviços Municipalizados de Águeda
159	G-03	O2/196/032		Fermentelos	Borehole	10/10/94	Serviços Municipalizados de Águeda
160	G-07	O2/196/033		Fermentelos	Borehole	10/10/94	Serviços Municipalizados de Águeda
161	G-09	O2/196/034		Fermentelos	Borehole	10/10/94	Serviços Municipalizados de Águeda
162	MM1	O2/206/001		Seixo de Mira	Borehole		Manuel Martins
163	SJS1	O2/206/002		Lentisqueira, Mira	Borehole	21/06/98	Manuel Jesus Silva
164	ASS1	O2/206/003		Zona Industrial Mira	Borehole	23/06/99	Leal & Soares, Lda
165	SJS2	O2/207/001		Chousa, Cov. Lobo	Borehole	25/05/91	Manuel Custódio Francisco Pinheiro
166	SJS3	O2/207/002		Andal, Cov. Lobo	Borehole	28/03/91	Manuel Augusto dos Santos Pires
167	SJS4	O2/207/003		Chousa, Cov. Lobo	Borehole	22/04/91	João Augusto Domingues Quintas
168	SJS3	O2/207/004		Malhapãozinho	Borehole	14/06/91	Adelino Domingues Pimentel
169	JK1	O2/207/005	207/001	Levira	Borehole	21/10/70	Serviços Mun. Aqua e Saneamento de Anadia
170	CA14	O2/207/006		Moita, Covão do Lobo	Borehole	09/11/98	Mindacris - Padaria e Pastelaria, Lda
171	TC1	O2/207/007		Samel, Vilarinho Bairro	Borehole	30/11/95	Centrovin - Produção e Comércio de Vinhos, Lda
172	LS1	O2/207/008		Mesas, Santa Catarina	Borehole	20/01/99	Eusébio Areias de Oliveira
173	JK3	O2/207/009	207/003	Levira	Borehole	25/04/71	Serviços Mun. Água e Saneamento de Anadia
174	LS1	O2/208/001		Perboi de Baixo	Borehole	30/07/97	Indústria de Cordas em Tripa de S. Caetano, Lda
175	SJS1	O2/208/002		Alpalhão	Borehole	21/12/83	Amilcar Fernandes Bártolo
176	SJS6	O2/208/003		Alféolas, Anadia	Borehole	26/06/91	Vidromax - Vidros e Espelhos, Lda
177	SO1	O2/217/001		Tocha	Borehole	10/08/95	Lactogal Produtos Alimentares, SA
178	JK1	O2/217/002	217/010	Tocha	Borehole	20/12/60	Colónia Rovisco Pais
179	JK2	O2/217/003	217/011	Tocha	Borehole	07/02/68	Colónia Rovisco Pais
180	AC1	O2/218/001		Cantanhede	Borehole	13/06/70	COBAI - Coop. Hortofruticultores da Bairrada
181	AC2	O2/218/002		Cantanhede	Borehole	13/06/70	COBAI - Coop. Hortofruticultores da Bairrada
182	SN1	O2/218/003		Póvoa do Bispo	Borehole	14/04/99	Carlos Alberto Barros Pereira
183	SJS1	O2/218/004	218/004	Olho de Aljuriça	Borehole	31/08/91	José Barreto Fernandes Sardão
184	SO1	O2/218/005		Póvoa do Bispo	Borehole	04/11/85	Fernando de Jesus Oliveira
185	JK12	O2/185/061		Aveiro	Borehole	14/08/00	Serviços Municipalizados de Aveiro

Well Ref	Map_N	Map_Scale	Gauss_M	Gauss_P	UTM_X	UTM_Y	ZM (m)	ZR (m)	Drilling_Company
1	162A	1/25 000	151940	421120	525253	4512111	5	1	Sondagens e Fundações A. Cavaco, Lda.
2	162A	1/25 000	151800	421610	525108	4512600	6	1	Johann Keller S.R.L.
3	162A	1/25 000	151400	420750	524717	4511736	7	0	D.R.A.Recursos Naturais Centro
4	162A	1/25 000	151875	420613	525193	4511604	12	1	D.R.A.Recursos Naturais Centro
5	162A	1/25 000	151850	420450	525170	4511441	12	1	D.R.A.Recursos Naturais Centro
6	162A	1/25 000	151980	421850	525286	4512841	6	0	Johann Keller S.R.L.
7	162A	1/25 000	151825	420600	525143	4511590	5	1	D.R.A.Recursos Naturais Centro
8	163	1/25 000	159730	422720	533023	4513788	11	0	Sondagens e Fundações A. Cavaco, Lda.
9	163	1/25 000	156900	421390	530208	4512430	5	0	Sondagens e Fundações A. Cavaco, Lda.
10	163	1/25 000	154950	422500	528248	4513521	2	0	Sondagens e Fundações A. Cavaco, Lda.
11	163	1/25 000	152080	424250	525362	4515241	4	0	Sondagens e Fundações A. Cavaco, Lda.
12	163	1/25 000	155130	421850	528434	4512873	2	0	Sondagens e Fundações A. Cavaco, Lda.
13	163	1/25 000	155530	421180	528841	4512207	2	0	Sondagens e Fundações A. Cavaco, Lda.
14	163	1/25 000	154620	424590	527897	4515606	2	0	Sondagens e Fundações A. Cavaco, Lda.
15	163	1/25 000	154910	420150	528231	4511171	3	0	Sondagens e Fundações A. Cavaco, Lda.
16	163	1/25 000	152070	420140	525393	4511133	5	0	Sondagens e Fundações A. Cavaco, Lda.
17	163	1/25 000	154750	420550	528067	4511569	3	1	Johann Keller S.R.L.
18	163	1/25 000	154620	424590	527897	4515606	2	2	Sondagens e Fundações A. Cavaco, Lda.
19	163	1/25 000	152080	424250	525362	4515241	7	0	Sondagens e Fundações A. Cavaco, Lda.
20	173	1/25 000	150120	412280	523521	4503258	7	1	Johann Keller S.R.L.
21	173	1/25 000	149150	410280	522571	4501249	6	0	Sondagens e Fundações A. Cavaco, Lda.
22	173	1/25 000	151750	416770	525300	4507800	3	1	D.R.A.Recursos Naturais Centro
23	174	1/25 000	159040	411240	532447	4502306	26	0	Sondagens e Fundações A. Cavaco, Lda.
24	174	1/25 000	159160	410260	532577	4501328	25	0	Sondagens e Fundações A. Cavaco, Lda.
25	174	1/25 000	158300	410730	531713	4501789	11	0	Sondagens e Fundações A. Cavaco, Lda.
26	174	1/25 000	157800	412600	531194	4503653	4	0	Sondagens e Fundações A. Cavaco, Lda.
27	174	1/25 000	158980	411720	532383	4502785	4	0	Sondagens e Fundações A. Cavaco, Lda.
28	174	1/25 000	160980	413130	534368	4504214	12	0	Sondagens e Fundações A. Cavaco, Lda.
29	174	1/25 000	159830	411020	533239	4502094	30	0	Sondagens e Fundações A. Cavaco, Lda.
30	174	1/25 000	154880	419450	528208	4510471	2	0	Sondagens e Fundações A. Cavaco, Lda.
31	174	1/25 000	157830	412600	531224	4503654	4	1	Sondagens e Fundações A. Cavaco, Lda.
32	174	1/25 000	158260	410820	531672	4501879	3	0	Sondagens e Fundações A. Cavaco, Lda.
33	173	1/25 000	159500	411000	532909	4502071	31	1	Johann Keller S.R.L.
34	174	1/25 000	157930	411690	531333	4502745	10	0	Sondagens e Fundações A. Cavaco, Lda.
35	174	1/25 000	159360	411720	532762	4502789	26	0	Sondagens e Fundações A. Cavaco, Lda.
36	174	1/25 000	159140	411560	532544	4502627	26	0	Sondagens e Fundações A. Cavaco, Lda.
37	174	1/25 000	159230	415540	532595	4506606	5	1	Persona - Soc. Perfurações e Sondagens, SA
38	174	1/25 000	158200	411700	531603	4502758	10	0	Sondagens e Fundações A. Cavaco, Lda.
39	174	1/25 000	157880	412580	531275	4503634	10	0	Sondagens e Fundações A. Cavaco, Lda.
40	174	1/25 000	158300	410730	531713	4501789	11	0	Sondagens e Fundações A. Cavaco, Lda.
41	174	1/25 000	159700	411440	533105	4502513	30	0	Captágua - Captações de Água, Lda
42	174	1/25 000	159420	411610	532823	4502680	26	0	Fundágua, SA
43	174	1/25 000	159050	411400	532456	4502466	26	0	Silvino J. Silva
44	174	1/25 000	159100	411080	532509	4502147	24	0	Persona - Soc. Perfurações e Sondagens, SA
45	174	1/25 000	159600	410600	533013	4501672	31	0	Captágua - Captações de Água, Lda
46	174	1/25 000	159350	410050	532769	4501120	26	0	Captágua - Captações de Água, Lda
47	174	1/25 000	159710	411410	533115	4502483	28	0	Captágua - Captações de Água, Lda
48	174	1/25 000	158402	411425	531808	4502485	18	0	Sondagens e Fundações A. Cavaco, Lda.
49	174	1/25 000	159159	412125	532557	4503192	18	0	Sondagens e Fundações A. Cavaco, Lda.
50	174	1/25 000	158780	411788	532182	4502852	18	0	Sondagens e Fundações A. Cavaco, Lda.
51	184	1/25 000	150570	404900	524044	4495885	10	0	Sondagens e Fundações A. Cavaco, Lda.
52	184	1/25 000	151900	408900	525334	4499897	3	1	Sondagens e Fundações A. Cavaco, Lda.
53	184	1/25 000	151700	408700	525136	4499695	3	0	Sondagens e Fundações A. Cavaco, Lda.
54	184	1/25 000	151500	408700	524936	4499693	3	0	Sondagens e Fundações A. Cavaco, Lda.
55	184	1/25 000	150630	407000	524083	4497985	3	0	Sondagens e Fundações A. Cavaco, Lda.
56	184	1/25 000	151980	405560	525447	4496559	10	1	Johann Keller S.R.L.
57	184	1/25 000	149780	408200	523222	4499176	2	0	Sondagens e Fundações A. Cavaco, Lda.
58	184	1/25 000	148420	407960	521865	4498923	2	0	Sondagens e Fundações A. Cavaco, Lda.
59	184	1/25 000	151430	409230	524861	4500222	3	0	Persona - Soc. Perfurações e Sondagens, SA
60	184	1/25 000	149800	408200	523242	4499176	3	0	Persona - Soc. Perfurações e Sondagens, SA
61	184	1/25 000	148565	407896	522010	4498860	2	0	Persona - Soc. Perfurações e Sondagens, SA
62	184	1/25 000	151625	408776	525060	4499770	2	0	Persona - Soc. Perfurações e Sondagens, SA
63	185	1/25 000	156370	406980	529820	4498022	15	0	Sondagens e Fundações A. Cavaco, Lda.
64	185	1/25 000	166850	400720	540357	4491868	6	0	Johann Keller S.R.L.
65	185	1/25 000	156400	406370	529857	4497412	12	0	Sondagens e Fundações A. Cavaco, Lda.
66	185	1/25 000	158450	408800	531882	4499861	10	0	Sondagens e Fundações A. Cavaco, Lda.
67	185	1/25 000	155025	403760	528508	4494790	18	0	Sondagens e Fundações A. Cavaco, Lda.
68	185	1/25 000	155100	403330	528587	4494361	14	0	Sondagens e Fundações A. Cavaco, Lda.
69	185	1/25 000	160200	409260	533626	4500338	42	0	Sondagens e Fundações A. Cavaco, Lda.
70	185	1/25 000	159750	404430	533224	4495506	57	0	Johann Keller S.R.L.
71	185	1/25 000	156350	406970	529801	4498012	13	0	Johann Keller S.R.L.
72	185	1/25 000	158430	405890	531890	4496953	45	0	Sondagens e Fundações A. Cavaco, Lda.
73	185	1/25 000	158840	402830	532330	4493898	50	0	Sondagens e Fundações A. Cavaco, Lda.
74	185	1/25 000	155630	405560	529095	4496595	18	0	D.R.A.Recursos Naturais Centro
75	185	1/25 000	153250	402450	526747	4493463	7	0	Sondagens e Fundações A. Cavaco, Lda.
76	185	1/25 000	156330	406100	529789	4497142	15	0	Sondagens e Fundações A. Cavaco, Lda.
77	185	1/25 000	152160	408350	525599	4499350	3	0	Sondagens e Fundações A. Cavaco, Lda.
78	185	1/25 000	152080	408950	525513	4499948	3	0	Sondagens e Fundações A. Cavaco, Lda.
79	185	1/25 000	157070	400750	530582	4491801	46	1	Johann Keller S.R.L.
80	185	1/25 000	152260	404620	525736	4495622	8	0	Sondagens e Fundações A. Cavaco, Lda.
81	185	1/25 000	153260	402540	526756	4493553	7	0	Sondagens e Fundações A. Cavaco, Lda.
82	185	1/25 000	159810	404320	533285	4495397	56	0	Sondagens e Fundações A. Cavaco, Lda.
83	185	1/25 000	161750	401530	535252	4492627	57	0	Sondagens e Fundações A. Cavaco, Lda.
84	185	1/25 000	156330	407070	529780	4498111	13	0	Sondagens e Fundações A. Cavaco, Lda.
85	185	1/25 000	155500	407180	528949	4498213	7	0	Johann Keller S.R.L.
86	185	1/25 000	161395	403354	534879	4494447	40	1	Johann Keller S.R.L.
87	185	1/25 000	159037	407340	532483	4498408	40	1	Johann Keller S.R.L.
88	185	1/25 000	162036	404427	535509	4495526	33	1	Johann Keller S.R.L.
89	185	1/25 000	153560	402480	527056	4493496	14	0	Sondagens e Fundações A. Cavaco, Lda.

Well Ref	Map_N	Map_Scale	Gauss_M	Gauss_P	UTM_X	UTM_Y	ZM (m)	ZR (m)	Drilling_Company
90	185	1/25 000	154500	407900	527942	4498923	5	0	Sondagens e Fundações A. Cavaco, Lda.
91	185	1/25 000	156366	407024	529816	4498066	15	1	Johann Keller S.R.L.
92	185	1/25 000	158439	407512	531883	4498574	16	1	Johann Keller S.R.L.
93	185	1/25 000	156380	404550	529854	4495593	25	1	Persona - Soc. Perfurações e Sondagens, SA
94	185	1/25 000	163700	400760	537208	4491877	26	0	Johann Keller S.R.L.
95	185	1/25 000	158440	408960	531870	4500021	20	0	Sondagens e Fundações A. Cavaco, Lda.
96	185	1/25 000	158500	405880	531960	4496943	45	0	Sondagens e Fundações A. Cavaco, Lda.
97	185	1/25 000	152300	408500	525737	4499501	2	0	Leiria Fernandes
98	185	1/25 000	152900	407500	526347	4498507	2	0	Duarte Pinto
99	185	1/25 000	160650	407630	534092	4498714	42	1	D.R.A.Recursos Naturais Centro
100	185	1/25 000	156300	407010	529750	4498051	18	0	Silvino J. Silva
101	185	1/25 000	163130	405780	536589	4496889	25	0	Sondagens e Fundações A. Cavaco, Lda.
102	185	1/25 000	161800	409820	535220	4500914	13	0	Captágua - Captações de Água, Lda
103	185	1/25 000	166700	400500	540210	4491646	22	0	Silvino J. Silva
104	185	1/25 000	166800	400080	540314	4491228	23	0	Silvino J. Silva
105	185	1/25 000	156600	403880	530081	4494925	25	0	Silvino J. Silva
106	185	1/25 000	156700	403700	530183	4494746	25	0	Silvino J. Silva
107	185	1/25 000	153475	407667	526920	4498680	2	0	Persona - Soc. Perfurações e Sondagens, SA
108	185	1/25 000	152260	408250	525700	4499251	3	0	Sondagens Perpétuo
109	185	1/25 000	152560	407740	526005	4498744	3	0	Sondagens Perpétuo
110	185	1/25 000	156140	404230	529618	4495271	21	1	Johann Keller S.R.L.
111	185	1/25 000	160090	408740	533521	4499818	41	0	Sondagens e Fundações A. Cavaco, Lda.
112	185	1/25 000	160180	409100	533608	4500178	42	0	Fundágua, SA
113	185	1/25 000	154370	404700	527844	4495723	12	0	Captágua - Captações de Água, Lda
114	185	1/25 000	153200	400060	526720	4491074	12	0	Captágua - Captações de Água, Lda
115	185	1/25 000	152470	408000	525912	4499003	2	0	Captágua - Captações de Água, Lda
116	185	1/25 000	157300	408700	530733	4499750	14	0	Sondagens e Fundações A. Cavaco, Lda.
117	185	1/25 000	154160	404820	527633	4495841	2	0	Captágua - Captações de Água, Lda
118	185	1/25 000	157500	403950	530980	4495004	40	0	Captágua - Captações de Água, Lda
119	185	1/25 000	152650	407750	526095	4498755	3	0	Captágua - Captações de Água, Lda
120	185	1/25 000	152540	407920	525983	4498923	3	0	Captágua - Captações de Água, Lda
121	185	1/25 000	153050	400750	526563	4491762	6	0	Captágua - Captações de Água, Lda
122	185	1/25 000	160200	409130	533628	4500209	42	0	Arménio da Silva Santos
123	195	1/25 000	150670	398130	524210	4489120	7	0	Silvino J. Silva
124	195	1/25 000	150650	398150	524190	4489139	7	0	Silvino J. Silva
125	195	1/25 000	149250	398275	522790	4489251	15	1	Persona - Soc. Perfurações e Sondagens, SA
126	195	1/25 000	150300	398140	523840	4489126	18	0	Captágua - Captações de Água, Lda
127	195	1/25 000	150330	397970	523872	4488956	13	0	Captágua - Captações de Água, Lda
128	196	1/25 000	154000	399970	527521	4490992	6	0	Sondagens e Fundações A. Cavaco, Lda.
129	196	1/25 000	165500	399100	539024	4490235	20	1	Johann Keller S.R.L.
130	196	1/25 000	165000	399200	538523	4490330	18	1	Johann Keller S.R.L.
131	196	1/25 000	163820	399350	537342	4490469	6	0	Arménio da Silva Santos
132	196	1/25 000	166000	395430	539560	4486572	30	0	Multiambiente - Téc. Ambiente e Geologia Lda
133	196	1/25 000	160825	396609	534376	4487699	57	1	Johann Keller S.R.L.
134	196	1/25 000	156900	397250	530446	4488301	57	1	Persona - Soc. Perfurações e Sondagens, SA
135	196	1/25 000	165280	398760	538807	4489893	25	0	Tecnifuro - Furos, Sondagens e Cap. Água, Lda
136	196	1/25 000	160300	395900	533858	4486986	50	0	Johann Keller S.R.L.
137	196	1/25 000	163200	392000	536795	4483116	61	1	Johann Keller S.R.L.
138	185	1/25 000	166850	400720	540357	4491868	7	1	Johann Keller S.R.L.
139	196	1/25 000	166900	396550	540449	4487700	72	0	Captágua - Captações de Água, Lda
140	196	1/25 000	164630	397200	538173	4488328	45	0	D.R.A.Recursos Naturais Centro
141	196	1/25 000	161500	392200	535094	4483299	64	0	D.R.A.Recursos Naturais Centro
142	196	1/25 000	163690	392470	537280	4483590	50	0	
143	196	1/25 000	163620	392730	537208	4483850	57	0	Tecnifuro - Furos, Sondagens e Cap. Água, Lda
144	196	1/25 000	156250	392000	529848	4483047	25	0	Silvino J. Silva
145	196	1/25 000	164450	397080	537994	4488206	55	0	Silvino J. Silva
146	196	1/25 000	164800	392800	538386	4483931	52	0	Silvino J. Silva
147	196	1/25 000	163500	399660	537019	4490775	12	0	Silvino J. Silva
148	196	1/25 000	167100	391680	540696	4482834	70	0	Silvino J. Silva
149	196	1/25 000	161630	396950	535177	4488048	52	0	Silvino J. Silva
150	196	1/25 000	160380	399020	533907	4490105	24	0	Silvino J. Silva
151	196	1/25 000	164300	398600	537830	4489724	13	0	Fundágua, SA
152	196	1/25 000	160500	392000	534096	4483089	56	0	Fundágua, SA
153	196	1/25 000	159200	394380	532773	4485455	41	0	Not known
154	196	1/25 000	167400	396450	540949	4487605	60	0	Sondagens e Fundações A. Cavaco, Lda.
155	196	1/25 000	167900	395900	541454	4487060	25	0	Tecnifuro - Furos, Sondagens e Cap. Água, Lda
156	185	1/25 000	166180	399400	539701	4490542	37	0	Johann Keller S.R.L.
157	196	1/25 000	161430	393000	535016	4484098	62	0	Johann Keller S.R.L.
158	196	1/25 000	165600	398970	539150	4490138	28	0	Geopesquisa - Sond. Captação de Água. Lda
159	196	1/25 000	165530	399100	539050	4490225	22	0	Geopesquisa - Sond. Captação de Água. Lda
160	196	1/25 000	165430	398920	538963	4490063	19	0	Geopesquisa - Sond. Captação de Água. Lda
161	196	1/25 000	165510	398820	539063	4489963	28	0	Geopesquisa - Sond. Captação de Água. Lda
162	206	1/25 000	149525	388200	523164	4479183	24	0	
163	206	1/25 000	152000	381000	525708	4472011	57	1	Silvino J. Silva
164	206	1/25 000	151270	387550	524914	4478551	39	0	Arménio da Silva Santos
165	207	1/25 000	157300	386100	530956	4477160	54	0	Silvino J. Silva
166	207	1/25 000	157200	388100	530836	4479159	43	0	Silvino J. Silva
167	207	1/25 000	157150	386000	530807	4477059	54	0	Silvino J. Silva
168	207	1/25 000	163370	389000	536994	4480119	51	0	Silvino J. Silva
169	207	1/25 000	164680	386910	538324	4478043	45	1	Johann Keller S.R.L.
170	207	1/25 000	155730	385920	529388	4476965	57	0	Captágua - Captações de Água, Lda
171	207	1/25 000	162600	388200	536233	4479312	69	0	Tecnifuro - Furos, Sondagens e Cap. Água, Lda
172	207	1/25 000	157860	389460	531482	4480524	47	0	Leirisonda - Captações Água e Mont. Bombas
173	207	1/25 000	164750	386750	538396	4477883	45	1	Johann Keller S.R.L.
174	208	1/25 000	154510	379960	528227	4470996	60	0	Leirisonda - Captações Água e Mont. Bombas
175	208	1/25 000	173550	381600	547243	4472822	60	0	Silvino J. Silva
176	208	1/25 000	173670	388000	547300	4479221	23	0	Silvino J. Silva
177	217	1/25 000	147480	371100	521287	4462071	69	0	Sondagens do Oeste, Lda
178	217	1/25 000	146125	370925	519935	4461883	59	0	Johann Keller S.R.L.
179	217	1/25 000	146100	370900	519910	4461858	59	0	Johann Keller S.R.L.
180	218	1/25 000	160450	376380	534200	4467476	57	0	Sondagens e Fundações A. Cavaco, Lda.
181	218	1/25 000	160280	376460	534029	4467554	57	0	Sondagens e Fundações A. Cavaco, Lda.
182	218	1/25 000	164460	379570	538177	4470704	80	0	Sondagens Neto
183	218	1/25 000	154900	372850	528687	4463893	62	0	Silvino J. Silva
184	218	1/25 000	164660	379770	538374	4470906	80	0	Sondagens do Oeste, Lda
185	185	1/25 000	156375	407025	529825	4498088	18	1	Johann Keller S.R.L.

Well Ref	Drilling_Method	Depth (m)	Initial Diameter (m)	Final Diameter (m)	Well_Use	Water_Use	Discharge Rate ($L\ s^{-1}$)	Pump_Depth (m)	HSL (m)
1	Rotary	201.0	0.381	0.251	Abandoned	None	5		5.60
2	Rotary	256.0	0.305	0.152	Piezometer	No specific use			-3.40
3	Rotary	202.0	0.219	0.165	Monitoring	No specific use	17		5.15
4	Rotary	204.0	0.200	0.165	Abandoned	None			
5	Rotary	205.0	0.200	0.160	Water supply	Domestic supply			
6	Rotary	172.0	0.305	0.254	Water supply	Public supply	15	30	-3.00
7	Rotary	182.0	0.381	0.311	Water supply	Domestic supply	15	30	-7.70
8	Mec. perc. & rotary	83.9	0.521	0.311	Abandoned	None			
9	Mec. perc. & rotary	145.0	0.356	0.102	Water supply	Industrial supply	5	40	-7.30
10	Mec. perc. & rotary	180.0	0.356	0.152	Piezometer	No specific use	20	50	-2.80
11	Rotary	229.0	0.127	0.076	Piezometer	No specific use			2.70
12	Reverse rotary	208.0	0.356	0.203	Water supply	Industrial supply	60	55	-5.60
13	Reverse rotary	158.0	0.356	0.203	Water supply	Industrial supply	60	55	-6.20
14	Reverse rotary	174.0	0.356	0.203	Monitoring	No specific use			-0.40
15	Reverse rotary	166.5	0.356	0.203	Piezometer	No specific use	80	55	-7.80
16	Rotary	134.0	0.559	0.254	Abandoned	None	3		-11.30
17	Reverse rotary	167.0	0.356	0.203	Water supply	Public supply	20	45	-18.00
18	Reverse rotary	164.0	0.102	0.051	Piezometer	No specific use			-0.40
19	Rotary	88.5	0.038	0.038	Monitoring	No specific use			0.00
20	Reverse rotary	349.5	0.445	0.152	Water supply	Public supply	12	71	2.00
21	Rotary	285.0	0.305	0.203	Water supply	Domestic supply	15	98	2.60
22	Rotary	235.0	0.203	0.152	Water supply	Domestic supply	3	66	
23	Reverse rotary	164.0	0.305	0.152	Water supply	Industrial supply	10	47	-18.10
24	Rotary	121.0	0.254	0.152	Water supply	Industrial supply	15	40	-22.50
25	Mec. perc. & rotary	132.0	0.305	0.152	Abandoned	None	28	45	-17.30
26	Mec. perc. & rotary	113.0	0.305	0.203	Abandoned	None	15	45	-14.90
27	Mec. perc. & rotary	126.0	0.305	0.203	Abandoned	None	28	50	-18.00
28	Mec. perc. & rotary	42.0	0.203	0.203	Abandoned	None	2	40	-4.40
29	Rotary	151.0	0.254	0.152	Water supply	Industrial supply	10	40	-21.26
30	Reverse rotary	198.5	0.356	0.203	Piezometer	No specific use	60	55	-11.20
31	Rotary	112.0	0.305	0.203	Water supply	Industrial supply	28	50	-17.40
32	Rotary	130.5	0.305	0.203	Water supply	Industrial supply	28	50	-23.80
33	Reverse rotary	150.0	0.305	0.203	Piezometer	No specific use	20	52	-30.78
34	Reverse rotary	126.0	0.305	0.203	Water supply	Industrial supply	30	53	-27.10
35	Reverse rotary	150.0	0.305	0.203	Water supply	Industrial supply	11	50	-28.30
36	Rotary	155.0	0.254	0.203	Water supply	Industrial supply	15	55	-34.40
37	Rotary	174.0	0.250	0.160	Water supply	Industrial supply	3	90	-1.32
38	Rotary	173.5	0.305	0.203	Abandoned	None			
39	Rotary	175.5	0.305	0.203	Abandoned	None			
40	Rotary				Abandoned	None			
41	Rotary	130.0	0.200	0.160	Water supply	Industrial supply	4	80	-36.00
42	Rotary	140.0	0.203	0.152	Water supply	Industrial supply	8	53	-26.00
43	Rotary	176.0	0.250	0.200	Water supply	Industrial supply	17	62	-37.42
44	Reverse rotary	121.0	0.305	0.203	Water supply	Industrial supply	20	54	-30.15
45	Rotary	116.0	0.140	0.140	Water supply	Industrial supply	2	70	-24.00
46	Rotary	110.0	0.140	0.140	Water supply	Domestic supply	1	54	-32.00
47	Rotary	132.0	0.380	0.160	Water supply	Industrial supply	3	77	-37.50
48	Mechanical percussion	19.4	0.368	0.251	Monitoring	No specific use			-0.60
49	Mechanical percussion	20.0	0.368	0.251	Monitoring	No specific use			
50	Mechanical percussion	35.3	0.368	0.251	Monitoring	No specific use			-16.30
51	Rotary	210.3	0.301	0.100	Monitoring	No specific use	5		6.40
52	Rotary	253.0	0.254	0.152	Water supply	Industrial supply	20		6.90
53	Rotary	270.0	0.305	0.152	Water supply	Industrial supply	15	50	3.10
54	Rotary	266.0	0.305	0.152	Water supply	Industrial supply	15	50	2.26
55	Rotary	277.5	0.356	0.152	Water supply	Public supply	25	50	-4.60
56	Reverse rotary	276.0	0.305	0.203	Water supply	Public supply	15	78	-19.91
57	Reverse rotary	270.0	0.254	0.203	Abandoned	None	20	30	-7.20
58	Reverse rotary	256.0	0.305	0.203	Water supply	Public supply	25	60	5.00
59	Reverse rotary	260.0	0.356	0.203	Water supply	Industrial supply	25	60	-15.57
60	Reverse rotary	298.0	0.356	0.203	Water supply	Industrial supply	15	60	-15.50
61	Reverse rotary	336	0.305	0.203	Water supply	Public supply	40	72	-10.05
62	Reverse rotary	272.0	0.305	0.203	Water supply	Industrial supply	30	72	-19.28
63	Rotary	240.0	0.521	0.305	Abandoned	None	35		-8.40
64	Rotary	25.5	0.305	0.305	Water supply	Public supply	4		-6.40
65	Rotary	281.5	0.356	0.152	Water supply	Public supply	21	62	-14.50
66	Rotary	139.5	0.356	0.203	Abandoned	None	28	77	-14.50
67	Rotary	292.0	0.356	0.152	Water supply	Public supply	25		-4.50
68	Rotary	302.0	0.356	0.152	Water supply	Public supply	25		0.00
69	Rotary	140.0	0.203	0.152	Water supply	Industrial supply	8	53	-40.50
70	Reverse rotary	233.9	0.305	0.152	Water supply	Public supply	15	77	-51.50
71	Reverse rotary	261.5	0.330	0.152	Abandoned	None			-28.45
72	Reverse rotary	239.0	0.356	0.203	Water supply	Public supply	20	80	-56.00
73	Reverse rotary	247.5	0.356	0.203	Water supply	Public supply	20	80	-49.00
74	Rotary	265.6	0.210	0.102	Abandoned	None	10		-25.00
75	Rotary	294.0	0.305	0.152	Water supply	Industrial supply	20	48	0.55
76	Rotary	183.0	0.203	0.203	Water supply	Industrial supply	8	60	-39.70
77	Rotary	264.0	0.305	0.152	Water supply	Industrial supply	15	30	-7.00
78	Rotary	252.0	0.254	0.152	Water supply	Industrial supply	20	40	-8.00
79	Reverse rotary	237.0	0.305	0.152	Water supply	Public supply	25	65	-46.20
80	Rotary	300.0	0.305	0.152	Water supply	Industrial supply	20	75	-10.30
81	Reverse rotary	295.0	0.305	0.152	Water supply	Industrial supply	20	67	-18.20
82	Reverse rotary	208.0	0.305	0.203	Water supply	Public supply	15	85	-64.30
83	Reverse rotary	194.0	0.305	0.203	Water supply	Public supply	15	83	-60.90
84	Reverse rotary	290.0	0.521	0.375	Abandoned	None			
85	Reverse rotary	194.5	0.254	0.152	Water supply	Public supply	10	62	-34.02
86	Reverse rotary	150.0	0.254	0.203	Water supply	Public supply	7	69	-30.70
87	Reverse rotary	196.0	0.254	0.152	Water supply	Public supply	28	80	-62.00
88	Reverse rotary	138.0	0.305	0.203	Abandoned	None	1		
89	Reverse rotary	298.0	0.305	0.152	Water supply	Industrial supply	20	66	-21.60

Well Ref	Drilling_Method	Depth (m)	Initial Diameter (m)	Final Diameter (m)	Well_Use	Water_Use	Discharge Rate ($L\ s^{-1}$)	Pump_Depth (m)	HSL (m)
90	Reverse rotary	226.0	0.254	0.203	Water supply	Industrial supply	4	98	-35.40
91	Reverse rotary	216.0	0.356	0.203	Water supply	Public supply	28	78	-47.05
92	Reverse rotary	233.0	0.305	0.203	Water supply	Public supply	27	88	-63.00
93	Reverse rotary	220.0	0.356	0.203	Water supply	Public supply	13	90	-66.84
94	Reverse rotary	156.0	0.305	0.203	Water supply	Public supply	3	90	-23.10
95	Reverse rotary	140.0	0.356	0.203	Water supply	Public supply	25	86	-57.75
96	Rotary	204.0	0.356	0.203	Water supply	Public supply	12	79	-69.20
97	Rotary	180.0	0.280	0.152	Water supply	Industrial supply			
98	Rotary	145.7	0.254	0.203	Water supply	Industrial supply			
99	Rotary	176.0	0.165	0.165	Monitoring	No specific use			-43.60
100	Rotary	175.0	0.320	0.140	Water supply	Irrigation	5	88	-61.00
101	Rotary	77.0	0.160	0.160	Water supply	Industrial supply	1	52	-20.20
102	Rotary	60.0	0.140	0.140	Water supply	Domestic supply	1	39	-18.00
103	Rotary	36.0	0.320	0.140	Water supply	Domestic supply			-15.00
104	Rotary	130.0	0.300	0.140	Water supply	Domestic supply	1		
105	Mec. perc. & rotary	158.0	0.140	0.140	Water supply	Industrial supply			-60.00
106	Rotary	238.0	0.300	0.160	Water supply	Industrial supply			-61.30
107	Reverse rotary	228.0	0.356	0.203	Water supply	Industrial supply	13	72	-27.90
108	Rotary	244.0	0.180	0.180	Water supply	Industrial supply	13	150	-8.00
109	Rotary	220.0	0.180	0.180	Water supply	Industrial supply	10	150	
110	Reverse rotary	218.0	0.254	0.152	Water supply	Industrial supply	5	56	-41.35
111	Rotary	125.0	0.152	0.152	Water supply	Industrial supply	10	80	-48.35
112	Rotary	147.0	0.203	0.152	Water supply	Industrial supply	4	60	-43.00
113	Rotary	224.0	0.160	0.160	Water supply	Industrial supply	3	70	-28.00
114	Rotary	210.0	0.160	0.160	Water supply	Domestic supply	1	60	-8.00
115	Rotary	220.0	0.200	0.160	Water supply	Industrial supply	5	85	-37.00
116	Rotary	181.8	0.254	0.152	Water supply	Industrial supply	17		-16.20
117	Rotary	220.0	0.140	0.140	Water supply	Industrial supply	3	55	-32.00
118	Rotary	210.0	0.140	0.140	Water supply	Domestic supply	1	90	-70.60
119	Rotary	215.0	0.140	0.140	Water supply	Industrial supply	3	85	-35.00
120	Rotary	230.0	0.200	0.160	Water supply	Industrial supply	4	85	-27.00
121	Rotary	220.0	0.140	0.140	Water supply	Domestic supply	1	60	-6.00
122	Rotary	150.0	0.180	0.180	Water supply	Industrial supply	7	100	
123	Rotary	292.0	0.305	0.203	Water supply	Industrial supply	3	150	-20.00
124	Rotary	300.0	0.254	0.203	Water supply	Industrial supply	21	60	-16.38
125	Reverse rotary	340.0	0.305	0.203	Water supply	Public supply	25	60	-13.14
126	Rotary	265.0	0.140	0.140	Water supply	Industrial supply	2	50	-6.00
127	Rotary	265.0	0.140	0.140	Water supply	Industrial supply	3	45	-11.00
128	Reverse rotary	294.0	0.305	0.203	Water supply	Industrial supply	28	20	5.00
129	Reverse rotary	124.0	0.305	0.203	Water supply	Public supply	5		-7.00
130	Reverse rotary	105.0	0.305	0.203	Water supply	Public supply	3		-3.60
131	Rotary	120.0	0.300	0.140	Water supply	Industrial supply	28		
132	Rotary	165.0	0.250	0.250	Abandoned	None	8	75	0.00
133	Reverse rotary	178.0	0.521	0.203	Water supply	Public supply	3	93	-57.00
134	Rotary	232.0	0.305	0.203	Water supply	Public supply	20	130	-50.10
135	Rotary	120.0	0.140	0.140	Water supply	Industrial supply	3	100	-20.00
136	Reverse rotary	68.0	0.254	0.203	Water supply	Public supply	4	52	-30.77
137	Reverse rotary	156.0	0.305	0.203	Abandoned	None	2	88	-15.00
138	Rotary	14.1	0.254	0.254	Water supply	Public supply	2		-1.65
139	Rotary	67.0	0.140	0.140	Water supply	No specific use	0	65	-22.00
140	Rotary	148.0	0.165	0.165	Monitoring	No specific use			-51.40
141	Rotary	220.0	0.200	0.200	Monitoring	No specific use			-18.83
142	Rotary	109.0			Water supply	Domestic supply			
143	Mec. perc. & rotary	60.0	0.140	0.140	Water supply	Domestic supply	8		-3.10
144	Mec. perc. & rotary	147.0	0.140	0.140	Water supply	Domestic supply			
145	Rotary	100.0	0.140	0.140	Water supply	Domestic supply	6		
146	Rotary	101.0	0.140	0.140	Water supply	Domestic supply			
147	Rotary	160.0	0.180	0.180	Water supply	Industrial supply	9		0.00
148	Mec. perc. & rotary	53.0	0.230	0.140	Water supply	Domestic supply	1	45	-18.00
149	Mec. perc. & rotary	107.0	0.140	0.140	Water supply	Public supply			
150	Mec. perc. & rotary	106.0	0.230	0.140	Water supply	Domestic supply	3	70	
151	Rotary	141.0	0.203	0.152	Water supply	Public supply	7	90	-14.60
152	Rotary	108.0	0.180	0.180	Water supply	Public supply	6	83	-14.00
153	Rotary	75.0			Water supply	Domestic supply			
154	Rotary	74.0	0.203	0.152	Water supply	Industrial supply			
155	Rotary	185.0	0.140	0.140	Water supply	Public supply	1	100	-7.00
156	Rotary	92.2	0.521	0.419	Abandoned	None			
157	Reverse rotary	150.0	0.521	0.375	Abandoned	None			
158	Mec. perc. & rotary	27.0	0.200	0.140	Monitoring	No specific use	6		
159	Mec. perc. & rotary	22.0	0.230	0.200	Monitoring	No specific use	6		-10.55
160	Mec. perc. & rotary	29.0	0.230	0.200	Water supply	Public supply	10		-9.63
161	Mec. perc. & rotary	31.5	0.230	0.140	Monitoring	No specific use	3		-15.96
162	Rotary	170.0			Water supply	Irrigation			
163	Rotary	100.0	0.140	0.140	Water supply	Domestic supply	1	100	-15.00
164	Rotary	200.0	0.140	0.140	Water supply	Industrial supply	8	100	
165	Rotary	202.0	0.140	0.140	Water supply	Domestic supply			
166	Rotary	218.0	0.140	0.140	Water supply	Domestic supply			-6.00
167	Rotary	208.0	0.140	0.140	Water supply	Domestic supply			
168	Rotary	85.0	0.140	0.140	Water supply	Domestic supply	1		
169	Rotary	32.0	0.254	0.254	Water supply	No specific use	20		0.20
170	Rotary	215.0	0.140	0.140	Water supply	Industrial supply	1	35	-23.00
171	Rotary	100.0	0.140	0.140	Water supply	Industrial supply	5	80	-27.00
172	Rotary	142.0	0.160	0.160	Water supply	Domestic supply	4	100	-9.70
173	Rotary	40.0	0.279	0.279	Water supply	Public supply	20		-0.10
174	Rotary	120.0	0.160	0.160	Water supply	Industrial supply	4	100	-42.00
175	Rotary	85.0	0.140	0.140	Water supply	Irrigation	2	50	-20.00
176	Rotary	107.0	0.140	0.140	Water supply	Industrial supply	3		
177	Rotary	203.0	0.200	0.200	Water supply	Industrial supply	17		
178	Rotary	93.0	0.235	0.152	Abandoned	None	8	58	-4.00
179	Rotary	96.0	0.305	0.203	Abandoned	None	5	60	-4.50
180	Rotary	169.0	0.203	0.102	Abandoned	None	10	25	-1.40
181	Rotary	137.3	0.254	0.152	Abandoned	None	20	20	-2.25
182	Rotary	132.0	0.140	0.140	Water supply	Domestic supply	4		-30.00
183	Rotary	190.0	0.140	0.140	Water supply	Domestic supply			
184	Rotary	116.0	0.140	0.140	Water supply	Domestic supply	5		
185	Reverse rotary	218.0	0.400	0.225	Water supply	Public supply	28	84	-47.00

A.2 GEOPHYSICAL AND GEOLOGICAL LOGS

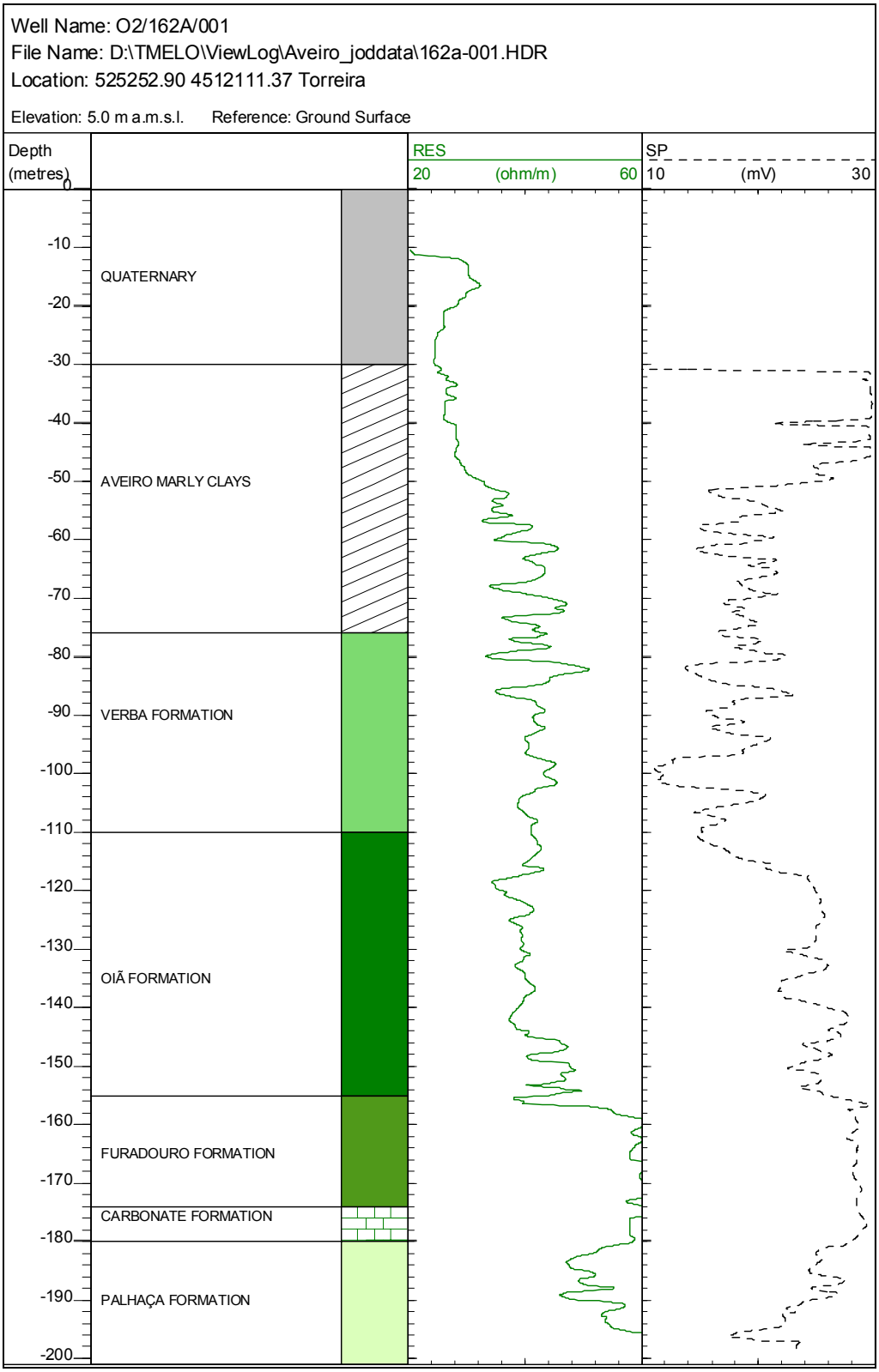

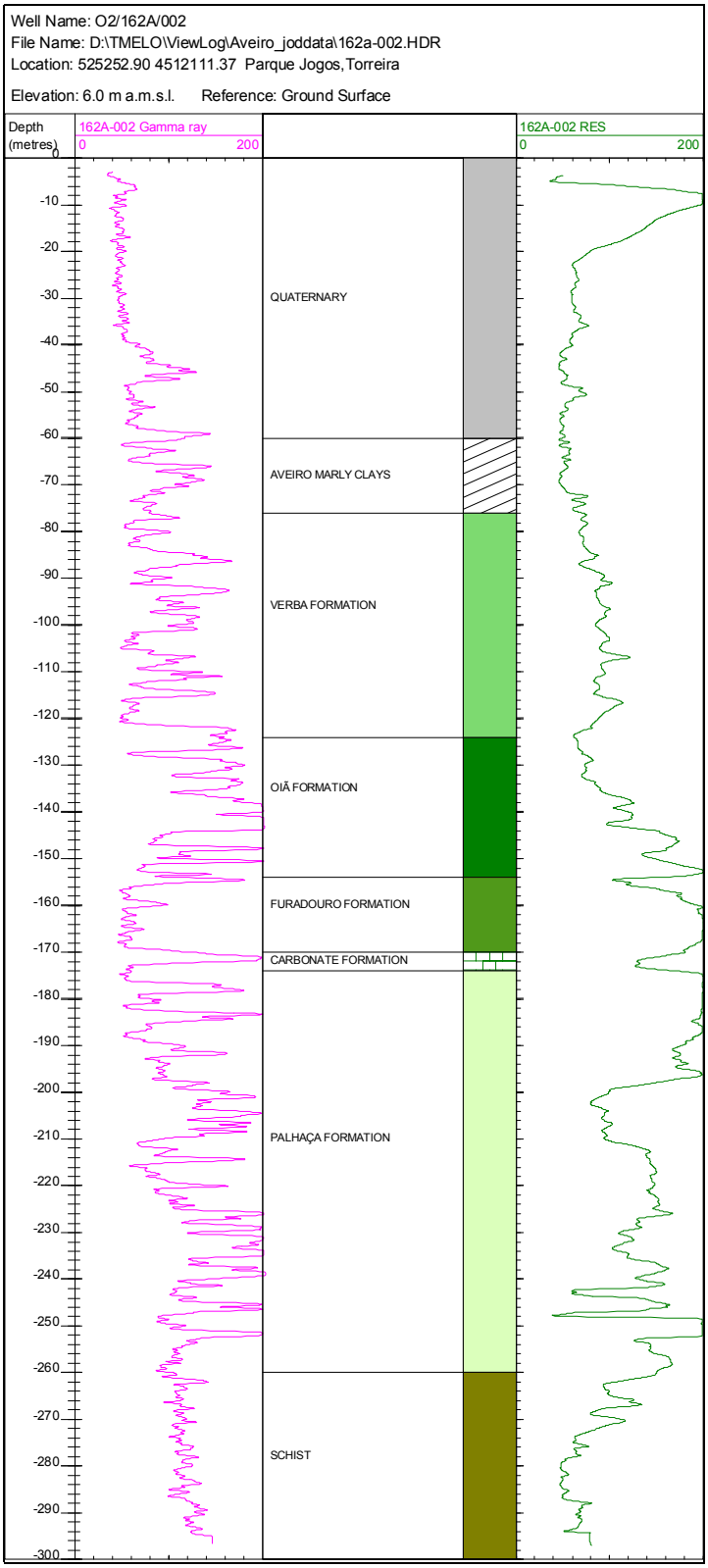
Well Name: O2/162A/002
File Name: D:\TMELO\ViewLog\Aveiro_joddata\162a-002.HDR
Location: 525252.90 4512111.37 Parque Jogos,Torreira
Elevation: 6.0 m a.m.s.l. Reference: Ground Surface
Depth (metres)
162A-002 Gamma ray
0
200
162A-002 RES
0
200
0
-10
-20
-30
-40
-50
-60
-70
-80
-90
-100
-110
-120
-130
-140
-150
-160
-170
-180
-190
-200
-210
-220
-230
-240
-250
-260
-270
-280
-290
-300
QUATERNARY
AVEIRO MARLY CLAYS
VERBA FORMATION
OIÃ FORMATION
FURADOURO FORMATION
CARBONATE FORMATION
PALHAÇA FORMATION
SCHIST

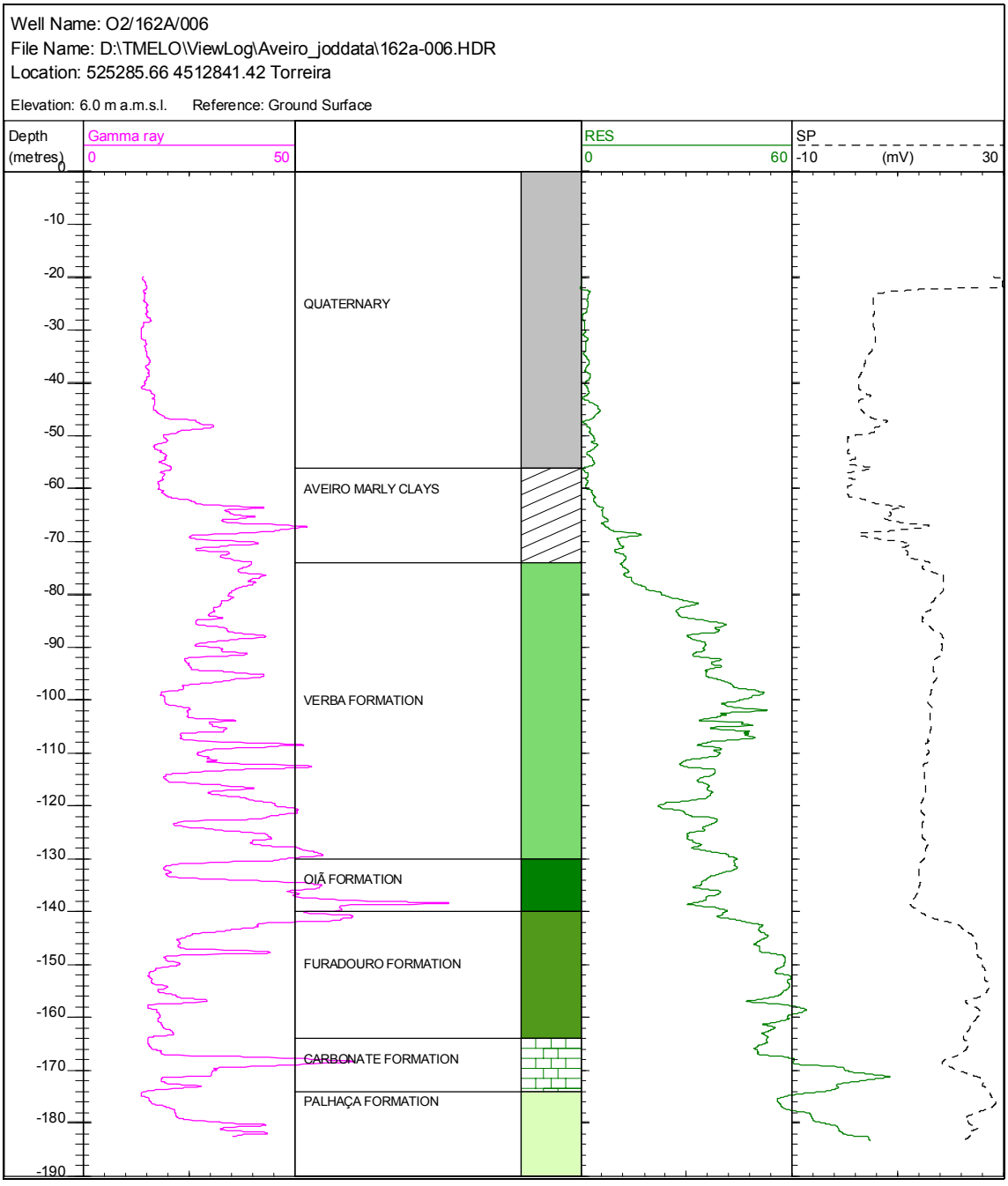
Well Name: O2/162A/006
File Name: D:\TMELO\ViewLog\Aveiro_joddata\162a-006.HDR
Location: 525285.66 4512841.42 Torreira
Elevation: 6.0 m a.m.s.l. Reference: Ground Surface
Depth (metres)
Gamma ray
0
50
RES
0
60
SP
-10
(mV)
30
0
-10
-20
-30
-40
-50
-60
-70
-80
-90
-100
-110
-120
-130
-140
-150
-160
-170
-180
-190
QUATERNARY
AVEIRO MARLY CLAYS
VERBA FORMATION
OIÃ FORMATION
FURADOURO FORMATION
CARBONATE FORMATION
PALHAÇA FORMATION

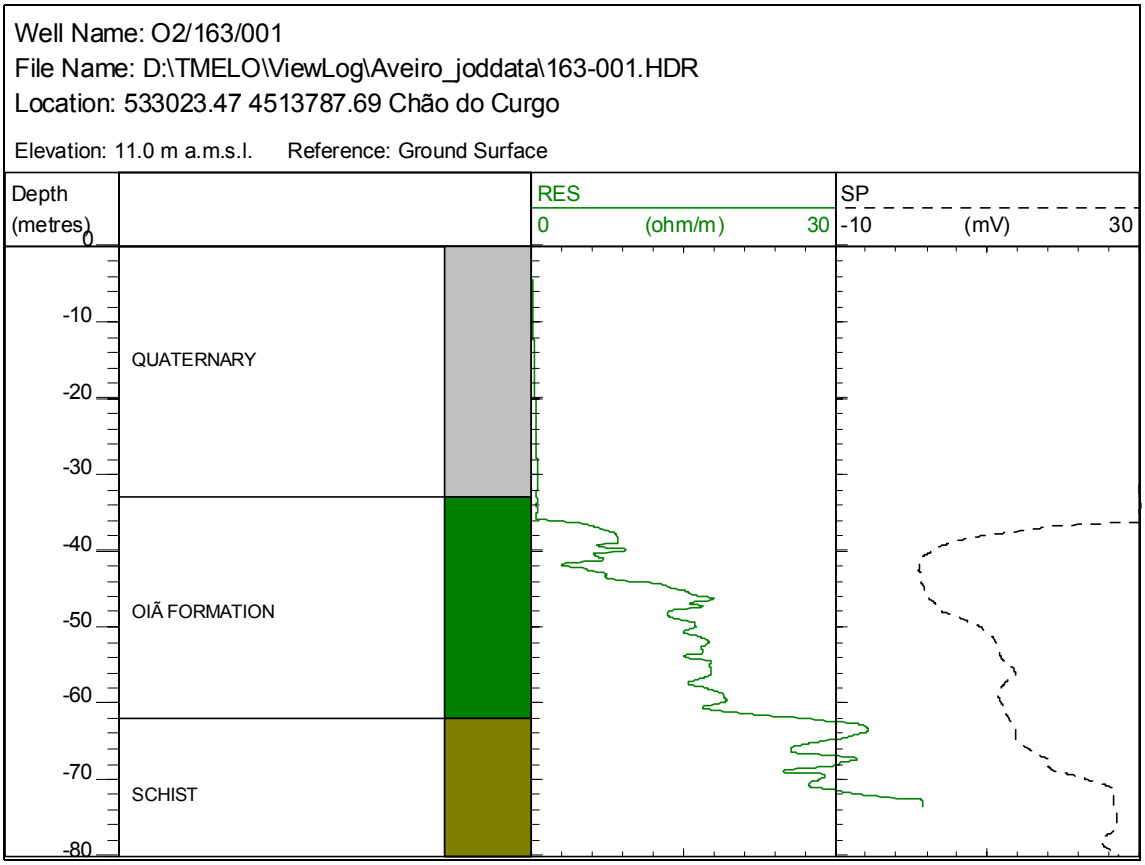
Well Name: O2/163/001
File Name: D:\TMELO\ViewLog\Aveiro_joddata\163-001.HDR
Location: 533023.47 4513787.69 Chão do Curgo
Elevation: 11.0 m a.m.s.l. Reference: Ground Surface
Depth (metres)
RES
0 (ohm/m) 30
SP
-10 (mV) 30
0
-10
-20
-30
-40
-50
-60
-70
-80
QUATERNARY
OIÃ FORMATION
SCHIST

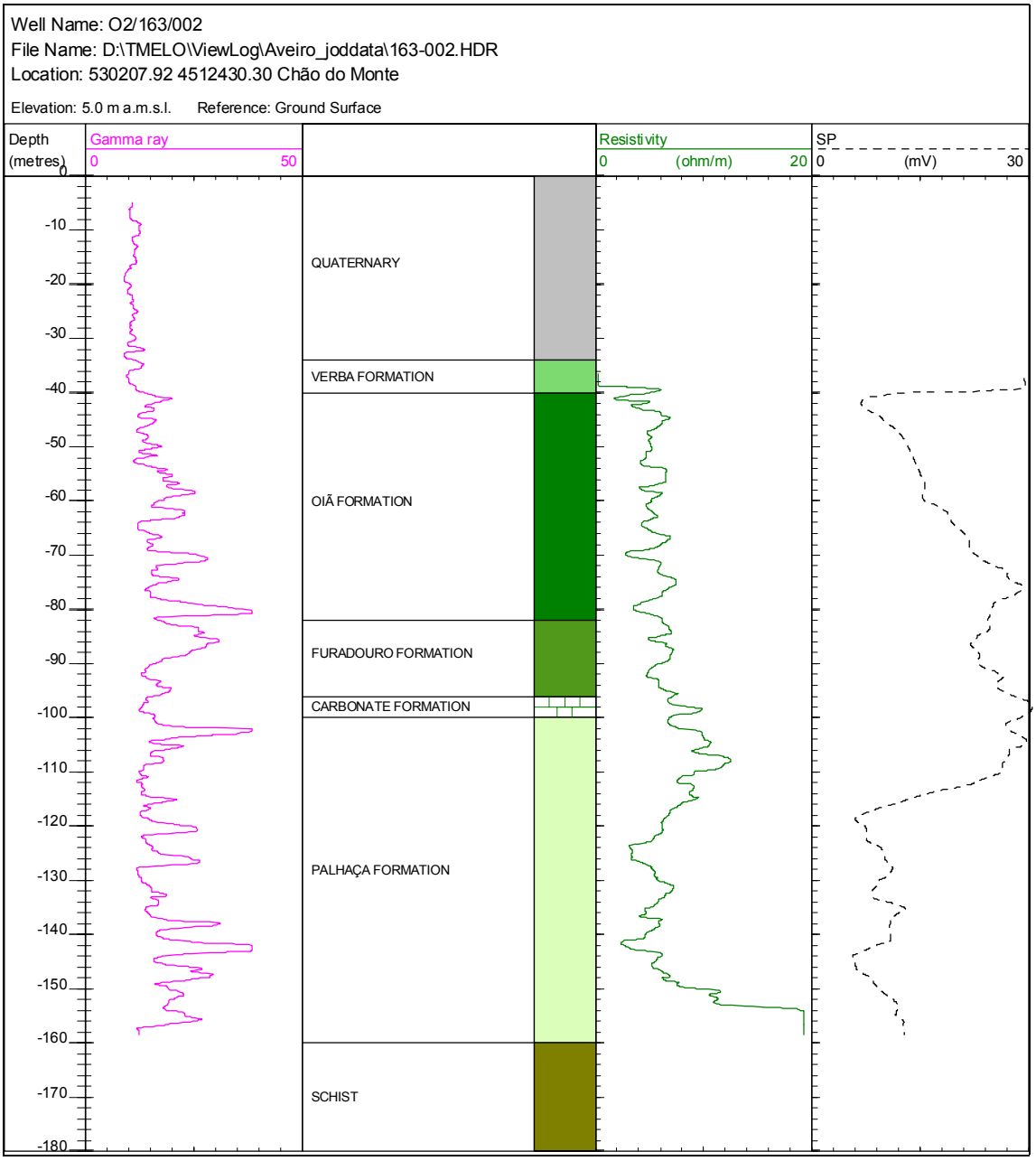
Well Name: O2/163/002
File Name: D:\TMELO\ViewLog\Aveiro_joddata\163-002.HDR
Location: 530207.92 4512430.30 Chão do Monte
Elevation: 5.0 m a.m.s.l. Reference: Ground Surface
Depth (metres)
Gamma ray
0
50
Resistivity
0
(ohm/m)
20
SP
0
(mV)
30
0
-10
-20
-30
-40
-50
-60
-70
-80
-90
-100
-110
-120
-130
-140
-150
-160
-170
-180
QUATERNARY
VERBA FORMATION
OIÃ FORMATION
FURADOURO FORMATION
CARBONATE FORMATION
PALHAÇA FORMATION
SCHIST

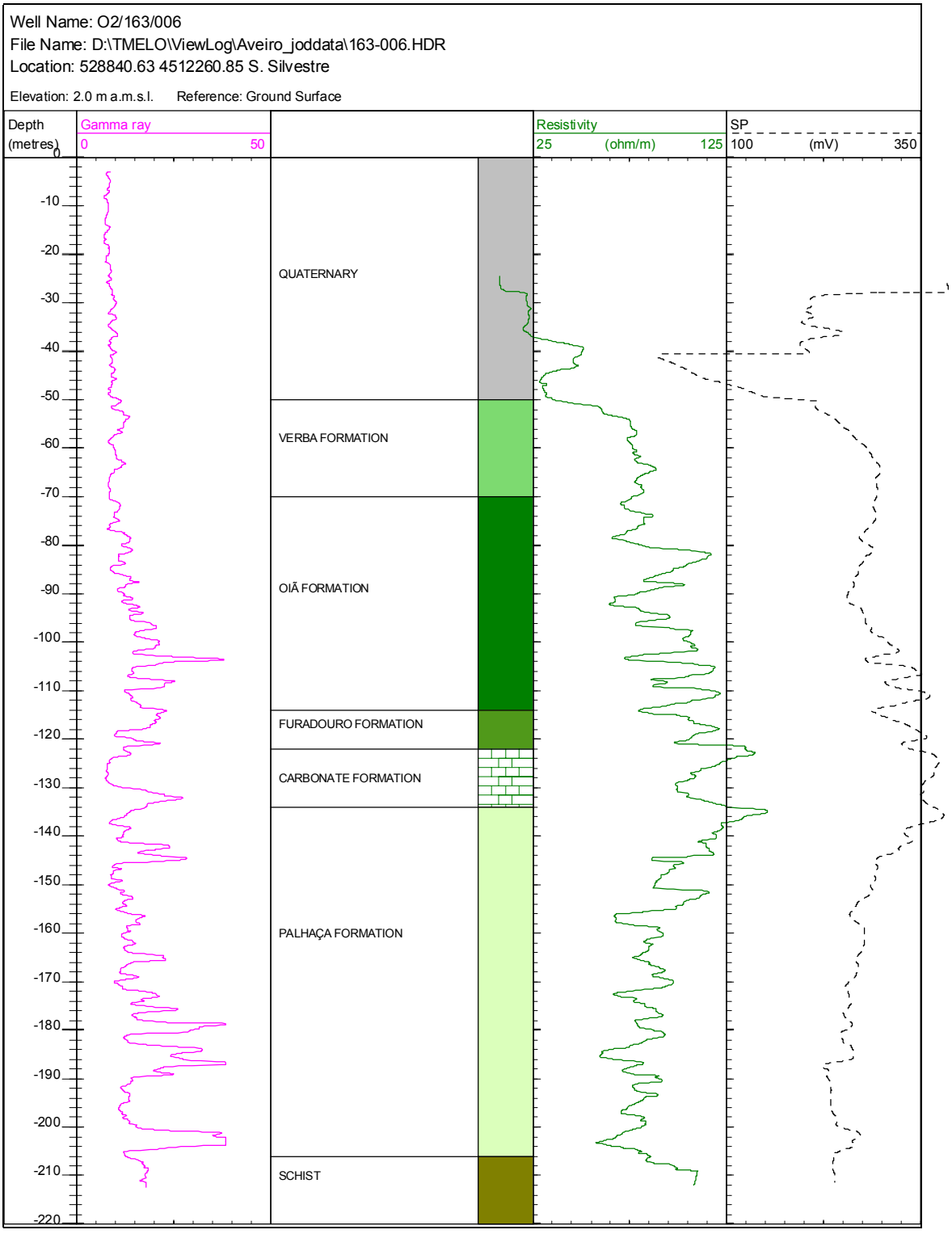
Well Name: O2/163/006
File Name: D:\TMELO\ViewLog\Aveiro_joddata\163-006.HDR
Location: 528840.63 4512260.85 S. Silvestre
Elevation: 2.0 m a.m.s.l.
Reference: Ground Surface
Depth (metres)
Gamma ray
0
50
Resistivity
25
(ohm/m)
125
SP
100
(mV)
350
0
-10
-20
-30
-40
-50
-60
-70
-80
-90
-100
-110
-120
-130
-140
-150
-160
-170
-180
-190
-200
-210
-220
QUATERNARY
VERBA FORMATION
OIÃ FORMATION
FURADOURO FORMATION
CARBONATE FORMATION
PALHAÇA FORMATION
SCHIST

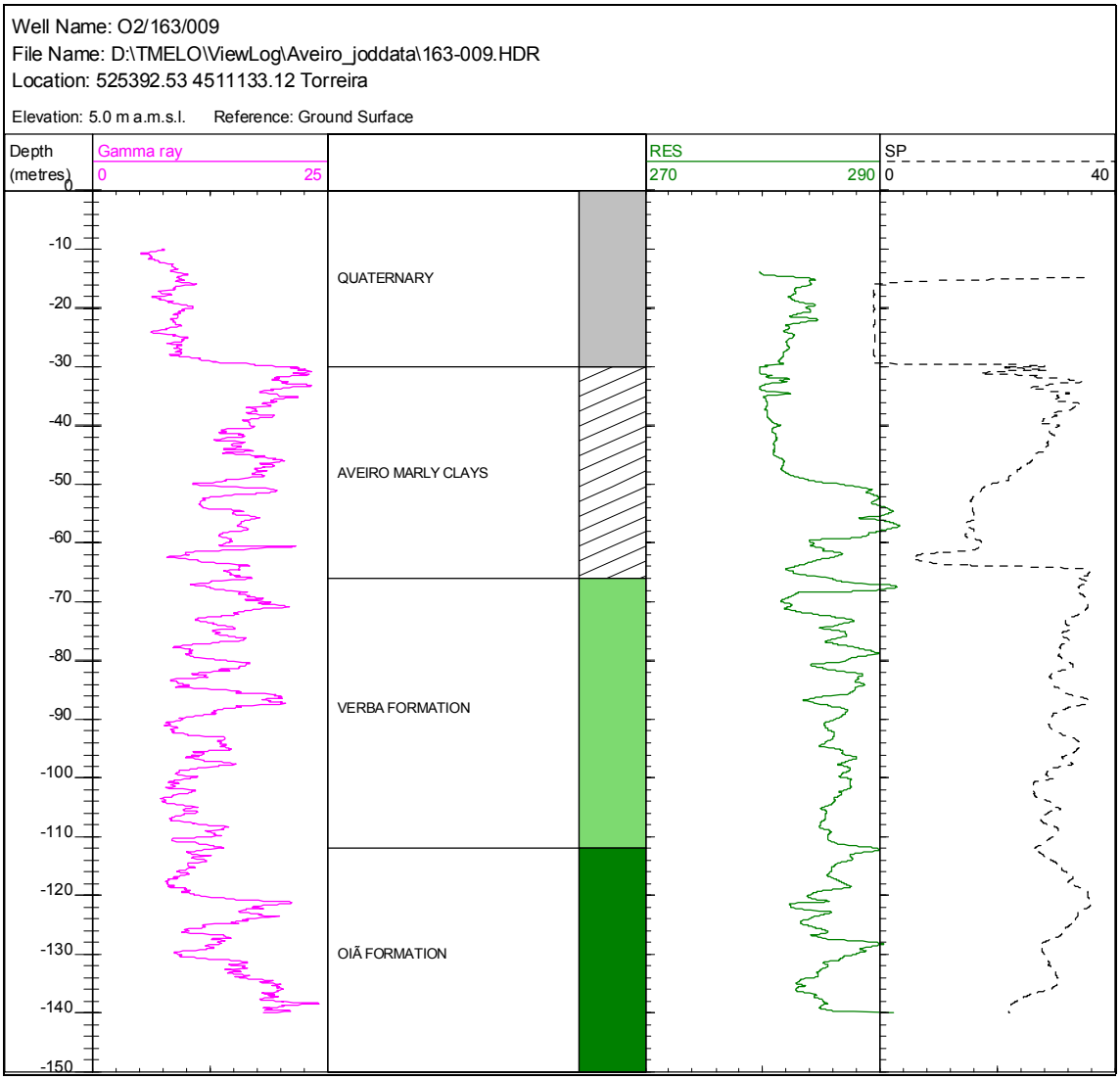
Well Name: O2/163/009
File Name: D:\TMELO\ViewLog\Aveiro_joddata\163-009.HDR
Location: 525392.53 4511133.12 Torreira
Elevation: 5.0 m a.m.s.l. Reference: Ground Surface
Depth (metres)
Gamma ray
0
25
RES
270
290
SP
0
40
0
-10
-20
-30
-40
-50
-60
-70
-80
-90
-100
-110
-120
-130
-140
-150
QUATERNARY
AVEIRO MARLY CLAYS
VERBA FORMATION
OIÃ FORMATION

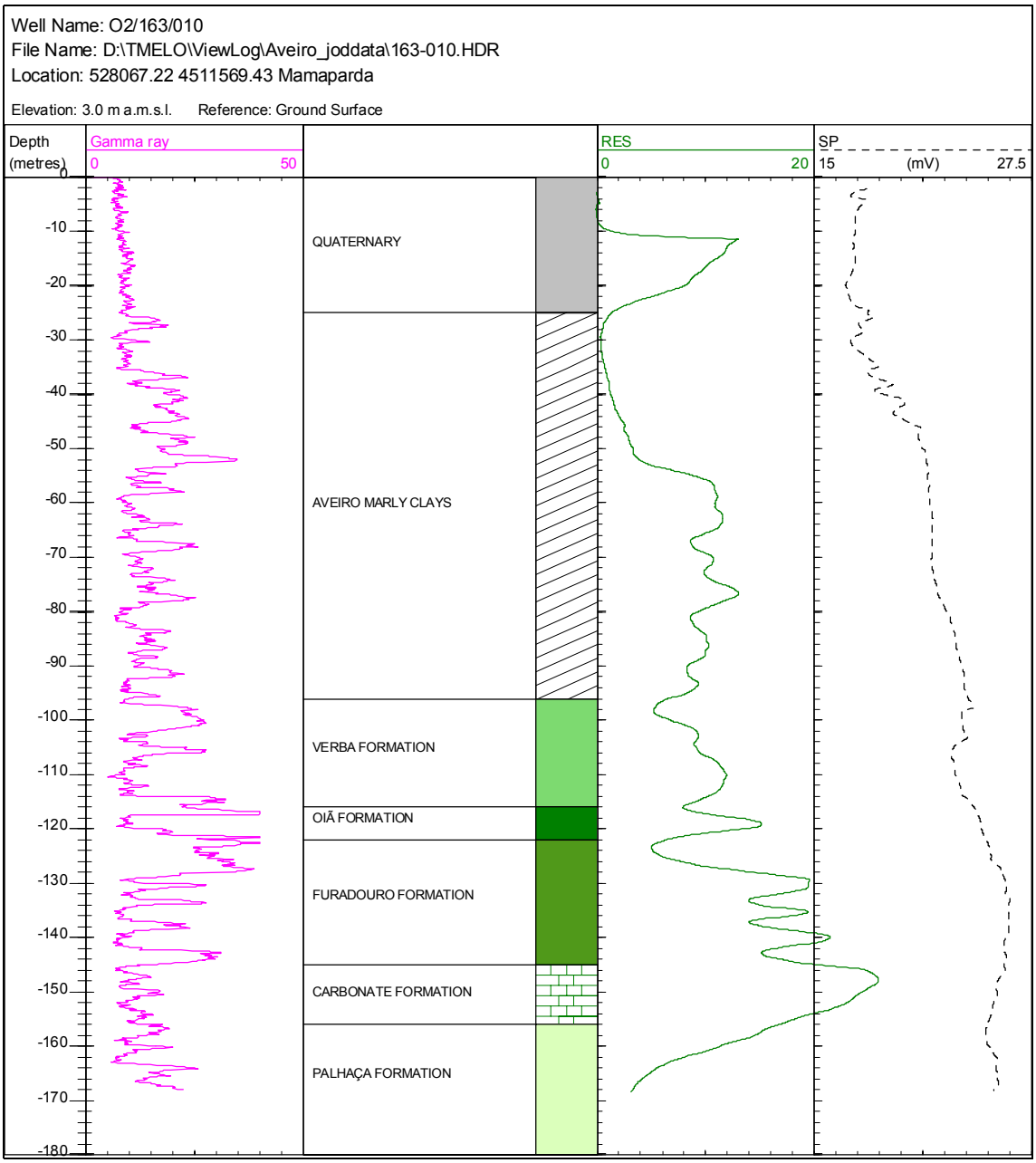
Well Name: O2/163/010
File Name: D:\TMELO\ViewLog\Aveiro_joddata\163-010.HDR
Location: 528067.22 4511569.43 Mamaparda
Elevation: 3.0 m a.m.s.l. Reference: Ground Surface
Depth (metres)
Gamma ray
0
50
RES
0
20
SP
15
(mV)
27.5
0
-10
-20
-30
-40
-50
-60
-70
-80
-90
-100
-110
-120
-130
-140
-150
-160
-170
-180
QUATERNARY
AVEIRO MARLY CLAYS
VERBA FORMATION
OIÃ FORMATION
FURADOURO FORMATION
CARBONATE FORMATION
PALHAÇA FORMATION

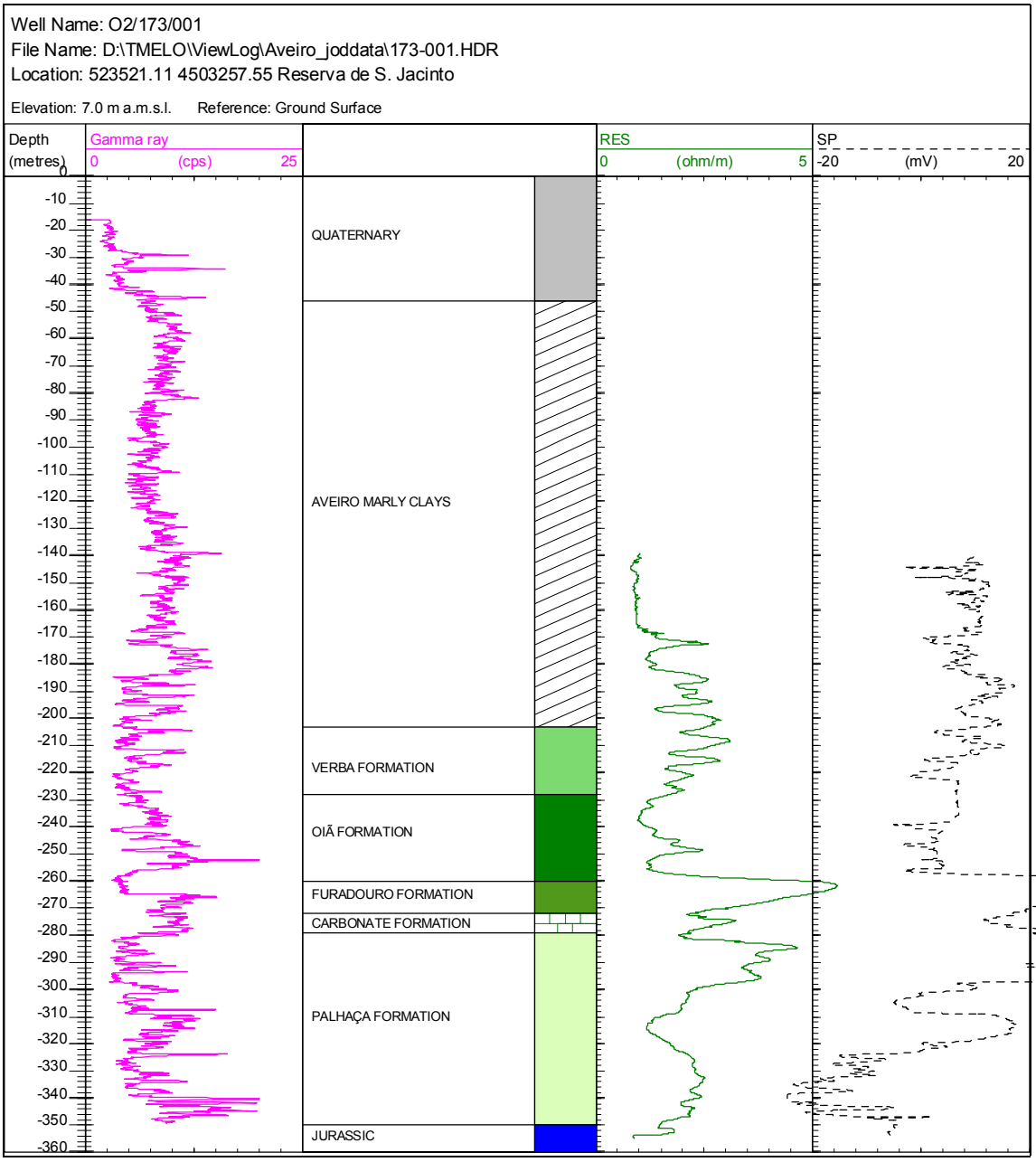
Well Name: O2/173/001
File Name: D:\TMELO\ViewLog\Aveiro_joddata\173-001.HDR
Location: 523521.11 4503257.55 Reserva de S. Jacinto
Elevation: 7.0 m a.m.s.l. Reference: Ground Surface
Depth (metres)
Gamma ray
0 (cps) 25
RES
0 (ohm/m) 5
SP
-20 (mV) 20
QUATERNARY
AVEIRO MARLY CLAYS
VERBA FORMATION
OIÃ FORMATION
FURADOURO FORMATION
CARBONATE FORMATION
PALHAÇA FORMATION
JURASSIC

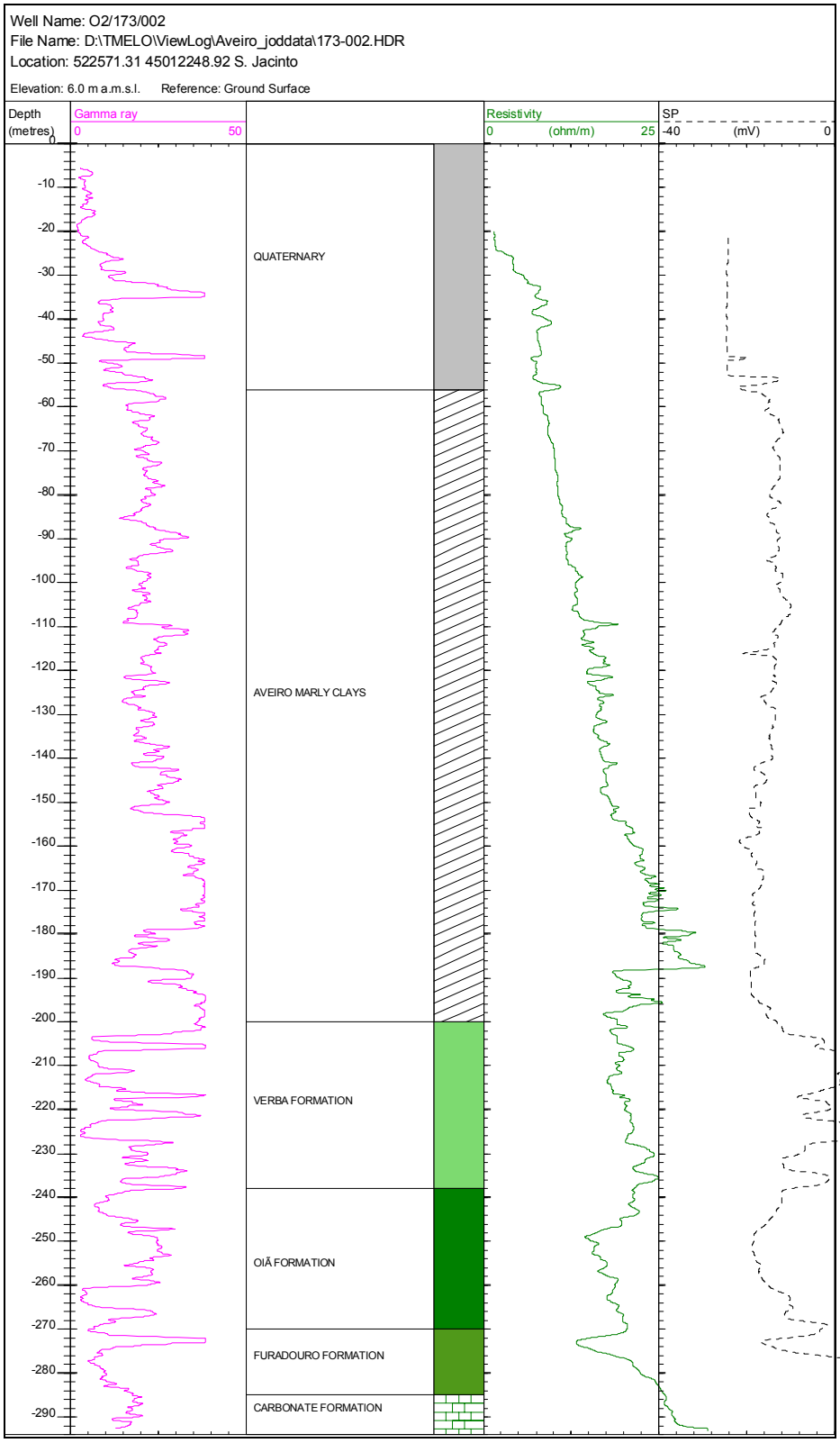
Well Name: O2/173/002
File Name: D:\TMELO\ViewLog\Aveiro_joddata\173-002.HDR
Location: 522571.31 45012248.92 S. Jacinto
Elevation: 6.0 m a.m.s.l. Reference: Ground Surface
Depth (metres)
Gamma ray
0
50
Resistivity
0
(ohm/m)
25
SP
-40
(mV)
0
QUATERNARY
AVEIRO MARLY CLAYS
VERBA FORMATION
OIÃ FORMATION
FURADOURO FORMATION
CARBONATE FORMATION

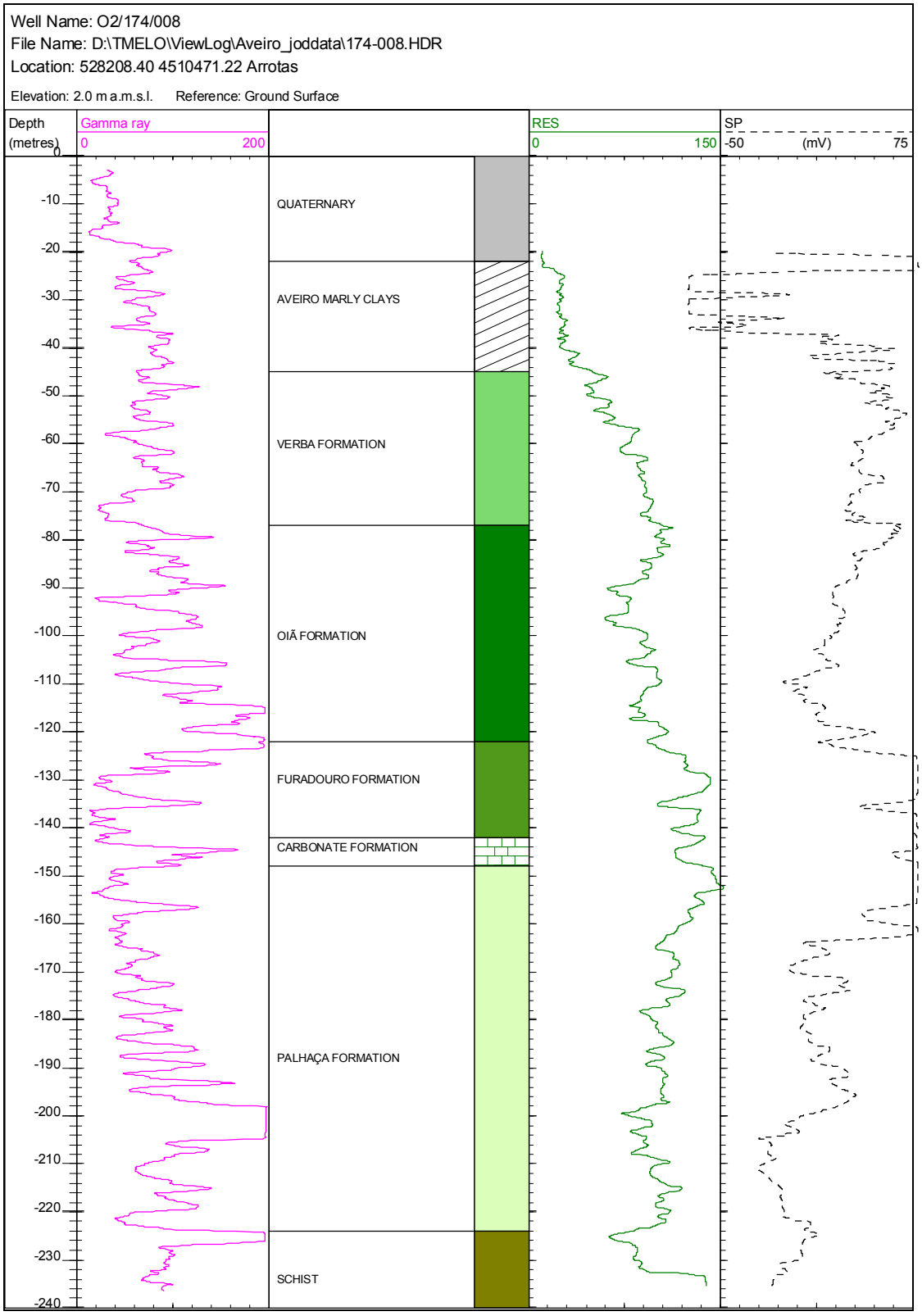
Well Name: O2/174/008
File Name: D:\TMELO\ViewLog\Aveiro_joddata\174-008.HDR
Location: 528208.40 4510471.22 Arrotas
Elevation: 2.0 m a.m.s.l. Reference: Ground Surface
Depth (metres)
Gamma ray
0
200
RES
0
150
SP
-50
(mV)
75
QUATERNARY
AVEIRO MARLY CLAYS
VERBA FORMATION
OIÃ FORMATION
FURADOURO FORMATION
CARBONATE FORMATION
PALHAÇA FORMATION
SCHIST

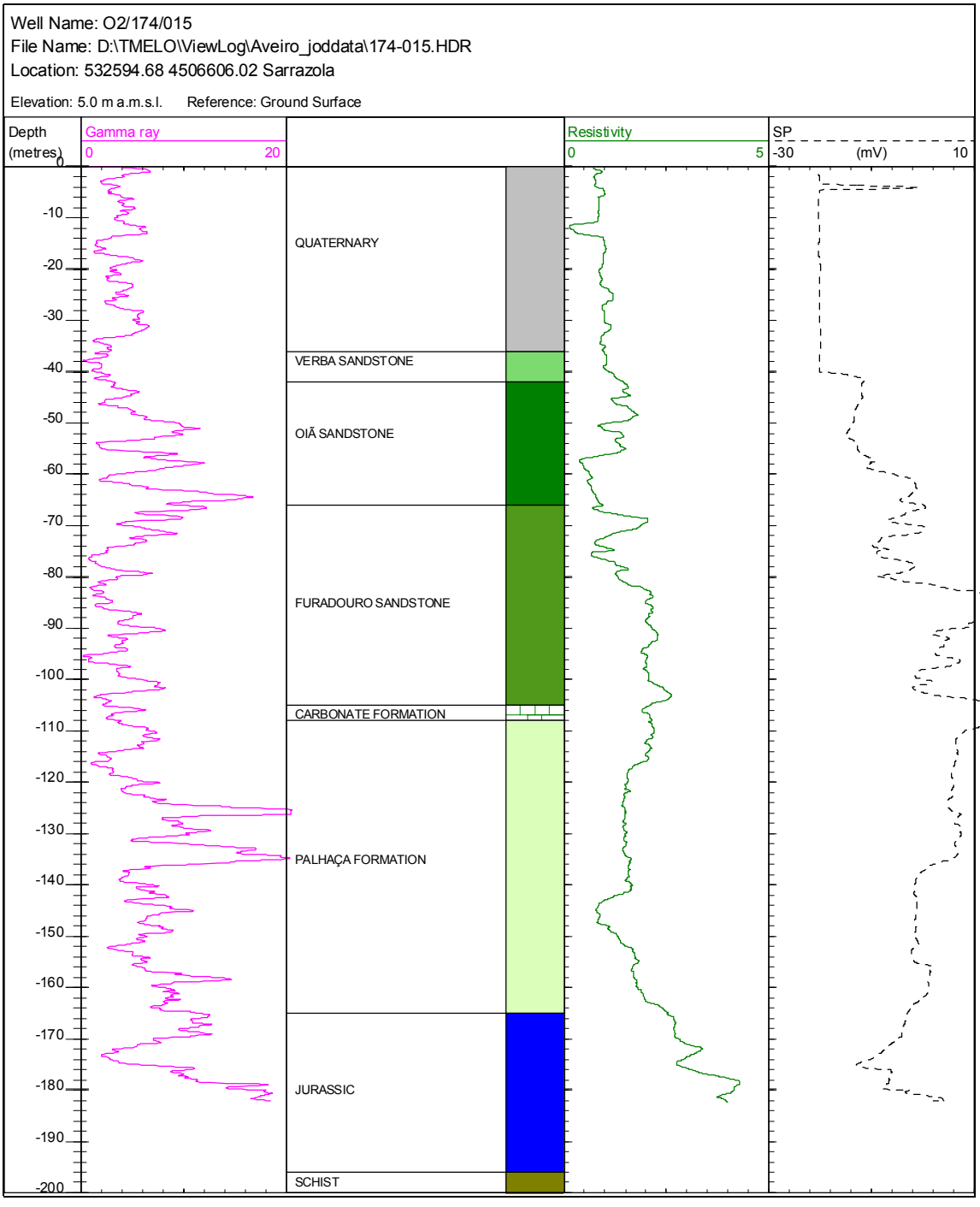
Well Name: O2/174/015
File Name: D:\TMELO\ViewLog\Aveiro_joddata\174-015.HDR
Location: 532594.68 4506606.02 Sarrazola
Elevation: 5.0 m a.m.s.l. Reference: Ground Surface
Depth (metres)
Gamma ray
0
20
Resistivity
0
5
SP
-30
(mV)
10
0
-10
-20
-30
-40
-50
-60
-70
-80
-90
-100
-110
-120
-130
-140
-150
-160
-170
-180
-190
-200
QUATERNARY
VERBA SANDSTONE
OIÃ SANDSTONE
FURADOURO SANDSTONE
CARBONATE FORMATION
PALHAÇA FORMATION
JURASSIC
SCHIST

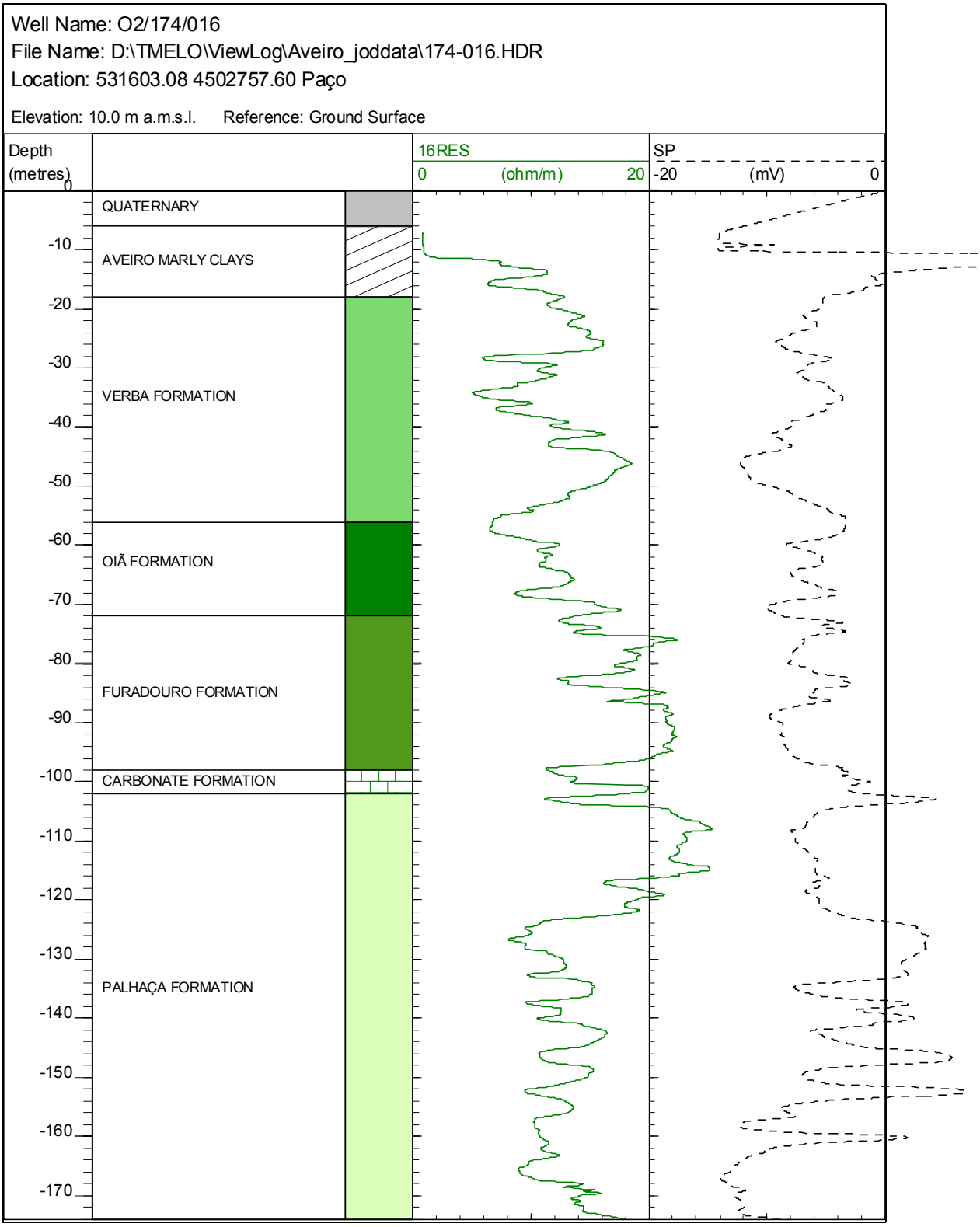
Well Name: O2/174/016
File Name: D:\TMELO\ViewLog\Aveiro_joddata\174-016.HDR
Location: 531603.08 4502757.60 Paço
Elevation: 10.0 m a.m.s.l. Reference: Ground Surface
Depth (metres)
16RES
0 (ohm/m) 20
SP
-20 (mV) 0
0
-10
-20
-30
-40
-50
-60
-70
-80
-90
-100
-110
-120
-130
-140
-150
-160
-170
QUATERNARY
AVEIRO MARLY CLAYS
VERBA FORMATION
OIÃ FORMATION
FURADOURO FORMATION
CARBONATE FORMATION
PALHAÇA FORMATION

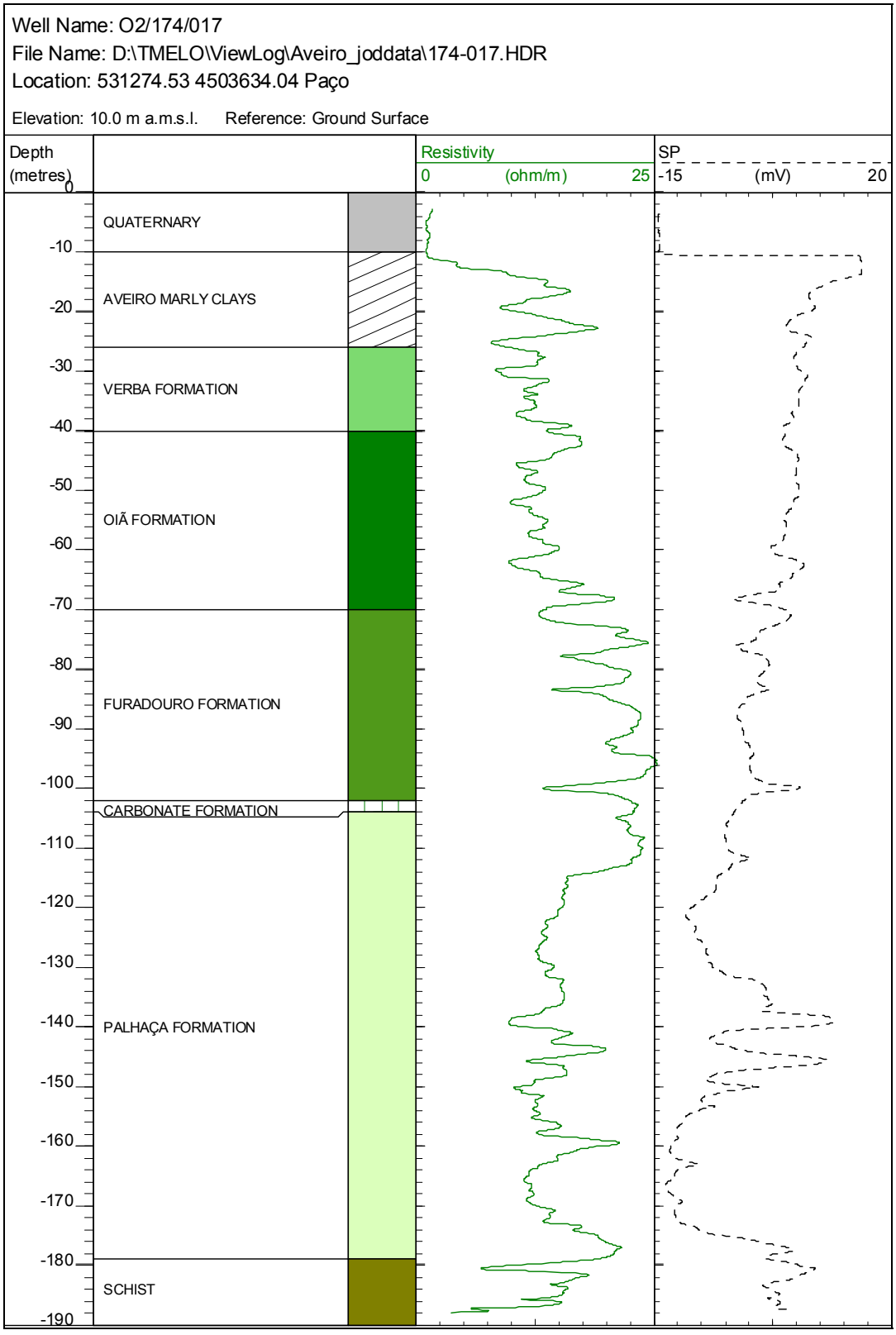
Well Name: O2/174/017
File Name: D:\TMELO\ViewLog\Aveiro_joddata\174-017.HDR
Location: 531274.53 4503634.04 Paço
Elevation: 10.0 m a.m.s.l. Reference: Ground Surface
Depth (metres)
Resistivity
0 (ohm/m) 25
SP
-15 (mV) 20
0
-10
-20
-30
-40
-50
-60
-70
-80
-90
-100
-110
-120
-130
-140
-150
-160
-170
-180
-190
QUATERNARY
AVEIRO MARLY CLAYS
VERBA FORMATION
OIÃ FORMATION
FURADOURO FORMATION
CARBONATE FORMATION
PALHAÇA FORMATION
SCHIST

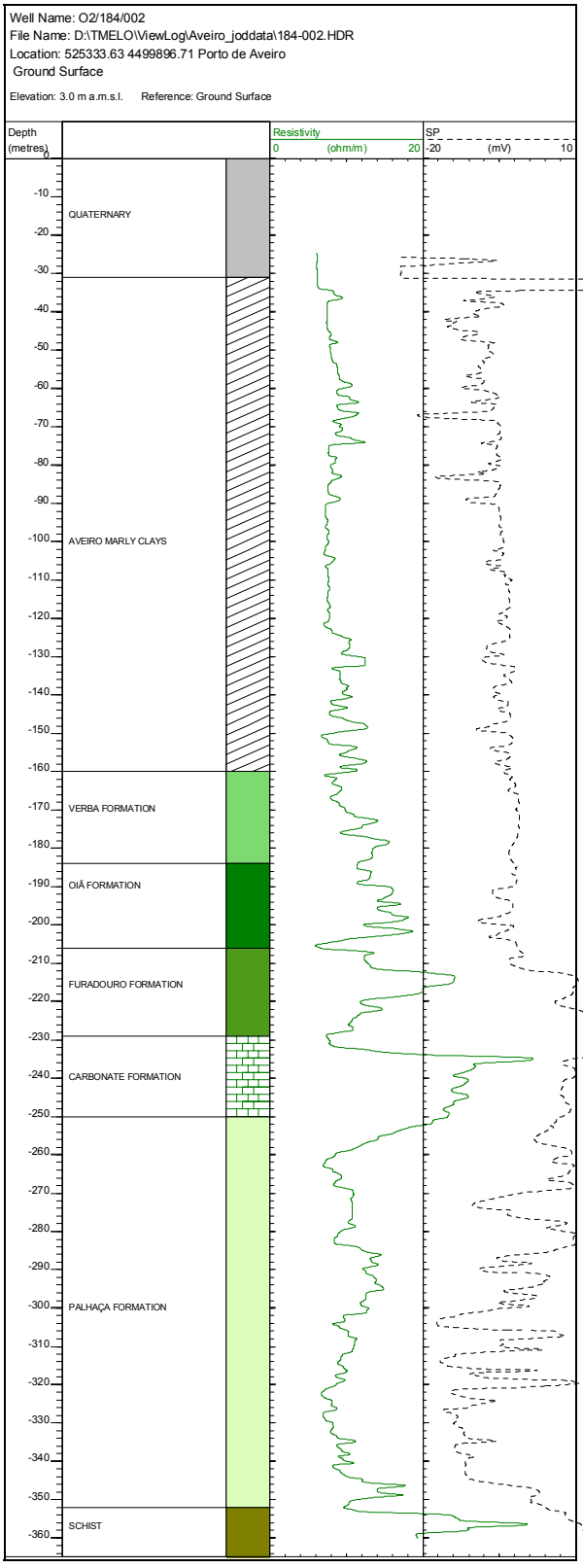
Well Name: O2/184/002
File Name: D:\TMELO\ViewLog\Aveiro_joddata\184-002.HDR
Location: 525333.63 4499896.71 Porto de Aveiro
Ground Surface
Elevation: 3.0 m a.m.s.l. Reference: Ground Surface
Depth (metres)
Resistivity
0 (ohm/m) 20
SP
-20 (mV) 10
QUATERNARY
AVEIRO MARLY CLAYS
VERBA FORMATION
OIÃ FORMATION
FURADOURO FORMATION
CARBONATE FORMATION
PALHAÇA FORMATION
SCHIST

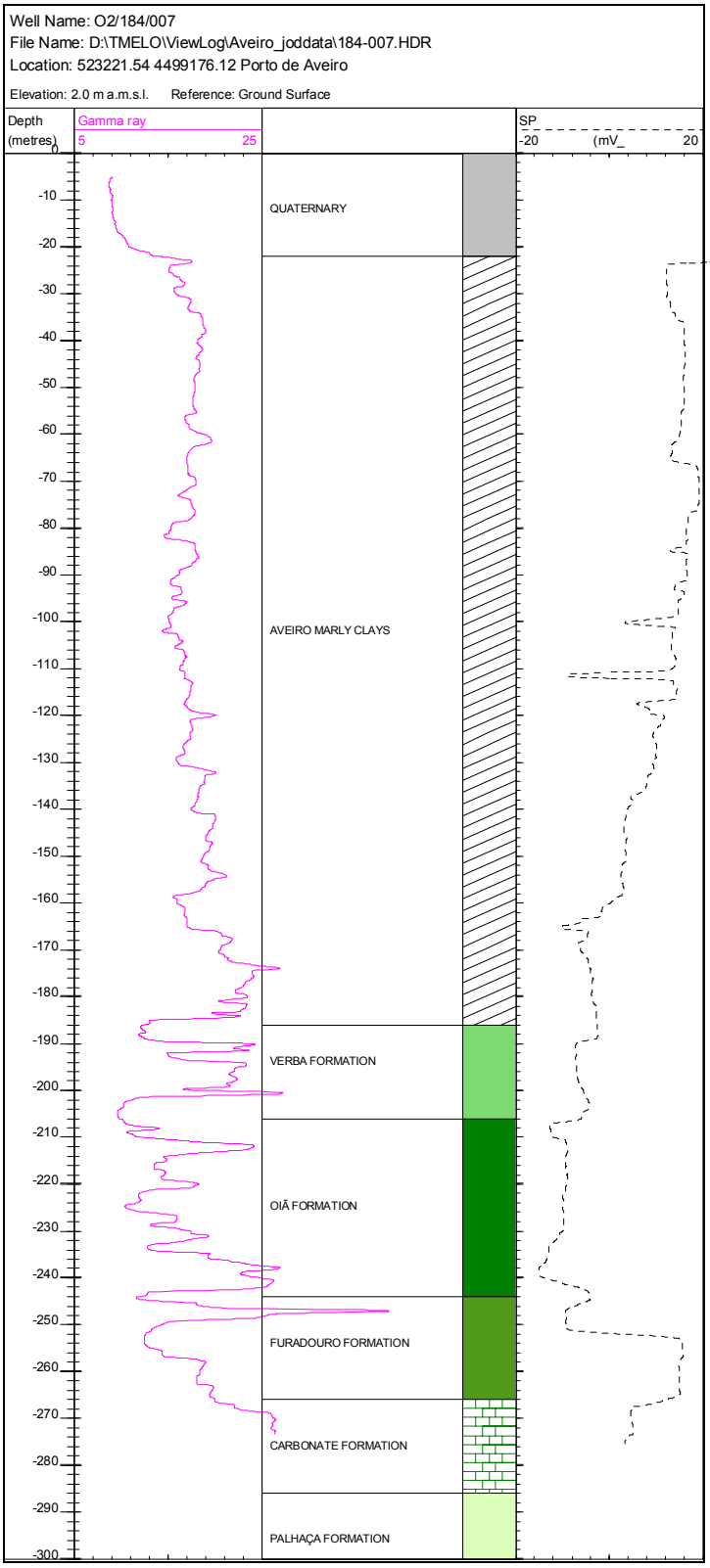
Well Name: O2/184/007
File Name: D:\TMELO\ViewLog\Aveiro_joddata\184-007.HDR
Location: 523221.54 4499176.12 Porto de Aveiro
Elevation: 2.0 m a.m.s.l. Reference: Ground Surface
Depth (metres)
Gamma ray
5
25
SP
-20
(mV_
20
0
-10
-20
-30
-40
-50
-60
-70
-80
-90
-100
-110
-120
-130
-140
-150
-160
-170
-180
-190
-200
-210
-220
-230
-240
-250
-260
-270
-280
-290
-300
QUATERNARY
AVEIRO MARLY CLAYS
VERBA FORMATION
OIÃ FORMATION
FURADOURO FORMATION
CARBONATE FORMATION
PALHAÇA FORMATION

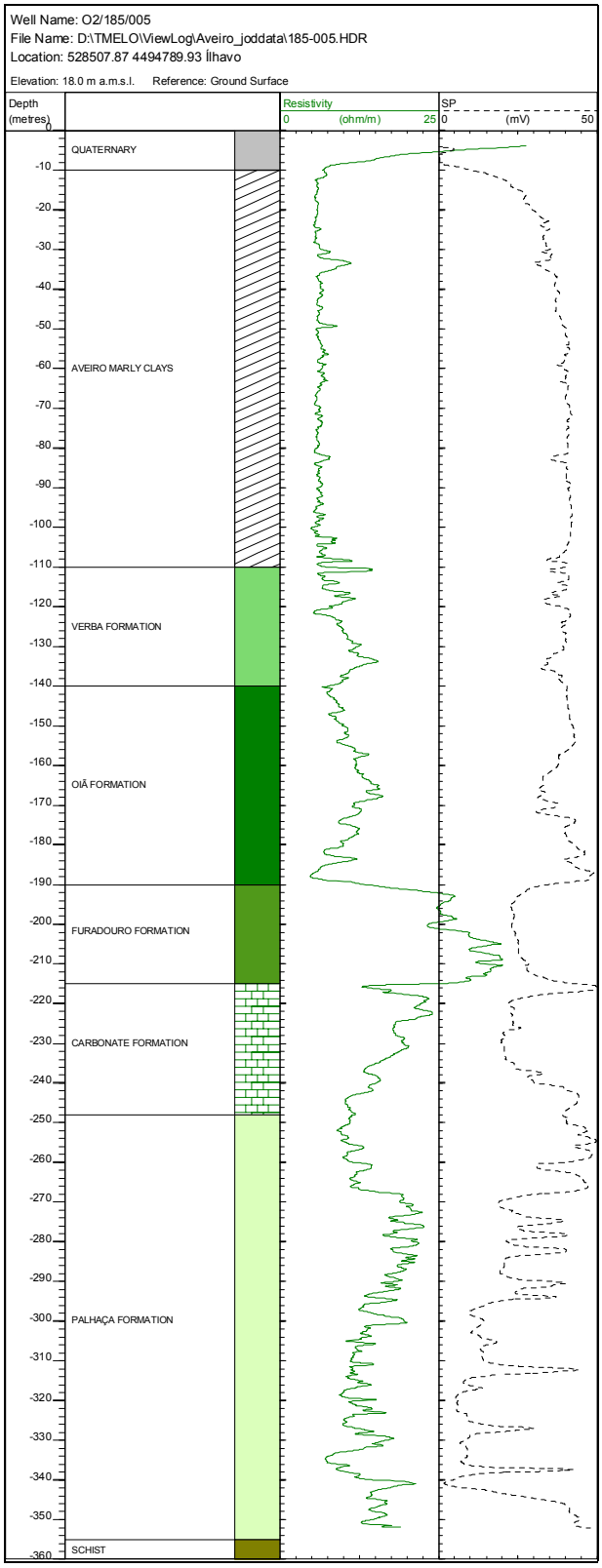
Well Name: O2/185/005
File Name: D:\TMELO\ViewLog\Aveiro_joddata\185-005.HDR
Location: 528507.87 4494789.93 Ílhavo
Elevation: 18.0 m a.m.s.l. Reference: Ground Surface
Depth (metres)
Resistivity
0 (ohm/m) 25
SP
0 (mV) 50
QUATERNARY
AVEIRO MARLY CLAYS
VERBA FORMATION
OIÃ FORMATION
FURADOURO FORMATION
CARBONATE FORMATION
PALHAÇA FORMATION
SCHIST

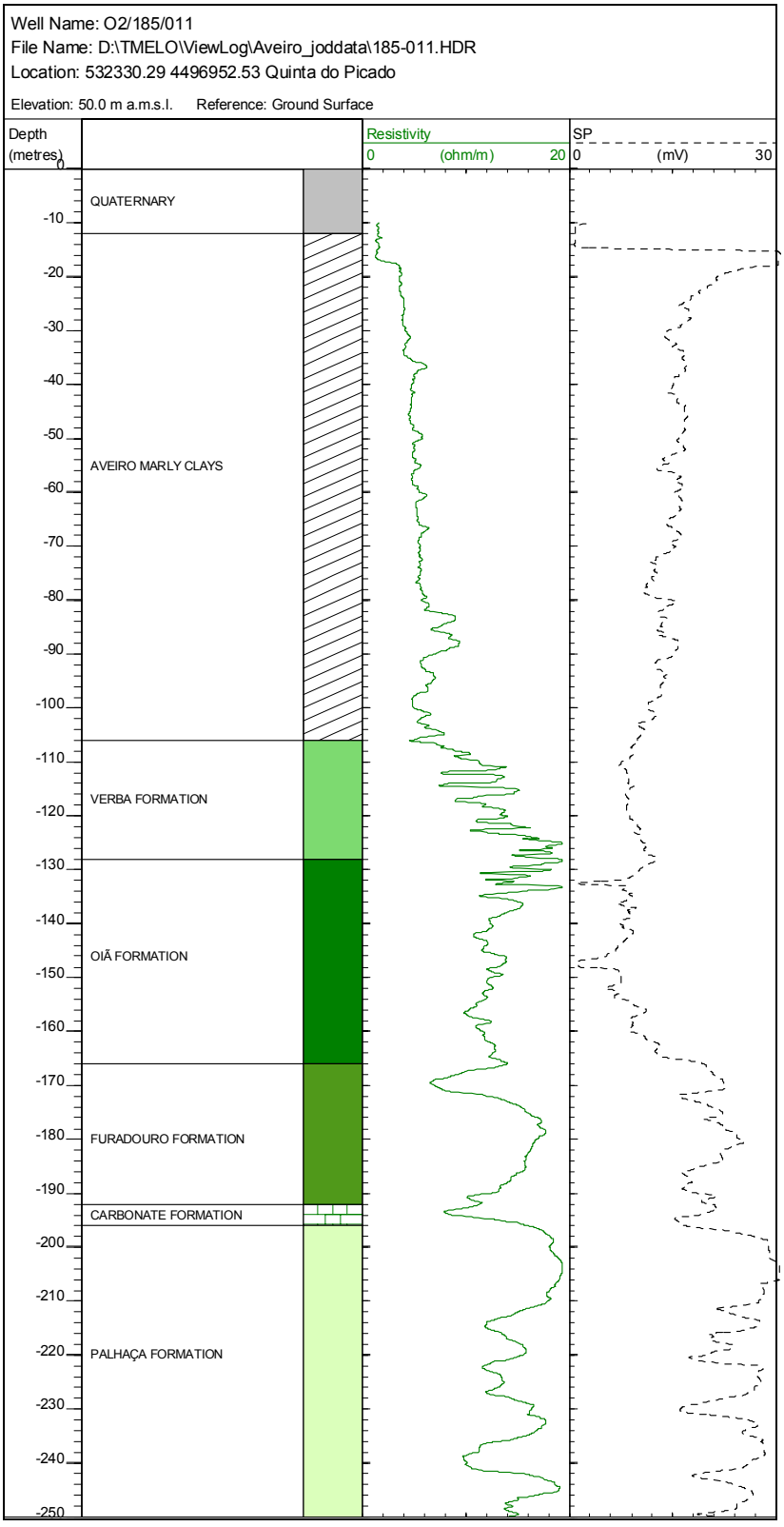
Well Name: O2/185/011
File Name: D:\TMELO\ViewLog\Aveiro_joddata\185-011.HDR
Location: 532330.29 4496952.53 Quinta do Picado
Elevation: 50.0 m a.m.s.l. Reference: Ground Surface
Depth (metres)
Resistivity
0 (ohm/m) 20
SP
0 (mV) 30
0
-10
-20
-30
-40
-50
-60
-70
-80
-90
-100
-110
-120
-130
-140
-150
-160
-170
-180
-190
-200
-210
-220
-230
-240
-250
QUATERNARY
AVEIRO MARLY CLAYS
VERBA FORMATION
OIÃ FORMATION
FURADOURO FORMATION
CARBONATE FORMATION
PALHAÇA FORMATION

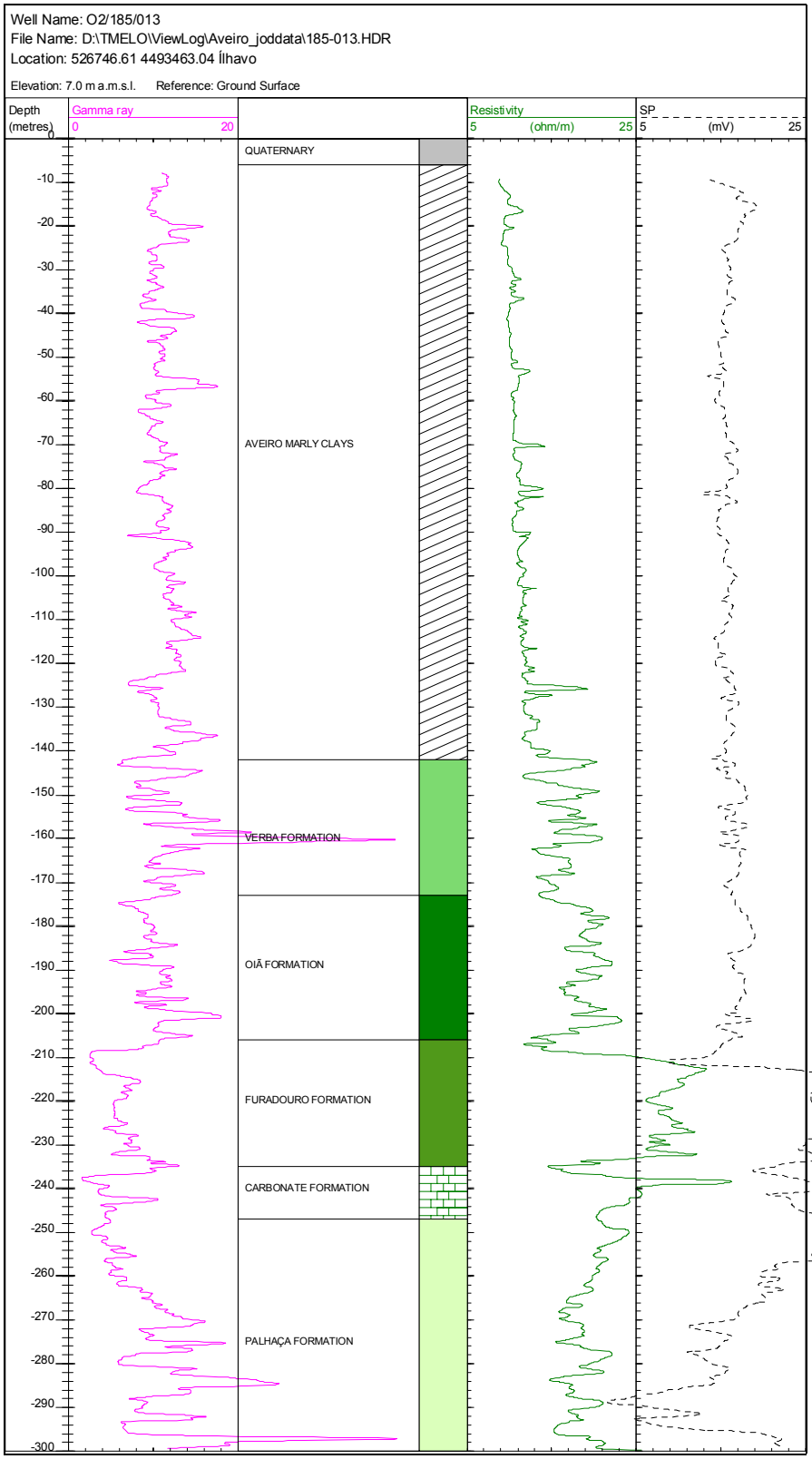
Well Name: O2/185/013
File Name: D:\TMELO\ViewLog\Aveiro_joddata\185-013.HDR
Location: 526746.61 4493463.04 Ílhavo
Elevation: 7.0 m a.m.s.l. Reference: Ground Surface
Depth (metres)
Gamma ray
0
20
Resistivity
5
(ohm/m)
25
SP
5
(mV)
25
QUATERNARY
AVEIRO MARLY CLAYS
VERBA FORMATION
OIÃ FORMATION
FURADOURO FORMATION
CARBONATE FORMATION
PALHAÇA FORMATION

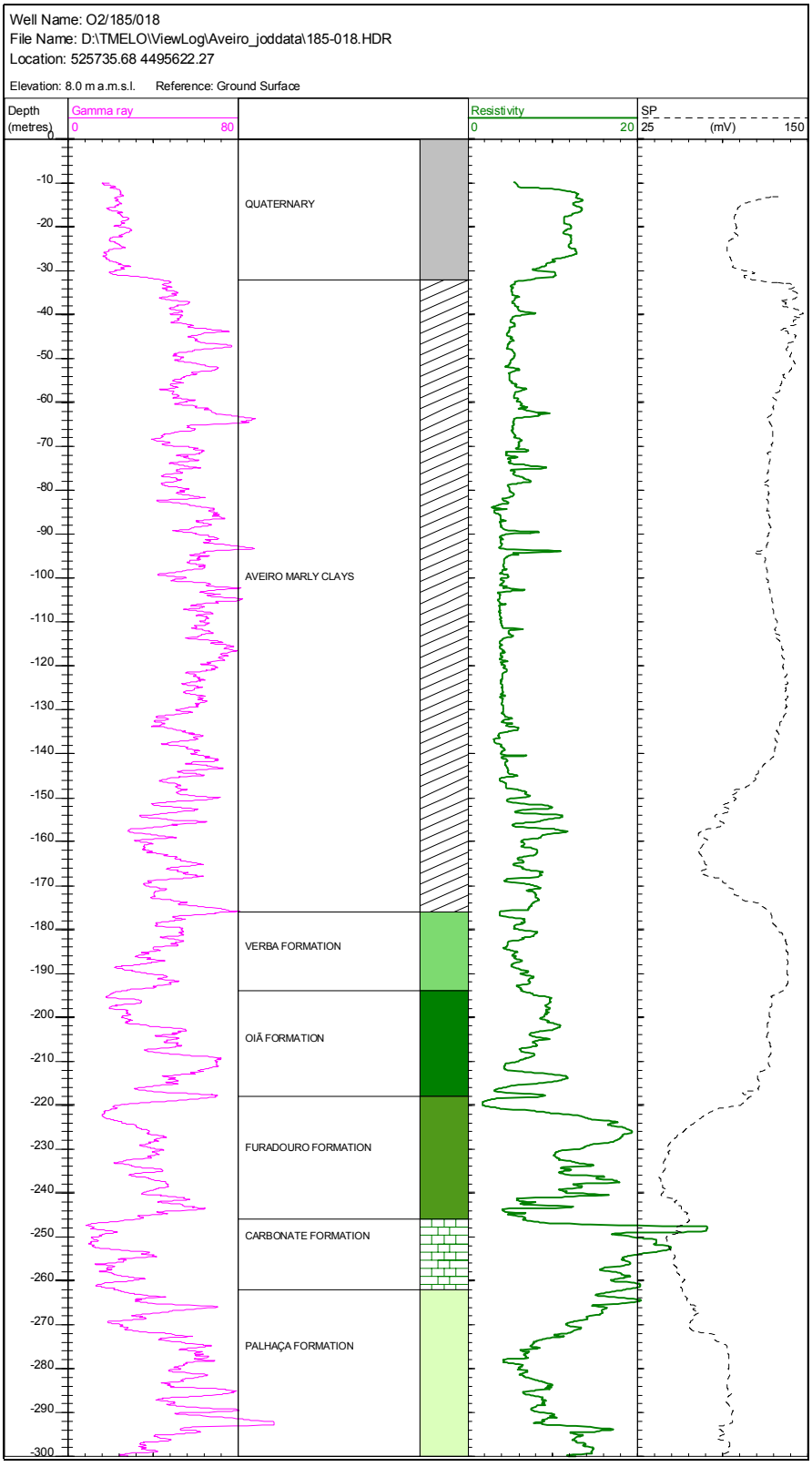
Well Name: O2/185/018
File Name: D:\TMELO\ViewLog\Aveiro_joddata\185-018.HDR
Location: 525735.68 4495622.27
Elevation: 8.0 m a.m.s.l. Reference: Ground Surface
Depth (metres)
Gamma ray
0
80
Resistivity
0
20
SP
25
(mV)
150
QUATERNARY
AVEIRO MARLY CLAYS
VERBA FORMATION
OIÃ FORMATION
FURADOURO FORMATION
CARBONATE FORMATION
PALHAÇA FORMATION

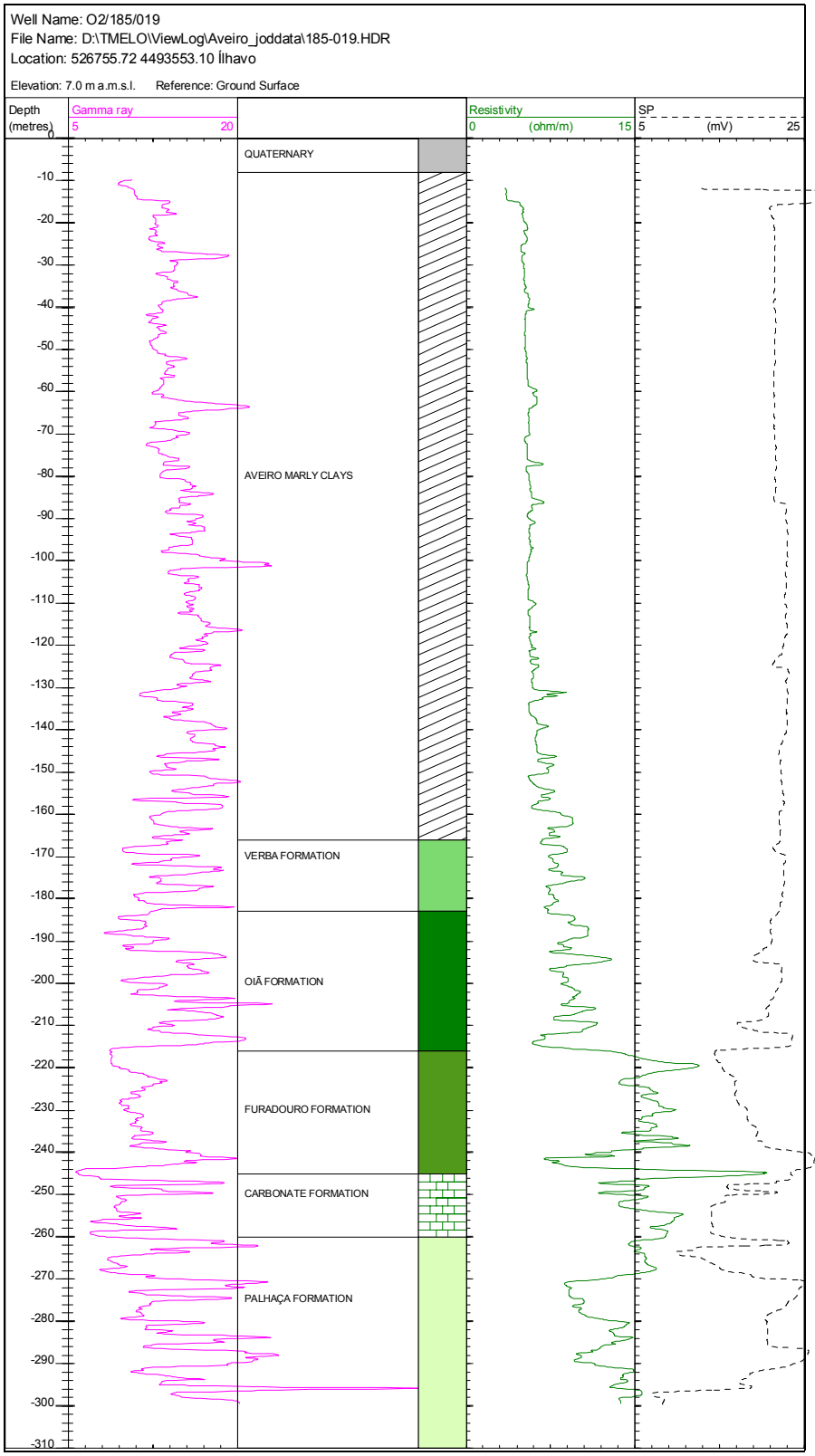
Well Name: O2/185/019
File Name: D:\TMELO\ViewLog\Aveiro_joddata\185-019.HDR
Location: 526755.72 4493553.10 Ílhavo
Elevation: 7.0 m a.m.s.l. Reference: Ground Surface
Depth (metres)
Gamma ray
5
20
Resistivity
0
(ohm/m)
15
SP
5
(mV)
25
QUATERNARY
AVEIRO MARLY CLAYS
VERBA FORMATION
OIÃ FORMATION
FURADOURO FORMATION
CARBONATE FORMATION
PALHAÇA FORMATION

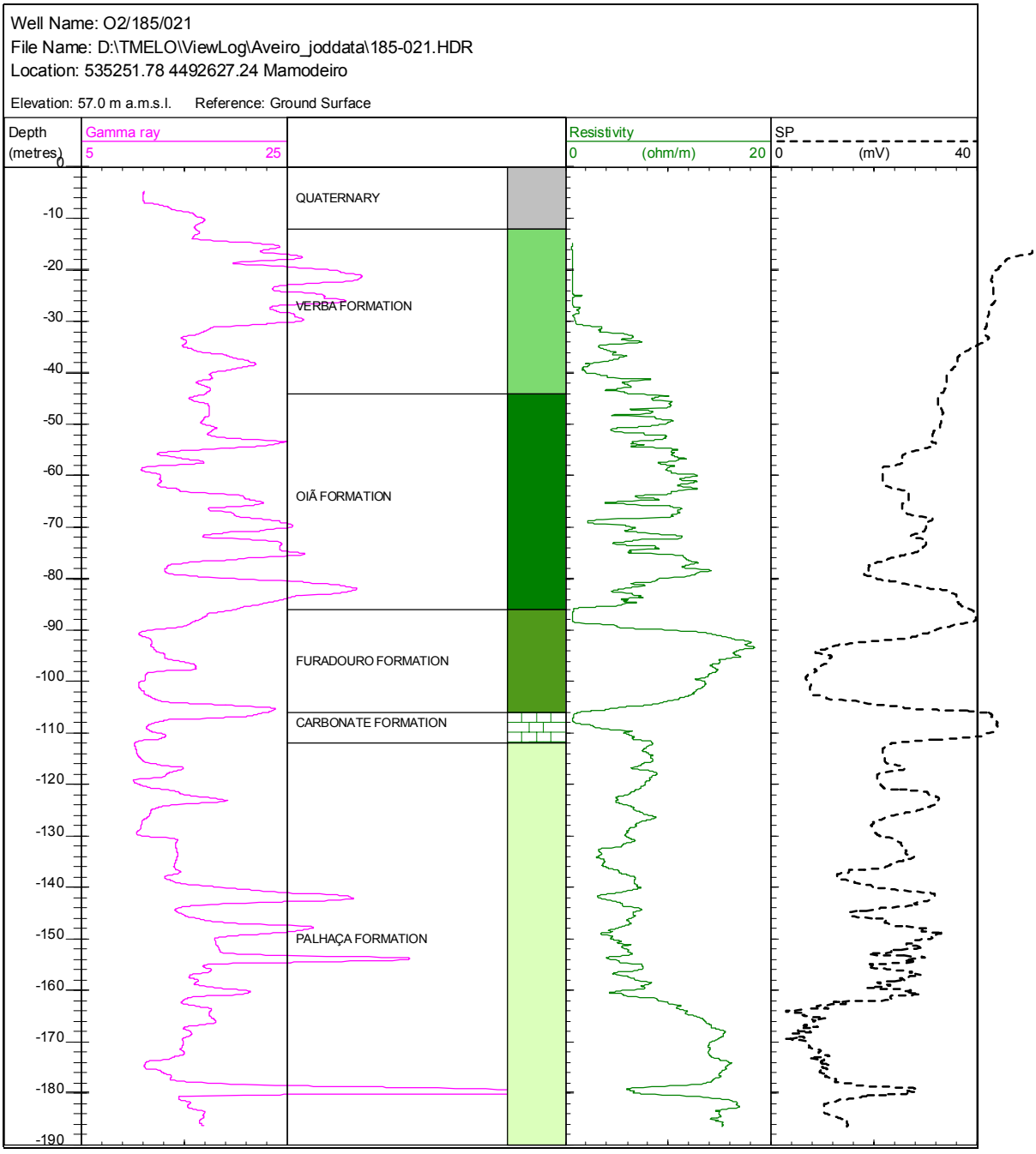
Well Name: O2/185/021
File Name: D:\TMELO\ViewLog\Aveiro_joddata\185-021.HDR
Location: 535251.78 4492627.24 Mamodeiro
Elevation: 57.0 m a.m.s.l. Reference: Ground Surface
Depth (metres)
Gamma ray
5
25
Resistivity
0
(ohm/m)
20
SP
0
(mV)
40
0
-10
-20
-30
-40
-50
-60
-70
-80
-90
-100
-110
-120
-130
-140
-150
-160
-170
-180
-190
QUATERNARY
VERBA FORMATION
OIÃ FORMATION
FURADOURO FORMATION
CARBONATE FORMATION
PALHAÇA FORMATION

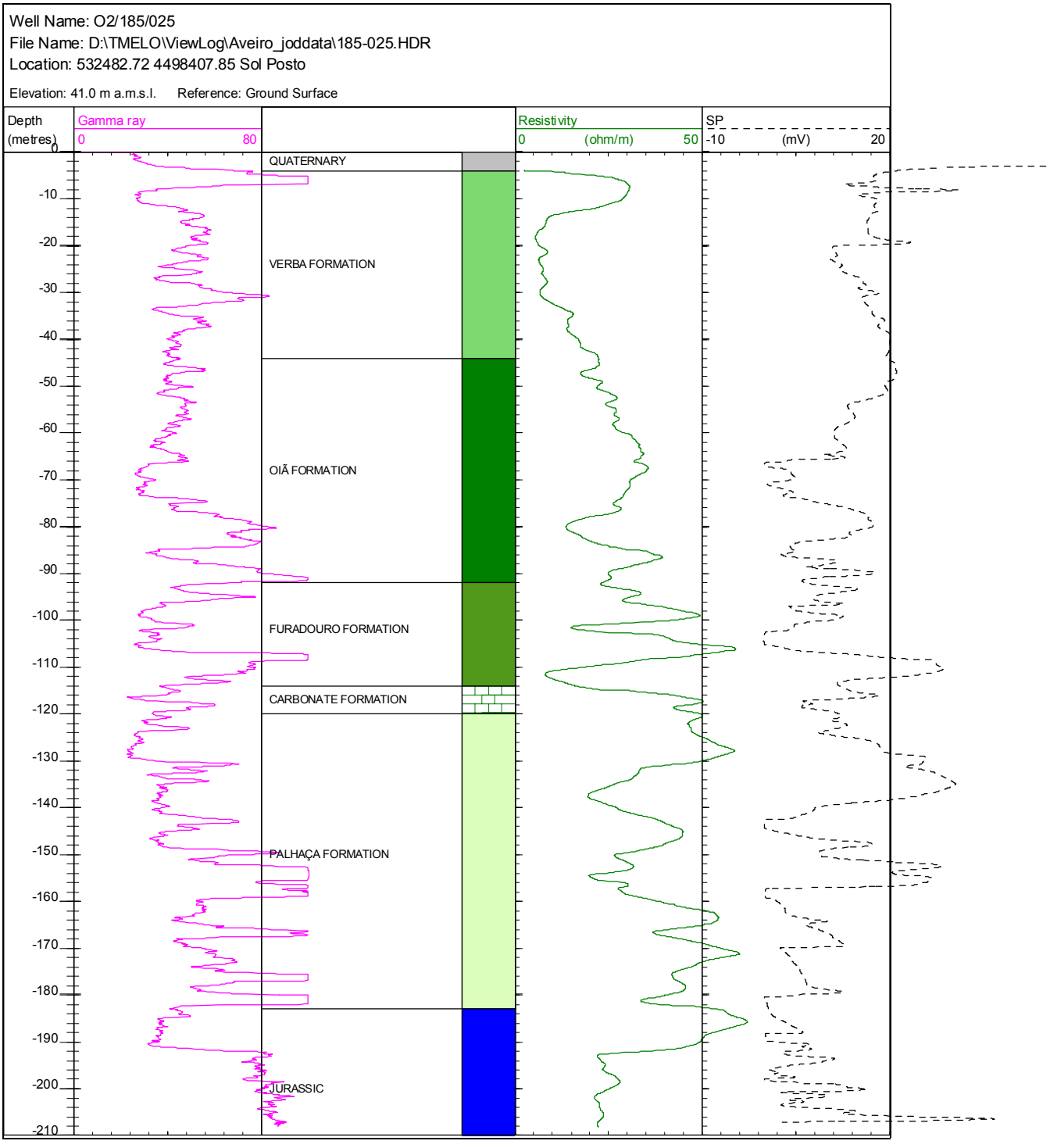
Well Name: O2/185/025
File Name: D:\TMELO\ViewLog\Aveiro_joddata\185-025.HDR
Location: 532482.72 4498407.85 Sol Posto
Elevation: 41.0 m a.m.s.l. Reference: Ground Surface
Depth (metres)
Gamma ray
0
80
Resistivity
0
(ohm/m)
50
SP
-10
(mV)
20
QUATERNARY
VERBA FORMATION
OIÃ FORMATION
FURADOURO FORMATION
CARBONATE FORMATION
PALHAÇA FORMATION
JURASSIC
0
-10
-20
-30
-40
-50
-60
-70
-80
-90
-100
-110
-120
-130
-140
-150
-160
-170
-180
-190
-200
-210

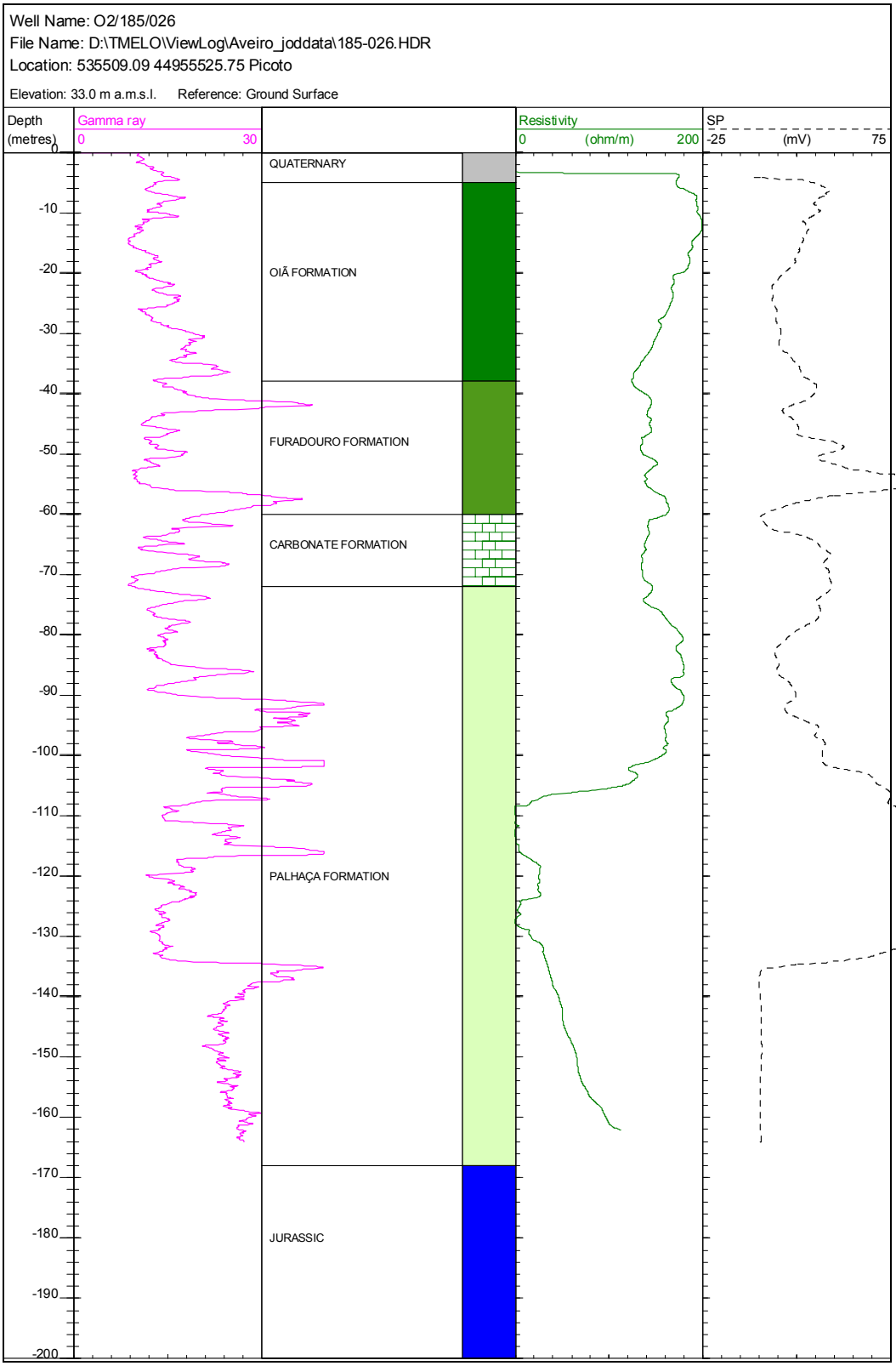
Well Name: O2/185/026
File Name: D:\TMELO\ViewLog\Aveiro_joddata\185-026.HDR
Location: 535509.09 44955525.75 Picoto
Elevation: 33.0 m a.m.s.l. Reference: Ground Surface
Depth (metres)
Gamma ray
0
30
Resistivity
0
(ohm/m)
200
SP
-25
(mV)
75
0
-10
-20
-30
-40
-50
-60
-70
-80
-90
-100
-110
-120
-130
-140
-150
-160
-170
-180
-190
-200
QUATERNARY
OIÃ FORMATION
FURADOURO FORMATION
CARBONATE FORMATION
PALHAÇA FORMATION
JURASSIC

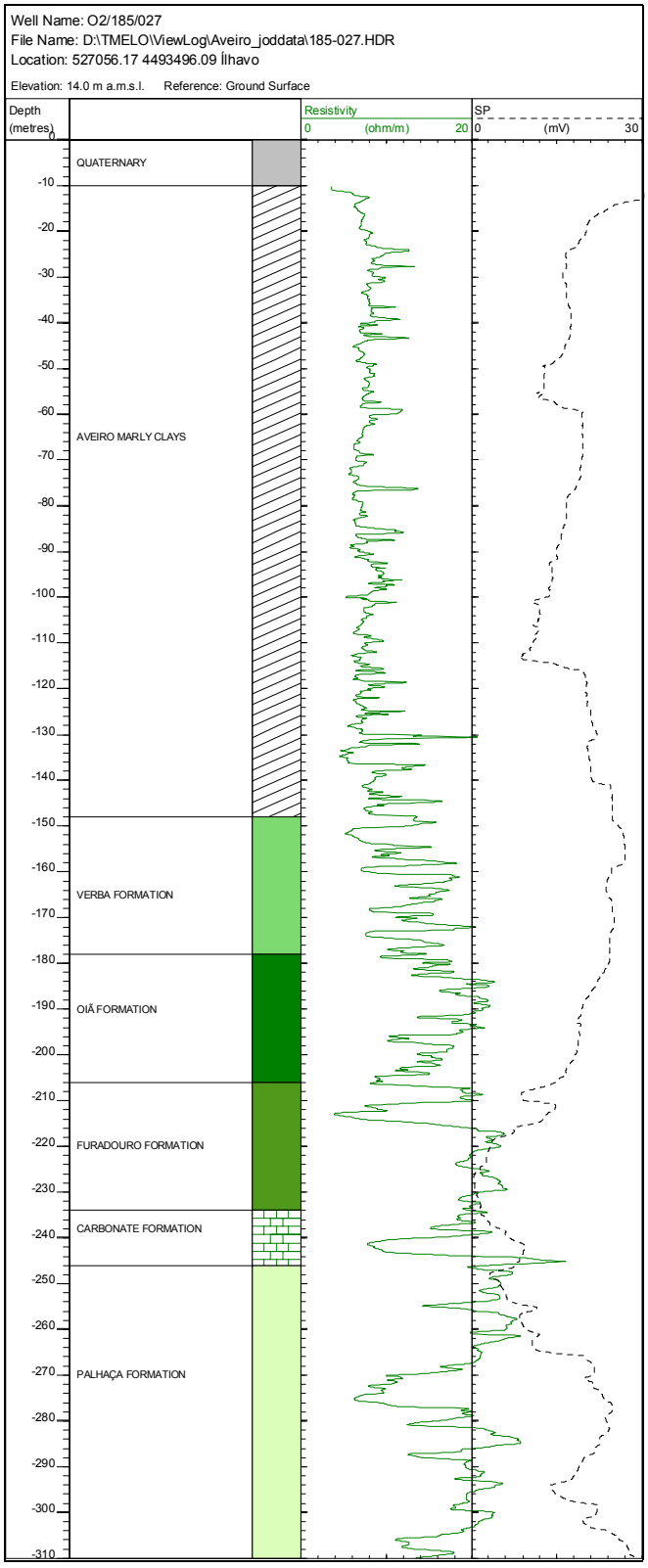
Well Name: O2/185/027
File Name: D:\TMELO\ViewLog\Aveiro_joddata\185-027.HDR
Location: 527056.17 4493496.09 Ílhavo
Elevation: 14.0 m a.m.s.l. Reference: Ground Surface
Depth (metres)
Resistivity
0 (ohm/m) 20
SP
0 (mV) 30
QUATERNARY
AVEIRO MARLY CLAYS
VERBA FORMATION
OIÃ FORMATION
FURADOURO FORMATION
CARBONATE FORMATION
PALHAÇA FORMATION
0
-10
-20
-30
-40
-50
-60
-70
-80
-90
-100
-110
-120
-130
-140
-150
-160
-170
-180
-190
-200
-210
-220
-230
-240
-250
-260
-270
-280
-290
-300
-310

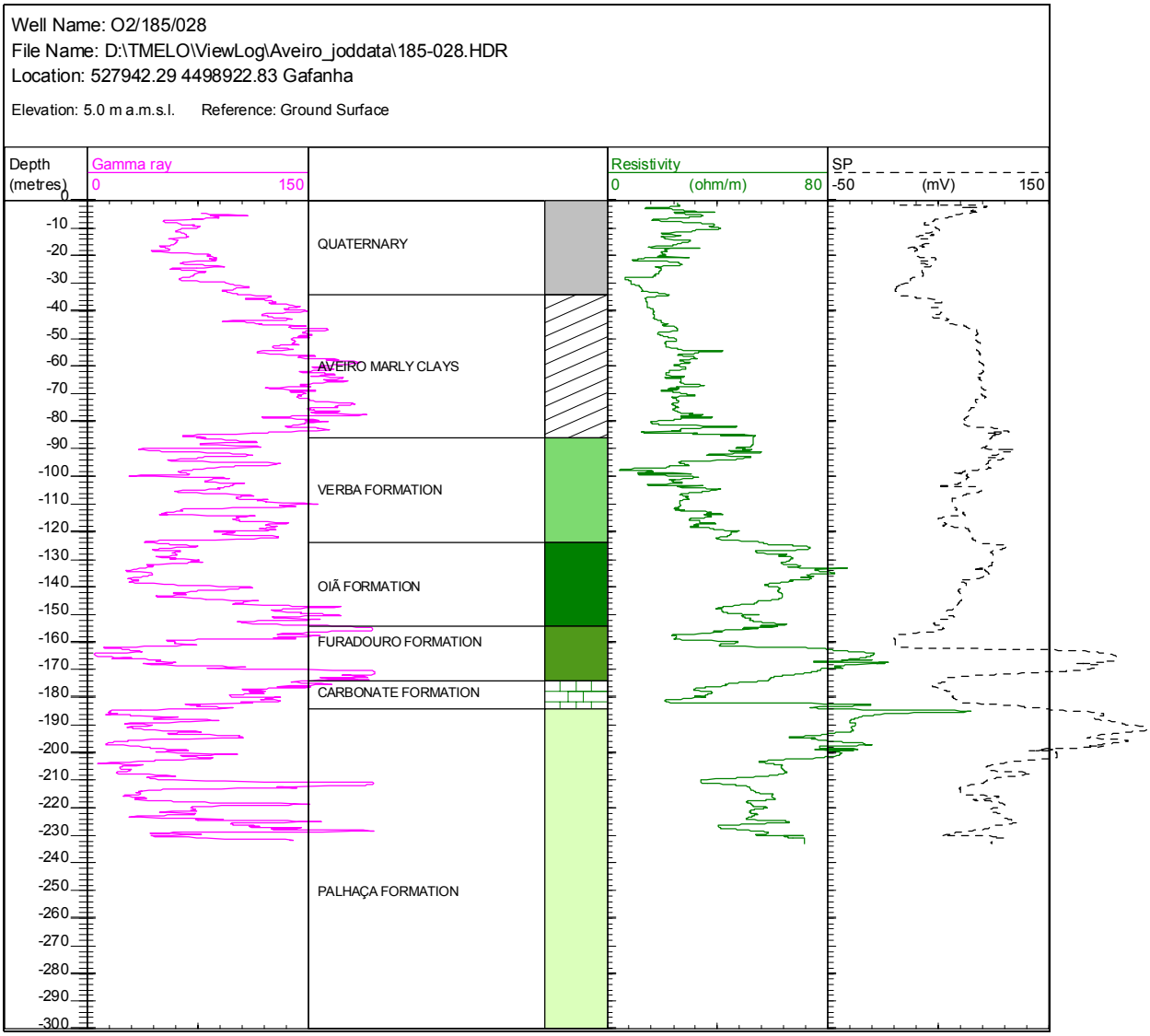
Well Name: O2/185/028
File Name: D:\TMELO\ViewLog\Aveiro_joddata\185-028.HDR
Location: 527942.29 4498922.83 Gafanha
Elevation: 5.0 m a.m.s.l. Reference: Ground Surface
Depth (metres)
Gamma ray
0
150
Resistivity
0
(ohm/m)
80
SP
-50
(mV)
150
0
-10
-20
-30
-40
-50
-60
-70
-80
-90
-100
-110
-120
-130
-140
-150
-160
-170
-180
-190
-200
-210
-220
-230
-240
-250
-260
-270
-280
-290
-300
QUATERNARY
AVEIRO MARLY CLAYS
VERBA FORMATION
OIÃ FORMATION
FURADOURO FORMATION
CARBONATE FORMATION
PALHAÇA FORMATION

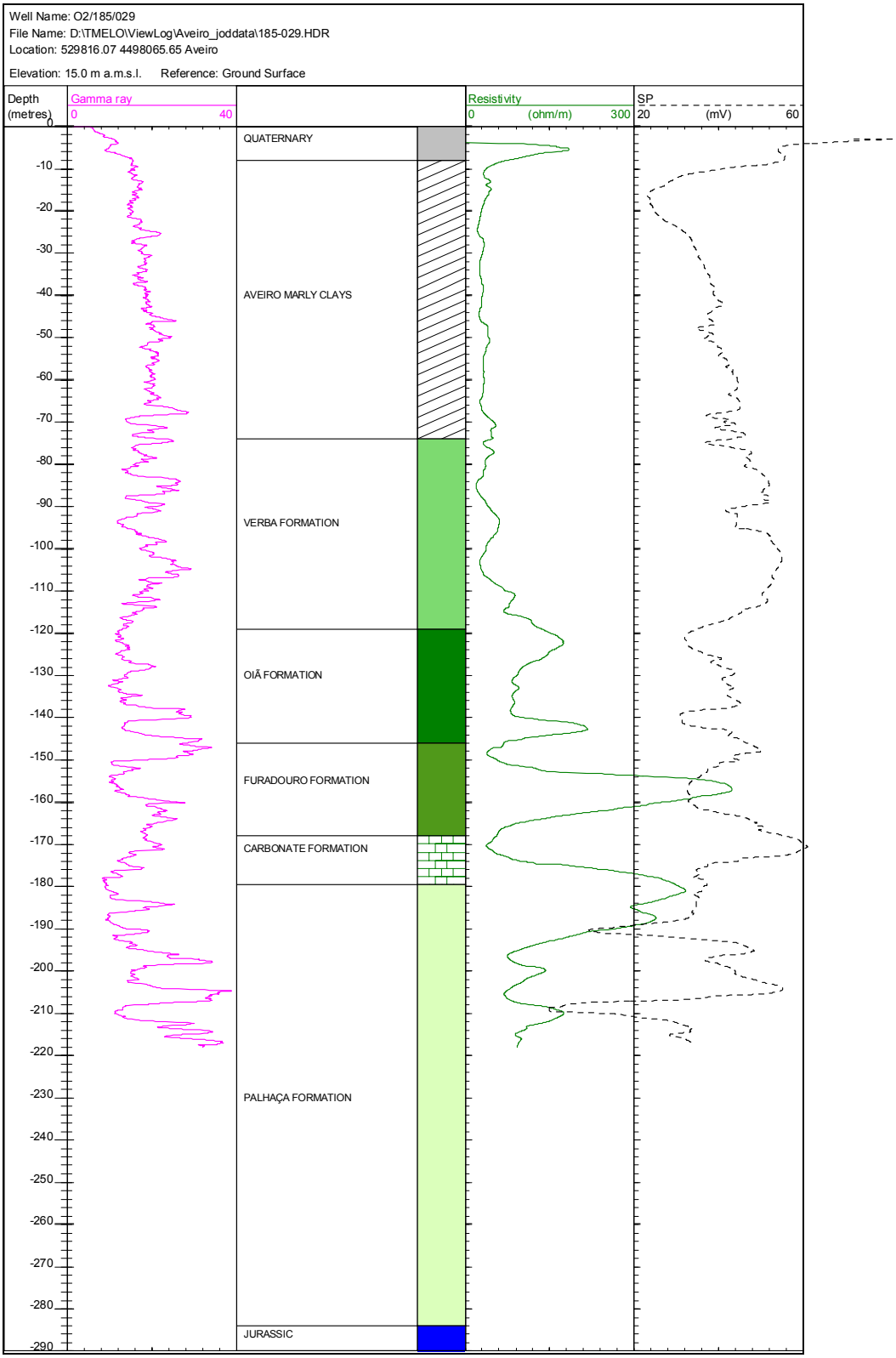
Well Name: O2/185/029
File Name: D:\TMELO\ViewLog\Aveiro_joddata\185-029.HDR
Location: 529816.07 4498065.65 Aveiro
Elevation: 15.0 m a.m.s.l. Reference: Ground Surface
Depth (metres)
Gamma ray
0
40
Resistivity
0
(ohm/m)
300
SP
20
(mV)
60
0
-10
-20
-30
-40
-50
-60
-70
-80
-90
-100
-110
-120
-130
-140
-150
-160
-170
-180
-190
-200
-210
-220
-230
-240
-250
-260
-270
-280
-290
QUATERNARY
AVEIRO MARLY CLAYS
VERBA FORMATION
OIÃ FORMATION
FURADOURO FORMATION
CARBONATE FORMATION
PALHAÇA FORMATION
JURASSIC

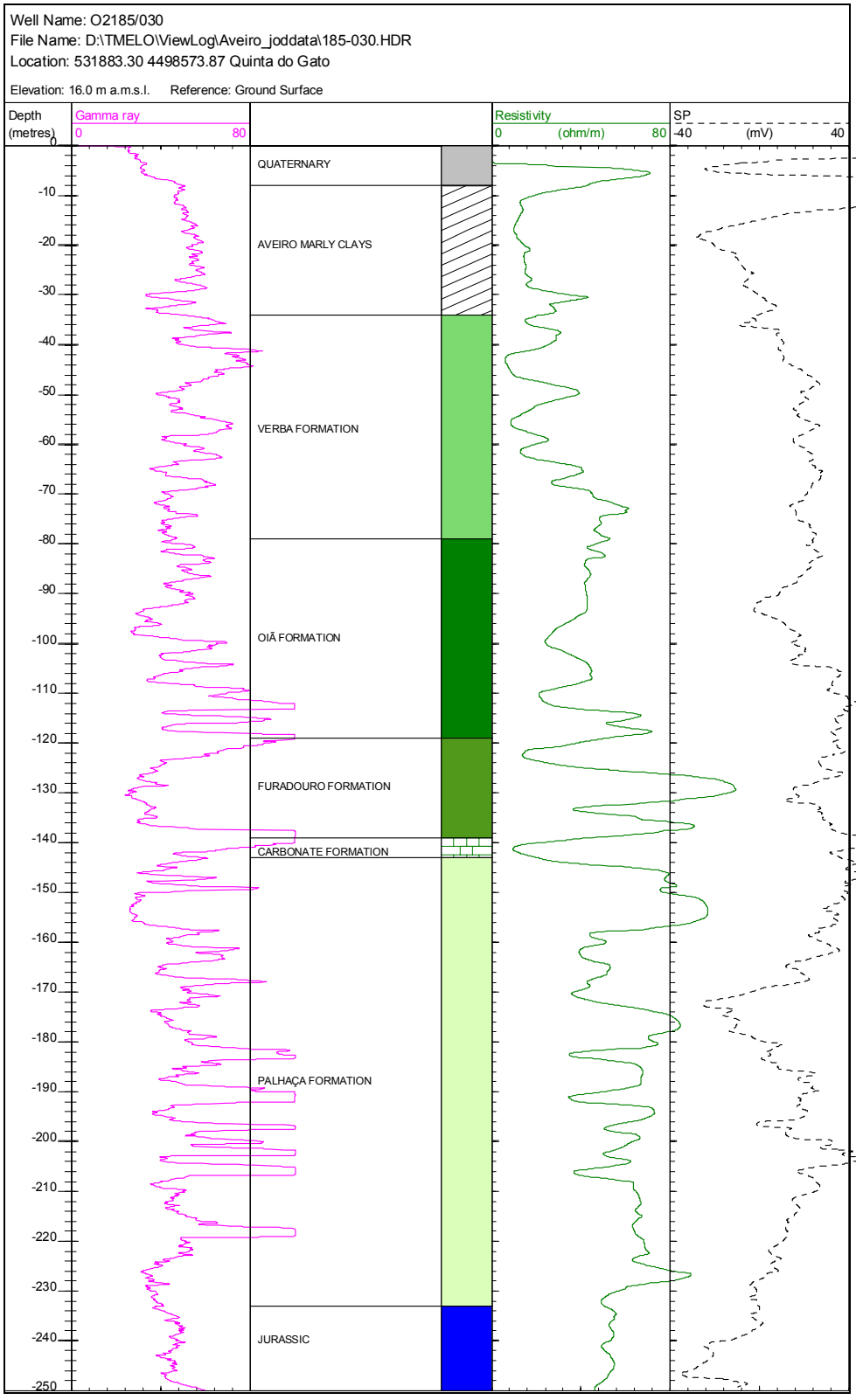
Well Name: O2185/030
File Name: D:\TMELO\ViewLog\Aveiro_joddata\185-030.HDR
Location: 531883.30 4498573.87 Quinta do Gato
Elevation: 16.0 m a.m.s.l. Reference: Ground Surface
Depth (metres)
Gamma ray
0
80
Resistivity
0
(ohm/m)
80
SP
-40
(mV)
40
QUATERNARY
AVEIRO MARLY CLAYS
VERBA FORMATION
OIÃ FORMATION
FURADOURO FORMATION
CARBONATE FORMATION
PALHAÇA FORMATION
JURASSIC
0
-10
-20
-30
-40
-50
-60
-70
-80
-90
-100
-110
-120
-130
-140
-150
-160
-170
-180
-190
-200
-210
-220
-230
-240
-250

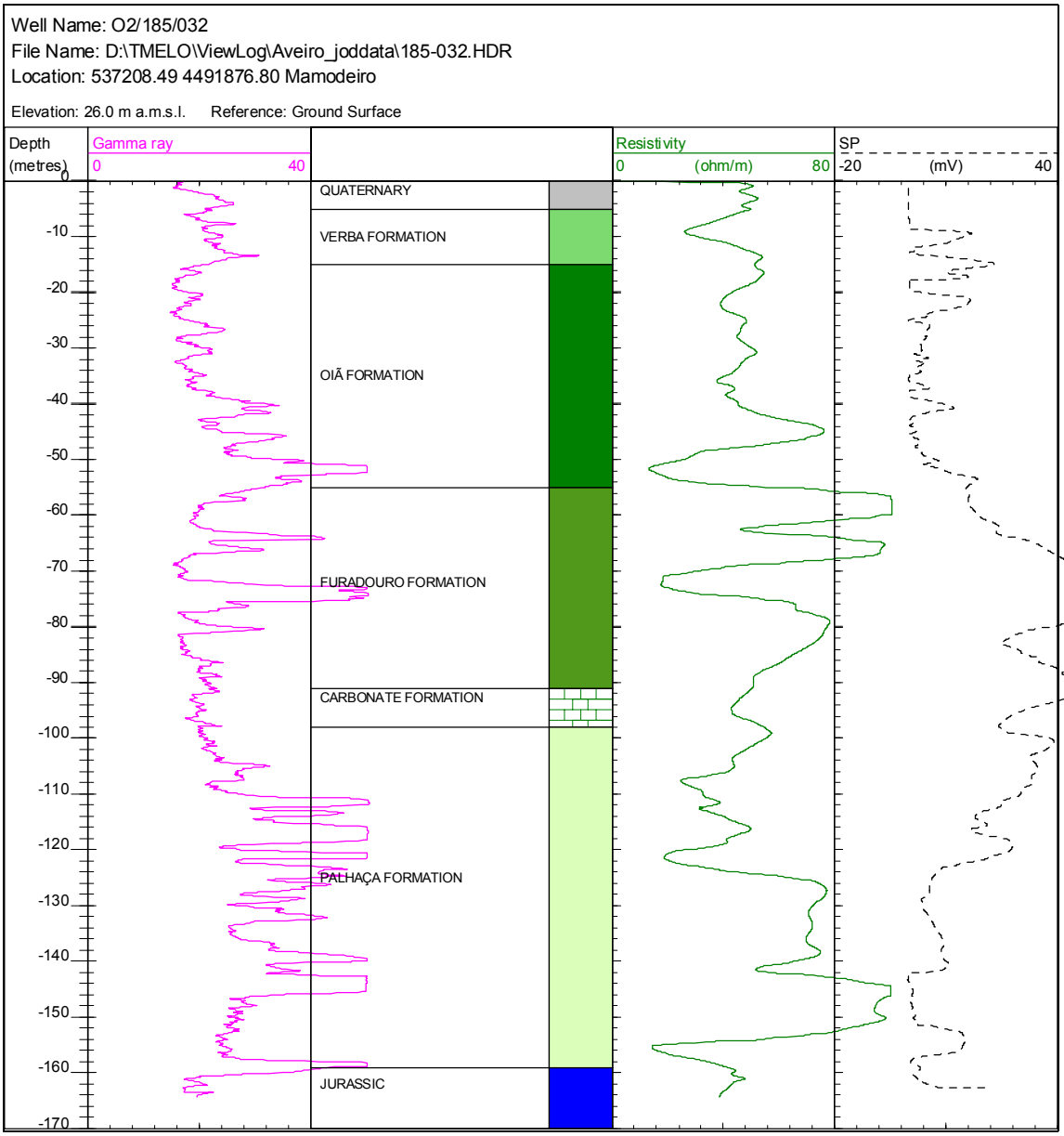
Well Name: O2/185/032
File Name: D:\TMELO\ViewLog\Aveiro_joddata\185-032.HDR
Location: 537208.49 4491876.80 Mamodeiro
Elevation: 26.0 m a.m.s.l. Reference: Ground Surface
Depth (metres)
Gamma ray
0
40
Resistivity
0
(ohm/m)
80
SP
-20
(mV)
40
0
-10
-20
-30
-40
-50
-60
-70
-80
-90
-100
-110
-120
-130
-140
-150
-160
-170
QUATERNARY
VERBA FORMATION
OIÃ FORMATION
FURADOURO FORMATION
CARBONATE FORMATION
PALHAÇA FORMATION
JURASSIC

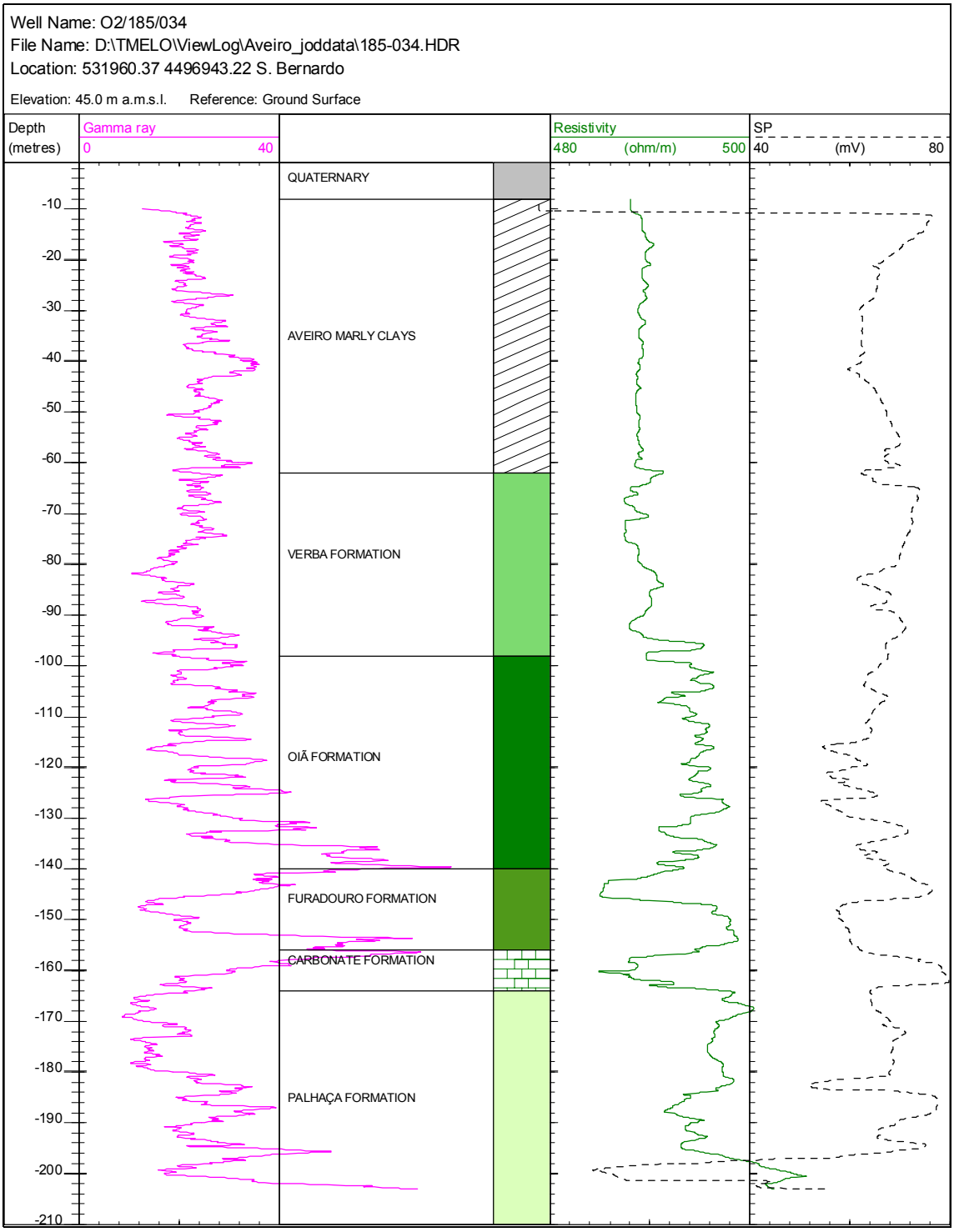
Well Name: O2/185/034
File Name: D:\TMELO\ViewLog\Aveiro_joddata\185-034.HDR
Location: 531960.37 4496943.22 S. Bernardo
Elevation: 45.0 m a.m.s.l. Reference: Ground Surface
Depth (metres)
Gamma ray
0
40
Resistivity
480
(ohm/m)
500
SP
40
(mV)
80
QUATERNARY
AVEIRO MARLY CLAYS
VERBA FORMATION
OIÃ FORMATION
FURADOURO FORMATION
CARBONATE FORMATION
PALHAÇA FORMATION
-10
-20
-30
-40
-50
-60
-70
-80
-90
-100
-110
-120
-130
-140
-150
-160
-170
-180
-190
-200
-210

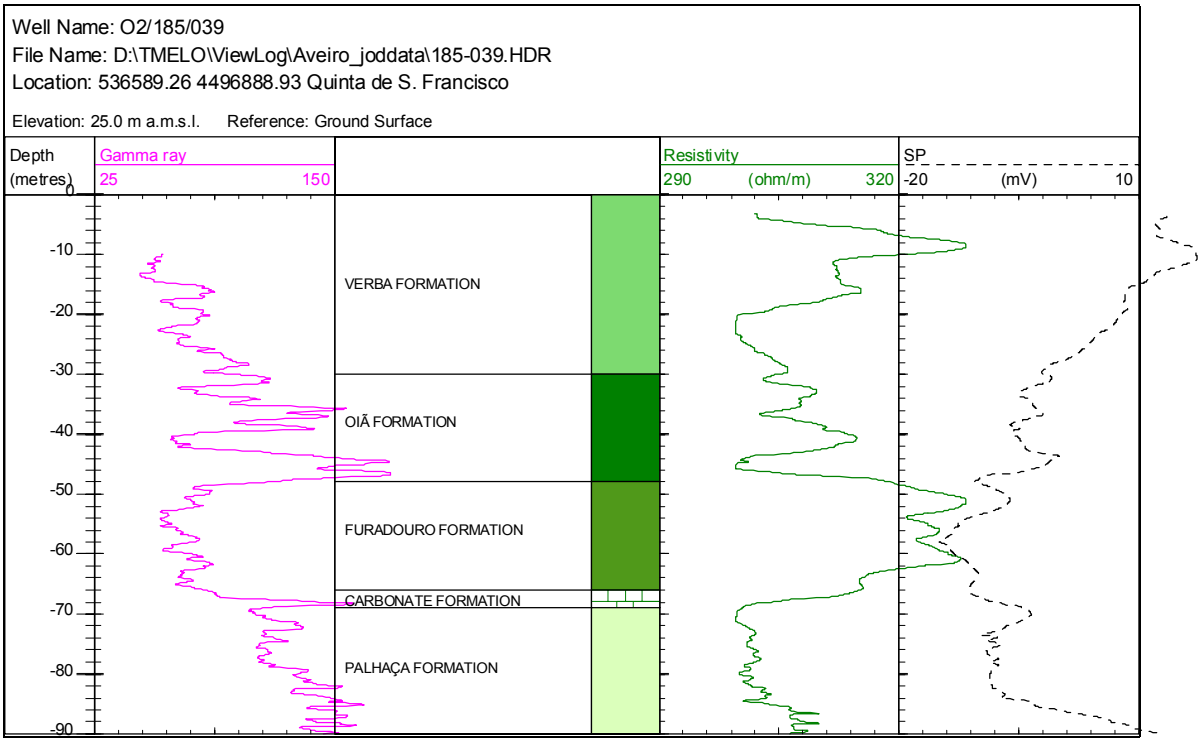
Well Name: O2/185/039
File Name: D:\TMELO\ViewLog\Aveiro_joddata\185-039.HDR
Location: 536589.26 4496888.93 Quinta de S. Francisco
Elevation: 25.0 m a.m.s.l. Reference: Ground Surface
Depth (metres)
Gamma ray
25
150
Resistivity
290
(ohm/m)
320
SP
-20
(mV)
10
0
-10
-20
-30
-40
-50
-60
-70
-80
-90
VERBA FORMATION
OIÃ FORMATION
FURADOURO FORMATION
CARBONATE FORMATION
PALHAÇA FORMATION

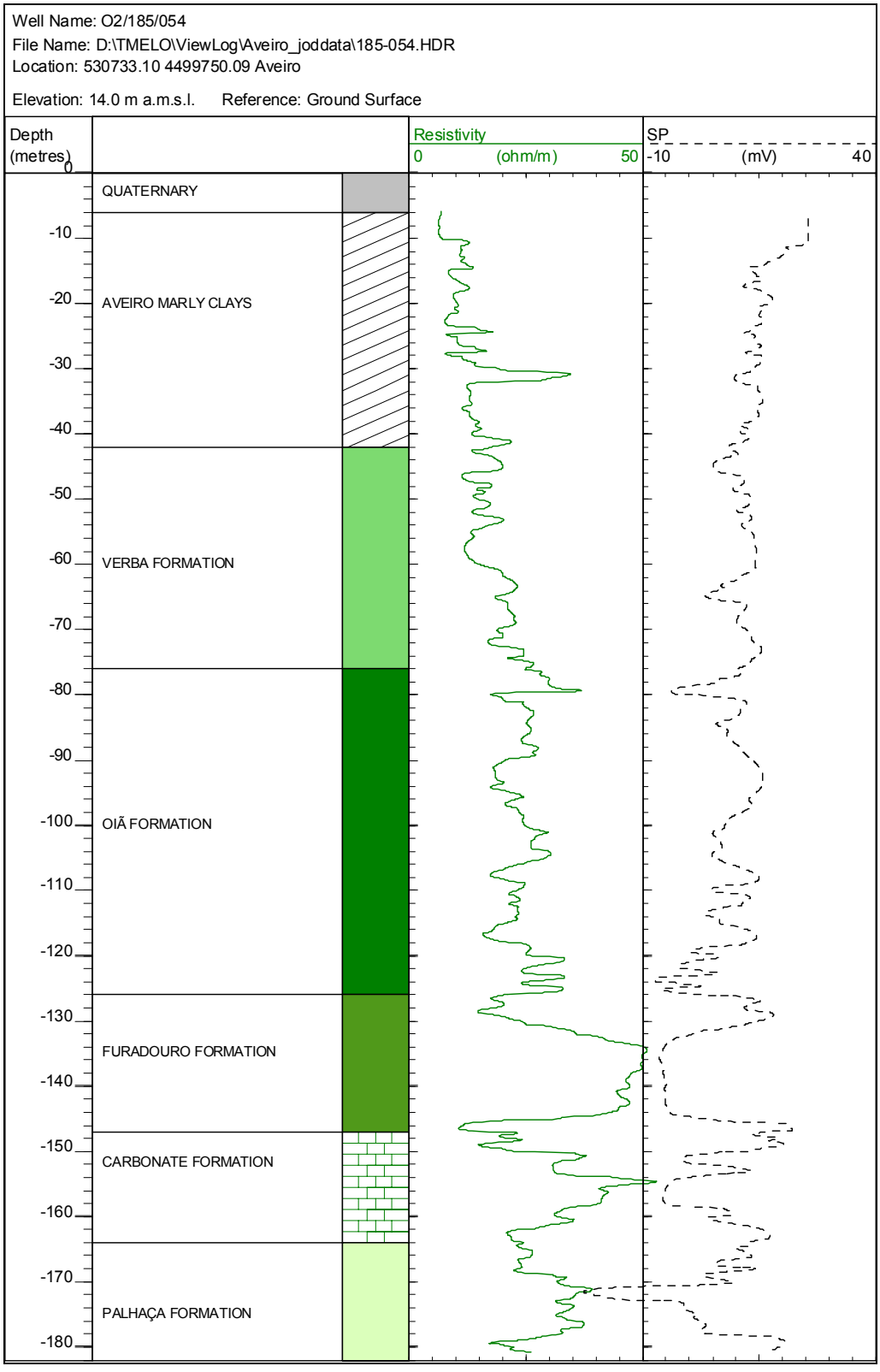
Well Name: O2/185/054
File Name: D:\TMELO\ViewLog\Aveiro_joddata\185-054.HDR
Location: 530733.10 4499750.09 Aveiro
Elevation: 14.0 m a.m.s.l. Reference: Ground Surface
Depth (metres)
Resistivity
0 (ohm/m) 50
SP
-10 (mV) 40
0
-10
-20
-30
-40
-50
-60
-70
-80
-90
-100
-110
-120
-130
-140
-150
-160
-170
-180
QUATERNARY
AVEIRO MARLY CLAYS
VERBA FORMATION
OIÃ FORMATION
FURADOURO FORMATION
CARBONATE FORMATION
PALHAÇA FORMATION

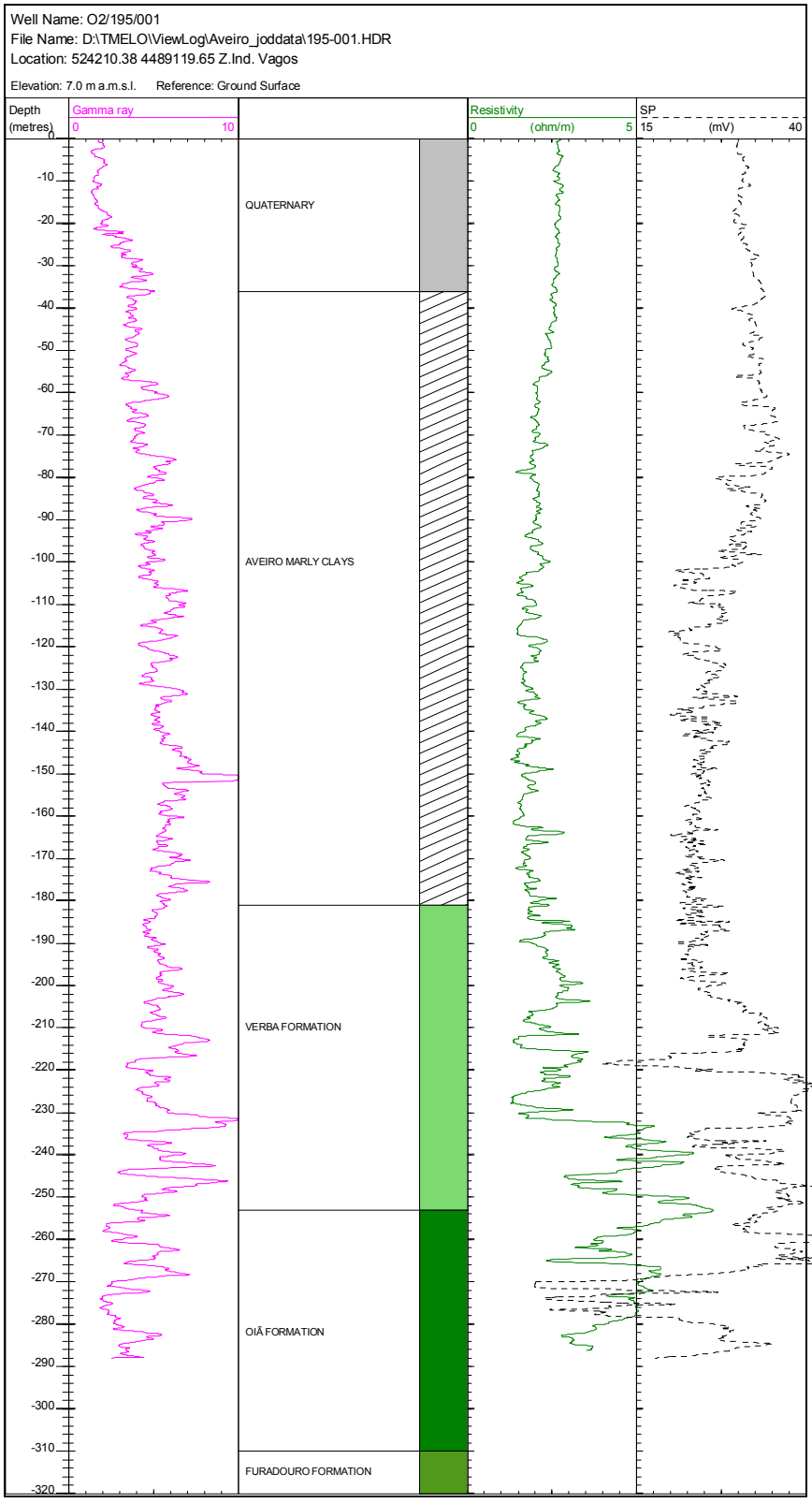
Well Name: O2/195/001
File Name: D:\TMELO\ViewLog\Aveiro_joddata\195-001.HDR
Location: 524210.38 4489119.65 Z.Ind. Vagos
Elevation: 7.0 m a.m.s.l. Reference: Ground Surface
Depth (metres)
Gamma ray
0
10
Resistivity
0
(ohm/m)
5
SP
15
(mV)
40
QUATERNARY
AVEIRO MARLY CLAYS
VERBA FORMATION
OIÃ FORMATION
FURADOURO FORMATION

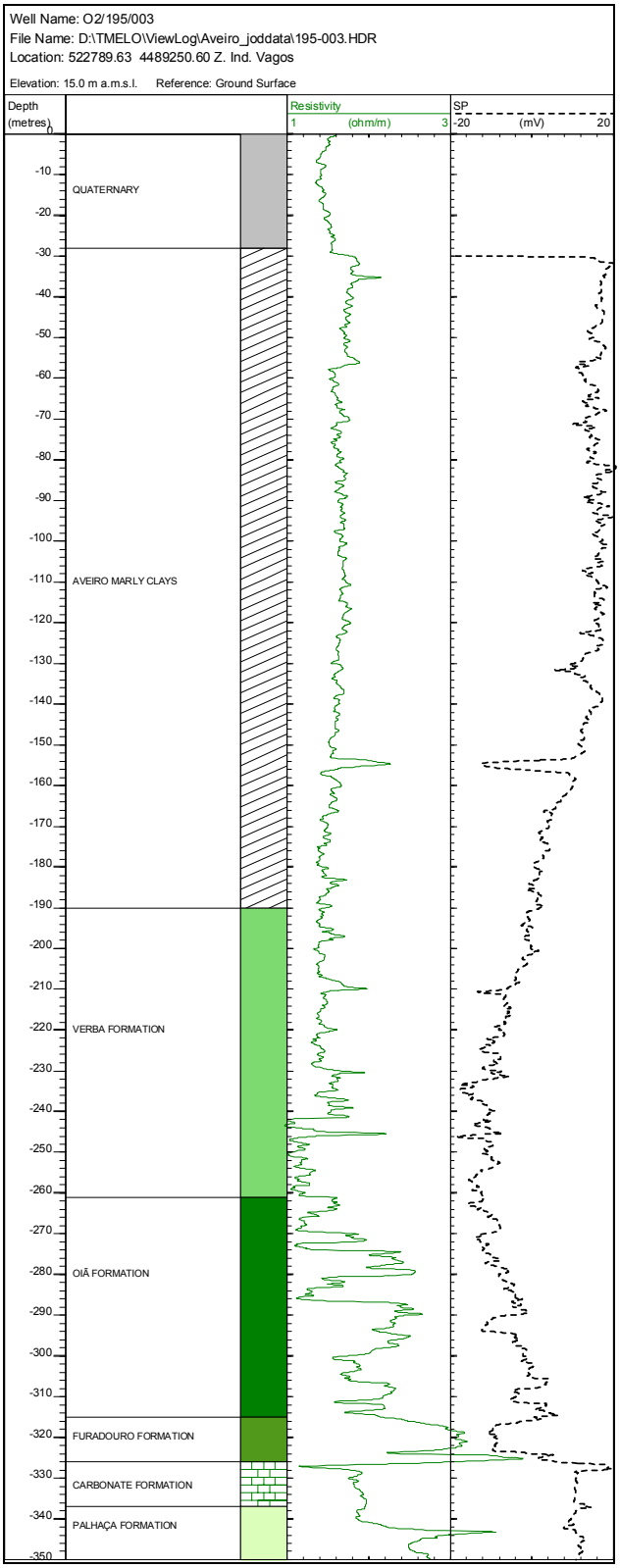
Well Name: O2/195/003
File Name: D:\TMELO\ViewLog\Aveiro_joddata\195-003.HDR
Location: 522789.63 4489250.60 Z. Ind. Vagos
Elevation: 15.0 m a.m.s.l. Reference: Ground Surface
Depth (metres)
Resistivity
1 (ohm/m) 3
SP
-20 (mV) 20
QUATERNARY
AVEIRO MARLY CLAYS
VERBA FORMATION
OIÃ FORMATION
FURADOURO FORMATION
CARBONATE FORMATION
PALHAÇA FORMATION

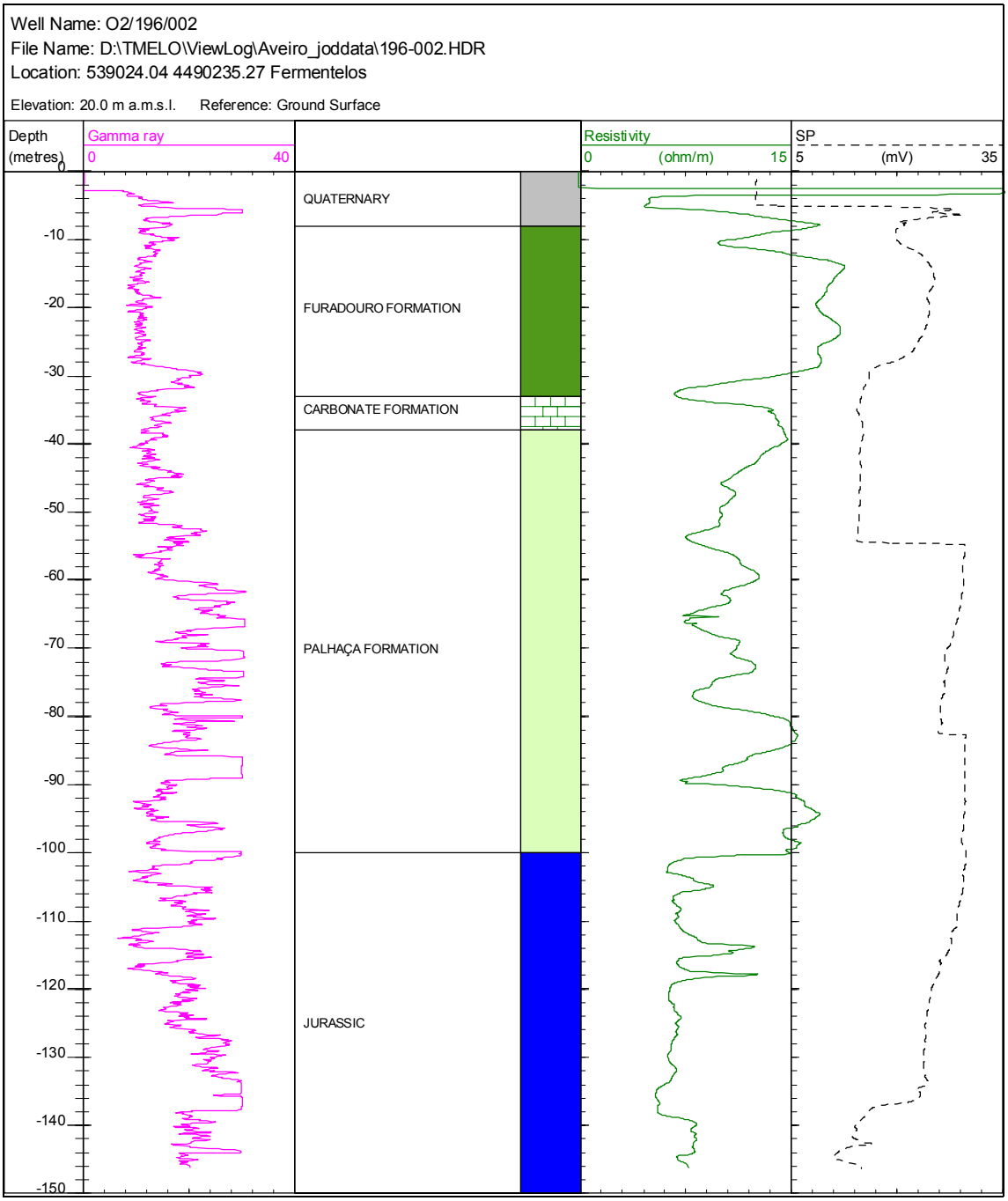
Well Name: O2/196/002
File Name: D:\TMELO\ViewLog\Aveiro_joddata\196-002.HDR
Location: 539024.04 4490235.27 Fermentelos
Elevation: 20.0 m a.m.s.l. Reference: Ground Surface
Depth (metres)
Gamma ray
0
40
Resistivity
0
(ohm/m)
15
SP
5
(mV)
35
0
-10
-20
-30
-40
-50
-60
-70
-80
-90
-100
-110
-120
-130
-140
-150
QUATERNARY
FURADOURO FORMATION
CARBONATE FORMATION
PALHAÇA FORMATION
JURASSIC

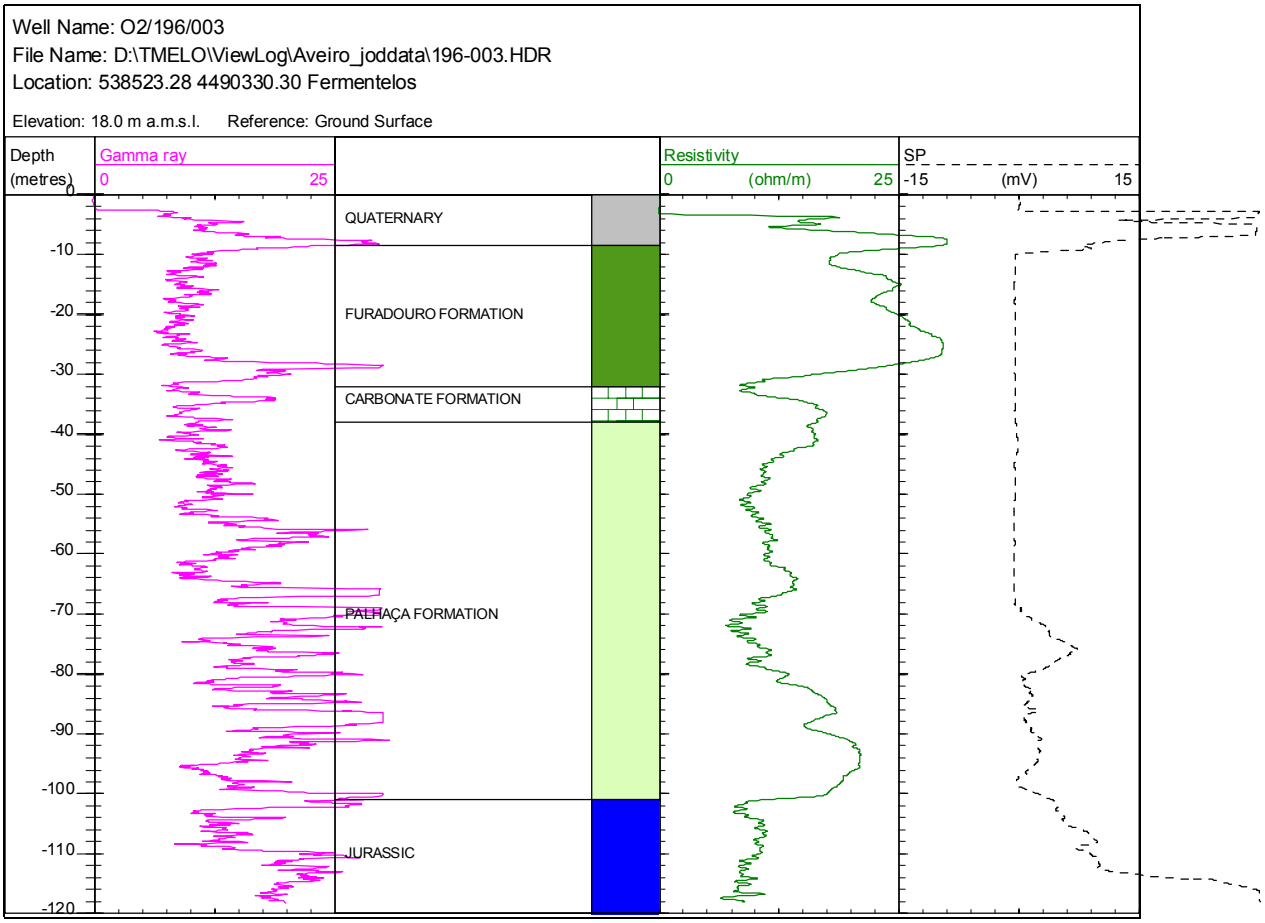
Well Name: O2/196/003
File Name: D:\TMELO\ViewLog\Aveiro_joddata\196-003.HDR
Location: 538523.28 4490330.30 Fermentelos
Elevation: 18.0 m a.m.s.l. Reference: Ground Surface
Depth (metres)
Gamma ray
0
25
Resistivity
0
(ohm/m)
25
SP
-15
(mV)
15
0
-10
-20
-30
-40
-50
-60
-70
-80
-90
-100
-110
-120
QUATERNARY
FURADOURO FORMATION
CARBONATE FORMATION
PALHAÇA FORMATION
JURASSIC

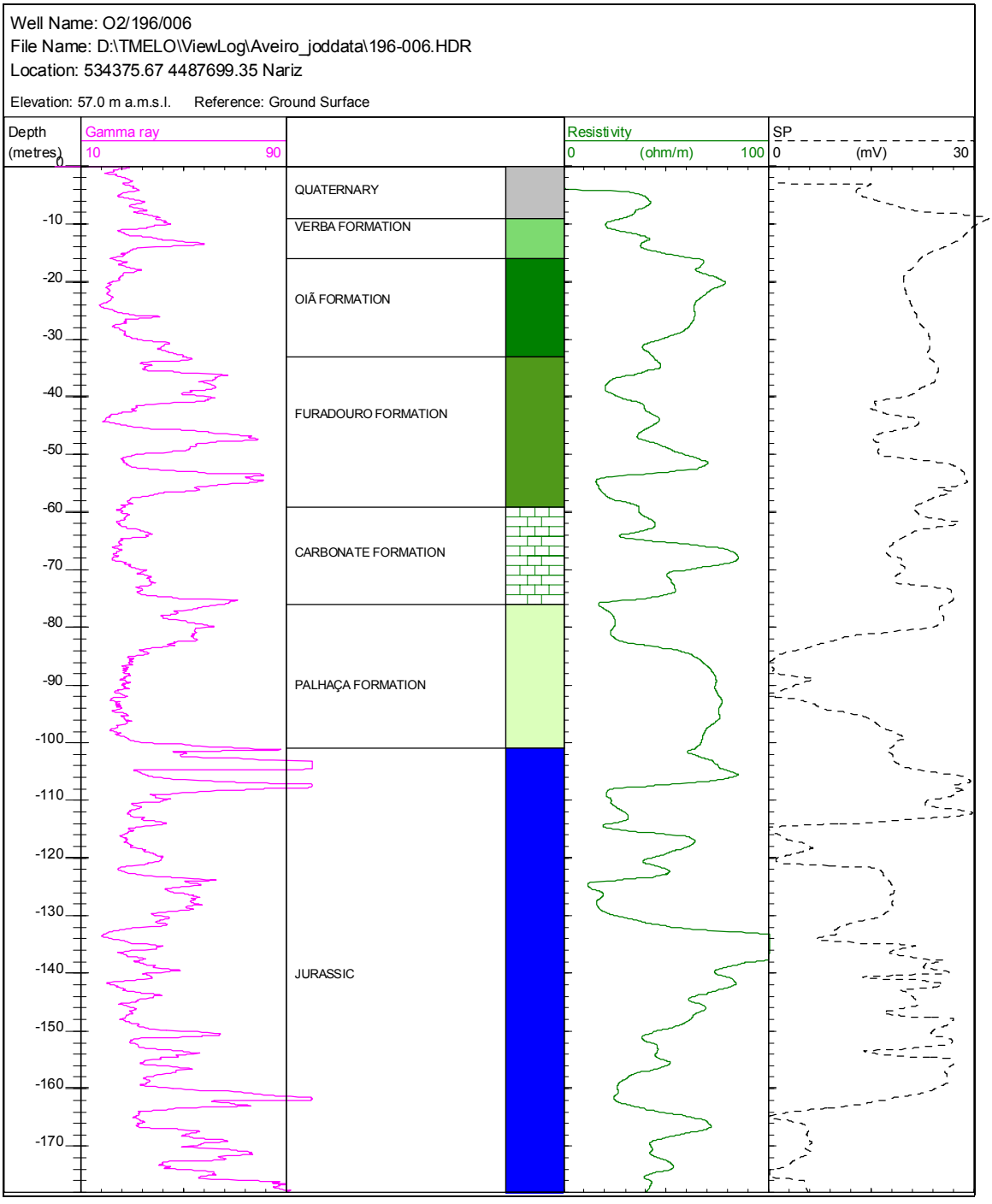
Well Name: O2/196/006
File Name: D:\TMELO\ViewLog\Aveiro_joddata\196-006.HDR
Location: 534375.67 4487699.35 Nariz
Elevation: 57.0 m a.m.s.l. Reference: Ground Surface
Depth (metres)
Gamma ray
10
90
Resistivity
0
(ohm/m)
100
SP
0
(mV)
30
0
-10
-20
-30
-40
-50
-60
-70
-80
-90
-100
-110
-120
-130
-140
-150
-160
-170
QUATERNARY
VERBA FORMATION
OIÃ FORMATION
FURADOURO FORMATION
CARBONATE FORMATION
PALHAÇA FORMATION
JURASSIC

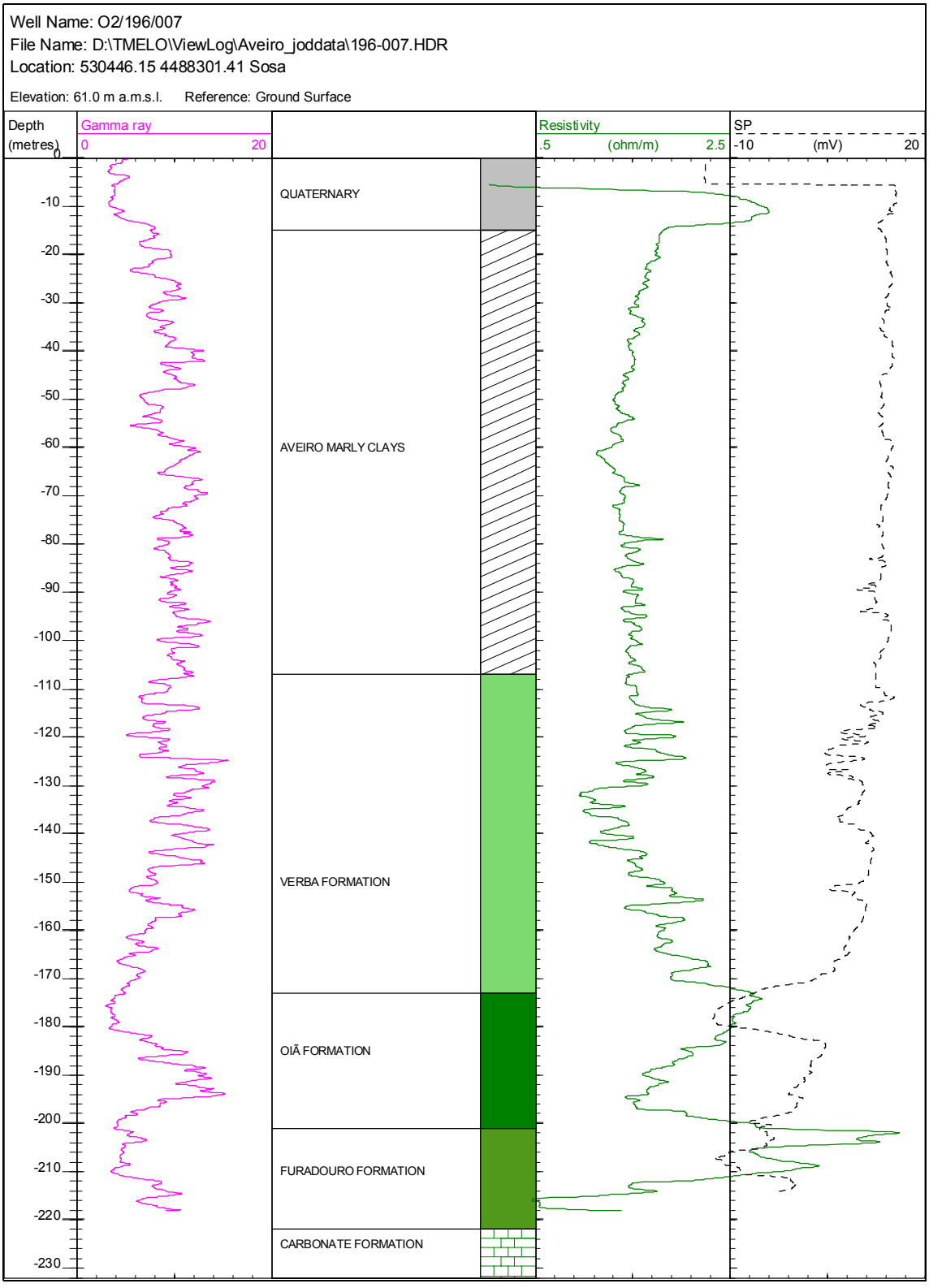
Well Name: O2/196/007
File Name: D:\TMELO\ViewLog\Aveiro_joddata\196-007.HDR
Location: 530446.15 4488301.41 Sosa
Elevation: 61.0 m a.m.s.l. Reference: Ground Surface
Depth (metres)
Gamma ray
0
20
Resistivity
.5
(ohm/m)
2.5
SP
-10
(mV)
20
0
-10
-20
-30
-40
-50
-60
-70
-80
-90
-100
-110
-120
-130
-140
-150
-160
-170
-180
-190
-200
-210
-220
-230
QUATERNARY
AVEIRO MARLY CLAYS
VERBA FORMATION
OIÃ FORMATION
FURADOURO FORMATION
CARBONATE FORMATION

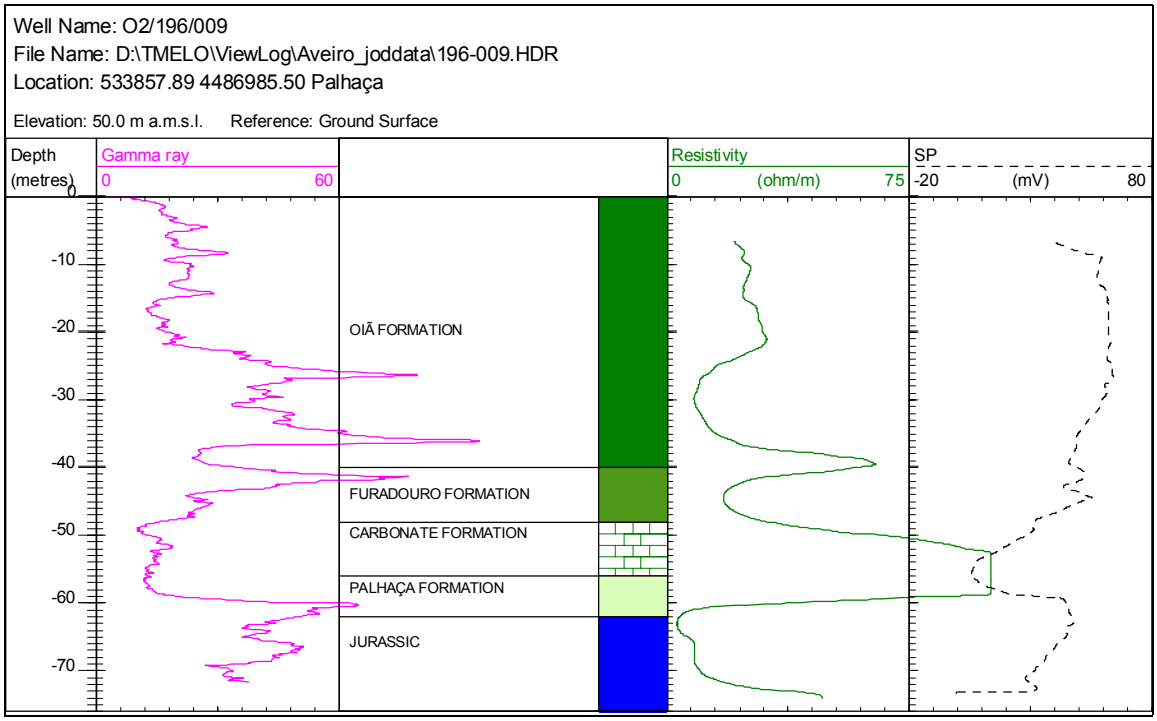
Well Name: O2/196/009
File Name: D:\TMELO\ViewLog\Aveiro_joddata\196-009.HDR
Location: 533857.89 4486985.50 Palhaça
Elevation: 50.0 m a.m.s.l. Reference: Ground Surface
Depth (metres)
Gamma ray
0
60
Resistivity
0
(ohm/m)
75
SP
-20
(mV)
80
0
-10
-20
-30
-40
-50
-60
-70
OIÃ FORMATION
FURADOURO FORMATION
CARBONATE FORMATION
PALHAÇA FORMATION
JURASSIC

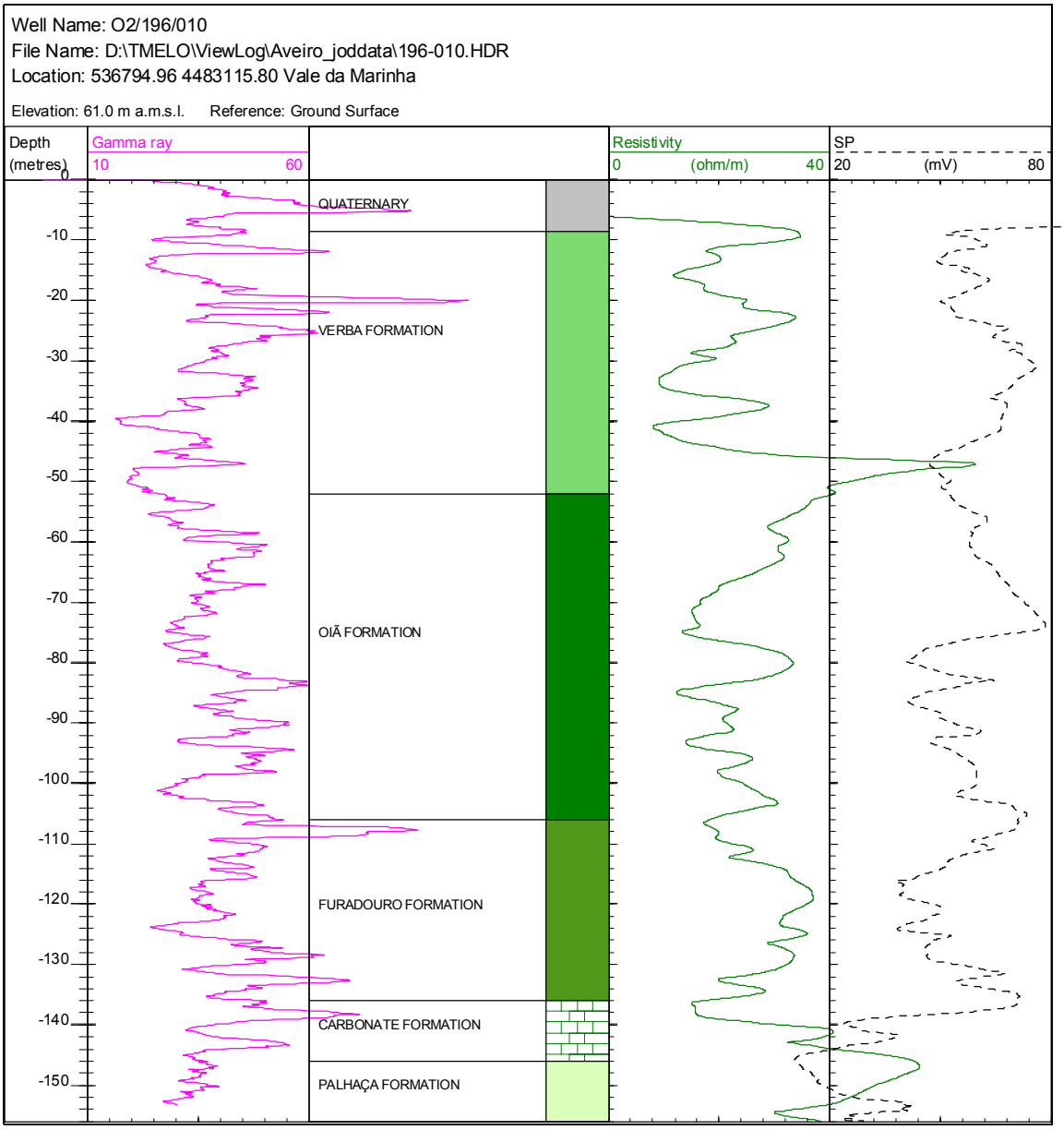
Well Name: O2/196/010
File Name: D:\TMELO\ViewLog\Aveiro_joddata\196-010.HDR
Location: 536794.96 4483115.80 Vale da Marinha
Elevation: 61.0 m a.m.s.l. Reference: Ground Surface
Depth (metres)
Gamma ray
10
60
Resistivity
0
(ohm/m)
40
SP
20
(mV)
80
0
-10
-20
-30
-40
-50
-60
-70
-80
-90
-100
-110
-120
-130
-140
-150
QUATERNARY
VERBA FORMATION
OIÃ FORMATION
FURADOURO FORMATION
CARBONATE FORMATION
PALHAÇA FORMATION

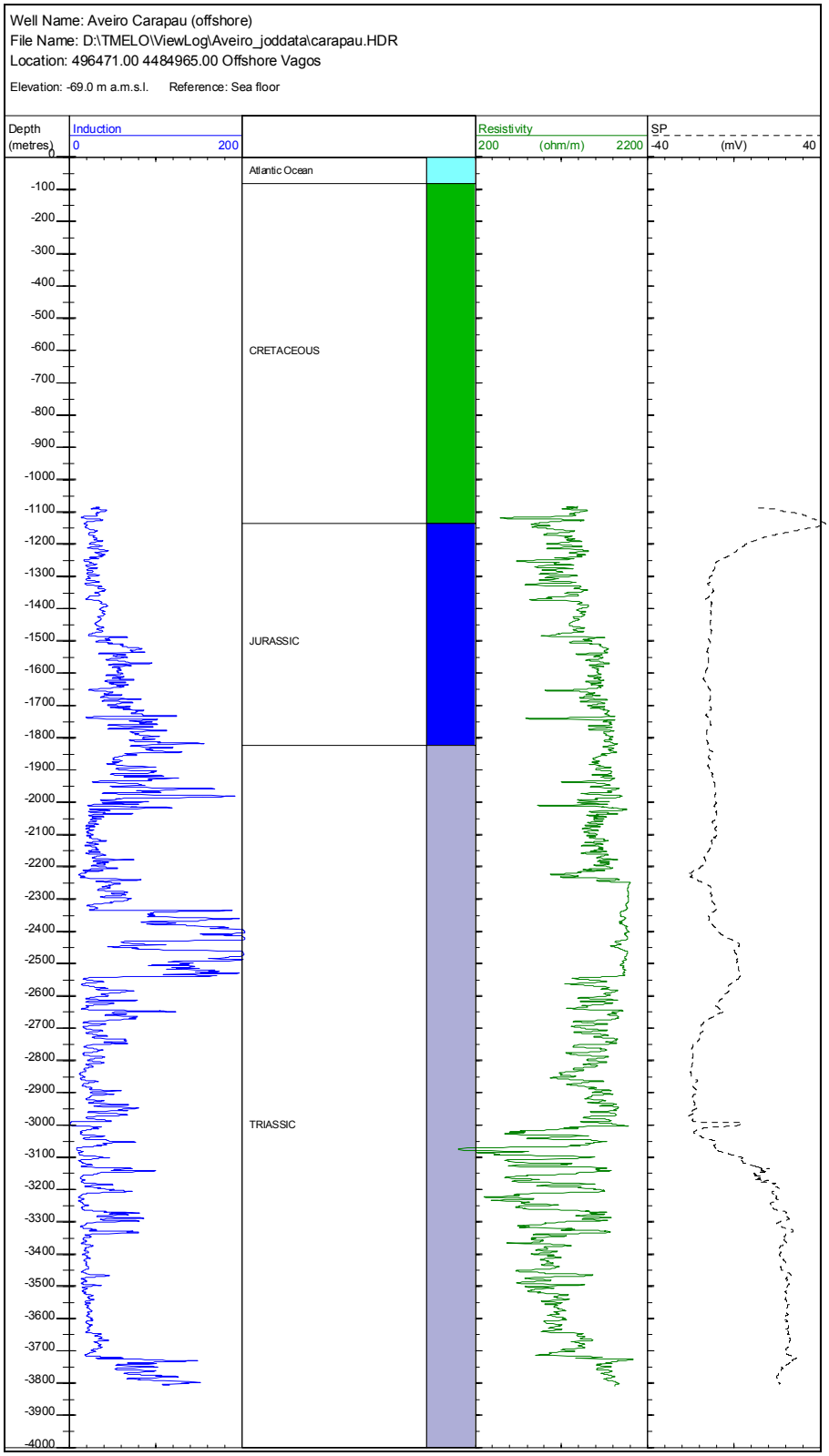
Well Name: Aveiro Carapau (offshore)
File Name: D:\TMELO\ViewLog\Aveiro_joddata\carapau.HDR
Location: 496471.00 4484965.00 Offshore Vagos
Elevation: -69.0 m a.m.s.l. Reference: Sea floor
Depth (metres)
Induction
0
200
Resistivity
200
(ohm/m)
2200
SP
-40
(mV)
40
Atlantic Ocean
CRETACEOUS
JURASSIC
TRIASSIC
0
-100
-200
-300
-400
-500
-600
-700
-800
-900
-1000
-1100
-1200
-1300
-1400
-1500
-1600
-1700
-1800
-1900
-2000
-2100
-2200
-2300
-2400
-2500
-2600
-2700
-2800
-2900
-3000
-3100
-3200
-3300
-3400
-3500
-3600
-3700
-3800
-3900
-4000

A.3 LONG-TERM GROUNDWATER LEVEL MONITORING DATA

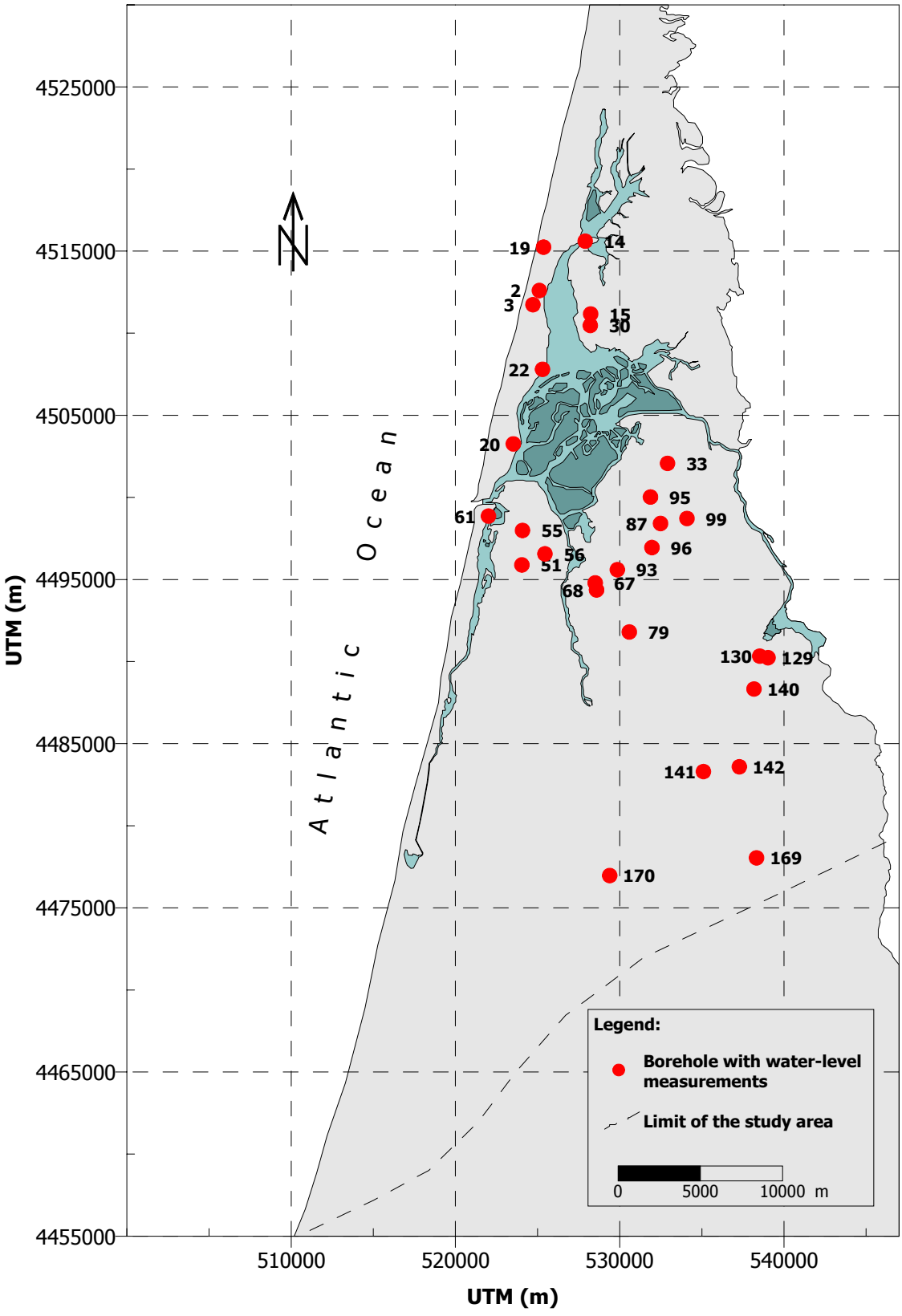

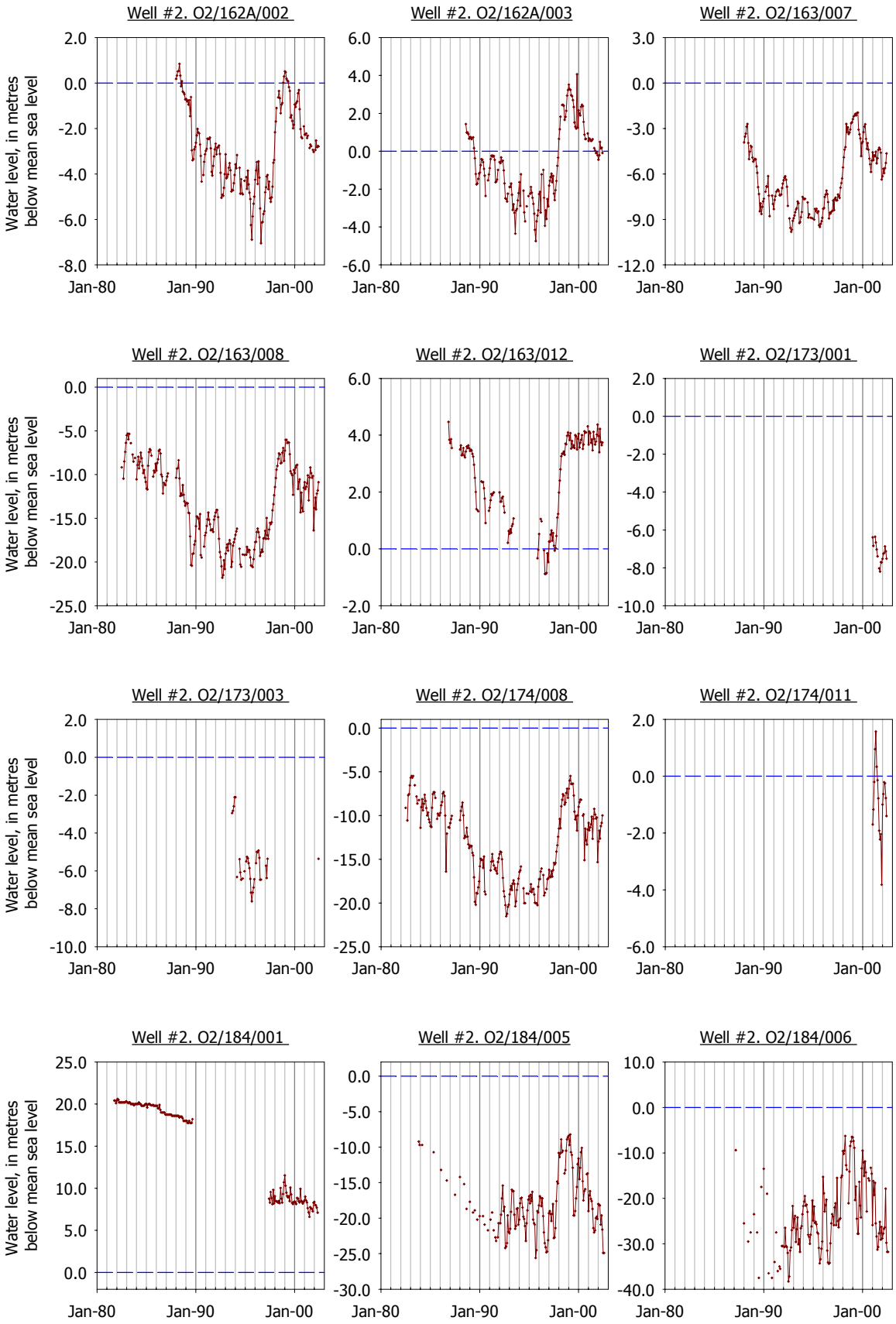
Well #2. O2/162A/002
Well #2. O2/162A/003
Well #2. O2/163/007
Well #2. O2/163/008
Well #2. O2/163/012
Well #2. O2/173/001
Well #2. O2/173/003
Well #2. O2/174/008
Well #2. O2/174/011
Well #2. O2/184/001
Well #2. O2/184/005
Well #2. O2/184/006
Water level, in metres below mean sea level
Jan-80
Jan-90
Jan-00

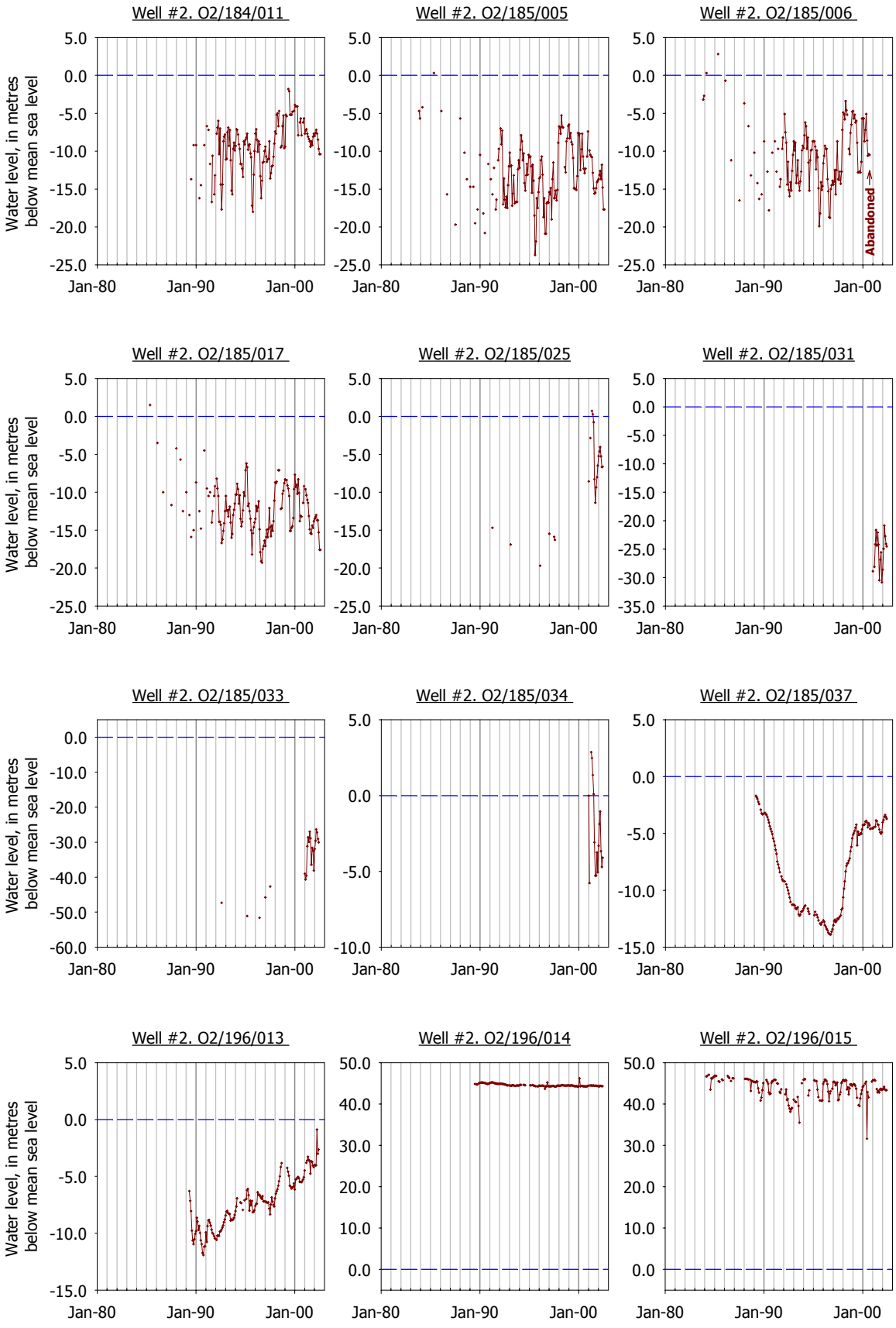
Well #2. O2/184/011
Well #2. O2/185/005
Well #2. O2/185/006
Abandoned
Well #2. O2/185/017
Well #2. O2/185/025
Well #2. O2/185/031
Well #2. O2/185/033
Well #2. O2/185/034
Well #2. O2/185/037
Well #2. O2/196/013
Well #2. O2/196/014
Well #2. O2/196/015
Water level, in metres below mean sea level
Jan-80
Jan-90
Jan-00

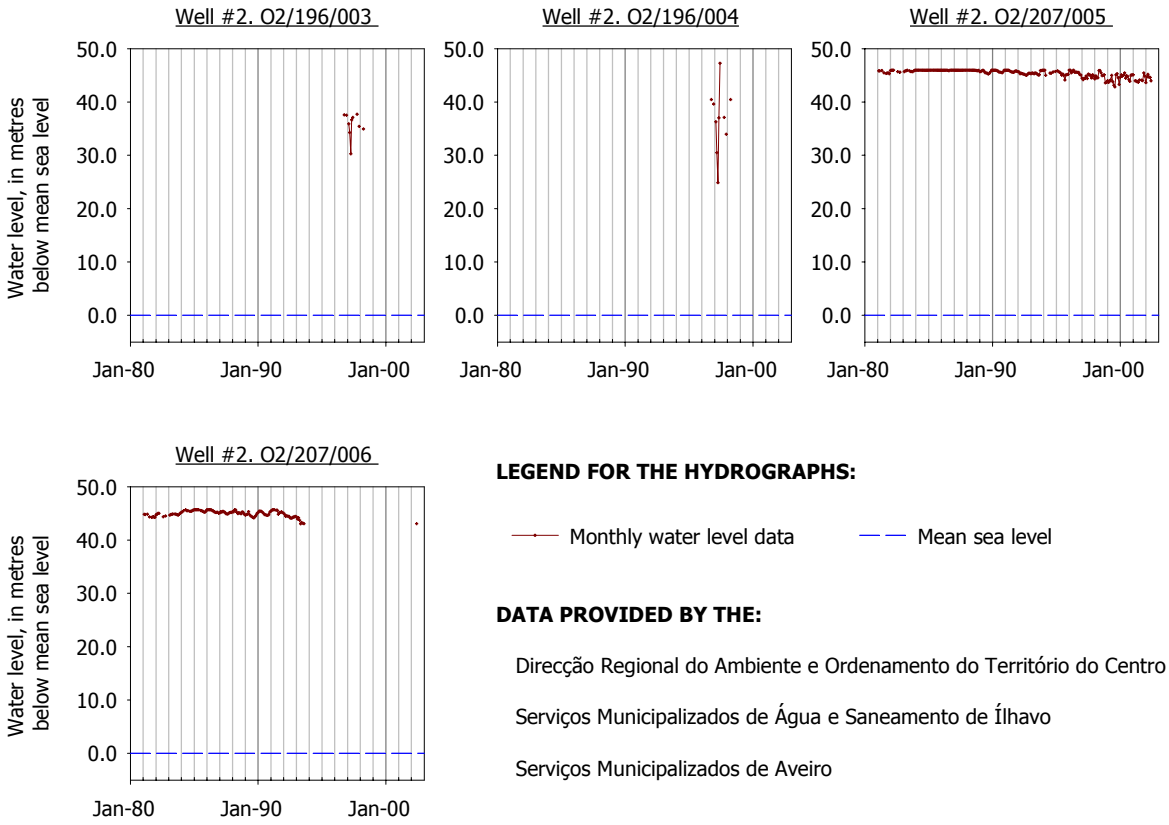

LEGEND FOR THE HYDROGRAPHS:

Monthly water level data — Mean sea level

DATA PROVIDED BY THE:

Direcção Regional do Ambiente e Ordenamento do Território do Centro

Serviços Municipalizados de Água e Saneamento de Ílhavo

Serviços Municipalizados de Aveiro

B

HYDROGEOCHEMICAL DATABASE

B.1 AVEIRO CRETACEOUS AQUIFER HYDROGEOCHEMICAL DATABASE

Well Ref	UAVR_N	Date	T	pH	Eh (mV)	O_2	SEC	Na	K	Ca	Mg	Si	HCO_3	SO_4	Cl	F	I	Br
6	O2/162A/006	31/07/00		7.51				538.0	27.4	27.2	45.10	5.26	91.6	132.0	941.0	0.18	0.018	3.15
7	O2/162A/007	19/09/97	17.5	7.72	36	0.1	1050	179.0	11.6	5.2	4.98	5.21	99.0	50.5	202.0	0.28	0.003	0.67
11	O2/163/004	16/12/00	19.5	7.97	-9	0.0	1850	359.1	17.6	4.49	5.50	4.70	171.4	120.0	467.1	3.70	0.009	1.13
12	O2/163/005	23/09/97	18.9	7.06	48	0.1	550	99.4	12.5	6.9	7.17	5.34	93.0	23.5	118.0	0.28	0.003	0.31
15	O2/163/008	15/12/00	18.7	7.54	16	0.1	550	93.8	11.7	3.86	4.50	5.86	106.1	6.6	118.0	0.40	0.006	0.31
17	O2/163/010	31/07/00	20.6	7.24	32	0.0	541	102.0	9.7	4.2	4.40	6.26	116.4	14.6	101.0	0.45	0.016	0.29
20	O2/173/001	25/09/96	22.9	8.90	55	1.4	518	119.0	4.7	1.2	0.68	4.96	164.0	38.1	71.9	0.96	0.004	0.26
21	O2/173/002	31/07/00	23.6	7.97	136	6.4	1058	250.0	8.0	1.2	0.98	5.28	230.0	73.8	181.0	3.50	0.008	0.60
22	O2/173/003	19/09/97	21.5	8.43	-84	0.7	1270	245.0	9.4	4.6	2.90	4.46	251.0	67.4	191.0	1.02	0.003	0.64
24	O2/174/002	31/07/00		6.70				31.8	9.8	16.1	7.70	6.34	131.1	12.7	32.9	0.36	0.029	0.15
34	O2/174/012	19/09/97	19.2	6.88	91	0.1	321	57.2	8.2	6.9	3.70	5.72	82.0	30.0	44.0	0.36	0.002	0.13
36	O2/174/014	19/09/97	18.4	6.56	93	0.2	662	92.0	15.3	25.9	15.20	5.28	119.0	101.0	105.0	0.50	0.011	0.31
41	O2/174/019	22/09/97	18.0	6.28	237	0.1	321	33.8	10.9	16.9	7.94	5.69	67.0	40.7	42.2	0.15	0.007	0.18
44	O2/174/022	31/07/00	19.4	6.74	187	12.6	433	39.9	11.6	23.2	12.00	6.00	126.2	37.9	50.7	0.41	0.028	0.18
51	O2/184/001	11/12/00	21.2	8.16	27	0.0	1710	378.0	12.4	4.48	2.63	6.00	431.9	164.0	233.0	2.20	0.006	0.73
52	O2/184/002	22/09/97	23.5	8.28	-26	0.6	368	85.3	4.0	1.5	0.63	5.73	109.0	58.5	31.4	0.20	0.002	0.11
53	O2/184/003	23/10/96	23.2	8.11	-45	1.5	364	82.1	5.2	1.7	0.74	5.08	120.0	49.3	35.4	0.23	0.003	0.13
55	O2/184/005	09/10/96	23.8	8.08	-60	1.1	467	81.5	8.4	7.7	3.20	5.00	138.0	55.8	40.1	0.40	0.002	0.13
56	O2/184/006	24/09/97	23.8	7.60	108	0.9	349	71.8	8.4	6.0	2.52	5.42	133.0	41.9	28.8	0.27	0.002	0.10
57	O2/184/007	22/09/97	22.3	8.10	-53	0.0	1590	314.0	9.3	2.3	1.94	4.7	284.0	106.0	220.0	3.50	0.006	0.76
58	O2/184/008	09/10/96	23.7	8.18	-46	0.9	1320	251.0	9.6	2.7	2.24	4.66	240.0	83.2	210.0	3.10	0.007	0.70
61	O2/184/011	04/08/00	26.0	8.15	-5	0.5	401	69.1	6.6	9.5	3.18	5.76	114.0	50.2	35.0	0.22	0.006	0.12
62	O2/184/012	12/12/00	21.9	8.15	-15	0.0	431	85.3	5.3	1.71	0.54	7.25	109.2	67.8	35.8	0.15	0.004	0.11
65	O2/185/003	25/09/96	21.3	8.07	-28	4.4	619	104.0	10.9	19.3	7.72	5.12	134.0	53.5	111.0	0.57	0.005	0.29
67	O2/185/005	09/10/96	23.1	7.71	-25	2.1	441	57.1	7.6	26.8	8.29	5.51	141.0	47.3	52.9	0.27	0.005	0.15
69	O2/185/007	29/10/96	17.6	6.60	13	1.6	248	22.5	7.4	14.3	6.50	6.10	73.0	4.7	42.7	0.32	0.004	0.26
70	O2/185/008	25/09/96	19.2	7.44	3	1.5	397	27.8	10.2	41.9	11.50	5.79	214.0	16.5	28.4	0.25	0.014	0.09
73	O2/185/011	24/09/97	21.5	6.98	91	0.1	411	30.7	9.2	48.5	10.40	5.93	205.0	17.8	29.4	0.21	0.004	0.09
76	O2/185/014	03/08/00	21.9	7.58	52	0.0	516	82.2	9.3	21.8	5.76	6.75	128.6	45.0	68.1	0.33	0.012	0.18
78	O2/185/016	22/09/97	23.6	8.06	-28	0.1	358	83.3	4.0	1.5	0.55	5.58	104.0	51.6	31.6	0.34	0.002	0.10
79	O2/185/017	09/10/96	23.2	7.82	-4	1.1	402	53.0	5.2	30.0	5.97	4.99	159.0	48.2	33.1	0.30	0.010	0.11
80	O2/185/018	23/10/96	24.2	8.01	-88	0.2	404	61.5	8.3	16.3	6.42	5.26	135.0	54.1	37.7	0.26	0.004	0.13
81	O2/185/019	23/10/96	25.4	7.90	-75	3.2	401	52.9	7.2	25.6	6.63	5.70	139.0	67.2	26.7	0.26	0.004	0.09
83	O2/185/021	25/09/96	18.4	6.82	188	1.6	218	16.5	6.0	19.1	5.56	6.27	85.4	14.1	23.8	0.25	0.006	0.09
85	O2/185/023	28/07/00	22.8	7.24	54	0.0	354	76.9	8.3	6.5	2.73	6.45	123.0	47.1	28.9	0.30	0.005	0.10
86	O2/185/024	25/09/96	18.8	7.42	23	3.5	364	40.5	12.6	23.8	8.21	5.12	136.0	47.3	29.8	0.26	0.007	0.10
87	O2/185/025	25/09/96	18.6	7.12	19	4.8	228	20.6	7.3	15.3	5.91	6.39	82.0	16.8	26.9	0.35	0.004	0.11
89	O2/185/027	23/10/96	23.6	9.15	-133	1.1	345	56.9	6.8	13.3	5.63	3.24	137.0	43.1	30.3	0.27	0.008	0.10
90	O2/185/028	23/10/96	21.0	7.81	-140	3.5	1770	291.0	8.9	15.8	22.50	4.49	438.0	23.9	300.0	2.30	0.147	1.31
91	O2/185/029	25/09/96	20.8	7.65	21	1.4	680	128.0	10.4	13.0	6.44	5.25	136.0	68.6	132.0	0.52	0.005	0.32
92	O2/185/030	25/09/96	19.5	7.67	13	2.1	502	34.9	8.9	26.2	7.22	5.05	146.0	29.5	26.7	0.19	0.004	0.10
93	O2/185/031	25/09/96	21.4	8.12	10	1.4	333	85.9	10.1	15.4	5.79	5.22	137.0	55.5	70.0	0.61	0.005	0.18
94	O2/185/032	24/09/97	17.8	6.49	95	0.3	225	13.5	4.4	26.2	3.75	6.28	92.0	9.1	23.5	0.04	0.002	0.10
95	O2/185/033	25/09/96	18.5	7.46	-18	0.9	364	52.9	9.3	15.2	5.92	5.44	136.0	28.3	39.6	0.36	0.005	0.12
96	O2/185/034	25/09/96	20.0	7.70	43	2.7	325	41.2	10.2	19.4	6.41	5.36	154.0	20.6	27.9	0.28	0.005	0.10
101	O2/185/039	22/09/97	16.7	6.00	254	0.2	141	17.3	8.5	3.6	2.46	6.65	31.0	17.4	15.9	0.15	0.001	0.04
104	O2/185/042	01/08/00	20.7	6.69	372	0.6	1293	190.0	18.3	79.6	23.70	7.51	131.7	260.0	213.0	0.28	0.011	0.41
105	O2/185/043	01/08/00	22.7	7.40	168		380	43.0	6.5	29.4	6.06	6.53	158.5	24.1	26.8	0.29	0.011	0.10
111	O2/185/049	31/07/00	19.1	6.58	129	1.9	284	21.9	7.8	17.5	8.27	6.82	97.5	4.9	41.1	0.42	0.009	0.23
113	O2/185/051	01/08/00	24.1	7.97	125	0.8	370	44.2	8.5	17.6	6.56	5.18	109.7	37.9	39.0	0.22	0.005	0.12
114	O2/185/052	03/08/00	21.5	6.81	375	3.7	722	57.5	6.6	93.8	8.01	5.91	262.7	64.2	52.3	0.24	0.106	0.25
116	O2/185/054	19/09/97	19.8	7.09	114	2.1	318	58.2	9.0	8.0	3.35	6.0	101.0	36.4	29.3	0.36	0.001	0.10
121	O2/185/059	02/08/00	26.0	8.21	337	0.7	1423	332.0	8.9	7.0	3.85	5.33	345.0	180.0	174.0	2.27	0.014	0.50
122	O2/185/060	28/07/00	20.3	6.18	314	0.6	234	23.5	6.8	11.9	5.05	7.47	44.5	12.0	39.5	0.30	0.004	0.24
123	O2/195/001	23/09/97	28.2	8.12	43	0.1	740	175.0	5.8	3.4	1.57	5.38	177.0	77.3	109.0	1.74	0.004	0.35
125	O2/195/003	23/09/97	30.8	7.78	-18	0.1	548	83.3	7.3	30.6	8.24	6.29	124.0	111.0	51.5	0.57	0.004	0.16
127	O2/195/005	28/07/00	27.1	7.84	209	0.0	1680	389.0	10.6	15.5	8.19	5.59	171.3	188.0	387.0	2.11	0.010	1.23
128	O2/196/001	22/09/97	25.3	7.67	15	1.0	580	91.8	7.2	35.7	7.42	5.57	151.0	131.0	44.0	0.43	0.003	0.15
129	O2/196/002	25/10/96	17.9	7.25	136	3.7	821	112.0	9.9	48.1	16.50	4.45	118.0	225.0	81.9	0.55	0.009	0.30
130	O2/196/003	25/10/96	17.9	6.55	262	1.2	326	27.6	6.9	24.1	9.80	4.39	77.1	49.7	33.5	0.22	0.008	0.16
131	O2/196/004	23/10/96	18.3	6.84	-6	2.1	316	17.2	5.9	39.4	6.74	6.38	157.0	16.4	25.2	0.12	0.005	0.08
134	O2/196/007	01/08/00	24.4	7.79	91	2.2	445	54.6	5.9	29.6	8.67	8.82	140.2	57.2	31.2	0.19	0.007	0.09
135	O2/196/008	29/10/96	17.1	5.00	342	5.2	148	13.5	2.9	6.0	4.54	4.88	4.2	23.0	24.4	0.03	0.008	0.20
136	O2/196/009	25/09/97	17.0	6.39	104	3.9	179	14.9	3.9	17.8	3.48	5.7	61.0	7.3	20.8	0.04	0.003	0.16
142	O2/196/015	26/09/97	18.1	6.87	169	2.7	631	17.7	2.8	125.0	8.29	4.54	217.0	99.8	30.6	0.04	0.004	0.15
144	O2/196/017	01/08/00	21.9	6.32	172	1.2	227	17.6	4.3	21.6	3.57	9.10	60.4	26.0	24.5	0.10	0.005	0.08
146	O2/196/019	26/09/97	18.0	6.32	46	0.2	215	21.5	9.9	10.1	5.20	9.52	39.5	22.1	43.4	0.07	0.003	0.14
147	O2/196/020	24/09/97	19.2	6.75	244		284	16.5	5.3	39.4	5.13	6.30	129.0	14.6	23.6	0.06	0.004	0.08
148	O2/196/021	25/09/97	16.7	6.61	215	5.4	518	21.8	3.8	73.3	15.70	4.27	159.0	33.2	39.0	0.02	0.007	0.19
149	O2/196/022	24/09/97	18.9	7.38	71	1.3	449	26.6	7.1	59.3	15.30	6.04	242.0	12.5	33.9	0.22	0.004	0.10
150	O2/196/023	26/09/97	19.8	7.06	203	0.3	504	41.6	5.4	69.0	8.49	6.52	223.0	21.6	53.9	0.19	0.013	0.22
151	O2/196/024	25/09/97	18.0	6.17	328	2.9	477	36.1	6.1	37.1	5.61	6.97	93.0	66.6	46.5	0.03	0.009	0.18
152	O2/196/025	25/09/97	18.4	6.44	334	5.1	241	14.9	2.8	29.1	5.25	4.41	77.0	19.4	24.8	0.04	0.004	0.13
153	O2/196/026	23/10/96	18.9	8.06	111	0.0	1500	219.0	9.2	36.5	27.70	4.28	356.0	51.4	240.0	2.20	0.014	0.36
154	O2/196/027	01/08/00	18.5	5.34	474	6.7	163	15.0	2.0	4.9	4.38	4.13	7.1	12.8	20.4	0.05	0.026	0.22
155	O2/196/028	01/08/00	19.7	6.17	366	11.1	333	43.1	7.1	115.0	9.51	8.71	69.5	325.0	43.7	0.14	0.009	0.13
162	O2/206/001	23/09/97	18.1	6.81	366	1.1	430	66.7	13.0	17.6	6.04	2.86	146.0	29.7	42.0	0.22	0.006	0.20
163	O2/206/002	04/08/00	23.0	6.77	376	4.6	169	13.8	2.3	13.3	3.20	6.89	37.2	19.4	20.4	0.09	0.005	0.06
164	O2/206/003	04/08/00	27.0	7.05	195	4.4	362	62.8	3.5	7.1	2.62	7.53	73.8	43.1	39.2	0.30	0.006	0.12
166	O2/207/002	23/09/97	21.7	7.41	77	0.1	490	16.9	5.6	75.8	15.40	5.67	141.0	125.0	23.9	0.05	0.004	0.07
167	O2/207/003	23/09/97	21.9	7.25	98	0.1	708	19.8	4.4	121.0	21.90	5.91	172.0	234.0	26.7	0.09	0.004	0.09
168	O2/207/004	26/09/97	17.5	5.77	190	0.3	483	54.3	10.4	33.0	17.60	9.74	12.5	160.0	46.2	0.05	0.002	0.19
172	O2/207/008	02/08/00	22.0	8.34	251	15.6	1205	225.0	18.7	96.4	32.40	6.31	230.4	128.0	365.0	0.41	0.061	0.80
174	O2/208/001	04/08/00	23.1	6.91	178	6.5	322	23.4	5.1	20.9	6.78	6.47	73.2	16.5	45.8	0.19	0.007	0.30
175	O2/208/002	02/08/00	18.0	7.18	390	2.8	498	14.7	2.3	55.1	16.20	5.24	212.5	51.2	21.1	0.22	0.011	0.09
176	O2/208/003	03/08/00	17.2	6.26	424	9.8	188	17.7	2.3	12.7	4.42	10.40	37.8	0.8	25.5	0.07	0.008	0.12
177	O2/217/001	04/08/00	21.3	7.30	218	2.0	538	38.7	3.8	59.8	10.60	7.32	195.1	21.5	62.9	0.11	0.012	0.16
182	O2/218/003	04/08/00	19.8	7.21	147	0.7	317	44.6	7.36	16.50	2.66	5.45	96.3	13.2	41.7	0.26	0.010	0.12
183	O2/218/004	04/08/00	22.0	7.10	336	4.0	613	28.0	9.6	74.5	7.06	3.05	145.1	65.3	56.9	0.14	0.011	0.16
185	O2/185/061	13/12/00	18.2	7.54	37	0.0	1540	272.0	22.3	16.70	11.10	5.63	103.7	129.0	360.9	3.20	0.007	0.78

Comments: (1) all the data are in mg L^{-1} if other units are not indicated

Well Ref	UAVR_N	NO_3_N	NO_2_N	NH_4_N	P_{total}	DOC	Ag	Al	As	B	Ba	Be	Bi	Cd
6	O2/162A/006	-0.50	-0.003	0.21	-0.10	7.9	-0.00020	0.00285	0.00024	0.292	0.100	0.00015	-0.00001	-0.00001
7	O2/162A/007	-0.01	-0.005	-0.01	-0.20		-0.00002	0.00047	0.00166	0.180	0.090	-0.00001	-0.00009	-0.00004
11	O2/163/004	-0.30	-0.400		-3.00		-0.00020	0.00244	0.00161		0.077	-0.00010	0.00001	0.00002
12	O2/163/005	-0.01	-0.005	-0.01	0.30		-0.00002	0.00392	-0.00076	0.190	0.144	0.00027	-0.00017	-0.00003
15	O2/163/008	-0.30	-0.400		-3.00		-0.00020	0.00439	0.00038		0.031	0.00016	-0.00001	0.00002
17	O2/163/010	-0.50	-0.003	-0.02	-0.10	0.8	-0.00020	0.49300	0.00138	0.268	0.199	0.00095	0.00001	0.00002
20	O2/173/001	-0.02		-0.01	-0.20		-0.00004	0.01294	0.00098	0.430	0.217	0.00008	-0.00002	0.00004
21	O2/173/002	-0.50	-0.003	-0.02	0.10	5.3	-0.00020	0.00320	0.00096	1.250	0.007	-0.00010	-0.00001	-0.00001
22	O2/173/003	-0.01	-0.005	-0.01	-0.20		-0.00002	0.01221	0.00131	0.800	0.054	0.00020	-0.00017	-0.00003
24	O2/174/002	-0.50	-0.003	-0.02	0.10	1.5	-0.00020	0.00637	0.01999	0.105	0.147	0.00223	-0.00001	0.00003
34	O2/174/012	-0.01	-0.005	-0.01	0.80		-0.00002	0.00492	0.00458	0.120	0.090	0.00030	-0.00017	-0.00003
36	O2/174/014	-0.01	-0.005	-0.01	-0.20		-0.00002	0.00535	0.03321	0.210	0.169	0.00020	-0.00017	-0.00003
41	O2/174/019	0.68	0.013	-0.01	0.40		-0.00002	0.00503	0.02213	0.060	0.122	0.00005	-0.00017	-0.00003
44	O2/174/022	-0.50	-0.003	0.02	-0.10	1.7	-0.00020	-0.00200	0.02709	0.117	0.202	0.00020	-0.00001	-0.00001
51	O2/184/001	-0.30	-0.400		-3.00		-0.00020	0.00691	0.00135		0.013	-0.00010	0.00024	0.00008
52	O2/184/002	-0.01	-0.005	-0.01	-0.20		-0.00002	0.00537	-0.00076	0.100	0.029	0.00014	-0.00017	-0.00003
53	O2/184/003	-0.02		-0.01	-0.20		-0.00004	0.00186	0.00184	0.110	0.034	0.00008	-0.00002	-0.00003
55	O2/184/005	-0.02		-0.01	-0.20		-0.00004	0.00189	0.00167	0.200	0.123	0.00009	-0.00002	-0.00003
56	O2/184/006	-0.01	-0.005	-0.01	-0.20		-0.00002	0.00041	0.00249	0.120	0.083	0.00016	-0.00009	-0.00004
57	O2/184/007	-0.01	-0.005	-0.01	-0.20		-0.00002	0.00864	0.00160	1.350	0.006	0.00027	-0.00017	-0.00003
58	O2/184/008	-0.02		-0.01	-0.20		-0.00004	0.00507	0.00506	1.040	0.020	0.00005	0.00003	0.00005
61	O2/184/011	-0.20	-0.003	-0.02	-0.10	1.0	-0.00020	0.00897	0.00083	0.126	0.066	0.00019	-0.00001	-0.00001
62	O2/184/012	-0.03	-0.040		-0.30		-0.00020	0.01053	0.00030		0.030	0.00018	0.00004	-0.00001
65	O2/185/003	-0.02		-0.01	-0.20		-0.00004	0.00315	0.00452	0.250	0.112	0.00023	-0.00002	-0.00003
67	O2/185/005	-0.02		-0.01	-0.20		-0.00004	0.00223	0.00416	0.110	0.104	0.00023	-0.00002	-0.00003
69	O2/185/007	-0.02		-0.01	-0.20		-0.00004	0.00230	0.03410	0.060	0.112	0.00010	-0.00002	-0.00003
70	O2/185/008	-0.02		-0.01	-0.20		-0.00004	0.00248	0.00237	0.070	0.264	0.00024	-0.00002	0.00003
73	O2/185/011	-0.01	-0.005	-0.01	-0.20		-0.00002	0.00582	0.00144	0.090	0.229	0.00037	-0.00017	-0.00003
76	O2/185/014	-0.20	-0.003	-0.02	-0.10	0.3	-0.00020	0.00279	0.00130	0.232	0.129	0.00026	-0.00001	-0.00001
78	O2/185/016	-0.01	-0.005	-0.01	-0.20		-0.00002	0.00564	-0.00076	0.120	0.033	0.00017	-0.00017	-0.00003
79	O2/185/017	-0.02		-0.01	-0.20		-0.00004	0.00238	0.00307	0.160	0.073	-0.00001	-0.00002	-0.00003
80	O2/185/018	-0.02		-0.01	-0.20		-0.00004	0.00199	0.00232	0.110	0.142	0.00015	-0.00002	-0.00003
81	O2/185/019	-0.02		-0.01	-0.20		-0.00004	0.00220	0.00370	0.080	0.141	0.00009	-0.00002	-0.00003
83	O2/185/021	0.04		-0.01	-0.20		-0.00004	0.00445	0.00220	0.040	0.069	0.00017	-0.00002	-0.00003
85	O2/185/023	-0.50	-0.003	-0.02	0.10	0.7	-0.00020	0.00229	0.00189	0.138	0.065	0.00039	-0.00001	0.00001
86	O2/185/024	-0.02		-0.01	-0.20		-0.00004	0.00288	0.00548	0.120	0.115	0.00016	-0.00002	0.00003
87	O2/185/025	-0.02		-0.01	-0.20		-0.00004	0.00637	0.00353	0.080	0.108	0.00085	-0.00002	-0.00003
89	O2/185/027	-0.02		0.01	-0.20		-0.00004	0.00128	0.00312	0.090	0.089	0.00002	-0.00002	-0.00003
90	O2/185/028	-0.02		1.77	0.20		-0.00004	0.00335	0.01030	1.190	0.305	0.00002	-0.00002	0.00006
91	O2/185/029	-0.02		-0.01	-0.20		0.00006	0.00530	0.00333	0.220	0.065	0.00030	-0.00002	0.00100
92	O2/185/030	-0.02		-0.01	-0.20		0.00004	0.00190	0.00311	0.100	0.137	0.00014	-0.00002	0.00034
93	O2/185/031	-0.02		-0.01	-0.20		-0.00004	0.00492	0.00959	0.280	0.118	0.00031	-0.00002	-0.00003
94	O2/185/032	-0.01	-0.005	-0.01	0.20		-0.00002	0.00773	-0.00076	0.016	0.089	0.00027	-0.00017	-0.00003
95	O2/185/033	-0.02		-0.01	-0.20		-0.00004	0.00523	0.00457	0.110	0.110	0.00030	-0.00002	-0.00003
96	O2/185/034	-0.02		-0.01	-0.20		-0.00004	0.00396	0.00176	0.100	0.194	0.00025	-0.00002	-0.00003
101	O2/185/039	-0.01	-0.005	-0.01	0.50		-0.00002	0.00591	0.01544	0.090	0.072	0.00101	-0.00017	-0.00003
104	O2/185/042	-0.50	-0.003	-0.02	-0.10	1.8	-0.00020	0.00398	0.00272	0.272	0.070	0.00117	-0.00001	-0.00001
105	O2/185/043	-0.50	-0.003	-0.02	-0.10	1.7	-0.00020	0.00234	0.00158	0.179	0.147	0.00034	-0.00001	-0.00001
111	O2/185/049	-0.50	-0.003	-0.02	-0.10	0.8	-0.00020	0.00391	0.00679	0.124	0.152	0.00024	-0.00001	-0.00001
113	O2/185/051	-0.50	-0.003	-0.02	-0.10	2.8	-0.00020	0.00302	0.00158	0.169	0.142	0.00011	-0.00001	-0.00001
114	O2/185/052	9.30	-0.003	-0.02	-0.10	7.2	-0.00020	0.00901	0.00124	0.277	0.045	-0.00010	-0.00001	0.00005
116	O2/185/054	-0.01	-0.005	-0.01	-0.20		-0.00002	0.00209	0.00344	0.120	0.108	0.00062	-0.00009	-0.00004
121	O2/185/059	-0.50	-0.003	-0.02	-0.10	0.9	-0.00020	0.00550	0.00202	1.200	0.022	-0.00010	-0.00001	0.00001
122	O2/185/060	-0.50	-0.003	-0.02	-0.10	0.9	-0.00020	-0.00200	0.00449	0.076	0.114	0.00013	0.00002	0.00004
123	O2/195/001	-0.01	-0.005	-0.01	-0.20		-0.00002	0.00627	-0.00076	0.550	0.006	0.00014	-0.00017	-0.00003
125	O2/195/003	-0.01	-0.005	-0.01	-0.20		-0.00002	0.00672	-0.00076	0.190	0.030	0.00029	-0.00017	-0.00003
127	O2/195/005	-0.50	-0.003	-0.02	-0.10	2.3	-0.00020	0.00697	0.00192	0.828	0.007	-0.00010	0.00002	0.00001
128	O2/196/001	-0.01	-0.005	-0.01	-0.20		-0.00002	0.00513	0.00186	0.160	0.100	0.00006	-0.00017	-0.00003
129	O2/196/002	0.90		-0.01	-0.20		-0.00004	0.01233	0.00299	0.310	0.038	0.00026	-0.00002	-0.00003
130	O2/196/003	2.90		0.04	-0.20		-0.00004	0.03746	0.00142	0.110	0.096	0.00074	-0.00002	-0.00003
131	O2/196/004	-0.02		-0.01	-0.20		-0.00004	0.00143	0.00146	0.020	0.084	0.00086	-0.00002	-0.00003
134	O2/196/007	-0.50	-0.003	-0.02	-0.10	0.9	-0.00020	0.00340	0.00048	0.113	0.067	0.00015	-0.00001	-0.00001
135	O2/196/008	1.80		-0.01	-0.20		-0.00004	0.04696	0.00175	-0.010	0.071	0.00180	-0.00002	0.00003
136	O2/196/009	0.15	-0.005	-0.01	-0.20		-0.00002	0.01032	-0.00076	0.013	0.067	0.00092	-0.00017	-0.00003
142	O2/196/015	9.80	0.005	-0.01	-0.20		-0.00002	0.00617	-0.00076	0.019	0.110	0.00007	-0.00017	-0.00003
144	O2/196/017	-0.50	-0.003	-0.02	-0.10	0.8	-0.00020	-0.00200	0.00046	0.037	0.067	0.00050	-0.00001	0.00002
146	O2/196/019	0.06	0.010	-0.01	-0.20		-0.00002	0.00792	0.00090	0.040	0.097	0.01739	-0.00009	0.00024
147	O2/196/020	-0.01	-0.005	-0.01	-0.20		-0.00002	-0.00032	0.00086	0.020	0.079	0.00223	-0.00009	-0.00004
148	O2/196/021	17.70	0.010	-0.01	-0.20		-0.00002	0.00622	-0.00076	0.015	0.090	0.00020	-0.00017	-0.00003
149	O2/196/022	-0.01	-0.005	-0.01	-0.20		-0.00002	-0.00032	0.00076	0.140	0.233	0.00015	-0.00009	-0.00004
150	O2/196/023	-0.01	-0.005	0.02	-0.20		-0.00002	0.00078	0.00138	0.070	0.167	0.00014	-0.00009	-0.00004
151	O2/196/024	3.20	0.008	-0.01	-0.20		-0.00002	0.01043	-0.00076	0.017	0.071	0.00256	-0.00017	0.00004
152	O2/196/025	1.21	-0.005	-0.01	-0.20		0.00005	0.00689	-0.00076	0.014	0.052	0.00009	-0.00017	-0.00003
153	O2/196/026	0.23		0.01	-0.20		-0.00004	0.01465	0.00270	0.560	0.030	0.00004	0.00003	0.00009
154	O2/196/027	5.40	-0.003	-0.02	-0.10	4.1	-0.00020	0.02752	0.00013	0.025	0.044	0.00044	-0.00001	0.00002
155	O2/196/028	-0.50	-0.003	-0.02	-0.10	0.7	-0.00020	0.02100	0.00067	0.121	0.039	0.00109	-0.00001	0.00006
162	O2/206/001	4.20	-0.005	0.28	0.30		-0.00002	0.00535	0.00095	0.220	0.058	0.00016	-0.00017	-0.00003
163	O2/206/002	-0.50	-0.003	-0.02	-0.10	0.3	-0.00020	0.00288	0.00089	0.050	0.019	0.00014	-0.00001	-0.00001
164	O2/206/003	-0.50	-0.003	-0.02	0.40	3.5	-0.00020	-0.00200	0.00105	0.143	0.032	-0.00010	-0.00001	-0.00001
166	O2/207/002	-0.01	-0.005	-0.01	-0.20		-0.00002	0.00888	-0.00076	0.040	0.031	0.00012	-0.00017	-0.00003
167	O2/207/003	-0.01	-0.005	-0.01	0.20		-0.00002	0.07650	-0.00076	0.040	0.028	0.00030	-0.00017	-0.00003
168	O2/207/004	4.80	-0.005	-0.01	-0.20		-0.00002	0.01261	0.00121	0.022	0.061	0.00314	-0.00017	0.00623
172	O2/207/008	-0.50	-0.003	-0.02	-0.10	11.0	-0.00020	0.00536	0.00078	0.372	0.287	0.00050	-0.00001	0.00003
174	O2/208/001	-0.50	-0.003	-0.02	0.10	1.6	-0.00020	0.02252	0.02456	0.164	0.022	-0.00010	-0.00001	-0.00001
175	O2/208/002	-0.50	-0.003	-0.02	-0.10	0.8	-0.00020	0.01032	0.00039	0.063	0.045	-0.00010	-0.00001	-0.00001
176	O2/208/003	4.70	-0.003	0.07	-0.10	0.1	-0.00020	0.07074	0.00024	0.035	0.054	0.00038	-0.00001	0.00003
177	O2/217/001	2.00	-0.003	-0.02	-0.10	2.2	-0.00020	0.00783	0.00328	0.050	0.062	0.00024	-0.00001	0.00002
182	O2/218/003	-0.20	-0.003	-0.02	-0.10	0.6	-0.00020	0.03301	0.00034	0.117	0.063	0.00014	-0.00001	-0.00001
183	O2/218/004	11.80	-0.003	-0.02	-0.10	2.8	-0.00020	0.00936	0.00020	0.053	0.028	-0.00010	-0.00001	0.00003
185	O2/185/061	-0.30	-0.400		-3.00		-0.00020	0.02747	0.01316		0.035	0.00033	0.00002	0.00008

Comments:

(1) all the data are in mg L^{-1} if other units are not indicated

(2) the symbol - before a number indicates below detection limit

(3) isotopic values in italic are from Carreira Paquete (1998)

Well Ref	UAVR_N	Co	Cr	Cs	Cu	Fe	Ga	Ge	Li	Mn	Mo	Ni	Pb	Rb
6	O2/162A/006	0.00006	-0.00050	0.00026	0.00565	2.060	0.00001	0.00009	0.075	0.072	0.00013	0.00306	-0.00010	0.012
7	O2/162A/007	-0.00002	-0.00004	0.00010	0.00022	0.352	-0.00004	0.00011	0.034	0.033	0.00023	0.00019	0.00031	0.005
11	O2/163/004	0.00002	0.00972	0.00013	0.00753	0.321	0.00010	0.00020	0.042	0.007	0.00623	0.07852	0.00030	0.008
12	O2/163/005	-0.00002	-0.00020	0.00024	-0.00028	0.535	-0.00004	0.00017	0.018	0.043	0.00023	0.00015	-0.00005	0.009
15	O2/163/008	0.00008	0.00490	0.00019	0.00176	0.248	0.00002	0.00034	0.022	0.044	0.00038	0.01565	0.00032	0.007
17	O2/163/010	0.00033	0.00998	0.00047	0.00147	1.160	0.00021	0.00034	0.031	0.056	0.00023	0.00236	0.00082	0.009
20	O2/173/001	0.00002	0.00012	0.00006	0.00162	0.069	0.00010	0.00018	0.008	0.005	0.00073	0.00033	0.00041	0.002
21	O2/173/002	0.00001	0.00206	0.00008	0.00278	0.077	0.00012	0.00033	0.029	0.001	0.00222	0.00318	-0.00010	0.003
22	O2/173/003	-0.00002	-0.00020	0.00013	-0.00028	0.110	0.00007	0.00045	0.016	0.009	0.00201	0.00026	0.00005	0.005
24	O2/174/002	0.00128	0.00148	0.00107	0.00697	4.550	-0.00001	0.00019	0.008	0.133	-0.00010	0.00192	0.00029	0.038
34	O2/174/012	0.00021	-0.00020	0.00099	-0.00028	1.670	-0.00004	0.00026	0.008	0.049	-0.00021	0.00211	-0.00005	0.018
36	O2/174/014	0.00281	-0.00020	0.00249	0.00083	7.530	0.00005	0.00014	0.006	0.212	0.00040	0.00259	0.00023	0.045
41	O2/174/019	0.00039	-0.00020	0.00116	0.00031	2.670	-0.00004	0.00018	0.008	0.098	-0.00021	0.00111	0.00019	0.030
44	O2/174/022	0.00315	0.00173	0.00191	0.00057	4.030	-0.00001	0.00019	0.003	0.142	-0.00010	0.00267	-0.00010	0.052
51	O2/184/001	0.00003	-0.00050	0.00016	0.00568	0.299	0.00010	0.00024	0.040	0.005	0.00356	0.03656	0.00023	0.006
52	O2/184/002	-0.00002	-0.00020	-0.00004	-0.00028	0.120	0.00006	0.00033	0.009	0.003	-0.00021	0.00025	-0.00005	0.002
53	O2/184/003	-0.00001	0.00006	0.00006	0.00017	0.129	0.00005	0.00012	0.010	0.002	0.00016	-0.00015	0.00008	0.002
55	O2/184/005	0.00003	0.00012	0.00008	0.00030	0.039	0.00005	0.00008	0.012	0.005	0.00033	0.00028	0.00009	0.004
56	O2/184/006	-0.00002	-0.00004	0.00005	0.00085	0.082	-0.00004	0.00014	0.013	0.006	0.00017	0.00011	0.00009	0.004
57	O2/184/007	-0.00002	-0.00020	0.00013	0.00028	0.185	0.00007	0.00025	0.023	0.002	0.00278	0.00010	-0.00005	0.005
58	O2/184/008	0.00002	0.00015	0.00011	0.00094	0.068	0.00008	0.00018	0.017	0.001	0.00211	-0.00015	0.00021	0.004
61	O2/184/011	0.00003	0.00096	0.00007	0.00119	0.079	0.00006	0.00029	0.016	0.006	0.00010	0.00152	-0.00010	0.005
62	O2/184/012	0.00003	-0.00050	0.00005	0.00145	0.242	0.00007	0.00019	0.013	0.008	0.00023	0.01307	0.00022	0.002
65	O2/185/003	0.00008	0.00011	0.00027	0.00056	0.476	0.00004	0.00009	0.014	0.023	0.00037	0.00088	0.00022	0.008
67	O2/185/005	0.00012	0.00007	0.00018	0.00081	0.255	0.00002	0.00010	0.012	0.027	0.00028	0.00142	0.00035	0.006
69	O2/185/007	0.00190	0.00008	0.00065	0.00014	3.550	0.00001	0.00019	0.006	0.106	-0.00011	0.00104	0.00005	0.021
70	O2/185/008	0.00015	-0.00004	0.00054	0.00063	0.578	0.00003	0.00008	0.009	0.053	-0.00011	0.00216	0.00009	0.015
73	O2/185/011	0.00012	-0.00020	0.00043	-0.00028	0.571	-0.00004	0.00010	0.014	0.042	-0.00021	0.00181	0.00007	0.013
76	O2/185/014	0.00004	0.00097	0.00020	0.00106	0.126	0.00003	0.00022	0.022	0.032	0.00025	0.00049	-0.00010	0.010
78	O2/185/016	-0.00002	-0.00020	-0.00004	-0.00028	0.142	0.00006	0.00024	0.010	0.005	-0.00021	0.00006	0.00011	0.002
79	O2/185/017	0.00021	0.00009	0.00008	0.00028	0.031	-0.00001	0.00002	0.013	0.012	0.00039	0.00213	0.00017	0.007
80	O2/185/018	0.00005	0.00006	0.00011	0.00021	0.089	0.00004	0.00007	0.013	0.013	0.00024	0.00074	0.00014	0.005
81	O2/185/019	0.00011	0.00008	0.00019	0.00032	0.033	0.00002	0.00006	0.011	0.025	0.00024	0.00189	0.00018	0.007
83	O2/185/021	0.00083	0.00013	0.00073	0.00070	0.088	-0.00001	0.00003	0.003	0.007	-0.00011	0.00218	0.00027	0.021
85	O2/185/023	0.00001	0.00079	0.00017	0.00120	0.288	0.00003	0.00022	0.020	0.021	0.00018	0.00474	0.00010	0.007
86	O2/185/024	0.00009	0.00009	0.00023	0.00076	0.723	-0.00001	0.00012	0.027	0.031	-0.00011	0.00314	0.00024	0.017
87	O2/185/025	0.00038	0.00011	0.00065	0.00094	0.973	0.00002	0.00013	0.009	0.048	0.00024	0.00131	0.00025	0.020
89	O2/185/027	0.00005	0.00005	0.00010	0.00016	0.116	0.00001	0.00008	0.012	0.026	0.00030	0.00055	0.00003	0.006
90	O2/185/028	0.00011	0.00018	0.00013	0.00040	1.180	0.00006	0.00010	0.032	0.014	0.00072	0.00092	0.00026	0.005
91	O2/185/029	0.00006	0.00601	0.00028	0.00098	0.322	0.00003	0.00019	0.018	0.024	0.00044	0.00064	0.00045	0.008
92	O2/185/030	0.00010	0.00026	0.00017	0.00097	0.238	0.00003	0.00017	0.011	0.056	0.00026	0.00228	0.00023	0.006
93	O2/185/031	0.00013	0.00036	0.00045	0.00114	0.418	0.00002	0.00015	0.022	0.026	0.00215	0.00406	0.00034	0.011
94	O2/185/032	0.00011	-0.00020	0.00022	-0.00028	5.470	-0.00004	0.00035	0.026	0.065	-0.00021	0.00253	0.00008	0.013
95	O2/185/033	0.00131	0.00013	0.00052	0.00165	0.821	0.00002	0.00016	0.010	0.040	0.00027	0.00162	0.00011	0.014
96	O2/185/034	0.00021	0.00008	0.00024	0.00634	0.158	0.00002	0.00010	0.013	0.030	0.00013	0.00132	0.00060	0.007
101	O2/185/039	0.00004	-0.00020	0.00030	-0.00028	0.525	-0.00004	0.00017	0.060	0.032	-0.00021	0.00541	0.00013	0.010
104	O2/185/042	0.00027	0.00063	0.00056	0.00300	0.054	-0.00001	0.00010	0.274	0.016	0.00060	0.00388	0.00025	0.020
105	O2/185/043	0.00004	0.00107	0.00024	0.00072	0.161	0.00002	0.00013	0.016	0.016	0.00028	0.00108	0.00027	0.008
111	O2/185/049	0.00079	0.00106	0.00068	0.00056	3.280	-0.00001	0.00018	0.010	0.107	-0.00010	0.00126	-0.00010	0.024
113	O2/185/051	0.00003	0.00122	0.00013	0.00104	0.025	0.00007	0.00021	0.012	0.015	0.00032	0.00033	-0.00010	0.005
114	O2/185/052	0.00027	-0.00050	0.00007	0.01513	0.072	0.00001	0.00003	0.006	0.002	0.00031	0.00112	0.00062	0.010
116	O2/185/054	0.00006	0.00110	0.00017	0.00107	0.640	-0.00004	0.00017	0.019	0.024	0.00036	0.00022	0.00042	0.008
121	O2/185/059	0.00003	0.00131	0.00021	0.00550	0.028	0.00012	0.00020	0.080	0.007	0.00227	0.01059	0.00046	0.005
122	O2/185/060	0.00178	-0.00050	0.00101	0.01494	0.013	-0.00001	0.00025	0.007	0.072	0.00012	0.00440	-0.00010	0.026
123	O2/195/001	-0.00002	-0.00020	0.00023	-0.00028	0.049	0.00010	0.00019	0.017	0.004	0.00105	0.00017	-0.00005	0.004
125	O2/195/003	0.00006	-0.00020	0.00041	-0.00028	0.118	0.00006	0.00019	0.014	0.027	0.00026	0.00106	-0.00005	0.007
127	O2/195/005	0.00002	0.00331	0.00030	0.00356	0.023	0.00008	0.00017	0.108	0.006	0.00155	0.00666	-0.00010	0.007
128	O2/196/001	0.00006	-0.00020	0.00026	-0.00028	0.327	-0.00004	0.00010	0.015	0.017	0.00076	0.00097	0.00005	0.008
129	O2/196/002	0.00101	0.00007	0.00024	0.00045	0.109	0.00004	0.00010	0.071	0.012	0.00012	0.00332	0.00006	0.011
130	O2/196/003	0.00265	0.00009	0.00035	0.00040	0.064	0.00028	0.00010	0.023	0.027	-0.00011	0.00229	0.00107	0.013
131	O2/196/004	0.00016	0.00007	0.00029	0.00025	1.730	0.00001	0.00014	0.018	0.084	-0.00011	0.00211	0.00004	0.013
134	O2/196/007	0.00004	0.00122	0.00027	0.00136	0.058	0.00002	0.00025	0.022	0.001	0.00012	0.00088	0.00027	0.007
135	O2/196/008	0.00293	0.00010	0.00058	0.00351	-0.006	0.00011	0.00003	0.005	0.018	-0.00011	0.00156	0.00032	0.016
136	O2/196/009	0.00047	-0.00020	0.00036	0.00108	0.099	-0.00004	0.00006	0.011	0.011	-0.00021	0.00265	0.00071	0.015
142	O2/196/015	0.00043	-0.00020	0.00006	0.00241	-0.006	-0.00004	0.00007	0.013	0.000	-0.00021	0.00769	0.00012	0.007
144	O2/196/017	0.00029	0.00116	0.00006	0.00218	0.196	-0.00001	0.00009	0.014	0.003	-0.00010	0.00096	0.00031	0.010
146	O2/196/019	0.02110	-0.00004	0.00155	0.03865	0.079	-0.00004	0.00043	0.047	0.020	-0.00014	0.01035	0.02231	0.051
147	O2/196/020	0.00003	-0.00004	0.00009	0.00031	1.180	-0.00004	0.00014	0.011	0.042	-0.00014	0.00040	0.00005	0.010
148	O2/196/021	0.00026	-0.00020	0.00010	0.00084	0.009	-0.00004	-0.00005	0.003	0.001	-0.00021	0.00451	-0.00005	0.008
149	O2/196/022	0.00013	0.00006	0.00015	0.00050	0.566	-0.00004	0.00016	0.014	0.013	-0.00014	0.00085	0.00182	0.007
150	O2/196/023	0.00007	-0.00004	0.00015	0.03361	0.109	-0.00004	0.00009	0.025	0.003	0.00015	0.00163	0.00060	0.008
151	O2/196/024	0.01622	-0.00020	0.00103	0.00163	0.009	-0.00004	0.00035	0.026	0.009	-0.00021	0.01202	0.00112	0.024
152	O2/196/025	0.00015	0.00036	0.00027	0.00344	0.026	-0.00004	0.00010	0.001	0.001	-0.00021	0.00187	0.00079	0.012
153	O2/196/026	0.00034	0.00015	0.00008	0.00053	0.034	0.00004	0.00020	0.084	0.003	0.00068	0.00223	0.00020	0.005
154	O2/196/027	0.00152	0.00073	0.00020	0.02287	0.009	-0.00001	-0.00001	0.002	0.017	-0.00010	0.00363	0.00135	0.009
155	O2/196/028	0.00212	0.00092	0.00043	0.00280	0.105	-0.00001	0.00029	0.115	0.034	0.00019	0.00254	0.00056	0.013
162	O2/206/001	0.00024	-0.00020	0.00028	0.00213	0.006	0.00006	0.00018	0.010	0.011	0.00062	0.00131	0.00014	0.014
163	O2/206/002	0.00066	0.00066	0.00010	0.01660	0.011	-0.00001	0.00007	0.009	0.005	-0.00010	0.00135	0.00050	0.008
164	O2/206/003	0.00004	-0.00050	0.00005	0.00118	0.052	0.00001	0.00034	0.020	0.019	0.00018	0.00179	-0.00010	0.005
166	O2/207/002	0.00015	-0.00020	0.00010	-0.00028	0.170	-0.00004	0.00008	0.019	0.005	0.00035	0.00237	-0.00005	0.009
167	O2/207/003	0.00035	-0.00020	0.00019	0.00080	0.439	-0.00004	0.00014	0.011	0.019	0.00021	0.00411	0.00035	0.010
168	O2/207/004	0.05249	0.00086	0.00021	0.00753	0.054	-0.00004	0.00010	0.030	0.082	-0.00021	0.04499	0.02733	0.010
172	O2/207/008	0.00434	-0.00050	0.00011	0.01549	0.313	0.00001	0.00008	0.082	0.242	0.00089	0.00576	0.00058	0.016
174	O2/208/001	0.00037	0.00054	0.00018	0.00097	1.530	0.00001	0.00020	0.016	0.056	0.00044	0.00127	0.00014	0.011
175	O2/208/002	0.00011	0.00066	0.00007	0.00069	0.083	-0.00001	0.00002	0.007	0.001	0.00048	-0.00030	-0.00010	0.004
176	O2/208/003	0.00018	0.00363	0.00004	0.01833	0.044	0.00002	0.00001	0.008	0.005	-0.00010	0.00171	0.00099	0.007
177	O2/217/001	0.00020	0.00060	0.00009	0.00156	0.259	-0.00001	0.00009	0.015	0.025	0.00016	0.00063	0.00024	0.010
182	O2/218/003	0.00012	0.00113	0.00006	0.00141	0.181	0.00003	0.00011	0.024	0.005	-0.00010	0.00070	-0.00010	0.008
183	O2/218/004	0.00035	0.00063	0.00006	0.00932	0.110	-0.00001	-0.00001	0.006	0.006	0.00088	0.00163	0.00117	0.015
185	O2/185/061	0.00003	0.00490	0.00048	0.00581	0.072	0.00007	0.00012	0.035	0.014	0.00311	0.05751	0.00070	0.013

Comments:

(1) all the data are in mg L^{-1} if other units are not indicated

(2) the symbol - before a number indicates below detection limit

(3) isotopic values in italic are from Carreira Paquete (1998)

Well Ref	UAVR_N	Sb	Sc	Se	Sr	Th	Ti	U	V	Y	Zn	Zr	La
6	O2/162A/006	-0.00001	0.00105	0.00389	0.33400	0.00003	0.00101	0.00000	-0.00005	0.00001	0.00900	0.00004	0.000005
7	O2/162A/007	-0.00094	-0.00080	0.00345	0.04710	-0.00004	-0.00003	-0.00005	-0.00600	-0.00001	1.53341	-0.00600	-0.000006
11	O2/163/004	0.00003	0.00126	0.00227	0.06254	0.00001	0.00102	0.00006	0.00267	0.00001	0.00775	0.00003	0.000006
12	O2/163/005	-0.00122	-0.00080	-0.00230	0.07220	-0.00013	-0.00004	-0.00007	-0.00600	-0.00001	0.00297	-0.00600	-0.000008
15	O2/163/008	0.00003	0.00147	0.00076	0.03955	0.00001	0.00097	0.00000	0.00146	0.00001	0.00929	-0.00001	0.000005
17	O2/163/010	0.00002	-0.00100	0.00253	0.04840	0.00040	0.01413	0.00014	0.00363	0.00030	0.04400	0.00044	0.000751
20	O2/173/001	-0.00005	-0.00080	0.00335	0.01090	0.00002	-0.00001	0.00003	-0.00600	0.00001	0.02073	-0.00600	0.000053
21	O2/173/002	-0.00001	0.00116	0.00311	0.02280	0.00001	0.00116	0.00001	0.00071	0.00000	0.01500	0.00002	0.000002
22	O2/173/003	-0.00122	-0.00080	-0.00230	0.03830	-0.00013	-0.00004	0.00012	-0.00600	0.00001	-0.00123	0.02900	0.000043
24	O2/174/002	0.00001	0.00172	-0.00020	0.09890	0.00001	0.00169	0.00002	0.00049	0.00002	0.16300	0.00027	0.000004
34	O2/174/012	-0.00122	-0.00080	-0.00230	0.04470	-0.00013	0.00005	-0.00007	-0.00600	-0.00001	0.01454	-0.00600	0.000009
36	O2/174/014	-0.00122	-0.00080	-0.00230	0.16700	-0.00013	0.00029	-0.00007	-0.00600	0.00001	0.05029	-0.00600	0.000014
41	O2/174/019	-0.00122	-0.00080	-0.00230	0.09850	-0.00013	0.00015	-0.00007	-0.00600	0.00001	0.00333	-0.00600	0.000026
44	O2/174/022	-0.00001	0.00149	-0.00020	0.14900	0.00001	0.00132	0.00000	0.00056	0.00002	0.03000	0.00002	0.000002
51	O2/184/001	0.00003	0.00188	-0.00020	0.10383	0.00004	0.00134	0.00040	-0.00005	0.00003	1.06000	0.00010	0.000021
52	O2/184/002	-0.00122	-0.00080	-0.00230	0.01020	-0.00013	-0.00004	-0.00007	-0.00600	-0.00001	-0.00123	-0.00600	-0.000008
53	O2/184/003	0.00008	-0.00080	0.00418	0.01000	0.00001	-0.00001	0.00000	-0.00600	0.00000	0.00213	-0.00600	-0.000004
55	O2/184/005	-0.00005	-0.00080	0.00441	0.04500	0.00001	-0.00001	0.00001	-0.00600	0.00000	0.00335	-0.00600	0.000005
56	O2/184/006	-0.00094	-0.00080	0.00073	0.03940	-0.00004	-0.00003	-0.00005	-0.00600	-0.00001	0.01496	-0.00600	-0.000006
57	O2/184/007	-0.00122	-0.00080	0.00318	0.04950	-0.00013	-0.00004	-0.00007	-0.00600	-0.00001	-0.00123	0.17900	-0.000008
58	O2/184/008	-0.00005	-0.00080	0.02093	0.04960	0.00005	-0.00001	0.00001	-0.00600	0.00000	0.00338	-0.00600	-0.000004
61	O2/184/011	-0.00001	0.00211	0.00049	0.05850	0.00000	0.00161	0.00002	0.00035	0.00001	0.01600	-0.00001	0.000019
62	O2/184/012	0.00002	0.00147	-0.00020	0.00821	0.00004	0.00165	0.00003	-0.00005	0.00005	0.37254	0.00003	0.000044
65	O2/185/003	-0.00005	-0.00080	0.00388	0.14900	0.00002	-0.00001	0.00001	-0.00600	0.00001	0.01205	-0.00600	0.000008
67	O2/185/005	-0.00005	-0.00080	0.00429	0.16300	0.00001	-0.00001	0.00001	-0.00600	0.00003	0.01544	-0.00600	0.000016
69	O2/185/007	-0.00005	-0.00080	0.00953	0.08270	0.00001	0.00007	0.00002	-0.00600	0.00001	0.00288	-0.00600	0.000012
70	O2/185/008	-0.00005	-0.00080	0.00117	0.21700	0.00001	0.00001	0.00005	-0.00600	0.00002	0.00540	-0.00600	0.000009
73	O2/185/011	-0.00122	-0.00080	-0.00230	0.23500	-0.00013	-0.00004	0.00008	-0.00600	0.00003	0.02687	-0.00600	0.000010
76	O2/185/014	-0.00001	0.00244	-0.00020	0.12700	0.00000	0.00163	0.00003	0.00036	0.00001	0.01800	0.00001	0.000003
78	O2/185/016	-0.00122	-0.00080	-0.00230	0.00870	-0.00013	-0.00004	-0.00007	-0.00600	0.00010	0.00200	-0.00600	0.000045
79	O2/185/017	-0.00005	-0.00080	0.00400	0.15600	0.00001	0.00003	0.00140	-0.00600	0.00001	0.01430	-0.00600	0.000006
80	O2/185/018	-0.00005	-0.00080	0.00282	0.11200	0.00000	-0.00001	0.00001	-0.00600	0.00001	0.00217	-0.00600	0.000006
81	O2/185/019	0.00008	-0.00080	0.00377	0.14300	0.00001	0.00002	0.00001	-0.00600	0.00001	0.00143	-0.00600	0.000006
83	O2/185/021	-0.00005	-0.00080	0.00194	0.07340	0.00001	0.00028	0.00123	-0.00600	0.00013	0.02253	-0.00600	0.000049
85	O2/185/023	-0.00001	0.00130	0.00106	0.04490	0.00000	0.00119	0.00001	0.00026	0.00000	0.03800	0.00004	0.000001
86	O2/185/024	-0.00005	-0.00080	0.00190	0.11300	0.00001	-0.00001	0.00005	-0.00600	0.00002	0.01940	-0.00600	0.000010
87	O2/185/025	-0.00005	-0.00080	0.00150	0.07970	0.00001	0.00005	0.00001	-0.00600	0.00001	0.01724	-0.00600	0.000006
89	O2/185/027	-0.00005	-0.00080	0.00165	0.11500	0.00000	0.00001	0.00000	-0.00600	0.00001	0.00165	-0.00600	-0.000004
90	O2/185/028	-0.00005	-0.00080	0.02405	0.24200	0.00003	-0.00001	0.00010	-0.00600	0.00001	0.01370	0.00800	0.000013
91	O2/185/029	0.00014	-0.00080	0.00364	0.11500	0.00001	-0.00001	0.00006	-0.00600	0.00001	0.01804	0.01000	-0.000004
92	O2/185/030	-0.00005	-0.00080	0.00515	0.14500	0.00001	-0.00001	0.00002	-0.00600	0.00001	0.00380	-0.00600	0.000005
93	O2/185/031	-0.00005	-0.00080	0.00194	0.10300	0.00002	-0.00001	0.00002	-0.00600	0.00001	0.01304	0.01200	0.000015
94	O2/185/032	-0.00122	-0.00080	-0.00230	0.06980	-0.00013	-0.00004	-0.00007	-0.00600	-0.00001	0.01171	0.00600	-0.000008
95	O2/185/033	-0.00005	-0.00080	0.00234	0.09170	0.00001	0.00005	0.00001	-0.00600	0.00003	0.01582	-0.00600	0.000015
96	O2/185/034	-0.00005	-0.00080	0.00102	0.11600	0.00001	0.00002	0.00005	-0.00600	0.00004	0.01419	-0.00600	0.000025
101	O2/185/039	-0.00122	-0.00080	-0.00230	0.03780	-0.00013	-0.00004	-0.00007	-0.00600	0.00001	0.00380	-0.00600	-0.000008
104	O2/185/042	0.00007	0.00224	0.00088	0.42000	0.00000	0.00170	0.00408	0.00035	0.00004	0.03300	0.00001	0.000008
105	O2/185/043	-0.00001	0.00205	-0.00020	0.16600	0.00000	0.00164	0.00045	0.00060	0.00000	0.00700	0.00004	0.000002
111	O2/185/049	-0.00001	0.00202	-0.00020	0.11400	0.00000	0.00164	0.00005	0.00034	0.00001	0.01800	0.00023	0.000003
113	O2/185/051	-0.00001	0.00154	0.00028	0.10900	0.00000	0.00105	0.00003	0.00045	0.00001	0.01000	0.00003	0.000003
114	O2/185/052	0.00019	0.00202	0.00084	0.21400	0.00001	0.00164	0.00161	0.00173	0.00021	0.05100	0.00009	0.000133
116	O2/185/054	-0.00094	-0.00080	0.00056	0.05250	-0.00004	-0.00003	-0.00005	-0.00600	-0.00001	0.21964	0.00800	-0.000006
121	O2/185/059	-0.00001	0.00159	0.00088	0.07810	0.00000	0.00126	0.00053	0.00047	0.00001	0.02200	0.00004	0.000003
122	O2/185/060	0.00002	0.00193	0.00136	0.06490	0.00001	0.00129	0.00003	0.00019	0.00000	0.14600	-0.00001	0.000003
123	O2/195/001	-0.00122	-0.00080	-0.00230	0.03420	-0.00013	-0.00004	-0.00007	-0.00600	-0.00001	0.00624	0.01700	-0.000008
125	O2/195/003	-0.00122	-0.00080	-0.00230	0.17400	-0.00013	-0.00004	-0.00007	-0.00600	0.00001	0.00189	-0.00600	-0.000008
127	O2/195/005	-0.00001	0.00136	0.00525	0.25700	0.00002	0.00103	0.00007	0.00104	0.00001	0.00800	0.00001	0.000005
128	O2/196/001	-0.00122	-0.00080	-0.00230	0.18900	-0.00013	-0.00004	0.00016	-0.00600	-0.00001	0.00361	-0.00600	-0.000008
129	O2/196/002	-0.00005	-0.00080	0.01007	0.41400	0.00002	0.00004	0.00022	-0.00600	0.00100	0.09414	-0.00600	0.000421
130	O2/196/003	0.00007	-0.00080	0.00520	0.16000	0.00000	0.00011	0.00074	-0.00600	0.00660	0.03085	-0.00600	0.002515
131	O2/196/004	-0.00005	-0.00080	0.00167	0.10500	0.00001	0.00002	0.00011	-0.00600	0.00002	0.00283	0.00800	-0.000004
134	O2/196/007	-0.00001	0.00219	0.00058	0.20700	0.00000	0.00160	0.00004	0.00043	0.00001	0.01200	0.00001	0.000004
135	O2/196/008	-0.00005	-0.00080	0.00841	0.04630	0.00001	0.00037	0.00089	-0.00600	0.00412	0.01113	-0.00600	0.000732
136	O2/196/009	-0.00122	-0.00080	-0.00230	0.05350	-0.00013	0.00016	0.00080	-0.00600	0.00004	0.10456	-0.00600	-0.000008
142	O2/196/015	-0.00122	-0.00080	-0.00230	0.32000	-0.00013	0.00008	0.00313	-0.00600	0.00002	0.02557	0.00800	-0.000008
144	O2/196/017	-0.00001	0.00212	0.00144	0.09000	0.00000	0.00155	0.00073	0.00044	0.00001	0.04800	0.00004	0.000002
146	O2/196/019	-0.00094	-0.00080	0.00155	0.06110	-0.00004	0.00123	0.02245	-0.00600	0.00035	0.03540	-0.00600	0.000046
147	O2/196/020	-0.00094	-0.00080	0.00067	0.09690	-0.00004	-0.00003	0.00016	-0.00600	0.00001	0.00378	-0.00600	-0.000006
148	O2/196/021	-0.00122	-0.00080	-0.00230	0.15500	-0.00013	0.00005	0.00038	-0.00600	0.00013	-0.00123	-0.00600	0.000089
149	O2/196/022	-0.00094	-0.00080	0.00072	0.36900	-0.00004	-0.00003	0.00024	-0.00600	-0.00001	0.02209	-0.00600	0.000006
150	O2/196/023	-0.00094	-0.00080	0.00142	0.26500	-0.00004	0.00004	0.00250	-0.00600	0.00007	0.07272	0.00900	0.000017
151	O2/196/024	-0.00122	-0.00080	0.00506	0.12400	-0.00013	0.00083	0.00124	-0.00600	0.00059	0.91224	-0.00600	0.000460
152	O2/196/025	-0.00122	-0.00080	-0.00230	0.09770	-0.00013	0.00013	0.00119	-0.00600	0.00002	0.12237	-0.00600	-0.000008
153	O2/196/026	0.00005	-0.00080	0.00743	0.30400	0.00004	-0.00001	0.04275	-0.00600	0.00002	0.00346	-0.00600	0.000021
154	O2/196/027	0.00001	0.00132	0.00081	0.04470	0.00000	0.00099	0.00096	0.00029	0.00065	0.01800	-0.00001	0.000176
155	O2/196/028	0.00004	0.00204	0.00081	0.57600	0.00001	0.00213	0.00230	0.00054	0.00025	0.02000	0.00003	0.000051
162	O2/206/001	-0.00122	-0.00080	0.00243	0.07880	-0.00013	0.00009	0.00029	-0.00600	0.00132	0.00675	-0.00600	0.000283
163	O2/206/002	0.00001	0.00233	0.00361	0.07730	0.00000	0.00156	0.00039	0.00053	0.00001	0.03800	0.00001	0.000008
164	O2/206/003	-0.00001	0.00269	0.00032	0.05560	0.00000	0.00348	0.00002	0.00016	0.00000	0.00388	-0.00001	0.000002
166	O2/207/002	-0.00122	-0.00080	-0.00230	0.27800	-0.00013	-0.00004	0.00007	-0.00600	0.00001	-0.00123	0.00800	0.000009
167	O2/207/003	-0.00122	-0.00080	-0.00230	0.53200	-0.00013	-0.00004	0.00090	-0.00600	0.00014	-0.00123	-0.00600	0.000270
168	O2/207/004	-0.00122	-0.00080	-0.00230	0.16600	-0.00013	0.00099	0.00009	-0.00600	0.00006	0.67773	-0.00600	0.000020
172	O2/207/008	0.00018	0.00231	-0.00020	0.50200	0.00001	0.00184	0.01164	0.00062	0.00019	0.07700	0.00036	0.000055
174	O2/208/001	-0.00001	0.00241	0.00022	0.15700	0.00001	0.00228	0.00015	0.00020	0.00003	0.02400	0.00002	0.000020
175	O2/208/002	-0.00001	0.00196	0.00025	0.31000	0.00000	0.00147	0.00018	0.00037	0.00002	0.00700	0.00002	0.000011
176	O2/208/003	0.00001	0.00439	0.00048	0.04790	0.00001	0.00420	0.00005	0.00099	0.00016	0.02200	0.00004	0.000073
177	O2/217/001	0.00001	0.00245	0.00046	0.15300	0.00000	0.00180	0.00065	0.00057	0.00011	0.08400	-0.00001	0.000018
182	O2/218/003	-0.00001	0.00207	0.00057	0.08390	0.00001	0.00219	0.00021	0.00036	0.00004	0.00600	0.00003	0.000027
183	O2/218/004	0.00015	0.00127	0.00140	0.15400	0.00001	0.00102	0.01544	0.00037	0.00004	1.56000	0.00005	0.000020
185	O2/185/061	0.00009	0.00146	-0.00020	0.21111	0.00002	0.00145	0.00005	0.00135	0.00002	0.01862	0.00007	0.000023

Comments:

(1) all the data are in mg L^{-1} if other units are not indicated

(2) the symbol - before a number indicates below detection limit

(3) isotopic values in italic are from Carreira Paquete (1998)

Well Ref	UAVR_N	Ce	Pr	Nd	Sm	Eu	Gd	Tb	Dy	Ho	Er
6	O2/162A/006	0.000011	0.000001	0.000006	0.000003	0.000007	-0.000002	-0.000001	0.000001	-0.000001	-0.000001
7	O2/162A/007	0.000009	-0.000005	0.000018	-0.000007	-0.000004	-0.000008	-0.000003	-0.000009	-0.000001	-0.000005
11	O2/163/004	0.000011	-0.000001	-0.000004	0.000002	0.000003	-0.000002	-0.000001	-0.000001	-0.000001	-0.000001
12	O2/163/005	-0.000056	-0.000054	-0.000064	-0.000089	-0.000065	-0.000083	-0.000059	-0.000051	-0.000058	-0.000062
15	O2/163/008	0.000011	0.000001	0.000004	-0.000002	0.000002	-0.000002	-0.000001	-0.000001	-0.000001	-0.000001
17	O2/163/010	0.002012	0.000262	0.001069	0.000260	0.000051	0.000208	0.000026	0.000083	0.000012	0.000034
20	O2/173/001	0.000089	0.000011	0.000052	-0.000008	-0.000004	-0.000010	-0.000003	-0.000007	-0.000002	-0.000007
21	O2/173/002	0.000003	-0.000001	-0.000004	-0.000002	0.000001	-0.000002	-0.000001	-0.000001	-0.000001	-0.000001
22	O2/173/003	-0.000056	-0.000054	-0.000064	-0.000089	-0.000065	-0.000083	-0.000059	-0.000051	-0.000058	-0.000062
24	O2/174/002	0.000007	0.000003	0.000006	0.000003	0.000011	0.000003	-0.000001	0.000003	-0.000001	-0.000001
34	O2/174/012	-0.000056	-0.000054	-0.000064	-0.000089	-0.000065	-0.000083	-0.000059	-0.000051	-0.000058	-0.000062
36	O2/174/014	-0.000056	-0.000054	-0.000064	-0.000089	-0.000065	-0.000083	-0.000059	-0.000051	-0.000058	-0.000062
41	O2/174/019	-0.000056	-0.000054	-0.000064	-0.000089	-0.000065	-0.000083	-0.000059	-0.000051	-0.000058	-0.000062
44	O2/174/022	0.000003	-0.000001	-0.000004	0.000002	0.000017	-0.000002	-0.000001	0.000001	-0.000001	-0.000001
51	O2/184/001	0.000055	0.000007	0.000028	0.000007	0.000002	0.000005	0.000001	0.000004	0.000002	0.000002
52	O2/184/002	-0.000056	-0.000054	-0.000064	-0.000089	-0.000065	-0.000083	-0.000059	-0.000051	-0.000058	-0.000062
53	O2/184/003	0.000005	-0.000004	-0.000009	-0.000008	-0.000004	-0.000010	-0.000003	-0.000007	-0.000002	-0.000007
55	O2/184/005	0.000004	-0.000004	-0.000009	-0.000008	-0.000004	-0.000010	-0.000003	-0.000007	-0.000002	-0.000007
56	O2/184/006	-0.000005	-0.000005	-0.000013	-0.000007	-0.000004	-0.000008	-0.000003	-0.000009	-0.000001	-0.000005
57	O2/184/007	-0.000056	-0.000054	-0.000064	-0.000089	-0.000065	-0.000083	-0.000059	-0.000051	-0.000058	-0.000062
58	O2/184/008	0.000015	0.000004	-0.000009	0.000011	-0.000004	-0.000010	-0.000003	-0.000007	-0.000002	-0.000007
61	O2/184/011	0.000036	0.000005	0.000020	0.000005	0.000008	0.000004	-0.000001	0.000002	-0.000001	-0.000001
62	O2/184/012	0.000124	0.000016	0.000072	0.000020	0.000006	0.000019	0.000001	0.000009	0.000002	0.000003
65	O2/185/003	0.000007	-0.000004	-0.000009	-0.000008	-0.000004	-0.000010	-0.000003	-0.000007	-0.000002	-0.000007
67	O2/185/005	0.000012	-0.000004	-0.000009	-0.000008	-0.000004	0.000010	-0.000003	-0.000007	-0.000002	-0.000007
69	O2/185/007	0.000020	-0.000004	-0.000009	-0.000008	-0.000004	-0.000010	-0.000003	-0.000007	-0.000002	-0.000007
70	O2/185/008	0.000008	-0.000004	-0.000009	-0.000008	-0.000004	0.000010	-0.000003	-0.000007	-0.000002	-0.000007
73	O2/185/011	-0.000056	-0.000054	-0.000064	-0.000089	-0.000065	-0.000083	-0.000059	-0.000051	-0.000058	-0.000062
76	O2/185/014	-0.000002	-0.000001	-0.000004	-0.000002	0.000014	-0.000002	-0.000001	-0.000001	-0.000001	-0.000001
78	O2/185/016	0.000097	-0.000054	0.000084	-0.000089	-0.000065	-0.000083	-0.000059	-0.000051	-0.000058	-0.000062
79	O2/185/017	-0.000004	-0.000004	-0.000009	0.000016	-0.000004	-0.000010	-0.000003	-0.000007	-0.000002	-0.000007
80	O2/185/018	0.000007	-0.000004	-0.000009	-0.000008	-0.000004	-0.000010	-0.000003	-0.000007	-0.000002	-0.000007
81	O2/185/019	-0.000004	-0.000004	-0.000009	-0.000008	-0.000004	-0.000010	-0.000003	-0.000007	-0.000002	-0.000007
83	O2/185/021	0.000136	0.000017	0.000083	0.000009	-0.000004	0.000033	0.000004	0.000010	0.000006	0.000008
85	O2/185/023	0.000003	-0.000001	-0.000004	-0.000002	0.000004	-0.000002	-0.000001	-0.000001	-0.000001	-0.000001
86	O2/185/024	0.000019	0.000005	-0.000009	-0.000008	-0.000004	0.000012	-0.000003	-0.000007	-0.000002	-0.000007
87	O2/185/025	0.000005	-0.000004	-0.000009	-0.000008	-0.000004	-0.000010	-0.000003	-0.000007	-0.000002	-0.000007
89	O2/185/027	-0.000004	-0.000004	-0.000009	-0.000008	-0.000004	-0.000010	-0.000003	-0.000007	-0.000002	-0.000007
90	O2/185/028	0.000006	-0.000004	0.000012	-0.000008	-0.000004	-0.000010	-0.000003	-0.000007	-0.000002	-0.000007
91	O2/185/029	0.000014	-0.000004	-0.000009	-0.000008	-0.000004	-0.000010	-0.000003	-0.000007	-0.000002	-0.000007
92	O2/185/030	0.000005	-0.000004	-0.000009	-0.000008	-0.000004	-0.000010	-0.000003	-0.000007	-0.000002	-0.000007
93	O2/185/031	0.000013	0.000006	-0.000009	-0.000008	-0.000004	-0.000010	-0.000003	-0.000007	-0.000002	-0.000007
94	O2/185/032	-0.000056	-0.000054	-0.000064	-0.000089	-0.000065	-0.000083	-0.000059	-0.000051	-0.000058	-0.000062
95	O2/185/033	0.000042	0.000007	0.000017	-0.000008	-0.000004	-0.000010	-0.000003	-0.000007	-0.000002	-0.000007
96	O2/185/034	0.000021	0.000006	0.000014	-0.000008	-0.000004	-0.000010	-0.000003	-0.000007	-0.000002	-0.000007
101	O2/185/039	-0.000056	-0.000054	-0.000064	-0.000089	-0.000065	-0.000083	-0.000059	-0.000051	-0.000058	-0.000062
104	O2/185/042	0.000009	0.000003	0.000019	0.000005	0.000007	0.000005	-0.000001	0.000003	-0.000001	0.000002
105	O2/185/043	-0.000002	-0.000001	-0.000004	-0.000002	0.000016	-0.000002	-0.000001	-0.000001	-0.000001	-0.000001
111	O2/185/049	0.000009	-0.000001	0.000005	0.000002	0.000015	0.000002	-0.000001	-0.000001	-0.000001	-0.000001
113	O2/185/051	0.000003	-0.000001	-0.000004	-0.000002	0.000012	-0.000002	-0.000001	-0.000001	-0.000001	-0.000001
114	O2/185/052	0.000021	0.000038	0.000184	0.000042	0.000015	0.000041	0.000005	0.000022	0.000005	0.000015
116	O2/185/054	-0.000005	-0.000005	-0.000013	-0.000007	-0.000004	-0.000008	-0.000003	-0.000009	-0.000001	-0.000005
121	O2/185/059	0.000006	-0.000001	-0.000004	0.000002	0.000002	-0.000002	-0.000001	0.000002	-0.000001	-0.000001
122	O2/185/060	0.000004	0.000001	-0.000004	-0.000002	0.000010	-0.000002	-0.000001	-0.000001	-0.000001	-0.000001
123	O2/195/001	-0.000056	-0.000054	-0.000064	-0.000089	-0.000065	-0.000083	-0.000059	-0.000051	-0.000058	-0.000062
125	O2/195/003	-0.000056	-0.000054	-0.000064	-0.000089	-0.000065	-0.000083	-0.000059	-0.000051	-0.000058	-0.000062
127	O2/195/005	0.000009	0.000002	0.000006	-0.000002	-0.000001	0.000002	-0.000001	-0.000001	-0.000001	-0.000001
128	O2/196/001	-0.000056	-0.000054	-0.000064	-0.000089	-0.000065	-0.000083	-0.000059	-0.000051	-0.000058	-0.000062
129	O2/196/002	0.001182	0.000207	0.000956	0.000192	0.000044	0.000216	0.000032	0.000145	0.000033	0.000077
130	O2/196/003	0.006845	0.001554	0.009061	0.002339	0.000460	0.002480	0.000312	0.001554	0.000235	0.000653
131	O2/196/004	-0.000004	-0.000004	-0.000009	-0.000008	-0.000004	-0.000010	-0.000003	-0.000007	-0.000002	-0.000007
134	O2/196/007	0.000008	0.000001	-0.000004	-0.000002	0.000006	-0.000002	-0.000001	-0.000001	-0.000001	-0.000001
135	O2/196/008	0.002190	0.000609	0.003784	0.001104	0.000274	0.001357	0.000166	0.000794	0.000144	0.000378
136	O2/196/009	-0.000056	-0.000054	-0.000064	-0.000089	-0.000065	-0.000083	-0.000059	-0.000051	-0.000058	-0.000062
142	O2/196/015	-0.000056	-0.000054	-0.000064	-0.000089	-0.000065	-0.000083	-0.000059	-0.000051	-0.000058	-0.000062
144	O2/196/017	0.000004	-0.000001	-0.000004	-0.000002	0.000006	-0.000002	-0.000001	-0.000001	-0.000001	-0.000001
146	O2/196/019	0.000102	0.000009	0.000069	0.000012	-0.000004	0.000035	0.000005	0.000033	0.000009	0.000028
147	O2/196/020	-0.000005	-0.000005	-0.000013	-0.000007	-0.000004	-0.000008	-0.000003	-0.000009	-0.000001	-0.000005
148	O2/196/021	-0.000056	-0.000054	0.000102	-0.000089	-0.000065	-0.000083	-0.000059	-0.000051	-0.000058	-0.000062
149	O2/196/022	0.000007	-0.000005	-0.000013	-0.000007	-0.000004	-0.000008	-0.000003	-0.000009	0.000002	-0.000005
150	O2/196/023	0.000013	0.000008	0.000014	-0.000007	-0.000004	-0.000008	-0.000003	-0.000009	0.000002	-0.000005
151	O2/196/024	0.000488	0.000135	0.000556	0.000128	-0.000065	0.000166	-0.000059	0.000093	-0.000058	-0.000062
152	O2/196/025	-0.000056	-0.000054	-0.000064	-0.000089	-0.000065	-0.000083	-0.000059	-0.000051	-0.000058	-0.000062
153	O2/196/026	0.000033	0.000007	-0.000009	-0.000008	-0.000004	0.000011	-0.000003	-0.000007	-0.000002	-0.000007
154	O2/196/027	0.000199	0.000102	0.000555	0.000168	0.000046	0.000175	0.000026	0.000116	0.000021	0.000051
155	O2/196/028	0.000096	0.000019	0.000107	0.000041	0.000012	0.000047	0.000006	0.000029	0.000006	0.000017
162	O2/206/001	0.000358	0.000161	0.001058	0.000305	0.000072	0.000269	-0.000059	0.000173	-0.000058	0.000165
163	O2/206/002	0.000010	0.000001	0.000005	-0.000002	0.000002	0.000002	-0.000001	-0.000001	-0.000001	-0.000001
164	O2/206/003	0.000002	-0.000001	-0.000004	-0.000002	0.000003	-0.000002	-0.000001	-0.000001	-0.000001	-0.000001
166	O2/207/002	-0.000056	-0.000054	-0.000064	-0.000089	-0.000065	-0.000083	-0.000059	-0.000051	-0.000058	-0.000062
167	O2/207/003	0.000644	0.000098	0.000341	-0.000089	-0.000065	0.000089	-0.000059	-0.000051	-0.000058	-0.000062
168	O2/207/004	-0.000056	-0.000054	-0.000064	-0.000089	-0.000065	-0.000083	-0.000059	-0.000051	-0.000058	-0.000062
172	O2/207/008	0.000116	0.000017	0.000082	0.000025	0.000036	0.000028	0.000004	0.000021	0.000005	0.000013
174	O2/208/001	0.000048	0.000006	0.000025	0.000006	0.000003	0.000006	-0.000001	0.000003	-0.000001	0.000001
175	O2/208/002	0.000014	0.000003	0.000013	0.000004	0.000005	0.000004	-0.000001	0.000002	-0.000001	0.000002
176	O2/208/003	0.000090	0.000027	0.000125	0.000033	0.000014	0.000038	0.000005	0.000024	0.000004	0.000013
177	O2/217/001	0.000023	0.000007	0.000035	0.000011	0.000008	0.000013	0.000002	0.000011	0.000003	0.000008
182	O2/218/003	0.000067	0.000010	0.000046	0.000014	0.000008	0.000010	0.000002	0.000005	-0.000001	0.000003
183	O2/218/004	0.000019	0.000005	0.000017	0.000007	0.000005	0.000006	-0.000001	0.000005	0.000001	0.000003
185	O2/185/061	0.000051	0.000006	0.000021	0.000005	0.000004	0.000005	-0.000001	0.000002	-0.000001	0.000001

Comments:

(1) all the data are in mg L^{-1} if other units are not indicated

(2) the symbol - before a number indicates below detection limit

(3) isotopic values in italic are from Carreira Paquete (1998)

Well Ref	UAVR_N	Tm	Yb	Lu	^{18}O (‰)	^{2}H (‰)	^{13}C (‰)	^{14}C (pmc)	σ	NGT (ºC)	σ	He
6	O2/162A/006	-0.000001	-0.000001	-0.000001	-4.28	-22.7	-9.34					
7	O2/162A/007	-0.000003	-0.000004	-0.000001	-4.43	-25.7	-11.94	2.74				
11	O2/163/004	-0.000001	0.000001	-0.000001	-4.18	-24.6	-10.42					
12	O2/163/005	-0.000060	-0.000064	-0.000054	-4.43	-25.6	-13.90	3.50				
15	O2/163/008	-0.000001	-0.000001	-0.000001	-4.33	-20.7	-14.42					
17	O2/163/010	0.000003	0.000021	0.000003	-4.59	-23.8	-14.04					
20	O2/173/001	-0.000002	-0.000006	-0.000002	*-4.40*	*-23.3*	*-9.78*	*5.15*	*0.89*			
21	O2/173/002	-0.000001	-0.000001	-0.000001	-4.34	-26.2	-11.23	*1.84*	*0.34*	*8.5*	*0.4*	*1.06E-06*
22	O2/173/003	-0.000060	-0.000064	-0.000054	-4.09	-20.5	-10.24	1.93				
24	O2/174/002	-0.000001	-0.000001	-0.000001	-4.78	-26.0	-10.96					
34	O2/174/012	-0.000060	-0.000064	-0.000054	-4.69	-23.2	-11.79	3.68				
36	O2/174/014	-0.000060	-0.000064	-0.000054	-4.71	-25.6	-15.37					
41	O2/174/019	-0.000060	-0.000064	-0.000054	-5.05	-30.4	-13.53					
44	O2/174/022	-0.000001	-0.000001	-0.000001	-4.75	-25.3	-10.71					
51	O2/184/001	-0.000001	0.000001	-0.000001	-4.88	-25.6	-8.99					
52	O2/184/002	-0.000060	-0.000064	-0.000054	-5.04	-27.1	-12.02					
53	O2/184/003	-0.000002	-0.000006	-0.000002								
55	O2/184/005	-0.000002	-0.000006	-0.000002	*-4.52*	*-23.9*	*-9.63*	*3.39*	*0.50*	*9.0*	*0.7*	*1.38E-06*
56	O2/184/006	-0.000003	-0.000004	-0.000001	-4.63	-25.9	-12.36					
57	O2/184/007	-0.000060	-0.000064	-0.000054	-4.92	-27.0	-11.14					
58	O2/184/008	0.000003	-0.000006	-0.000002	*-4.71*	*-25.9*	*-9.87*	*0.91*	*0.31*	*9.3*	*0.5*	*1.43E-06*
61	O2/184/011	-0.000001	-0.000001	-0.000001	-4.52	-24.2	-10.70					
62	O2/184/012	-0.000001	0.000002	-0.000001	-4.47	-24.3	-10.27					
65	O2/185/003	-0.000002	-0.000006	-0.000002	*-4.46*	*-24.5*	*-14.00*	*9.52*	*2.92*	*9.2*	*0.4*	*3.93E-06*
67	O2/185/005	-0.000002	-0.000006	-0.000002								
69	O2/185/007	-0.000002	-0.000006	-0.000002	*-4.70*	*-24.6*	*-18.54*	*73.29*	*1.17*			
70	O2/185/008	-0.000002	-0.000006	-0.000002								
73	O2/185/011	-0.000060	-0.000064	-0.000054	-5.03	-26.7	-11.68					
76	O2/185/014	-0.000001	-0.000001	-0.000001	-4.40	-24.2	-10.13					
78	O2/185/016	-0.000060	-0.000064	-0.000054	-5.02	-27.8	-11.54					
79	O2/185/017	-0.000002	-0.000006	-0.000002	*-4.50*	*-25.3*	*-9.42*	*8.07*	*0.47*	*10.4*	*0.5*	*2.82E-07*
80	O2/185/018	-0.000002	-0.000006	-0.000002	*-4.44*	*-23.8*	*-9.94*	*7.29*	*0.69*			
81	O2/185/019	-0.000002	-0.000006	-0.000002	*-4.46*	*-24.2*	*-8.89*	*6.23*	*0.49*	*9.6*	*0.6*	*5.53E-07*
83	O2/185/021	-0.000002	0.000006	0.000002	*-4.84*	*-27.8*	*-14.75*	*43.63*	*0.44*	*14.2*	*0.6*	*7.39E-08*
85	O2/185/023	-0.000001	-0.000001	-0.000001	-4.52	-25.5	-10.21					
86	O2/185/024	-0.000002	-0.000006	-0.000002								
87	O2/185/025	-0.000002	-0.000006	-0.000002	*-4.70*	*-26.2*	*-15.30*	*37.14*	*0.66*	*13.2*	*0.7*	*2.13E-07*
89	O2/185/027	-0.000002	-0.000006	-0.000002								
90	O2/185/028	-0.000002	-0.000006	-0.000002								
91	O2/185/029	-0.000002	-0.000006	-0.000002	*-4.52*	*-24.5*	*-10.20*	*6.58*	*0.90*	*8.3*	*0.6*	*3.71E-06*
92	O2/185/030	-0.000002	-0.000006	-0.000002								
93	O2/185/031	-0.000002	-0.000006	-0.000002								
94	O2/185/032	-0.000060	-0.000064	-0.000054	-4.99	-28.7	-16.62	52.21				
95	O2/185/033	0.000002	-0.000006	-0.000002	*-4.44*	*-24.9*	*-9.79*	*6.87*	*0.74*			
96	O2/185/034	-0.000002	-0.000006	-0.000002	*-4.57*	*-25.1*	*-8.70*	*12.48*	*0.89*	*10.0*	*0.7*	*5.18E-07*
101	O2/185/039	-0.000060	-0.000064	-0.000054	-4.92	-25.3	-20.84					
104	O2/185/042	-0.000001	0.000002	-0.000001	-4.45	-23.1	-17.25					
105	O2/185/043	-0.000001	-0.000001	-0.000001	-4.82	-26.6	-7.32					
111	O2/185/049	-0.000001	-0.000001	-0.000001	-4.37	-27.4	-15.82					
113	O2/185/051	-0.000001	-0.000001	-0.000001	-4.56	-24.8	-11.62					
114	O2/185/052	0.000002	0.000015	0.000002	-4.24	-23.3	-17.49					
116	O2/185/054	-0.000003	-0.000004	-0.000001	-4.44	-22.0	-12.09					
121	O2/185/059	-0.000001	0.000001	-0.000001	-5.02	-28.4	-10.19					
122	O2/185/060	-0.000001	-0.000001	-0.000001	-4.80	-27.5	-18.57					
123	O2/195/001	-0.000060	-0.000064	-0.000054	-4.40	-24.7	-12.51	1.92				
125	O2/195/003	-0.000060	-0.000064	-0.000054	-4.84	-27.8	-11.86	7.28				
127	O2/195/005	-0.000001	0.000001	-0.000001	-4.77	-25.9	-11.32					
128	O2/196/001	-0.000060	-0.000064	-0.000054	-4.82	-26.1	-12.17					
129	O2/196/002	0.000005	0.000067	0.000008								
130	O2/196/003	0.000081	0.000469	0.000072								
131	O2/196/004	-0.000002	-0.000006	-0.000002	*-4.74*	*-25.7*	*-14.24*	*37.50*	*0.44*	*14.2*	*0.6*	*1.17E-07*
134	O2/196/007	-0.000001	-0.000001	-0.000001	-4.73	-24.1	-10.23					
135	O2/196/008	0.000045	0.000275	0.000040								
136	O2/196/009	-0.000060	-0.000064	-0.000054	-5.37	-28.9	-18.08					
142	O2/196/015	-0.000060	-0.000064	-0.000054	-5.11	-28.9	-13.66					
144	O2/196/017	-0.000001	-0.000001	-0.000001	-4.84	-24.7	-16.02					
146	O2/196/019	-0.000003	0.000007	-0.000001	-5.02	-24.9	-20.73					
147	O2/196/020	-0.000003	-0.000004	-0.000001	-4.98	-27.5	-15.32					
148	O2/196/021	-0.000060	-0.000064	-0.000054	-5.27	-33.0	-13.23					
149	O2/196/022	-0.000003	-0.000004	-0.000001	-4.75	-25.8	-11.12	28.15				
150	O2/196/023	-0.000003	-0.000004	-0.000001	-4.76	-27.6	-13.59					
151	O2/196/024	-0.000060	-0.000064	-0.000054	-4.81	-28.8	-17.60					
152	O2/196/025	-0.000060	-0.000064	-0.000054	-4.62	-22.9	-16.64					
153	O2/196/026	-0.000002	-0.000006	-0.000002								
154	O2/196/027	0.000007	0.000045	0.000007	-4.86	-27.5	-17.99					
155	O2/196/028	0.000002	0.000014	0.000002	-4.81	-26.9	-17.12					
162	O2/206/001	-0.000060	0.000177	-0.000054	-4.54	-26.3	-15.77					
163	O2/206/002	-0.000001	-0.000001	-0.000001	-4.70	-28.2	-17.64					
164	O2/206/003	-0.000001	-0.000001	-0.000001	-4.54	-25.3	-16.40					
166	O2/207/002	-0.000060	-0.000064	-0.000054	-4.80	-28.5	-13.43					
167	O2/207/003	-0.000060	-0.000064	-0.000054	-4.77	-28.5	-11.94	34.23				
168	O2/207/004	-0.000060	-0.000064	-0.000054	-4.76	-28.7	-25.02					
172	O2/207/008	0.000002	0.000014	0.000003	-4.25	-22.3	-14.52					
174	O2/208/001	-0.000001	0.000001	-0.000001	-5.60	-27.8	-16.67					
175	O2/208/002	-0.000001	0.000001	-0.000001	-4.77	-26.6	-10.20					
176	O2/208/003	0.000002	0.000012	0.000003	-4.85	-24.1	-18.69					
177	O2/217/001	0.000001	0.000010	0.000002	-4.62	-26.8	-13.58					
182	O2/218/003	-0.000001	0.000003	-0.000001	-4.80	-24.3	-15.25					
183	O2/218/004	-0.000001	0.000006	-0.000001	-4.20	-24.0	-13.51					
185	O2/185/061	-0.000001	0.000001	-0.000001	-4.75	-25.4	-14.35					

Comments:

(1) all the data are in mg L^{-1} if other units are not indicated

(2) the symbol - before a number indicates below detection limit

(3) isotopic values in italic are from Carreira Paquete (1998)

B.2 AVEIRO CRETACEOUS AQUIFER BASELINE VALUES

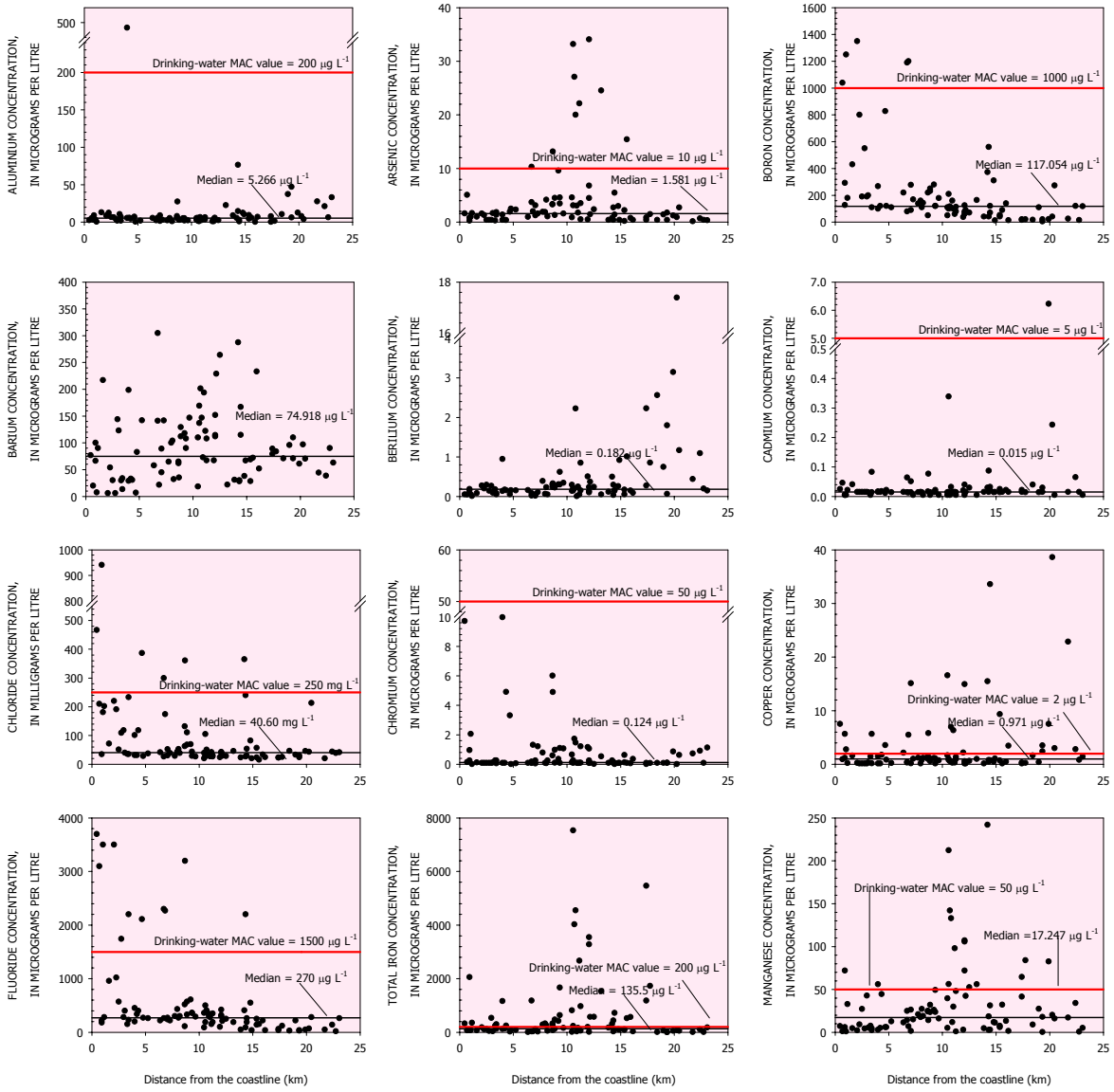

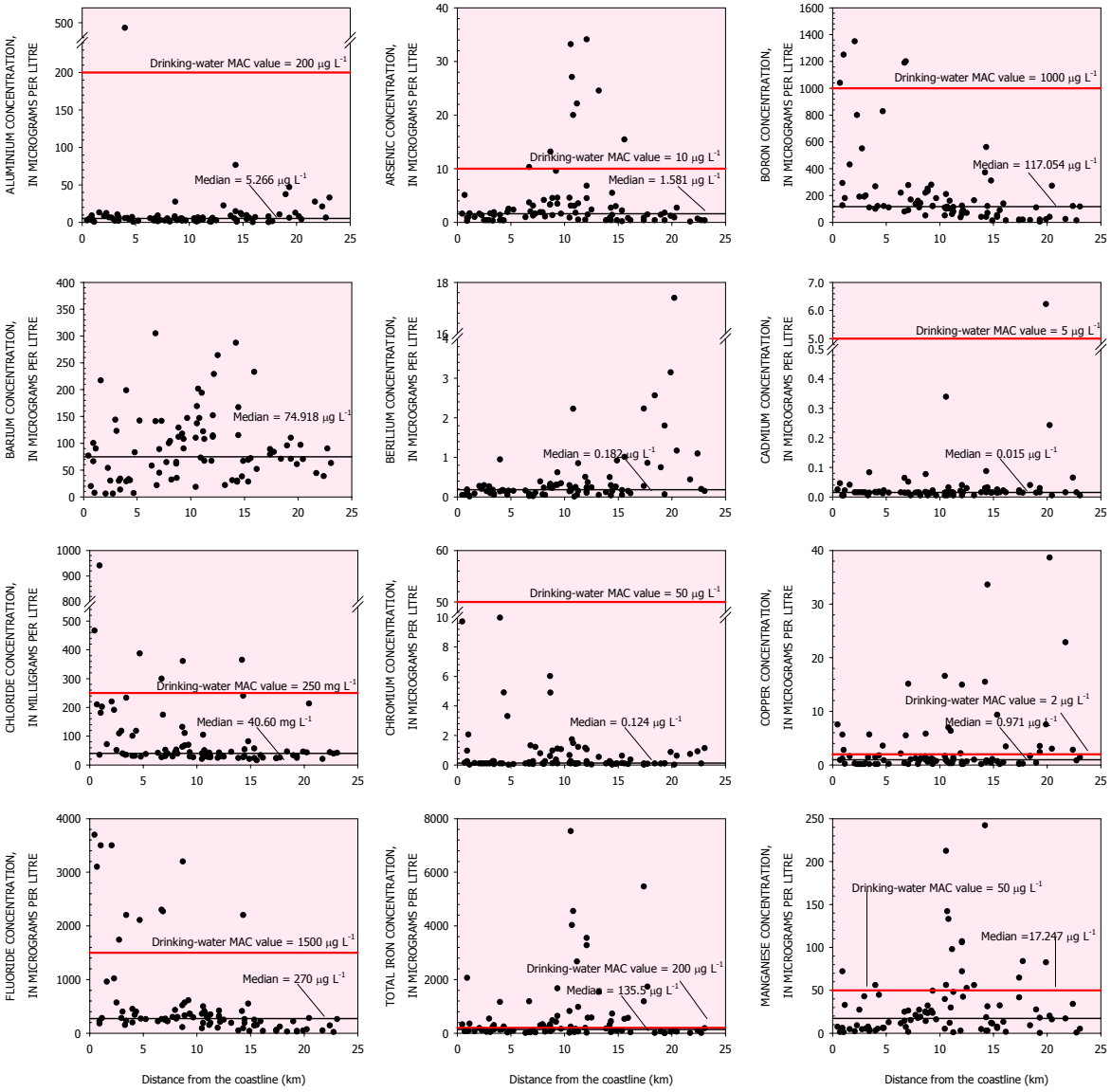
ALUMINIUM CONCENTRATION, IN MICROGRAMS PER LITRE
Drinking-water MAC value = 200 µg L-1
Median = 5.266 µg L-1
ARSENIC CONCENTRATION, IN MICROGRAMS PER LITRE
Drinking-water MAC value = 10 µg L-1
Median = 1.581 µg L-1
BORON CONCENTRATION, IN MICROGRAMS PER LITRE
Drinking-water MAC value = 1000 µg L-1
Median = 117.054 µg L-1
BARIUM CONCENTRATION, IN MICROGRAMS PER LITRE
Median = 74.918 µg L-1
BERILLIUM CONCENTRATION, IN MICROGRAMS PER LITRE
Median = 0.182 µg L-1
CADMIUM CONCENTRATION, IN MICROGRAMS PER LITRE
Drinking-water MAC value = 5 µg L-1
Median = 0.015 µg L-1
CHLORIDE CONCENTRATION, IN MILLIGRAMS PER LITRE
Drinking-water MAC value = 250 mg L-1
Median = 40.60 mg L-1
CHROMIUM CONCENTRATION, IN MICROGRAMS PER LITRE
Drinking-water MAC value = 50 µg L-1
Median = 0.124 µg L-1
COPPER CONCENTRATION, IN MICROGRAMS PER LITRE
Drinking-water MAC value = 2 µg L-1
Median = 0.971 µg L-1
FLUORIDE CONCENTRATION, IN MICROGRAMS PER LITRE
Drinking-water MAC value = 1500 µg L-1
Median = 270 µg L-1
TOTAL IRON CONCENTRATION, IN MICROGRAMS PER LITRE
Drinking-water MAC value = 200 µg L-1
Median = 135.5 µg L-1
MANGANESE CONCENTRATION, IN MICROGRAMS PER LITRE
Drinking-water MAC value = 50 µg L-1
Median =17.247 µg L-1
Distance from the coastline (km)
Distance from the coastline (km)
Distance from the coastline (km)

B.3 MODIFIED STIFF DIAGRAMS

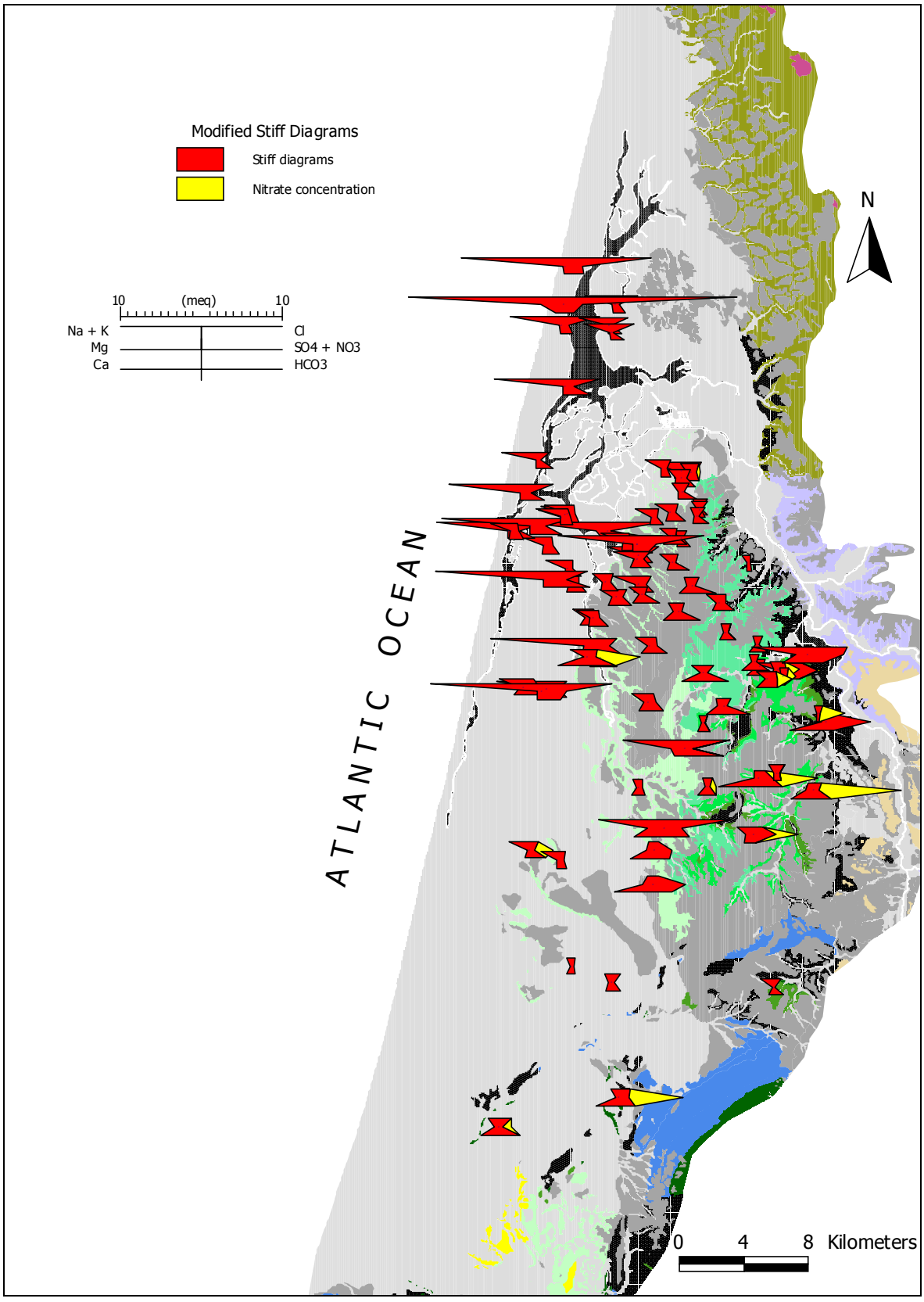

C

DEPTH SAMPLING CAMPAIGN

C.1 DEPTH SAMPLING CAMPAIGN IN THE AVEIRO CRETACEOUS AQUIFER

Seven non-equipped boreholes (#11, #15, #33, #51, #62, #140, #185) located across the study area were initially selected for the investigation of the aquifer vertical stratification, but only four of them were indeed depth-sampled. The rest had to be abandoned due to technical limitations of the equipment available. In borehole #140 (6RN Oiã) the static water level was initially at 50.2 mbd (metres below datum) but drew down to pump suction immediately before discharge appeared at the surface and could not therefore be pumped or sampled with the pumping equipment available. In borehole #33 (JK4 Cacia) and #11 (ACC01A Quintas do Sul) the pumps were still installed but had to be abandoned for pumping too much sand. However, in all these three boreholes was still possible to run some geophysical logs and in borehole #11 was even possible to collect a sample from discharge while initially pumping.

The four boreholes depth-sampled were #15 (ACCP5 Bestida), #51 (AC1 Gafanha da Encarnação), #62 (PS1 Gafanha da Nazaré) and #185 (JK12 Aveiro). These boreholes were first geophysically logged to characterise the aquifer formation, check borehole construction details (casing and wellscreen diameters and positions, and total depth), characterise the fluid vertical salinity and temperature, and to identify the relative productivity of individual aquifer layers and eventual vertical fluid movements.

The formation measurements made depended on the type of lining of the boreholes, and for instance, induction resistivity (IND) and magnetic susceptibility (MSUS) logs were just run in borehole #185 because it was the only one equipped with PVC casing. Most of the probes and pumps used during the geophysical and depth sampling campaign are shown in Fig. C.1.

Fig. C.1 Geophysical logging probes used for the depth sampling campaign in the Aveiro Cretaceous aquifer. From left to right: (1) French BRGM Romulus® magnetic susceptibility/induction resistivity probe; (2) Comprobe® Inc water sampler; (3) Focused resistivity/gamma ray probe; (4) Heat-pulse flowmeter probe (fitted with centralisers); (5) Caliper, NGAM, SP, point RES probe; (6) MLS single caliper; (7) SIE® single gamma ray (detector at base); (8 & 9) Sondex® inline spinner flowmeters (50mm, 30mm) and (10) Geovista® spinner flowmeter 75mm cage fitted.

The rest of the logs were run in all boreholes and included the fluid electrical conductivity (EC25, normalised to 25ºC) and temperature (TEMP) measurements that were made first downhole before any disturbance of the borehole fluid. Then, caliper (CAL), natural gamma (NGAM), point resistance (SPR) and spontaneous potential (SP) measurements that were made in a single log run and recorded whilst logging uphole. The impeller flowmeter measurements were made during both runs, down (DownlogQ) and uphole (UplogQ).

Once logged, boreholes were then pumped generally for up to 300 minutes, at rates ranging from 6.7–20 $m^3 h^{-1}$, long enough to purge the well, removing several well volumes. While pumping, salinity fluid electrical conductivity (ECQ25), temperature (TEMPQ) logs and impeller flowmeter measurements were repeated.

Discharge water was monitored for SEC, T, pH, Eh and DO, and sampled for chemical and isotopic analysis (Fig. C.2). Samples were also collected whilst pumping from depths chosen from interpretation of the fluid ECQ/TQ and flowmeter logging using a Comprobe® water sampler fitted, with a 2.5 L sample chamber. The samples were usually collected from just above or within identified producing wellscreens, to characterise the individual groundwaters.

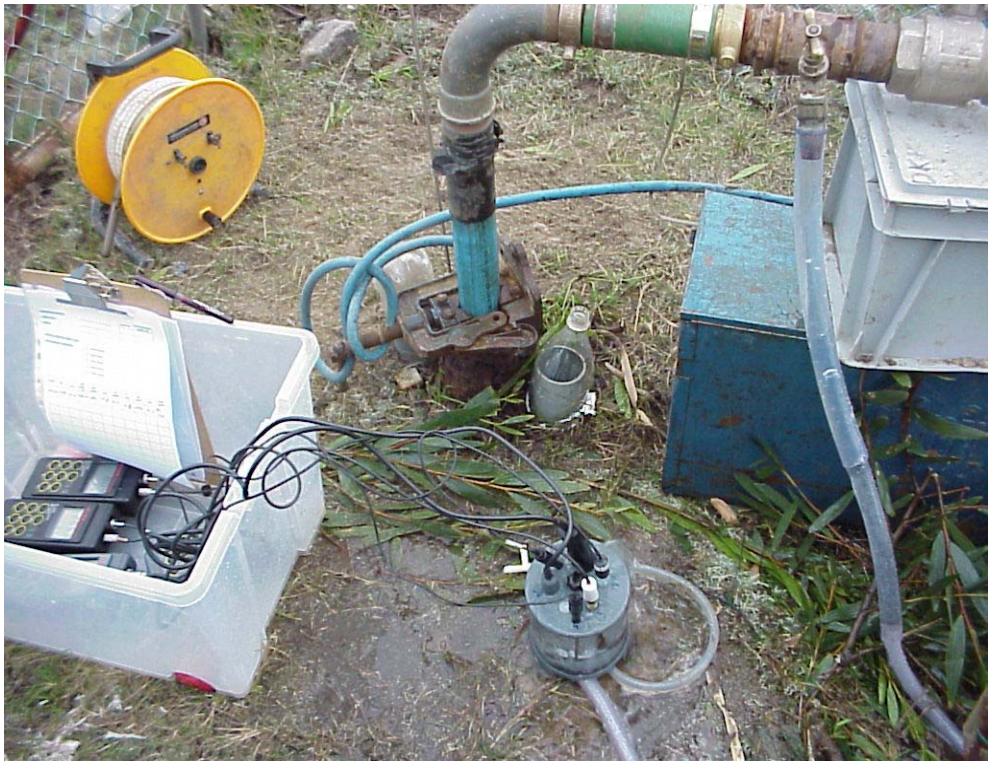

Fig. C.2 Monitoring of the principal field parameters (T, pH, SEC, Eh, DO) in the discharge water while carrying out the geophysical logging and depth sampling.

C.1.1 **Borehole #11 (ACC01A Quintas do Sul)**

Borehole ACC01A is located only a few hundred metres away from the coastline in the sand dunes and is the most northerly borehole of the study area. It was drilled in August 1981 up to 263 m and is part of a piezometer nest installed in the gravel pack in the open hole. There are two piezometers (88 m and 37 m deep, respectively) installed alongside the main borehole which penetrated Quaternary sediments (0-54 m), Cretaceous sediments (54-236 m) and entered basement schist from 236-263 m. Important to say that in this part of the aquifer the confining aquifer layer was not identified.

Measurements during drilling indicated fresher water in the Cretaceous sediments from 115 to 168 m (corresponding to the bottom of the 'Oiã sandstone formation' and to the "Furadouro sandstone formation"), and higher salinity from 182 to 226 m ('Palhaça sandstone formation'). The borehole was artesian after drilling and the head increased when drilled below 183 m, which indicates higher hydraulic heads in this layer, but these days is no longer artesian and the static water level (SWL) when logged (16/12/2000) was at –0.9 m below mean sea level.

Geophysical logs were run in the main borehole but the fluid EC/T probe could only run to 48.9 m where there was a blockage. The larger NGAM/CALIPER probe was run, with the caliper arms closed, to try to clear the blockage but only reached 53 m. A 75 mm diameter submersible pump was then installed to 24 m but pumped a large quantity of sand. Eventually, a 100 mm diameter submersible pump better able to cope with the sand was installed, and gradually cleared the borehole to 128 m, allowing the collection of a water sample from the discharge and the monitoring of the principal field parameters (Fig. C.3).

Fig. C.3 Borehole #11 (ACC01A Quintas do Sul) with the 100 mm diameter submersible pump installed to 24 m pumping a variable quantity of sand but able to gradually clear the borehole up to 128 m.

The flow sample obtained has a Na-Cl facies with a moderate salinity (SEC=1850 μS cm^{-1}), a chloride content of 467 mg L^{-1} but a total hardness of less than 35 mg L^{-1}. The groundwater pH is around 8.0 and temperature is 19.5ºC, which discards the hypothesis of being from the Quaternary aquifer. Eh negative values and DO null values also indicate totally anaerobic conditions. This sample shows some enrichment in trace elements such as Cr, F, Ni or Mo when compared to aquifer median values and is probably related to longer residence times. Fluoride gets as high as 3.70 mg L^{-1}, which is the highest value observed for the aquifer.

C.1.2 **Borehole #15 (ACCP5 Bestida)**

Borehole #15 (ACCP5 Bestida) is located in the north part of the study area at about 4.3 km from the coastline and is used as a piezometer for the National Groundwater Level Monitoring Network. It was drilled in August 1982 up to 180 m and penetrated Quaternary sediments (0-28 m), the Aveiro clays formation (28-52 m), 'Verba sandstone formation' (52-68 m), 'Oiã sandstone formation' (68-112 m), 'Furadouro sandstone formation' (112-146 m), 'Palhaça sandstone formation' (146-164 m) and entered Triassic sandstone formation from 164-180 m.

The caliper log shows Ø350 mm blank casing up to 60 m below which there is a dropset to Ø190 mm casing, screened in nine intervals: 89-93, 115-117, 121-123, 128-131, 134-140, 146-148, 150-153, 155-159 and 161.5-163.5 m (Fig. C.4). The static water level (SWL) was at 15.2 mbd, approximately 12.2 m below mean sea level in the region.

Fluid EC/TEMP logs ran prior to pumping show groundwater temperature increasing steadily from 16.5ºC at the initial metres to 20ºC at the deepest accessible part of the borehole. The fluid EC profile reveals high salinity water (>15,000 μS cm^{-1}) inside the blank casing from 30-60 m reducing to 3750 μS cm^{-1} at 91 m at wellscreen 1, and reaching a minimum of 600 μS cm^{-1} from 146 to 156 m, coinciding with the last three wellscreens. The high EC fluid at shallow depths must be a result of a leak at a joint in the blank casing (at 34 m as suggested by the caliper log) allowing high salinity water to enter from the Quaternary sediments and then diffusing along the borehole due to density settling.

The pumped fluid ECQ and TEMPQ logs were obtained while the borehole was pumped at 20 m^3 h^{-1} using a Ø150 mm submersible pump installed to 24 m. On pumping, the ECQ and TQ profiles indicate that most of the water movement up to the pump coming from the screens in front of the 'Furadouro sandstone formation' (wellscreen 5 and above). Eventually some inflow can also be identified from wellscreen 8 (155-159 m). The average pumping fluid ECQ was then 1125 μS cm^{-1}, and replaced quickly the high salinity waters (>15,000 μS cm^{-1}) observed in the blank casing before pumping.

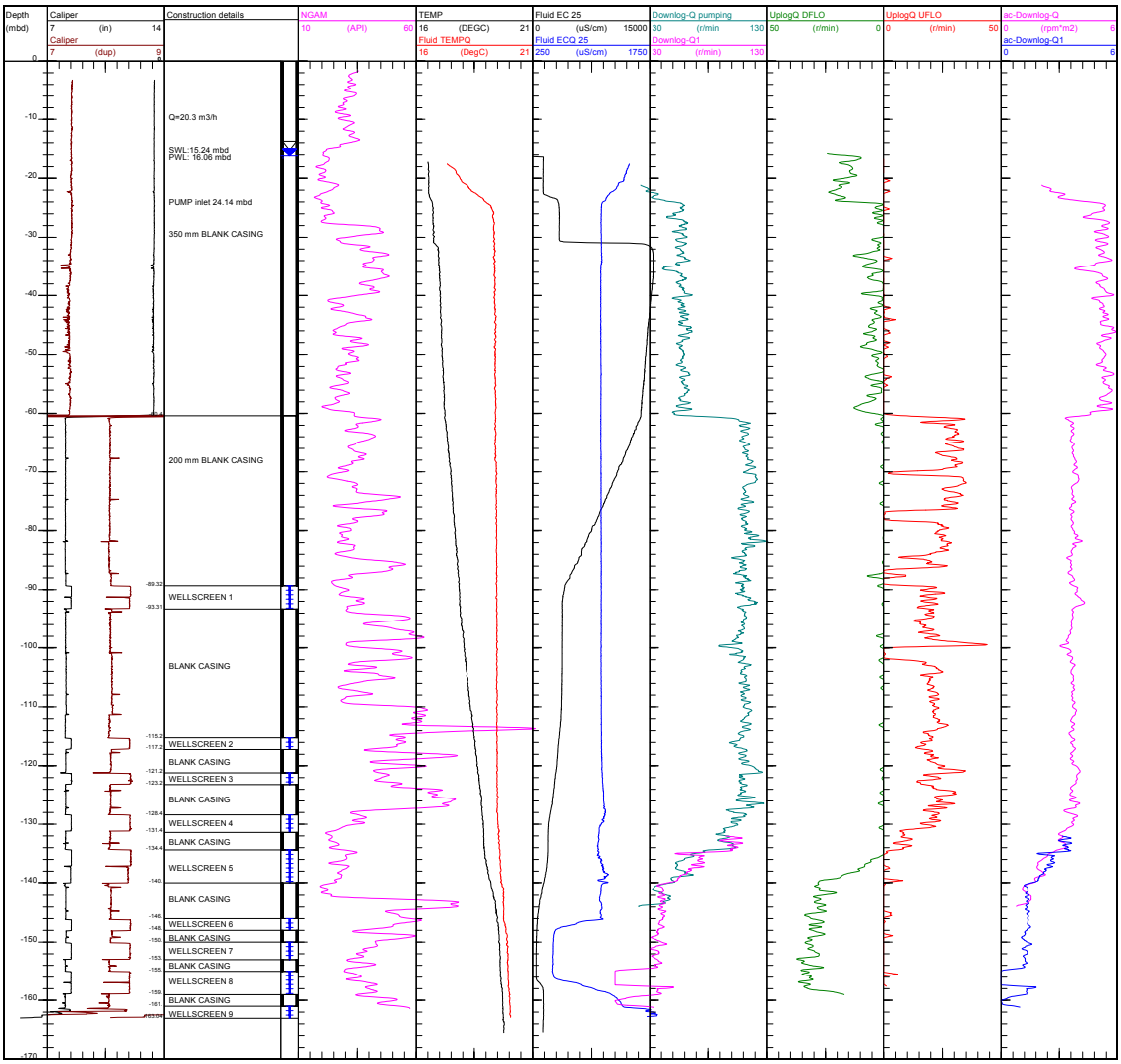

Fig. C.4 Geophysical and fluid logs for borehole #15 (ACCP5 Bestida).

While pumping, the depth samples were collected from three different depths. The first sample was collected at 40 m just after the supposed leaking joint, and so was expected to correspond to a mixture of Quaternary and Cretaceous groundwaters. The second sample was collected from 134 m, at the top of screen 5 where the main inflow has been identified, and should correspond to the water coming from the 'Furadouro sandstone formation'. The last and deepest sample was collected at 152 m where just a minimal inflow is recognised but in an attempt to get a sample representative of the 'Palhaça sandstone formation'. As a term for comparison, a sample was collected from the borehole discharge while pumping that should correspond to a depth of approximately 128 m. The major ions and stable isotopic compositions for the four samples collected are plotted in Fig. C.5.

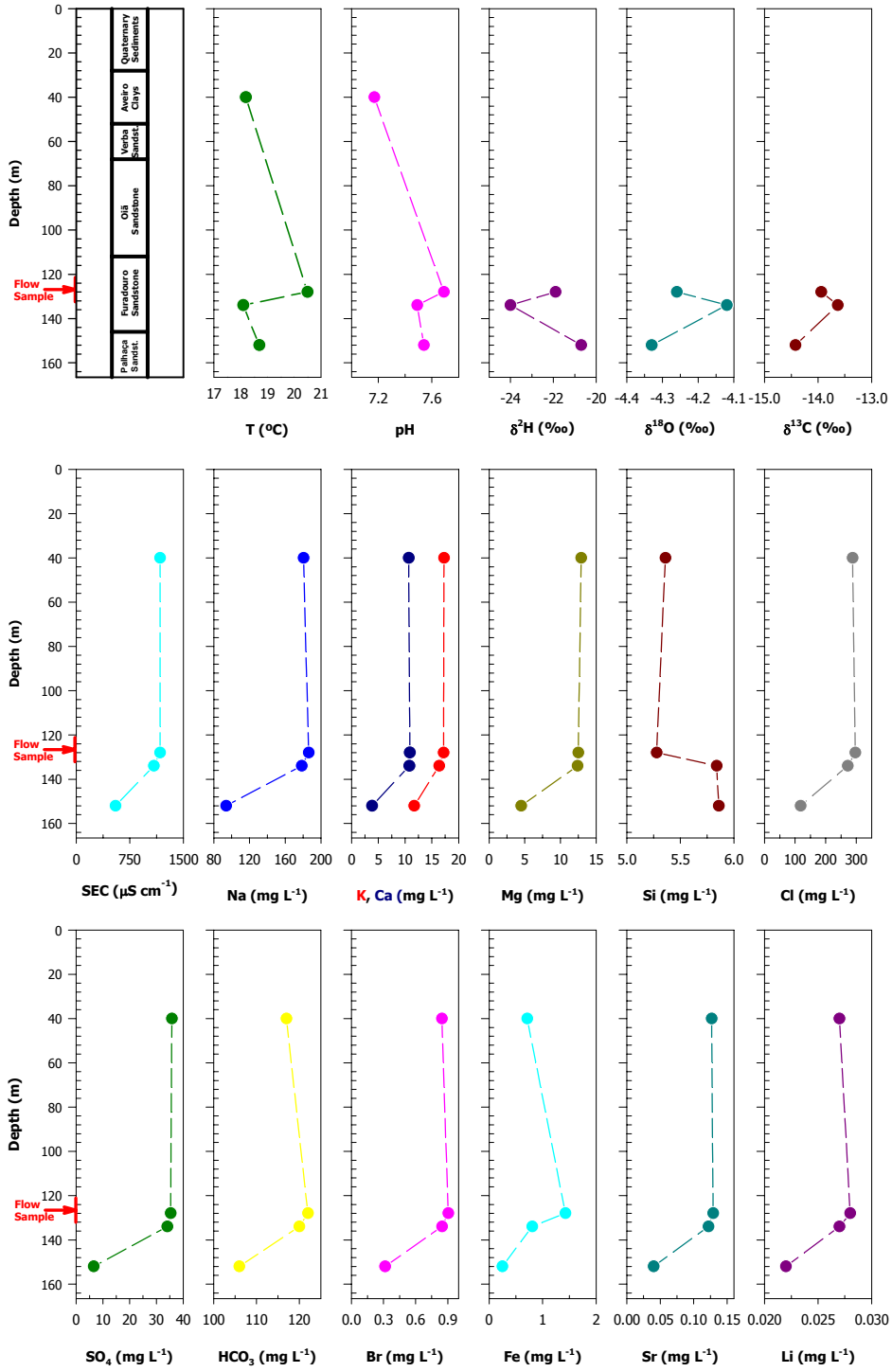

Fig. C.5 Variation in groundwater geochemical composition in depth samples and flow samples for borehole #15 (ACCP5 Bestida).

Groundwater sampled in the upper zone at –40 m is chemically identical to the one sampled at –134 m on the 'Furadouro sandstone formation', and to the pumped groundwater. These three samples are moderately fresh (SEC~1,100 µS cm^{-1}) but show chloride concentrations already higher than 270 mg L^{-1}, falling into the Na-Cl type waters. However, the fourth sample

collected at –154 m is of much lower salinity (with a SEC of 550 μS cm^{-1}, almost half of the average SEC value for the other samples) and chemically distinct from the others.

These results indicate: (1) that the very high salinity water from the Quaternary aquifer (SEC>15,000 μS cm^{-1}) that has been leaking into the borehole was replaced in the initial 60 metres by pumped groundwater; (2) this pumped water is a mixture of fresh Cretaceous aquifer water (~95%) and leaking water from the Quaternary aquifer (~5%), that penetrated into the most permeable aquifer layer, the 'Furadouro sandstone formation', due to favourable hydraulic heads. For this reason, pumped water and water sampled at 134 m has higher specific electrical conductance than the baseline values for the aquifer in the region (430 μS cm^{-1}).

For the pumping rates used, pumped groundwater is mostly supplied by wellscreen 6 and above, that is to say, by the 'Furadouro sandstone formation'. The isotopic signature of the water sampled at 134 m supports evidence of a relatively modern age coinciding with the local meteoric water line which confirms that there is mixture with Quaternary water. However, the flow sample shows some isotopic enrichment, which could indicate that the percentage of mixture with modern water is slightly less in this sample than in the depth sample. These samples have much higher iron contents and are enriched in most minor and trace elements when compared to the deeper sample.

Fresh Na-Cl type groundwater of an older generation appears to exist in the deeper aquifer layer. The sample collected down to 152 m is fresh groundwater (SEC~550 μS cm^{-1}) with chloride contents of 118 mg L^{-1}, less than half of the chloride content of the samples collected in the intermediate zone. It has also the particularity of showing very low SO_4^{2-}. Its isotopic signature shows an enrichment in deuterium relative to present modern recharge indicative of Late Pleistocene-Early Holocene waters. Unfortunately there are no ^{14}C determinations available to confirm the age. This aquifer layer also shows enrichment in some minor elements such as As, Be, Co, Ge and Si that could be due to increasing residence time and water-rock reaction.

C.1.3 **Borehole #51 (AC1 Gafanha da Encarnação)**

Borehole #51 (AC1 Gafanha da Encarnação) is located in a forested area, at about 3.4 km from the coast in the western part of the study area. This borehole was one of the first ones drilled in the aquifer in August 1962 and has always been used as observation well. It was drilled up to 228.30 m and penetrated Quaternary sediments (0-31 m), the Aveiro clays formation (31-164 m), "Verba sandstone formation" (164-204 m), 'Oiã sandstone formation' (204-228 m) but not reaching the most productive aquifer layers. This borehole is one of the very few that provide information about water flowing within the "Verba sandstone formation" (Fig. C.6).

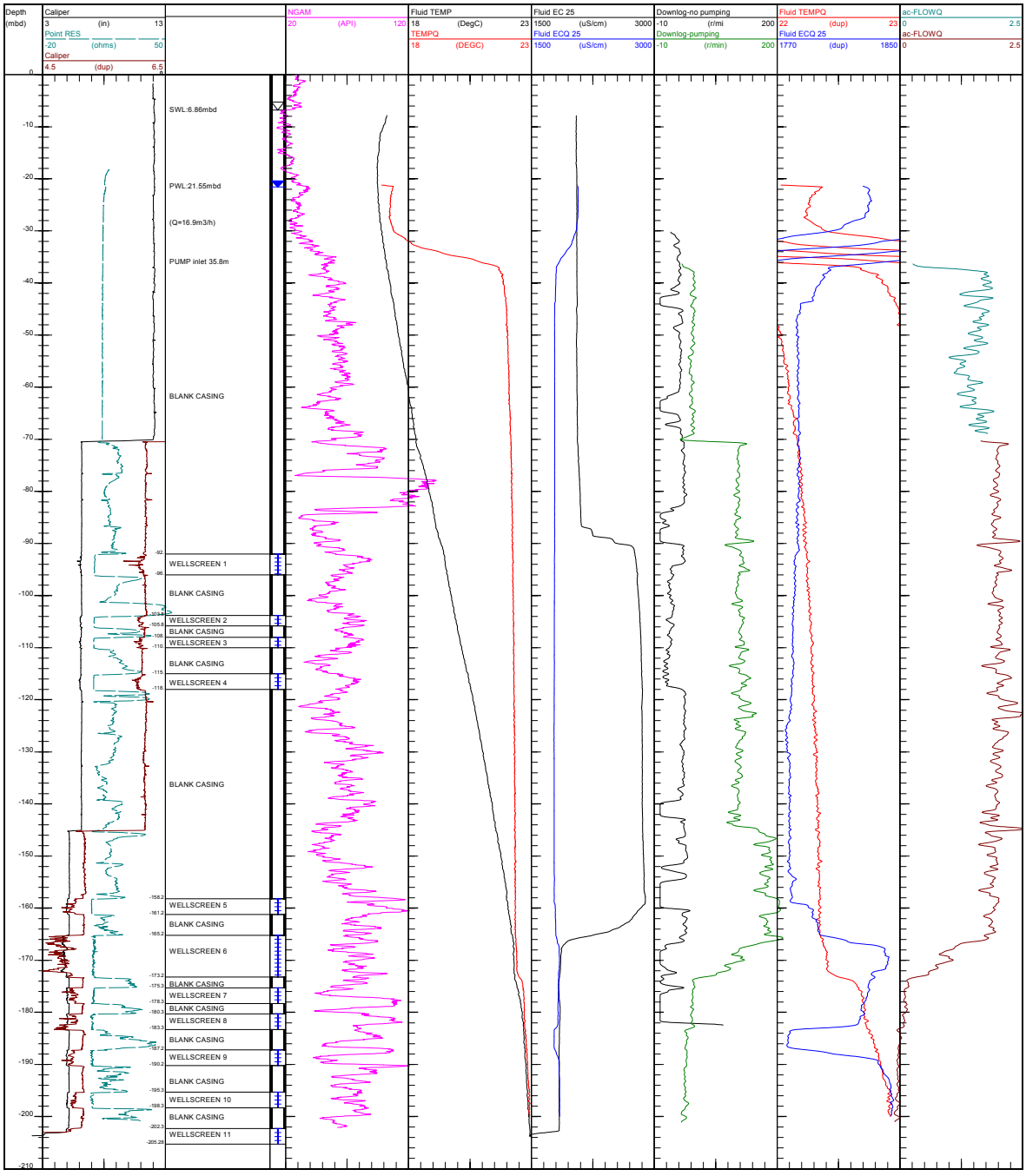

Fig. C.6 Geophysical and fluid logs for borehole #51 (AC1 Gafanha da Encarnação).

The caliper log shows a telescopic blank casing construction of Ø300 mm up to 70.7 m below which there is a dropset to Ø150 mm casing screened in nine intervals (92.3-96.3, 104.3-106.3, 108.3-110.3, 115.3-118.3, 158.3-161.3, 165.3-173.3, 175.3-178.3, 180.3-183.3, 187.3-190.3, 195.3-198.3 and 202.3-205.3 m). This borehole was artesian at the time it was drilled but nowadays the water level (SWL) is at 6.9 mbd, still 3 metres above mean sea level.

Fluid EC/TEMP logs ran prior to pumping show groundwater temperature increasing with depth from 16.8°C to 23°C, with a slightly cooler water from 165-173 m (wellscreen 6), corresponding to the principal inflow area. The fluid EC profile reveals a higher salinity water between 90-164 m (wellscreens 1 to 5), and lower salinity water below and above this region (~1600 μS cm^{-1}).

The pumped fluid ECQ and TQ logs were obtained while the borehole was pumped at 14.7 m^3 h^{-1} using a Ø100 mm submersible pump installed to 35.9 m. On pumping, the ECQ and TQ profiles indicate that most of the water movement up to the pump coming from wellscreens 6 (higher salinity) and 8 (lower salinity). The average pumping fluid ECQ is 1790 μS cm^{-1} and above 164 m is distributed uniformly along the borehole.

Two samples were collected from this borehole and are both representative of the upper aquifer layer, the "Verba sandstone formation", known by its high clay content and consequent low productivity. The first sample was collected from the discharge and should correspond to the water coming from the main inflow area at 166 m. A second sample was collected at 194 m, the bottom of "Verba sandstone formation" and where the EC and ECQ logs identified slightly higher salinity water.

The principal major and minor elements and some field parameters determined in the two collected samples are plotted in Fig. C.7 and confirm the higher salinity of the deeper sample. Both samples are Na-HCO_3-Cl type anoxic groundwaters with very similar chemical compositions, showing moderate chloride concentrations (~250 mg L^{-1}) but high HCO_3 (~430 mg L^{-1}) contents which is in agreement with a freshening water. The determined pH values are high (pH>8.1) and the waters are in equilibrium with calcite and potassium feldspar.

This aquifer layer shows enrichment in several minor elements such as Bi, Br, Cu, F, Mo, Ni, Rb, Sr, Th, Ti, Zn. when compared to baseline values. Fluoride concentrations are particularly high (>2.0 mg L^{-1}) exceeding clearly the maximum admissible concentration (MAC) for human consumption. This enrichment reflects the aquifer layer mineralogy and is a result of time-dependent water-rock interaction in this low permeability layer. Iron and manganese are present in low concentrations and are not a water quality constraint.

Considering the observed unusual depletion in both ^{18}O and ^{2}H with respect to modern waters observed in both samples it is probable that they postdate glaciation and may have been recharged by infiltrating rainfall that for some reason reflected isotopically depleted glacial meltwater. These groundwaters also show some enrichment in $\delta^{13}C$ due to water-rock interaction.

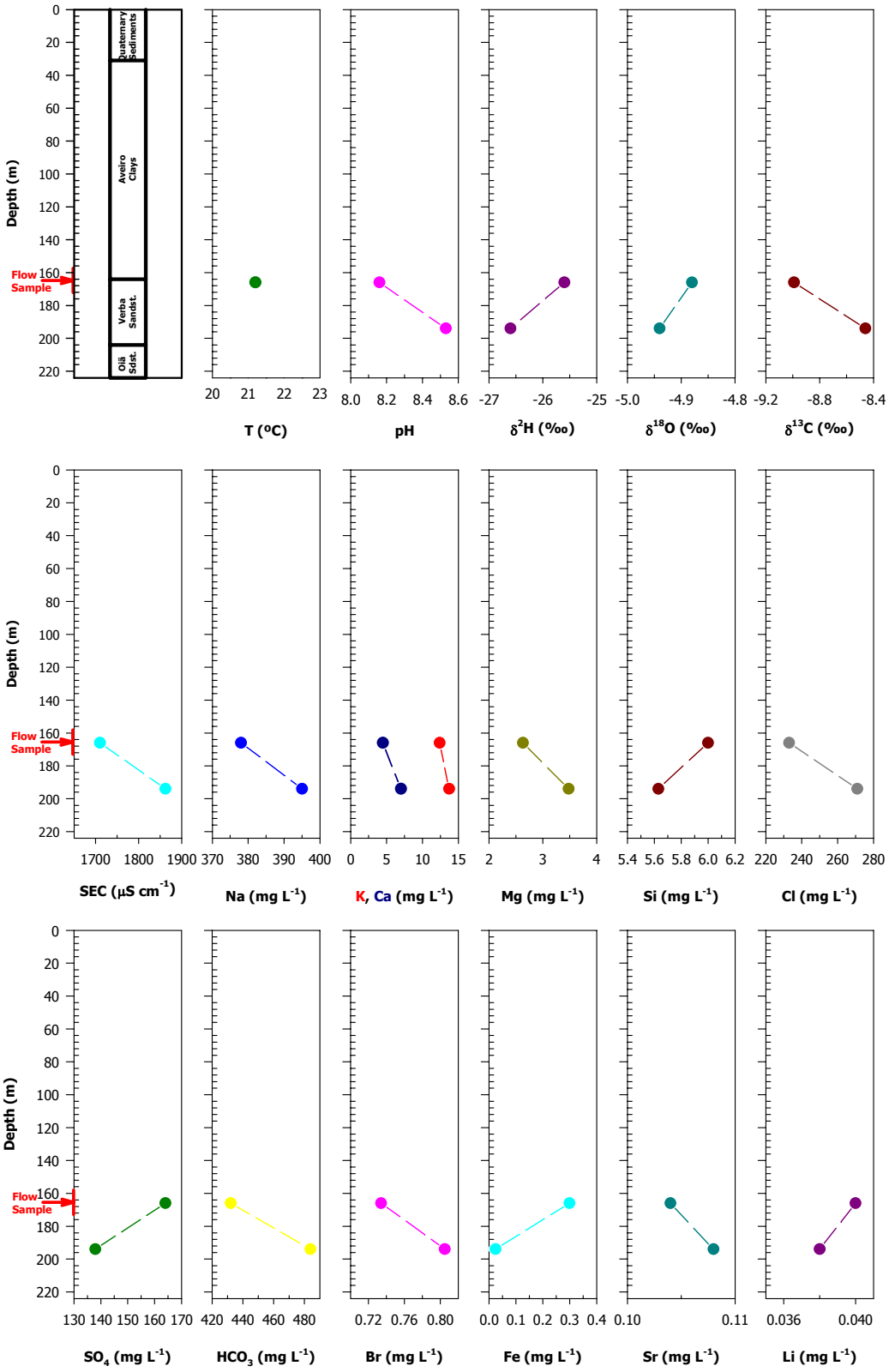

Fig. C.7 Variation in groundwater geochemical composition in depth and flow samples for borehole #51 (AC1 Gafanha da Encarnação).

C.1.4 **Borehole #62 (PS1 Gafanha da Nazaré)**

Borehole #62 (PS1 Gafanha da Nazaré) is located in an industrial area next to Aveiro harbour about 3.3 km from the coastline. This borehole was drilled on September 2000, just three months before the logs were run. It was drilled up to 276 m and penetrated Quaternary sediments (0-53 m), the Aveiro clays formation (53-146 m), 'Verba sandstone formation' (146-194 m), 'Oiã sandstone formation' (194-216 m), 'Furadouro sandstone formation' (216-238 m), 'Mamarrosa limestone formation' (238-246 m) and in the deepest part, the 'Palhaça sandstone formation' (246-276 m).

The caliper logs indicates a blank casing up to 93.50 m, with a Ø300 mm in the initial 51 m and of Ø250 mm in the following 42.2 m. At 93.50 m there is a dropset to Ø200 mm casing screened in seven intervals (202-205, 217.5-220.5, 221-224, 242.5-244.5,255-256, 256.5-259.5, 261-262, 262.5-265.5 and 267-269 m) as shown in Fig. C.8.

The static water level was at 22.5 mbd and to save time it was decided not to run a EC/TEMP log before pumping. Two submersible pumps were placed at 35 m and pumped at a combined rate of 15.0 $m^3 h^{-1}$.

The fluid ECQ25 log displays a uniform ECQ of 420 $\mu S\ cm^{-1}$ from 200 m up to the pump. Changes in ECQ can be identified alongside most of the wellscreens, although in greater extent along wellscreens 4, 3, 2 and 1. Flowmeter profiles recorded whilst pumping indicate the major inflow at 220–225 depth, from wellscreens 2 and 3 in the Furadouro sandstone, and a minor inflow from wellscreen 5 in the Palhaça sandstone.

During the pumping, water samples were collected from the discharge and depth samples were collected from 194 m (above wellscreen 1), 210 m (below wellscreen 1), 230 m (below the main inflow from wellscreen 3) and from 250 m (the contribution below wellscreen 4). The chemical and isotopic results obtained are plotted in Fig. C.9.

The four groundwater samples have a Na-HCO_3 water type indicative that calcium is taken up by cation exchange from water, in return for sodium, and that any remaining seawater is being flushed by fresh water. This evidence is confirmed by the low salinity of the samples (SEC<440 $\mu S\ cm^{-1}$) with chloride contents lower than 40 $mg\ L^{-1}$, which is remarkably low for a coastal aquifer.

There is not a significant vertical stratification of the aquifer water quality but small differences can be inferred from Fig. C.9. The sample corresponding to the 'Furadouro sandstone formation' has slightly lower SO_4^{2-} and a Cl- concentration than the others, but on the contrary shows higher Ca^{2+}, Mg^{2+}, HCO_3^- and Li^+ concentrations in solution. Also, total Fe is almost two times higher that in the waters flowing in the other aquifer layers, exceeding even the VMA value for human consumption.

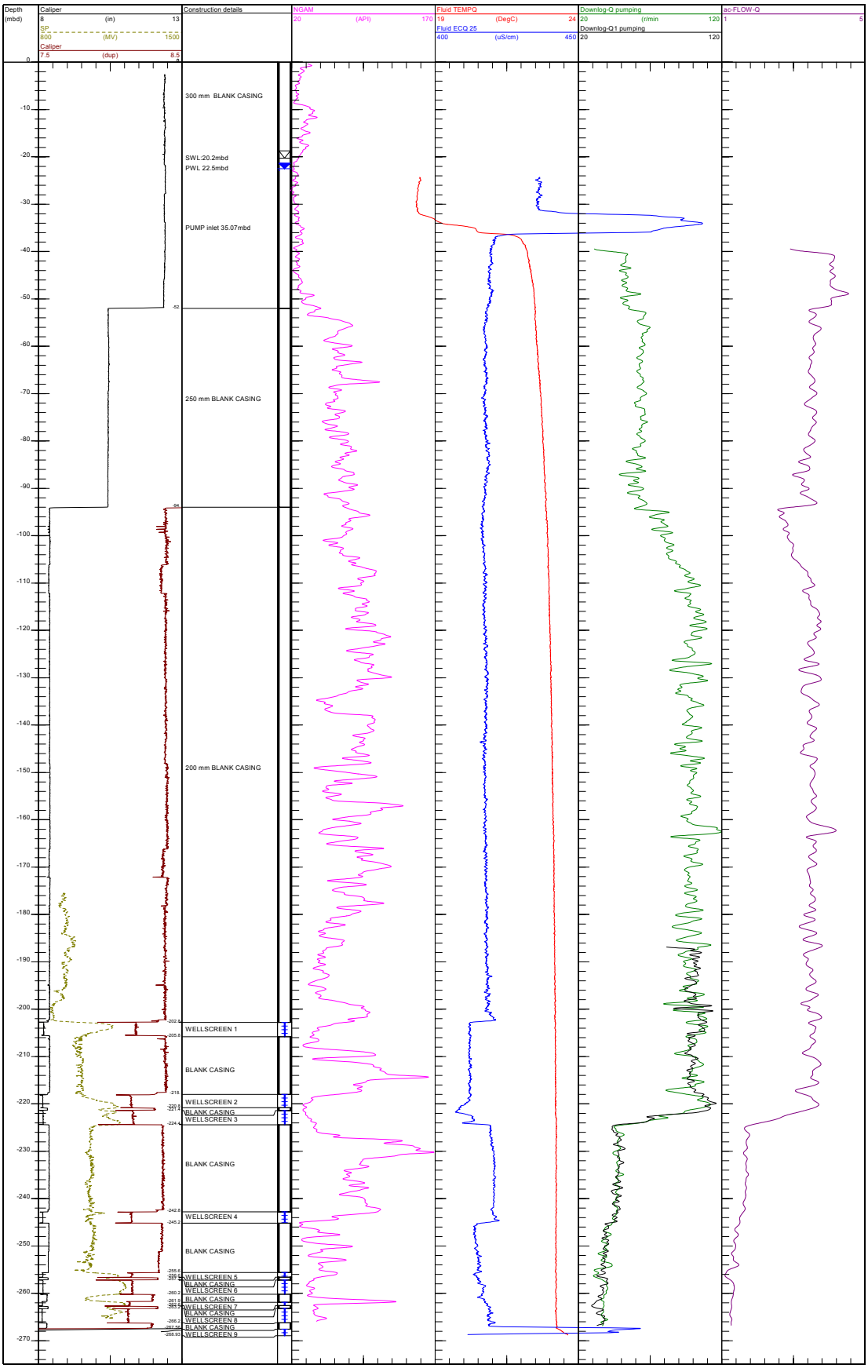

Fig. C.8 Geophysical and fluid logs for borehole #62 (PS1 Gafanha da Nazaré).

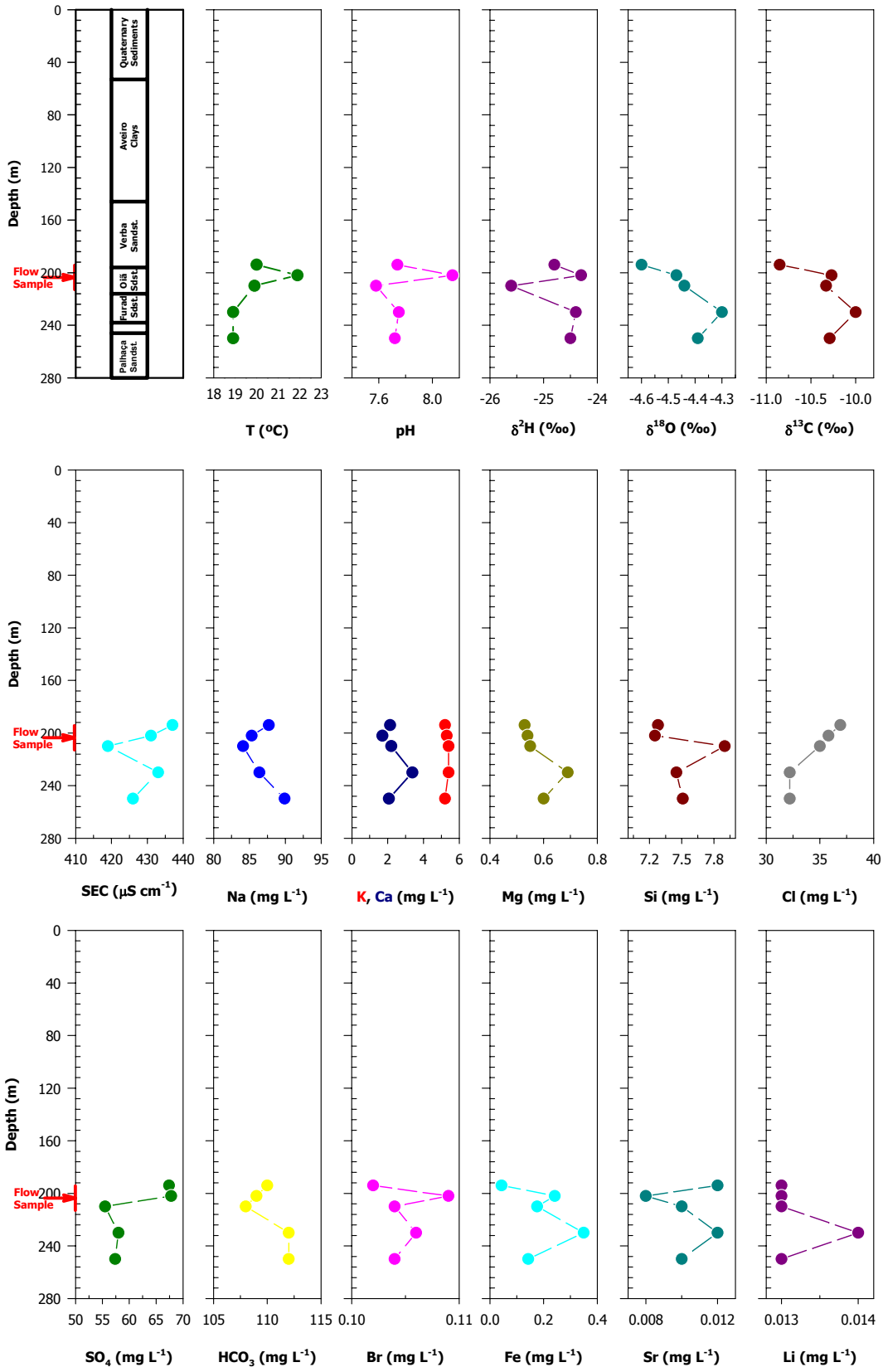

Fig. C.9 Variation in groundwater geochemical composition in depth and flow samples for borehole #62 (PS1 Gafanha da Nazaré).

Comparing now the average concentrations obtained for this borehole with the aquifer background values it is observed that Na^+ and SO_4^{2-} are present in higher concentrations than the aquifer baseline values, respectively 54.5 and 46 mg L^{-1}. On the contrary, calcium has been almost removed from solution with average concentrations of less than 3.5 mg L^{-1}. Silicon also shows a notable enrichment indicative that silicate weathering processes are important for the whole chemistry of the aquifer.

Determined isotopic contents are just slightly enriched when compared to modern recharge, and the deeper samples representative of the more permeable formations (Furadouro and Palhaça sandstone) almost coincide with the local meteoric water line, which could indicate shorter residence times than those from the 'Oiã sandstone formation'. These waters must be Holocene waters coming from the most permeable aquifer layers though the most exploited.

C.1.5 **Borehole #185 (JK12 Aveiro)**

Borehole JK12 was drilled on August 1999 in a Municipal Pumping Station located in Aveiro next to another two production boreholes drilled in 1975 (JK3) and in 1991 (JK9). It has just been used so far as an observation borehole because for some reason is pumping water with more than 400 mg L^{-1} of chloride.

The borehole was drilled up to 240 m and penetrated Quaternary sediments (0-9.5 m), the Aveiro clays formation (9.5-76 m), 'Verba sandstone formation' (76-118 m), 'Oiã sandstone formation' (118-145 m), 'Furadouro sandstone formation' (145-170 m), 'Mamarrosa limestone formation' (170-178 m) and in the deepest part, the 'Palhaça sandstone formation' (>178 m). It is equipped with PVC blank (0-130 m) and slotted casing.

Caliper log shows the design is telescopic without any change in diameter alongside the reported slotted intervals, and the joints are at 4 m intervals. It is noted that the screen positions thus identified are approximately 4 m lower than indicated in the completion record (145-148, 154-159, 163-167, 180-184, 186-190, 196-204, 210-215) and might represent a simple error in the recording of the casing lengths (Fig. C.10).

The fluid TEMP, EC25 and flowmeter measurements were made prior to pumping. The fluid TEMP log shows coolest water (~18^{o}C) at the water level (45.3 mbd), increasing with depth down to 156 m below which there is a constant temperature (22^{o}C) till the bottom (220 m). The pre-pumping flowmeter log reveals up-flow taking place from 220-156 m (from wellscreen 7 to wellscreen 2) and inflow at wellscreen 4 and 5.

The fluid EC25 log reveals that the inflows alongside these two wellscreens in the Palhaça sandstone increase the fluid EC from 1250 μS cm^{-1} to 3600 μS cm^{-1}. This relatively high EC fluid

exits the borehole at 156 m via wellscreen 2 in the Furadouro Sandstone, where it is presumably drawn into an adjacent abstraction borehole. Above wellscreen 2 the fluid EC reduces to 1200 μS cm^{-1} and then to ~800 μS cm^{-1} alongside wellscreen 1.

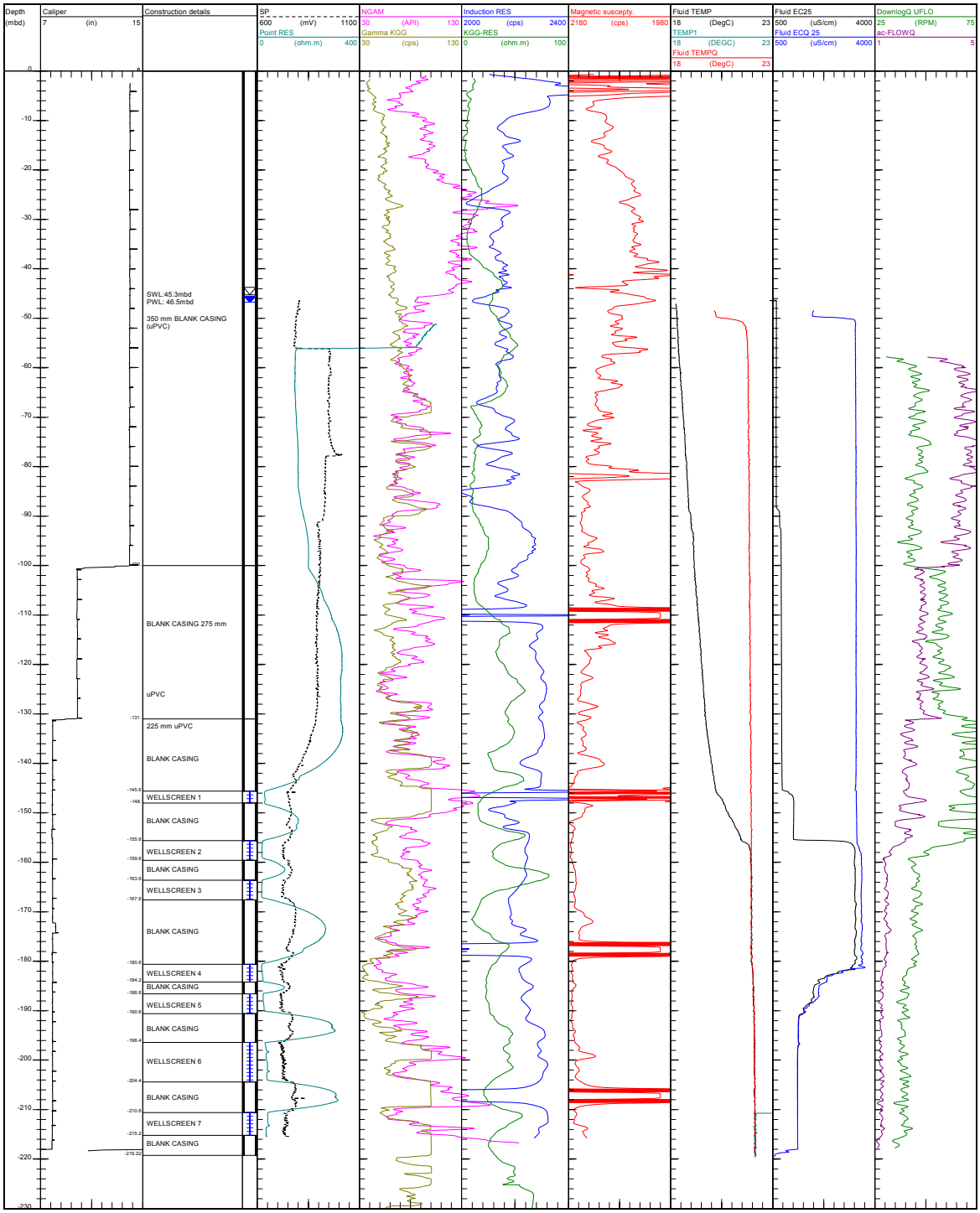

Fig. C.10 Geophysical and fluid logs for borehole #185 (JK12 Aveiro).

Two pumps were installed to 50 m and the borehole was pumped at 10 $m^3 h^{-1}$, when fluid ECQ, fluid TQ and impeller flowmeter and thermal flowmeter logs were run. The impeller flowmeter log reveals the main inflow is at 156 m (Furadouro sandstone aquifer layer) and in the fluid ECQ logs two other inflows at 181 m (wellscreen 4) and at 190 m (wellscreen 5) can also be confirmed.

On pumping the fluid temperature below 156 m did not change because the water was already flowing upwards over this interval. Above 156 m the fluid temperature remained similar (~22^0C) right up to the pump suction. Similarly the ECQ profile did not change below 156 m but showed a slight reduction at wellscreen 2 and continued up to the pump at ~3300 $\mu S\ cm^{-1}$. The logs show the source of this relatively high EC water is at wellscreen 4 and 5 within the Palhaça sandstone unit. The ECQ25 log indicates the fluid EC of water pumped from the borehole is ~3300 $\mu S\ cm^{-1}$.

While pumping, groundwater samples were collected from the discharge and at different depths, at 150 m (above wellscreen 1), 168 m (below wellscreen 3) and at 200 m (the contribution below wellscreen 6 and to differentiate the chemical composition of the bottom and top of the 'Palhaça sandstone formation'). The principal chemical and isotopic results obtained are plotted in Fig. C.11.

The four samples are Na-Cl type waters but three of them have high salinity (SEC>3,000 $\mu S\ cm^{-1}$) and chloride contents of ~850 mg L^{-1} while the deeper one, is moderately fresh groundwater with chloride contents of ~360 mg L^{-1}. The typical chloride values in this area should be around 100 mg L^{-1} but the high salinity upflow is completely altering the aquifer background. Due to their higher salinity these samples are enriched in most of the minor and trace elements when compared to aquifer background values, with several elements such as As, Cu, F, Fe, Mn and Ni exceeding the MAC values for human consumption.

High salinity waters are coming into the borehole through the screens positioned in front of the top part of 'Palhaça sandstone formation'. This aquifer layer is usually less exploited than the overlaying Furadouro sandstone unit and for this reason has these days higher groundwater potentials that may create favourable conditions for upflow to occur from one aquifer layer to the other, leading to the vertical mixing of water of different qualities.

The identified salinity in this borehole could probably be reduced if the borehole is sealed below 180 depth (below wellscreen 4) and the fluid ECQ in both the observation borehole and the abstraction borehole should be improved. However, unless there are clay seals placed in the gravel pack to prevent water movement, the higher salinity water could simply move up the gravel pack annulus to be drawn across to the abstraction borehole. Despite this action, it would be advisable to seal the other adjacent deactivated boreholes.

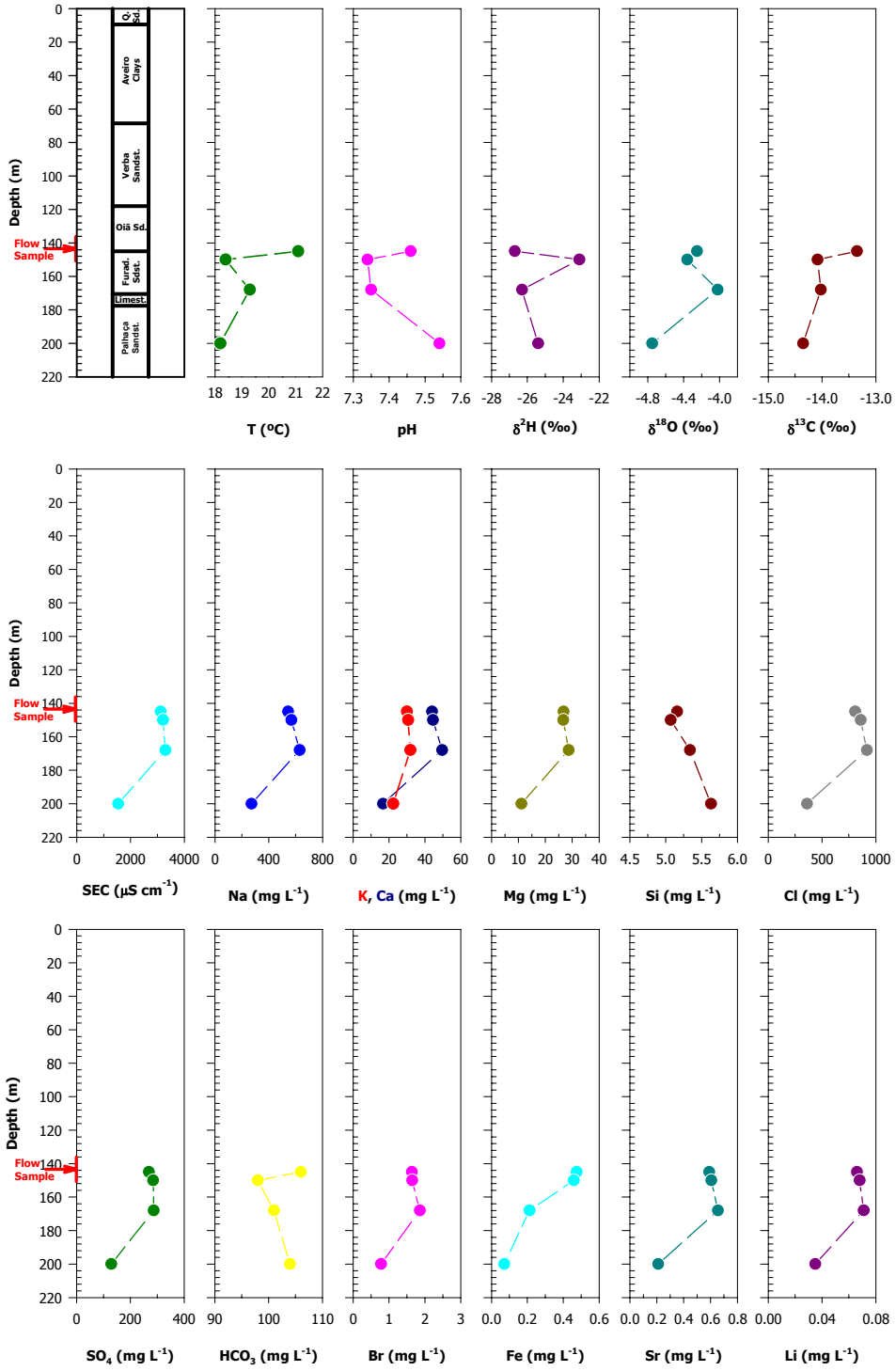

Fig. C.11 Variation in groundwater geochemical composition in depth and flow samples for borehole #185 (JK12 Aveiro).

Isotopically, all the samples show a slight isotopic enrichment. The older sample seems to be the one sampled at the bottom of the 'Furadouro sandstone formation'. It is isotopically enriched compared to the present LMWL and to the other samples, corresponding probably to Late Pleistocene-Early Holocene water.

D

CONTOUR MAPS

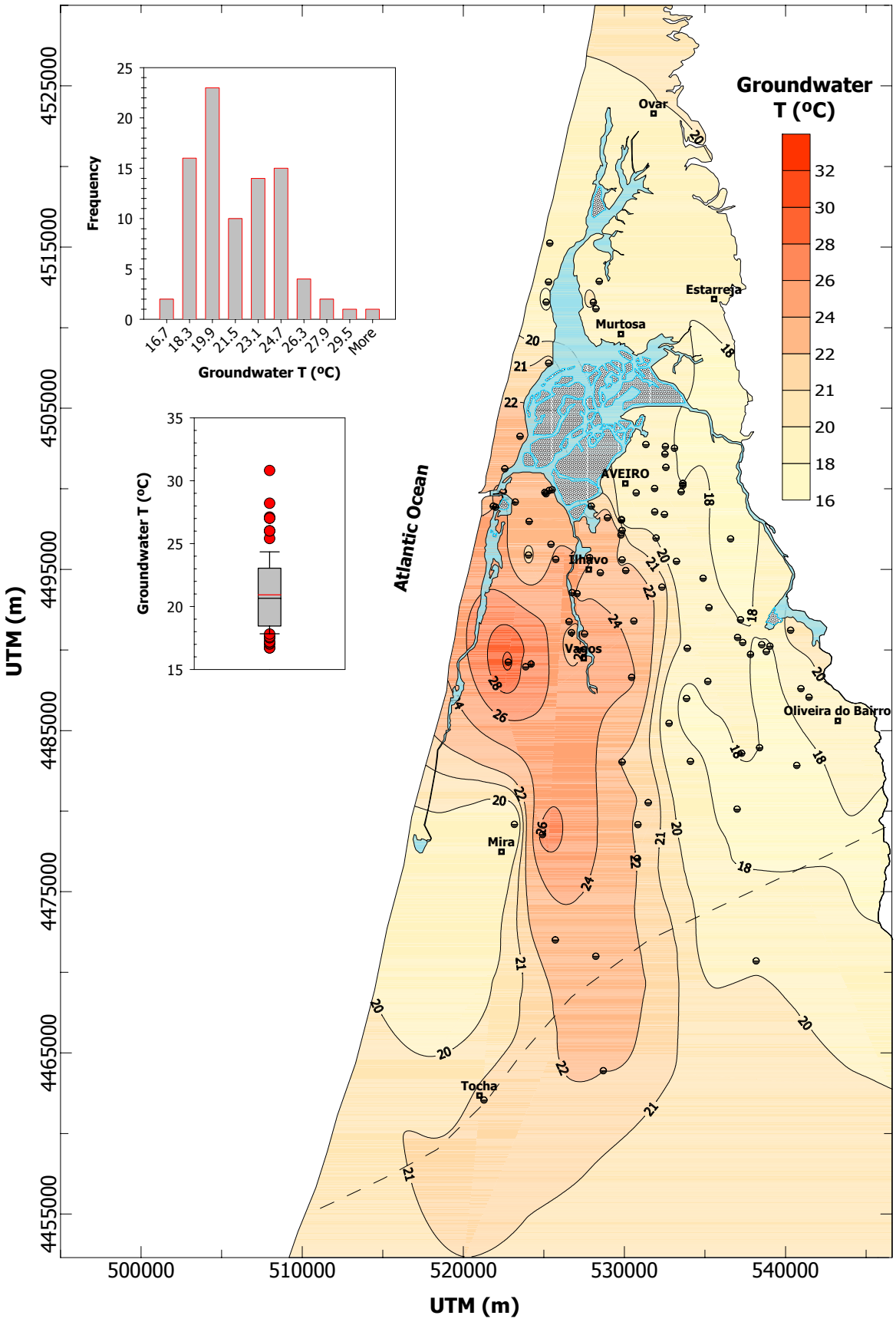
Groundwater T (ºC)
32
30
28
26
24
22
21
20
18
16
Ovar
Estarreja
Murtosa
AVEIRO
Ilhavo
Vagos
Oliveira do Bairro
Mira
Tocha
Atlantic Ocean
Frequency
Groundwater T (ºC)
16.7
18.3
19.9
21.5
23.1
24.7
26.3
27.9
29.5
More
UTM (m)
UTM (m)
4525000
4515000
4505000
4495000
4485000
4475000
4465000
4455000
500000
510000
520000
530000
540000

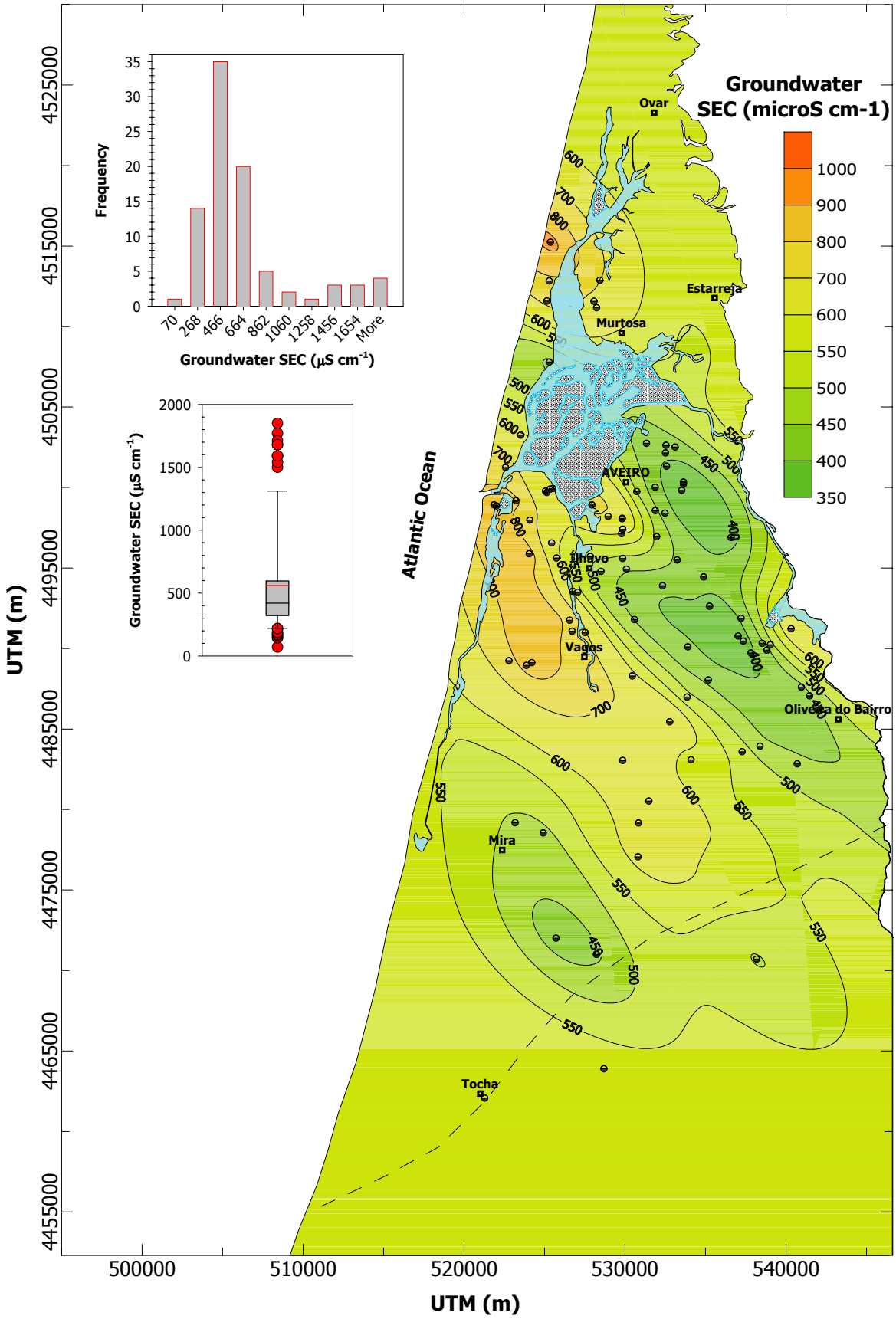
Groundwater SEC (microS cm-1)
1000
900
800
700
600
550
500
450
400
350
Ovar
Estarreja
Murtosa
AVEIRO
Ilhavo
Vagos
Oliveira do Bairro
Mira
Tocha
Atlantic Ocean
Frequency
Groundwater SEC (µS cm-1)
70
268
466
664
862
1060
1258
1456
1654
More
Groundwater SEC (µS cm-1)
UTM (m)
UTM (m)
500000
510000
520000
530000
540000
4455000
4465000
4475000
4485000
4495000
4505000
4515000
4525000

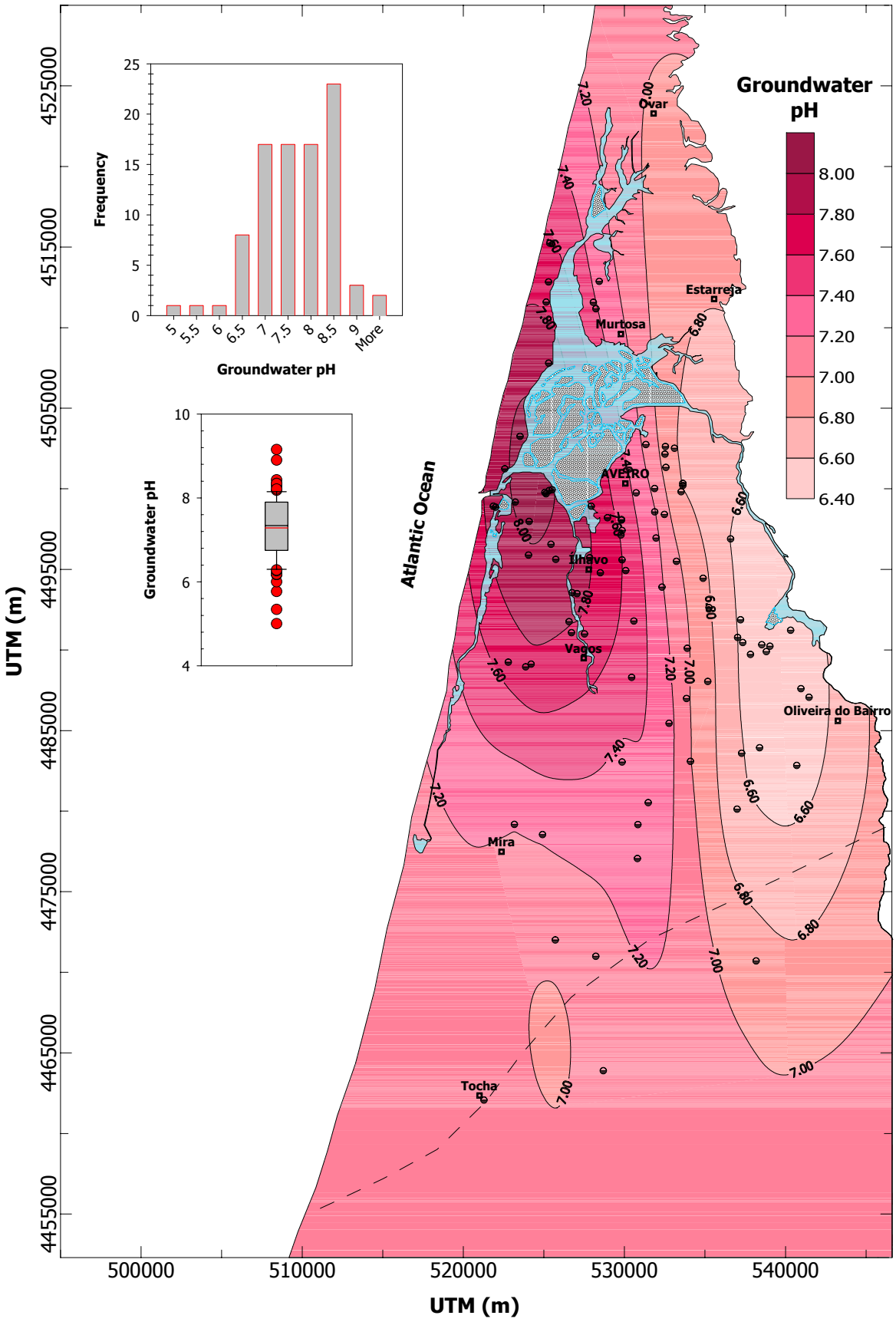
Groundwater pH
8.00
7.80
7.60
7.40
7.20
7.00
6.80
6.60
6.40
Frequency
Groundwater pH
Groundwater pH
Atlantic Ocean
Ovar
Estarreja
Murtosa
AVEIRO
Ílhavo
Vagos
Oliveira do Bairro
Mira
Tocha
UTM (m)
UTM (m)
4525000
4515000
4505000
4495000
4485000
4475000
4465000
4455000
500000
510000
520000
530000
540000

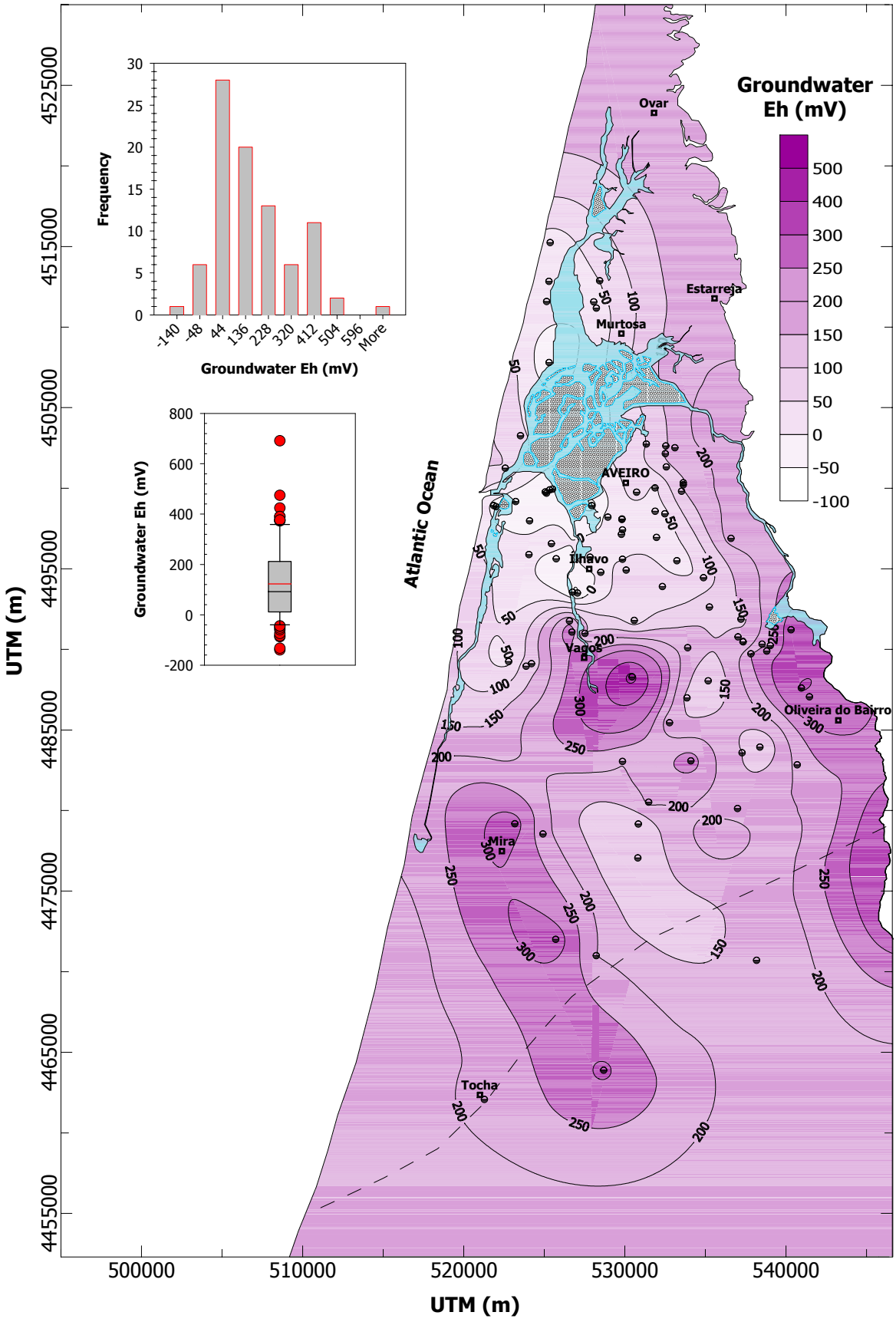
Groundwater Eh (mV)
500
400
300
250
200
150
100
50
0
-50
-100
Ovar
Estarreja
Murtosa
AVEIRO
Ilhavo
Vagos
Oliveira do Bairro
Mira
Tocha
Atlantic Ocean
Frequency
Groundwater Eh (mV)
-140
-48
44
136
228
320
412
504
596
More
Groundwater Eh (mV)
UTM (m)
UTM (m)
4525000
4515000
4505000
4495000
4485000
4475000
4465000
4455000
500000
510000
520000
530000
540000

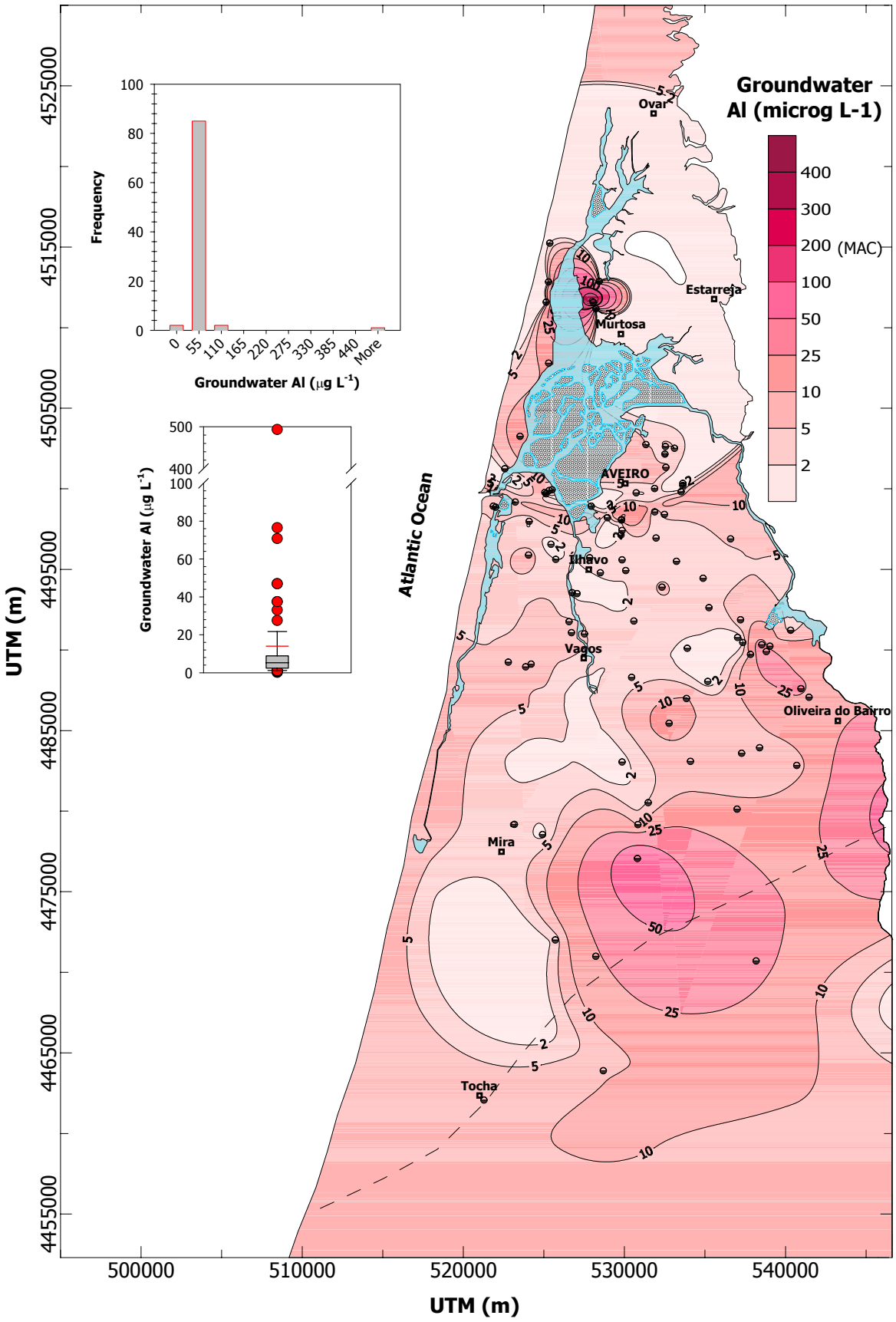
Groundwater Al (microg L-1)
400
300
200 (MAC)
100
50
25
10
5
2
Ovar
Estarreja
Murtosa
AVEIRO
Ilhavo
Vagos
Oliveira do Bairro
Mira
Tocha
Atlantic Ocean
Frequency
Groundwater Al (µg L-1)
0
55
110
165
220
275
330
385
440
More
UTM (m)
UTM (m)
500000
510000
520000
530000
540000
4525000
4515000
4505000
4495000
4485000
4475000
4465000
4455000

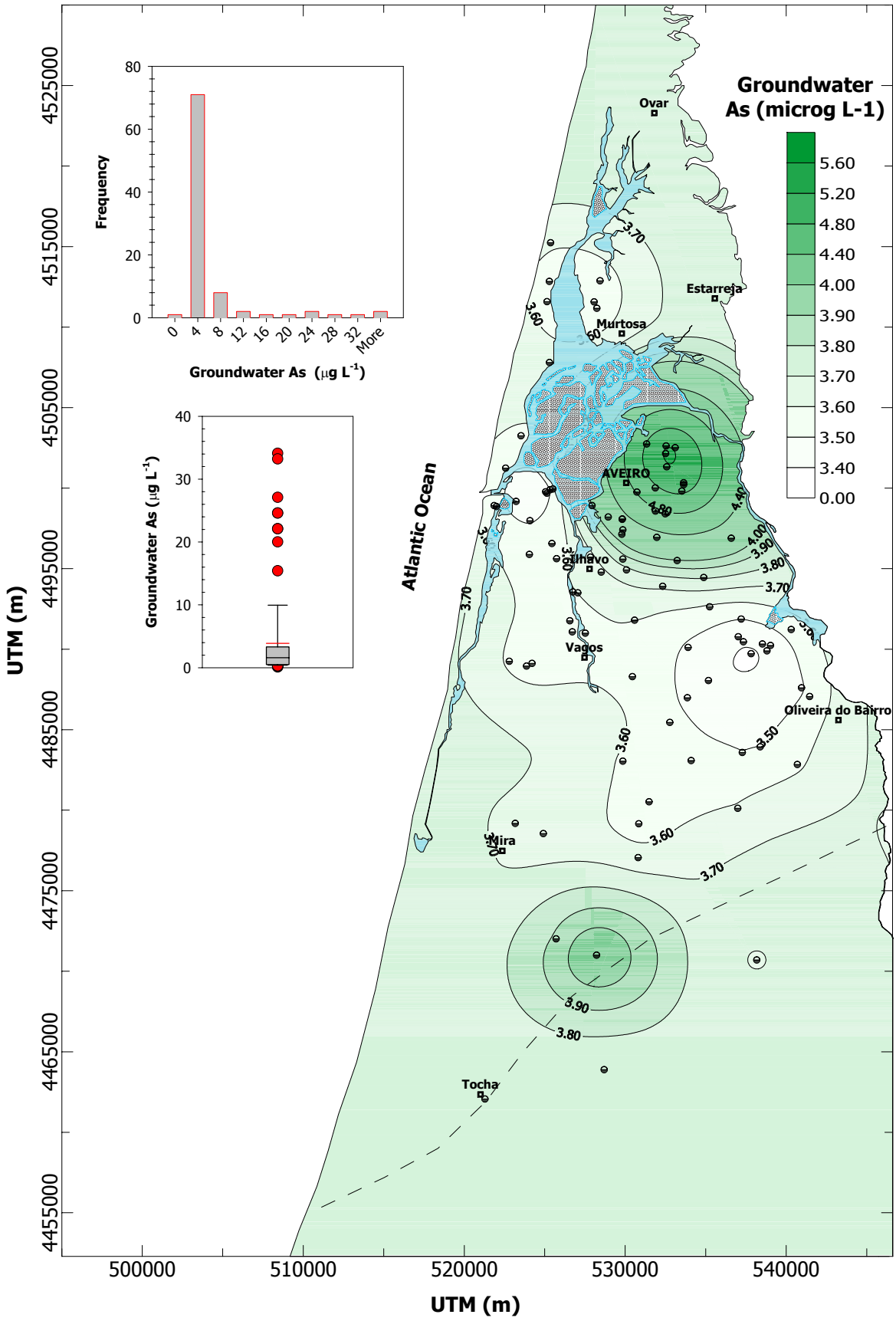
Groundwater As (microg L-1)
5.60
5.20
4.80
4.40
4.00
3.90
3.80
3.70
3.60
3.50
3.40
0.00
Frequency
Groundwater As (µg L-1)
0
4
8
12
16
20
24
28
32
More
Groundwater As (µg L-1)
Ovar
Estarreja
Murtosa
AVEIRO
Ílhavo
Vagos
Oliveira do Bairro
Mira
Tocha
Atlantic Ocean
UTM (m)
UTM (m)
4525000
4515000
4505000
4495000
4485000
4475000
4465000
4455000
500000
510000
520000
530000
540000

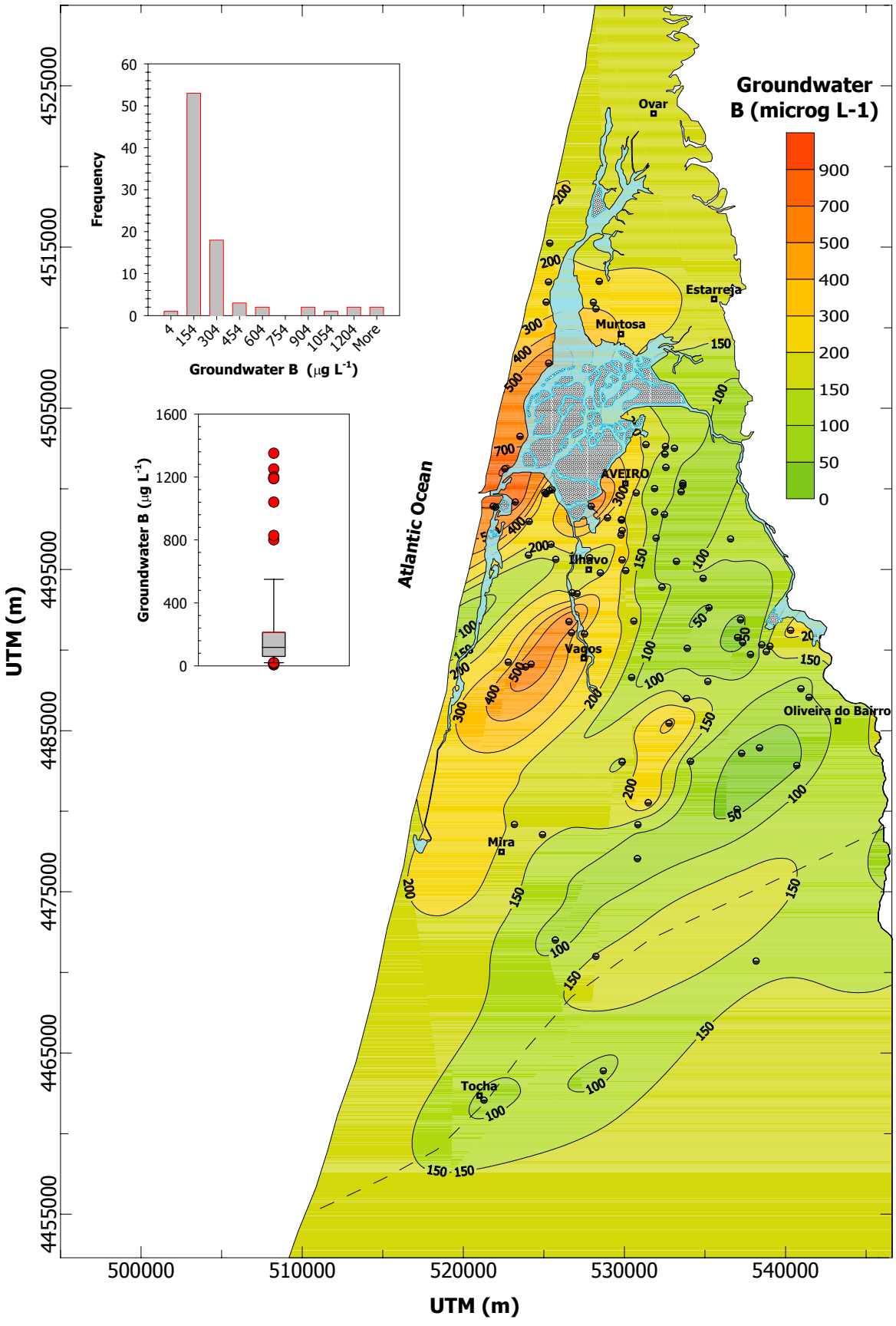
Groundwater B (microg L-1)
900
700
500
400
300
200
150
100
50
0
Ovar
Estarreja
Murtosa
AVEIRO
Ilhavo
Vagos
Oliveira do Bairro
Mira
Tocha
Atlantic Ocean
Frequency
Groundwater B (µg L-1)
4
154
304
454
604
754
904
1054
1204
More
Groundwater B (µg L-1)
UTM (m)
UTM (m)
500000
510000
520000
530000
540000
4525000
4515000
4505000
4495000
4485000
4475000
4465000
4455000

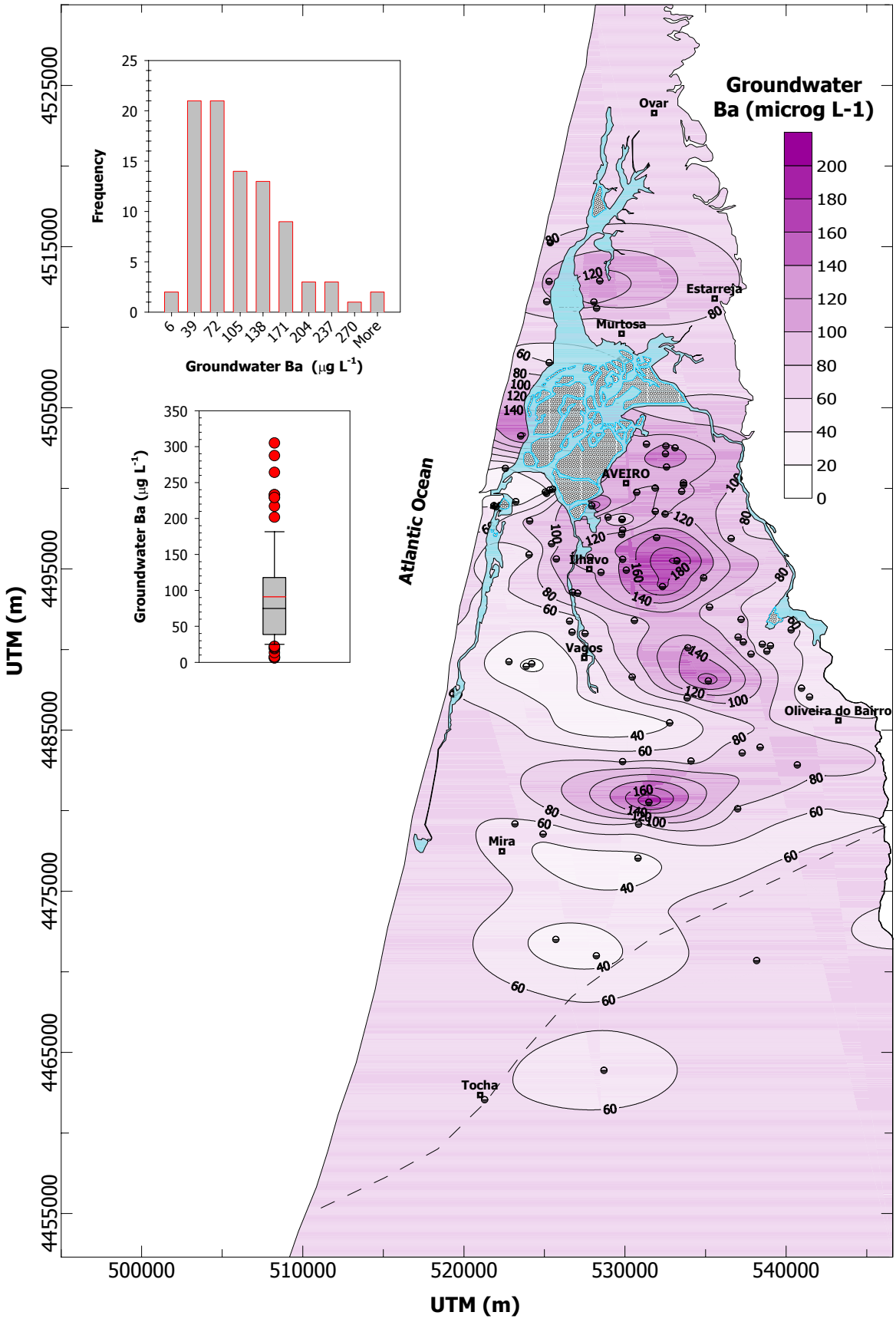
Groundwater Ba (microg L-1)
200
180
160
140
120
100
80
60
40
20
0
Ovar
Estarreja
Murtosa
AVEIRO
Ilhavo
Vagos
Oliveira do Bairro
Mira
Tocha
Atlantic Ocean
Frequency
25
20
15
10
5
0
6
39
72
105
138
171
204
237
270
More
Groundwater Ba (μg L-1)
Groundwater Ba (μg L-1)
350
300
250
200
150
100
50
0
UTM (m)
4525000
4515000
4505000
4495000
4485000
4475000
4465000
4455000
500000
510000
520000
530000
540000
UTM (m)

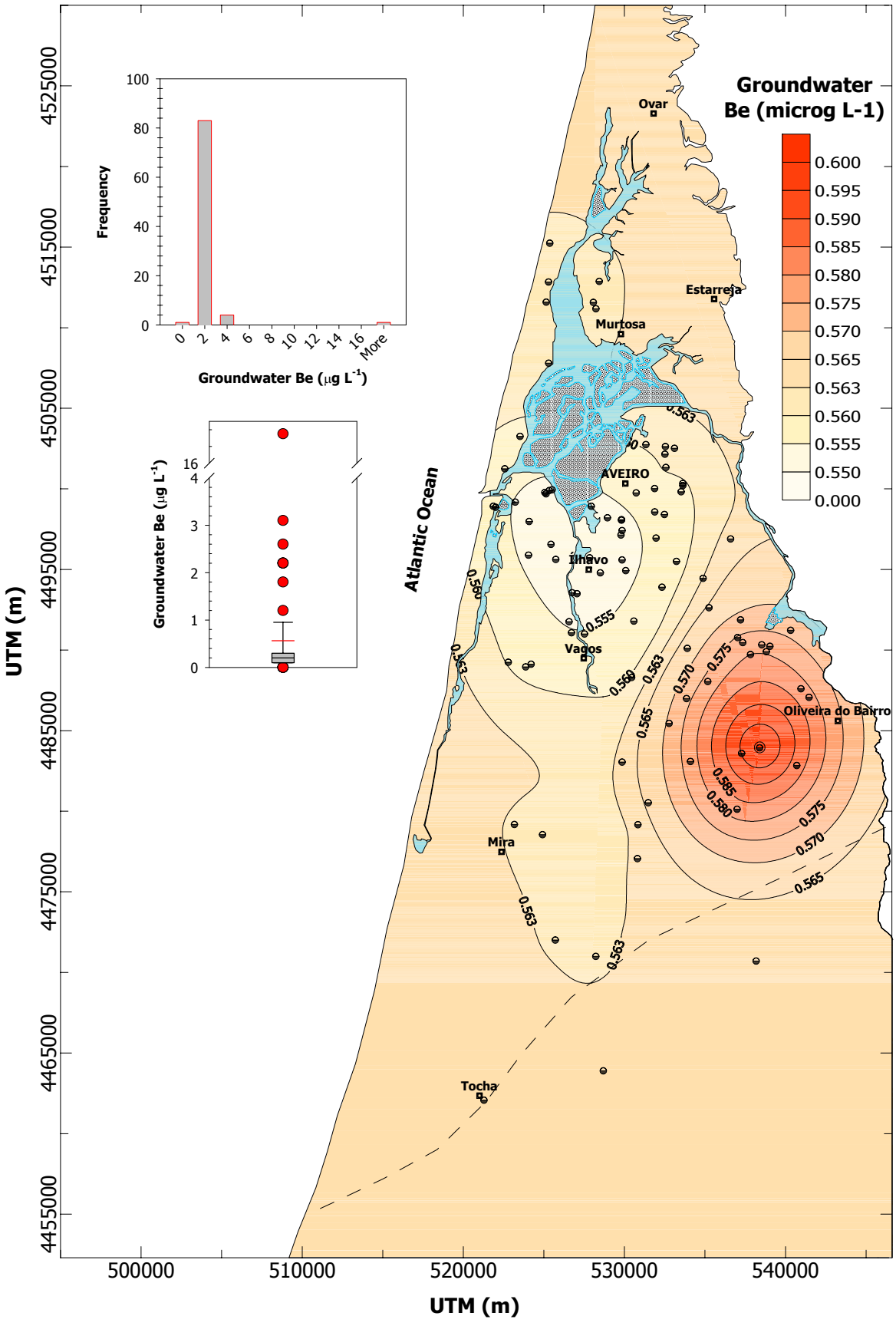
Groundwater Be (microg L-1)
0.600
0.595
0.590
0.585
0.580
0.575
0.570
0.565
0.563
0.560
0.555
0.550
0.000
Frequency
Groundwater Be (µg L-1)
Groundwater Be (µg L-1)
Atlantic Ocean
Ovar
Estarreja
Murtosa
AVEIRO
Ílhavo
Vagos
Oliveira do Bairro
Mira
Tocha
UTM (m)
UTM (m)
4525000
4515000
4505000
4495000
4485000
4475000
4465000
4455000
500000
510000
520000
530000
540000

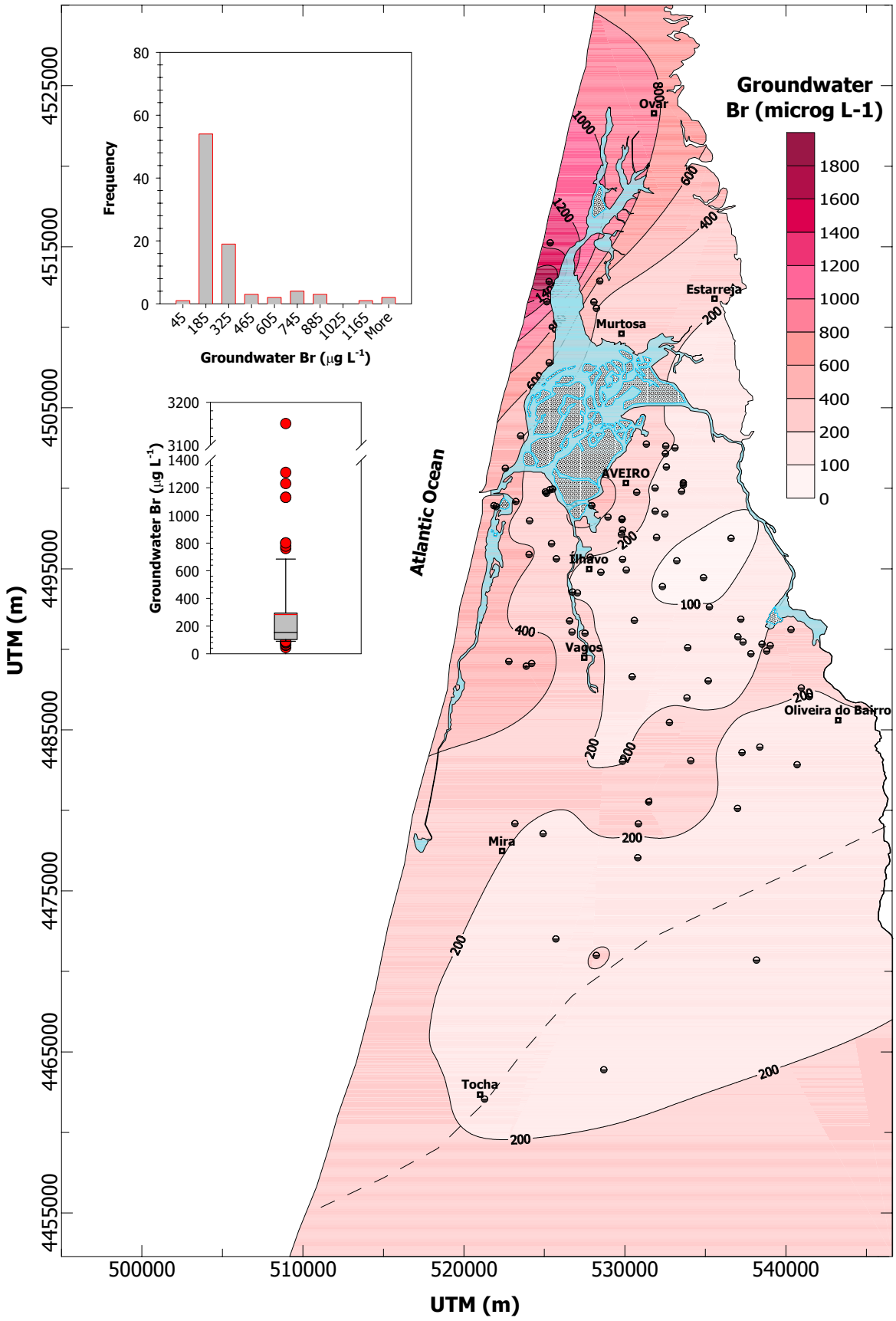
Groundwater Br (microg L-1)
1800
1600
1400
1200
1000
800
600
400
200
100
0
Frequency
Groundwater Br (µg L-1)
45
185
325
465
605
745
885
1025
1165
More
Groundwater Br (µg L-1)
Atlantic Ocean
Ovar
Estarreja
Murtosa
AVEIRO
Ílhavo
Vagos
Oliveira do Bairro
Mira
Tocha
UTM (m)
UTM (m)
4525000
4515000
4505000
4495000
4485000
4475000
4465000
4455000
500000
510000
520000
530000
540000

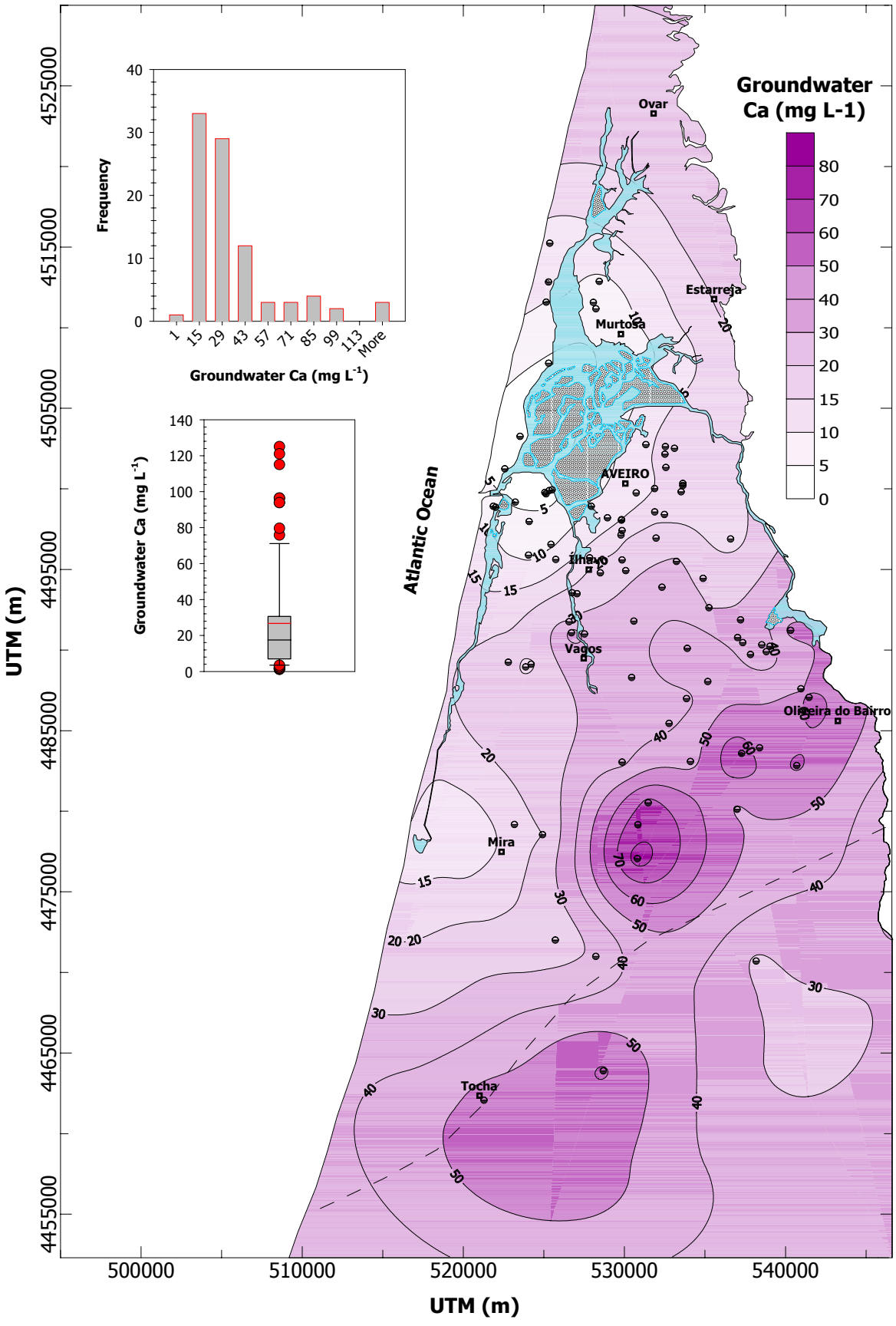
Groundwater Ca (mg L-1)
80
70
60
50
40
30
20
15
10
5
0
Ovar
Estarreja
Murtosa
AVEIRO
Ílhavo
Vagos
Oliveira do Bairro
Mira
Tocha
Atlantic Ocean
Frequency
Groundwater Ca (mg L-1)
1
15
29
43
57
71
85
99
113
More
Groundwater Ca (mg L-1)
UTM (m)
UTM (m)
500000
510000
520000
530000
540000
4525000
4515000
4505000
4495000
4485000
4475000
4465000
4455000

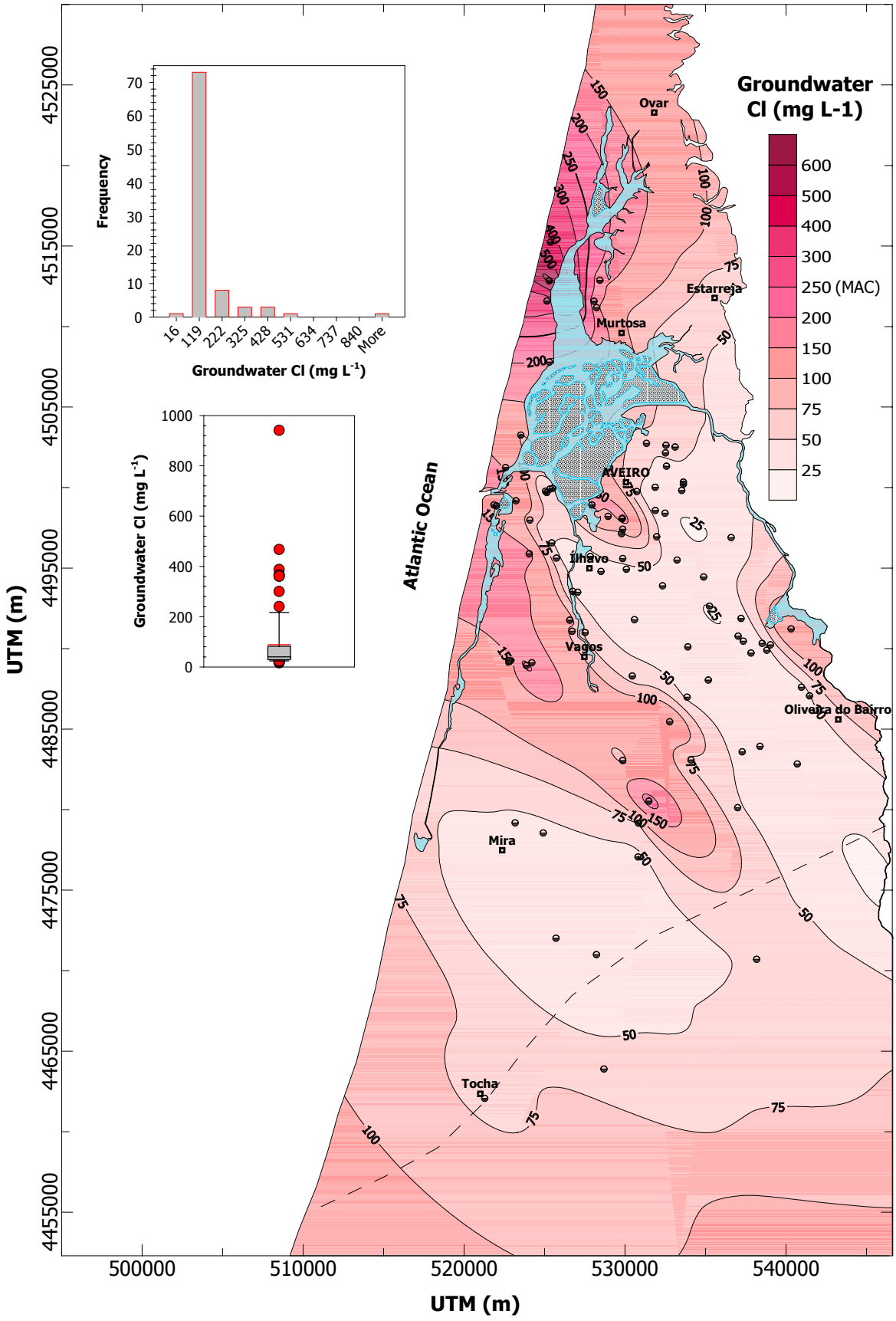
Groundwater Cl (mg L-1)
600
500
400
300
250 (MAC)
200
150
100
75
50
25
Atlantic Ocean
Ovar
Estarreja
Murtosa
AVEIRO
Ilhavo
Vagos
Oliveira do Bairro
Mira
Tocha
Frequency
Groundwater Cl (mg L-1)
16
119
222
325
428
531
634
737
840
More
Groundwater Cl (mg L-1)
UTM (m)
UTM (m)
4525000
4515000
4505000
4495000
4485000
4475000
4465000
4455000
500000
510000
520000
530000
540000

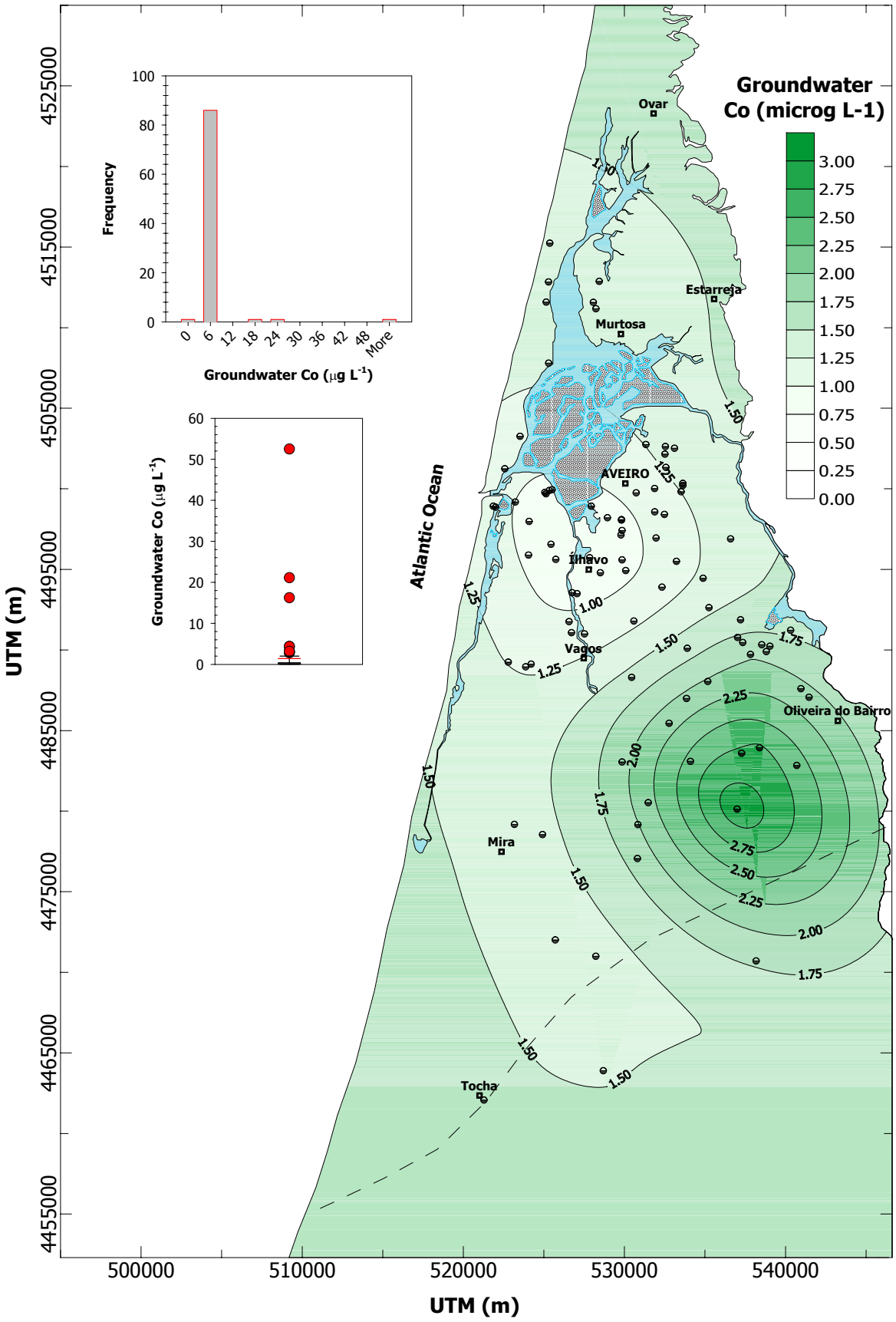
Groundwater Co (microg L-1)
3.00
2.75
2.50
2.25
2.00
1.75
1.50
1.25
1.00
0.75
0.50
0.25
0.00
Frequency
Groundwater Co (µg L-1)
0 6 12 18 24 30 36 42 48 More
Groundwater Co (µg L-1)
Atlantic Ocean
Ovar
Estarreja
Murtosa
AVEIRO
Ílhavo
Vagos
Oliveira do Bairro
Mira
Tocha
UTM (m)
UTM (m)
500000
510000
520000
530000
540000
4525000
4515000
4505000
4495000
4485000
4475000
4465000
4455000

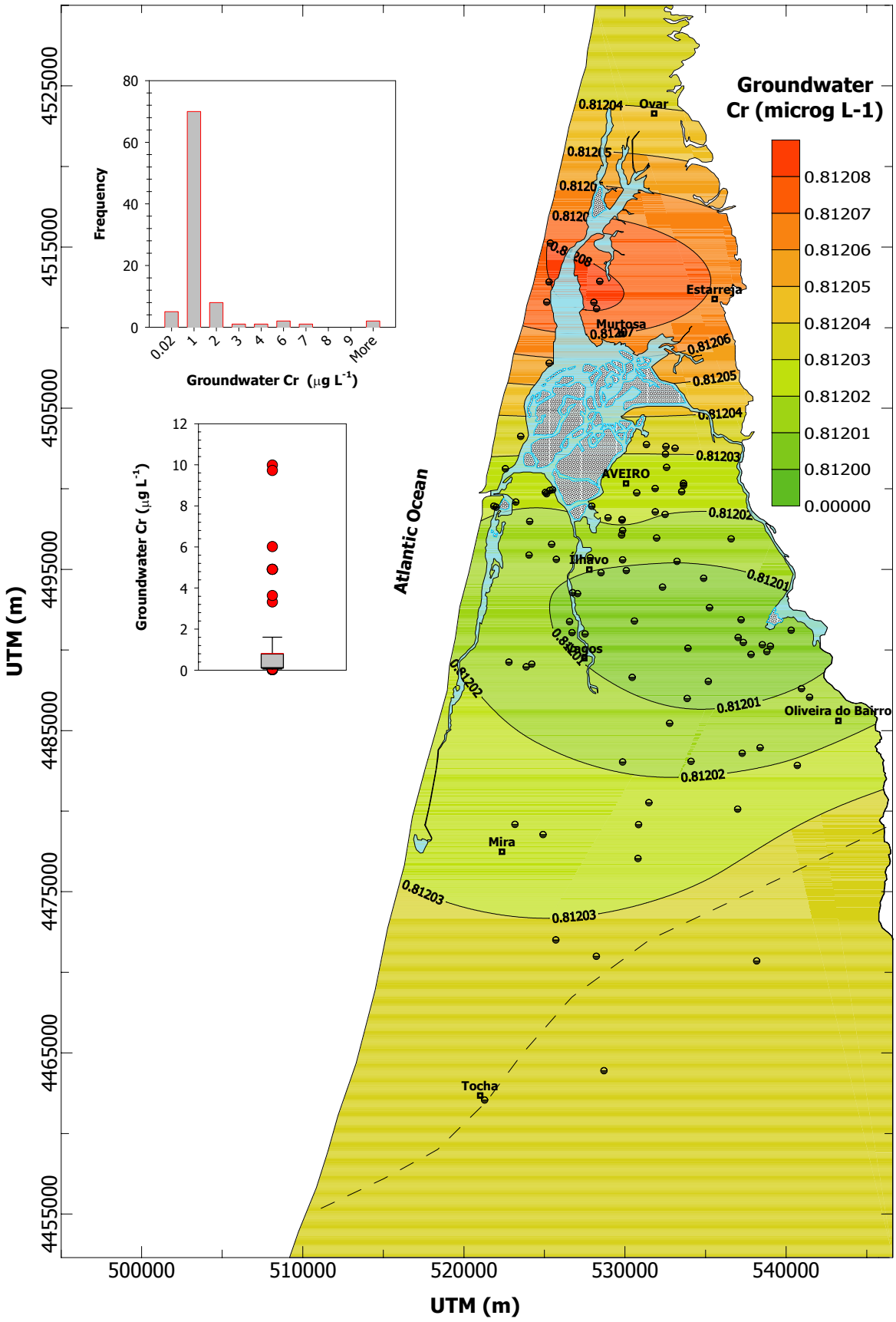
Groundwater Cr (microg L-1)
0.81208
0.81207
0.81206
0.81205
0.81204
0.81203
0.81202
0.81201
0.81200
0.00000
Frequency
Groundwater Cr (µg L-1)
0.02
1
2
3
4
6
7
8
9
More
Groundwater Cr (µg L-1)
Atlantic Ocean
Ovar
Estarreja
Murtosa
AVEIRO
Ilhavo
Oliveira do Bairro
Mira
Tocha
UTM (m)
UTM (m)
4525000
4515000
4505000
4495000
4485000
4475000
4465000
4455000
500000
510000
520000
530000
540000

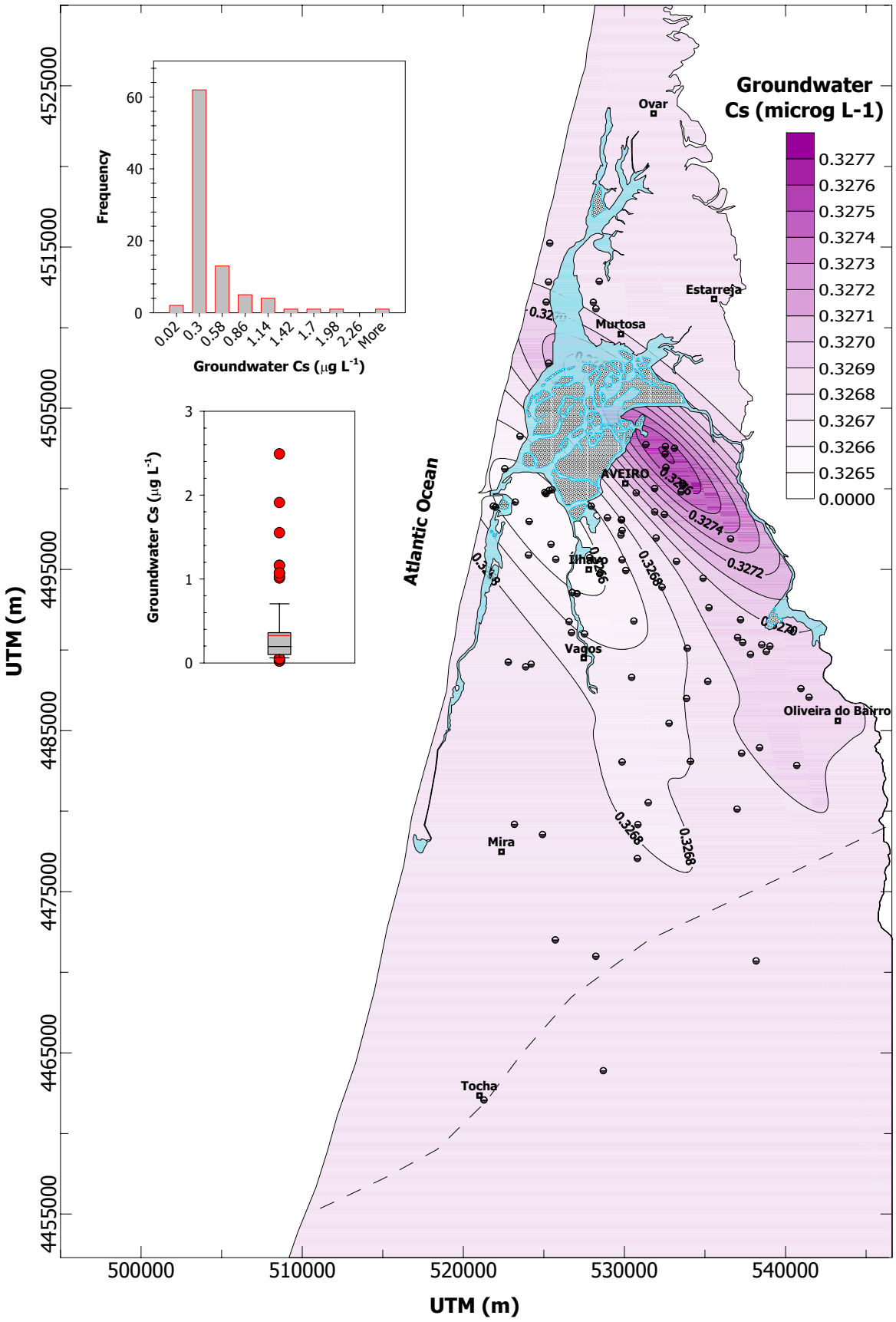
Groundwater Cs (microg L-1)
0.3277
0.3276
0.3275
0.3274
0.3273
0.3272
0.3271
0.3270
0.3269
0.3268
0.3267
0.3266
0.3265
0.0000
Frequency
Groundwater Cs (µg L-1)
0.02
0.3
0.58
0.86
1.14
1.42
1.7
1.98
2.26
More
Groundwater Cs (µg L-1)
Atlantic Ocean
Ovar
Estarreja
Murtosa
AVEIRO
Ilhavo
Vagos
Oliveira do Bairro
Mira
Tocha
UTM (m)
UTM (m)
4525000
4515000
4505000
4495000
4485000
4475000
4465000
4455000
500000
510000
520000
530000
540000

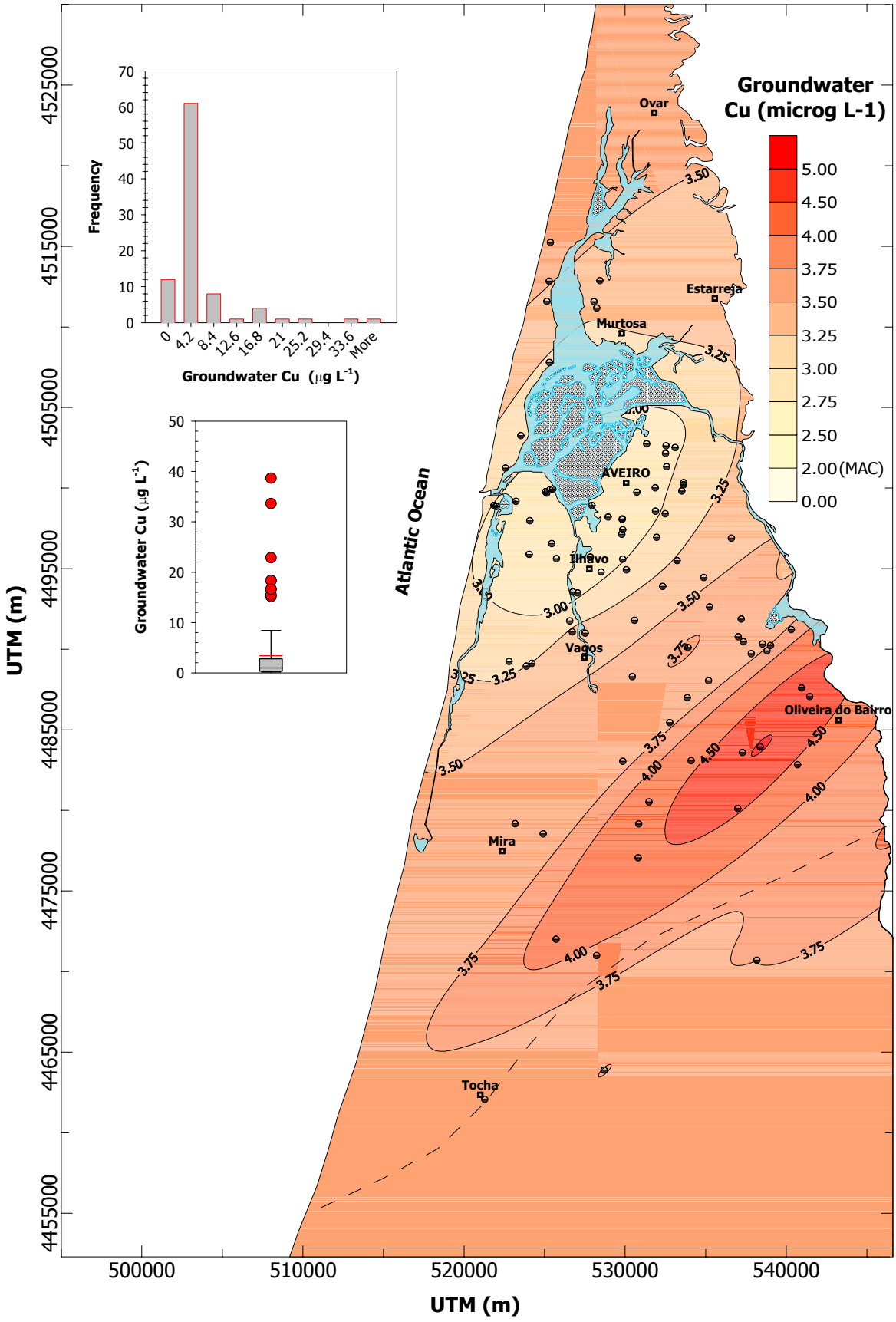
Groundwater Cu (microg L-1)
5.00
4.50
4.00
3.75
3.50
3.25
3.00
2.75
2.50
2.00 (MAC)
0.00
Frequency
Groundwater Cu (µg L-1)
0
4.2
8.4
12.6
16.8
21
25.2
29.4
33.6
More
Groundwater Cu (µg L-1)
Atlantic Ocean
Ovar
Estarreja
Murtosa
AVEIRO
Ilhavo
Vagos
Oliveira do Bairro
Mira
Tocha
UTM (m)
UTM (m)
4525000
4515000
4505000
4495000
4485000
4475000
4465000
4455000
500000
510000
520000
530000
540000

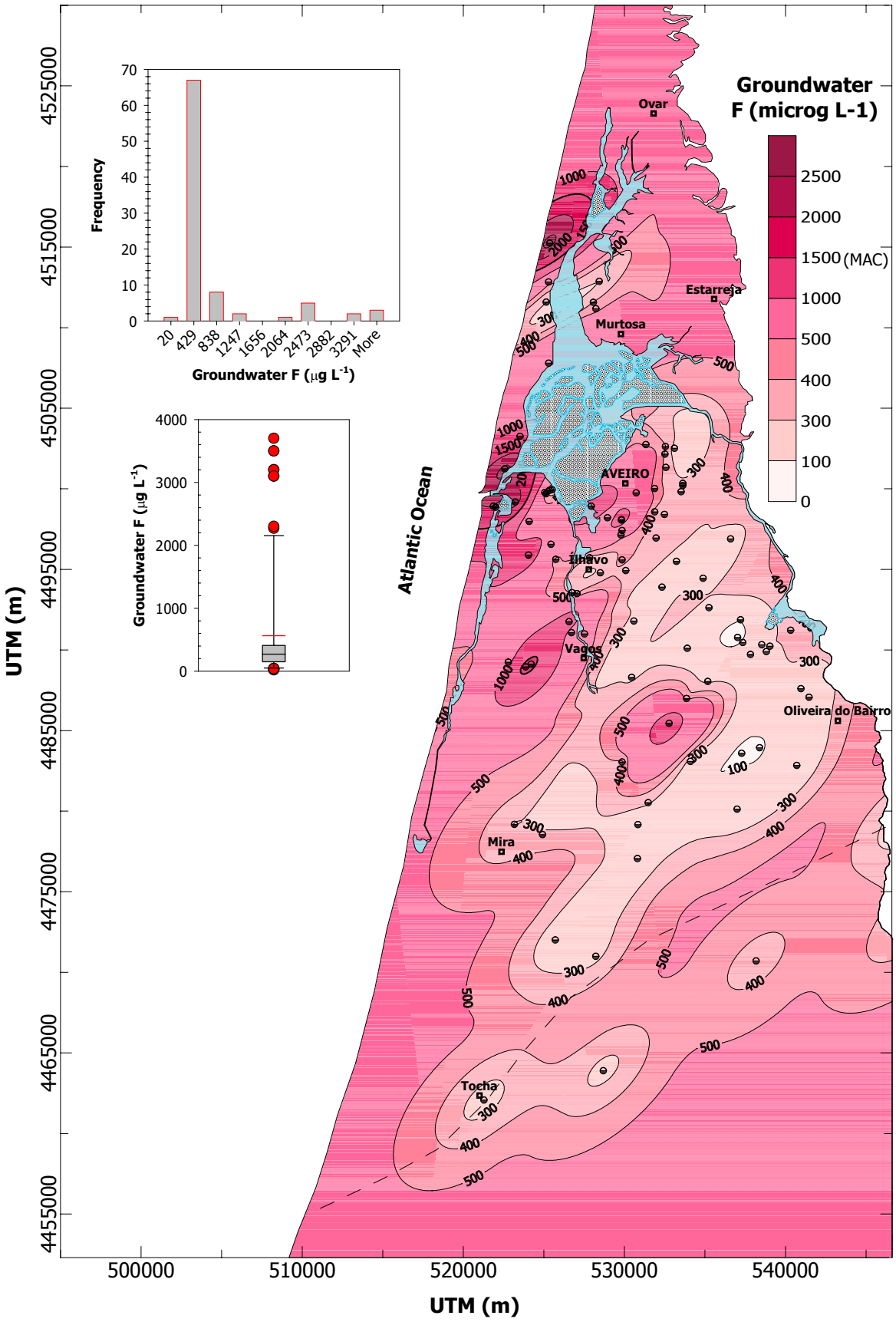
Groundwater
F (microg L-1)
2500
2000
1500 (MAC)
1000
500
400
300
100
0
Ovar
Estarreja
Murtosa
AVEIRO
Ilhavo
Vagos
Mira
Tocha
Oliveira do Bairro
Atlantic Ocean
Frequency
Groundwater F (μg L-1)
20
429
838
1247
1656
2064
2473
2882
3291
More
Groundwater F (μg L-1)
UTM (m)
UTM (m)
500000
510000
520000
530000
540000
4525000
4515000
4505000
4495000
4485000
4475000
4465000
4455000

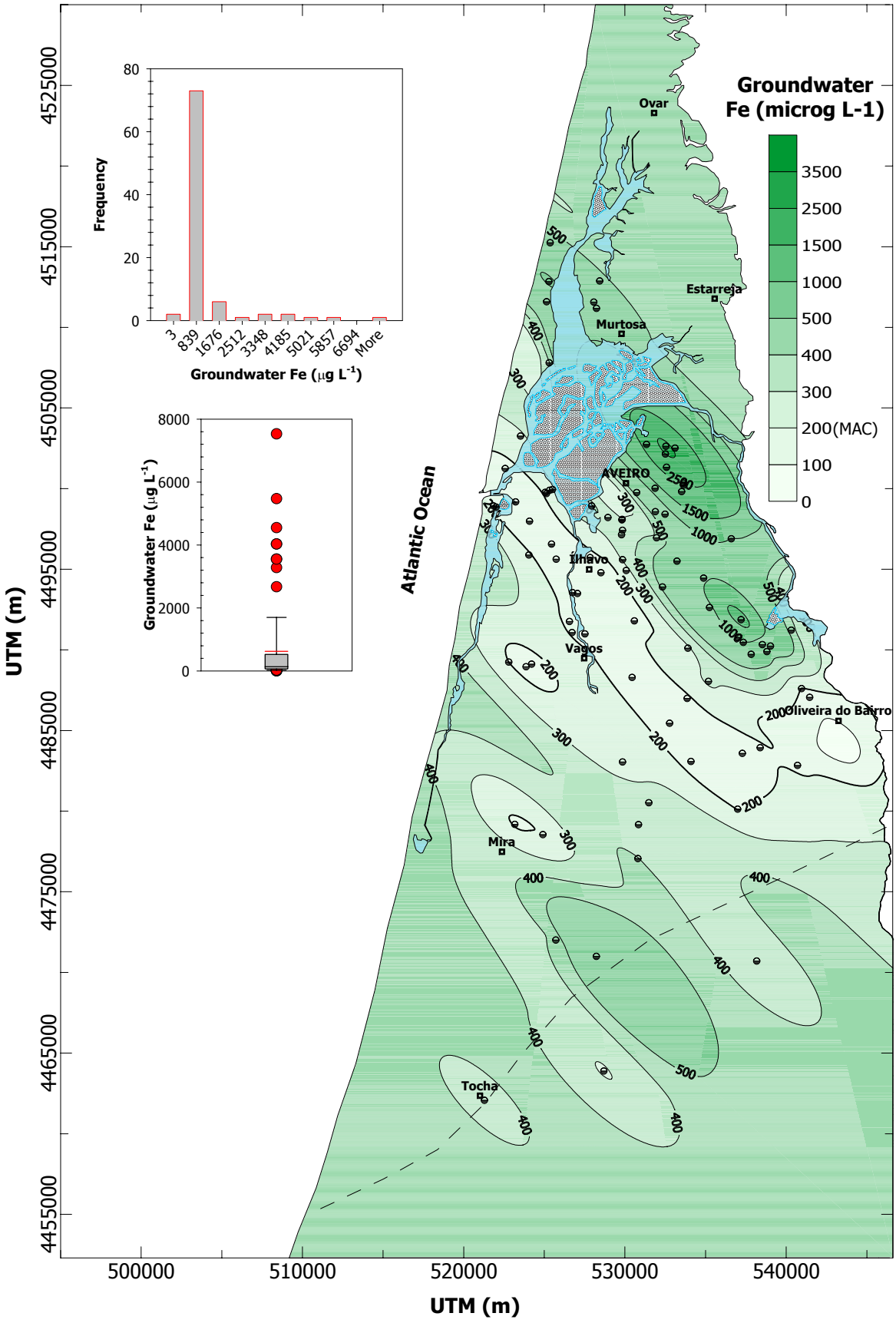
Groundwater Fe (microg L-1)
3500
2500
1500
1000
500
400
300
200(MAC)
100
0
Ovar
Estarreja
Murtosa
AVEIRO
Ilhavo
Vagos
Oliveira do Bairro
Mira
Tocha
Atlantic Ocean
Frequency
Groundwater Fe (μg L-1)
3
839
1676
2512
3348
4185
5021
5857
6694
More
UTM (m)
UTM (m)
500000
510000
520000
530000
540000
4525000
4515000
4505000
4495000
4485000
4475000
4465000
4455000

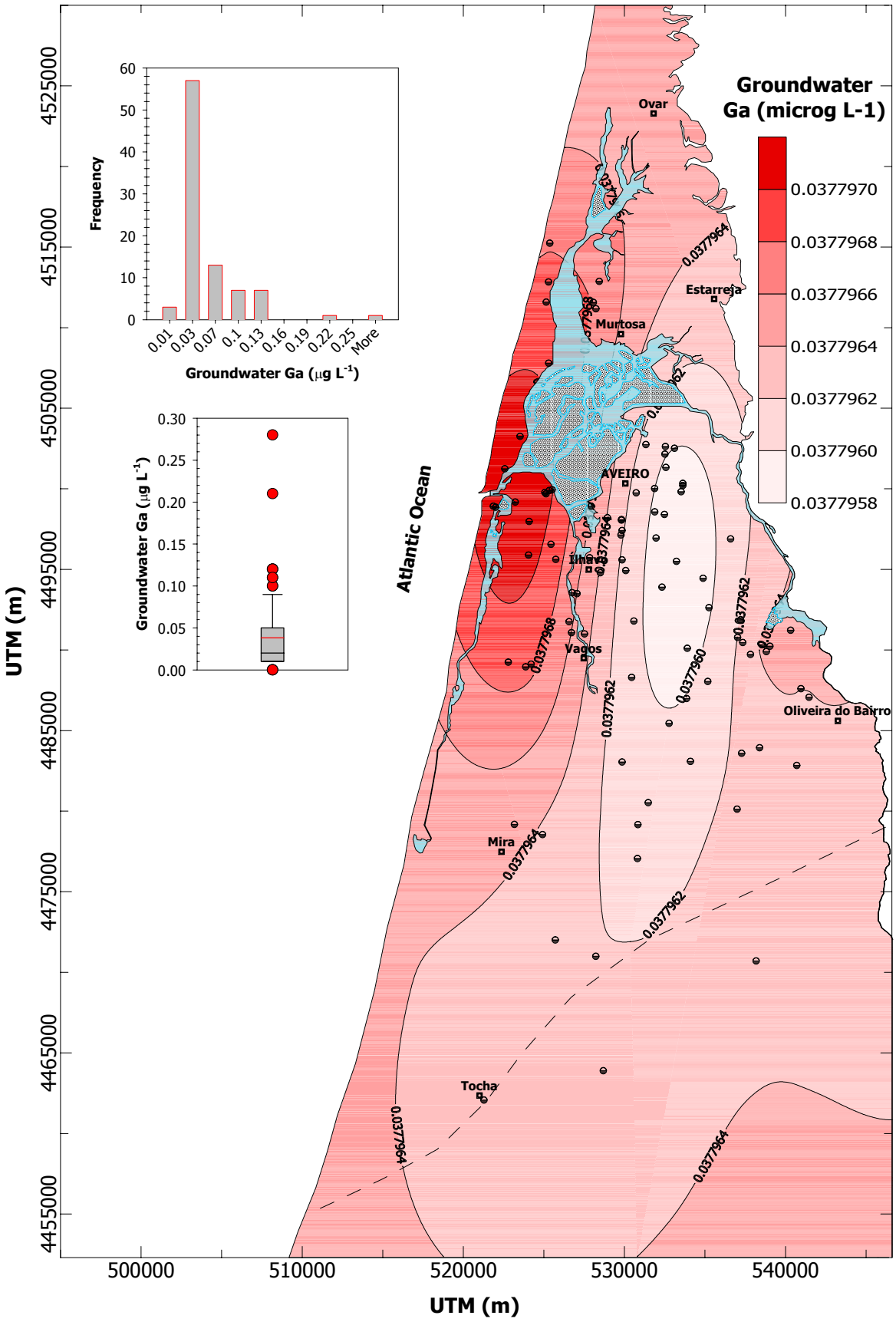
Groundwater
Ga (microg L-1)
0.0377970
0.0377968
0.0377966
0.0377964
0.0377962
0.0377960
0.0377958
Frequency
Groundwater Ga (µg L-1)
0.01
0.03
0.07
0.1
0.13
0.16
0.19
0.22
0.25
More
Groundwater Ga (µg L-1)
Atlantic Ocean
Ovar
Estarreja
Murtosa
AVEIRO
Ilhavo
Vagos
Oliveira do Bairro
Mira
Tocha
UTM (m)
UTM (m)
4525000
4515000
4505000
4495000
4485000
4475000
4465000
4455000
500000
510000
520000
530000
540000

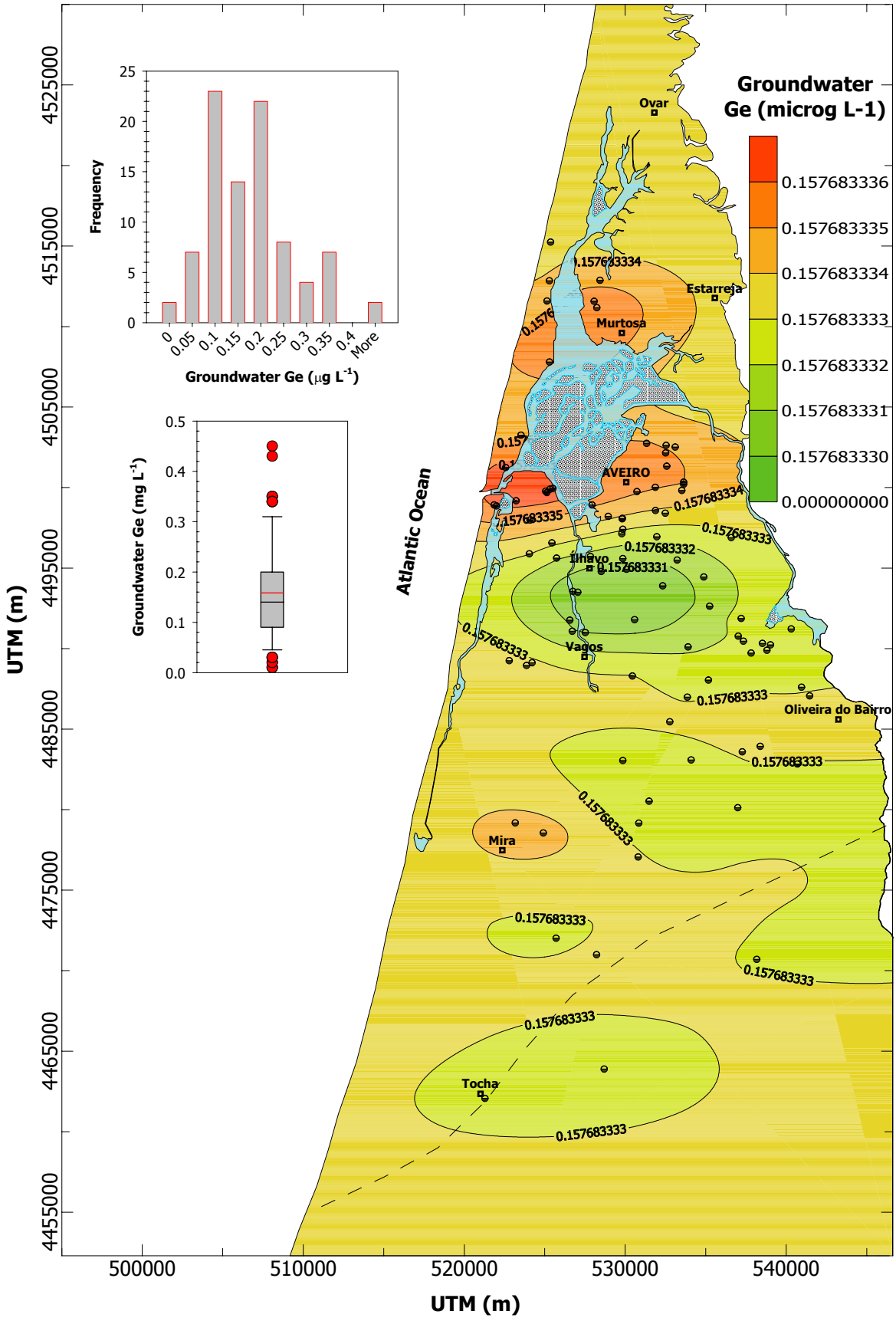
Groundwater Ge (microg L-1)
0.157683336
0.157683335
0.157683334
0.157683333
0.157683332
0.157683331
0.157683330
0.000000000
Frequency
Groundwater Ge (μg L-1)
Groundwater Ge (mg L-1)
Atlantic Ocean
Ovar
Estarreja
Murtosa
AVEIRO
Ilhavo
Vagos
Oliveira do Bairro
Mira
Tocha
UTM (m)
UTM (m)
4525000
4515000
4505000
4495000
4485000
4475000
4465000
4455000
500000
510000
520000
530000
540000

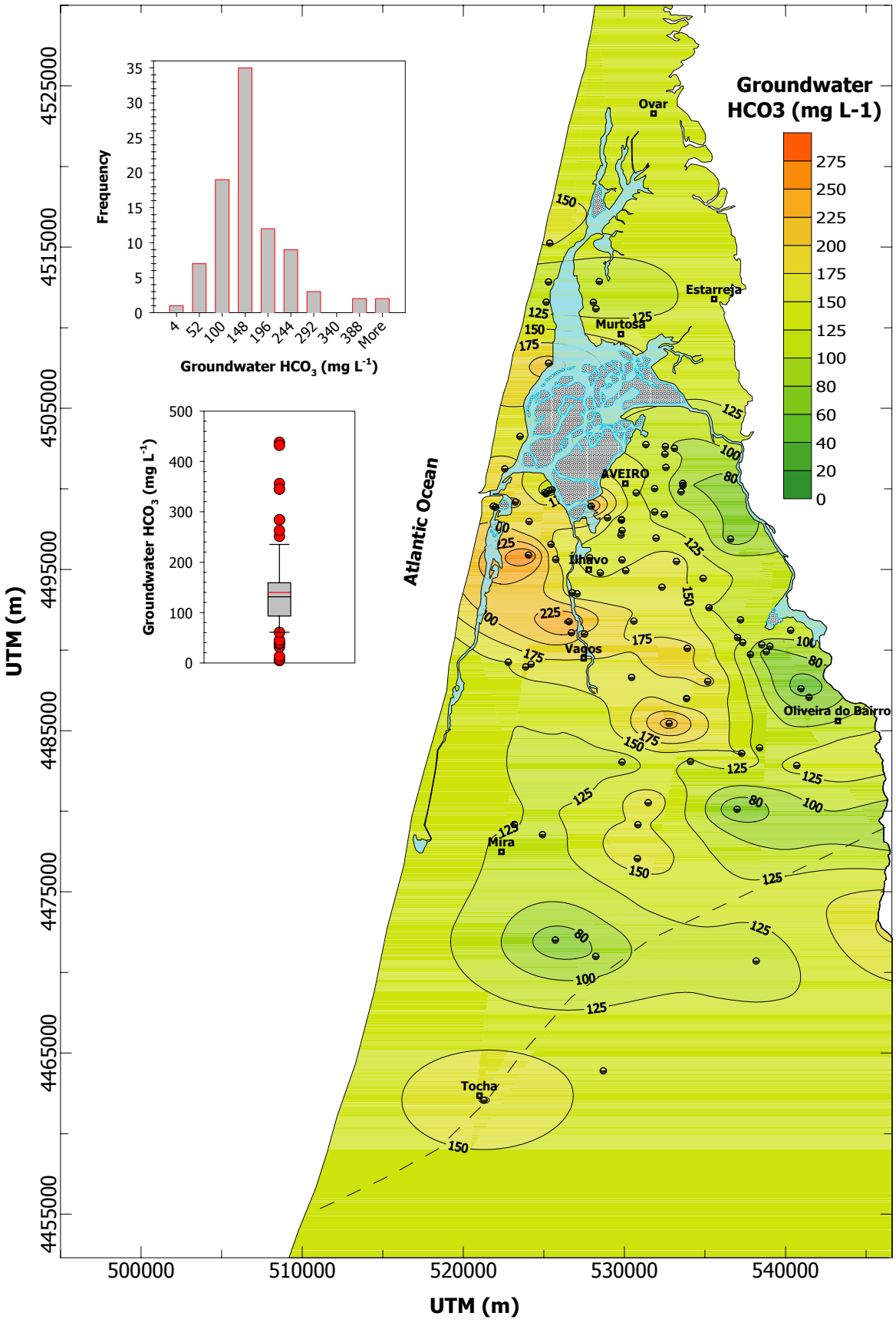
Groundwater HCO3 (mg L-1)
275
250
225
200
175
150
125
100
80
60
40
20
0
Ovar
Estarreja
Murtosa
AVEIRO
Ílhavo
Vagos
Oliveira do Bairro
Mira
Tocha
Atlantic Ocean
Frequency
Groundwater HCO3 (mg L-1)
4
52
100
148
196
244
292
340
388
More
Groundwater HCO3 (mg L-1)
UTM (m)
UTM (m)
500000
510000
520000
530000
540000
4525000
4515000
4505000
4495000
4485000
4475000
4465000
4455000

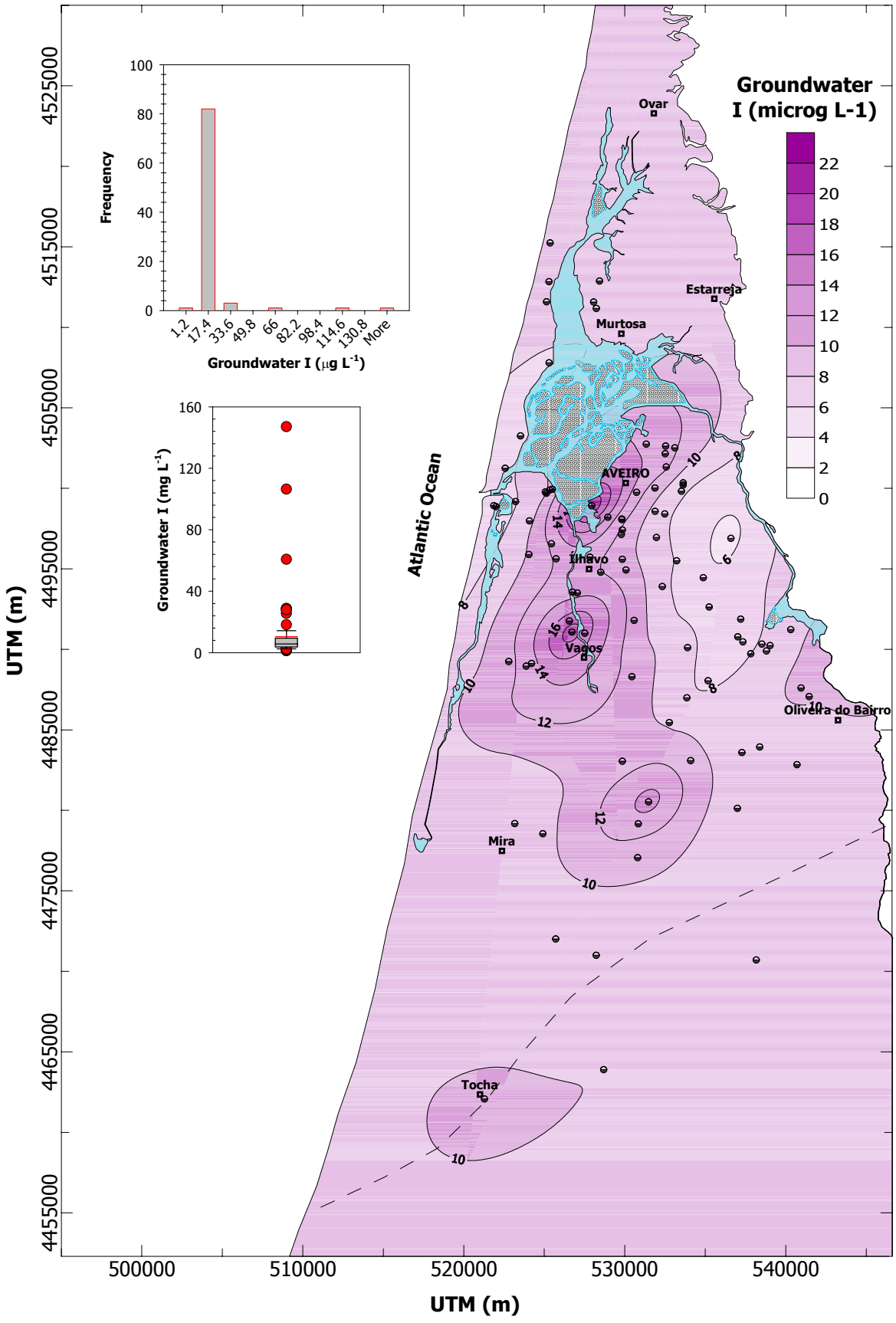
Groundwater I (microg L-1)
22
20
18
16
14
12
10
8
6
4
2
0
Ovar
Estarreja
Murtosa
AVEIRO
Ilhavo
Vagos
Oliveira do Bairro
Mira
Tocha
Atlantic Ocean
Frequency
100
80
60
40
20
0
1.2
17.4
33.6
49.8
66
82.2
98.4
114.6
130.8
More
Groundwater I (µg L-1)
Groundwater I (mg L-1)
160
120
80
40
0
UTM (m)
4525000
4515000
4505000
4495000
4485000
4475000
4465000
4455000
500000
510000
520000
530000
540000
UTM (m)

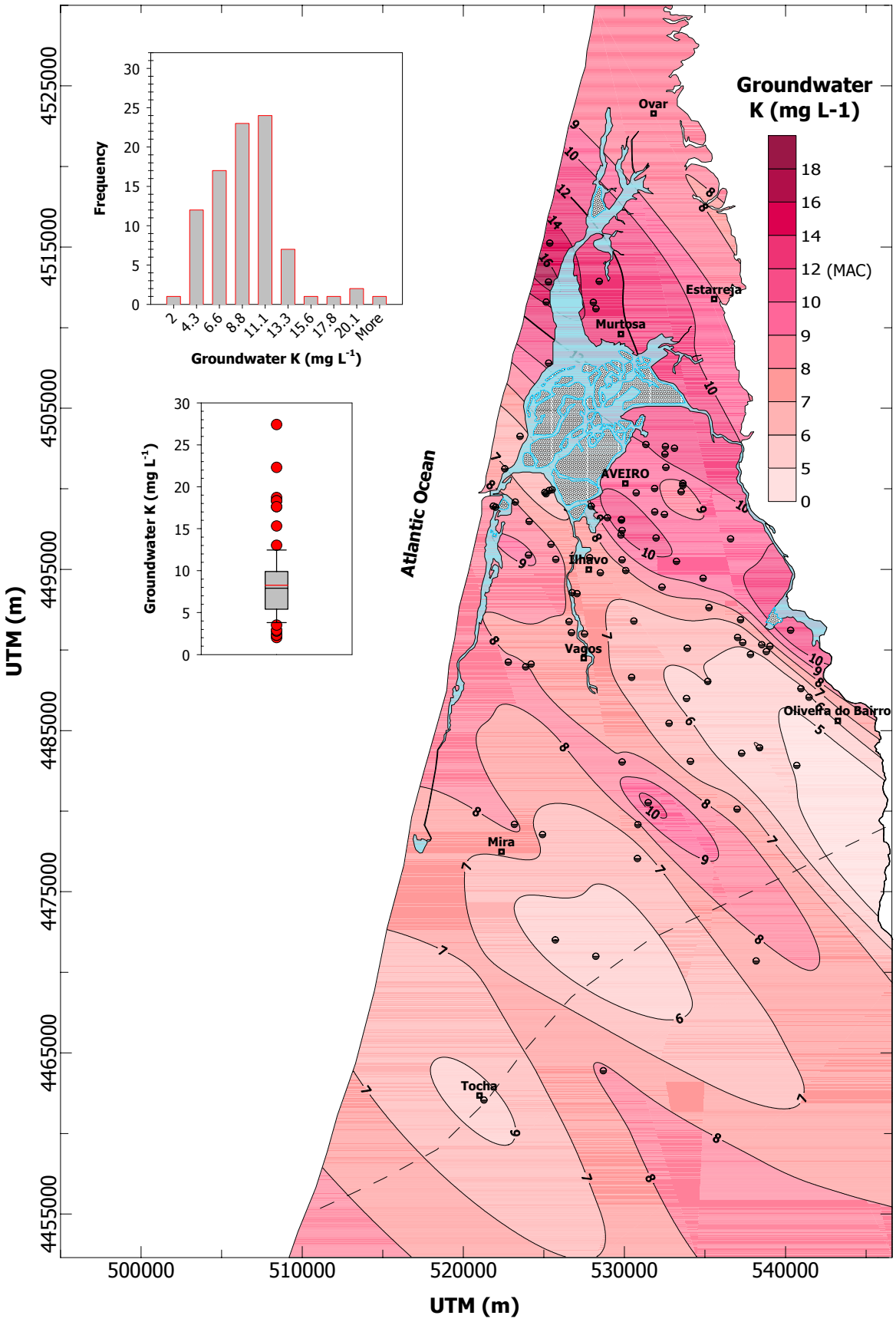
Groundwater
K (mg L-1)
18
16
14
12 (MAC)
10
9
8
7
6
5
0
Frequency
Groundwater K (mg L-1)
2
4.3
6.6
8.8
11.1
13.3
15.6
17.8
20.1
More
Groundwater K (mg L-1)
Atlantic Ocean
Ovar
Estarreja
Murtosa
AVEIRO
Ílhavo
Vagos
Oliveira do Bairro
Mira
Tocha
UTM (m)
4525000
4515000
4505000
4495000
4485000
4475000
4465000
4455000
500000
510000
520000
530000
540000
UTM (m)

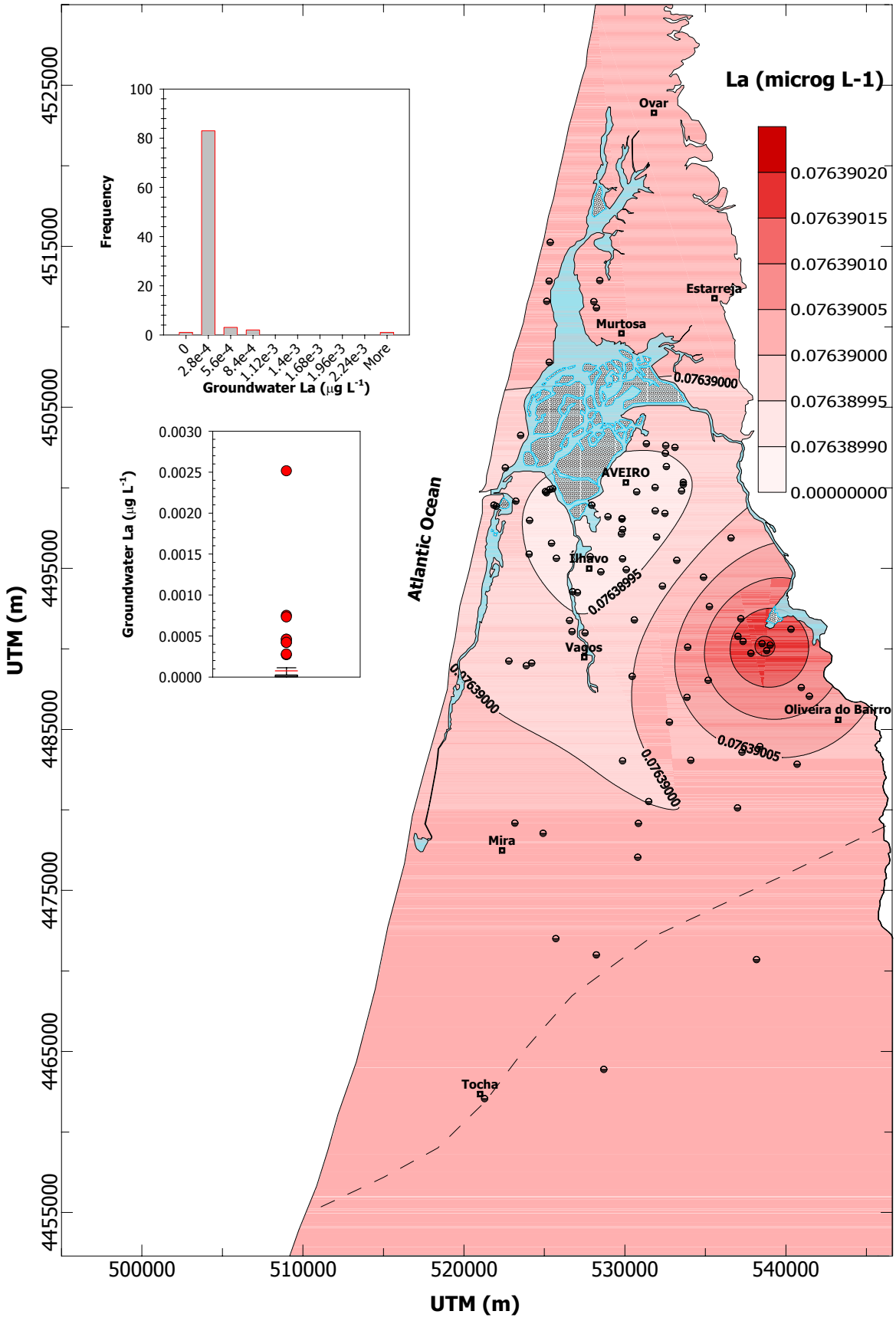
La (microg L-1)
0.07639020
0.07639015
0.07639010
0.07639005
0.07639000
0.07638995
0.07638990
0.00000000
Frequency
Groundwater La (µg L-1)
0
2.8e-4
5.6e-4
8.4e-4
1.12e-3
1.4e-3
1.68e-3
1.96e-3
2.24e-3
More
Groundwater La (µg L-1)
Atlantic Ocean
Ovar
Estarreja
Murtosa
AVEIRO
Ílhavo
Vagos
Oliveira do Bairro
Mira
Tocha
UTM (m)
UTM (m)
4525000
4515000
4505000
4495000
4485000
4475000
4465000
4455000
500000
510000
520000
530000
540000

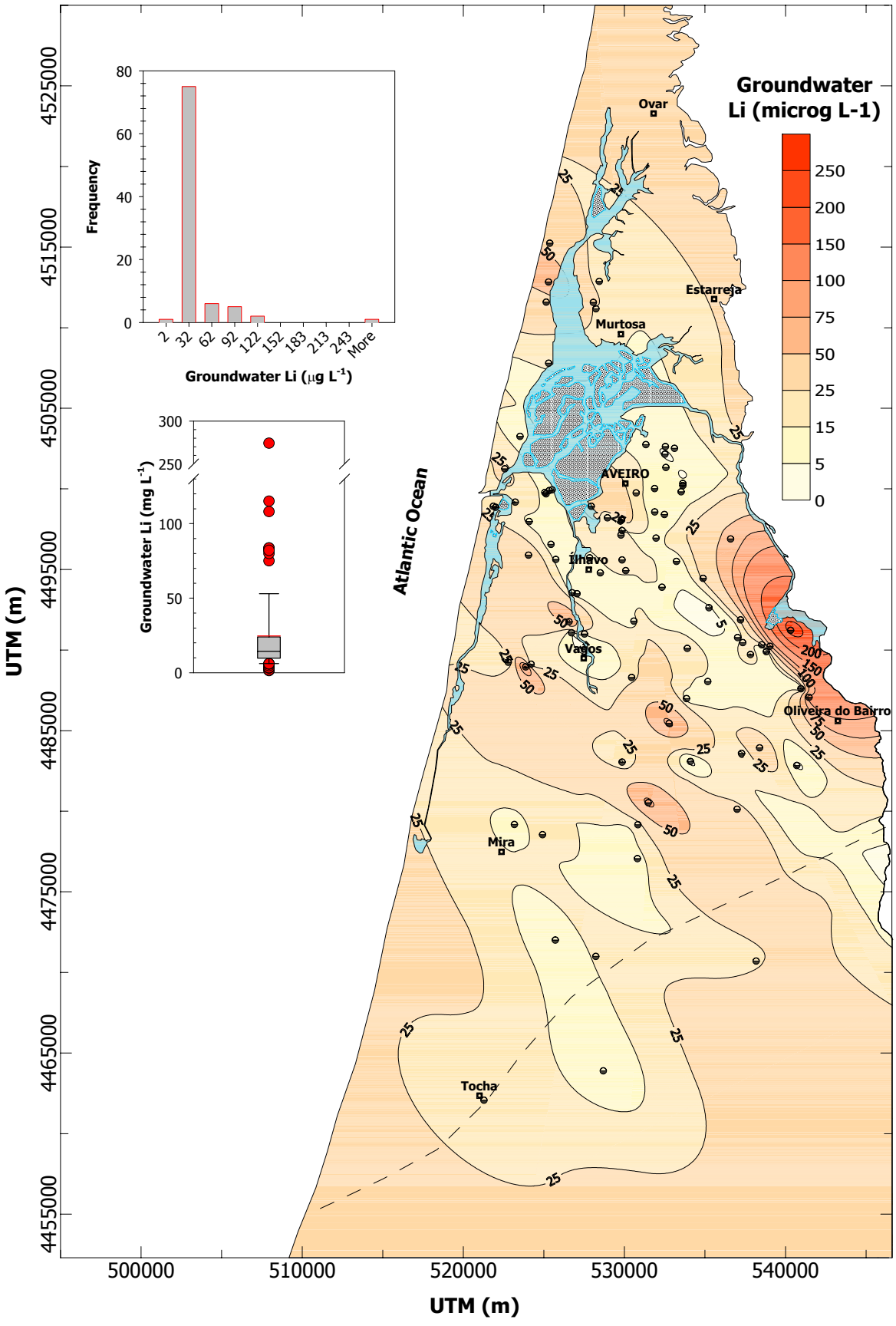
Groundwater
Li (microg L-1)
250
200
150
100
75
50
25
15
5
0
Ovar
Estarreja
Murtosa
AVEIRO
Ílhavo
Vagos
Oliveira do Bairro
Mira
Tocha
Atlantic Ocean
Frequency
Groundwater Li (μg L-1)
2
32
62
92
122
152
183
213
243
More
Groundwater Li (mg L-1)
UTM (m)
UTM (m)
500000
510000
520000
530000
540000
4455000
4465000
4475000
4485000
4495000
4505000
4515000
4525000

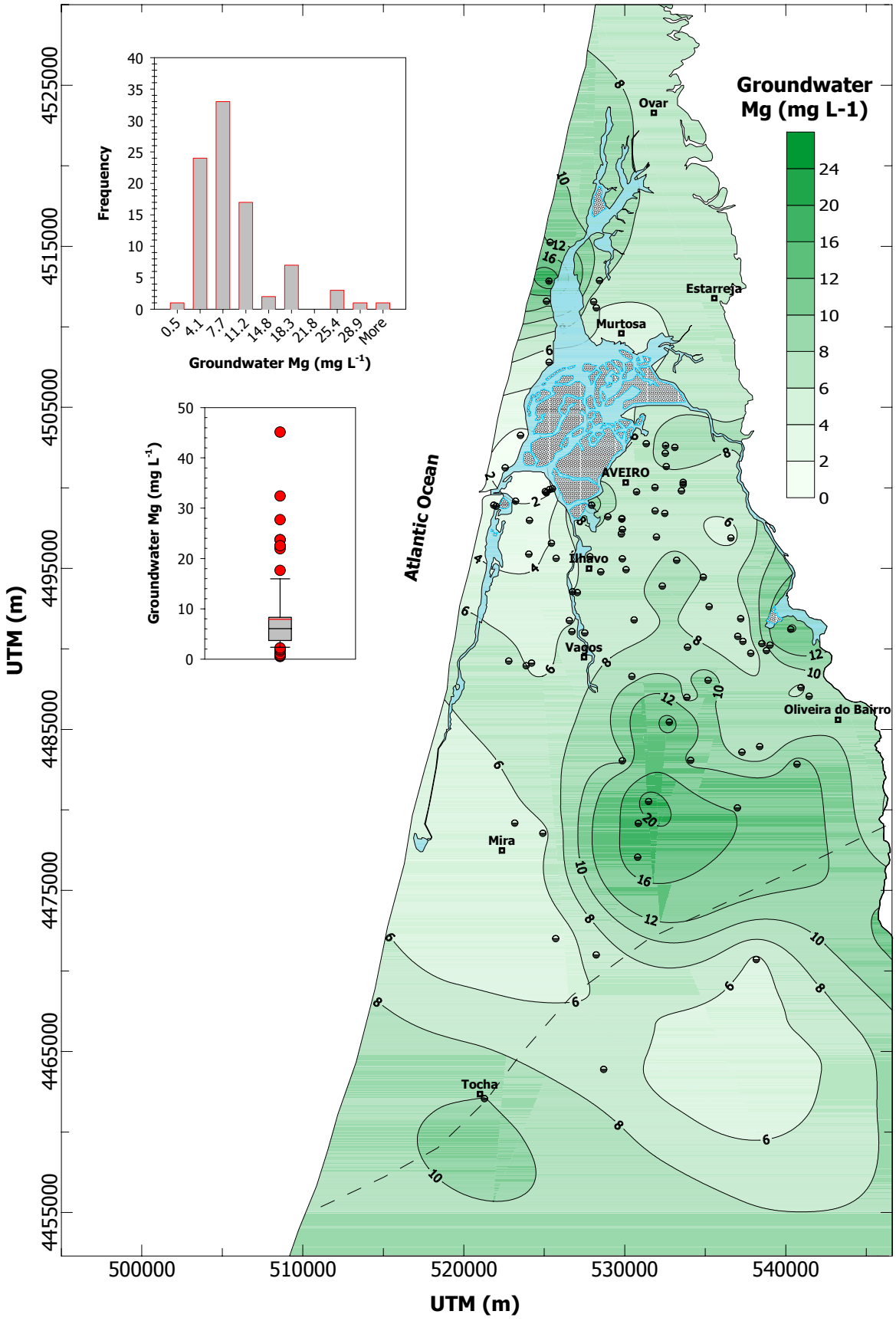
Groundwater Mg (mg L-1)
24
20
16
12
10
8
6
4
2
0
Ovar
Estarreja
Murtosa
AVEIRO
Ilhavo
Vagos
Oliveira do Bairro
Mira
Tocha
Atlantic Ocean
Frequency
0.5
4.1
7.7
11.2
14.8
18.3
21.8
25.4
28.9
More
Groundwater Mg (mg L-1)
Groundwater Mg (mg L-1)
UTM (m)
UTM (m)
4525000
4515000
4505000
4495000
4485000
4475000
4465000
4455000
500000
510000
520000
530000
540000

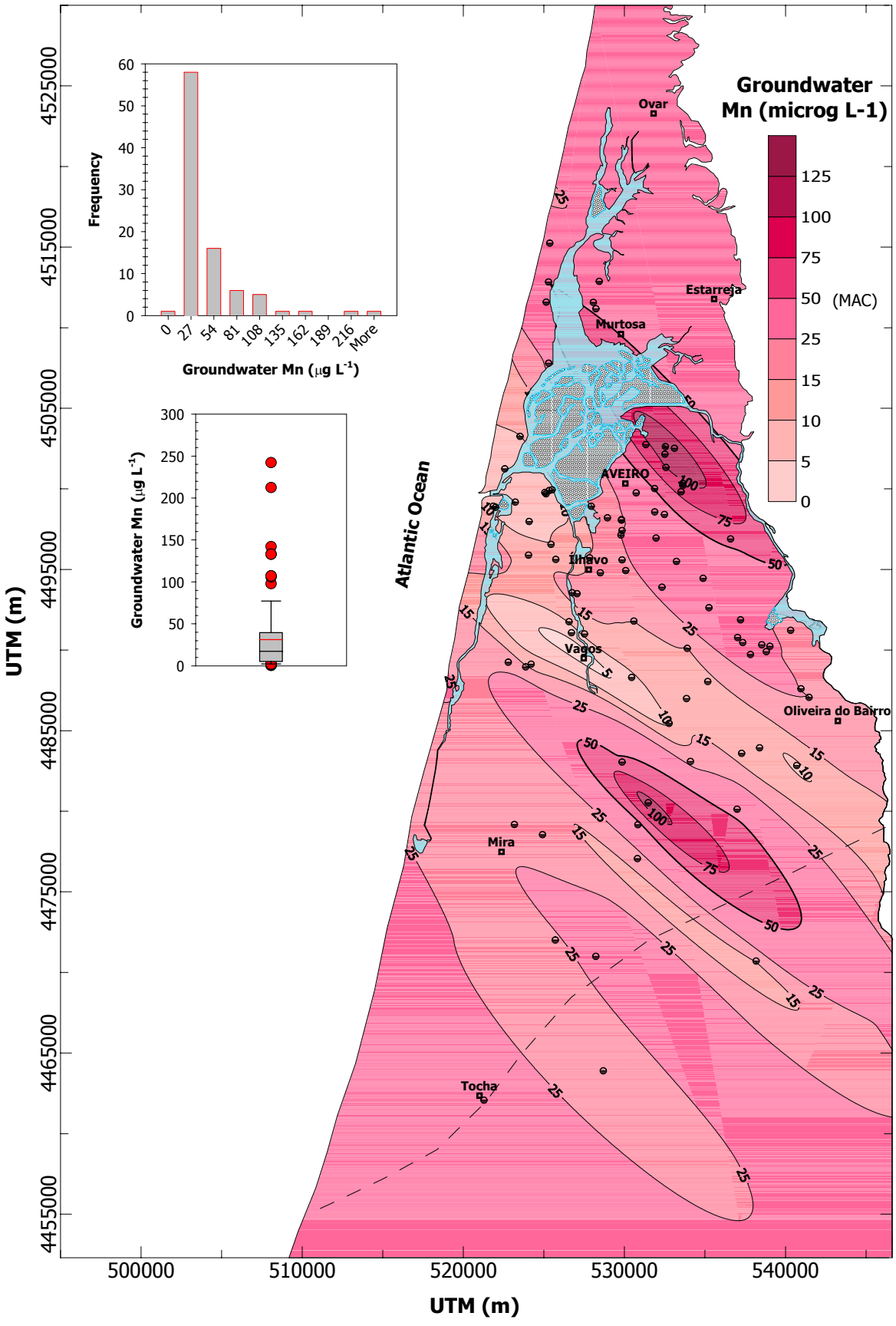
Groundwater
Mn (microg L-1)
125
100
75
50 (MAC)
25
15
10
5
0
Ovar
Estarreja
Murtosa
AVEIRO
Ílhavo
Vagos
Oliveira do Bairro
Mira
Tocha
Atlantic Ocean
Frequency
Groundwater Mn (μg L-1)
0
27
54
81
108
135
162
189
216
More
Groundwater Mn (μg L-1)
UTM (m)
UTM (m)
500000
510000
520000
530000
540000
4525000
4515000
4505000
4495000
4485000
4475000
4465000
4455000

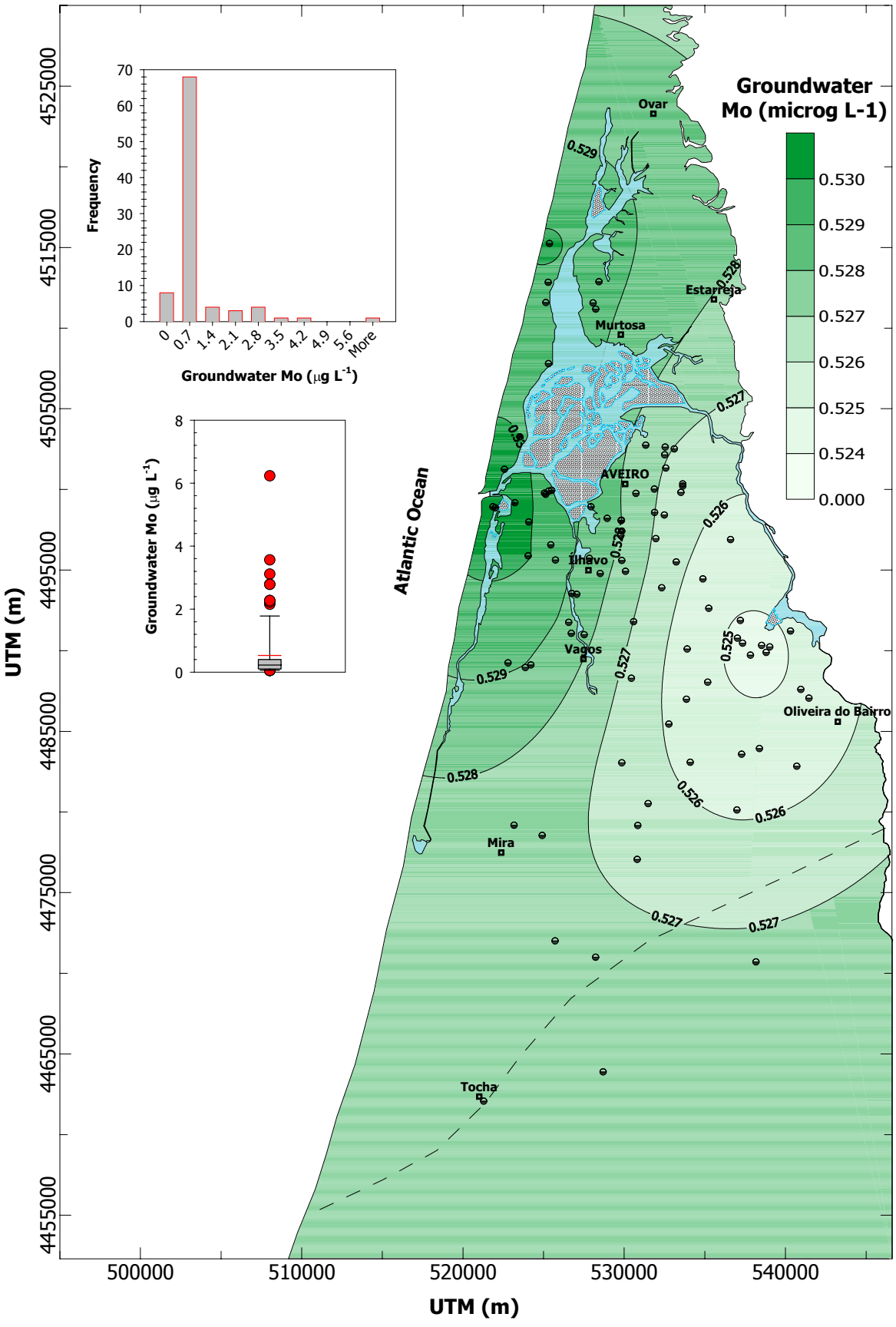
Groundwater Mo (microg L-1)
0.530
0.529
0.528
0.527
0.526
0.525
0.524
0.000
Frequency
Groundwater Mo (µg L-1)
0
0.7
1.4
2.1
2.8
3.5
4.2
4.9
5.6
More
Groundwater Mo (µg L-1)
Atlantic Ocean
Ovar
Estarreja
Murtosa
AVEIRO
Ilhavo
Vagos
Oliveira do Bairro
Mira
Tocha
0.529
0.528
0.527
0.526
0.525
UTM (m)
4525000
4515000
4505000
4495000
4485000
4475000
4465000
4455000
500000
510000
520000
530000
540000
UTM (m)

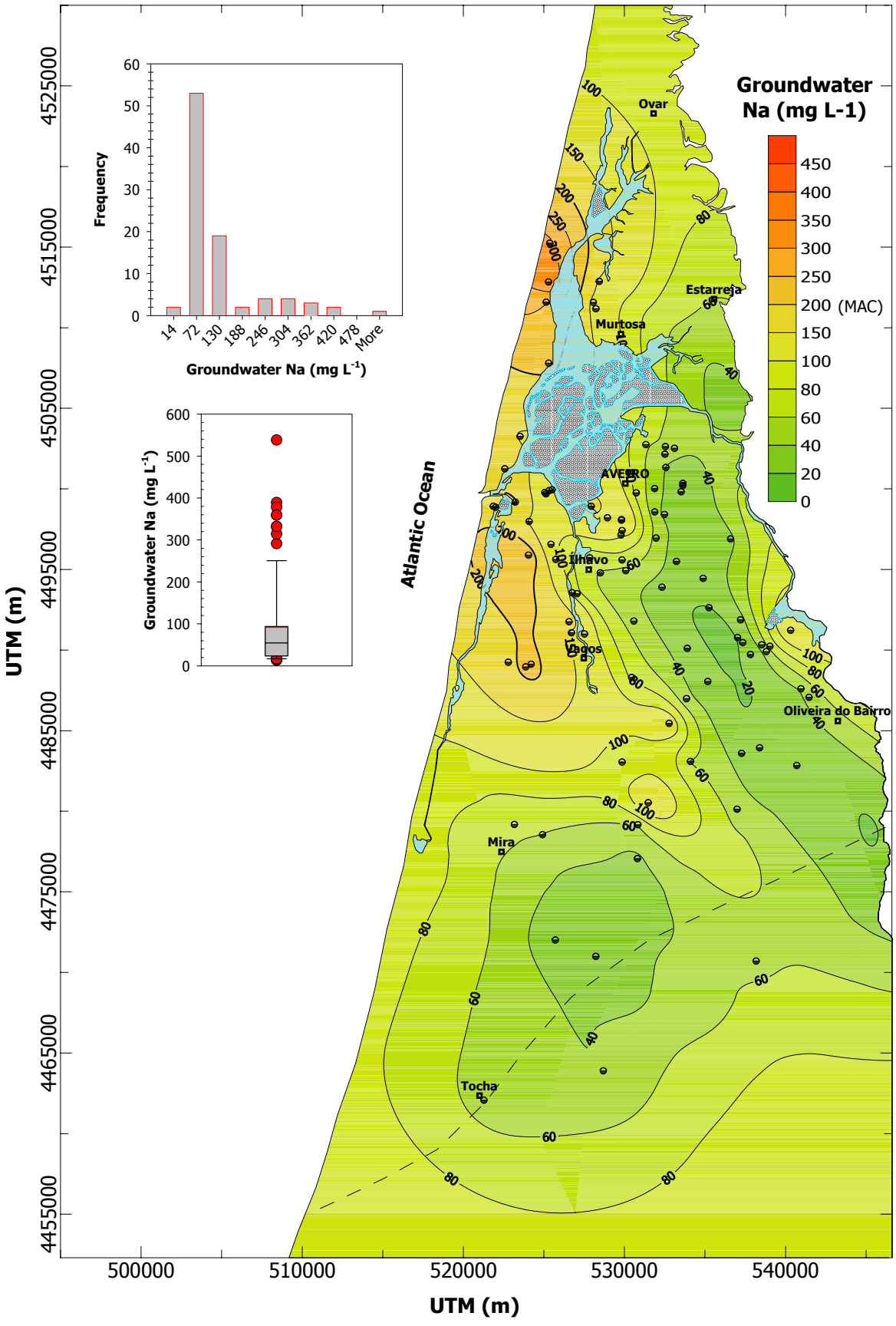
Groundwater Na (mg L-1)
450
400
350
300
250
200 (MAC)
150
100
80
60
40
20
0
Ovar
Estarreja
Murtosa
AVEIRO
Ilhavo
Vagos
Oliveira do Bairro
Mira
Tocha
Atlantic Ocean
Frequency
Groundwater Na (mg L-1)
14
72
130
188
246
304
362
420
478
More
Groundwater Na (mg L-1)
UTM (m)
4525000
4515000
4505000
4495000
4485000
4475000
4465000
4455000
500000
510000
520000
530000
540000
UTM (m)

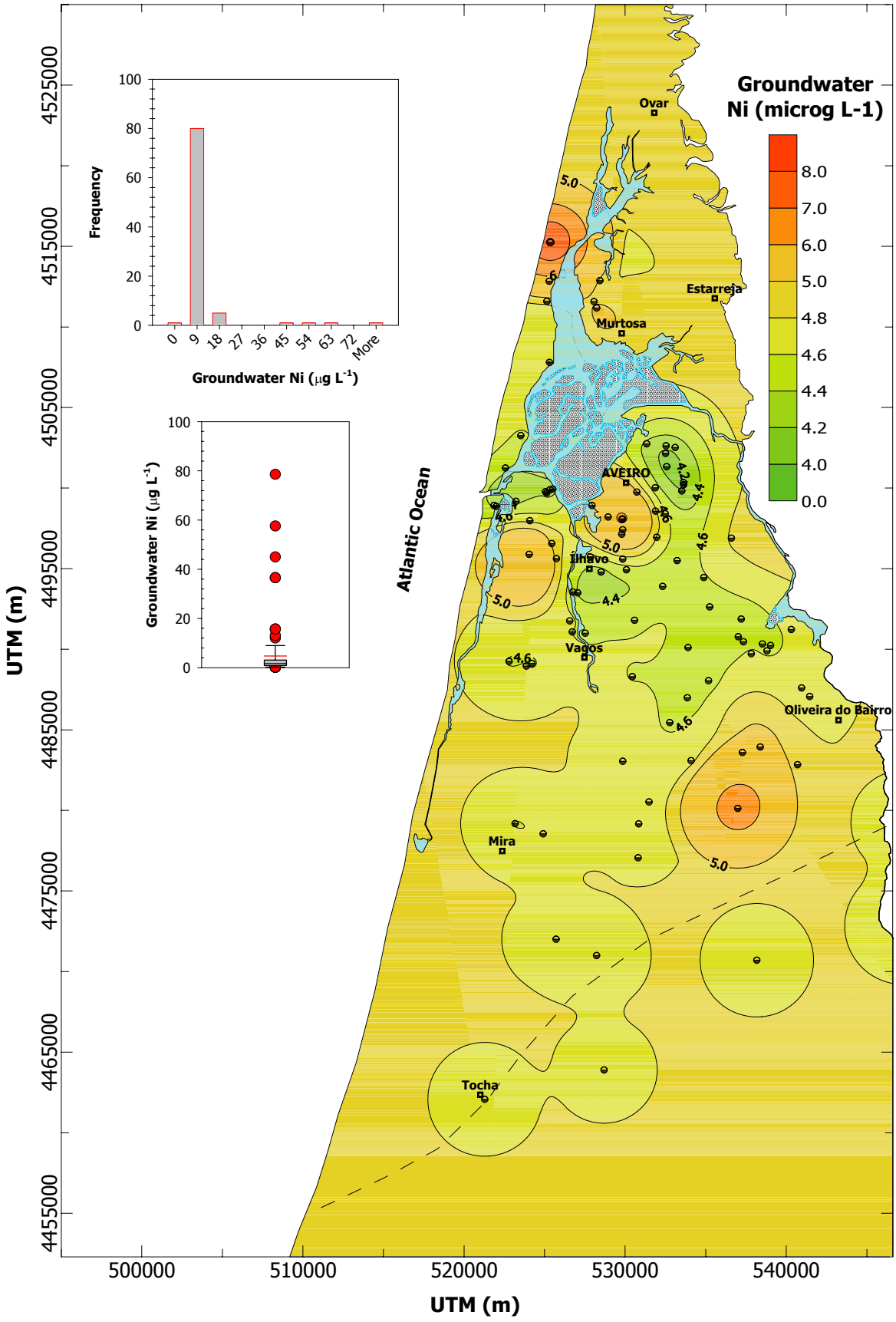
Groundwater
Ni (microg L-1)
8.0
7.0
6.0
5.0
4.8
4.6
4.4
4.2
4.0
0.0
Frequency
Groundwater Ni (µg L-1)
0 9 18 27 36 45 54 63 72 More
Groundwater Ni (µg L-1)
Atlantic Ocean
Ovar
Estarreja
Murtosa
AVEIRO
Ilhavo
Vagos
Oliveira do Bairro
Mira
Tocha
UTM (m)
4525000
4515000
4505000
4495000
4485000
4475000
4465000
4455000
500000
510000
520000
530000
540000
UTM (m)

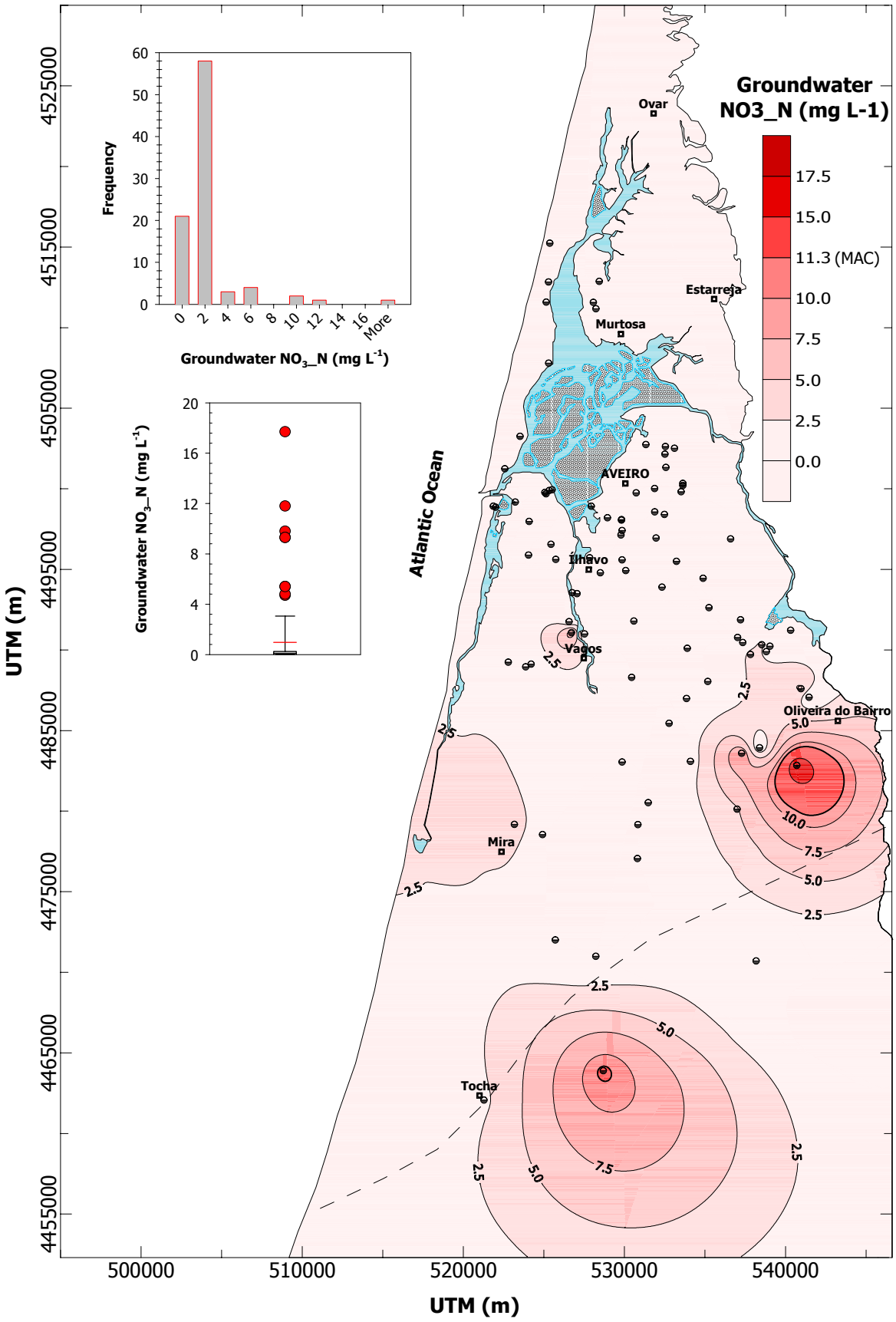
Groundwater
NO3_N (mg L-1)
17.5
15.0
11.3 (MAC)
10.0
7.5
5.0
2.5
0.0
Frequency
Groundwater NO3_N (mg L-1)
Groundwater NO3_N (mg L-1)
Atlantic Ocean
Ovar
Estarreja
Murtosa
AVEIRO
Ílhavo
Vagos
Oliveira do Bairro
Mira
Tocha
UTM (m)
UTM (m)
4525000
4515000
4505000
4495000
4485000
4475000
4465000
4455000
500000
510000
520000
530000
540000

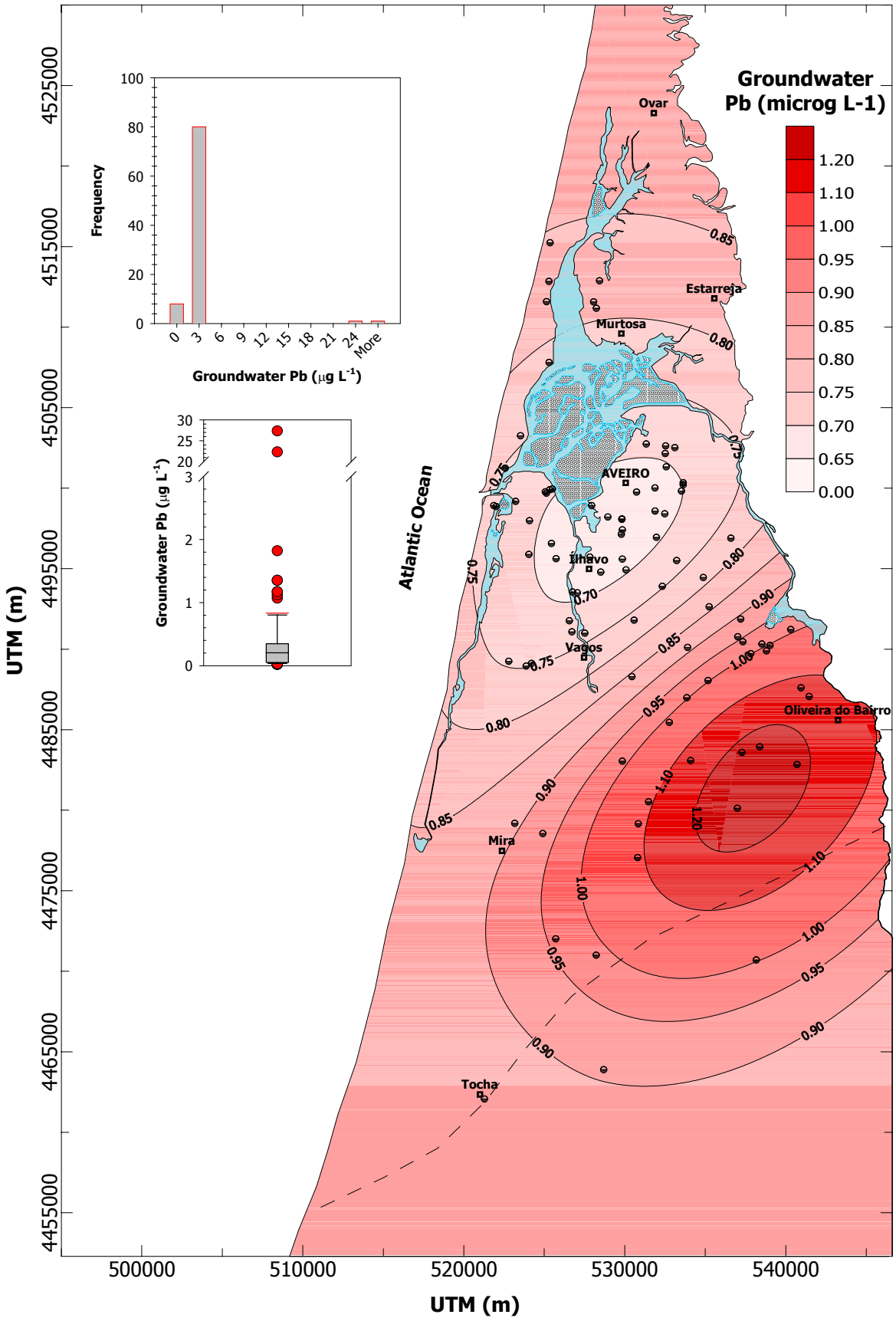
Groundwater Pb (microg L-1)
1.20
1.10
1.00
0.95
0.90
0.85
0.80
0.75
0.70
0.65
0.00
Ovar
Estarreja
Murtosa
AVEIRO
Ílhavo
Vagos
Oliveira do Bairro
Mira
Tocha
Atlantic Ocean
Frequency
Groundwater Pb (μg L-1)
0 3 6 9 12 15 18 21 24 More
Groundwater Pb (μg L-1)
UTM (m)
UTM (m)
4525000
4515000
4505000
4495000
4485000
4475000
4465000
4455000
500000
510000
520000
530000
540000

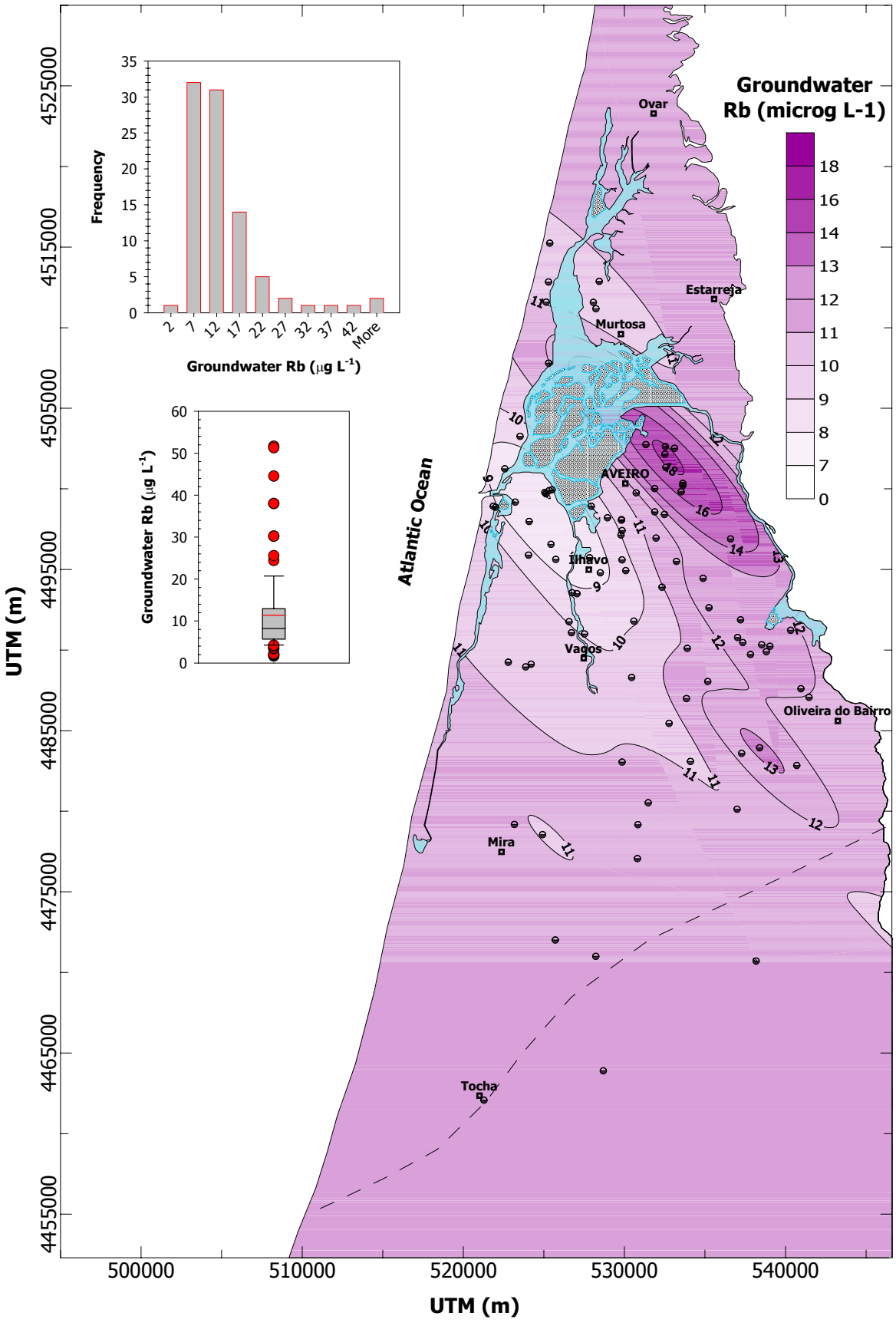
Groundwater
Rb (microg L-1)
18
16
14
13
12
11
10
9
8
7
0
Ovar
Estarreja
Murtosa
AVEIRO
Ílhavo
Vagos
Oliveira do Bairro
Mira
Tocha
Atlantic Ocean
Frequency
Groundwater Rb (μg L-1)
2
7
12
17
22
27
32
37
42
More
Groundwater Rb (μg L-1)
UTM (m)
UTM (m)
500000
510000
520000
530000
540000
4525000
4515000
4505000
4495000
4485000
4475000
4465000
4455000

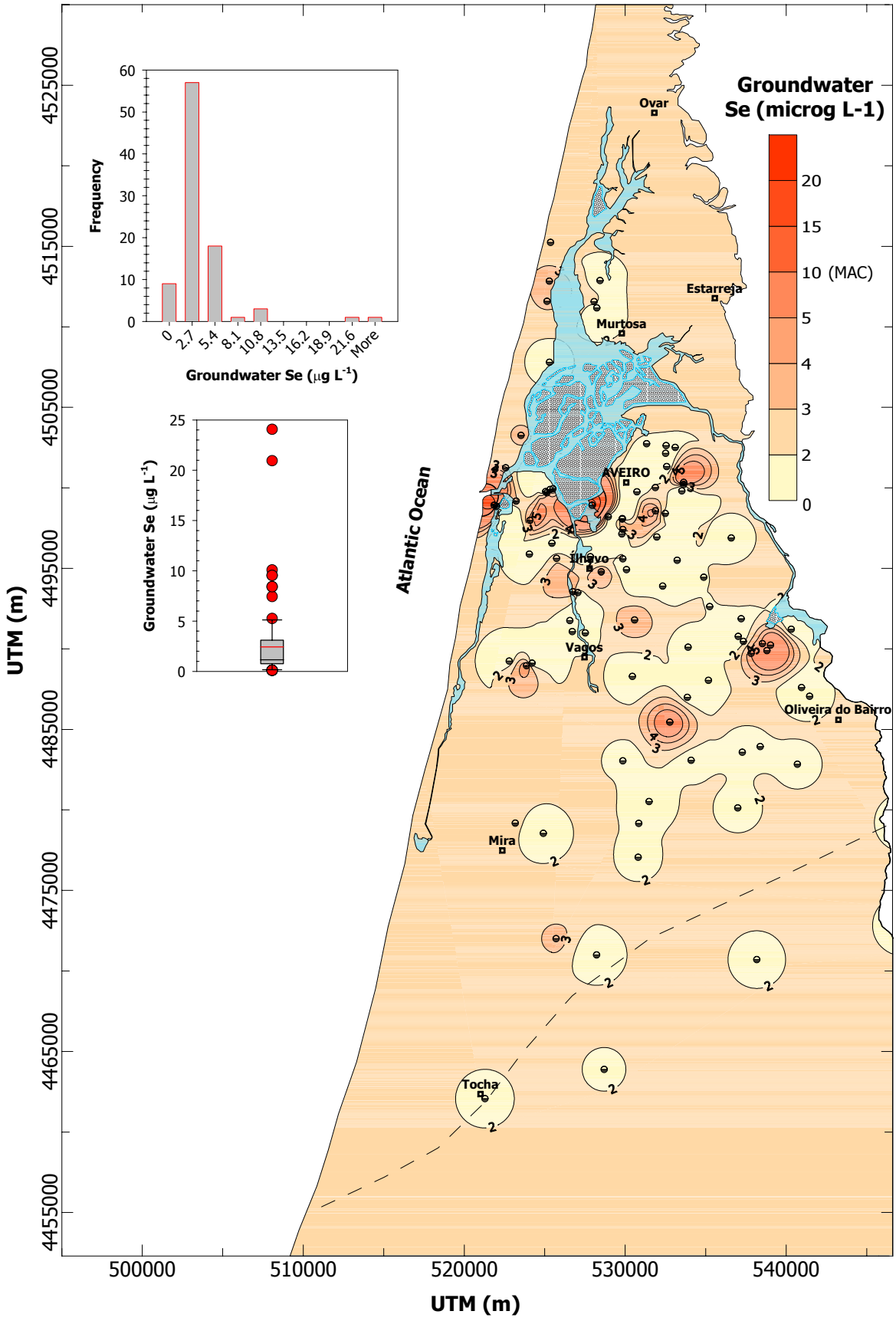
Groundwater Se (microg L-1)
20
15
10 (MAC)
5
4
3
2
0
Ovar
Estarreja
Murtosa
AVEIRO
Ílhavo
Vagos
Oliveira do Bairro
Mira
Tocha
Atlantic Ocean
Frequency
Groundwater Se (μg L-1)
0
2.7
5.4
8.1
10.8
13.5
16.2
18.9
21.6
More
Groundwater Se (μg L-1)
UTM (m)
UTM (m)
4525000
4515000
4505000
4495000
4485000
4475000
4465000
4455000
500000
510000
520000
530000
540000

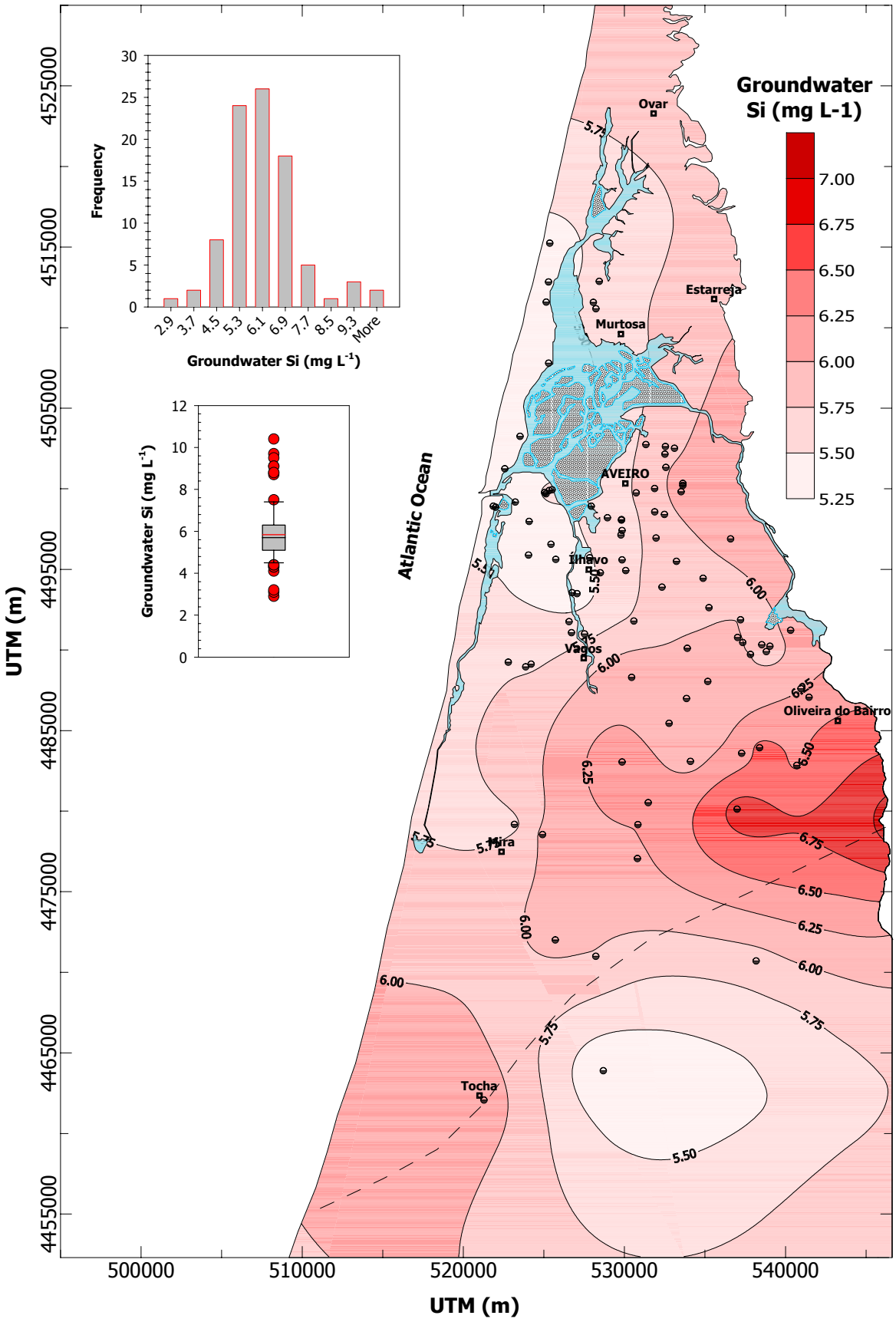
Groundwater Si (mg L-1)
7.00
6.75
6.50
6.25
6.00
5.75
5.50
5.25
Frequency
Groundwater Si (mg L-1)
2.9
3.7
4.5
5.3
6.1
6.9
7.7
8.5
9.3
More
Groundwater Si (mg L-1)
Atlantic Ocean
Ovar
Estarreja
Murtosa
AVEIRO
Ílhavo
Vagos
Oliveira do Bairro
Mira
Tocha
UTM (m)
UTM (m)
4525000
4515000
4505000
4495000
4485000
4475000
4465000
4455000
500000
510000
520000
530000
540000

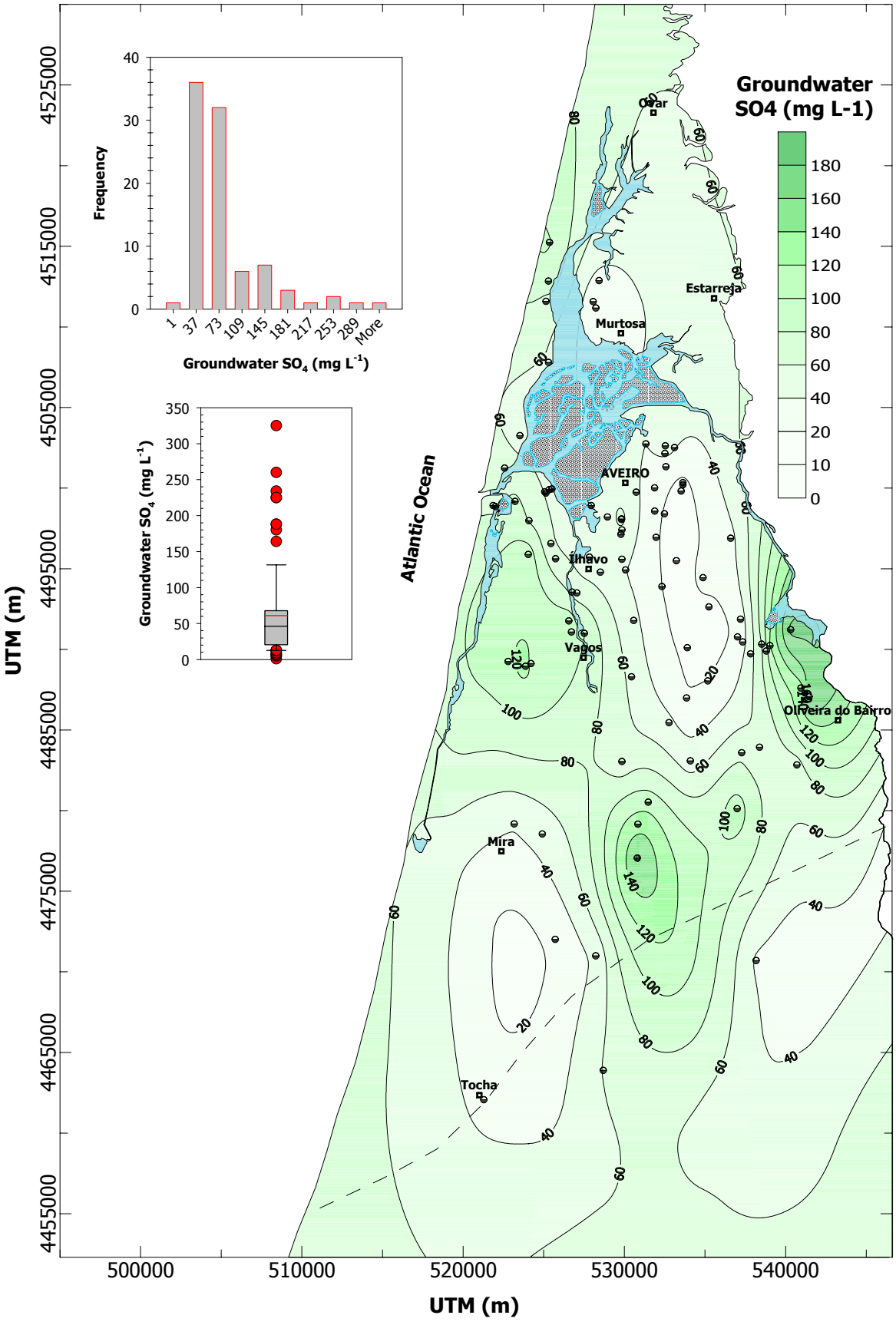
Groundwater SO4 (mg L-1)
180
160
140
120
100
80
60
40
20
10
0
Frequency
Groundwater SO4 (mg L-1)
1
37
73
109
145
181
217
253
289
More
Groundwater SO4 (mg L-1)
Atlantic Ocean
Ovar
Estarreja
Murtosa
AVEIRO
Ilhavo
Vagos
Oliveira do Bairro
Mira
Tocha
UTM (m)
UTM (m)
4525000
4515000
4505000
4495000
4485000
4475000
4465000
4455000
500000
510000
520000
530000
540000

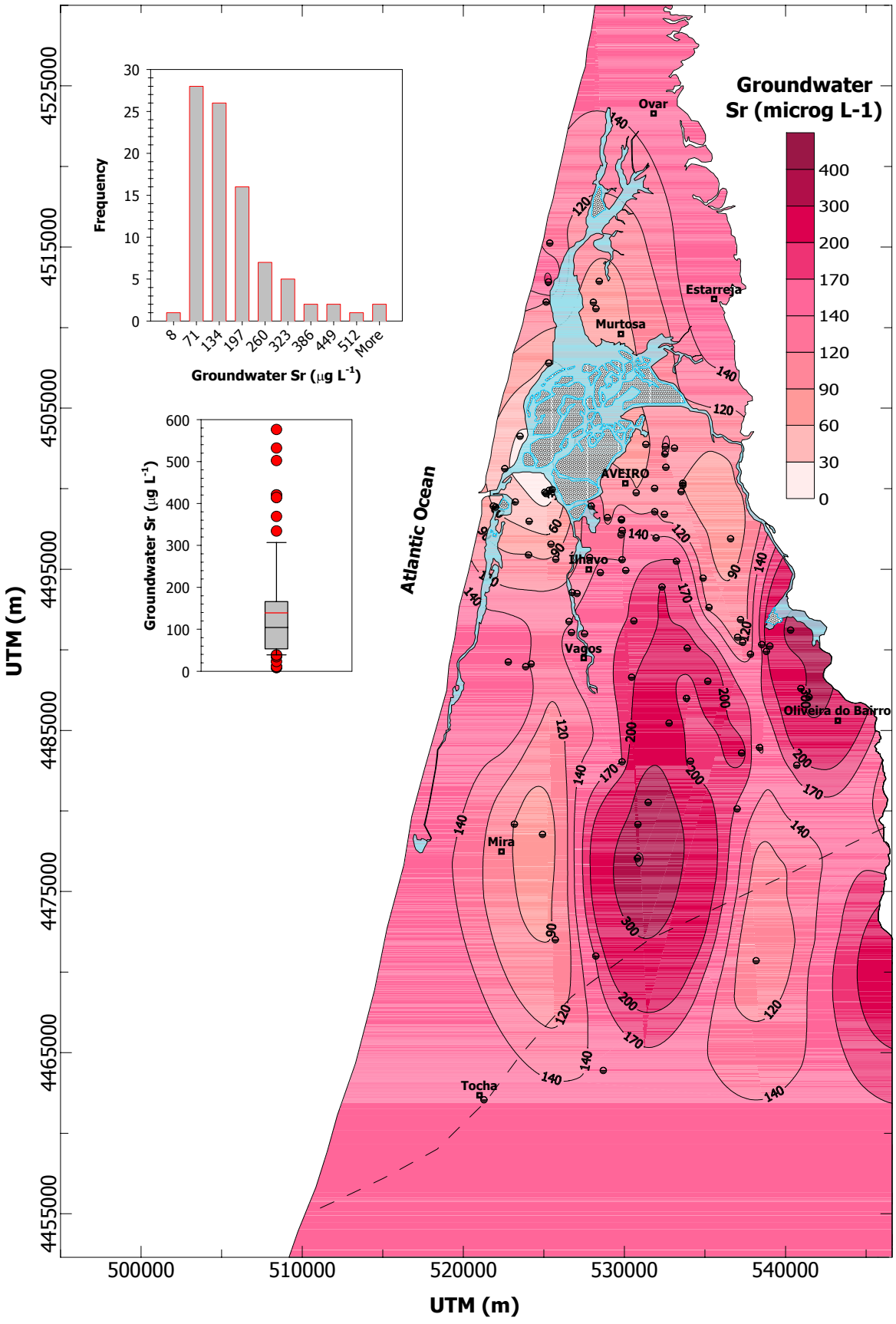
Groundwater Sr (microg L-1)
400
300
200
170
140
120
90
60
30
0
Atlantic Ocean
Ovar
Estarreja
Murtosa
AVEIRO
Ilhavo
Vagos
Oliveira do Bairro
Mira
Tocha
Frequency
Groundwater Sr (μg L-1)
8
71
134
197
260
323
386
449
512
More
UTM (m)
UTM (m)
500000
510000
520000
530000
540000
4525000
4515000
4505000
4495000
4485000
4475000
4465000
4455000

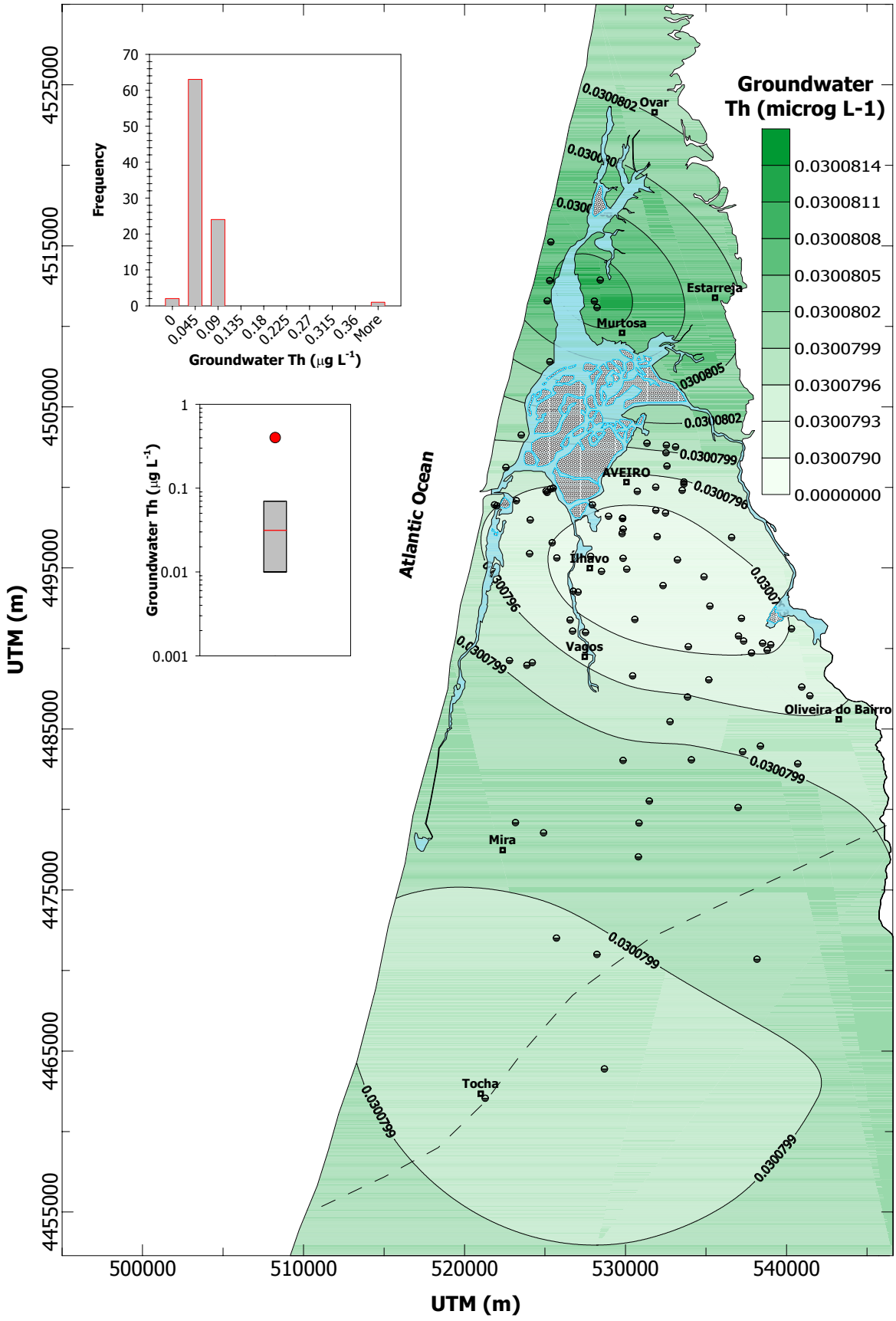
Groundwater Th (microg L-1)
0.0300814
0.0300811
0.0300808
0.0300805
0.0300802
0.0300799
0.0300796
0.0300793
0.0300790
0.0000000
Frequency
Groundwater Th (µg L-1)
0
0.045
0.09
0.135
0.18
0.225
0.27
0.315
0.36
More
Groundwater Th (µg L-1)
Atlantic Ocean
Ovar
Estarreja
Murtosa
AVEIRO
Ílhavo
Vagos
Oliveira do Bairro
Mira
Tocha
UTM (m)
UTM (m)
4525000
4515000
4505000
4495000
4485000
4475000
4465000
4455000
500000
510000
520000
530000
540000

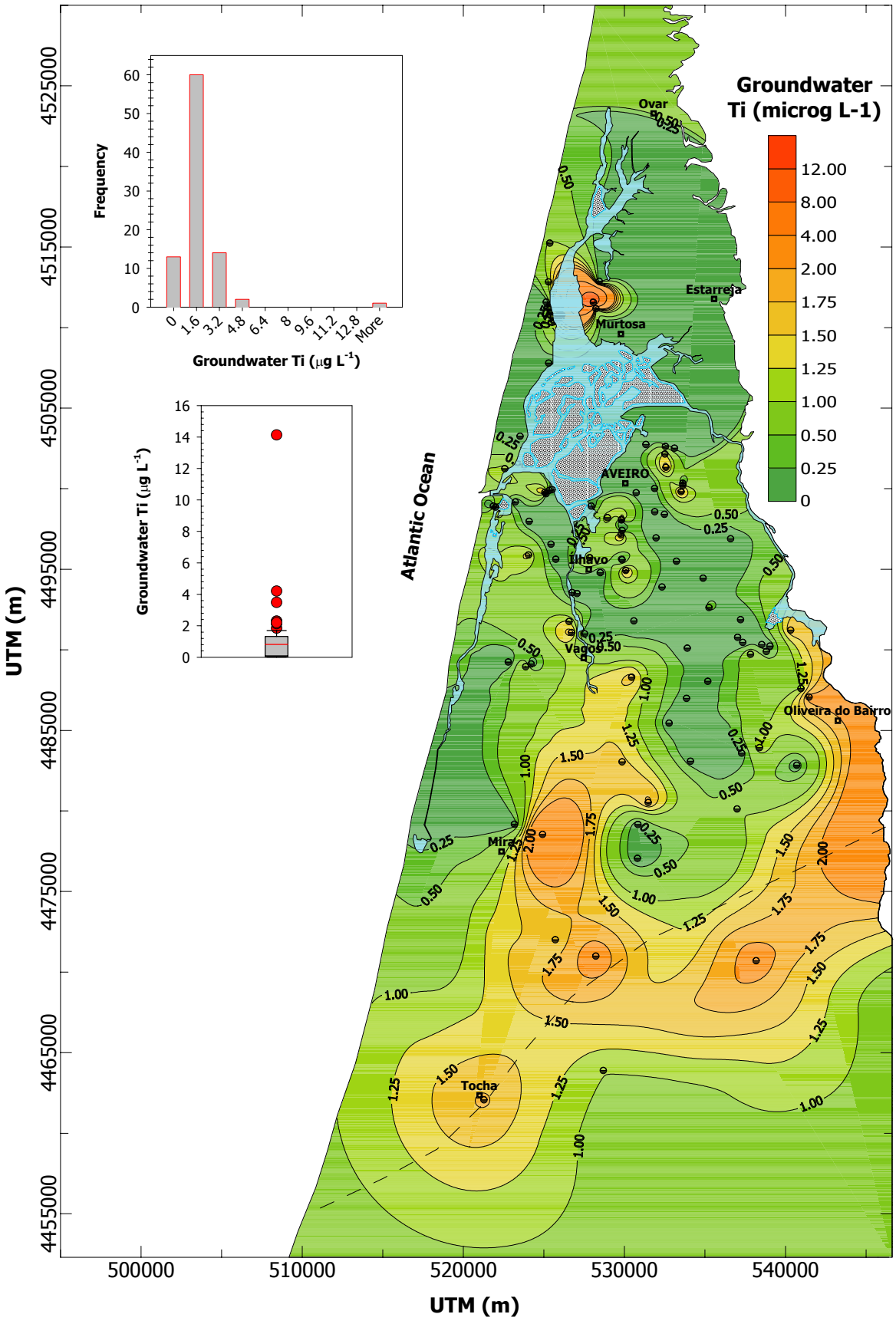
Groundwater Ti (microg L-1)
12.00
8.00
4.00
2.00
1.75
1.50
1.25
1.00
0.50
0.25
0
Frequency
Groundwater Ti (μg L-1)
0
1.6
3.2
4.8
6.4
8
9.6
11.2
12.8
More
Groundwater Ti (μg L-1)
Atlantic Ocean
Ovar
Estarreja
Murtosa
AVEIRO
Ilhavo
Vagos
Oliveira do Bairro
Mira
Tocha
UTM (m)
4525000
4515000
4505000
4495000
4485000
4475000
4465000
4455000
500000
510000
520000
530000
540000
UTM (m)

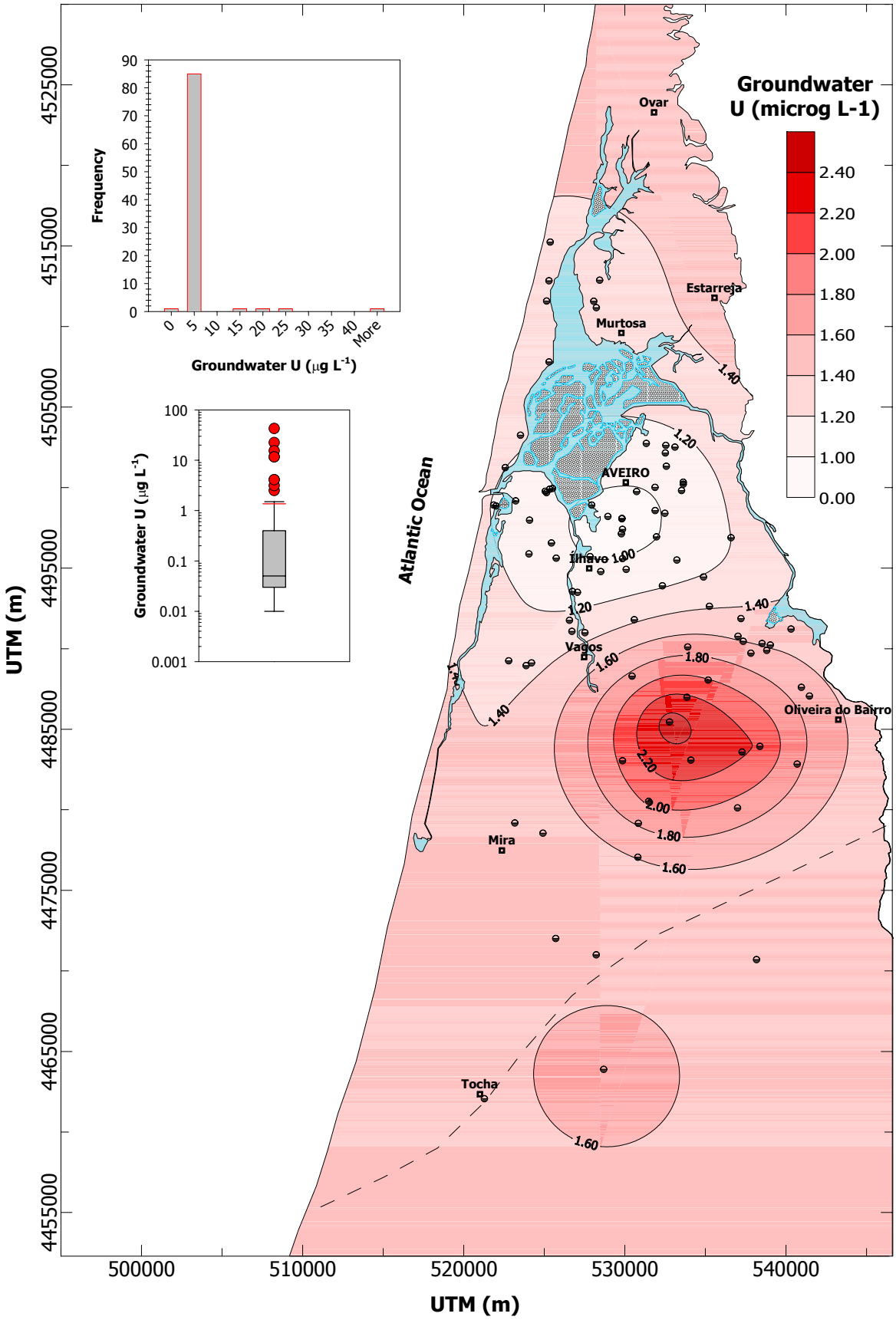
Groundwater U (microg L-1)
2.40
2.20
2.00
1.80
1.60
1.40
1.20
1.00
0.00
Frequency
Groundwater U (μg L-1)
Groundwater U (μg L-1)
Atlantic Ocean
Ovar
Estarreja
Murtosa
AVEIRO
Ilhavo
Vagos
Oliveira do Bairro
Mira
Tocha
UTM (m)
UTM (m)
500000
510000
520000
530000
540000
4455000
4465000
4475000
4485000
4495000
4505000
4515000
4525000

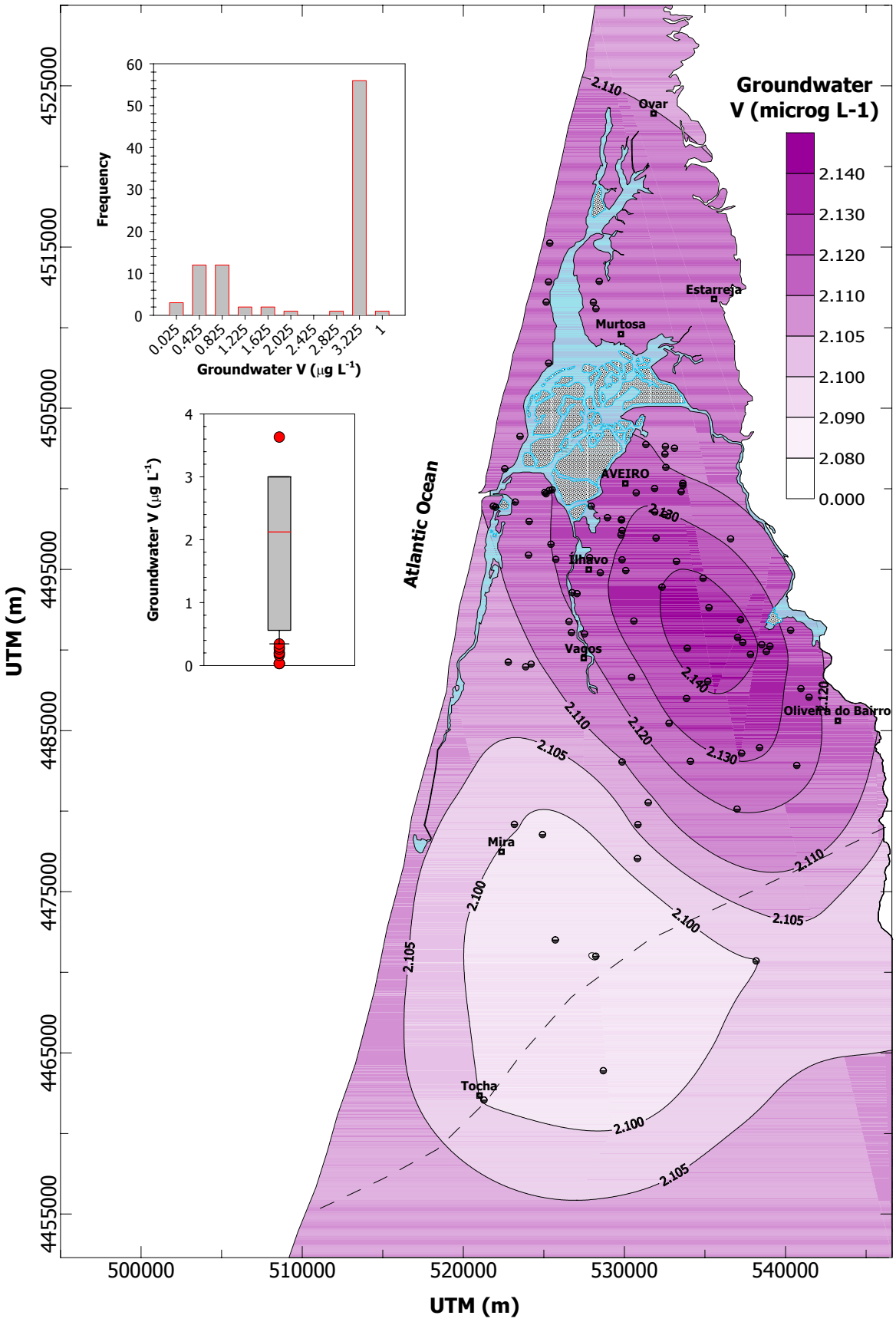
Groundwater V (microg L-1)
2.140
2.130
2.120
2.110
2.105
2.100
2.090
2.080
0.000
Frequency
Groundwater V (µg L-1)
0.025
0.425
0.825
1.225
1.625
2.025
2.425
2.825
3.225
1
Groundwater V (µg L-1)
Atlantic Ocean
Ovar
Estarreja
Murtosa
AVEIRO
Ílhavo
Vagos
Oliveira do Bairro
Mira
Tocha
UTM (m)
500000
510000
520000
530000
540000
4525000
4515000
4505000
4495000
4485000
4475000
4465000
4455000

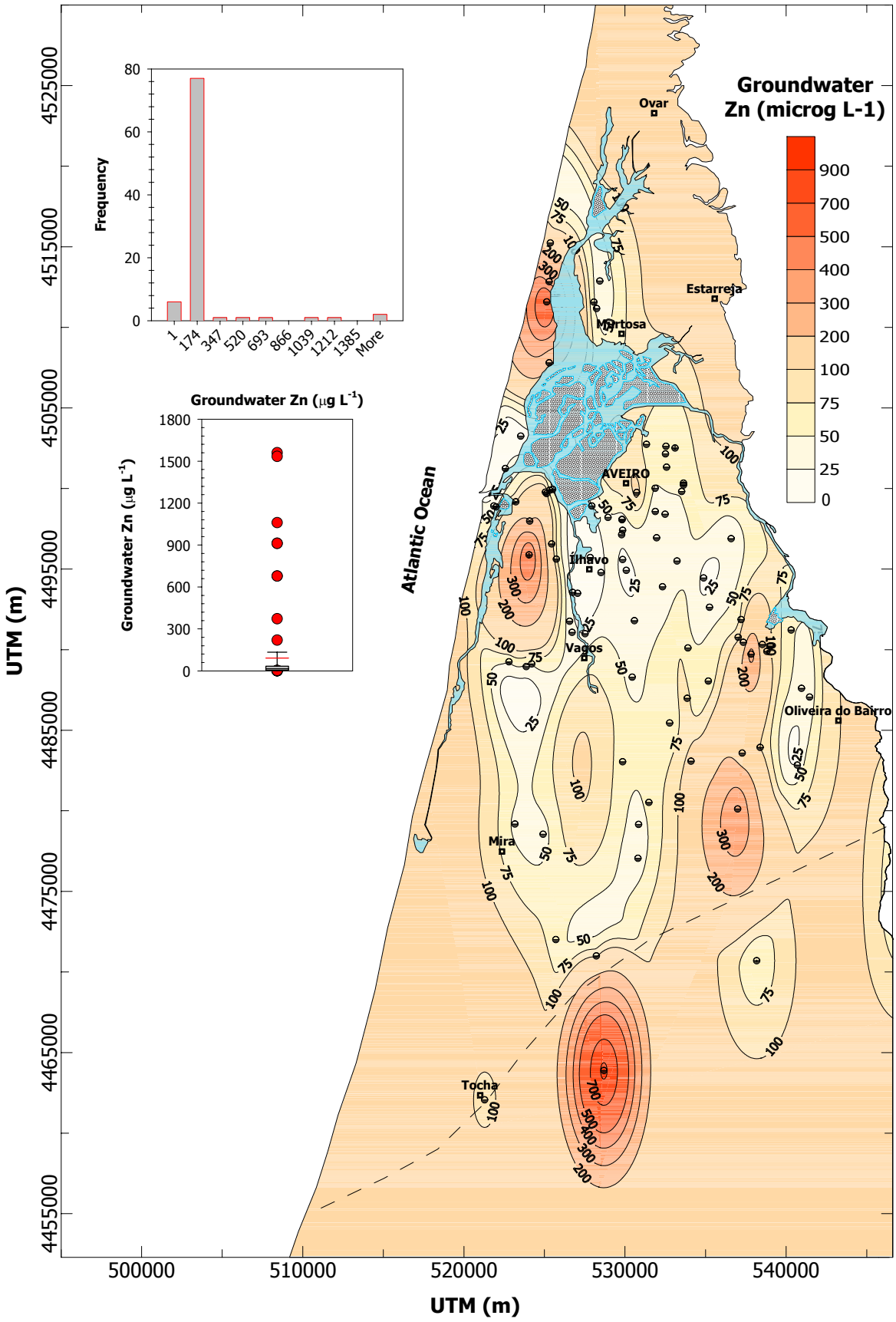
Groundwater Zn (microg L-1)
900
700
500
400
300
200
100
75
50
25
0
Ovar
Estarreja
Murtosa
AVEIRO
Ilhavo
Vagos
Oliveira do Bairro
Mira
Tocha
Atlantic Ocean
Frequency
80
60
40
20
0
1
174
347
520
693
866
1039
1212
1385
More
Groundwater Zn (µg L-1)
1800
1500
1200
900
600
300
0
Groundwater Zn (µg L-1)
UTM (m)
4525000
4515000
4505000
4495000
4485000
4475000
4465000
4455000
500000
510000
520000
530000
540000
UTM (m)

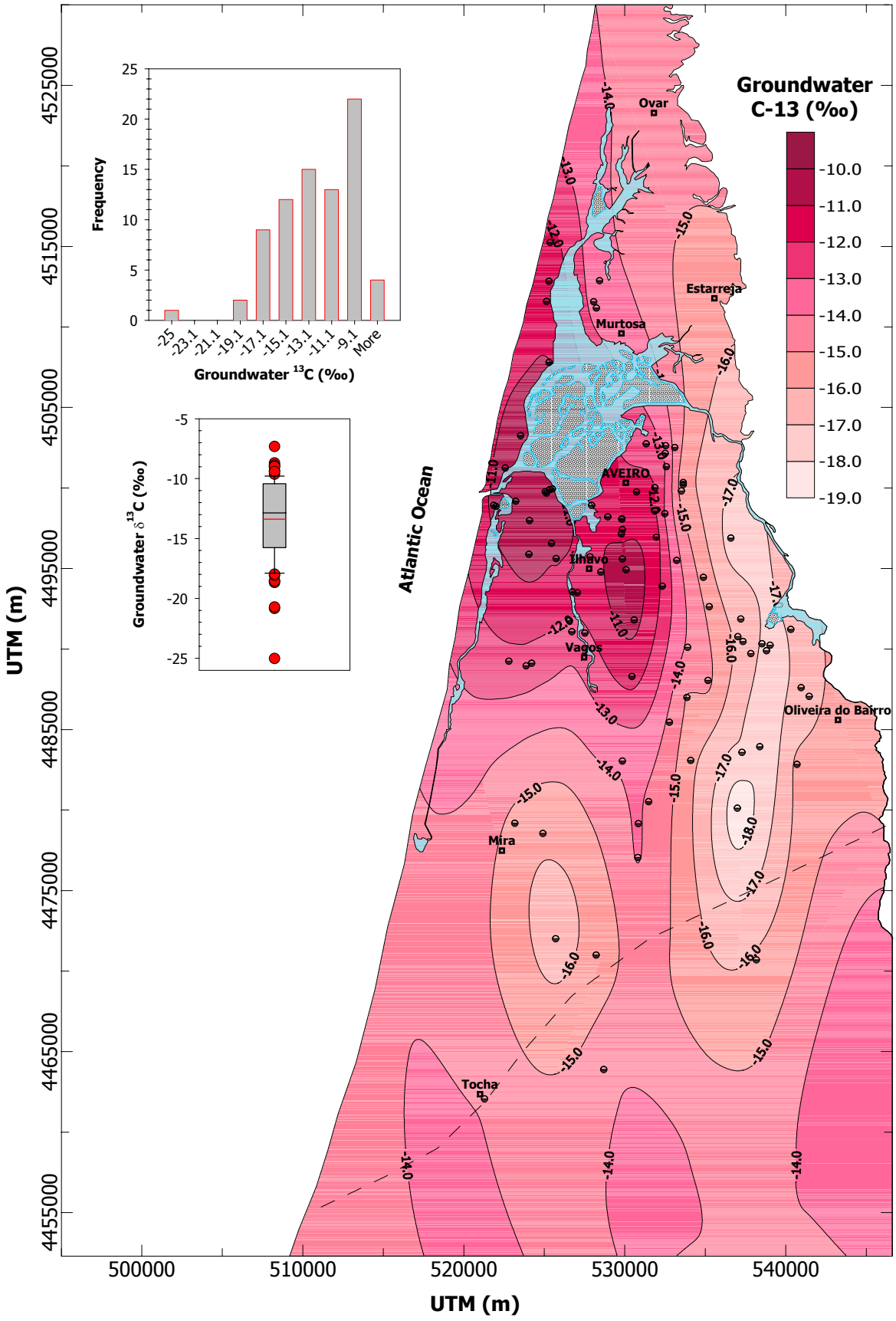
Groundwater C-13 (‰)
-10.0
-11.0
-12.0
-13.0
-14.0
-15.0
-16.0
-17.0
-18.0
-19.0
Frequency
Groundwater ^{13}C (‰)
Groundwater δ^{13}C (‰)
Atlantic Ocean
Ovar
Estarreja
Murtosa
AVEIRO
Ilhavo
Vagos
Oliveira do Bairro
Mira
Tocha
UTM (m)
UTM (m)
4525000
4515000
4505000
4495000
4485000
4475000
4465000
4455000
500000
510000
520000
530000
540000

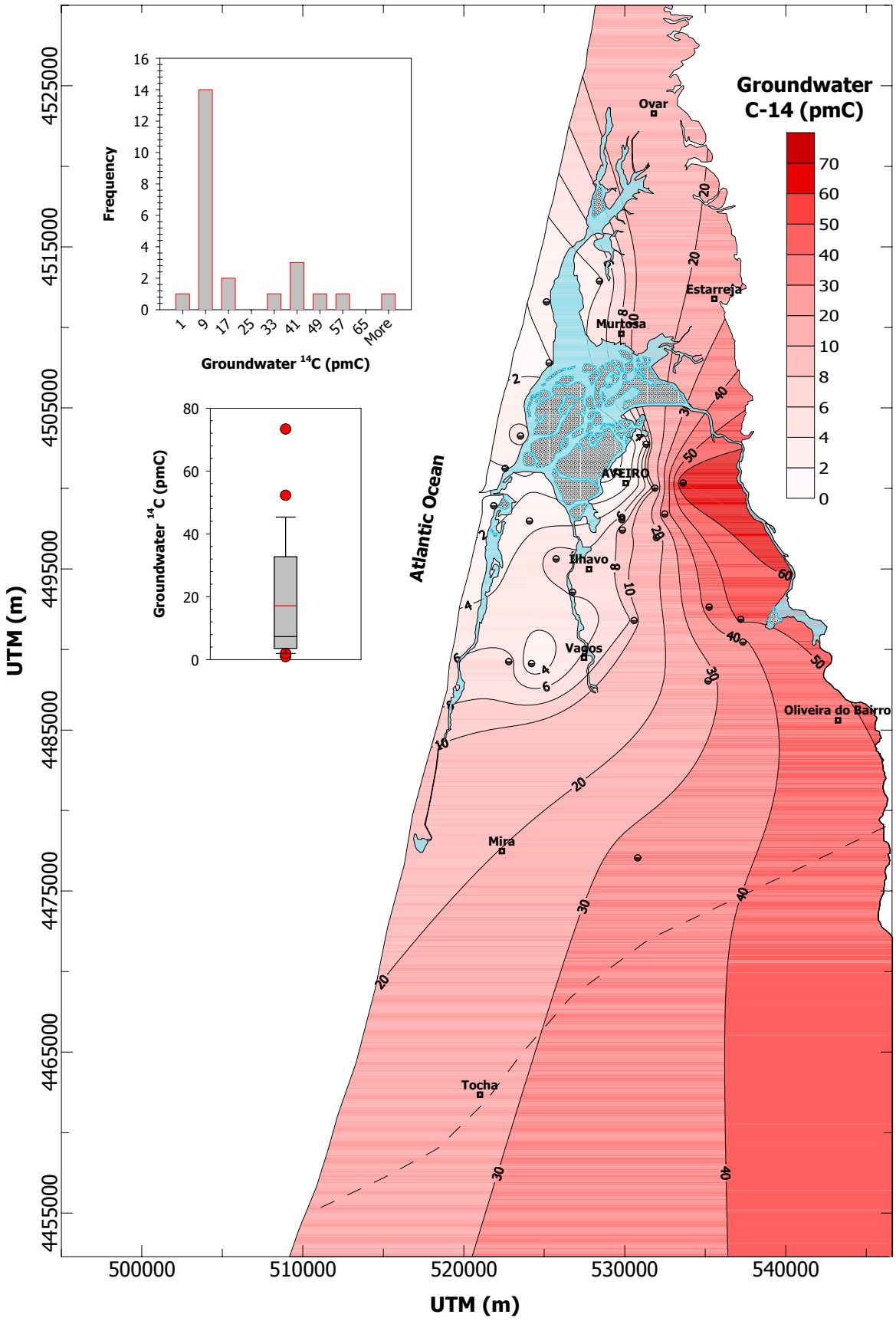
Groundwater
C-14 (pmC)
70
60
50
40
30
20
10
8
6
4
2
0
Ovar
Estarreja
Murtosa
AVEIRO
Ílhavo
Vagos
Oliveira do Bairro
Mira
Tocha
Atlantic Ocean
Frequency
Groundwater ^{14}C (pmC)
Groundwater ^{14}C (pmC)
UTM (m)
UTM (m)
4525000
4515000
4505000
4495000
4485000
4475000
4465000
4455000
500000
510000
520000
530000
540000

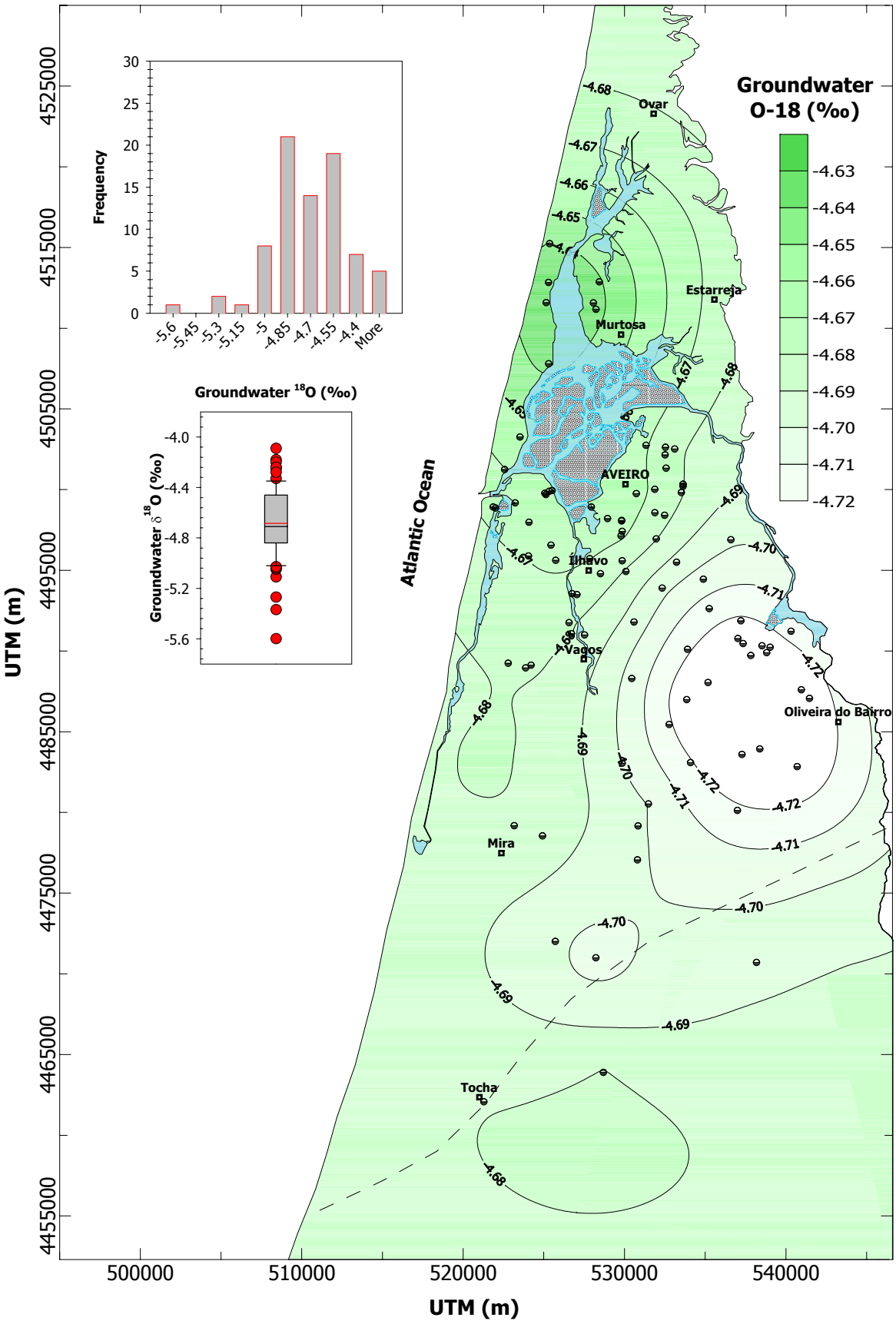
Groundwater
O-18 (‰)
-4.63
-4.64
-4.65
-4.66
-4.67
-4.68
-4.69
-4.70
-4.71
-4.72
Frequency
30
25
20
15
10
5
0
-5.6
-5.45
-5.3
-5.15
-5
-4.85
-4.7
-4.55
-4.4
More
Groundwater ^{18}O (‰)
Groundwater δ^{18}O (‰)
-4.0
-4.4
-4.8
-5.2
-5.6
Atlantic Ocean
Ovar
Estarreja
Murtosa
AVEIRO
Ílhavo
Vagos
Oliveira do Bairro
Mira
Tocha
-4.68
-4.67
-4.66
-4.65
-4.69
-4.70
-4.71
-4.72
UTM (m)
4525000
4515000
4505000
4495000
4485000
4475000
4465000
4455000
500000
510000
520000
530000
540000
UTM (m)

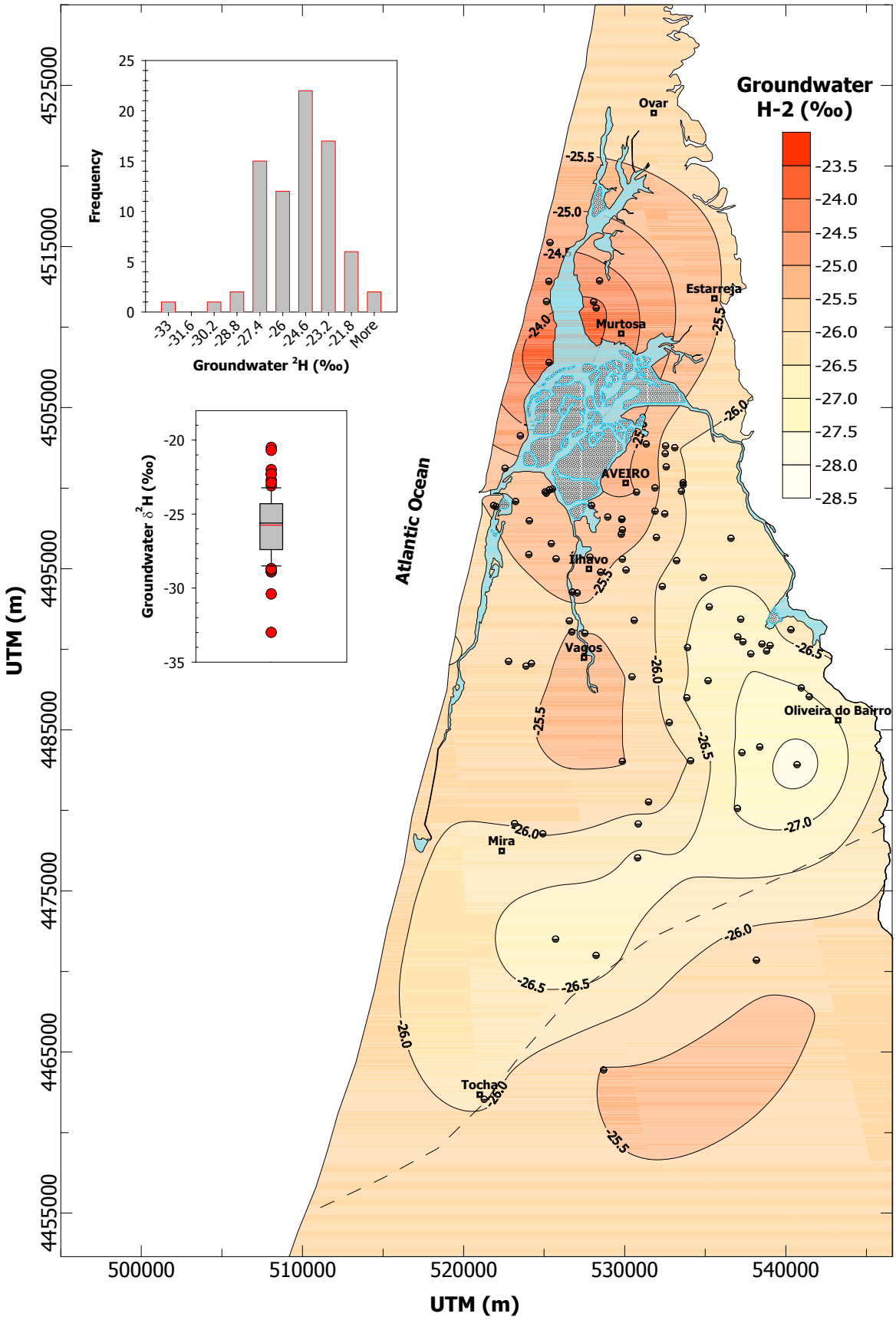
Groundwater
H-2 (‰)
-23.5
-24.0
-24.5
-25.0
-25.5
-26.0
-26.5
-27.0
-27.5
-28.0
-28.5
Ovar
Estarreja
Murtosa
AVEIRO
Ílhavo
Vagos
Mira
Oliveira do Bairro
Tocha
Atlantic Ocean
Frequency
Groundwater ²H (‰)
-33
-31.6
-30.2
-28.8
-27.4
-26
-24.6
-23.2
-21.8
More
Groundwater δ²H (‰)
UTM (m)
UTM (m)
4525000
4515000
4505000
4495000
4485000
4475000
4465000
4455000
500000
510000
520000
530000
540000

E

CLASSED POST MAPS

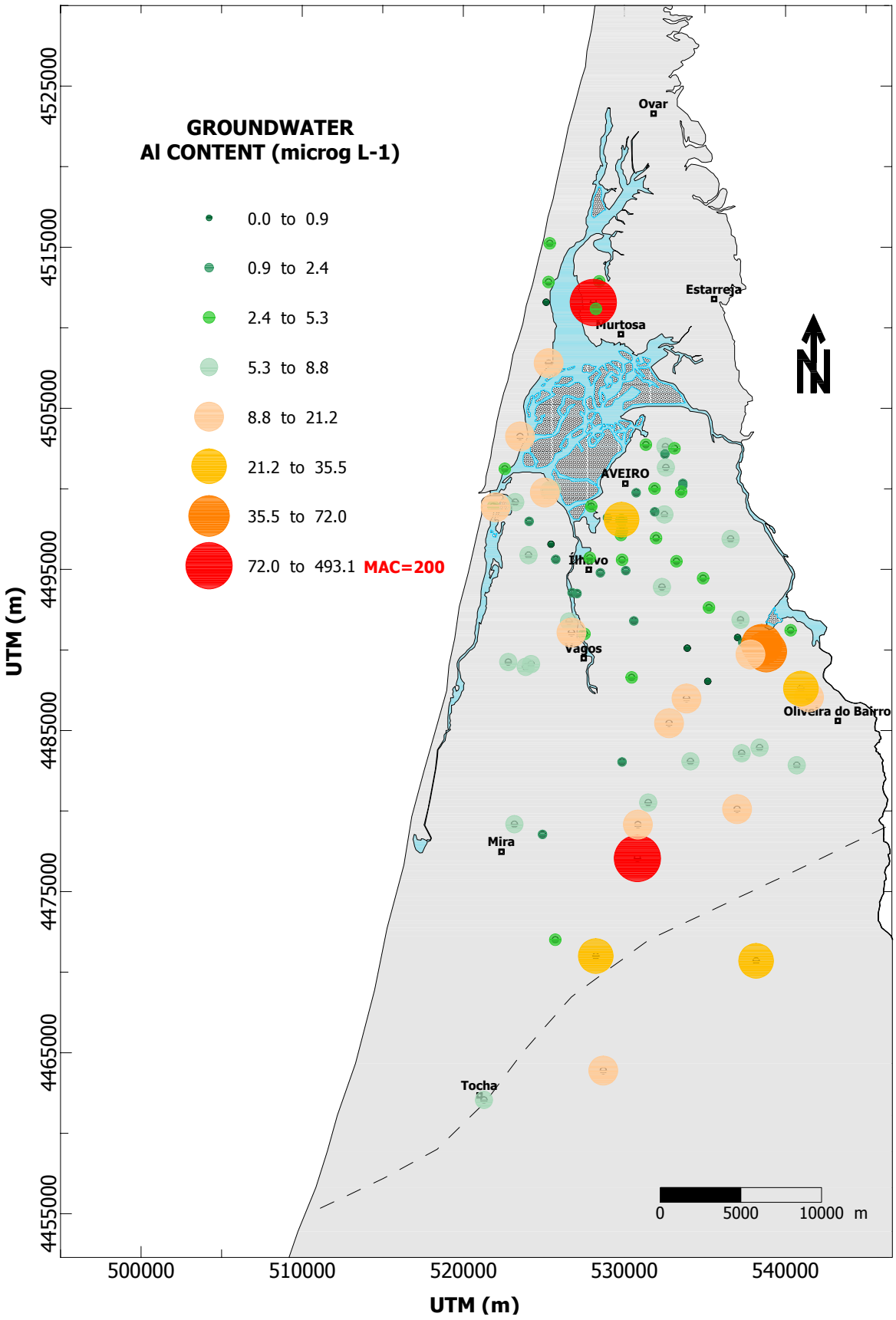
GROUNDWATER
Al CONTENT (microg L-1)
0.0 to 0.9
0.9 to 2.4
2.4 to 5.3
5.3 to 8.8
8.8 to 21.2
21.2 to 35.5
35.5 to 72.0
72.0 to 493.1 MAC=200
Ovar
Estarreja
Murtosa
AVEIRO
Ílhavo
Vagos
Oliveira do Bairro
Mira
Tocha
0
5000
10000 m
UTM (m)
UTM (m)
4525000
4515000
4505000
4495000
4485000
4475000
4465000
4455000
500000
510000
520000
530000
540000

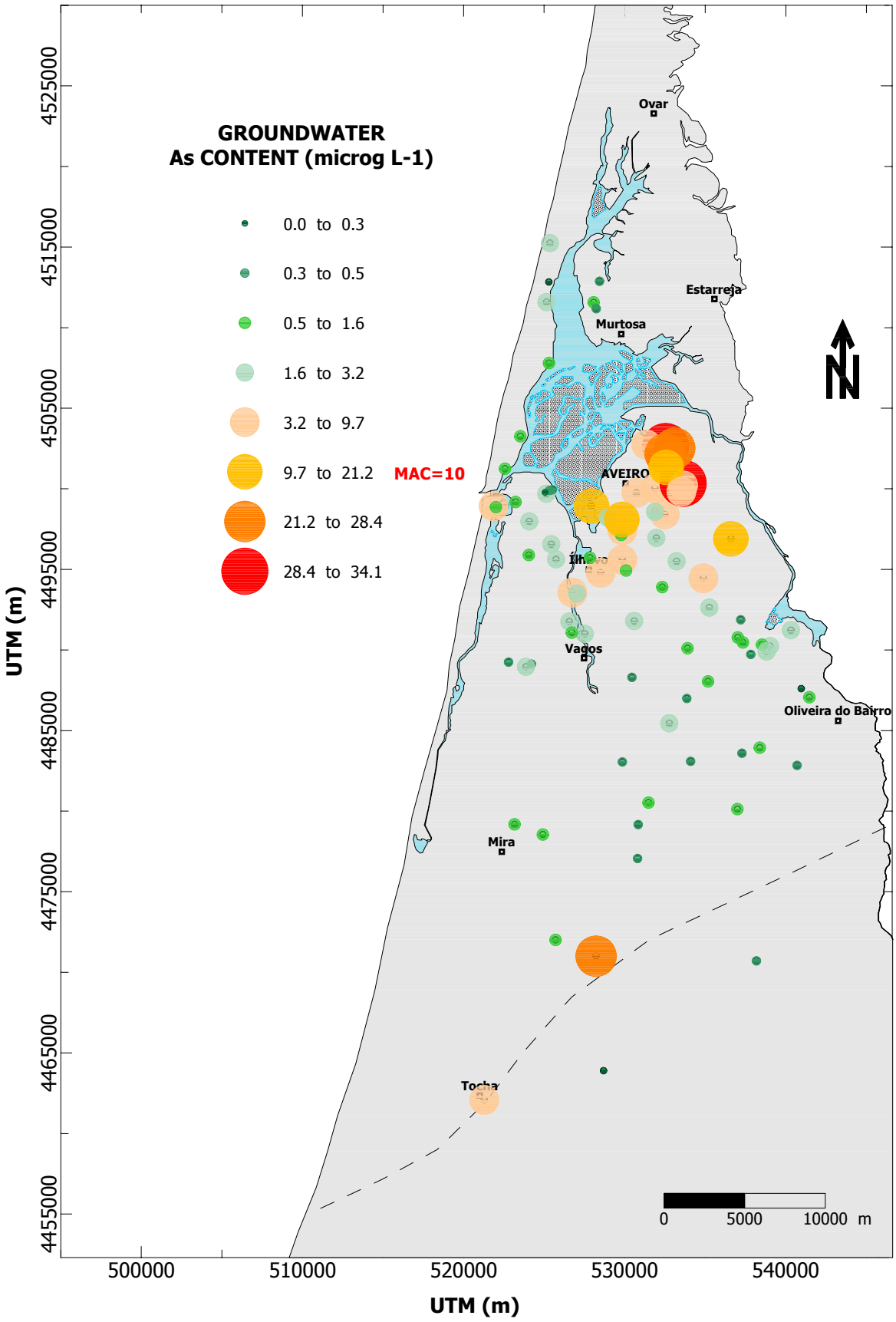
GROUNDWATER
As CONTENT (microg L-1)
0.0 to 0.3
0.3 to 0.5
0.5 to 1.6
1.6 to 3.2
3.2 to 9.7
9.7 to 21.2
MAC=10
21.2 to 28.4
28.4 to 34.1
Ovar
Estarreja
Murtosa
AVEIRO
Ílhavo
Vagos
Oliveira do Bairro
Mira
Tocha
0
5000
10000 m
4525000
4515000
4505000
4495000
4485000
4475000
4465000
4455000
500000
510000
520000
530000
540000
UTM (m)
UTM (m)

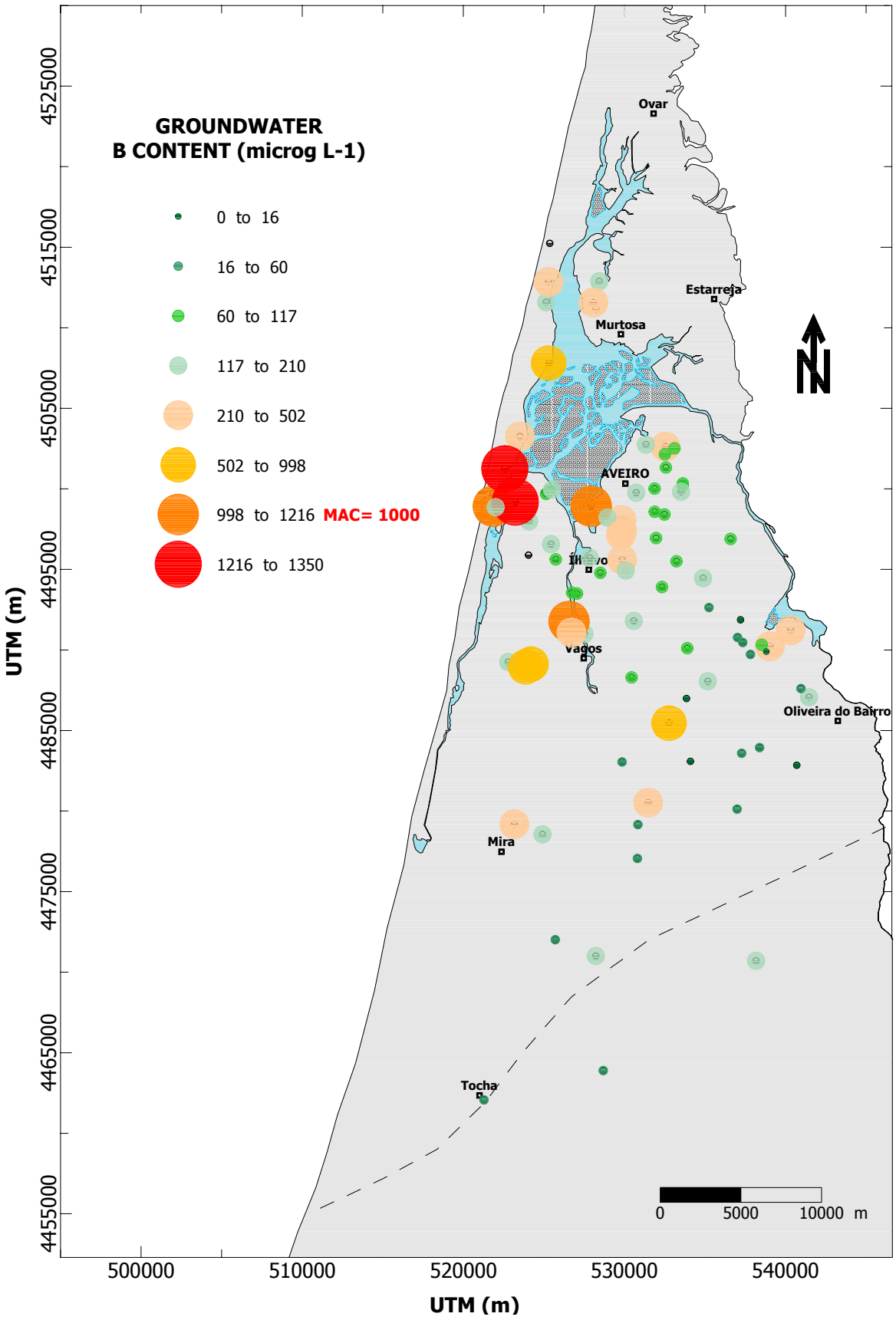
GROUNDWATER
B CONTENT (microg L-1)
0 to 16
16 to 60
60 to 117
117 to 210
210 to 502
502 to 998
998 to 1216 MAC= 1000
1216 to 1350
Ovar
Estarreja
Murtosa
AVEIRO
Vagos
Oliveira do Bairro
Mira
Tocha
0
5000
10000 m
UTM (m)
UTM (m)
4525000
4515000
4505000
4495000
4485000
4475000
4465000
4455000
500000
510000
520000
530000
540000

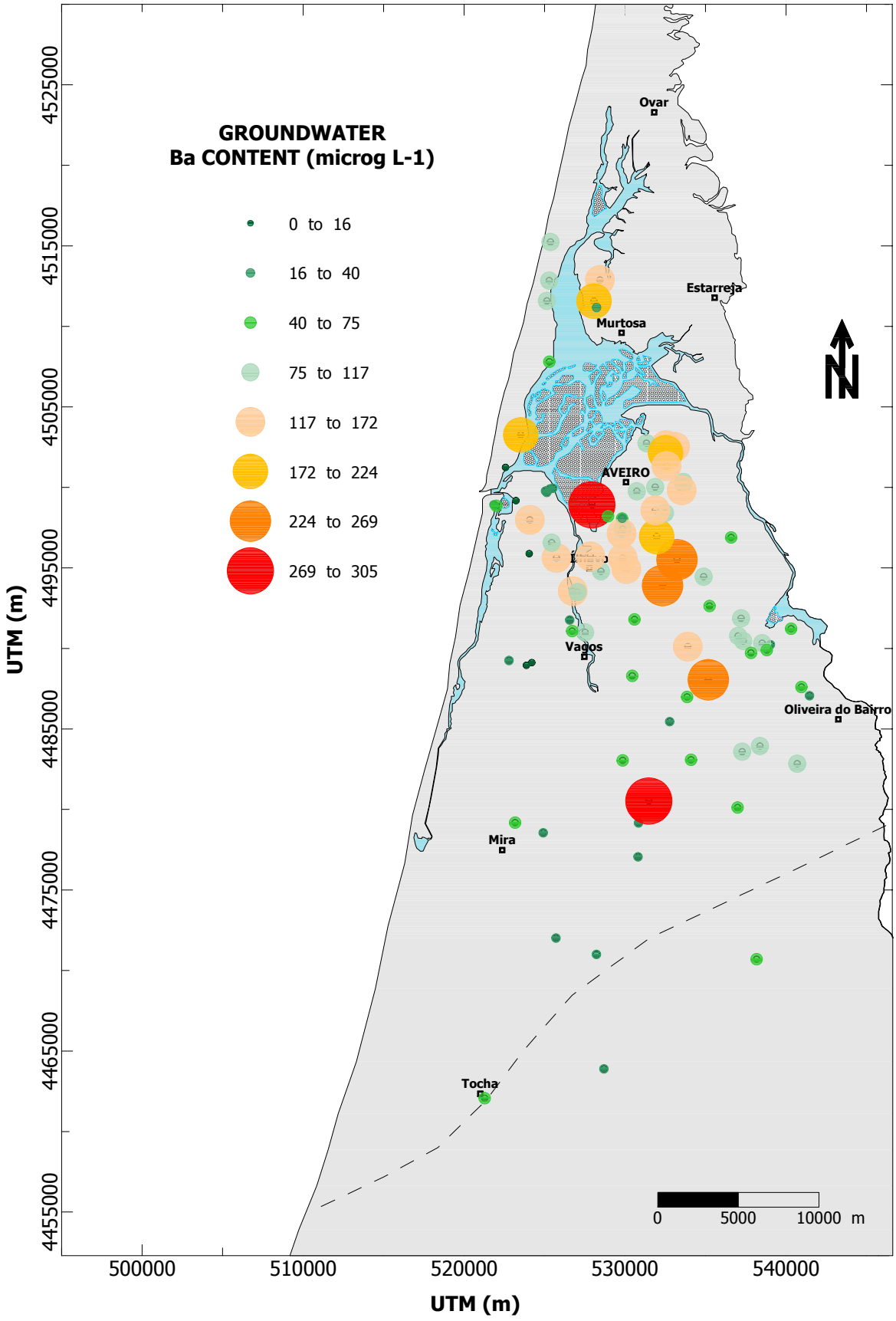
GROUNDWATER
Ba CONTENT (microg L-1)
0 to 16
16 to 40
40 to 75
75 to 117
117 to 172
172 to 224
224 to 269
269 to 305
Ovar
Estarreja
Murtosa
AVEIRO
Vagos
Oliveira do Bairro
Mira
Tocha
0
5000
10000 m
UTM (m)
UTM (m)
4525000
4515000
4505000
4495000
4485000
4475000
4465000
4455000
500000
510000
520000
530000
540000

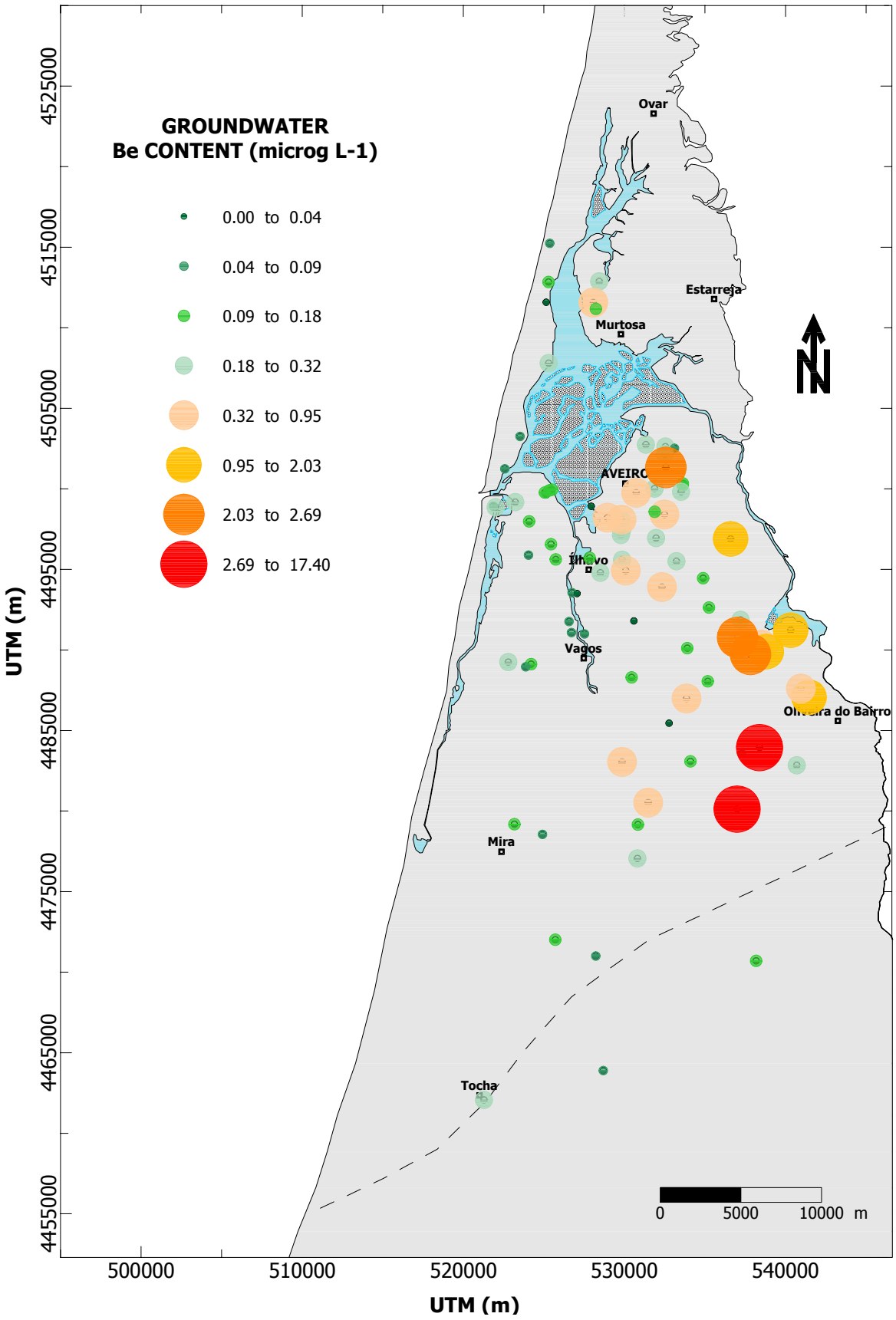
GROUNDWATER
Be CONTENT (microg L-1)
0.00 to 0.04
0.04 to 0.09
0.09 to 0.18
0.18 to 0.32
0.32 to 0.95
0.95 to 2.03
2.03 to 2.69
2.69 to 17.40
Ovar
Estarreja
Murtosa
AVEIRO
Ílhavo
Vagos
Mira
Tocha
0
5000
10000 m
UTM (m)
4525000
4515000
4505000
4495000
4485000
4475000
4465000
4455000
500000
510000
520000
530000
540000
UTM (m)

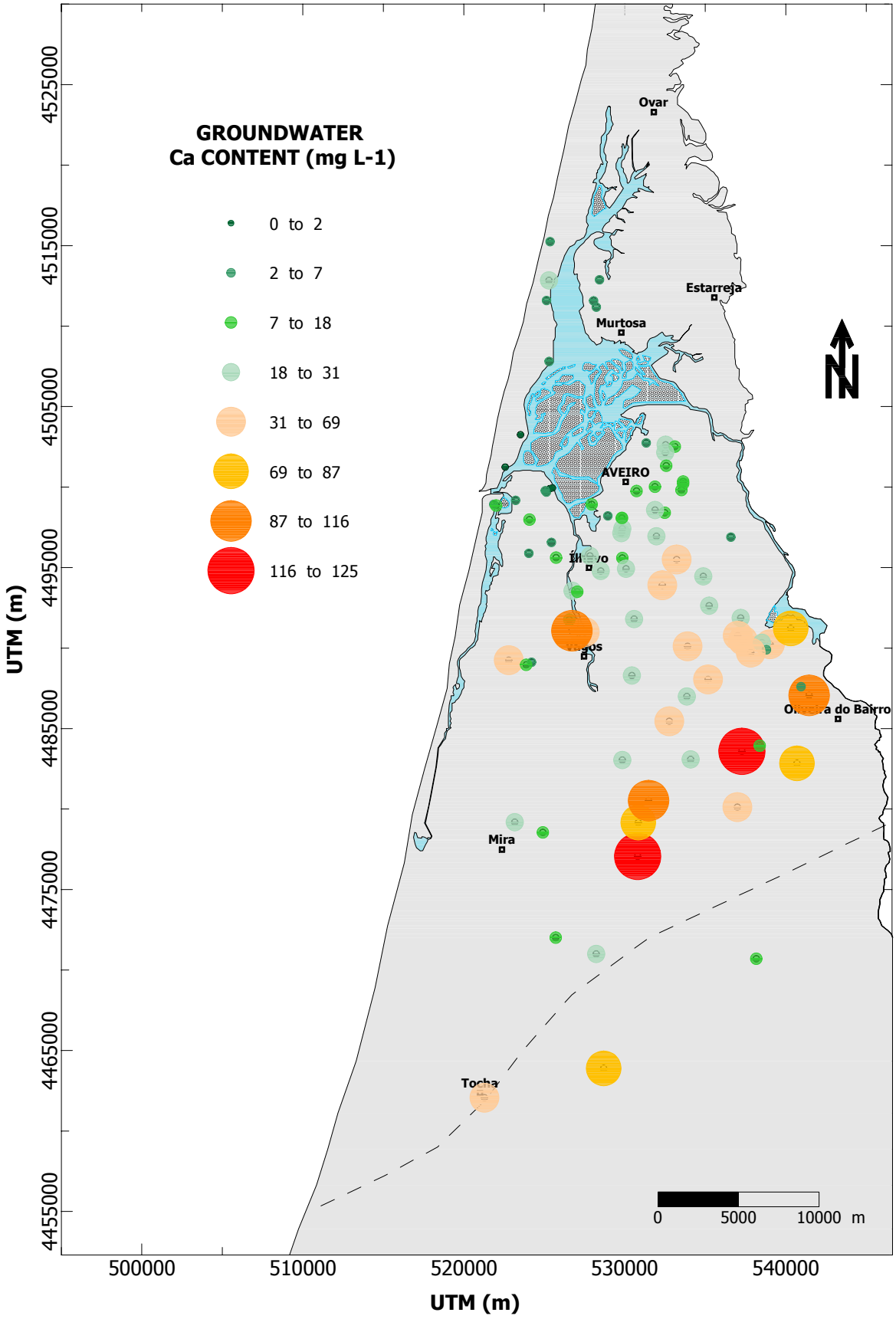
GROUNDWATER
Ca CONTENT (mg L-1)
0 to 2
2 to 7
7 to 18
18 to 31
31 to 69
69 to 87
87 to 116
116 to 125
Ovar
Estarreja
Murtosa
AVEIRO
Mira
Tocha
0
5000
10000 m
UTM (m)
UTM (m)
4525000
4515000
4505000
4495000
4485000
4475000
4465000
4455000
500000
510000
520000
530000
540000

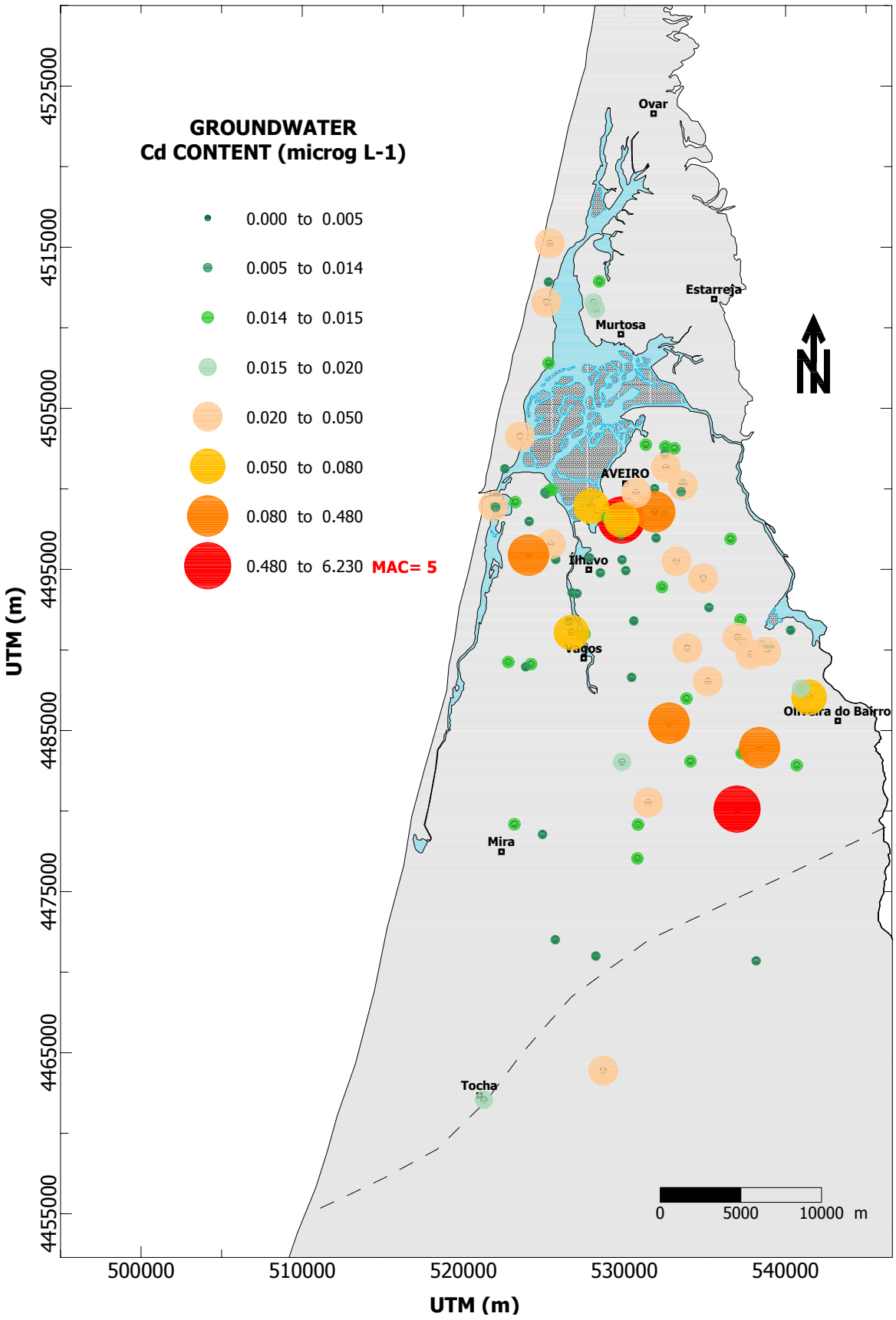
GROUNDWATER
Cd CONTENT (microg L-1)
0.000 to 0.005
0.005 to 0.014
0.014 to 0.015
0.015 to 0.020
0.020 to 0.050
0.050 to 0.080
0.080 to 0.480
0.480 to 6.230 MAC= 5
Ovar
Estarreja
Murtosa
AVEIRO
Ílhavo
Vagos
Mira
Tocha
0
5000
10000 m
UTM (m)
UTM (m)
4525000
4515000
4505000
4495000
4485000
4475000
4465000
4455000
500000
510000
520000
530000
540000

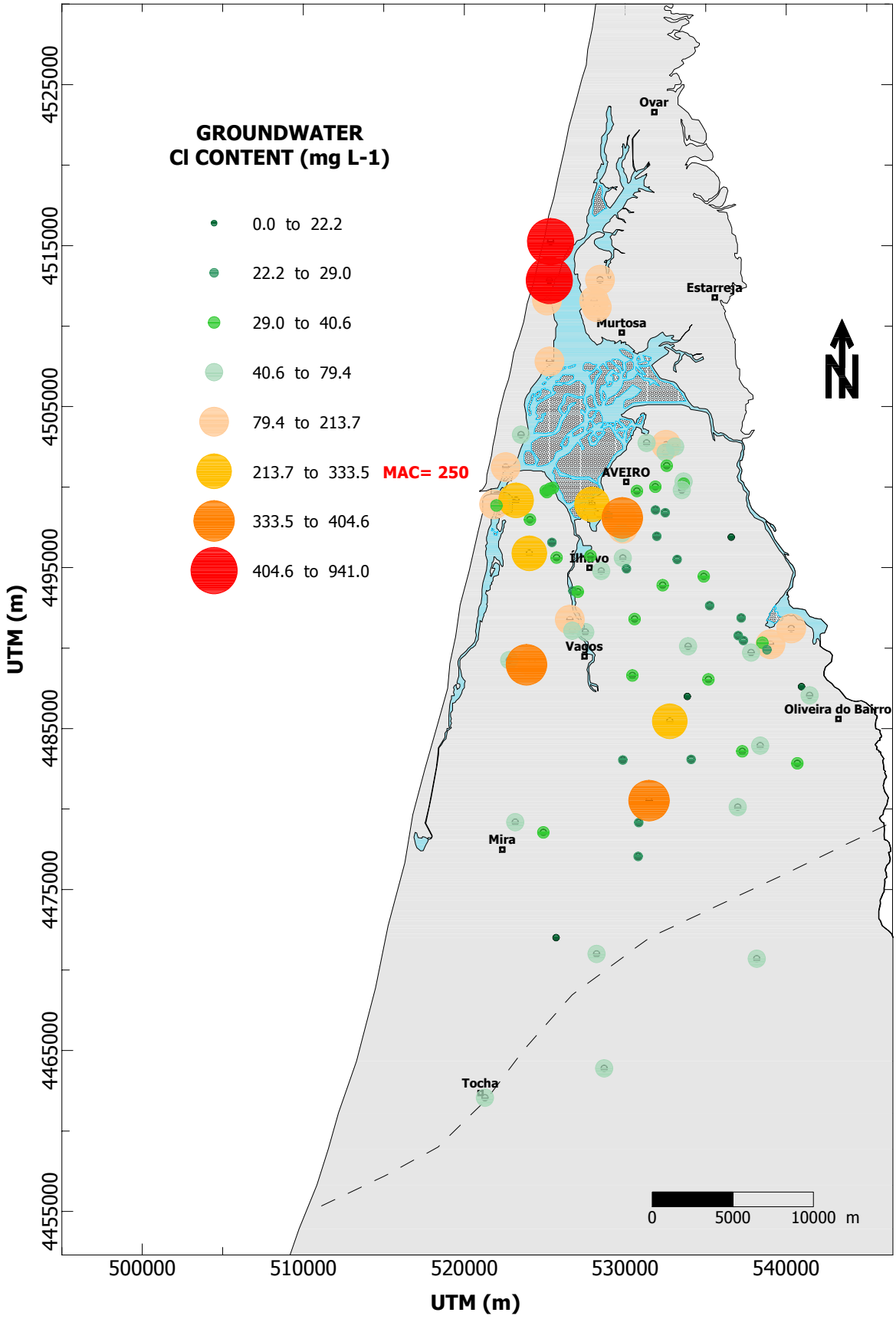
GROUNDWATER
Cl CONTENT (mg L-1)
0.0 to 22.2
22.2 to 29.0
29.0 to 40.6
40.6 to 79.4
79.4 to 213.7
213.7 to 333.5
MAC= 250
333.5 to 404.6
404.6 to 941.0
Ovar
Estarreja
Murtosa
AVEIRO
Ílhavo
Vagos
Oliveira do Bairro
Mira
Tocha
N
0
5000
10000 m
UTM (m)
4525000
4515000
4505000
4495000
4485000
4475000
4465000
4455000
500000
510000
520000
530000
540000
UTM (m)

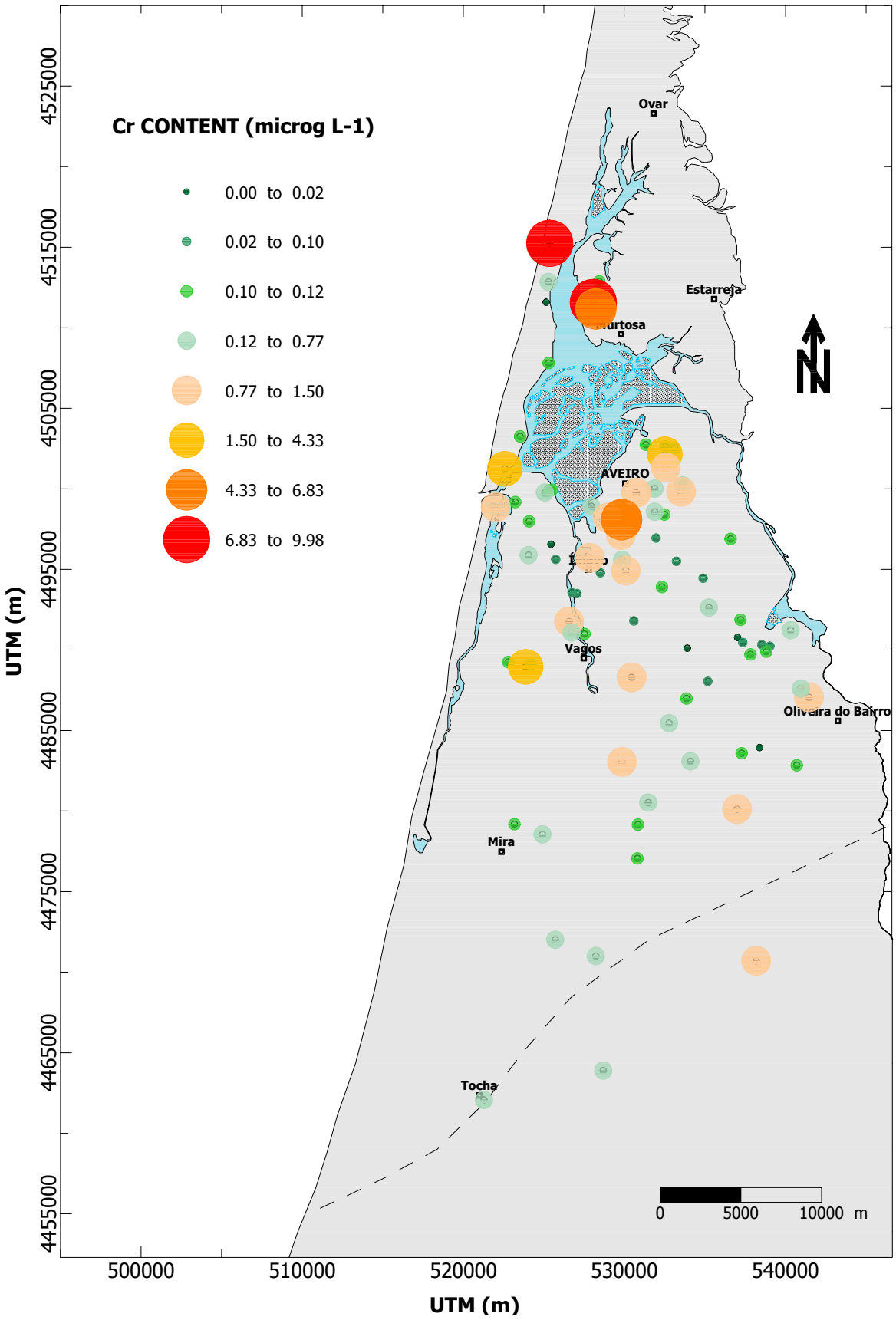
Cr CONTENT (microg L-1)
0.00 to 0.02
0.02 to 0.10
0.10 to 0.12
0.12 to 0.77
0.77 to 1.50
1.50 to 4.33
4.33 to 6.83
6.83 to 9.98
Ovar
Estarreja
AVEIRO
Vagos
Oliveira do Bairro
Mira
Tocha
0
5000
10000 m
UTM (m)
4525000
4515000
4505000
4495000
4485000
4475000
4465000
4455000
500000
510000
520000
530000
540000
UTM (m)

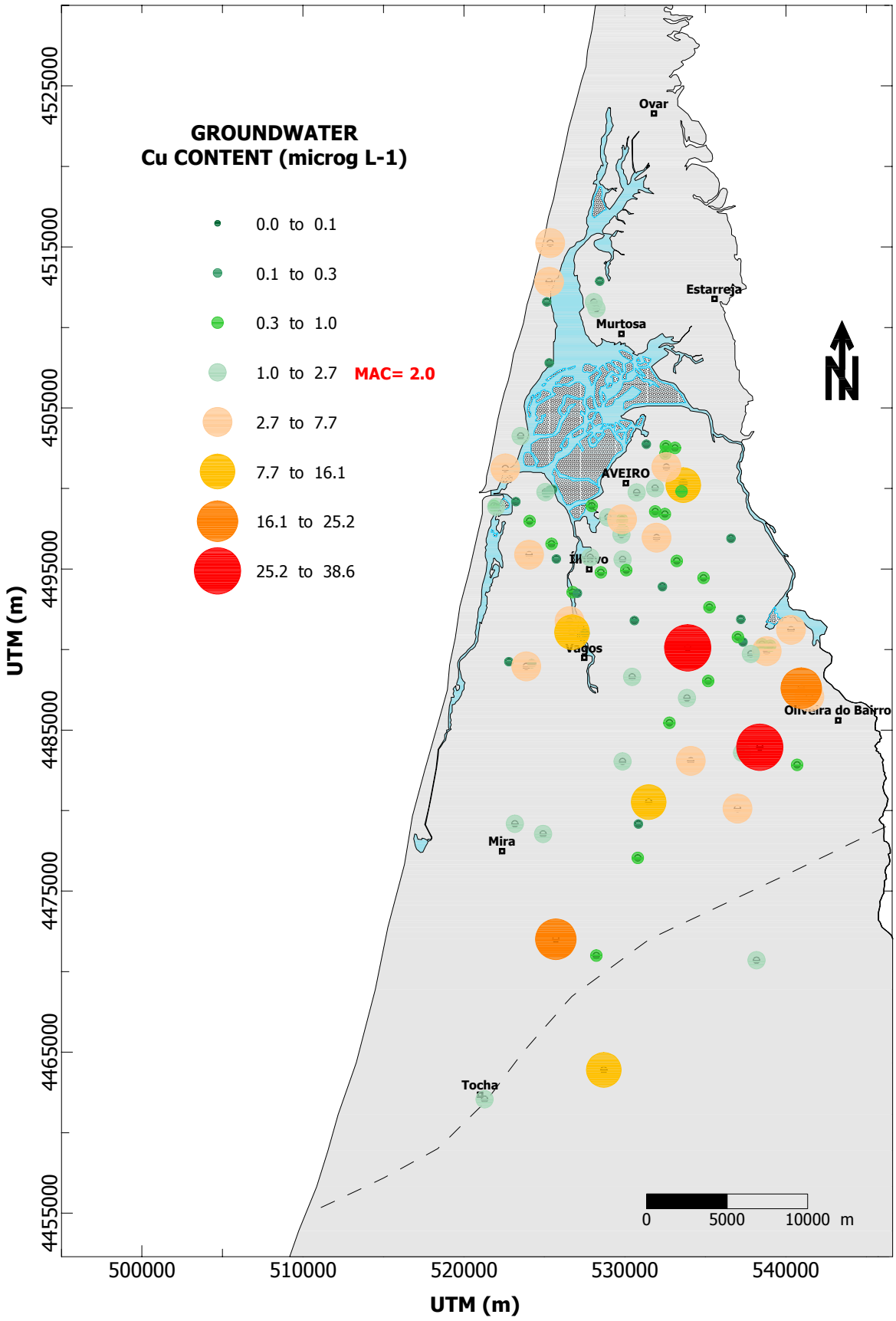
GROUNDWATER
Cu CONTENT (microg L-1)
0.0 to 0.1
0.1 to 0.3
0.3 to 1.0
1.0 to 2.7
MAC= 2.0
2.7 to 7.7
7.7 to 16.1
16.1 to 25.2
25.2 to 38.6
Ovar
Estarreja
Murtosa
AVEIRO
Vagos
Oliveira do Bairro
Mira
Tocha
0
5000
10000 m
4525000
4515000
4505000
4495000
4485000
4475000
4465000
4455000
UTM (m)
500000
510000
520000
530000
540000
UTM (m)

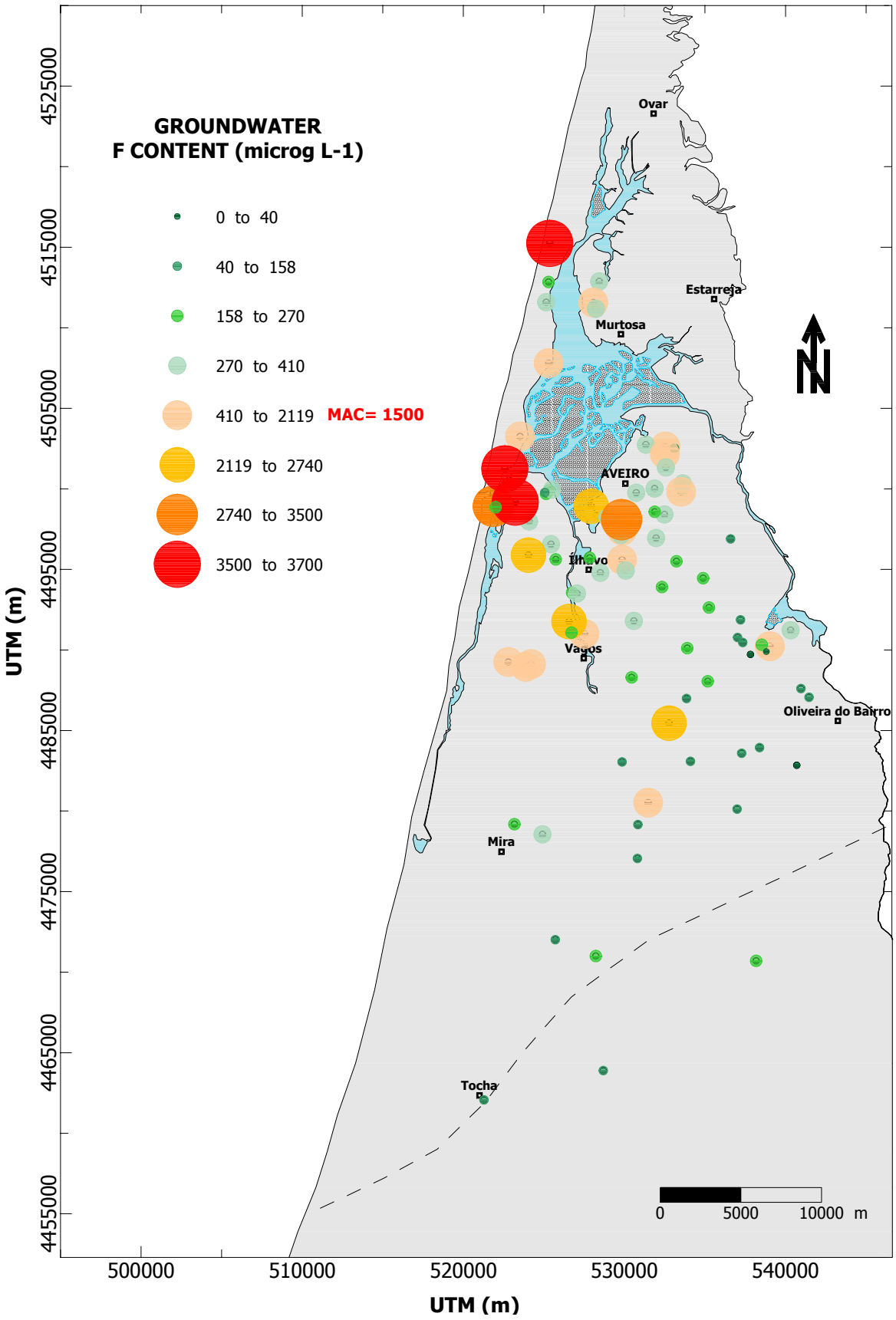
GROUNDWATER
F CONTENT (microg L-1)
0 to 40
40 to 158
158 to 270
270 to 410
410 to 2119
MAC= 1500
2119 to 2740
2740 to 3500
3500 to 3700
Ovar
Estarreja
Murtosa
AVEIRO
Ílhavo
Vagos
Oliveira do Bairro
Mira
Tocha
0
5000
10000 m
UTM (m)
4525000
4515000
4505000
4495000
4485000
4475000
4465000
4455000
500000
510000
520000
530000
540000
UTM (m)

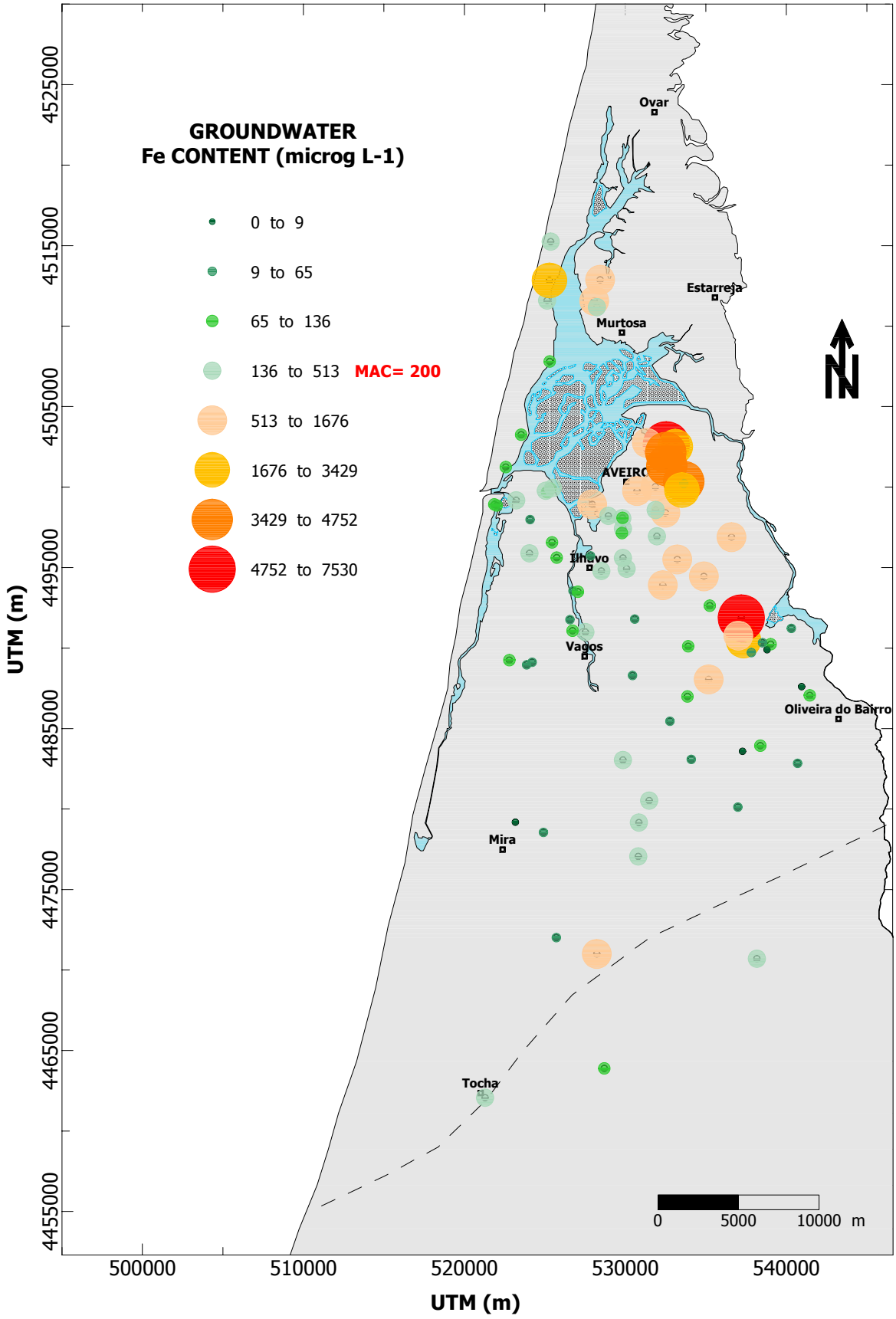
GROUNDWATER
Fe CONTENT (microg L-1)
0 to 9
9 to 65
65 to 136
136 to 513 MAC= 200
513 to 1676
1676 to 3429
3429 to 4752
4752 to 7530
Ovar
Estarreja
Murtosa
AVEIRO
Ílhavo
Vagos
Oliveira do Bairro
Mira
Tocha
0 5000 10000 m
UTM (m)
4525000
4515000
4505000
4495000
4485000
4475000
4465000
4455000
500000
510000
520000
530000
540000
UTM (m)

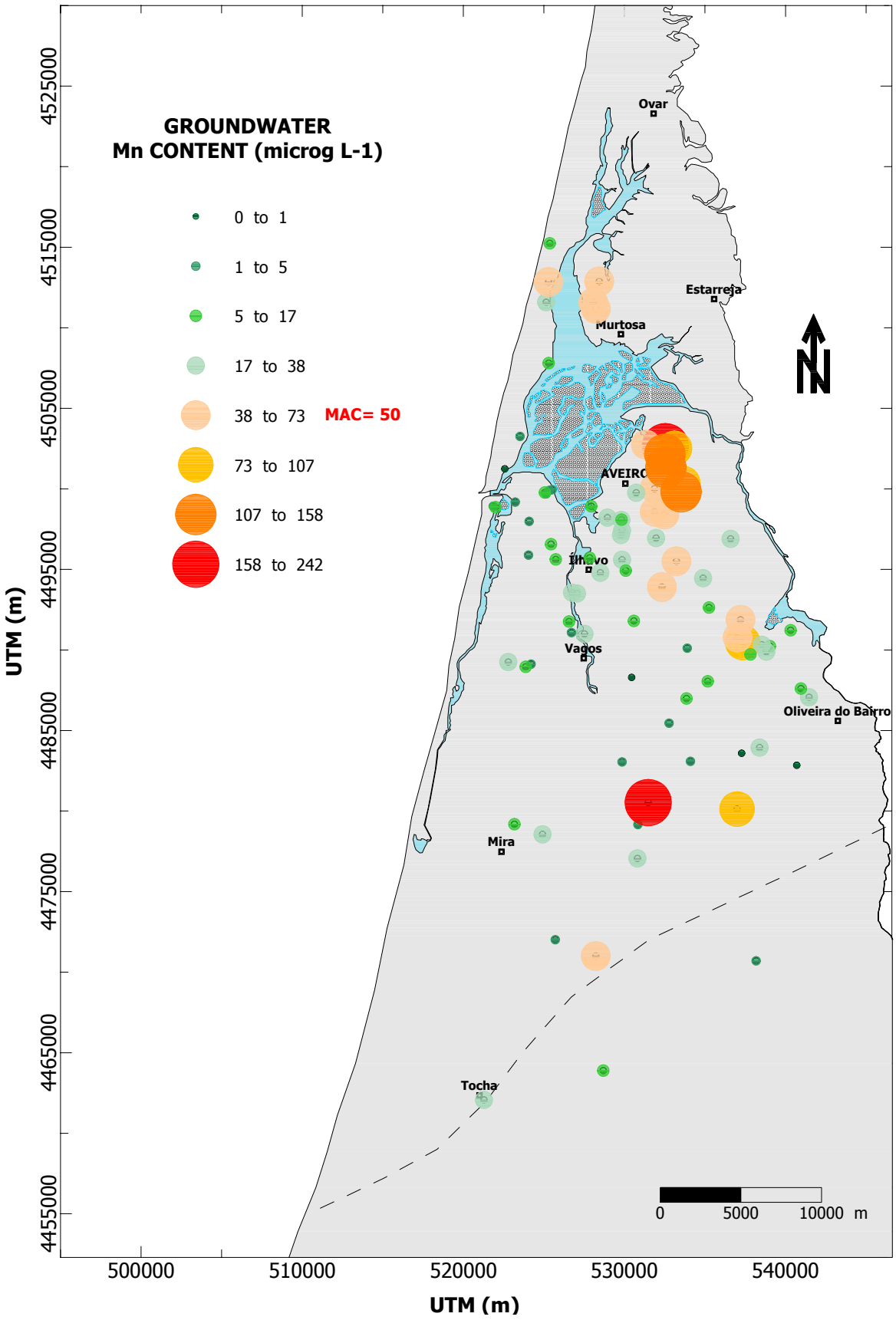
GROUNDWATER
Mn CONTENT (microg L-1)
0 to 1
1 to 5
5 to 17
17 to 38
38 to 73
MAC= 50
73 to 107
107 to 158
158 to 242
Ovar
Estarreja
Murtosa
AVEIRO
Ílhavo
Vagos
Oliveira do Bairro
Mira
Tocha
0
5000
10000 m
UTM (m)
UTM (m)
4525000
4515000
4505000
4495000
4485000
4475000
4465000
4455000
500000
510000
520000
530000
540000

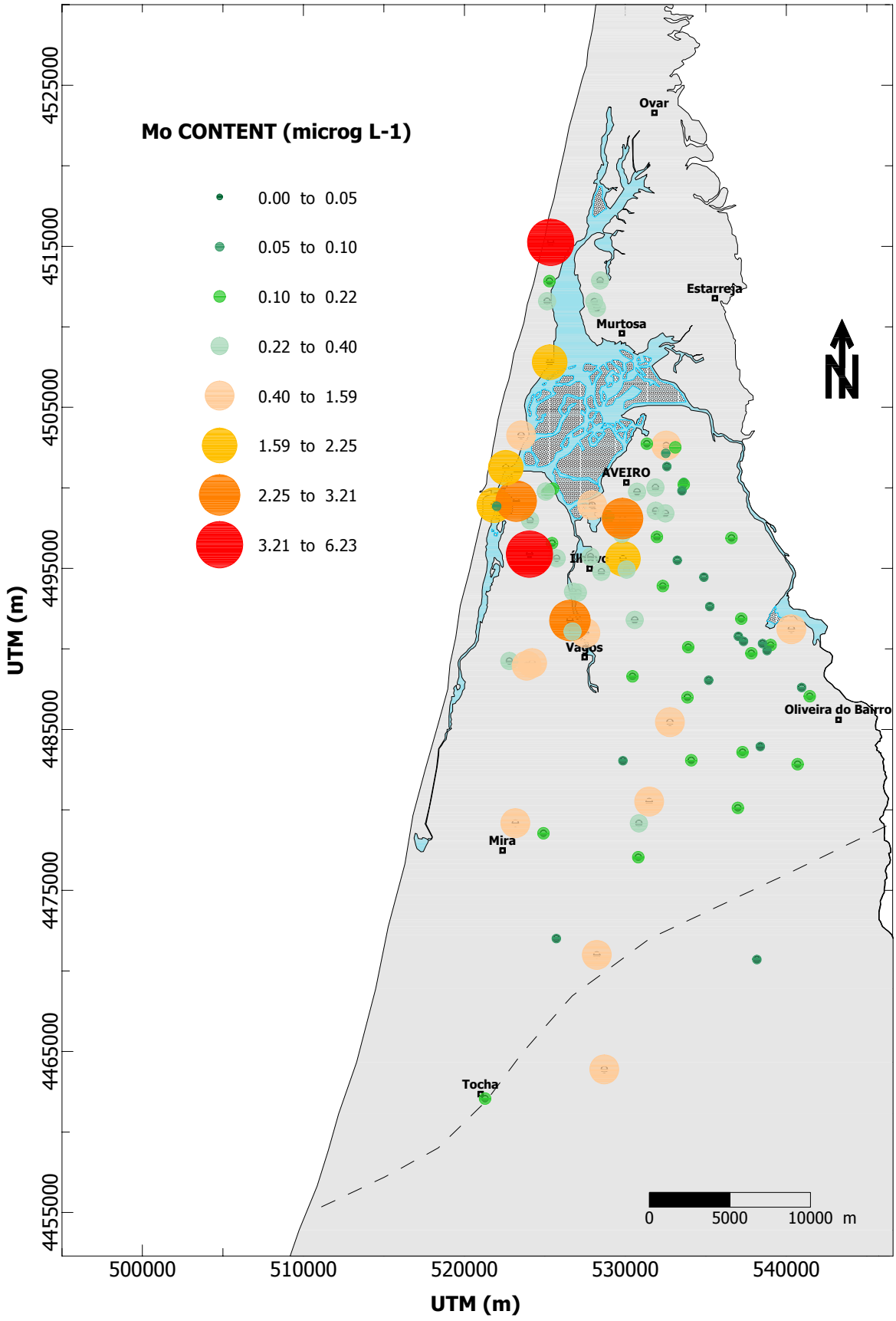
Mo CONTENT (microg L-1)
0.00 to 0.05
0.05 to 0.10
0.10 to 0.22
0.22 to 0.40
0.40 to 1.59
1.59 to 2.25
2.25 to 3.21
3.21 to 6.23
Ovar
Estarreja
Murtosa
AVEIRO
Vagos
Oliveira do Bairro
Mira
Tocha
0
5000
10000 m
4525000
4515000
4505000
4495000
4485000
4475000
4465000
4455000
500000
510000
520000
530000
540000
UTM (m)
UTM (m)

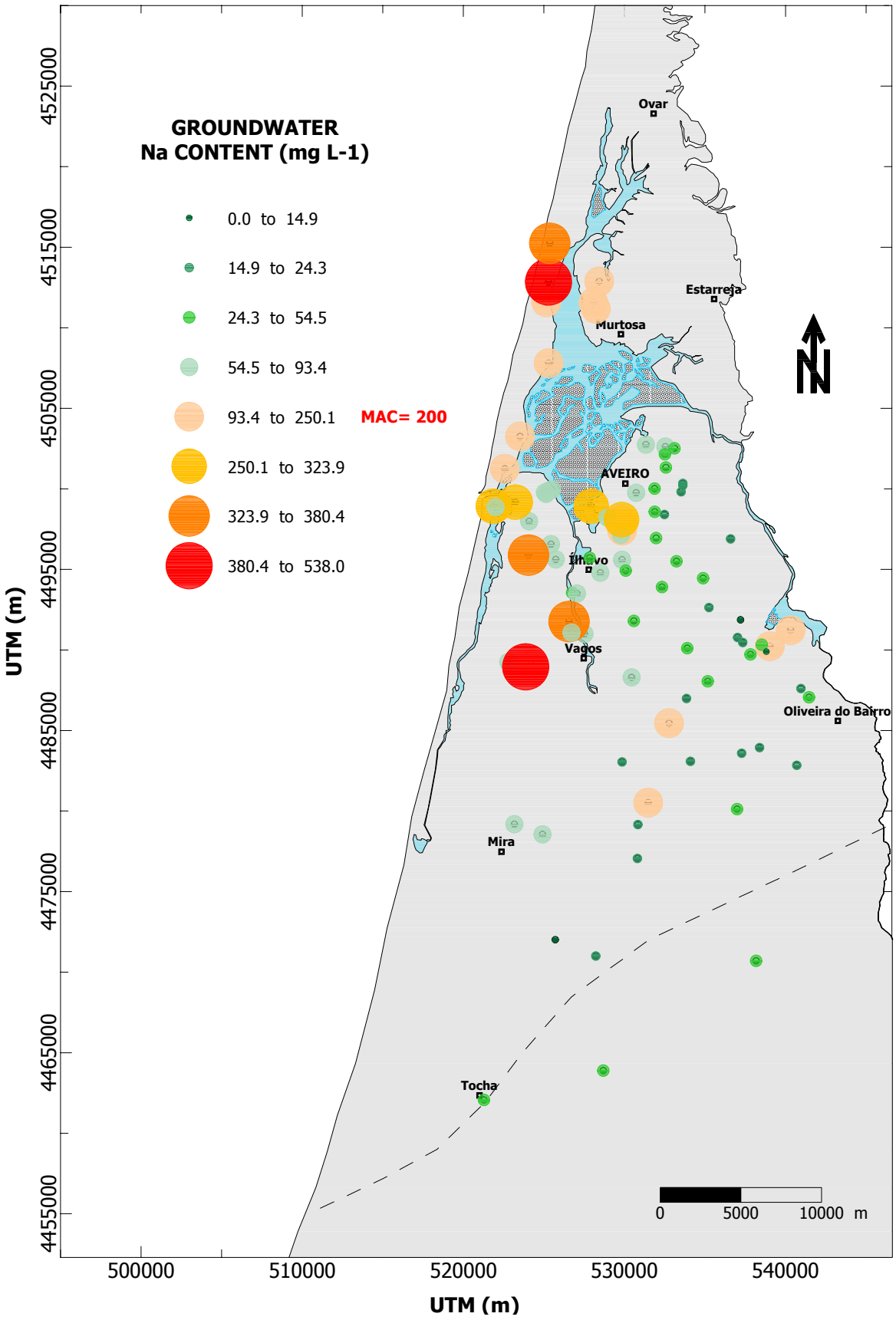
GROUNDWATER
Na CONTENT (mg L-1)
0.0 to 14.9
14.9 to 24.3
24.3 to 54.5
54.5 to 93.4
93.4 to 250.1
250.1 to 323.9
323.9 to 380.4
380.4 to 538.0
MAC= 200
Ovar
Estarreja
Murtosa
AVEIRO
Ílhavo
Vagos
Oliveira do Bairro
Mira
Tocha
0
5000
10000 m
UTM (m)
UTM (m)
4525000
4515000
4505000
4495000
4485000
4475000
4465000
4455000
500000
510000
520000
530000
540000

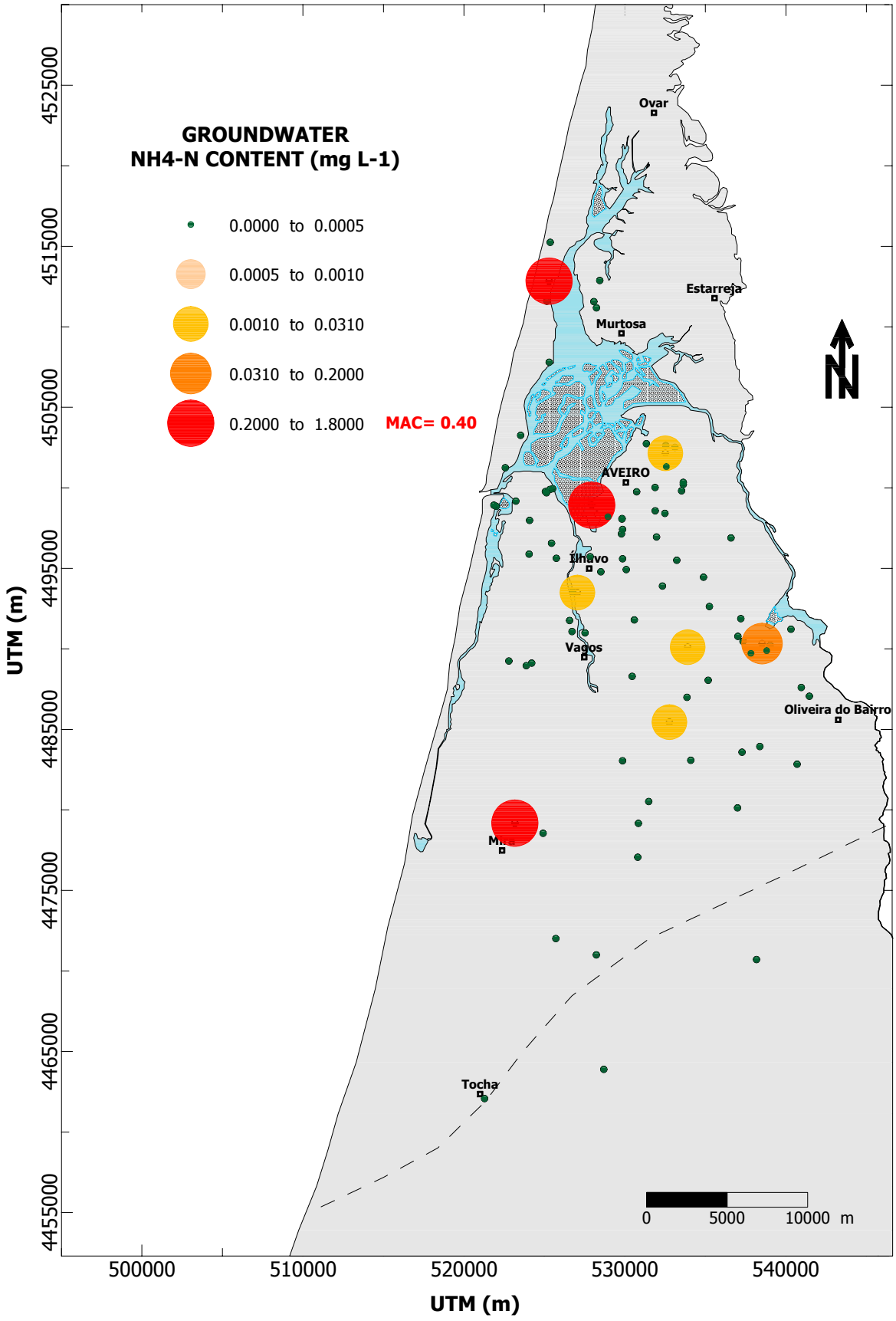
GROUNDWATER
NH4-N CONTENT (mg L-1)
0.0000 to 0.0005
0.0005 to 0.0010
0.0010 to 0.0310
0.0310 to 0.2000
0.2000 to 1.8000
MAC= 0.40
Ovar
Estarreja
Murtosa
AVEIRO
Ílhavo
Vagos
Oliveira do Bairro
Tocha
0
5000
10000 m
4525000
4515000
4505000
4495000
4485000
4475000
4465000
4455000
500000
510000
520000
530000
540000
UTM (m)
UTM (m)

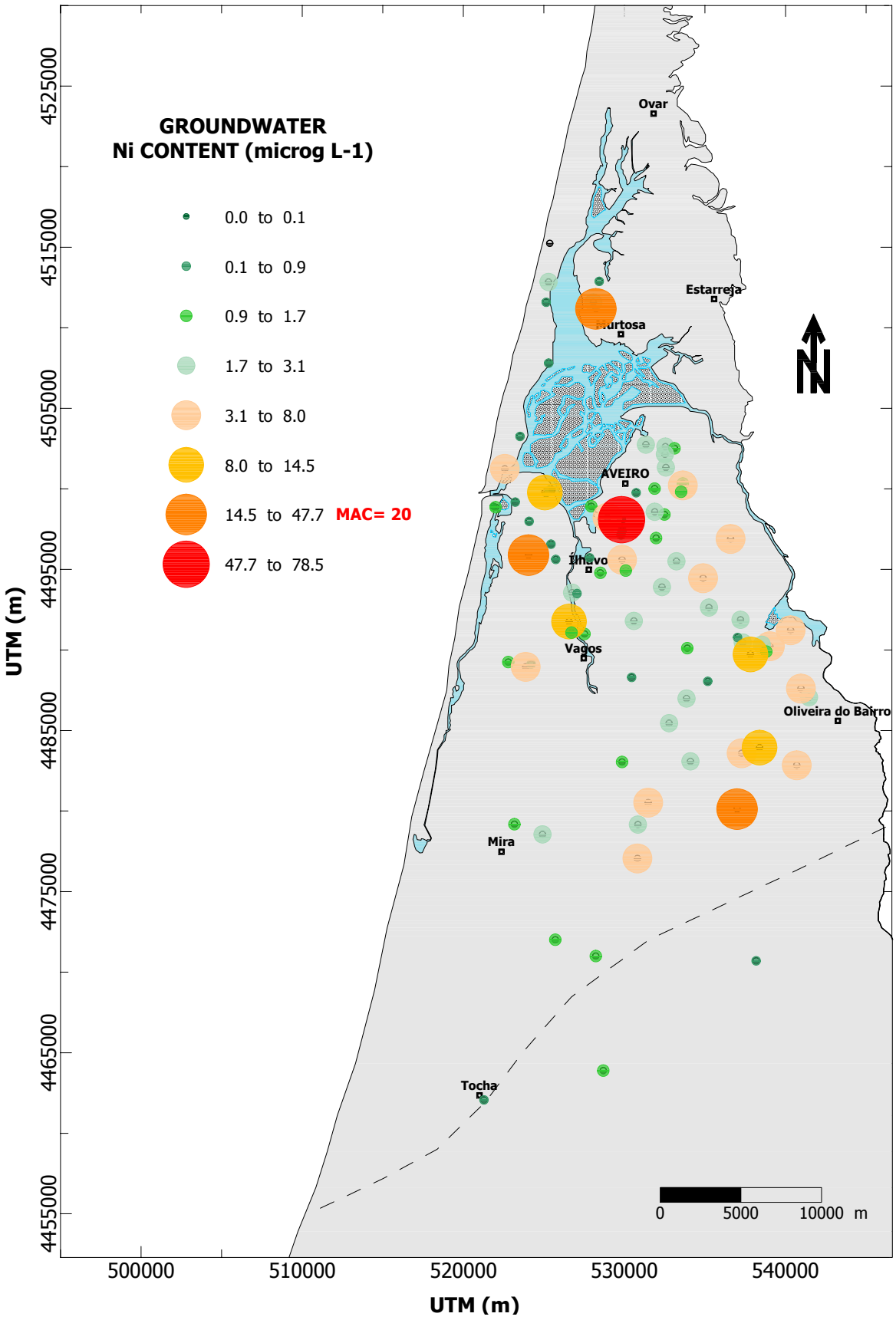
GROUNDWATER
Ni CONTENT (microg L-1)
0.0 to 0.1
0.1 to 0.9
0.9 to 1.7
1.7 to 3.1
3.1 to 8.0
8.0 to 14.5
14.5 to 47.7 MAC= 20
47.7 to 78.5
Ovar
Estarreja
Murtosa
AVEIRO
Ílhavo
Vagos
Oliveira do Bairro
Mira
Tocha
0
5000
10000 m
UTM (m)
UTM (m)
4525000
4515000
4505000
4495000
4485000
4475000
4465000
4455000
500000
510000
520000
530000
540000

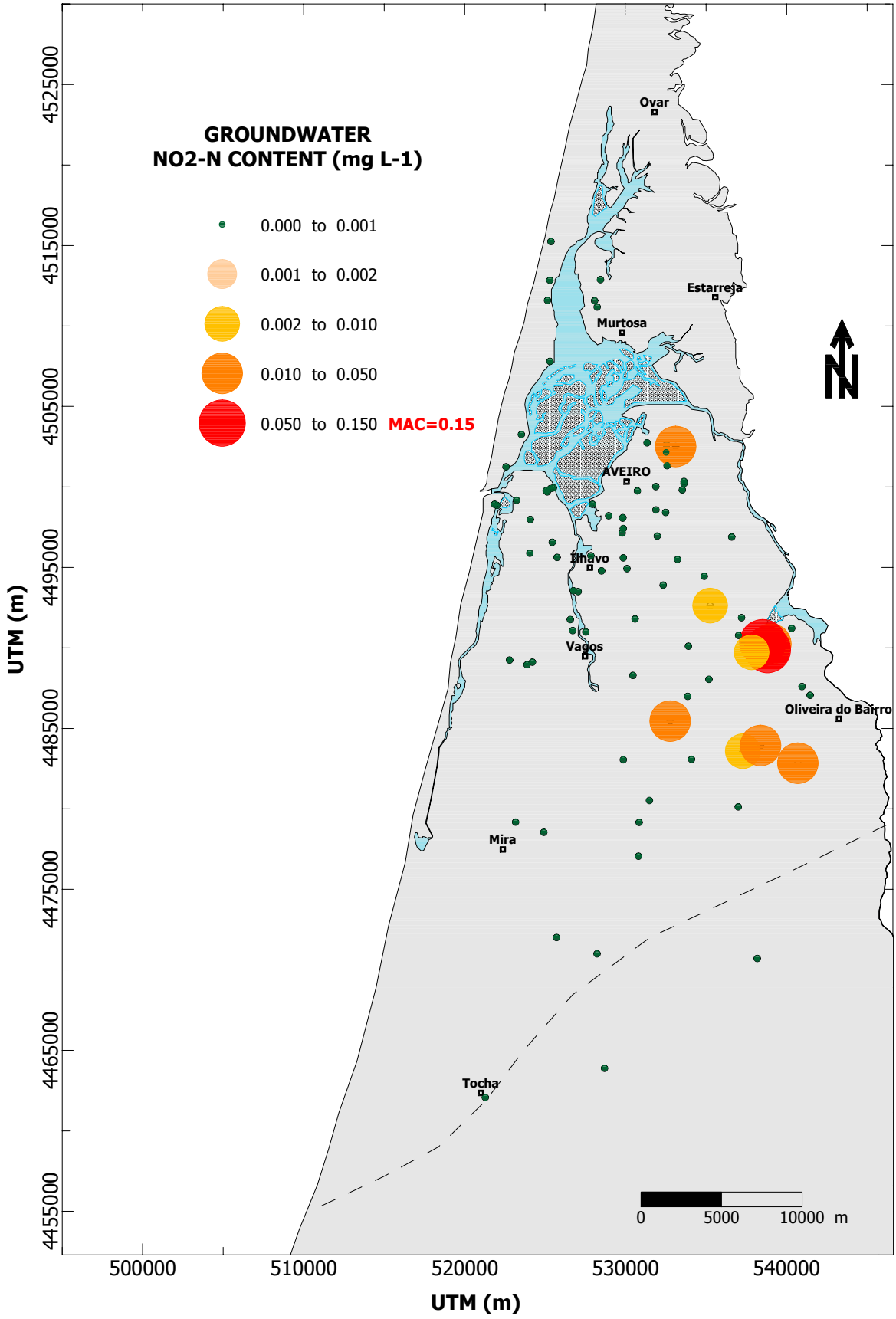
GROUNDWATER
NO2-N CONTENT (mg L-1)
0.000 to 0.001
0.001 to 0.002
0.002 to 0.010
0.010 to 0.050
0.050 to 0.150 MAC=0.15
Ovar
Estarreja
Murtosa
AVEIRO
Ílhavo
Vagos
Oliveira do Bairro
Mira
Tocha
0
5000
10000 m
UTM (m)
UTM (m)
4525000
4515000
4505000
4495000
4485000
4475000
4465000
4455000
500000
510000
520000
530000
540000

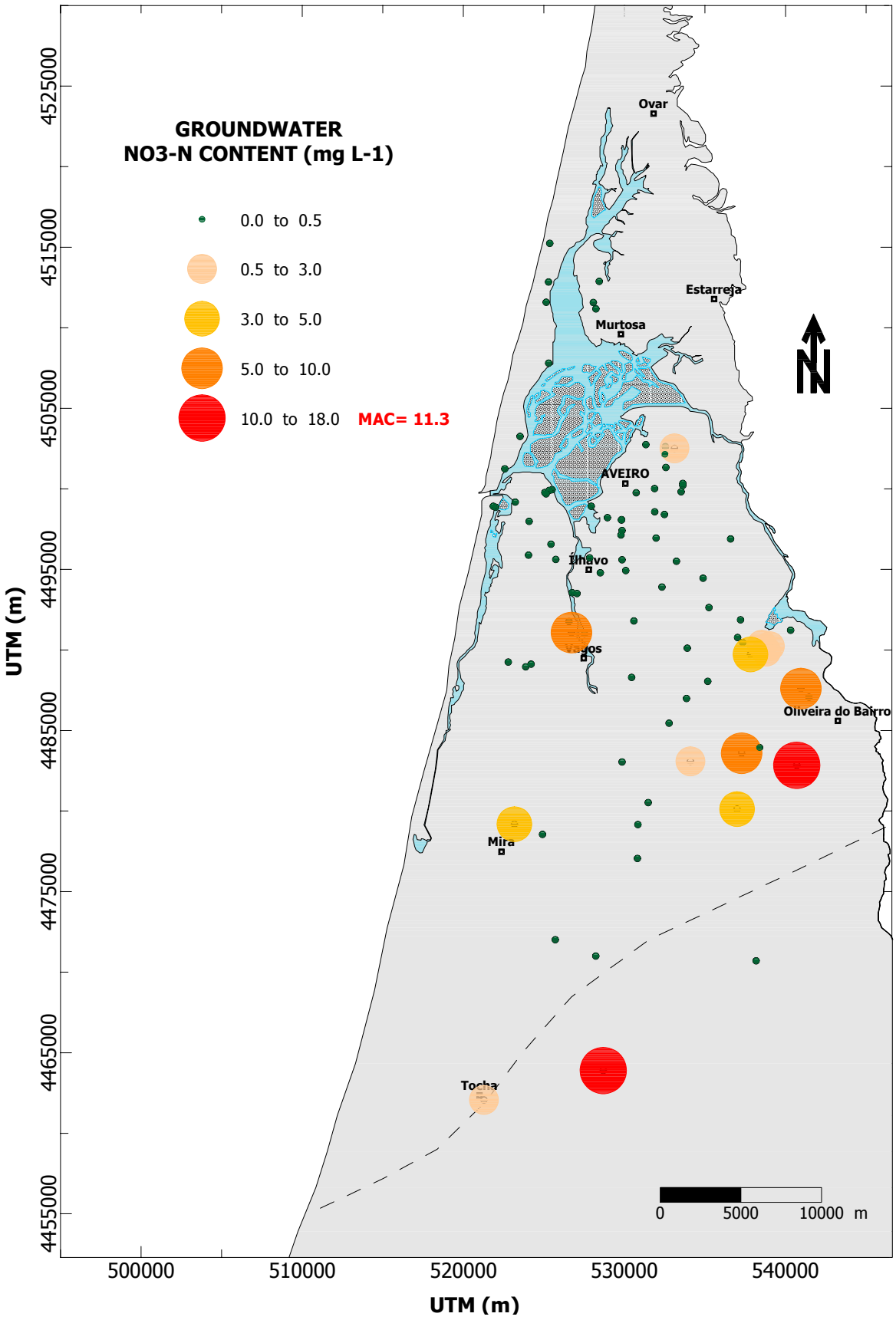
GROUNDWATER
NO3-N CONTENT (mg L-1)
0.0 to 0.5
0.5 to 3.0
3.0 to 5.0
5.0 to 10.0
10.0 to 18.0
MAC= 11.3
Ovar
Estarreja
Murtosa
AVEIRO
Ílhavo
Oliveira do Bairro
Mira
Tocha
0
5000
10000 m
UTM (m)
4525000
4515000
4505000
4495000
4485000
4475000
4465000
4455000
500000
510000
520000
530000
540000
UTM (m)

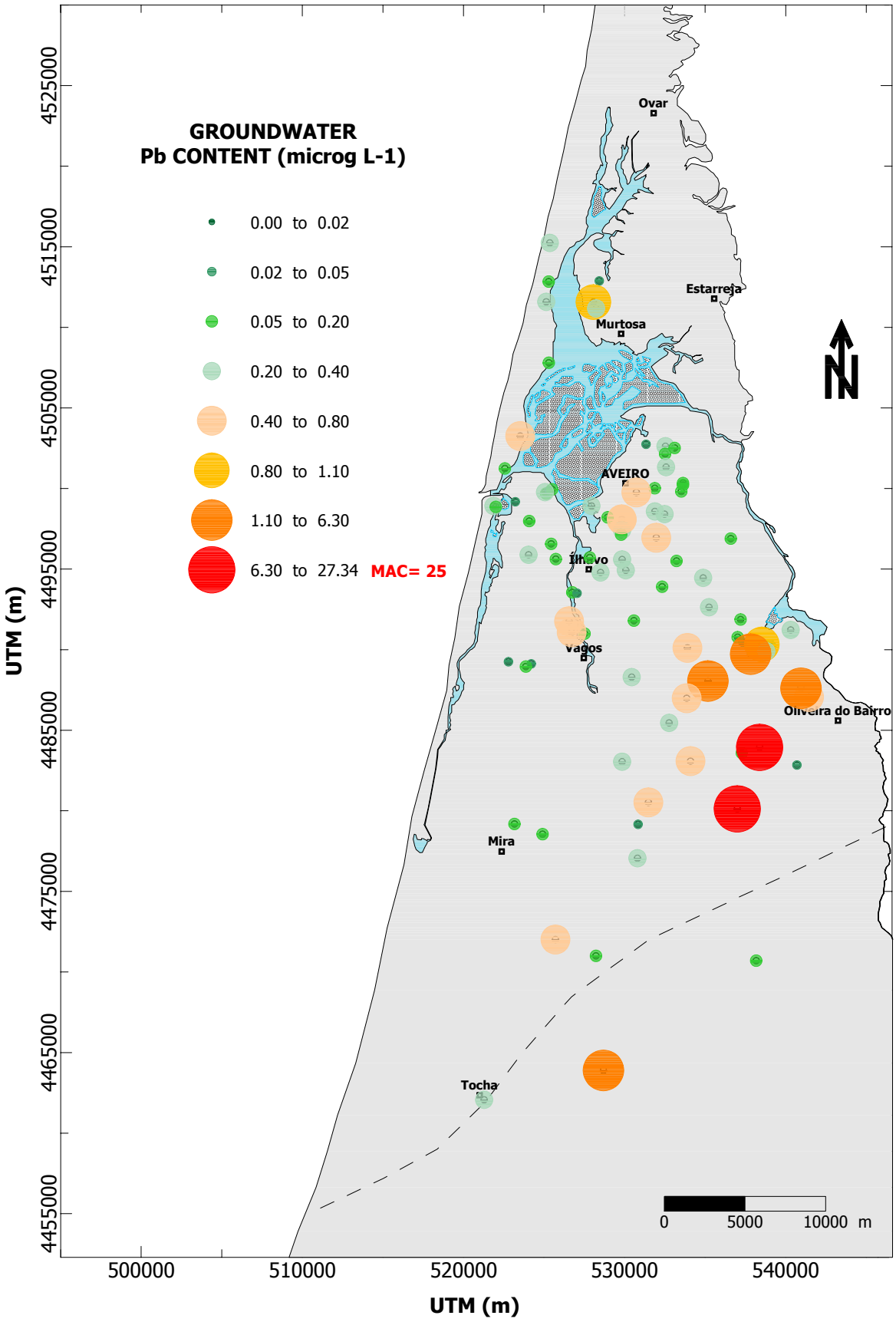
GROUNDWATER
Pb CONTENT (microg L-1)
0.00 to 0.02
0.02 to 0.05
0.05 to 0.20
0.20 to 0.40
0.40 to 0.80
0.80 to 1.10
1.10 to 6.30
6.30 to 27.34 MAC= 25
Ovar
Estarreja
Murtosa
AVEIRO
Ílhavo
Vagos
Oliveira do Bairro
Mira
Tocha
0 5000 10000 m
UTM (m)
4525000
4515000
4505000
4495000
4485000
4475000
4465000
4455000
500000
510000
520000
530000
540000
UTM (m)

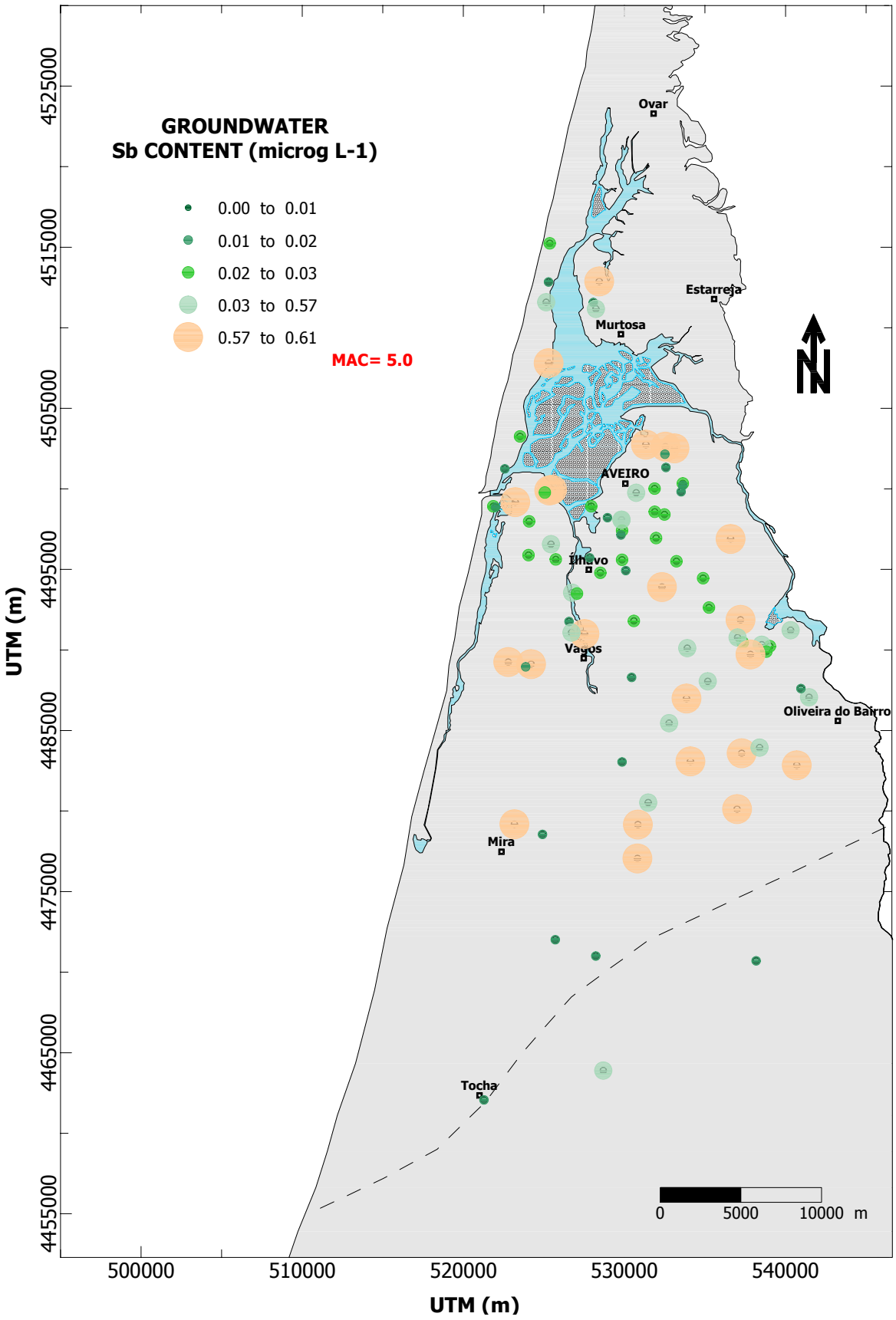
GROUNDWATER
Sb CONTENT (microg L-1)
0.00 to 0.01
0.01 to 0.02
0.02 to 0.03
0.03 to 0.57
0.57 to 0.61
MAC= 5.0
Ovar
Estarreja
Murtosa
AVEIRO
Ílhavo
Vagos
Oliveira do Bairro
Mira
Tocha
0
5000
10000 m
UTM (m)
4525000
4515000
4505000
4495000
4485000
4475000
4465000
4455000
500000
510000
520000
530000
540000
UTM (m)

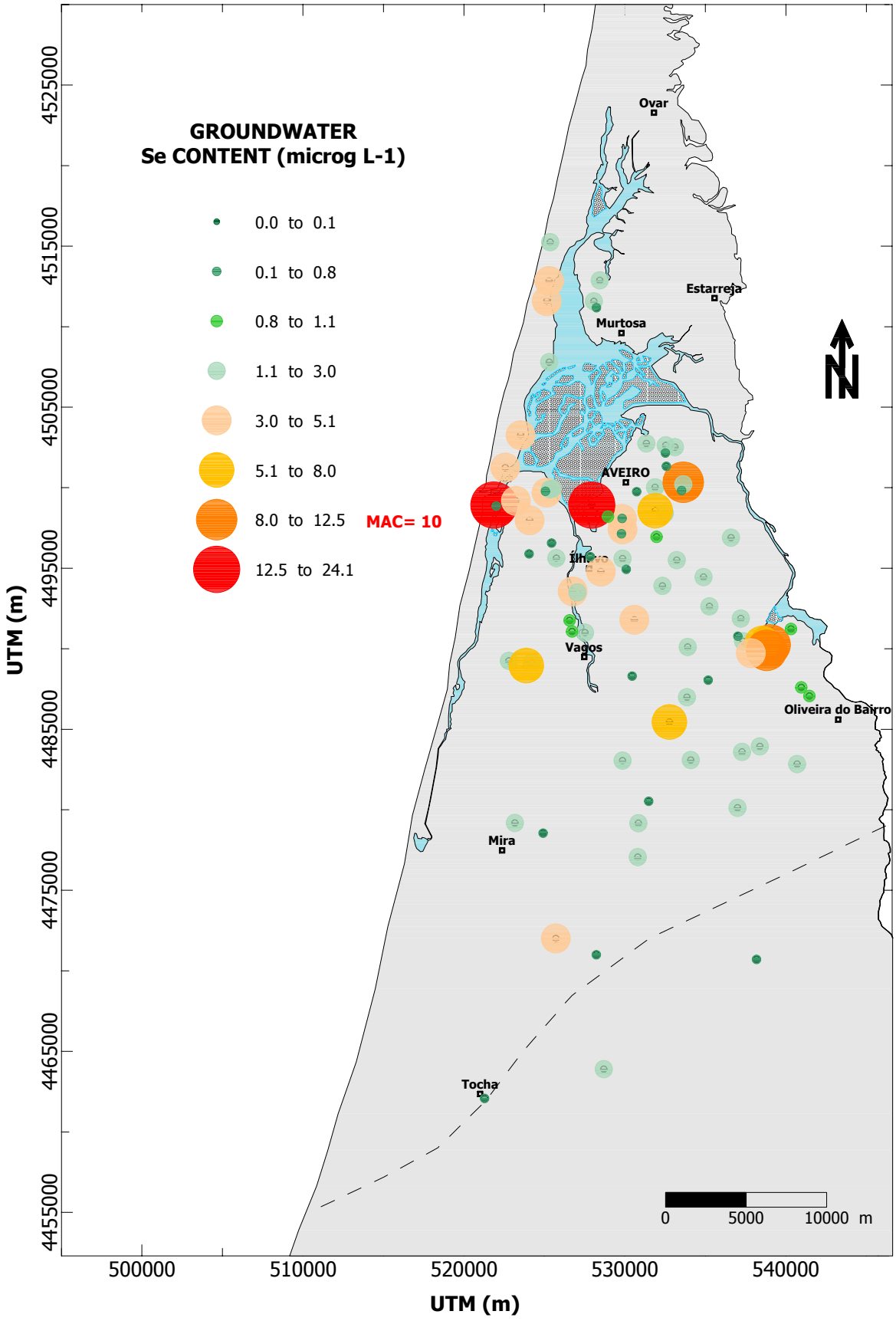
GROUNDWATER
Se CONTENT (microg L-1)
0.0 to 0.1
0.1 to 0.8
0.8 to 1.1
1.1 to 3.0
3.0 to 5.1
5.1 to 8.0
8.0 to 12.5
12.5 to 24.1
MAC= 10
Ovar
Estarreja
Murtosa
AVEIRO
Ílhavo
Vagos
Oliveira do Bairro
Mira
Tocha
N
0
5000
10000 m
4525000
4515000
4505000
4495000
4485000
4475000
4465000
4455000
500000
510000
520000
530000
540000
UTM (m)
UTM (m)

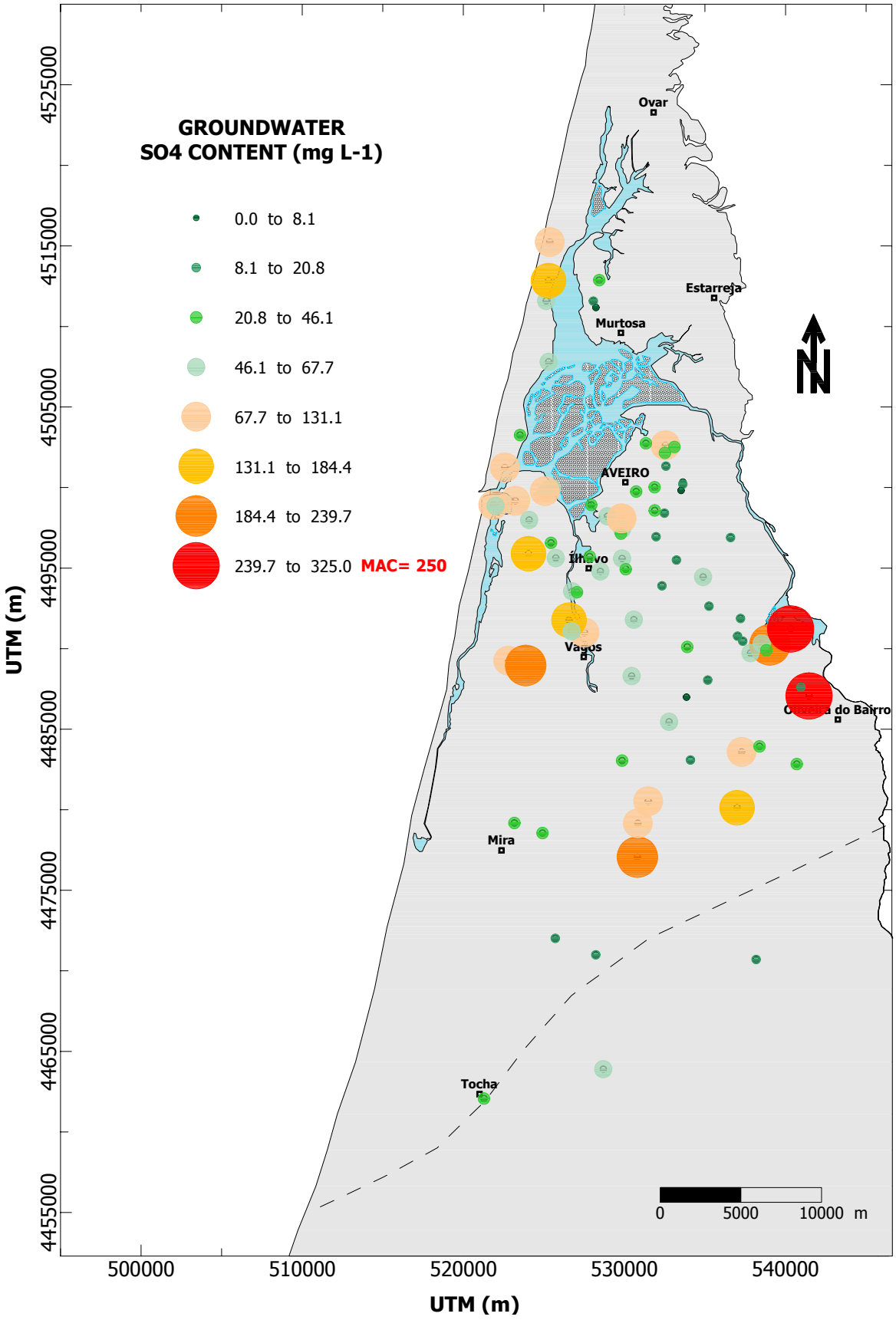
GROUNDWATER
SO4 CONTENT (mg L-1)
0.0 to 8.1
8.1 to 20.8
20.8 to 46.1
46.1 to 67.7
67.7 to 131.1
131.1 to 184.4
184.4 to 239.7
239.7 to 325.0 MAC= 250
Ovar
Estarreja
Murtosa
AVEIRO
Ílhavo
Vagos
Mira
Tocha
0 5000 10000 m
UTM (m)
4525000
4515000
4505000
4495000
4485000
4475000
4465000
4455000
500000
510000
520000
530000
540000
UTM (m)

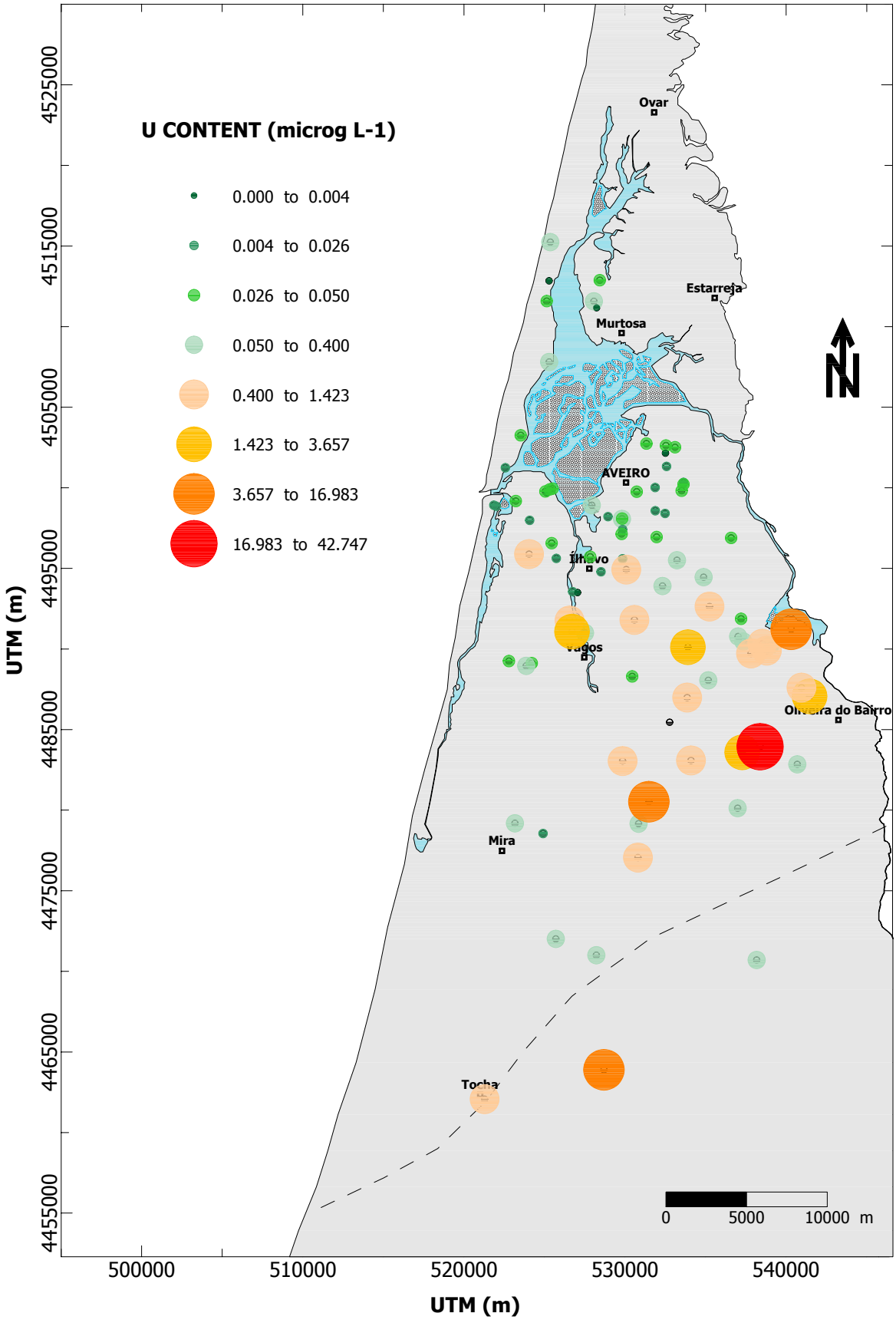
U CONTENT (microg L-1)
0.000 to 0.004
0.004 to 0.026
0.026 to 0.050
0.050 to 0.400
0.400 to 1.423
1.423 to 3.657
3.657 to 16.983
16.983 to 42.747
Ovar
Estarreja
Murtosa
AVEIRO
Ílhavo
Vagos
Oliveira do Bairro
Mira
Tocha
N
0
5000
10000 m
UTM (m)
4525000
4515000
4505000
4495000
4485000
4475000
4465000
4455000
500000
510000
520000
530000
540000
UTM (m)

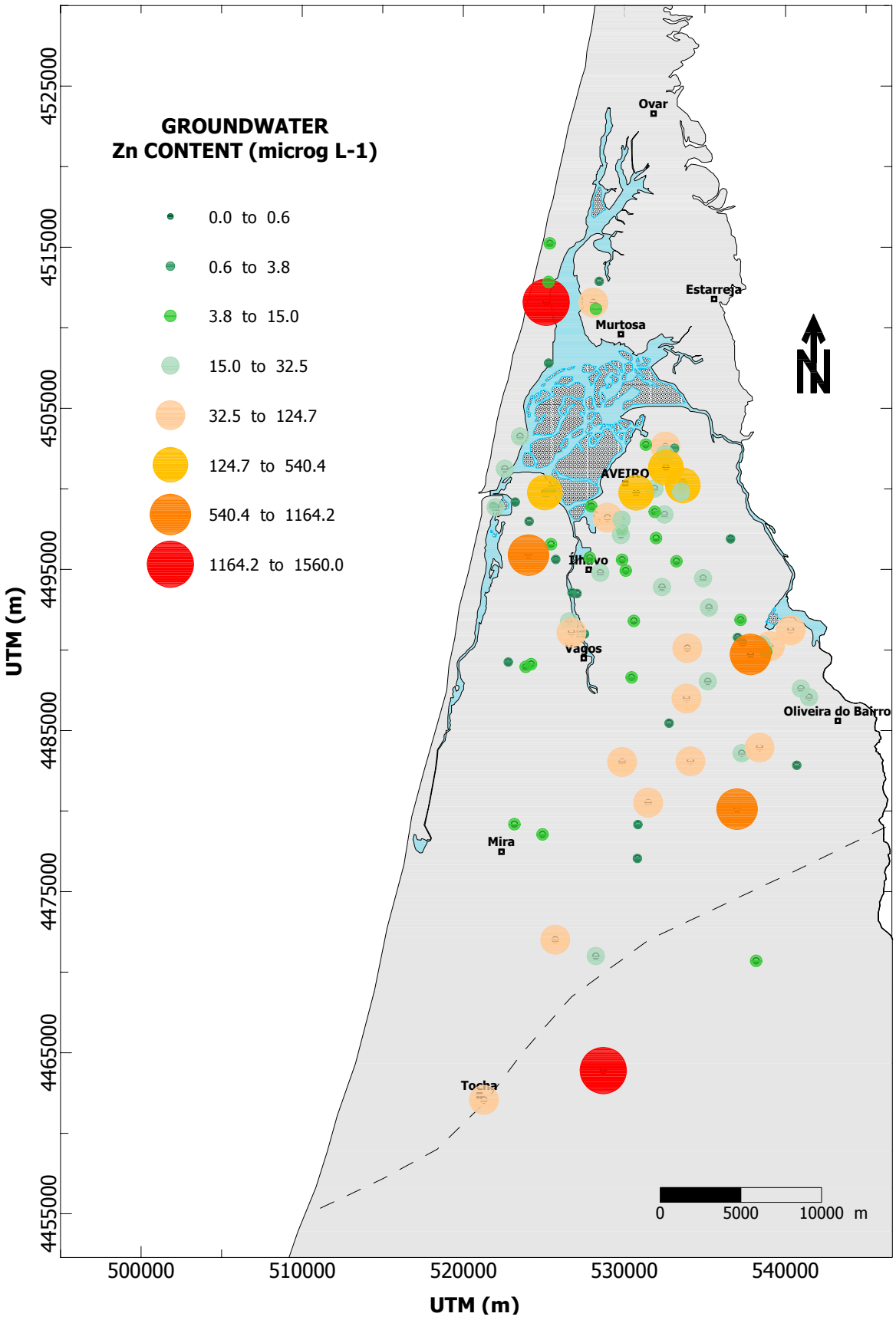
GROUNDWATER
Zn CONTENT (microg L-1)
0.0 to 0.6
0.6 to 3.8
3.8 to 15.0
15.0 to 32.5
32.5 to 124.7
124.7 to 540.4
540.4 to 1164.2
1164.2 to 1560.0
Ovar
Estarreja
Murtosa
AVEIRO
Ílhavo
Vagos
Oliveira do Bairro
Mira
Tocha
0
5000
10000 m
UTM (m)
4525000
4515000
4505000
4495000
4485000
4475000
4465000
4455000
500000
510000
520000
530000
540000
UTM (m)

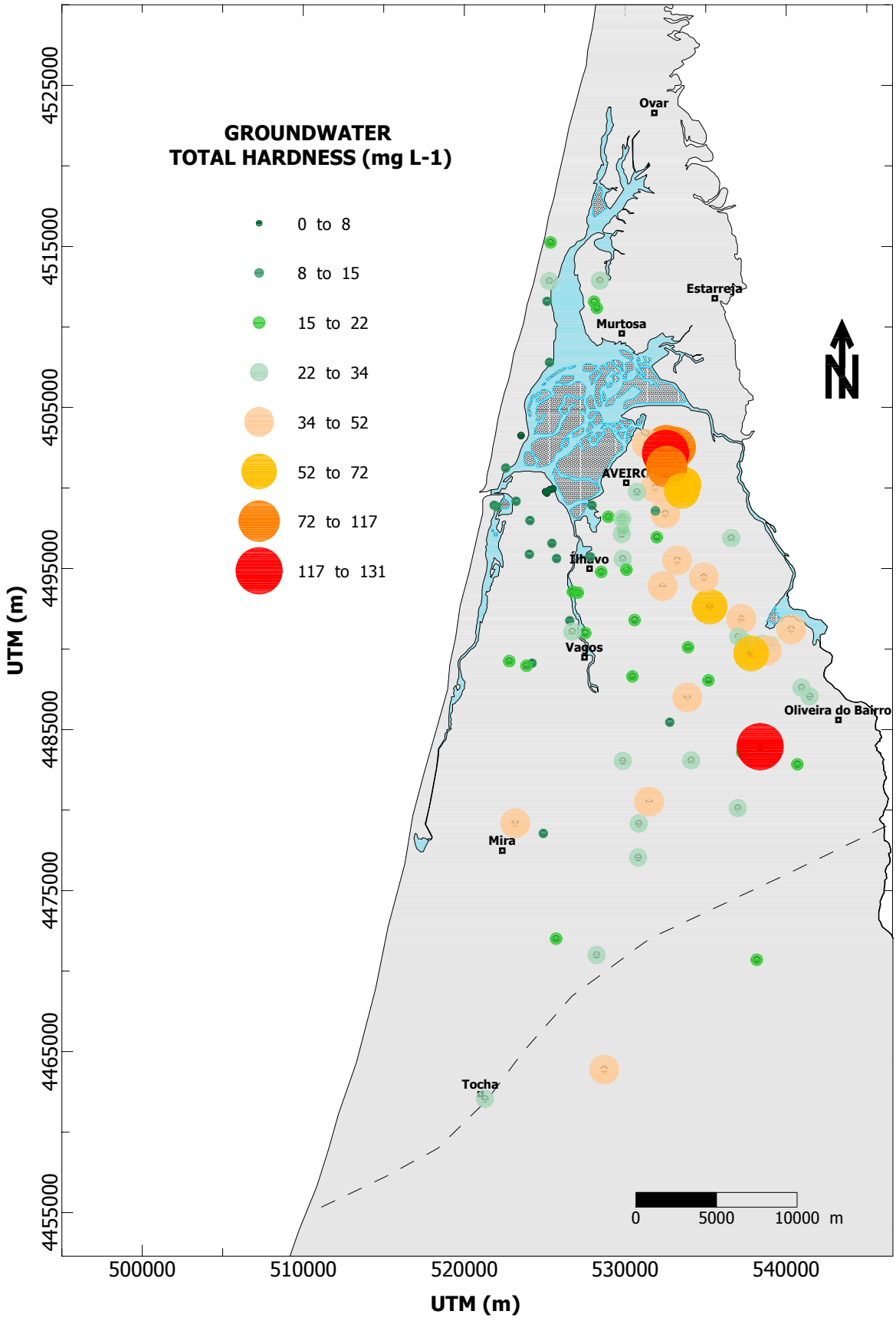
GROUNDWATER
TOTAL HARDNESS (mg L-1)
0 to 8
8 to 15
15 to 22
22 to 34
34 to 52
52 to 72
72 to 117
117 to 131
Ovar
Estarreja
Murtosa
AVEIRO
Ílhavo
Vagos
Oliveira do Bairro
Mira
Tocha
0
5000
10000 m
UTM (m)
UTM (m)
4525000
4515000
4505000
4495000
4485000
4475000
4465000
4455000
500000
510000
520000
530000
540000